

**Experimental and computational study of a solar
powered hydrogen production system for domestic
cooking applications in developing economies**

**A thesis submitted for the degree of
Doctor of Philosophy (PhD)**

by

Evangelia Vasiliki Topriska

College of Engineering, Design, and Physical Sciences

Brunel University London



Abstract

In many developing economies, a high percentage of domestic energy demand is for cooking based on fossil and biomass fuels. Their use has serious health consequences affecting almost 3 billion people. Cleaner cooking systems have been promoted in these countries such as solar cooking and smokeless stoves with varying degrees of success. In parallel, solar electrolytic hydrogen systems have been developed and increasingly used during the last 25 years for electricity, heat and automobile fueling applications.

This study has developed and tested experimentally in the laboratory a solar hydrogen plant numerical model suitable for small communities, to generate and store cooking fuel. The numerical model was developed in TRNSYS and consists of PV panels supplying a PEM electrolyser of 63.6% measured stack efficiency and hydrogen storage in metal hydride cylinders for household distribution. The model includes novel components for the operation of the PEM electrolyser, its controls and the metal hydride storage, developed based on data of hydrogen generation, stack temperature and energy use from a purpose constructed small-scale experimental rig. The model was validated by a second set of experiments that confirmed the accurate prediction of hydrogen generation and storage rates under direct power supply from PV panels.

Based on the validated model, large-scale case studies for communities of 20 houses were developed. The system was sized to generate enough hydrogen to provide for typical domestic cooking demand for three case-studies; Jamaica, Ghana and Indonesia. The daily cooking demands were calculated to be 2.5kWh/day for Ghana, 1.98kWh/day for Jamaica and 2kWh/day for Indonesia using data mining and a specific quantitative survey for Ghana. The suitability of weather data used in the model was evaluated through Finkelstein Schafer statistics based on composite and recent weather data and by comparing simulation results. A difference of 0.9% indicated that the composite data can be confidently used. Simulations results indicate that a direct connection system to the PV plant rather than using a battery is the optimal design option based on increased efficiency and associated costs. They also show that on average 10tonnes of CO₂/year/household can be saved by replacing biomass fuel with hydrogen. The potential of total savings in the three case-study countries is shown in the form of novel solar hydrogen potential maps. The results of this study are a contribution towards better understanding the use of hydrogen systems and enhancing their role in renewable energy policy.

Acknowledgments

I would like to express my appreciation and gratitude to my supervisor, Professor Maria Kolokotroni, who has given me the opportunity to work on this project. I would like to thank her for her trust in me, her guidance and for supporting my professional and educational development throughout all the years of my research. Also I would like to express my thankfulness to Dr Zahir Dehouche, for his scientific support and advice throughout the experimental part of this project.

I would like to thank the ACP Caribbean & Pacific Research Programme for Sustainable Development of the European Union (EuropeAid/130381/D/ACT/ACP) for funding this project and Dr Earl A. Wilson of the University of Technology in Kingston, Jamaica for leading the project and facilitating the collaborative research between Brunel and UTech.

I am thankful to the technicians of Brunel University: Mr C. Xanthos and Mr E. Wyse amongst others, for their technical help and to Dr Divine Noviето of Ho Polytechnic in Ghana for his aid with the conduction of the quantitative surveys in the Volta region. I would like to express my thanks to my colleagues and friends at Brunel for their support and for the time well spent working together and sharing our agonies and aspirations.

Finally, I would like to express my gratitude to my family and friends and especially my mother Sofia and my grandfather Pavlos, for their moral and emotional support. I am grateful that they aspired in me the will of constant self-improvement, educational achievements and development. I dedicate this thesis to them.

Contents

Chapter 1. Introduction	25
1.1 Research motivation	26
1.2 The Solar Hydrogen System.....	29
1.3 Objectives of the Research	33
1.4 Structure of this Thesis	34
1.5 Publications	37
Chapter 2. Background Information of Solar Hydrogen Systems	39
2.1 Introduction	40
2.2 Hydrogen production.....	40
2.3 Photovoltaic Panels	55
2.4 Hydrogen storage	57
2.5 Summary	60
Chapter 3. Experimental Components and Processes.....	61
3.1 Experimental Setup Introduction.....	62
3.2 Laboratory Safety and Equipment.....	62
3.3 Description of the Proton Exchange Membrane (PEM) electrolyser by Proton Onsite	64
3.4 Description of the Alkaline Solid Polymeric Membrane (ASPM) electrolyser by Acta	67
3.5 PV Data emulator	70
3.6 Metal hydride storage tank	76
3.7 Instrumentation.....	77
3.8 Experimental Steps for the Proton Exchange Membrane (PEM) Electrolyser experiments	79

3.9	Experimental Steps for the Alkaline Solid Polymeric Membrane (ASPM) Electrolyser experiments	82
3.10	Direct Stack Measurements	85
3.11	Metal hydride storage experimental process description	86
3.12	Summary	88
Chapter 4:	Analysis of Experimental Results and Numerical Model Development	89
4.1	Introduction	90
4.2	Hydrogen flow and stack measurements	90
4.3	Electrical Characteristics Measurements for the Start Up.....	96
4.4	Stack Direct Measurements	98
4.5	Metal Hydride Storage Experiment.....	100
4.6	Alkaline Solid Polymeric Membrane (ASPM) Electrolyser Experimental Measurements.....	112
4.7	Summary	116
Chapter 5:	Numerical Model Development.....	117
5.1	Introduction	118
5.2	Introduction to TRNSYS.....	118
5.3	Model Development Strategy.....	120
5.4	Model validation - Experimental Weather and PV Power Input Data	127
5.5	Experiments for the Numerical Model Validation	131
5.6	Experiments for the UK (London) Conditions.....	131
5.7	Experiments for the Jamaica Conditions.....	135
5.8	Effect of the irradiance input on the efficiency of the electrolyser	137
5.9	Numerical model validation	139
5.10	Statistical Validation of Models	142

5.11	Sensitivity Parametric Tests on the Hydrogen Generation Flow Rates of the PEM Electrolyser Model	145
5.12	ASPM Electrolyser day tests	147
5.13	Summary	149
Chapter 6:	Case Study Countries Presentation and Cooking Demand Calculation.....	150
6.1	Introduction	151
6.2	Ghana Case Study	151
6.3	Jamaica Case Study	183
6.4	Indonesia Case Study	187
6.5	Summary	191
Chapter 7:	Case Studies Numerical Model Development and Weather Data Effect on Simulation.....	192
7.1	Introduction	193
7.2	Design and Optimisation Methodology of the Solar Hydrogen system.....	193
7.3	Case Studies Development.....	198
7.4	Weather Data Effect on the Simulation.....	208
7.5	Weather Data Types	208
7.6	Meteonorm Weather Data	209
7.7	Suitable Weather Data Type for the Solar Hydrogen System Simulation	211
7.8	Comparison of the Meteonorm Weather Data with the Recent Weather Data for Kingston	212
7.9	Comparison of the Effect of the Composite and the Recent Weather Data on the Simulation Results.....	220
7.10	Comparison of the effect of the Future Weather Files on the Simulation Results 222	
7.11	Generation of Solar Hydrogen Potential Maps	226
7.12	Discussion of the Solar Hydrogen Potential Maps.....	229

7.13 Summary	230
Chapter 8. Techno-economic Analysis.....	231
8.1 Introduction	232
8.2 Ghana Case Studies Cost Analysis.....	232
8.3 Jamaica and Indonesia Case Studies Cost Analysis.....	243
8.4 Cost Benefit Analysis Results Discussion.....	243
8.5 Marginal Abatement Cost Curves	246
8.6 Summary	249
Chapter 9. Conclusions and Future Recommendations	250
9.1 Overview	251
9.2 Main Findings.....	253
9.3 Recommendations for Further Work.....	258
References	259

List of figures

Figure 1.1, The Energy Ladder: Household Energy and Development Linking	26
Figure 1.2, Annual Deaths Worldwide by Cause.....	27
Figure 1.3, Open Fire inside a house in rural India.....	28
Figure 1.4, The Long Term Perspective of Main Hydrogen Pathways	32
Figure 1.5, Future Potential Costs of Electrolytic Hydrogen.....	32
Figure 1.6, Main components of the solar hydrogen system for cooking.....	33
Figure 1.7, Research Methodology	36
Figure 2.1, World Hydrogen Consumption Rates.....	41
Figure 2.2, Non-refinery use of Hydrogen in the United States Market.....	41
Figure 2.3, Selected Hydrogen Production Methods	42
Figure 2.4, Alkaline Electrolysis Process	48
Figure 2.5, Monopolar and Bipolar Electrolyser cell arrangements	49
Figure 2.6, PEM Electrolysis process	50
Figure 2.7, Structure of the PEM electrolytic cell	51
Figure 2.8, Cost apportionment in a PEM electrolyser stack.....	51
Figure 2.9, The concept of Photo-electrolysis	53
Figure 2.10, The principle of Photo-biological hydrogen production	54
Figure 2.11, photovoltaic panel fundamental principles.....	56
Figure 3.1, Hydrogen Sensor installed in the Hydrogen Laboratory	63
Figure 3.2, Hydrogen Sensor Box installed in the entrance of the Hydrogen Lab	63
Figure 3.3: Representative I-V Polarization curve (at 13.8bar, 40°C).....	64
Figure 3.4, Internal Schematic of the PEM electrolyser, redrawn from original.....	66
Figure 3.5, Components of the hydrogen production and water and gases management of the PEM electrolyser	67
Figure 3.6, Representative I-V polarisation curve, at 20°C, 13.8bar	68

Figure 3.7, Left side and internal hydrogen generation components of the ASPM electrolyser	68
Figure 3.8, Internal Schematic of the ASPM electrolyser, redrawn from original	69
Figure 3.9, The Raspberry Pi used in the experiments	71
Figure 3.10, Raspberry Pi B schematich diagramm and ports	74
Figure 3.11, Digital to Analogue Converter used in the experiments.....	74
Figure 3.12, Power Envelope of the DC Power Supply Unit	75
Figure 3.13, Analogue controls connection at the back of the DC Power Supply Unit.....	75
Figure 3.14, Metal hydride storage tank	77
Figure 3.15, Thermocouple for the measuring of the temperature of the PEM electrolyser produced hydrogen.....	78
Figure 3.16, Experimental Setup of the PEM Electrolyser	81
Figure 3.17, Experimental Setup of the PEM Electrolyser	82
Figure 3.18, Experiment setup of the ASPM Electrolyser.....	84
Figure 3.19, Schematic Diagram of the Experimental Rigs.....	84
Figure 3.20, The complete Experimental Setup of PEM and ASPM Electrolyser	85
Figure 3.21, Direct stack measurements on the PEM electrolyser	86
Figure 3.22, Direct stack measurements on the ASPM electrolyser.....	86
Figures 4.1, hydrogen flow at the generating pressure of 13.8bar	92
Figure 4.2, Average hydrogen flow rates curve for the complete pressure range of the electrolyser, 3 to 13.8bar	93
Figure 4.3, Experimental temperature measurements for pressures of 5 to 13.8 bar.....	94
Figure 4.4, Experimentally measured energy use of the stack for pressures of 5 to 13.8bar	94
Figure 4.5, power of the electrolyser during start-up for the distinct pressures set-points of 5bar, 7bar, 10bar and 13.8bar	97
Figure 4.6, Experimental stack polarisation curve.....	98

Figure 4.7, Variable DC current and voltage to the stack while producing constant hydrogen at 13.8bar.....	99
Figure 4.8, Variable DC power to the stack while producing constant hydrogen at 13.8bar	99
Figure 4.9, Maximum DC current and voltage to the stack for maximum stack operation	100
Figure 4.10, Maximum DC power to the stack for maximum stack operation.....	100
Figure 4.11, Stack measurements	100
Figure 4.12, PCI of LaNi ₅	101
Figure 4.13, The experimental Metal Hydride Tank.....	101
Figure 4.14, The experimental setup for the metal hydride experiment	102
Figure 4.15, Hydrogen flow rates to the metal hydride tank from the electrolyser during absorption phase.....	103
Figure 4.16, Temperatures of the metal hydride tank from the electrolyser during absorption phase.....	104
Figure 4.17, measurement of the weight of the Metal Hydride tank at the beginning and at the end of the experiment.....	107
Figure 4.18, Mass of hydrogen stored in the metal hydride tank in relation to the supply pressure	108
Figure 4.19, Mass of stored hydrogen in the metal hydride tank in relation to the supply pressure	109
Figure 4.20, Volume of stored hydrogen in the metal hydride tank in relation to the supply pressure	109
Figure 4.21, Pressure increase over time in the metal hydride tank in relation to the hydrogen supply pressure.....	110
Figure 4.22, Hydrogen mass accumulated in the tank at pressure equilibrium point over the maximum mass	111
Figure 4.23, I-V Polarisation curve for the ASPM Stack at 25°C	112

Figure 4.24, I-V Polarisation curve for the ASPM Stack at 25°C, 29°C and 30°C.....	113
Figure 4.25, ASPM Electrolyser hydrogen flow rate and stack input power over time ...	114
Figure 4.26, Stack Voltage over Stack temperature.....	114
Figure 4.27, Stack input power over stack temperature for the ASPM electrolyser.....	115
Figure 4.28, Hydrogen flow rates over stack temperature for the ASPM electrolyser.....	115
Figure 5.1, TRNSYS PEM electrolyser component parameters.....	124
Figure 5.2, TRNSYS PEM electrolyser controls component inputs.....	125
Figure 5.3, TRNSYS metal hydride component outputs	126
Figure 5.4, Power output data of the PV array for the first week of June 2013 in United Kingdom.....	129
Figure 5.5, Power output and irradiance data of the PV array installed in University of Technology in Kingston for days in May 2013	130
Figure 5.6, Power output and irradiance data of the PV array installed in University of Technology in Kingston for days in December 2013	130
Figure 5.7, Hydrogen production rate in L/h at 5bar, 7bar,10bar,13.8bar pressure set points during day 1 that presents unstable irradiance levels.....	131
Figure 5.8, Hydrogen production rate in L/h at 5bar, 7bar,10bar,13.8bar pressure set points during day 4 that presents consistently high irradiance levels.....	132
Figure 5.9, Efficiency vs pressure set point for each day of the United Kingdom experimental days.....	132
Figure 5.10, kWh/kg vs pressure set point for each day of the United Kingdom experimental days.....	133
Figure 5.11, kWh/Nm ³ of H ₂ vs pressure set point for each day of the United Kingdom experimental days.....	133
Figure 5.12, Hydrogen production rate in L/h at 5bar, 7bar,10bar,13.8bar pressure set points during 12 th of May in Jamaica, that presents consistently high irradiance levels ..	135
Figure 5.13, Hydrogen production rate in L/h at 5bar, 7bar,10bar,13.8bar pressure set points during 17 th of May in Jamaica, that presents unstable irradiance levels	135

Figure 5.14, Efficiency vs pressure set point for each day of the Jamaica experimental days	136
Figure 5.15, kWh/kg vs pressure set point for each day of the Jamaica experimental days	136
Figure 5.16, kWh/Nm ³ vs pressure set point for each day of the Jamaica experimental day	137
Figure 5.17, TRNSYS model of the experimental setup for the validation.....	140
Figure 5.18, Comparison between TRNSYS and experimental results of produced hydrogen flow rates at 5bar.....	142
Figure 5.19, Comparison between TRNSYS and experimental results of produced hydrogen flow rates at 7bar.....	142
Figure 5.20, Comparison between TRNSYS and experimental results of produced hydrogen flow rates at 10bar.....	142
Figure 5.21, Comparison between TRNSYS and experimental results of produced hydrogen flow rates at 13.8bar.....	142
Figure 5.22, Experimental and numerical model stack power results	144
Figure 5.23, Sensitivity of hydrogen flow rates to hydrogen generation pressure	145
Figure 5.24, Sensitivity of hydrogen flow rates to stack current	146
Figure 5.25, Sensitivity of hydrogen flow rates to stack temperature	146
Figure 5.26, Hydrogen production rate in L/h Day 1 of the UK data, that presents unstable irradiance levels	147
Figure 5.27, Hydrogen production rate in L/h Day 2 of the UK data, that presents unstable irradiance levels	147
Figure 5.28, Hydrogen production rate in L/h Day 3 of the UK data, that presents unstable irradiance levels	148
Figure 5.29, Hydrogen production rate in L/h Day 4 of the UK data, that presents constantly high irradiance levels.....	148

Figure 5.30, Hydrogen production rate in L/h Day 5 of the UK data, that presents constantly high irradiance levels	148
Figure 5.31, Hydrogen production rate in L/h Day 6 of the UK data, that presents constantly high irradiance levels	148
Figure 6.1, Ghana location in Africa and country map.....	152
Figure 6.2, Ghana Final Energy Consumption	153
Figure 6.3, Ghana Energy Share by Type in 2012.....	153
Figure 6.4, Fuel Used for Cooking as percentage in Households in Ghana in 2010	154
Figure 6.5, LPG consumption Share in Ghana	155
Figure 6.6, LPG consumption Share in Ghana	155
Figure 6.7, Ghana map, location in Africa and the selected fieldwork locations	158
Figure 6.8, The Charcoal market in Akatsi	162
Figure 6.9, The firewood market in Keta.....	162
Figure 6.10, Percentage of households per main fuel use.....	163
Figure 6.11, Akatsi participants' educational attainment.....	164
Figure 6.12, Keta participants' educational attainment	164
Figure 6.13, Sogakope participants' educational attainment	164
Figure 6.14, Main fuel use according to the educational attainment	165
Figure 6.15, Main fuel use per area	166
Figure 6.16, Total fuel use per household.....	168
Figure 6.17, Total fuel use per educational attainment.....	169
Figure 6.18, Total fuel use per area	170
Figure 6.19, Cooking with local firewood stove.....	171
Figure 6.20, Charcoal pot.....	172
Figure 6.21, Firewood local stove.....	172
Figure 6.22, Firewood local stove.....	172

Figure 6.23, Firewood local stove.....	172
Figure 6.24, Age breakdown of the sample population	173
Figure 6.25, Trends in fuel use according to the household income.....	176
Figure 6.26, Representation of income percentages spent on cooking fuel for the total sample	177
Figure 6.27, Main fuel use according to the household income	178
Figure 6.28, Total fuel use according to the household income	178
Figure 6.29, Percentages of the reason for the main fuel selection accordance to the use of each fuel	179
Figure 6.30, Reasons to switch to hydrogen cooking gas	179
Figure 6.31, Percentage of the CO ₂ emissions for each fuel.....	182
Figure 6.32, Percentage of the CO emissions for each fuel	182
Figure 6.33, Jamaica Global Horizontal Irradiation.....	183
Figure 6.34, Breakdown of Energy Sources other than Oil	184
Figure 6.35, CO ₂ emissions in relation to fossil fuel consumption in Jamaica.....	185
Figure 6.36, Indonesia in the globe	187
Figure 6.37 Indonesia energy demand by sector in 2012.....	188
Figure 6.38, Indonesia primary energy demand mix in 2012	188
Figure 6.39, Indonesia energy mix share by 2015	189
Figure 7.1, Flowchart of the system design decision making	197
Figure 7.2, Ghana direct connection case study TRNSYS print screen	199
Figure 7.3, Ghana annual global horizontal irradiance and temperature values from Meteonorm file.....	202
Figure 7.4, TRNSYS simulation results for the Ghana direct connection case study for the month of May	204
Figure 7.5, Monthly demand and production of hydrogen and PV yield for the current conditions and after the panel degradation period for the Ghana case study.....	205

Figure 7.6, Meteorological Stations Map.....	210
Figure 7.7, Meteororm Typical Meteorological Year data generation process.....	210
Figure 7.8 ,Weather Station in the University of Technology, Jamaica	212
Figure 7.9, Comparison between the CDF curves for Global Horizontal Radiation for 2011	216
Figure 7.10, Comparison between the CDF curves for Global Horizontal Radiation for 2012.....	217
Figure 7.11, Comparison between the CDF curves for Global Horizontal Radiation for 2013.....	217
Figure 7.12, Comparison between the CDF curves for Global Horizontal Radiation for all the years	217
Figure 7.13, Comparison of the hydrogen generation results of the simulation with the Meteororm and the 2013 recent weather data	220
Figure 7.14, Comparison of the Irradiance with the Meteororm weather file and the morphed weather file.....	223
Figure 7.15, Comparison of the temperature with the Meteororm weather file and the morphed weather.....	223
Figure 7.16, Comparison between the CDF curves for Global Horizontal Irradiance for Typical Meteororm Year and Morphed Meteororm Year	225
Figure 7.17, Comparison between the CDF curves for Temperature for Typical Meteororm Year and Morphed Meteororm Year	225
Figure 7.18, Comparison of the hydrogen generation with the Meteororm weather file and the morphed weather file.....	226
Figure 7.19, Solar hydrogen potential maps for Ghana, Jamaica and Indonesia	228
Figure 8.1, Price history of silicon PV cells.....	246
Figure 8.2, Ghana case studies options MAC curves.....	247
Figure 8.3, Jamaica case studies options MAC curves	247
Figure 8.4, Indonesia case studies options MAC curves	247

List of Tables

Table 1.1, Properties of hydrogen	31
Table 1.2, Environmental Damage Factors	31
Table 2.1, Comparison of the natural gas hydrogen production methods	44
Table 2.2, Advantages and disadvantages of water electrolysis methods.....	55
Table 3.1, Electrical and Thermal characteristics of the UK PV modules used for the experimental PV emulator.....	71
Table 3.2, Typical example of current values used in the experiments	73
Table 4.1 Average flow rates, maximum temperature and stack efficiency	95
Table 4.2: Specific energy use of the stack per mass and per volume.....	96
Table 4.3, Maximum temperatures during absorption phases and the time to reach it, for each hydrogen supply pressure	104
Table 4.4, Time to complete storage process in relation to hydrogen supply pressure	107
Table 4.5, Hydrogen storage capacity (wt%) for each test	109
Table 4.6, Hydrogen mass accumulated in the tank at pressure equilibrium point over the maximum mass	110
Table 4.7, Reduction in the energy consumption of the stack with the increase in operating temperature.....	113
Table 5.1, Coefficient of performance of the PEM electrolyser operation.....	121
Table 5.2, Electrical and Thermal characteristics of the PV modules of the experimental PV emulator	128
Table 5.3, Stack efficiency improvement with pressure and irradiance profile.....	134
Table 5.4, Total generated hydrogen (L) for the UK representative experimental days .	139
Table 5.5, Total generated hydrogen (L) for the Jamaica representative experimental days	139
Table 5.6, Results of F-test and t-test for the model calculated parameters	145

Table 5.7, ASPM electrolyser efficiencies for each experimental day	148
Table 6.1 Fuel Used for Cooking as percentage in households in Ghana, 2000 and 2010	154
Table 6.2, Categories and numbers of stakeholders that participated in the Survey	161
Table 6.3, Percentage of the population in relation to their educational attainment and main fuel use	165
Table 6.4, LPG use and additional fuels	167
Table 6.5, Charcoal use and additional fuels	167
Table 6.6, Firewood use and additional fuels	167
Table 6.7, Percentage of the population in relation to their educational attainment and total fuel use	169
Table 6.8, Percentages of total fuel use in relation to each area and its population	170
Table 6.9, Cooking device use per fuel use	171
Table 6.10, Average yearly fuel consumption for a typical Ghanaian household, if the demand was satisfied only by one cooking fuel.....	174
Table 6.11, Type and costs of standard fuel purchased units.....	174
Table 6.12, Comparison between the fuel costs of the field study and reported 2005 data,	175
Table 6.13, Fuel costs per kWh for the total fuel use of each main fuel and total cost for the average household	176
Table 6.14, Extra costs spent for the acquisition of cooking fuel	178
Table 6.15, Ghana percentage share of gaseous emissions to the environment, 2000 – 2004	180
Table 6.16, GHG Emission forecast for 2015 and 2020 in CO ₂ equivalent.....	180
Table 6.17, Inventory data for cook-stove emissions (kg/MJ fuel)	181
Table 6.18, Annual CO ₂ emissions that correspond to the used fuels of the field study ..	181
Table 6.19, Distribution of households by source and use of energy for cooking,.....	185

Table 6.20, Size, Price and Durability of LPG Cylinders in Jamaica.....	186
Table 6.21, Size and durability of LPG and kerosene cylinders in Indonesia	190
Table 7.1, Each PEM electrolyzers’ parameters in the Ghana case study	201
Table 7.2, Ghana case study hydrogen production and PV yield at current and future conditions	205
Table 7.3, Ghana battery case study hydrogen production and PV yield at current and future conditions.....	206
Table 7.4, Jamaica case study hydrogen production and PV yield at current and future conditions	206
Table 7.5 Jamaica battery case study hydrogen production and PV yield at current and future conditions.....	207
Table 7.6, Indonesia case study hydrogen production and PV yield at current and future conditions	207
Table 7.7, Indonesia battery case study hydrogen production and PV yield at current and future conditions.....	207
Table 7.8, Jamaica Weather Station Information, source: (Meteotest, 2014).....	211
Table 7.9, Total FS Statistics of Recent Weather Data of Kingston compared with Meteorom Weather Data	218
Table 7.10, Hydrogen generation results of the simulation with the Meteorom and the 2013 recent weather data.....	221
Table 7.11, Total country solar hydrogen potential indicators	229
Table 8.1, Overview of commercially available electrolyser technologies, source: (Bertuccioli, et al., 2014).....	233
Table 8.2, Price apportionment for the PV system installation.....	234
Table 8.3, Scenario 1a - Distribution of costs	236
Table 8.4, Present cost analysis model for the solar hydrogen system, referring to scenario 1a.....	236
Table 8.5, Sensitivity analysis of the scenario 1a system	237

Table 8.6, Scenario 1b - Distribution of costs.....	238
Table 8.7, Present cost analysis model for the solar hydrogen system, referring to scenario 1b.....	238
Table 8.8, Sensitivity analysis of the scenario 1b system	239
Table 8.9, Scenario 1c - Distribution of costs	240
Table 8.10, Present cost analysis model for the solar hydrogen system, referring to scenario 1c.....	240
Table 8.11, Sensitivity analysis of the scenario 1c system	241
Table 8.12, Distribution of costs	242
Table 8.13, Hydrogen unit costs referring to the battery system configurations	242
Table 8.14, Comparison of the scenarios of each case study country.....	244

Abbreviations

AC	Alternative Current
ASPM	Alkaline Solid Polymeric Membrane
ATR	Autothermal Reforming
CCS	Carbon Capture and Storage
CDF	Cumulative Distribution Function
CGS	Compressed Gas Storage
DC	Direct Current
F	Faraday
FS	Finkelstein-Schafer
GHS	Ghanaian Cedi
IEA	International Energy Agency
LPG	Liquified Petroleum Gas
MH	Metal Hydride
MS	Middle school
PEM	Proton Exchange Membrane
POX	Partial Oxidation
PS	Primary school
PV	Photovoltaic
SH	Senior high school
SMR	Steam Reforming
TMY	Typical Meteorological Year
UN	United Nations
WHO	World Health Organisation

List of Symbols

ΔH	Enthalpy Difference (kJ)
a_{cat}	The charge transfer coefficients at the cathode (CTC)
CD	Average daily cooking demand (kWh/day)
CDay	Daily amount of charcoal used by each household (kg)
CDFm	Long term cumulative distribution factor
CDFy,m	Short term distribution factor, for year y
Ceff	Efficiency of the charcoal pot, equal to 18%
c_o	Performance coefficient of the electrolyser
CVC	Calorific value of charcoal, equal to 8.5kWh/kg
CVF	Calorific value of firewood, equal to 3.9kWh/kg
CVK	Calorific value of kerosene, equal to 12.7kWh/kg
CVLPG	Calorific value of LPG, equal to 13kWh/kg
E_{H_2}	Energy content of generated hydrogen (kWh)
F	The Faraday constant (96,485 C/mol)
FDay	Daily amount of firewood used by each household (kg)
Feff	Efficiency of the firewood stove, equal to 14%
FSweighted	FS statistic incorporating all the weather parameters multiplied by weighting factors
FSx	FS statistic for a particular weather parameter x
H_2	Generated hydrogen flow rates (ml/min)
H_{2Max}	Maximum hydrogen that can be stored in the metal hydride tank (Nm ³)
H2stored	Stored hydrogen in the metal hydride tank in (Nm ³) and (gr)
$H_{2stored}$	Hydrogen mass stored in the metal hydride tank for specific flow (kg)
Hf,products	Enthalpy of products (kJ)

Hf,reactants	Enthalpy of reactants (kJ)
HHV	Higher Heating Value (MJ/kg)
I	The current to the electrolyser stack (A)
I _L	PV module photocurrent (A)
I _o	Diode reverse saturation current (A)
j	The current density (A/cm)
j _{0,an}	The exchange current density at the anode (A/cm ²)
j _{0,cat}	The exchange current density at the cathode (A/cm ²)
k	Boltzmann constant [J/K]
Kcyl	Kerosene cylinder size (kg)
Keff	Efficiency of the kerosene stove, equal to 35%
LPGcyl	LPG cylinder size (kg)
LPGDay	Daily amount of LPG used by each household (kg)
LPGeff	Efficiency of the gas burner, equal to 45%
M	Number of parameters for the weighted Finkelstein-Schafer statistic
mTMAX	Hydrogen mass accumulated in the tank at pressure equilibrium point (gr)
mTOTAL	Stored hydrogen in the metal hydride tank (gr)
n	The number of electrons (2 for water electrolysis)
N	Number of daily readings in a month
N	Normal
n _c	The number of cells of the electrolyser stack
n _i	Diode ideality factor
N _s	Number of individual cells in series within a module
p	The atmospheric pressure (atm)
pH ₂	Hydrogen generation pressure (bar)

P_{H_2}	Stack Power (W)
q	Electrical charge (C/mol)
$Q_{convection}$	Convective heat transfer losses of the tank (W)
$Q_{radiation}$	Radiation heat transfer losses of the tank (W)
Q_{total}	Total heat transfer losses of the tank (W)
R	The ideal gas constant (0.0824 Latm/molK)
R_s	Module series resistance [Ω]
R_{sh}	Module shunt resistance [Ω]
$SH_{potential}$	Normalised solar hydrogen potential (thousand kg/km ² /year)
Solar	Solar potential
T	Temperature (K or C)
T_c	Module temperature [K]
V	Voltage (V)
$V_{activation}$	Activation Overvoltage (V)
V_{actual}	Actual hydrogen production (ml/min)
V_{cell}	Electrolytic cell voltage (V)
V_{H_2}	Theoretical hydrogen production (ml/min)
V_{Nernst}	Nernst Voltage (V)
V_{Ohmic}	Ohmic Resistance Overvoltage (V)
V_{rev}	Reversible cell voltage (V)
V_{stack}	Electrolytic stack voltage (V)
V_{th}	Thermoneutral cell voltage (V)
W_e	Work (W)
WF	Weighting factor for a specific weather parameter
WF_x	Weighting factor for a specific weather parameter

α_{an}	The charge transfer coefficients at the anode (CTC)
ΔG	Gibbs Free Energy (kJ)
ΔS	Entropy Difference J mol ⁻¹ K ⁻¹)
η_F	The Faraday efficiency of the electrolyser
ρ	Hydrogen density (kg/m ³)
σ	The conductivity of the membrane (Scm ⁻¹)
φ	The thickness of the electrolyte-membrane (178 μ m for Nafion TM 117)

Subscripts

an	Anode
cat	Cathode
cyl	cylinder
eff	efficiency
F	Farraday
rev	reversible - for the reversible cell voltage of the electrolytic cell
weighted	weighted FS statistic
x	Parameter in Finkelstein-Schafer statistics

Chapter 1. Introduction

1.1 Research motivation

Future global energy demand is predicted to increase; over 70% of this demand will be from developing economies (World Nuclear Association, 2014). Currently, over 2.5 billion people depend on firewood, charcoal, agricultural waste and animal dug as fuel for cooking; 87% of rural India and 93% of rural sub-Saharan Africa depend on these fuels. Figure 1.1 shows graphically that low income population depends on less clean and inefficient fuels. This number is predicted to increase further, and by 2030 over 2.7 billion people will depend on these fuels (IEA, 2006).

As a consequence, energy related greenhouse gas emissions are predicted to increase (Kaygusuz, 2011). According to the IEA, energy-related CO₂ emissions were 30.4Gt in 2010 and are predicted to rise to 36.4Gt in 2035 under the scenario which incorporates global energy policies to tackle climate change (International Energy Agency, 2011). Over three quarters of this growth come from developing economies with China leading the emissions on a global level.

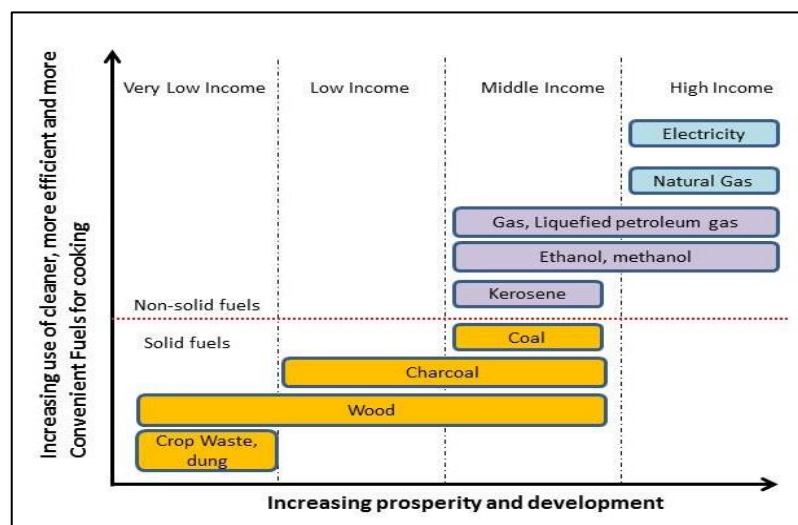


Figure 1.1, The Energy Ladder: Household Energy and Development Linking, source: (World Health Organisation, 2006)

Household energy use in the developing world represents 10% of the world's primary energy demand, according to the IEA (IEA, 2006). The main use of energy (90%) in households in developing economies is for cooking, followed by heating and lighting as due to location and climate space and water heating needs are very small. The majority of these countries are situated in sub-Saharan Africa and the rest in rural China, India, Asia

and Latin America. Electricity is more scarce and subject to regular power cuts with almost 1.5 billion with no access to electricity (Kaygusuz, 2011).

Therefore, cooking in developing economies depends on biomass based fuels. The use of wood, charcoal and biomass can prove extremely hazardous for health. In 2002, cooking with solid fuels contributed to nearly 800,000 deaths among children and more than 500,000 deaths among women (World Health Organisation, 2006). In developing economies death related to indoor air pollution from the use of solid fuels is rated fourth after human immunodeficiency virus infection and acquired immune deficiency syndrome (HIV/AIDS) and lack of clean water, and caused more fatalities than malaria and almost the same as tuberculosis (World Health Organisation, 2006). This is shown diagrammatically in Figure 1.2.

According to more recent data, this problem is continuing; the number of people that die every year due to exposure to indoor air pollution has increased to approximately 4 million (World Health Organisation, 2014). Poor ventilation and outdated cooking methods, as shown in Figure 1.3, result to numerous deaths directly related to cooking. (World Health Organisation, 2014).

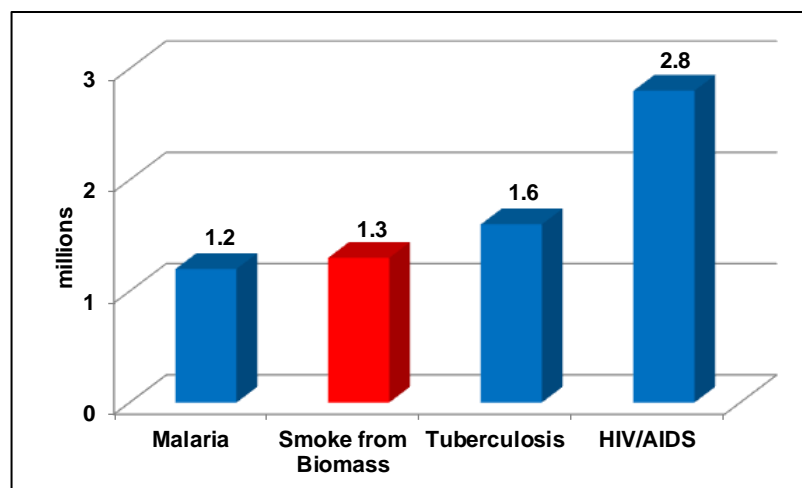


Figure 1.2, Annual Deaths Worldwide by Cause, redrawn from: (IEA, 2006)



Figure 1.3, Open Fire inside a house in rural India, source: (Massachusetts Academy of Math and Science, 2013, p. 168)

An additional consequence of using firewood and charcoal for cooking is deforestation leading to degradation of the local environment. A very characteristic example is Ghana where 70% of the fuel used is biomass and the average citizen uses approximately 640kg of wood per year while the forest growth is under half of the wood demand (Massachusetts Academy of Math and Science, 2013). Research indicates that a switch from firewood can save up to 2.4 million hectares of forests, which is almost half the global net deforestation per year (Johnson , 2012). A cost-effective analysis from the WHO has indicated also that it is worth investing in improving the cooking methods in developing economies. Fewer deaths and time gains from reduced illness, account for more than 95% of the benefits, (World Health Organisation, 2006).

Recently, a solution has been the replacement of solid fuels with Liquefied Petroleum Gas (LPG) or electricity (electric cooker). LPG provides a safer choice for cooking and has been promoted by many governments. According to the World LPG Association there is great potential in reducing CO₂ emissions by replacing firewood with LPG (Johnson , 2012). However, the increase in LPG prices in relation to the low per-capita income in developing economies has reversed the trend towards the use of biomass once again, such as in the case of Brazil (IEA, 2006).

At the beginning of the 21st century the UN Organisation launched the Millennium Project that sets the target of reducing by 50% by the year 2015 the number of households that use biomass as a primary source of fuel (United Nations, 2006). Moreover, the 17 sustainable development goals set in 2015 further promote access to affordable, reliable and

sustainable energy for all, with a focus on the cooking fuels and energy (United Nations, 2015). Solar powered electric cooking (United Nations in India, 2015), improved wood stoves (United Nations, 2015) and solar cooking projects (Programme, 2015) have been implemented by the UN as sustainable, clean and emissions free cooking methods. Beneficial outcomes have been reported by the use of solar cooking in refugee camps in Africa and multiple locations in Asia and South America where energy poverty was forcing people to use animal and agricultural waste (The UN Refugee Agency, 2004; Solar Cookers International, 2015). Solar cooking and modified charcoal stoves are also highly promoted through the Global Alliance for Clean Cookstoves (Global Alliance for Clean Cooking, 2015) with 11.7 million modified stoves distributed in seven countries in 2013. The solar cooking projects however, which were the most ambitious, have not reported particular successes. Their dependency on sunlight availability, as the energy storage option is rarely combined, their low efficiency which makes cooking time-consuming and the large space demand, especially in the case of parabolic or solar panel cookers (Solar cooker, 2015; Cuce & Cuce, 2012), pose hindrances for their use. Furthermore, solar cookers have not been widely accepted due to adverse social and cultural perceptions. This is because originally solar cooker projects targeted extreme energy poverty tackling which created a strong association with social discrimination and therefore have been met with reluctance and criticism by local societies (Piroschka Otte, 2013). Moreover, they limit the cooking place to specific areas outside the house and are difficult to cook at high temperatures to prepare traditional fried meals, to correspond with traditional cooking habits and meals (Piroschka Otte, 2013; Simon, et al., 2011).

1.2 The Solar Hydrogen System

It is suggested that a successful alternative cooking system should be easy to adopt and should not pose disruption to daily habits and cooking schedule of local residents that traditionally cook in stoves (IEA, 2006; Foell, et al., 2011). A study for the investigation of such a system was funded in 2010 by the European APC Caribbean & Pacific Research Programme for Sustainable Development programme to develop and test experimentally the application of solar-powered polymer electrolyte membrane (PEM) electrolyzers for the sustainable production of hydrogen gas a fuel for domestic cooking (ACP Science and Technology Programme, 2015). Within the scope of this project, this research focuses on

the evaluation of the potential to develop and apply solar-powered PEM electrolyser systems.

The developed solar hydrogen system consists of a photovoltaic panel array that powers a PEM electrolyser plant. Hydrogen gas is generated and distributed to households for use as an alternative clean and sustainable cooking fuel in modified gas stoves with a simple adaptation to burn hydrogen. The current cooking systems in countries selected for this study consist mainly of LPG, charcoal and firewood stoves and therefore the introduction of a modified gas stove is a solution that can be easily accepted by a wide range of the society in these countries.

Hydrogen has the biggest energy content per unit mass of any other fuel, (see Table 1.1). On a weight basis, hydrogen has energy content of 140.4 MJ/kg that is almost three times higher than the energy content of LPG, which is 46.4 MJ/kg. However, hydrogen has a very low volumetric density and this may affect applications where the size of the hydrogen storage is an issue. Nevertheless, it has many advantageous properties in comparison with fossil fuels. The most significant ones are the following:

- It diffuses through air faster than other gaseous fuels and also rises faster than methane, propane or gasoline vapour. This property of hydrogen to diffuse so fast is its greatest safety advantage.
- The flammability of hydrogen is much greater than that of methane or other fuels and is a function of concentration level.
- When its concentration is in the flammability range (4-75%), hydrogen can be ignited by a very small amount of energy due to its low ignition energy, much lower than that of gasoline and methane.
- It has a faster flame velocity than other fuels such as gasoline vapor and methane
- The hydrogen-air flame is hotter than methane-air flame and cooler than gasoline at stoichiometric conditions (Gupta, 2009).

Table 1.1, Properties of hydrogen, source: (Kirk-Othmer Encyclopedia of Chemical Technology, 1992, p. 631)

Property	Value
Molecular weight	2.01594
Density of gas at 0°C and 1 atm	0.08987 kg/m ³
Density of solid at -259°C	858 kg/m ³
Density of liquid at -253°C	708 kg/m ³
Flammability range	4-75%
Flame velocity	1.85m/s
Diffusion Coefficient in air	0.61 cm ² /s

Furthermore, hydrogen based systems have a very small environmental damage factor, as reported by Veziroglou and Sahin (Veziroglou & Sahin, 2008) and is shown in Table 1.2.

Table 1.2, Environmental Damage Factors, source: (Veziroglou & Sahin, 2008)

Energy System and Fuel	Environmental Damage (1998 US\$/GJ)
Fossil Fuel System	12.47
Coal	14.51
Oil	12.52
Natural Gas	8.26
Coal/Synthetic Fossil System	15.46
SynGas	20.34
SNG	13.49
<i>Solar Hydrogen Energy System</i>	<i>0.68</i>
<i>Hydrogen</i>	<i>0.68</i>

Use of electrolytic hydrogen is predicted to rise in the future, see Figure 1.4. The increasing use of electrolysis may lead to a reduction in costs, see Figure 1.5. Consequently this will increase the affordability of electrolytic hydrogen plants for uses other than electricity, such as for the provision of hydrogen as an alternative cooking fuel.

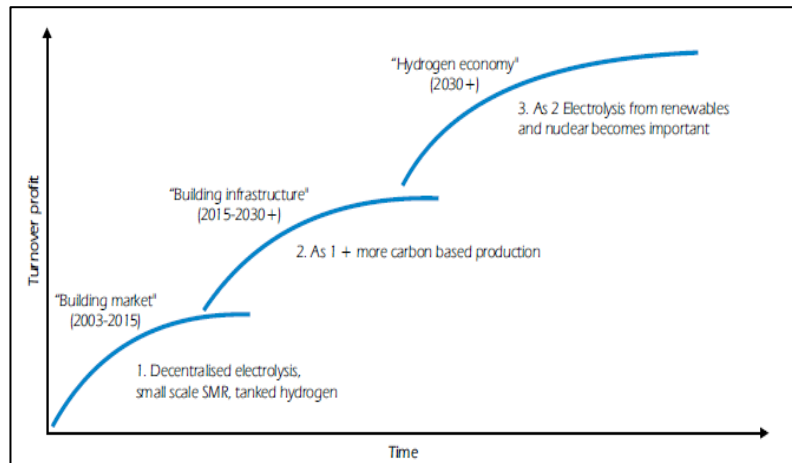


Figure 1.4, The Long Term Perspective of Main Hydrogen Pathways, source: (International Energy Agency, 2006)

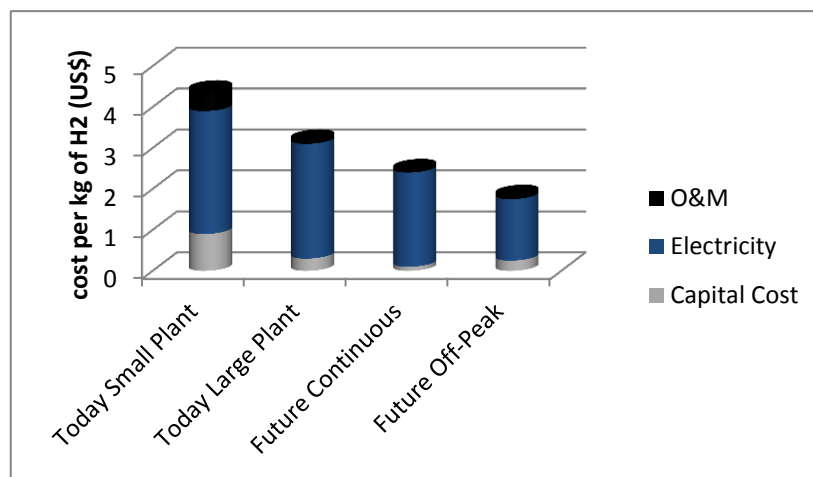


Figure 1.5, Future Potential Costs of Electrolytic Hydrogen, redrawn from: (International Energy Agency, 2006)

Safety of hydrogen use at home is an important issue considered in this project. Two alternative methods of storage were developed and assessed; a relatively low cost cascading system where hydrogen is stored in high pressure cylinders outside and is cascaded to lightweight low pressure containers suitable for transportation in private vehicles and used inside homes and (b) metal hydride storage which is more expensive and under development at present but is considered as a safer option. The system examined in this research focuses on the metal hydride storage. In addition, cookers need to be modified for burning hydrogen to which odour and flame colour is added for safety. A prototype of the modified cooker has been constructed and is being tested. Some visual information of the developed system can be seen in: (University of Technology, Jamaica, 2015).

1.3 Objectives of the Research

This research project was funded by ACP Caribbean & Pacific Research Programme for Sustainable Development of the European Union (EuropeAid/130381/D/ACT/ACP) (University of Technology Jamaica, 2014). The main objective of the funded project was to investigate the application of a novel stand-alone solar-powered PEM electrolyser plant to produce hydrogen gas at a scale suitable for storage and distribution to multiple households for cooking. The main components of the system can be seen in Figure 1.6.

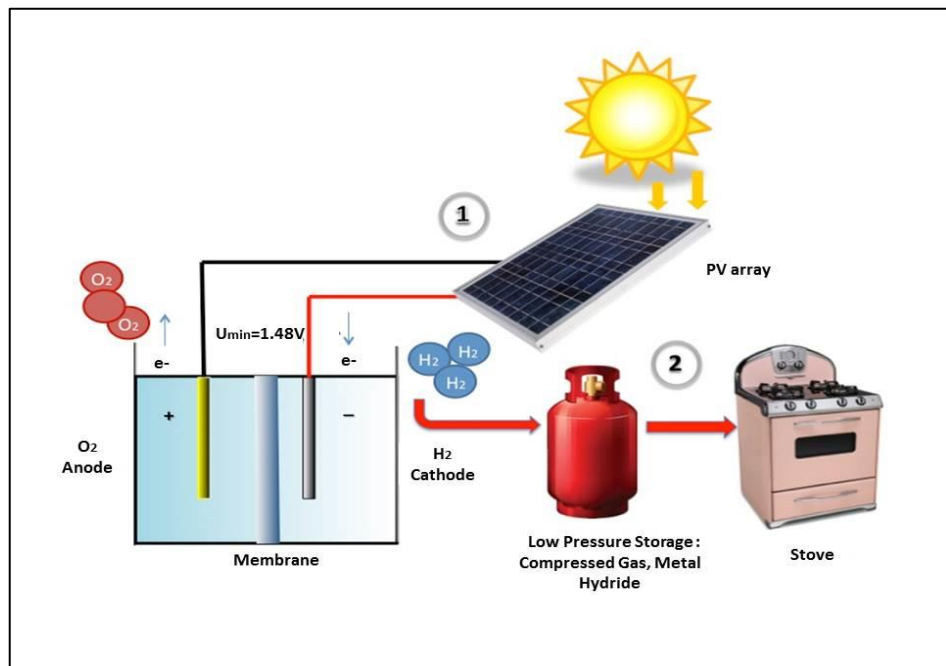


Figure 1.6, Main components of the solar hydrogen system for cooking

Within the overall funded project, this research project defined the following objectives:

- Extensive review of hydrogen generation systems and types, with a focus on solar powered electrolysis systems
- Design, construct and test the technical performance of an experimental PV panels-electrolyser setup that emulates the solar hydrogen system in a small scale (all components of Figure 1.6 excluding the stove).
- Develop a computer simulation model for the operation of the solar powered PEM electrolyser system for the production and storage of hydrogen as a cooking fuel
- Validation of the developed model

-
- Develop case studies of large-scale application by simulating communities in Jamaica as the project's main location and other selected developing economies, which are Ghana and Indonesia.
 - Evaluate the effect of the weather data on the simulation results
 - Cost Benefit Analysis of the developed system

1.4 Structure of this Thesis

This thesis is structured in ten chapters.

Chapter 1 gives an introduction and a description of the motivation of this research and the main objectives.

Chapter 2 presents a detailed overview of the solar hydrogen system applications with a special focus on each component of the system, highlighting the suitability of the selected electrolyser, PV panels and hydrogen storage types.

Chapter 3 presents the experimental procedure. It describes the components and measuring equipment of the experimental setup, as well as the construction process.

Chapter 4 discusses the experimental results. It covers the results of experiments for the electrical characterisation of the proton exchange membrane (PEM) electrolyser unit, the electrochemical operation of the stack, the storage of hydrogen in metal hydride and the interaction between the metal hydride tank and the electrolyser. It includes an extra set of experiments with an alkaline solid polymeric membrane (ASPM) electrolyser.

Chapter 5 presents the development of the numerical model of the solar hydrogen system in TRNSYS software, based on the results of Chapter 4. It describes the process of developing novel components that model the PEM stack operation, the PEM electrolyser controls and the metal hydride storage, in FORTRAN programming language, and the integration of the components in TRNSYS. Moreover, it presents the validation of the numerical model through a second set of experimental tests for the operation of the electrolyser and the balance-of-plant when it is coupled to a PV system.

Chapter 6 presents the three countries selected as case studies for the evaluation of the application of the solar hydrogen system: Ghana, Jamaica and Indonesia. Statistical

analyses are performed, and a specific quantitative study for Ghana and the domestic cooking demand profile is created for the three countries.

Chapter 7 presents the results of the case studies that are developed for small communities of 20 households in the selected countries with an aim to satisfy the cooking demands of the communities with the solar hydrogen system. In each case the core design consists in hydrogen being produced in a central plant, where the electrolysis process is powered by PV panels. A detailed description regarding the sizing of the system and its components of the numerical model is given for various versions of the system. The cooking demand profile is used to size solar hydrogen plant case studies based on the TRNSYS numerical model developed and presented in Chapter 4. The optimised system and its effectiveness are analysed through multiple sets of simulations in TRNSYS. Furthermore, the analysis of weather data used for the simulation of the solar hydrogen system in TRNSYS is presented. Recent weather data for Jamaica and weather data available from the Meteoronorm database are analysed and compared through the use of Finkelstein-Schafer Statistics. The effect of the weather data on the system operation is evaluated further through simulations with the different weather data sets. Moreover, the effect of the future weather data on the numerical model is also assessed. The potential to establish solar hydrogen plants in the case study countries is further estimated through the creation of novel solar hydrogen potential maps.

Chapter 8 presents the techno economic, analysis of the systems as sized and presented in Chapter 7, with a comparison of potential different hydrogen distribution methods. This chapter presents cost-benefit analyses (CBA) and marginal abatement cost (MAC) curves of the solar hydrogen system in comparison to the currently used cooking fuels in Jamaica, Ghana and Indonesia.

Chapter 9 presents the conclusions and suggestions for further research.

Figure 1.7 shows diagrammatically how the chapters are developed through the methodology followed for the development of this research.

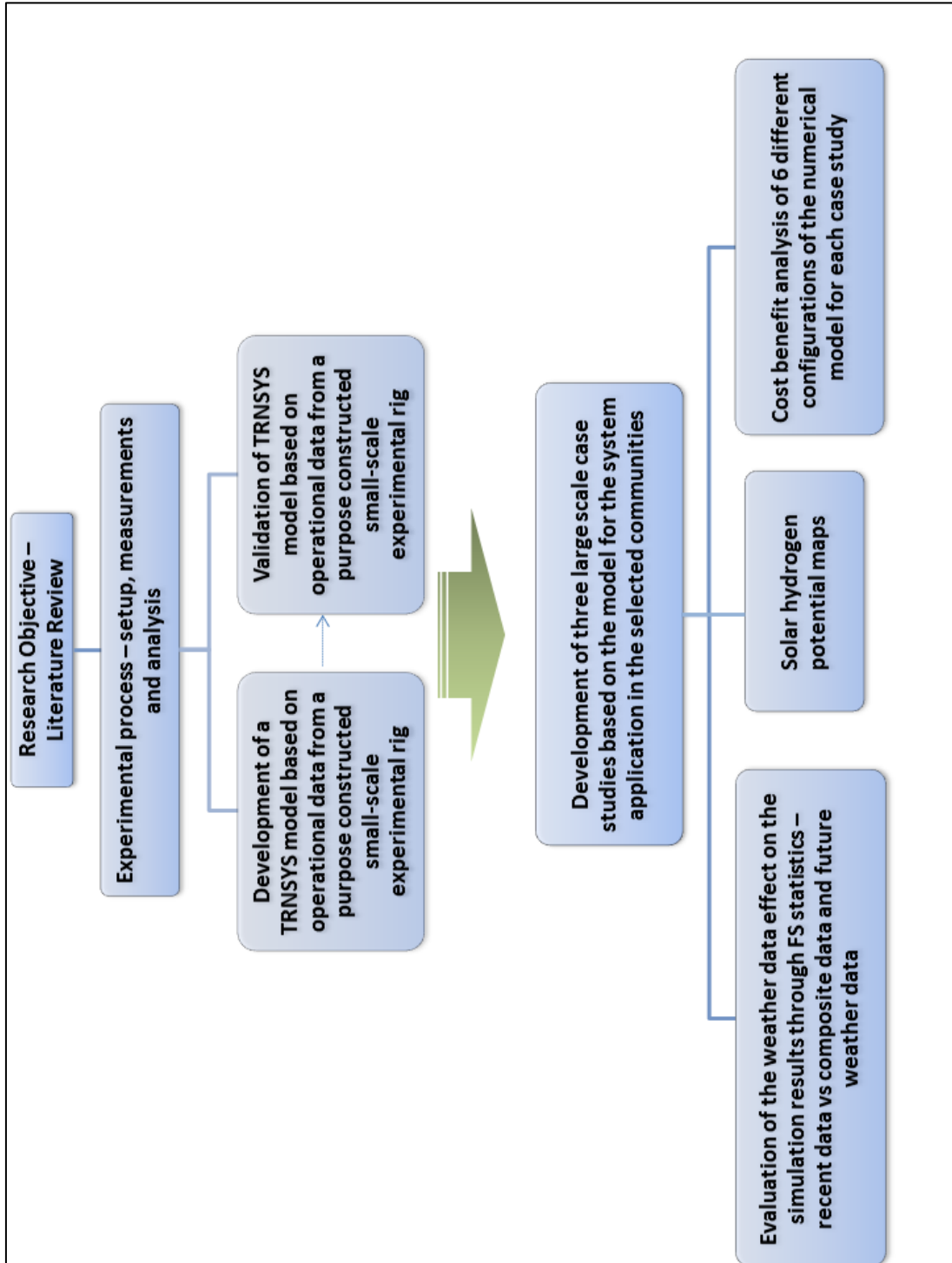


Figure 1.7, Research Methodology

1.5 Publications

Work carried out within this project resulted to the following publications:

Journal publications

1. Topriska EV Kolokotroni M, Dehouche Z. and Wilson E (2015), Solar hydrogen system for cooking applications: Experimental and numerical study. *Renewable Energy*, Vol 83, November 2015, Pages 717–728. (doi:10.1016/j.renene.2015.05.011)
2. Topriska EV Kolokotroni M, Dehouche Z. Divine T. Novieto and Wilson E (2015), The potential to generate solar hydrogen for cooking applications: Case studies of Ghana, Jamaica and Indonesia, *Renewable Energy*, Vol 95, September 2016, Pages 495–509. (doi:10.1016/j.renene.2016.04.060)

Book Chapters

3. E. Topriska, M. Kolokotroni, Z. Dehouche, R. Potopsingh, E. Wilson, The Application of Solar-Powered Polymer Electrolyte Membrane (PEM) Electrolysers for the Sustainable Production of Hydrogen Gas as Fuel for Domestic Cooking, Chapter 18, *Renewable Energy in the service of Mankind Vol 1: Selected Topics from the World Renewable Energy Congress WREC 2014*, ISBN 978-3-319-17777-9

Conference publications

4. E. Topriska, M. Kolokotroni, Z. Dehouche, R. Potopsingh, E. Wilson, The Application of Solar-Powered Polymer Electrolyte Membrane (PEM) Electrolysers for the Sustainable Production of Hydrogen Gas as Fuel for Domestic Cooking, *Proceedings of the World Renewable Energy Congress XIII* 3-8 August 2014, London, UK.
5. E. Topriska, M. Kolokotroni, Z. Dehouche, E. Wilson, D. Novieto, Analysis of domestic cooking fuels demand in Ghana: field work and case study application of

solar hydrogen cooking system, World Renewable Energy Congress WREC 2015, 8-12 June 2015, Bucharest, Romania

6. E. Topriska, M. Kolokotroni, Z. Dehouche, E. Wilson, Solar Powered Electrolysis for the Generation of Hydrogen as an Alternative Cooking Fuel, International Hydrogen Conference, The Hydrogen Economy – A Sustainable Energy Diversification Option for the Caribbean”, November 3-4, 2015 , University of Technology, Jamaica
7. E. Topriska, M. Kolokotroni, Z. Dehouche, E. Wilson, Solar Powered Electrolysis System for Cooking Applications, International Conference on Energy, Water & Environmental Sciences (ICEWES) 2015, December 15-17 2015, American University of Ras Al Khaimah UAE

Poster presentations

1. E. Topriska, M. Kolokotroni, Z. Dehouche, Solar Powered Polymer Electrolyte Membrane System for Cooking Applications, European Technical School on Hydrogen and Fuel Cells 2013, 23-27 September 2013, Crete, Greece – Participation with scholarship of the European Commission under the H2FC project (H2FC European Infrastructure Project, 2013)
2. E. Topriska, M. Kolokotroni, Z. Dehouche, Solar Powered Electrolysis for the Production of Hydrogen as a Domestic Cooking Fuel, EUED conference, July 2 2014, Lancaster UK
3. E. Topriska, M. Kolokotroni, Solar Powered Electrolysis for the Production of Hydrogen as a Domestic Cooking Fuel, CSEF Manchester conference, 14 January 2015, University of Manchester, Manchester, UK
4. E. Topriska, M. Kolokotroni, Z. Dehouche, E. Wilson, Solar Hydrogen System for Cooking Applications, CSEF Centre launch, 13 July 2014, Brunel University London, UK

Chapter 2. Background Information of Solar Hydrogen Systems

2.1 Introduction

The basic components of solar hydrogen production systems are presented in this chapter. The various processes related to hydrogen production methods are described with a special emphasis on water electrolysis and proton exchange membrane electrolysis. Additionally a complete review of the PV panel operation and hydrogen storage systems and the available technologies is given. The technologies selected for this research are highlighted in the view of the application of the system for domestic cooking. The most recent research advances and contribution in the related fields are discussed. The pioneer projects in solar hydrogen systems are summarized and presented in the final section of this chapter, as an indication of the progress and future potential in this field.

2.2 Hydrogen production

Hydrogen is one of the two vital energy carriers of the future (International Association for Hydrogen Energy, 2014). Some significant motivations that promote the use of hydrogen as energy carrier are:

- Diversification of the primary energy sources and enhancement of energy security. Hydrogen as an energy carrier can be produced from a variety of methods powered by renewable energy sources. In this way it can be produced locally without demand of fossil fuels
- Hydrogen can be stored long-term with negligible losses and also transported easily
- The use of hydrogen instead of fossil fuels reduces the greenhouse gases emissions
- Introducing a new energy carrier in the energy market will contribute to the increase of competitiveness and possible fuel price reductions

Hydrogen is an element that cannot be found naturally unbounded. Thus in order to use it, the first step is to produce it. Only 1% of the total hydrogen capacity is used directly as fuel, whereas the rest is destined for ammonia and fertiliser production as well as in oil refineries and metallurgical industries (Clarke, et al., 2009). Global hydrogen production is approximately 55 tonnes per year, and 95% of it comes from fossil fuels through steam reforming of natural gas and gasification of coal, (Clarke, et al., 2009). Figures 2.1 and 2.2 show data related to the US market, which indicate that the non-refinery use of hydrogen is mostly related to chemical processing.

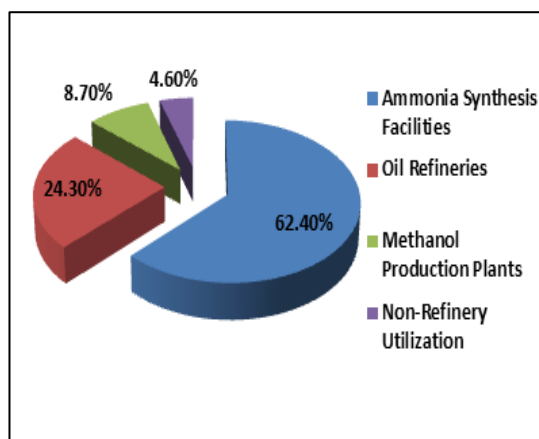


Figure 2.1, World Hydrogen Consumption Rates, source: (Gupta, 2009, p. 34)

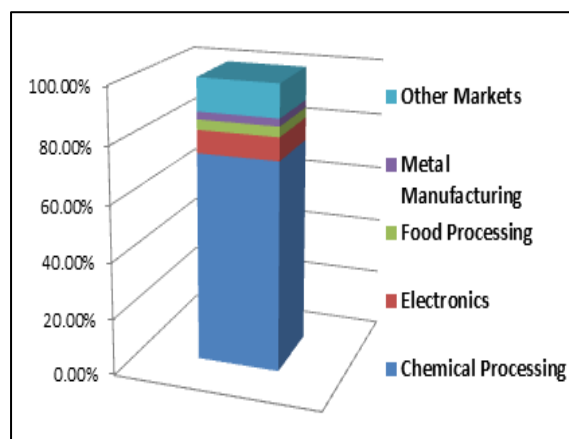


Figure 2.2, Non-refinery use of Hydrogen in the United States Market, source: (Gupta, 2009, p. 34)

There are various hydrogen production methods:

- Steam reforming of Natural Gas
- Gasification of Coal and Biomass
- Water Electrolysis
- Photochemical processes (photobiological water splitting, photocatalytic water splitting)
- High temperature decomposition – Thermolysis

The majority of hydrogen today is generated by fossil fuel based processes, and mainly steam reforming of natural gas. This technology has the advantage of using natural gas which is abundant, but at the same time it generates greenhouse gases. On the other hand, steam reforming has traditionally been the main production method for hydrogen that is meant to be used as part of ammonia production, and not as a fuel. The use of fossil fuels in general has the side effect of CO₂ emissions, apart from the cases that Carbon Capture and Storage (CCS) Technologies can be implemented. Streibel et al. recommend the CCS as a mean of reducing greenhouse gas emissions and present the case of an integrated carbon cycle for storage of electricity from wind and solar hydrogen in Germany (Streibel et al., 2013).

Water electrolysis on the other hand, is the oldest known technology to produce hydrogen, from the dissociation of water. It was the main production method since the early 1990's, until the fossil fuels began to dominate power generation, providing a much cheaper method. Electrolysis constitutes the cleanest hydrogen production method since no

gaseous by-products are emitted and also the most efficient of the rest of the water splitting processes (International Energy Agency, 2006).

A selection of the most common hydrogen production methods can be seen in Figure 2.3.

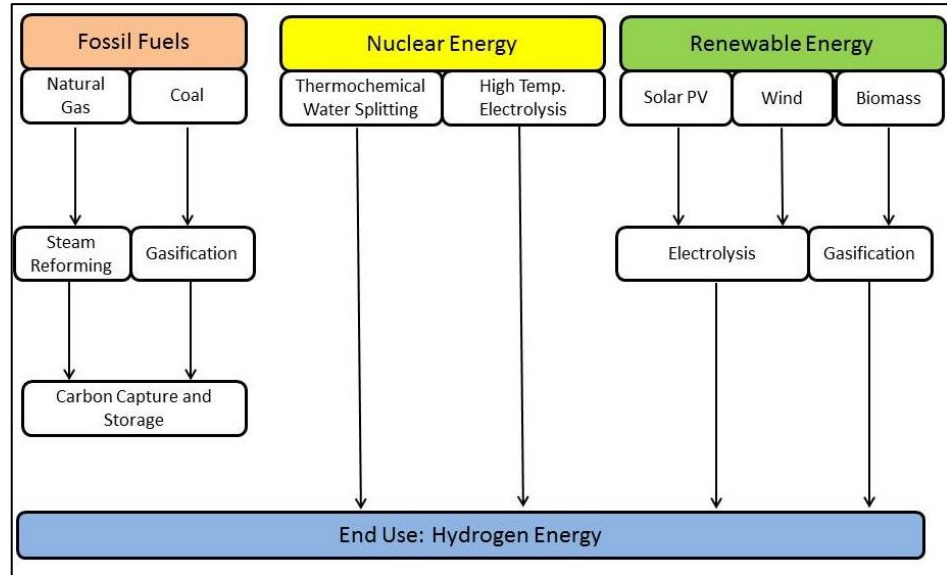


Figure 2.3, Selected Hydrogen Production Methods, redrawn from: (Acar & Dincer, 2013)

A detailed presentation of each technology, with a special focus on water electrolysis is presented in sections 2.2.1, 2.2.2 and 2.2.3.

2.2.1 Hydrogen Production from Natural Gas

The production of hydrogen from natural gas is a mature technology that has been used for many decades as part of the industrial production of ammonia. It can be distinguished in three different commercial chemical processes:

- Steam Reforming (Steam Methane Reforming-SMR)
- Partial Oxidation (POX)
- Autothermal Reforming (ATR)

(International Energy Agency, 2006, p. 7)

2.2.1.a Steam Reforming (SMR)

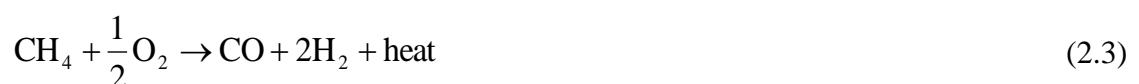
Steam reforming is the conversion of methane and water vapour into hydrogen and carbon monoxide, in the presence of high temperature (700 to 850°C) and pressures of 3 to 25bar. It is worth noting that in the United States 95% of the hydrogen production comes from Natural Gas Reforming (DOE, 2013). Purified natural gas is mixed with steam and sent through an extremely hot reactor where CO and hydrogen are generated. The gas products contain a small amount of CO, almost 12%, that can be further converted to CO₂ and water through a water-gas shift reaction that is described by Equations (2.1) and (2.2):



According to Spath and Mann (Spath & Mann, 2001) in a hydrogen plant operation, 74.8% of the total CO₂ emissions originate from the hydrogen production operation. This is equal to 8.895 kg of CO₂ per kg of net hydrogen produced. In total, a steam reforming hydrogen production plant has net greenhouse gas emissions of 11.888 kg of CO₂ per kg of net hydrogen produced. The water consumption of the system corresponds to 19.8 litres of water/ kg of hydrogen. Gupta states that the most modern SMR plants incorporate hydrogen purification facilities in order to remove CO, CO₂ and CH₄ impurities (Gupta, 2009, p. 42).

2.2.1.b Partial Oxidation (POX)

In this case hydrogen is produced through the partial combustion of methane with oxygen, with carbon monoxide and hydrogen as products. On the contrary to the steam reforming where heat acts catalytically in the development of the reaction, this process is exothermic. According to Welaya et al. when the catalyst reaches 800 °C, the partial oxidation reaction can be self-activated and the predetermined mixture of methane and air is fed to the reformer. This process results in less hydrogen per mole of methane feed, compared to steam reforming, but it has proved advantageous for small scale operation where efficiency is not such an issue (Welaya, et al., 2012). The process is characterised by Equation (2.3):



2.2.1.c Autothermal Reforming (ATR)

This process combines the above two, and is an exothermic reaction. The temperatures that characterise ATR are very high, ranging from 950 to 1100°C, at pressures as high as 100bar. In this case, the produced hydrogen needs to be further purified; having a negative effect on the cost and efficiency of the system (International Energy Agency, 2006, p. 8). A comparison between the advantages and the drawbacks of the natural gas hydrogen production technologies can be seen more clearly in Table 2.1:

Table 2.1, Comparison of the natural gas hydrogen production methods, source: (International Energy Agency, 2006)

Technology	SMR	POX and ATR
Benefits	High efficiency, 89% taking steam into consideration 79.2% steam not included	Small size units
	Small emissions	Cost for small units
	Cost for large units	Simple system
Drawbacks		
	Complexity of the system	Lower efficiency, 69.5%
	The process is highly sensitive to the qualities of natural gas	Higher emissions plus flaring
		Need for further H ₂ purification

The most important drawbacks of the natural gas hydrogen production methods are the greenhouse gas emissions, as well as the cost of the production that depends on the natural gas cost.

2.2.2 Hydrogen production from Coal

The procedure of producing hydrogen from coal can be efficient in terms of cost and also by taking advantage of the new methods of Carbon Capture and Storage (CCS). Coal is a plentiful natural source that it is established as a cost effective choice when it comes to fossil fuel decision. Hydrogen is produced from coal through a variety of gasification processes that are characterised by Equation (2.4):



Coal is converted into carbon monoxide and hydrogen and the higher the temperature of the reaction, the cleaner is the process. In more detail, reduction in phenols, tars and chars is achieved by providing the necessary heat input so that this endothermic reaction can occur in high temperatures. The following step of this reaction is to convert the CO into CO₂ and H₂ in the same way as in the steam reforming process, Equation (2.2).

Furthermore, the CO₂ that is produced can ideally be captured and stored by the CCS technology (International Energy Agency, 2006, p. 9).

2.2.3 Water Electrolysis

The most abundant element on the planet, hydrogen, can primarily be found in water. The process of splitting water into its two constituents is characterised by Equation (2.5):



An electric current has to pass through the water so that this reaction is achieved. The fundamental structure of an electrolyser is that an electric power source is connected to two parallel electrodes made from a noble metal and placed inside the water. The electric current enters the water from the cathode, which is negatively charged, and completes its way through the anode, which is positively charged. Hydrogen is formed at the cathode and oxygen at the anode. The electrical charge has to be above a certain limit so that electrolysis of pure water is achieved. In the case of sea water or water with the presence of salts as catalysts the electrical conductivity is much greater. The electrolysis of water requires a minimum of 286 kJ of electrical energy input to dissociate each water mole. Each water mole requires two moles of electrons and thus the specific electrical energy required is 143 kJ per mole. Faraday in 1832 proposed the two laws that characterise the electrolysis process:

1. “The quantity of the elements produced during electrolysis is directly proportional to the amount of electricity passing through the electrolytic cell”
2. “With a given quantity of electricity, the amount of elements produced is proportional to the equivalent weight of the element” (Zini & Tartarini, 2012)

Thermodynamics of Electrolysis

A chemical reaction is characterised by the enthalpy formation change between the reactants and the products of the reaction, as shown in Equation (2.6).

$$\Delta H = \sum H_{f,products} - \sum H_{f,reactants} \quad (2.6)$$

When this difference is negative, the reaction is exothermic and energy is released to the environment. The energy that is available to generate work throughout a reaction derives from the formation enthalpy difference after removing the effect of temperature (T) and entropy (S). What results is the Gibb's free energy, Equation (2.7):

$$\Delta G = \Delta H - T\Delta S - S\Delta T \quad (2.7)$$

If temperature is constant, for water:

$$\begin{aligned} \Delta G &= \Delta H - T\Delta S = -285.83 - 298.15 * (S_{water}^0 - S_{H_2}^0 - 0.5S_{O_2}^0) \Rightarrow \\ \Delta G &= -285.83 - 298.15 * (69.95 - 130.68 - 0.5 * 205.14) \Rightarrow \\ \Delta G &= -285.83 - 298.15 * (-163.3/1000) \Rightarrow \\ \Delta G &= -237.13kJ \end{aligned} \quad (2.8)$$

In the above equation the units of entropy are $J \text{ mol}^{-1}K^{-1}$ whereas the enthalpy units are $kJ \text{ mol}^{-1}K^{-1}$, this is because the value of entropy difference is divided by 1000. The Gibb's free energy is the energy that is released without considering pressure and volume work. If the Gibb's free energy is negative the reaction happens spontaneously. Electrolysis is not a spontaneous reaction and requires an external electric work to occur which is derived from Equation (2.9):

$$W_e = \Delta G = q * E = -n * F * E \quad (2.9)$$

$$\begin{aligned} \Delta G &= -n * F * V_{rev} \Rightarrow \\ V_{rev} &= -\frac{\Delta G}{n * F} = -\frac{(-237.13)}{2 * 96485} = 1.23V \end{aligned}$$

Where q is the electrical charge (C/mol) transferred to the cell from the external circuit and F is Faraday's constant. In water electrolysis one mole of water produces a charge that is composed of $n=2$ electrons, according to Faraday's law. The result of the above is the ideal cell voltage for electrolysis to occur and it is called reversible cell voltage, and is equal to 1,23V at 25°C. In reality a little overvoltage is required to carry out electrolysis.

When the energy dissipated to the surrounding environment is taken into consideration the minimum voltage to start electrolysis is given by Equation (2.10) and is equal to:

$$V_{th} = -\frac{\Delta H}{n * F} = -\frac{(-285.83)}{2 * 96485} = 1.48V \quad (2.10)$$

In this case, the process is considered to occur adiabatically since no heat is lost or added from the surroundings - the heat associated with the entropy change of the reaction $T\Delta S$ is not taken into consideration.

The electrolysis efficiency is defined as the ratio of the thermoneutral cell voltage over the operating cell voltage, as shown in Equation (2.11):

$$\eta_{electrolysis} = \frac{V_{th}}{V} = \frac{-n * F * \Delta H}{-n * F * \Delta G} = \frac{\Delta H}{\Delta G} \quad (2.11)$$

It is the HHV value of one mol of the product divided by the energy consumption. Isothermal operation, at applied cell voltage equal to V_{th} , results in efficiency 100%. In some cases, efficiencies higher than 100% can occur when the operating cell voltage is less than the thermoneutral voltage and higher than the reverse cell voltage. Typical example at 25°C where V_{th} is 1.48V and $V_{rev}=1.23$,

$$\eta_{electrolysis} = \frac{V_{th}}{V} = \frac{1.48}{1.23} = 120\%$$

In this case external heat is supplied to the cell to make up for the $-T\Delta S$ difference. But in the case that the operational cell voltage is increased above V_{rev} , the current density is also higher and therefore the production rate increased.

There are currently three main options commercially available for water electrolysis. These technologies are based on the same basic principle, but the application approach is different. The first one is alkaline electrolysis with the first systems to be developed in the late 1970's. The second technology is the proton exchange membrane, which is a more recent achievement (Zoulias, et al., 2005) and the third solid oxide electrolysis (Momirlan & Veziroglou, 2002). More details can be found in the following sections:

2.2.3.a Alkaline Electrolysis

Alkaline electrolysis is a mature technology for hydrogen production, and is the most common commercially available electrolytic technology. In the alkaline electrolyser the decomposition of water into H₂ and O₂ is achieved by passing an electric current between the electrodes, which are separated by an aqueous electrolyte with good ionic conductivity (in most cases aqueous potassium hydroxide KOH at a concentration of 20-30%), (Carmo, et al., 2013). Two water molecules are reduced to one hydrogen molecule and two hydroxyl molecules at the cathode. The hydrogen escapes at the surface of the cathode, whereas the hydroxyl ions migrate under the effect of the electric current, passing through the porous diaphragm to the anode, where they are reduced to one molecule of water and half a molecule of oxygen, as shown in Equations (2.12) and (2.13). This is shown diagrammatically in Figure 2.4.

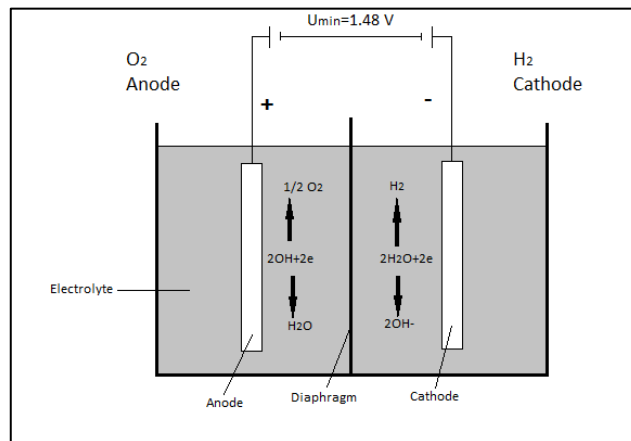


Figure 2.4, Alkaline Electrolysis Process, redrawn from Zoulias et al, “A review on water electrolysis”, (Zoulias et al)

The usual electrolysis temperatures are 70-90 °C at a cell voltage of 1.85 - 2.05 V (Zoulias, et al., 2005). Recent developed cells can reach temperatures of 150°C, at pressures 5 – 30bar. To reach higher pressures than the ones delivered directly by the electrolyser, further compression is needed. Alkaline electrolysis is characterised by efficiencies of 62% to 82% (Carmo, et al., 2013). There are two main designs in the alkaline electrolysis. In the monopolar electrolysers the electrodes are either positive or

negative, whereas at the bipolar arrangement, the electrodes are positive from the one side and negative on the other, as shown in Figure 2.5.

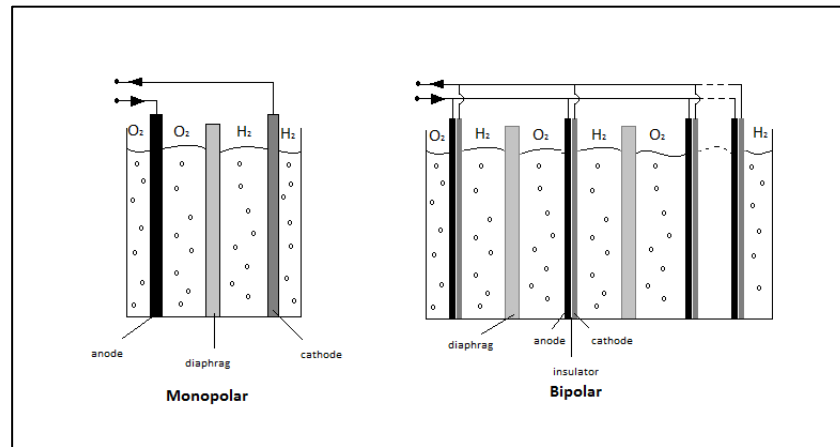


Figure 2.5, Monopolar and Bipolar Electrolyser cell arrangements, redrawn from: (Ulleberg, 1998)

The advantage of the bipolar systems is that they are more compact than the monopolar ones and can operate at higher pressures, thus reducing any external compression work required (Ulleberg, 1998; Zoulias, et al., 2005).

According to Manabe et al., great focus is given in the research and development of the alkaline electrolysis by big industries, like Kawasaki Heavy Industries and Chlorine Engineers Corp. Ltd (Manabe, et al., 2013). The most important aspects of alkaline electrolysis investigated by researchers are related to the improvement of partial load operation that leads to risky mixing of gases within the electrolyser and pressure levels operation (Carmo, et al., 2013). Efforts also focus on the efficiency improvement by electrode modifications as demonstrated by Zeng and Zhang, (Zeng & Zhang, 2014).

Alkaline electrolysis is a mature and highly used technology, and its use in combination with renewable energy primary sources indicates that it can have a significant role in the future of electrolytic hydrogen (Ursua, et al., 2013). Nevertheless, the toxicity of the aqueous electrolyte sets an important drawback in the environmental aspects of their use.

2.2.3.b Proton Exchange Membrane (PEM) Electrolysis

Proton exchange membrane electrolysis is based on the use of a polymeric proton exchange membrane as a solid electrolyte, and was originally proposed by General Electric. Further on, the technology of the PEM membrane has been evolved and

identified by DuPont and particularly the product Nafion 117 (DuPont, 2013; Zoulias, et al., 2005). Nafion is the prevailing membrane technology as it presents outstanding chemical and thermal stability, mechanical strength and high proton conductivity, boosting the efficiencies of PEM electrolyzers to higher than 85% (Carmo, et al., 2013). In fact, most PEM electrolyzers in the market today include the Nafion membrane. In such an electrolyser, the cathode consists of a porous graphite current collector with platinum or a mixed oxide as electrocatalyst.

The PEM electrolyzers present some basic advantages over the use of the alkaline ones:

- Greater safety and reliability since no caustic electrolyte is used
- Greater efficiency in preventing gas mixing
- The possibility to operate cells to several amperes per cm^2
- Good partial load response
- High operational pressures, (Carmo, et al., 2013; Zoulias, et al., 2005)

In the PEM electrolyser the reactions taking place are described by equations (2.14) and (2.15) and are graphically shown in Figures 2.6 and 2.7:

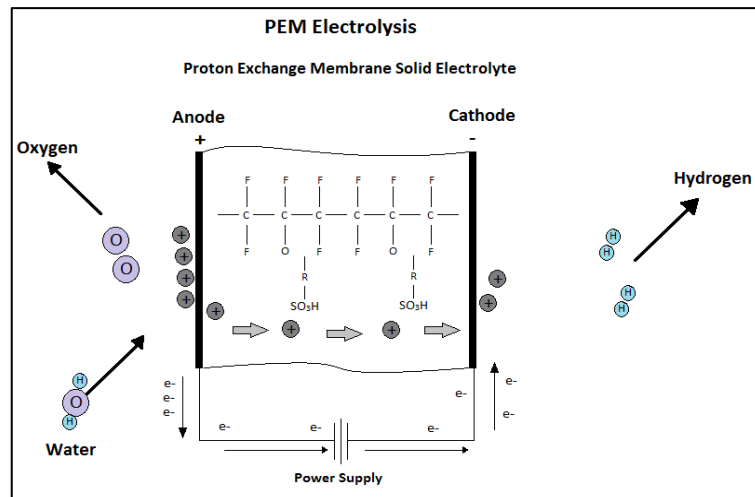
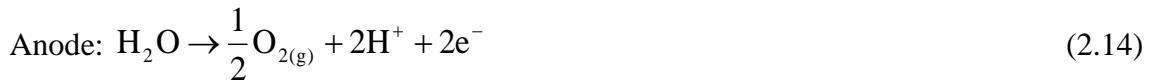


Figure 2.6, PEM Electrolysis process, redrawn from Barbir F, “PEM Electrolysis for production of hydrogen form renewable energy sources”, (Barbir, 2005)

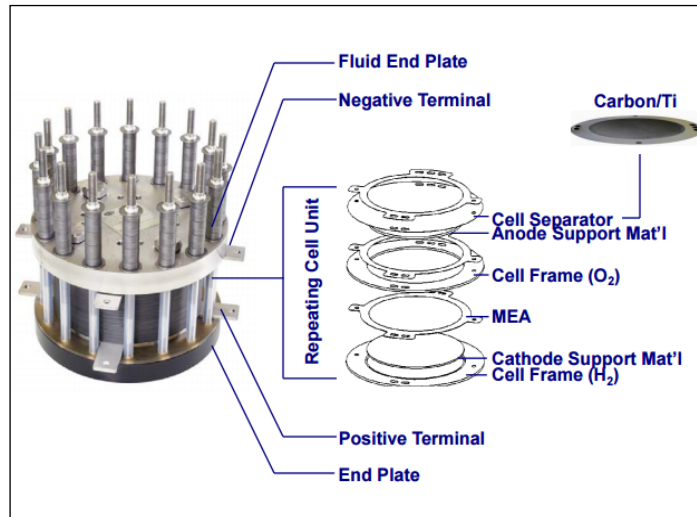


Figure 2.7, Structure of the PEM electrolytic cell, source: (Hamdan, 2011)

Major focus has been given on the reduction of the cost related to PEM electrolyzers. The corrosive acidic environment that is the result of the PEM membrane demands the use of distinct materials that can resist the low corrosive PH. These kinds of materials are scarce and expensive noble catalysts - Platinum (Pt), Iridium (Ir) and Ruthenium (Ru) - and titanium based current collectors and separator plates, (Carmo, et al., 2013). The cost apportionment of the PEM electrolyser stack is shown in Figure 2.8.

According to Ayers et al., (Ayers, et al., 2010) most recently, many researchers have investigated the performance of the electrocatalysts of the oxygen and hydrogen evolution reaction, (Chen, et al., 2002; de Oliveira-Souza, et al., 2000; Terezo, et al., 2001; Hinnemann, et al., 2005). Additionally the separator plates can contribute greatly to cost reduction in PEM electrolyzers and Ojong et al. presented a reaserch that can help towards that direction and improve performance (Ojong, et al., 2012).

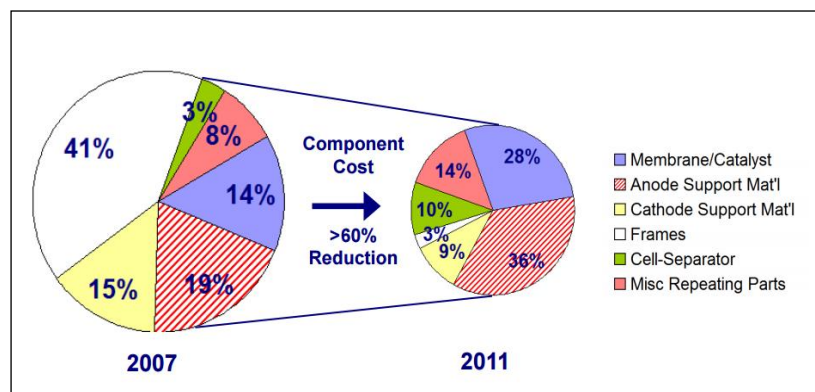


Figure 2.8, Cost apportionment in a PEM electrolyser stack, source: (Hamdan, 2011)

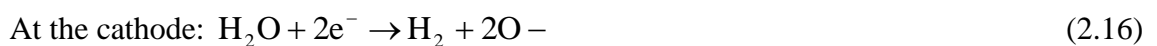
The advantages of PEM electrolysis regarding its efficiency, performance and environmental safety set it as the most sustainable electrolysis method. Regarding the solar powered system, these advantages in combination to the PEM electrolyser's valuable characteristics of low maintenance and longevity set them as the preferable electrolysis technology. Therefore, it is thus justified why PEM is the electrolysis process selected for the design and development of the solar powered electrolysis system for the generation of hydrogen as a cooking fuel.

2.2.3.c Solid Oxide Electrolysis

High temperature solid oxide electrolytic cells (SOEC) have the great advantage in comparison to the other electrolytic processes that they can be operated both in fuel cell mode and electrolysis mode (Nguyen et al., 2013). Solid oxide electrolysis has recently attracted great interest in the scientific community. According to Mocoteguy and Brisse, solid oxide electrolysis is thermodynamically and electrochemically superior to low temperature electrolysis thanks to the increased operating temperatures that result in low electrical demand (Mocoteguy & Brisse, 2013).

A solid oxide electrolyser consists of ceramic based cells that operate at very high temperatures, usually around 800°C. Water steam passes through the cathode to be reduced to hydrogen. Superoxide ions pass through the electrolyte to the anode where they recombine to oxygen molecules, with the simultaneous release of electrons (Mocoteguy & Brisse, 2013).

High temperature electrolysis can reach much greater efficiencies than normal electrolysis (International Energy Agency, 2006, p. 11). Acar and Dincer indicate the use of nuclear reactors as primary energy for high temperature electrolysis (Acar & Dincer, 2013), and they highlight the fact that in this case the efficiency of the electrolysis is immediately related to the efficiency of the nuclear reactor and can be 50% in temperatures around 950°C. The equations that characterise solid oxide electrolysis are Equations (2.16) and (2.17):



This dependence of the SOEC on very high temperatures sets them inappropriate for small-scale applications.

2.2.3.d Photo –Electrolysis (Photolysis)

Photo-electrolysis of water is the process where water is split into hydrogen and oxygen by the direct effect of light. It is a concept that can highly reduce the need of equipment and machinery for the hydrogen production such as in the cases of electrolysis or steam reforming. It is still a technology under development and very immature in relation to the rest, but it is one that has many promising perspectives. The basic concept is a photosensitive material that is immersed in water, and by reacting with the sunlight it induces water splitting, as shown diagrammatically in Figure 2.9.

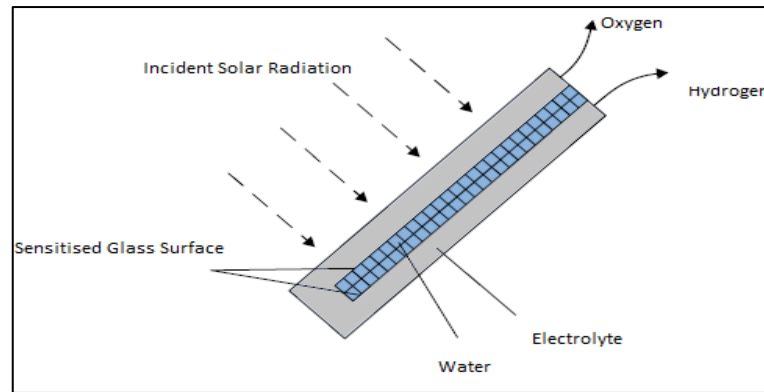


Figure 2.9, The concept of Photo-electrolysis, redrawn from (International Energy Agency, 2006, p. 12)

2.2.3.e Photo-biological production (biophotolysis)

Photo-biological production of hydrogen is based on the fundamental concept of photosynthesis (International Energy Agency, 2006). By simulating artificially the photosynthesis process, hydrogen can be created through the process described in Equations (2.18) and (2.19):



The concept of photo-biological hydrogen production is the use of green algae and cyanobacteria. These substances can act as catalysts in the generation of hydrogen through the process that can be seen in Figure 2.10:

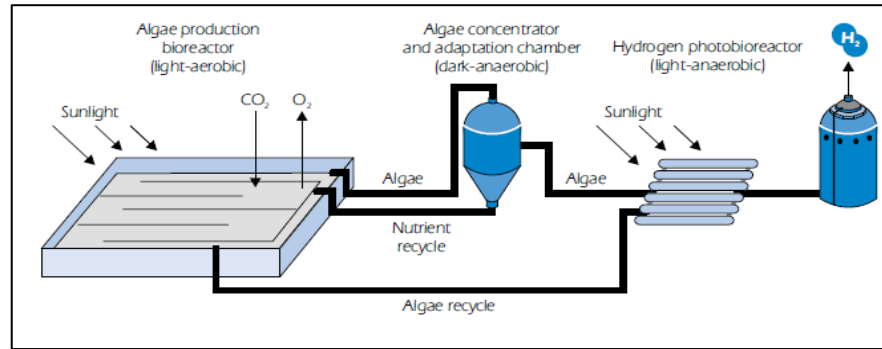


Figure 2.10, The principle of Photo-biological hydrogen production, source: (International Energy Agency, 2006, p. 13)

2.2.3.f High Temperature Decomposition

Water can be decomposed at around 3000°C. This temperature is extremely difficult to achieve and thus there are some methods that act catalytically in order to enhance the water splitting process. These can be:

- Thermochemical cycles
- Thermal decomposition in combination with electrolytic decomposition
- Plasma chemical decomposition in double stage CO₂ cycle
- Direct catalytic decomposition of water with the use of a ceramic membrane as diaphragm

These processes are characterised by efficiencies of around 50% and are not commonly used due to susceptibility of the electrodes to corrosion and in general the resistance of the materials involved in the process to high temperatures (International Energy Agency, 2006, p. 14).

Table 2.2 presents a summary of the main advantages and disadvantages of the presented water electrolysis methods.

Table 2.2, Advantages and disadvantages of water electrolysis methods, sources: (Carmo, et al., 2013; Zini & Tartarini, 2012)

Method	Advantages	Disadvantages
Alkaline electrolysis	High efficiencies	Low current densities
	Mature technology	Gas crossover
	Relatively low cost	Corrosive liquid electrolyte
		Low partial load range and low operational pressures
PEM electrolysis	High current densities	High cost of noble catalysts
	Good partial load operation	Low commercialisation in relation to Alkaline
	No caustic electrolyte present	
	High gas purity	
Solid Oxide Electrolysis	No noble catalysts	Still mainly at R&D stage
	High operating pressures	Bulky design
		Low durability
		High cost
Photo-electrolysis	Simple design	Still at R&D stage
		Low efficiencies
Biophotolysis	Capacity of auto organisation and regulation	Still at R&D stage
		Low efficiencies
High Temperature Decomposition	High efficiency	Difficult to achieve the necessary temperatures
		High cost

2.3 Photovoltaic Panels

Photovoltaic panels are an essential component for powering the electrolysis process in the solar hydrogen system. According to the Global Market Outlook for Photovoltaics for 2013-2017 the world's installed photovoltaic capacity was 102GW in 2012, and close to 200GW in 2015 (European Photovoltaic Industry Association, 2013). There are various photovoltaic panel technologies available in the market, all based on the same principle of operation, which is converting solar radiation into electricity through the use of semiconducting materials such as silicon or platinum. When these materials are exposed to light, photons are absorbed by the photovoltaic cell and the energy of each photon is

transferred to an electron of an atom of the cell. The excited electron escapes the atomic bond and generates an electric current. By leaving this position in the atom the electron creates a “hole”. Within the photovoltaic cell there is a layer that is formed by P-type and N-type semiconductors that creates an electric field. Electric current is produced when the electrons interact with this P-N junction and they move to the opposite direction of the “holes” (PVEducation.org, 2013; Encyclopaedia Britannica, 2014), shown in Figure 2.11.

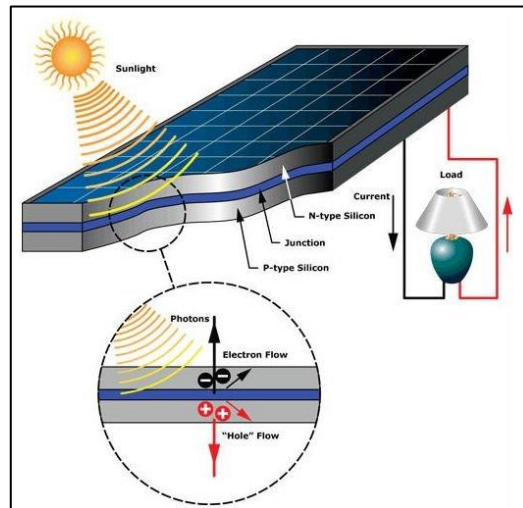


Figure 2.11, photovoltaic panel fundamental principles, source: (Electronics Hub, 2015)

Since 1839 that Edmund Becquerel discovered the existence of the photovoltaic effect, great progress has been noted in this field. Especially during the last half of the previous century since Pearson, Fuller and Chapin of Bell Laboratories designed the first solar cell of 6% efficiency (Inventors, 2015), the solar panels technology has been well established and developed. Most recently, one of the leading companies in the area, SunPower, has announced a world record panel efficiency of 24%, by improving the reflection inside the cells and the metal contacts (SunPower, 2014). The semiconducting materials that are used nowadays include monocrystalline silicon, polycrystalline silicon, amorphous silicon, and cadmium telluride and copper indium gallium selenide/sulphide.

2.3.1 Monocrystalline Panels

Monocrystalline solar cells present very high efficiency and high performance, thanks to the detailed and time consuming manufacturing process of monocrystalline silicon that results in regular pattern arranged atoms (Wenham, et al., 2007). Current conversion efficiency of monocrystalline solar cells is about 15% and laboratory results show efficiencies higher than 20%. Also, efficiencies up to 50% or more have been reported for

the space station applications. This technology because of its complications sets the panels very expensive and thus has become less preferred by the industry.

2.3.2 Polycrystalline Panels

Polycrystalline panels are currently the most rapidly developing solar cell technology as it is the one most applied by manufacturers. Polycrystalline silicon doesn't require the detail and tedious techniques that monocrystalline silicon production needs. As a result, polycrystalline panels present lower efficiencies than the monocrystalline ones but still high enough to set them commercially successful and are much more cost effective. (Wenham, et al., 2007). Current efficiencies range in the area of 14%. Ease in manufacturing, low cost and suitability for any size applications and popularity among the manufacturers set the polycrystalline panels the technology used as a PV power source for this research.

2.3.3 Thin film/ Amorphous Silicon

Amorphous silicon requires even less detail than polycrystalline silicon thus resulting in even lower capital related costs but also lower efficiencies. The thickness of the material required to construct an amorphous silicon cell is very small and this is why they are also called thin films (Wenham, et al., 2007). Thin film cells are used in the construction of flexible, light and thin materials where photovoltaic cells are employed. Typical applications are calculators, watches, tents, bags and any sort of outdoor application.

2.3.4 Multijunction Panels

As photovoltaic technology is developing rapidly, the advances and the breakthroughs are daily. The major milestone in recent research refers to multi-junction cells, that they present efficiencies higher than 40%. The multi-junction technology employs a set of junctions with different, but suitably selected, bandgap energies to better match the solar spectrum with maximum utilization (Rabady, 2013).

2.4 Hydrogen storage

2.4.1. Compressed Gas Storage and Liquefied storage

A safe and cost effective hydrogen system depends greatly on storage. Hydrogen storage is a key factor in safety and minimisation of inefficiencies and losses and is a process that

presents challenges. As hydrogen is characterised by such low density, storing requires either high-pressure solutions or high gravimetric capacity (Zini & Tartarini, 2012). The traditional hydrogen storage methods are high-pressure storage and cryogenic liquid storage. Liquid storage has the drawback of a refrigeration unit that is necessary to maintain hydrogen at cryogenic state, at 21.2K at ambient pressure, thus adding extra energy costs and complicating the system. The gas is first precooled and compressed and then cooled in a heat exchanger before undergoing an isenthalpic expansion (Zuttel, 2003). High-pressure storage is restricted by the cylinders weight and safety issues. Especially as compressed hydrogen storage is performed under pressures of the range 200-700bar, it is inappropriate for domestic applications (Zini & Tartarini, 2012).

2.4.2. Metal hydride Storage

Hydrogen reacts with many transition metals and their alloys at elevated temperatures or pressures to form solid hydrides (Zuttel, 2003). Metal hydrides present higher energy density (6.5 H atoms/cm³ for MgH₂) than compressed hydrogen gas (0.99 H atoms/cm³) and liquid hydrogen (4.2 H atoms/cm³) (Sakintuna, et al., 2007; Dehouche, et al., 2005). In this context the storage of hydrogen in metal hydride form presents a low-pressure safe and promising solution for stationary applications, such as domestic use and should be characterised by the following (Gupta, 2009, p. 382):

- High hydrogen capacity per unit mass and unit volume
- Low dissociation temperature
- Moderate dissociation pressure
- Low heat of formation to minimise the energy necessary for hydrogen release and low heat dissipation during the exothermic hydride formation
- Reversibility for limited energy loss during the charge and discharge cycles
- Fast kinetics
- High stability against oxygen and moisture to ensure long cycle life
- Low cost of recycling and charging infrastructures
- High safety

Metal hydrides are charged by absorbing pressurised hydrogen and during this process heat is released. The options of materials used for metal hydride storage is very wide since over 50 metallic elements of the periodic table show the ability to absorb hydrogen. What

is critical for the selection of suitable material is the hydrogen capacity, the charging and discharging temperatures and the charging and discharging pressures. In order to tailor the properties of metals so that they fit the applications requirements, alloys of various compositions are used and are classified as:

- AB_5
- AB
- A_2B
- AB_2

A typical example of the prevalence of metal hydride storage over traditional gas storage is the $LaNi_5H_{6.5}$ where the volumetric density at 2bar equals the volumetric density of gaseous molecular hydrogen at 1800bar (Larsen, et al., 2004). In general when compared to conventional high-pressure gas cylinders, metal hydride storage presents the following advantages:

- It needs much smaller volume in comparison to the traditional gas cylinders
- Typical pressure of absorption/desorption is 1-25 bar opposed to the 200 and 700 bar of typical gas cylinder applications

The method that is experimentally tested as hydrogen storage for the solar hydrogen system of this research is the metal hydride storage as it presents the greatest advantage in terms of safety of all the hydrogen storage methods, which is critical for stationary domestic applications. Furthermore, it shows great research development. A metal hydride cylinder developed in the Hydrogen laboratory of Brunel University, with $LaNi_5$ as alloy is used.

2.4.3. Other storage Options

There are other methods of hydrogen storage, which are not commonly used because of low efficiencies and difficulty in process, but nevertheless are here mentioned for completeness purposes. Glass and plastic containments can absorb hydrogen when heated and pressurised to a few hundreds of Celsius and a few MPa. Carbon nanotubes also, can bind with hydrogen atoms at high temperatures, as well as zeolites which are minerals that when heated can absorb hydrogen ions (Zini & Tartarini, 2012). In all these cases, hydrogen is released through reheating.

2.5 Summary

Hydrogen production systems that are based on a combination of the PV powered electrolysis with associated storage have been in the spotlight of the renewable energy sector in the past decades. They are the systems that offer the greatest flexibility and potential for development in stationary renewable energy systems (Zoulias & Lympelopoulou, 2008). The work of milestone projects on solar hydrogen systems is presented in Appendix A showing the significance and the application of the system..

Chapter 2 presented the concept of solar hydrogen systems with a focus on the individual components. Electrolysis theory was described and proton exchange membrane (PEM) electrolysis was highlighted. The advantages of PEM electrolysis over other electrolysis and hydrogen generation processes were emphasised; these are greater safety and reliability, no caustic electrolyte use, greater efficiency in preventing gas mixing, the possibility to operate cells to several amperes per cm², good partial load response and high operational pressures that can eliminate the need of a compression and reduce thus operational costs.

Polycrystalline cells were selected as the PV technology to be used because it is the most cost effective, broadly used and manufactured and with good efficiencies.

Finally, hydrogen storage options were evaluated and the metal hydride storage was selected as the most appropriate for safety reasons although it might not be the most cost effective.

Chapter 3 will describe the experimental setup and equipment used for the experiments that will provide the results for the development and validation of the solar hydrogen model for cooking gas.

**Chapter 3. Experimental Components and
Processes**

3.1 Experimental Setup Introduction

This chapter presents the experimental procedure and the components and equipment used. These experiments are the basis for the development and the validation of the numerical model used to size the solar hydrogen system.

The objective of this part of the project is to build a small scale laboratory experimental setup that represents the solar powered PEM electrolyser system, to evaluate the performance of the system and investigate its optimisation. The experiments have a dual focus, i) to evaluate the electrical performance of the electrolyser units as well as the electrochemical behaviour of the stack and create the basis of the numerical model development, and ii) to assess the operation of the electrolyser and the balance-of-plant when coupled to a PV system which will act as a validation of the numerical model.

Moreover, experiments are carried out with a metal hydride storage tank to investigate the storage process. Further tests were conducted with an Alkaline Solid Polymeric Membrane (ASPM) electrolyser, to compare efficiencies of the two electrolysers. In total regarding the PEM electrolyser, 24 tests were conducted for the characterisation, 52 tests for the model validation, and 17 tests for stack measurements. 13 tests were conducted for the ASPM electrolyser operation and 25 tests regarding the metal hydride storage interaction with the electrolyser. More details of the experiments type and number can be found in the Appendix D.

3.2 Laboratory Safety and Equipment

The hydrogen laboratory used for this research is specifically designed to accommodate devices that produce hydrogen gas and it is equipped with all the necessary safety equipment and gas sensors in order to prevent any hazardous circumstances. A hydrogen sensor is installed at ceiling height that measures the hydrogen volume in the air of the room; in the case of possible leak and if the percentage is higher or equal than 2% the alarm will be activated (Figures 3.1, 3.2) (Paterson Instruments, 2014; Gas Sense, 2014). Protection is provided by passive means (natural ventilation) to ensure that gas mixtures remain below the volume fraction of 2% hydrogen in air. In standard atmospheric conditions hydrogen can be flammable in concentrations between 4-75% (Gupta, 2009).



Figure 3.1, Hydrogen Sensor installed in the Hydrogen Laboratory



Figure 3.2, Hydrogen Sensor Box installed in the entrance of the Hydrogen Lab

Piping, fittings and joints for the experimental rig are selected to withstand the operating pressure and temperature of the produced hydrogen. Maximum operating pressures of the system do not overcome the pressure of 13.8bar or 200psig. Swagelok stainless steel equipment is selected with the characteristics demonstrated in Appendix C. All electrical equipment is properly earthed and data logging cables are screened to ensure maximum safety and no interference on the data logging signals.

3.3 Description of the Proton Exchange Membrane (PEM) electrolyser by Proton Onsite

The (PEM) electrolyser is manufactured by Proton Onsite, one of the leading companies in hydrogen production systems worldwide (Proton Onsite, 2014). It was selected after extensive market research and quotations from other leading PEM manufacturers and analysis of individual PEM electrolysers' characteristics. This selection procedure is included in Appendix B.

The selected PEM electrolyser consists of a 4-cell stack and is rated at a maximum hydrogen production of 600cc/min at a current of 30A DC. The I-V curve of the stack can be seen in Figure 3.3.

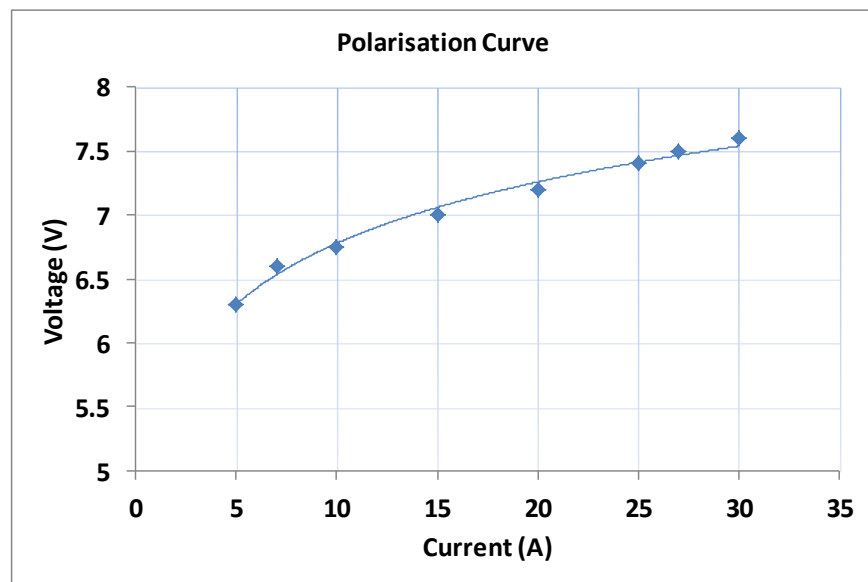


Figure 3.3: Representative I-V Polarization curve (at 13.8bar, 40°C)

The separation of the gases is performed by a Nafion membrane, which is a solid ion exchanging membrane (DuPont, 2013). The electrolyser is a compact commercial unit and apart from the stack it includes supplementary features for the necessary management of the produced gases and water. The water used is deionised with a conductivity of less than 1 μ S/cm, is inserted into a water tank inside the electrolyser, and is circulated by a small pump. It flows through the stack where it is separated into hydrogen and oxygen. Oxygen is vented to the ambient environment and hydrogen passes through a drying and purification module that removes the excess water. Hydrogen gas exits through a back-pressure control valve at pressures within the range of 3 to 13.8bar. This internal system is powered and controlled by a DC power supply unit that provides the necessary power to

each component. In order to characterise correctly the operation of the stack, it is necessary to evaluate the energy breakdown in the electrolyser as all the internal auxiliary components use extra energy. From the internal schematic of the PEM electrolyser as shown in Figure 3.4, and Figure 3.5, the internal components and their energy use are the following:

1. The water fill and oxygen vent
2. The water tank
3. The PEM Stack, that at maximum current input uses 300W
4. The purification system which operates at 273°C and includes a large electrical heating element to maintain this temperature has a demand of 500W
5. The hydrogen accumulator, where hydrogen is stored after the generation and the purity check is performed.
6. The impure hydrogen is vented through the perflex tubing
7. The normally open solenoid valve at the hydrogen vent, SV306 (Peter Paul 51X00560GB). The valve is rated at 12VDC and has a resistance of 26.5Ω. Thus, it is rated at ~5.43W.

The internal components of the electrolysers further include sensors and controls (30W in combination with the gear pump and solenoid valve) and the gear pump GP205.

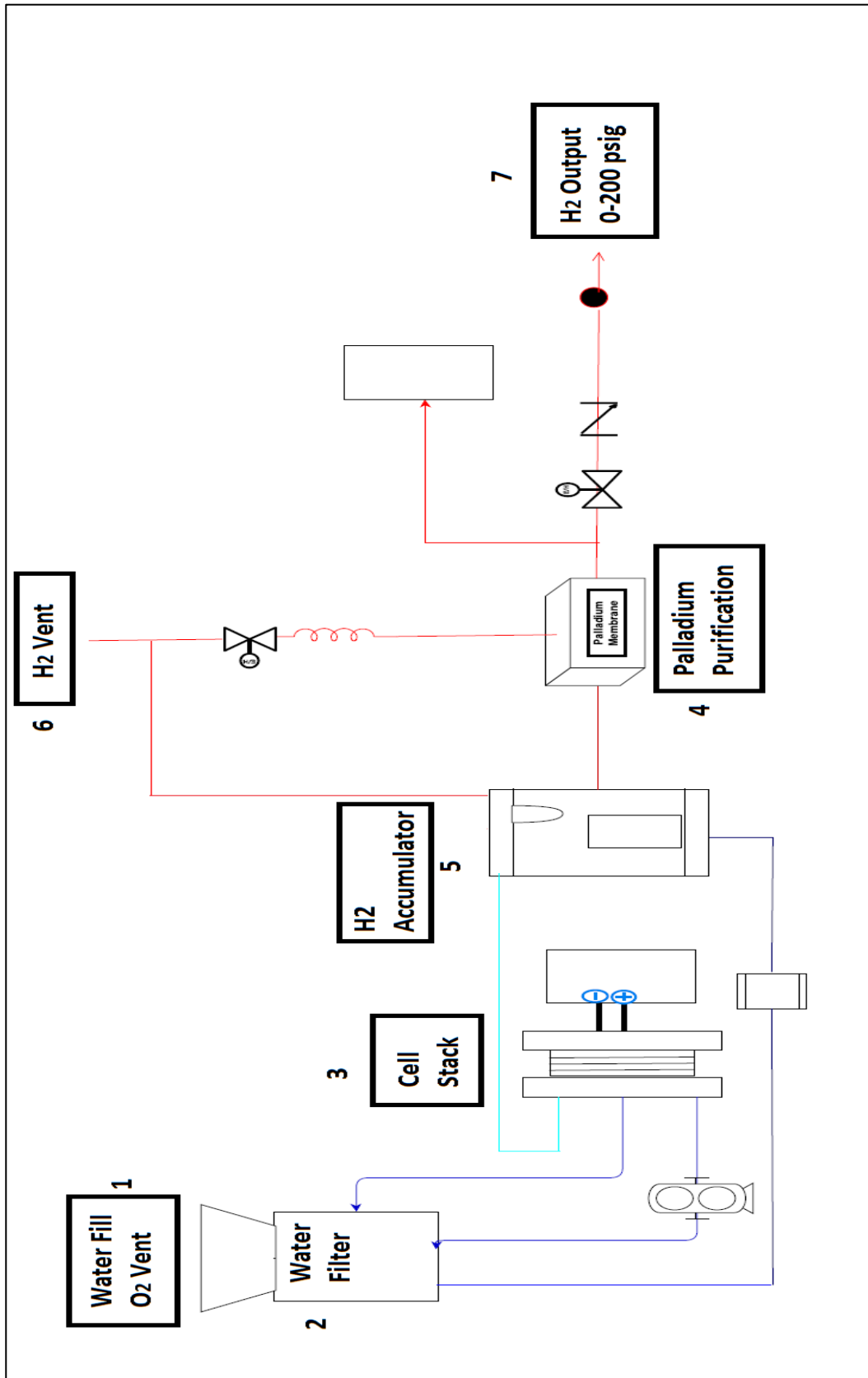


Figure 3.4, Internal Schematic of the PEM electrolyser, redrawn from original

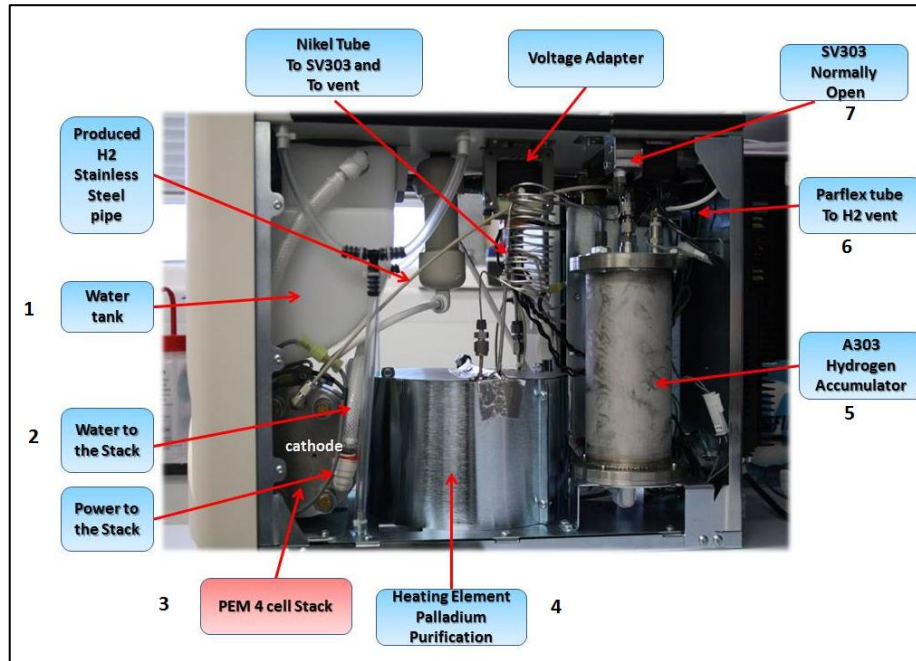


Figure 3.5, Components of the hydrogen production and water and gases management of the PEM electrolyser

3.4 Description of the Alkaline Solid Polymeric Membrane (ASPM) electrolyser by Acta

This electrolyser manufactured by ActaSpa is based on an Alkaline Solid Polymeric Membrane (ASPM), which combines the benefits of PEM electrolysis (no extra hydrogen compression required, small environmental impact), with the benefits of the alkaline electrolysis (no need of noble metals, low system cost) (ACTA, 2014). It employs an anion exchange membrane, an alkaline electrolyte solution of K_2CO_3 and low cost metal catalysts (Pavel, et al., 2013). The unit is rated at 100l/h hydrogen production.

The electrolyser consists of a 9 cell stack and as for the PEM electrolyser, supplementary components are responsible for the water and gas management, such as a water pump and solenoid valves. Figures 3.7 and 3.8 present the components of the ASPM electrolyser:

1. Water tank and filter
2. Cell stack
3. Power to the stack and internal components
4. Fan and heat exchanger
5. Hydrogen vent

Each cell accepts a maximum of 2.2V and 27A and the I-V curve of the stack is shown in Figure 3.6. The maximum power to the stack is 535W.

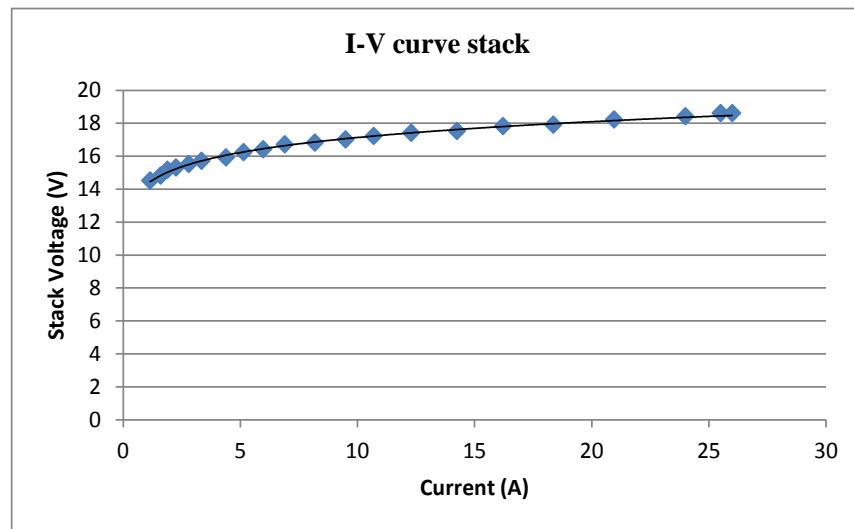


Figure 3.6, Representative I-V polarisation curve, at 20°C, 13.8bar

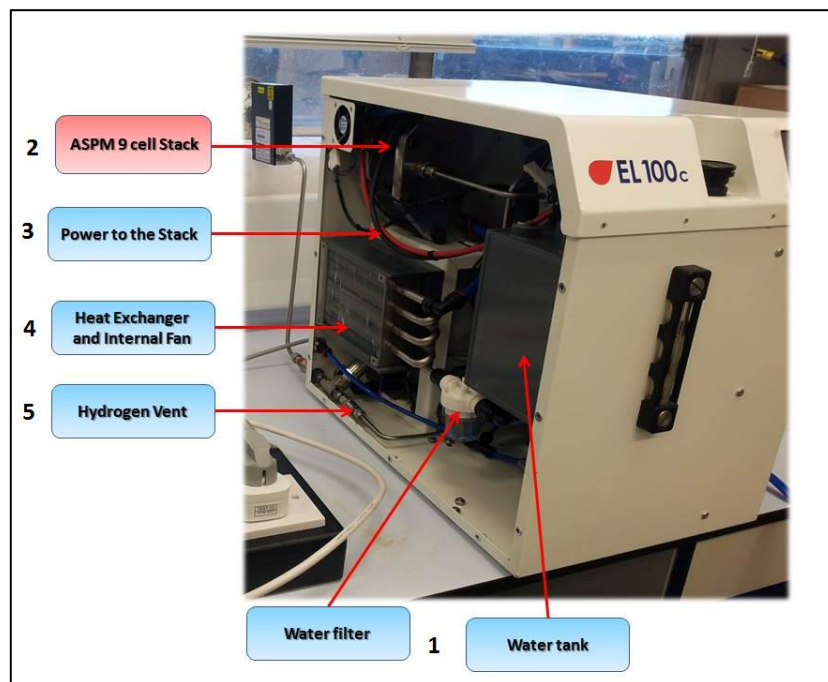


Figure 3.7, Left side and internal hydrogen generation components of the ASPM electrolyser

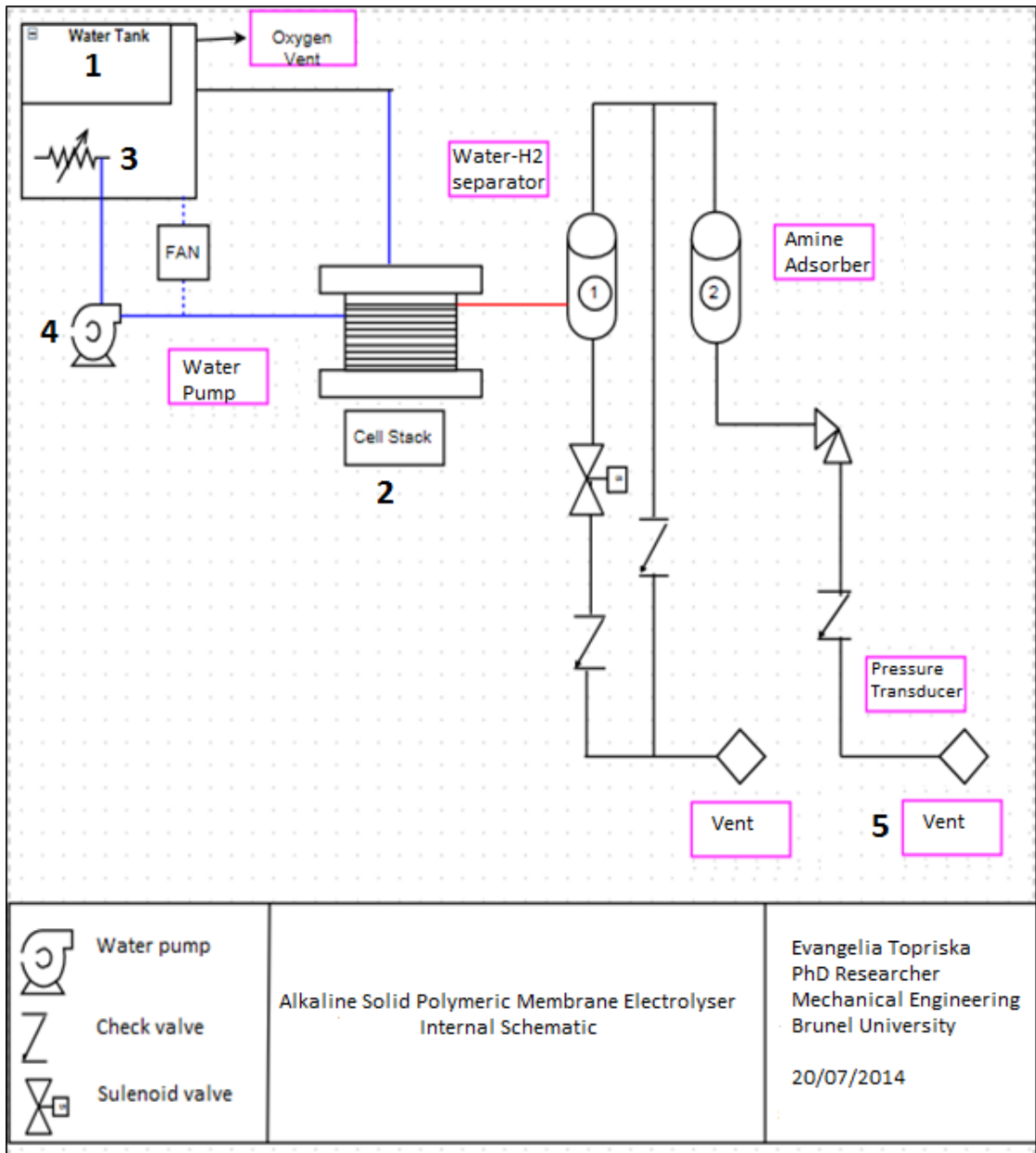


Figure 3.8, Internal Schematic of the ASPM electrolyser, redrawn from original

3.5 PV Data emulator

The purpose of the experiments is to characterise the operation of the PEM electrolyser and develop a numerical model in TRNSYS and to validate the model. The validation experiments are described in Chapter 5 and examine the performance of the electrolyser over a wide range of weather conditions so as to validate the model results. PV panels power the electrolysers, and therefore the irradiance and temperature levels directly affect the operation and performance of the system. It was necessary thus to design an experimental procedure that provides flexibility and allows for multiple and versatile tests. It is imperative to examine the performance of the system on days that are free of cloud and of high irradiance and on days that irradiance levels are volatile and subject to cloud coverage.

For this reason a PV emulator was constructed and used for the experiments. This emulator simulates the operation of PV panels and it consists of the following:

1. A 1200W DC Power Supply Unit, 60V and 50A maximum, within a power envelope
2. A Raspberry Pi computer
3. A 12bit digital to analogue converter
4. A 1500W, 24VDC to 240VAC Pure Sine Output Inverter

3.5.1 PV panels

Two sets of validation experiments are performed, for two different PV systems and two locations, Jamaica and London. The first set of experiments was conducted for London. Irradiance data from Brunel University's weather station and power data from a 1.765kW photovoltaic array installed by Brunel Institute of Power Systems (BIPS) was used. The available data has a time interval of 5 minutes. The array consists of 4 Sanyo HIT 210W modules of 16.8% efficiency, and 5 Sharp monoSi 185W modules of 14.1% efficiency. The PV panels' power output is emulated in the laboratory through the PV emulator designed and constructed for the tests.

For the Jamaica case, data from a PV array installed in the University of Technology in Kingston that supplies the PEM electrolyser in Jamaica is used. The PV array consists of 6

Trina Solar TSM-180DA01 panels rated at 180W and 14.1% efficiency. The characteristics of the modules are summarised in Table 3.1 and their detailed specifications can be found in the Appendix C. The data has a time interval of 15 minutes.

Table 3.1, Electrical and Thermal characteristics of the UK PV modules used for the experimental PV emulator

PV Type	Sanyo Heterojunction with Intrinsic Thin Layer (HIP)-210NHE1	Sharp MonoSi NUS5E3E	Trina Solar TSM-180DA01
Nominal Power Output P_{MP}	210	185	180
V_{MP} [V]	41.3	24	36.8
I_{MP} [A]	5.09	7.71	4.90
V_{OC} [V]	50.9	30.2	44.20
I_{SC} [A]	5.57	8.54	5.35
Temperature Coefficient of Power [%/°C]	-0.30	-0.485	-0.45

For the tests, the DC Power Supply Unit (section 3.5.4) is set at 24V constant to match the inverter specifications (section 3.5.5) and the current changes accordingly so that the unit operates as the PV array. Python coding is used and the unit is programmed through a Raspberry Pi B computer to use 5 and 15 min irradiance and power data.



Figure 3.9, The Raspberry Pi used in the experiments

3.5.2 Raspberry Pi b

A Raspberry Pi b computer is used for the programming purposes of the experiments. The Raspberry Pi is a credit card sized computer that can be connected to a screen and keyboard and can be used for programming in electronic projects. The Raspberry Pi b that was used in the experiments has a 512MB RAM, 2 USB ports and an Ethernet port and

can be seen in Figure 3.9 (Raspberry Pi, 2014). In order to optimise the experimental process for an automated flow of data of PV power output, it was necessary to find a method of setting the DC Power Supply Unit to automatically change its output every 5 and 15 minutes, to match the available data's interval.

The Raspberry Pi works on a Linux operational system. Python programming is used in order to develop a code that serves the purpose of sending signals to the DC Power Supply Unit; the complete code can be found in Appendix C

The main component of the PV emulator is the DC Power Supply Unit, which generates DC power. The Unit is connected to a 24VDC power inverter and for this reason its output is set at 24V. The reason for selecting a 24VDC power inverter is that the DC Unit works within a power envelope of 50A and 60V. This, in accordance with the power values of the PV array gives maximum DC current values of the range of 45A. Therefore, the DC voltage output of the DC unit is set at 24V constant and the power changes according to the changes in the DC current. The DC current values are derived from the DC Power output of the PV array and the DC voltage of the inverter, which is 24V.

The current values derive from analysis on the power data of the PV panels based on the process described by Equation (3.1):

$$I[A] = \frac{P[W]}{\eta \times V[V]} \quad (3.1)$$

Where:

P= Inverter power output in [W]

η = efficiency of the inverter

V=24V, the voltage of the inverter

I=current in [A]

Therefore, for each of the PV Power values there is a current value derived from Equation (3.1) used as an input. The inverter efficiency is a combination of the two inverter efficiencies, the laboratory inverter used for the experiments and the inverter used in the actual PV arrays. The calculations of the efficiency of the emulator inverter are shown in detail in Appendix C. The DC current values are controlled by signals sent to the DC Power Supply Unit through the Raspberry Pi and a digital to analogue converter. This

allows the process to be automated and to simulate more accurately the operation of PV panels. A typical example of current values derived from the above-described computational process is given in Table 3.2. More values can be found in Appendix D. The DC current values highlighted in red are the values that the current should take according to the DC power value and the 24VDC and are above the 50A current limit of the DC Power Supply Unit. These values are altered to smaller ones that the DC Power Supply Unit is able to provide and still correspond to PV power output high enough to emulate conditions similar to the original power output.

Table 3.2, Typical example of current values used in the experiments

Date	Time [hh:mm:ss]	Sanyo Power [W]	Sharp Power [W]	Total Power [W]	Voltage [V]	DC Power Output [W]	DC Current [A]
Sat, 1 June	11:00:00	446	453	899	24	1058	44.0
Sat, 1 June	11:05:00	375	383	758	24	892	37.2
Sat, 1 June	11:10:00	397	405	802	24	944	39.3
Sat, 1 June	11:15:00	462	470	932	24	1096	45.7
Sat, 1 June	11:25:00	578	595	1173	24	1380	57.5
Sat, 1 June	11:35:00	563	591	1154	24	1358	56.6
Sat, 1 June	11:40:00	527	530	1057	24	1244	51.8
Sat, 1 June	11:45:00	491	491	982	24	1155	48.1
Sat, 1 June	11:50:00	542	543	1085	24	1276	53.2
Sat, 1 June	11:55:00	544	526	1070	24	1259	52.5
Sat, 1 June	12:05:00	555	558	1113	24	1309	54.6
Sat, 1 June	12:10:00	634	633	1267	24	1491	62.1

As mentioned before the DC current values are sent from the Raspberry Pi computer through a digital to analogue converter to the DC Power Supply Unit, as described in section 3.5.3. The Raspberry Pi sends digital signals that the DC Power Supply Unit is not able to receive as it only accepts analogue control signals. For this reason the digital to analogue converter is essential, as it converts the digital signals to 0-5V analogue ones accepted by the DC Power Supply Unit. The Raspberry Pi is powered through the power slot of a regular mobile phone charger. The screen, keyboard and mouse are connected through the USB port. The detailed schematic diagram is shown in Figure 3.10.

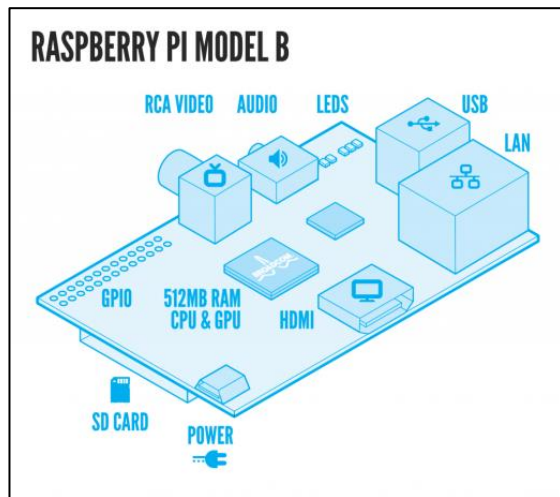


Figure 3.10, Raspberry Pi B schematich diagramm and ports

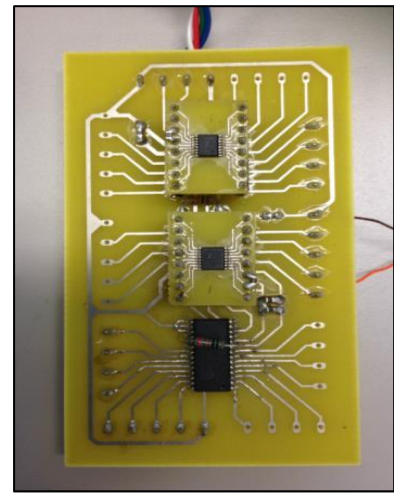


Figure 3.11, Digital to Analogue Converter used in the experiments

3.5.3 Digital to Analogue Converter

The signals from the Raspberry Pi are in digital form that requires further conversion as the DC Power Supply Unit accepts only analogue signal inputs. In order to overcome this, a digital to analogue converter was used. This was an AD5625R, nanoDAC low power, 12 bit converter that is demonstrated in Figure 3.11 (Analog Devices, 2007-2013). This converter is connected to the GPIO of the Raspberry Pi B.

3.5.4 DC Power Supply Unit

The DC Power Supply Unit used is the QPX1200S manufactured by AIM & THURLBY THANDAR Instruments (Aim & Thurlby Thandar Instruments, 2014). It is suitable for

laboratory bench top applications. It offers a wide range of current and voltage combinations and operates up to 60V and 50A within a power envelope, see Figure 3.12.

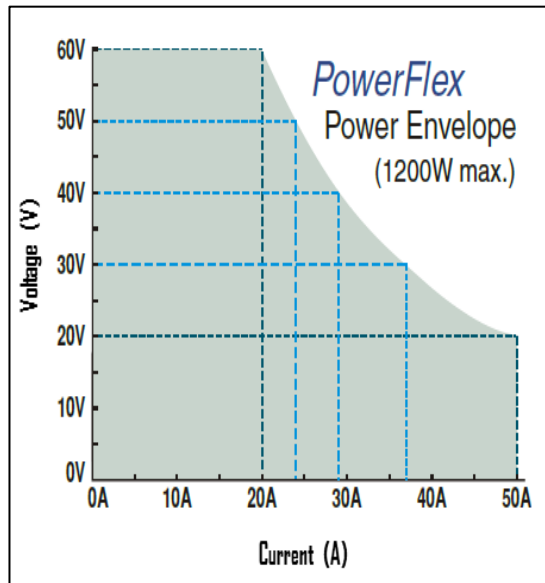


Figure 3.12, Power Envelope of the DC Power Supply Unit

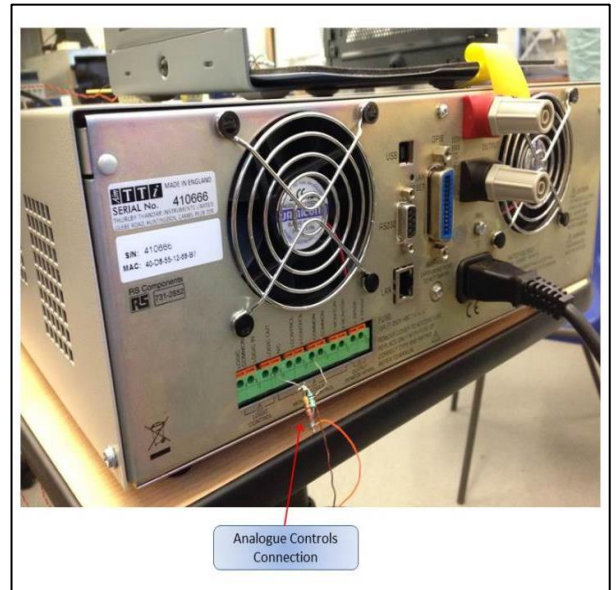


Figure 3.13, Analogue controls connection at the back of the DC Power Supply Unit

The DC Power Supply Unit has a digital display for clarity and ease of use and offers an analogue input control. The analogue input controls the current output with an accuracy of 0.3%. This is done by control voltages of scale 0-5V that are sent by the digital to analogue converter which “translates” the digital signals of the Raspberry Pi as shown in Figure 3.13.

3.5.6 Pure Sine Output Power Inverter

The inverter used for the experiment is a 1500W true pure sin wave, 24V input voltage inverter by LiveLife. The inverter’s input is connected to the DC Power Supply Unit and its output is connected to the electrolyser through a power analyser. The inverter accepts 24VDC by the DC Power Supply Unit at all times and the available energy varies according to the DC current. The electrolyser draws the necessary energy through the inverter, at the periods that this is available.

3.5.7 Overview of Energy Flow through the PV Emulator

The overview of energy flow through the system components of the PV emulator are described with an example: during the experiment of the 6th day of the first week of June 2013 for the UK case, the irradiance at 09.30 is 705.5W/m² and this corresponds to a PV power output of 629W. In order to emulate this with the PV emulator the following steps are carried out:

1. Equation (3.1) is used to calculate the current to be used as input in the Python code; the value is 30.83A
2. This value is inserted in the code
3. The code is read by the processor that sends digital signals of the read values with a defined time step of 5 minutes
4. The digital to analogue converter reads the digital signal of the 30.83 A, translates it to an analogue voltage signal within the range of 0 to 5 V and sends it to the DC Power Supply Unit.
5. The DC Power Supply Unit takes this signal as control input. Its settings are already customised to provide constant voltage output at 24V and to change the current output according to the input signal.
6. Thus the available power at that moment corresponds to a PV output of 629W and this is available to the electrolyser through the inverter, which has an AC output of 240V.

3.6 Metal hydride storage tank

The metal hydride storage tank used in the experiments is made of aluminium and all the fittings, valves, nuts gland and gasket are stainless steel from Swagelok, see Figure 3.14. Aluminium was chosen because it presents higher thermal conductivity (205 Wm⁻¹K⁻¹) in comparison to stainless steel (50.2 Wm⁻¹K⁻¹) (Hyper Physics, 2014).



Figure 3.14, Metal hydride storage tank

3.7 Instrumentation

The measuring equipment used in the experiments is described in this section. Detailed information and the degrees of accuracy of each instrument are given in Appendix B.

3.7.1 Digital Mass Flow Meter

The mass flow meter acquired is a digital one manufactured by Aalborg (Aalborg , 2014). It has a range of 0 to 1000ml/min and it shows the flow rate on a digital screen. It has the option of analogue and digital outputs. For the experiments the analogue outputs are selected and the flow rate readings are transferred to the computer through a 4-20mA analogue signal via a data logger.

3.7.2 Power Analyser

An AC power analyser is used to evaluate the energy use of the electrolysers during the experiments. The power analyser acquired is the ACM20-2-AC1-R-C from Murata Power Solution (Murata Power Solutions, 2014) . It displays information about:

- Input Voltage
- Input Current
- Input Active Power
- Power Factor

Its operating and measuring range is 0-10A and has a 0.001A resolution at 999.9 watts max, and 85-264AAC supply voltage. Its operation is based on a built-in current transformer.

The ACM20-2-AC1-R-C power meter does not offer the possibility to data log; therefore, a current transducer was used as is described in the following paragraph.

3.7.3 Current Transducer

The current transducer acquired for the experiments is the PM-CTR07 Current Transducer from Sontay; (Sontay, 2012). It provides accurate load trending information for currents 0-10A with an output of 0-5VDC connected to an analogue data logger. The current transducer is used to data log the input current to the electrolyzers so as to create the energy use profiles.

3.7.4 Thermocouple for the Temperature of the PEM produced Hydrogen

A thermocouple is installed at the exit of the produced hydrogen of the PEM electrolyser so that the temperature of the produced gas is measured. The thermocouple is installed in the steel pipe and is carefully situated in the middle of the pipe not to touch the metal and affect indication, see Figure 3.15. Thermocouples are also inserted in the water tank and record temperature corresponding to the stack.



Figure 3.15, Thermocouple for the measuring of the temperature of the PEM electrolyser produced hydrogen

3.7.5 Pico Data Loggers

A TC-08 thermocouple data logger is used to log data of the flow meter, current transducer and temperature.

It is designed to measure a wide range of temperatures using any thermocouple that has a miniature size thermocouple connector and can be connected to other sensors using a 70 mV range. In order to send the signals of 4-10mA from the flowmeter and 0-5V from the current transducer a USB TC-08 Single-Channel Terminal Board is used. The screw terminals allow wires to be attached to the data logger without soldering and enable the USB TC-08 to measure voltages from 0 to +5 V, or 4-20 mA loop current.

3.7.6 Digital Clamp Multi meter

The digital clamp multi meter is a TENMA made and is used to measure the DC current to the stack (Farnell, 2014). It is set at 40A mode and is clamped directly on the stack supply cable.

3.7.7 Digital Multi meter

A digital multi meter from SkyTronic is used to measure the stack voltage, and is set at 20VDC.

3.7.8 Pressure Gauge

The pressure gauge is used as an extra indication of the pressure of hydrogen gas in the pipe. It is Swagelok made, stainless steel, and can stand up to 360psi or 25bar.

3.8 Experimental Steps for the Proton Exchange Membrane (PEM) Electrolyser experiments

The experimental setup of the PEM electrolyser experiments can be seen in Figures 3.16 and 3.17. The experiments require specific procedures for measurement accuracy. Each test is performed on separate days because each experiment is time demanding (many hours) and the period between two consecutive days allows the electrolyser to cool down. The steps refer to the experimental processes of both the characterisation and the validation tests, and more specifically steps 5, 6, 7 and 14 are valid only for the validation experimental process:

-
1. Check all sensors and safety controls in the laboratory and confirm their correct performance. This is done through checking the monitoring board, as shown in Figure 3.2
 2. The digital mass flow meter is switched; it needs 6 minutes to warm up
 3. The computer is switched on and the software that performs data logging is loaded (Pico). For each experiment a file is created named after the date and experiment characteristics which are: test day and pressure set point for the characterisation experiments, test day from the selected PV input data and pressure set point for the validation experiments. The data logging interval is set at 1 second and the period is set at 36000 sec which corresponds to 10 hours covering the period of each experiment
 4. Two data loggers are used, one for logging the flow rate and one for logging the energy input to the electrolyser and the temperature of the produced hydrogen of the PEM electrolyser. Using separate loggers ensures that there is no interference between the signals logged
 5. The Raspberry Pi computer is switched on and the Python file is loaded which corresponds to the current data of the PV for each specific experimental day
 6. The DC Power Supply is switched on; it requires a few seconds for its software to start and get to operate condition
 7. The Python file of the Raspberry Pi starts running; the output of the DC unit connected to the inverter is switched on so that the energy flow through the inverter can initiate
 8. The electrolyser absorbs the necessary energy from the inverter and is switched on. The pressure set point is regulated to the selected for each experiment and the heat up process starts. This lasts for 7 minutes and 20 seconds regardless the selected pressure set point. During this period the heater of the purification system starts and needs to reach a temperature of 273°C
 9. After the heat up period the stack generation/ pressure build up period starts. This is different for each pressure set point and the higher the selected pressure the longer this period
 10. When the stack has generated enough hydrogen to reach the pressure set point at the stack output the flow of hydrogen is ready to start

-
11. Hydrogen starts flowing at the output and the stack generation is specified by the pressure at the output that has to be constant. The stack starts generating hydrogen at low flow rates that gradually increase until they reach steady state production
 12. Flow rates, energy consumption and hydrogen temperature are logged through the data loggers
 13. Throughout the experimental process the data is checked regularly as well as the temperature of the water tank
 14. In case that a day with variable PV output is tested during the validation tests there are occasions when the available PV energy is not enough and the electrolyser stops. These occasions are recorded as well as the periods they last. When the available energy is again at adequate levels the electrolyser is switched on. If the period that it was off is long the electrolyser requires again a heat up period, shorter than the original one. In any case the stack generates again until it reaches the point of the selected pressure and then the flow is ready to start again
 15. The efficiency of the inverter is also measured

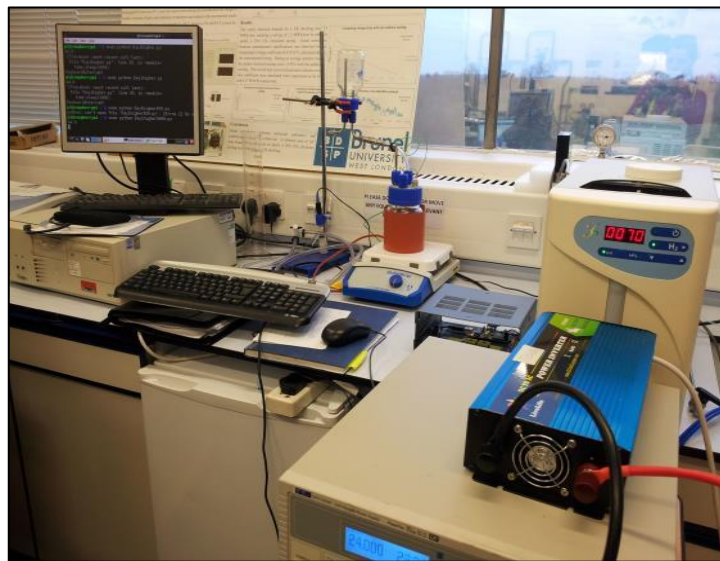


Figure 3.16, Experimental Setup of the PEM Electrolyser



Figure 3.17, Experimental Setup of the PEM Electrolyser

3.9 Experimental Steps for the Alkaline Solid Polymeric Membrane (ASPM) Electrolyser experiments

The experimental setup of the ASPM electrolyser experiments can be seen in Figure 3.18. As in the case of the PEM electrolyser experiments, the execution of the experiments requires specific procedures to take place in order for the measurements to be carried out correctly. Each experiment is performed on separate days for the same reasons as the PEM electrolyser. Steps 7, 8, 9 and 17 refer to the experimental process where the ASPM electrolyser is checked for operation during specific days.

1. Check all the sensors and safety controls in the laboratory and confirm their correct performance. This is done through the monitoring board shown in Figure 3.2
2. The flow meter is recorded through a monitoring software that can communicate with the electrolyser through a LAN connection cable.
3. The stack temperature and voltage are also recorded through the monitoring software
4. The stack current is recorded through a digital clamp multimeter clamped immediately on the stack supply cable
5. The computer is switched on and the software that performs data logging is loaded. (Pico). For each experiment a file is created that is named after the date and the

experiment characteristics. The data logging interval is set at 1 sec and the period is set at 36000 sec which corresponds to 10 hours and covers the period of each experiment

6. One data logger is used, for the logging of the energy input to the electrolyser.
7. The Raspberry Pi computer is switched on and the Python file is loaded which corresponds to the current data of the PV for each specific experimental day.
8. The DC Power Supply is switched on and it requires a few seconds for its software to start and get to ready to operate condition
9. The Python file of the Raspberry Pi starts running and the output of the DC unit that is connected to the inverter is switched to on and energy flows through the inverter
10. The electrolyser absorbs the necessary energy from the inverter and is switched on. In the beginning the stack is being hydrated and this lasts for 2.5 minutes
11. After the stack hydration period the stack generation starts
12. The stack starts generating hydrogen at low flow rates that gradually increase until they reach steady state production
13. Hydrogen flow rates, energy consumption and temperature are logged through the data logger and the monitoring software
16. Throughout the experimental process the data is checked regularly as well as the temperature of the water tank
17. In case that a day with variable PV output is tested there are moments where the available PV energy is not enough and the electrolyser stops. In this case these moments are recorded as well as the periods they last. When the available energy is again at adequate levels the electrolyser is switched on manually. In any case the stack generates again at lower flow rates at the beginning until it reaches the steady state point
18. The efficiency of the inverter is also measured

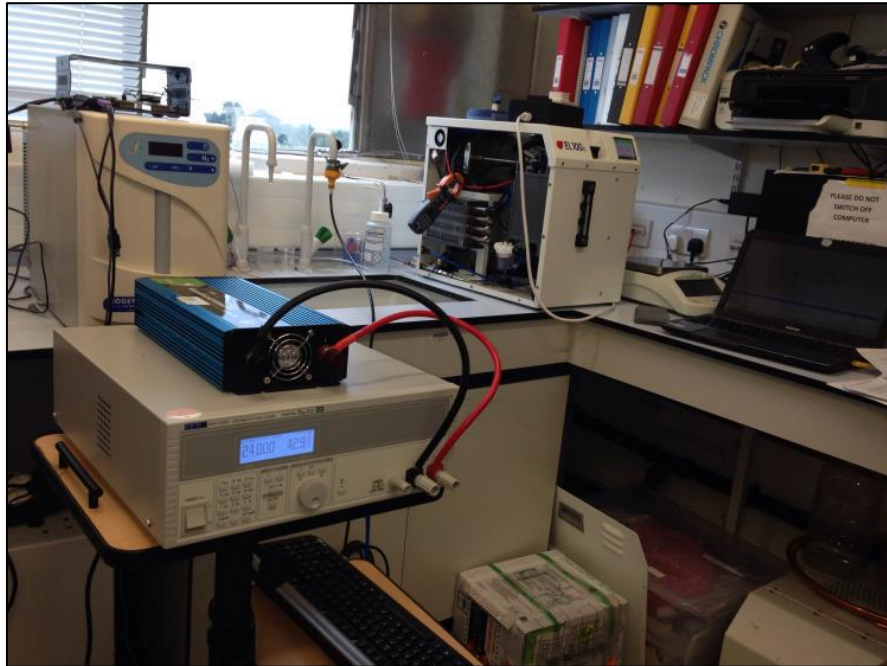


Figure 3.18, Experiment setup of the ASPM Electrolyser

The complete setup of the two experimental rigs can be seen in Figures 3.19 and 3.20.

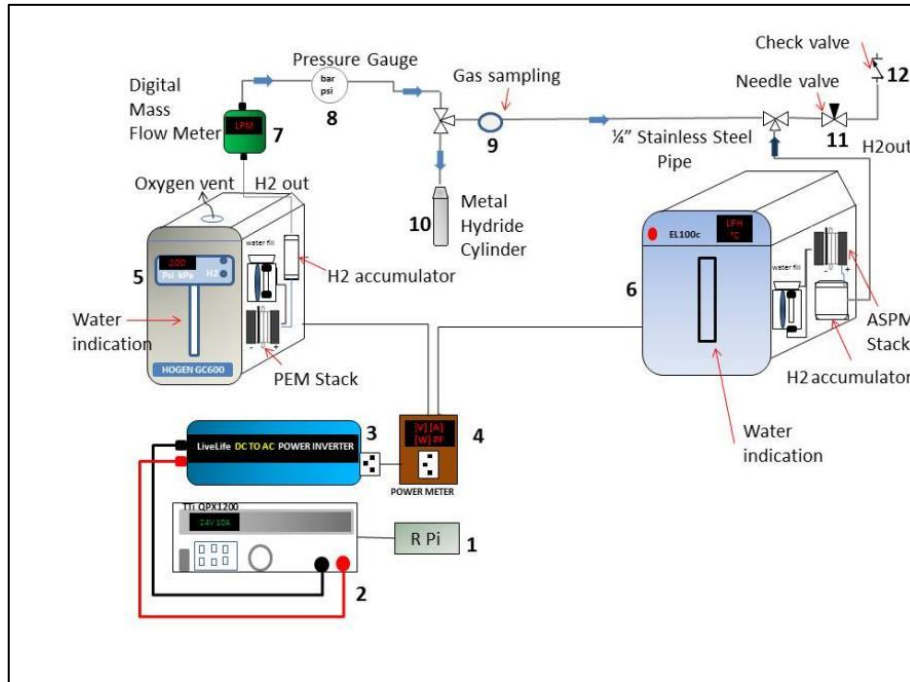


Figure 3.19, Schematic Diagram of the Experimental Rigs



Figure 3.20, The complete Experimental Setup of PEM and ASPM Electrolyser

3.10 Direct Stack Measurements

In order to conduct the direct stack measurements of the PEM and ASPM electrolyser the following procedure was followed:

1. A digital Clamp Multimeter was clamped directly on the supply cable of the stack. The setting was selected as 0-40A DC, so that the stack current could be measured
2. A digital Multimeter was attached to the supply of the stack, and the 20VDC setting was selected so that the stack voltage could be measured
3. The electrolyser was powered and the incremented values of the current and voltage to the stack were measured and recorded
4. The temperature of the stack was recorded
5. Each experiment was repeated five times so as to validate the results

The direct stack measurements are indicatively shown in Figures 3.21 and 3.22.

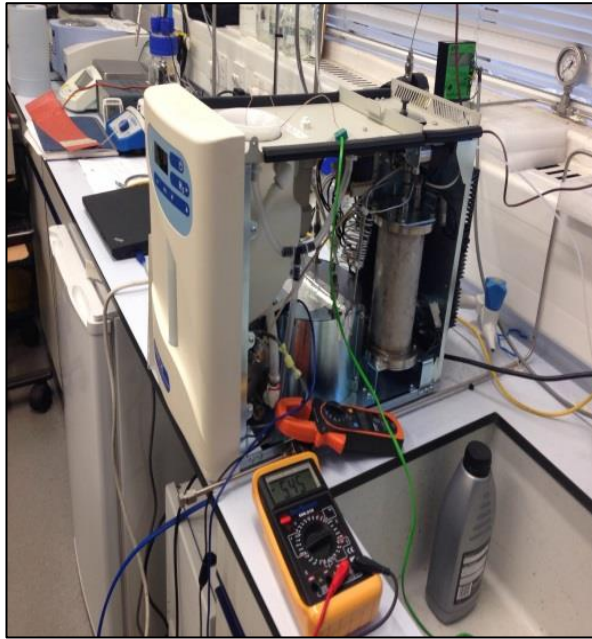


Figure 3.21, Direct stack measurements on the PEM electrolyser

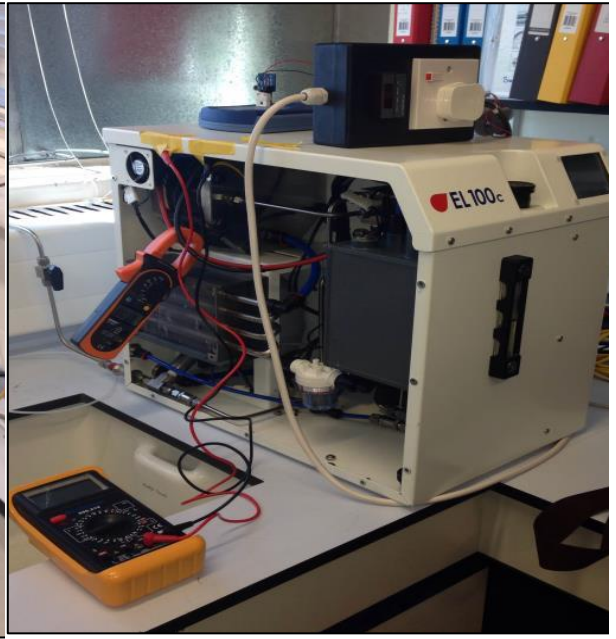


Figure 3.22, Direct stack measurements on the ASPM electrolyser

3.11 Metal hydride storage experimental process description

The hydrogen supply line from the PEM electrolyser is connected to the metal hydride cylinder through $\frac{1}{4}$ " inch tubes and $\frac{1}{4}$ " Swagelok stainless steel fittings. Thermocouples are placed on the bottom and walls of the metal hydride storage tank to measure the temperature data when the storage unit is in operation, during absorption and desorption. For the first time of operation of the metal hydride storage tank, the activation process has to be performed. After the activation is completed successfully, the material is ready to be used for absorption and desorption cycles, which are described below. (The activation process is similar as the absorption process)

Absorption Process Steps:

1. The metal hydride tank is weighted before the start of the experiment, still empty
2. The metal hydride tank is connected to the setup and it is closed
3. The pipelines are vacuumed and no air is present in the piping network
4. The hydrogen generation begins for the selected operating pressure
5. The three way valve is switched to allow the hydrogen to flow towards the metal hydride storage tank.

-
6. Hydrogen is now present in the line that connects the metal hydride tank
 7. The on-off valve of the metal hydride is switched to on and the pressurised hydrogen flows to the storage tank
 8. A pressure drop will be observed in the system as the pressurised hydrogen flows to the tank
 9. The generator will produce more hydrogen to compensate for the pressure drop and the pressure of the tank will eventually reach the selected hydrogen pressure
 10. Hydrogen flow rates, pressure and temperature are recorded through the data loggers
 11. The mass of the absorbed hydrogen is confirmed also by measuring the weight of the metal hydride tank upon completion of the absorption process.

Desorption Process Steps:

1. Upon completion of the absorption process, the tank is weighted to confirm full absorption potential
2. The on-off valve of the tank is closed and the line that connects it to the electrolyser and to ambient is vacuumed to ensure that no air is present
3. The metal hydride tank is opened and hydrogen is released in the line.
4. In order to trigger and enhance the desorption process heat transfer to the tank is used at a maximum temperature of 70°C (Souahlia, et al., 2014) , until the pressure inside the tank becomes constant and equal to 1bar.
5. The on-off valve of the tank is switched to off again and hydrogen is allowed after to flow to ambient without air contacting the tank interior.
6. Process is repeated until desorption is completed according to the weight of the tank and the temperature readings.

3.12 Summary

This chapter presents the procedures and equipment employed for the experiments of this research. The mechanical and electrical equipment was presented in detail as well as the measuring equipment. The basic experimental processes outlined are:

- Proton Exchange Membrane (PEM) Electrolyser experiments
- Alkaline Solid Polymeric Membrane (ASPM) Electrolyser Experiments
- Direct stack measurements
- Metal Hydride Storage of Hydrogen Gas

The next chapter gives a detailed presentation and discussion of the results of the experiments with the PEM electrolyser and hydrogen storage process. The experiments focus on hydrogen generation rates, temperatures, stack energy use and the interaction of the metal hydride storage with the electrolyser, in relation to the hydrogen generating pressure. Furthermore, an overview of a comparative experimental set with an Alkaline Solid Polymeric Membrane (ASPM) Electrolyser is presented.

**Chapter 4. Analysis of Experimental Results
and Numerical Model Development**

4.1 Introduction

This chapter presents the results of the experimental part of this research. The experimental setup and basic steps and guides for the experiments are described in Chapter 3. The experimental results are important for the development and validation of the numerical model to be presented in Chapter 5. The experiments had a dual purpose, to create the basis for the model development and also validate the model. First the experiments with the PEM electrolyser lead to information regarding: (a) efficiency of the hydrogen generation process in terms of stack and the complete electrolyser unit, (b) losses due to the hydrogen management systems, and (c) hydrogen temperature, all for different hydrogen generation pressure. This information is used as the basis for the development of the numerical model regarding the PEM electrolyser operation, its controls and the metal hydride storage. Experiments with the metal hydride storage provide information of the metal hydride tank filling time according to the hydrogen flow rates for the distinct generation pressure and also for the interaction between the electrolyser and the metal hydride tank.

Second, additional tests are performed to validate the model. The model is validated by an iterative procedure through which the model outputs are compared to the experimental data until errors between model and experiments are justified within confidence limits (Thomson, 2005). Once the model is validated, parametric analysis is performed to quantify the impact of the model varying parameters.

4.2 Hydrogen flow and stack measurements

The electrolyser is a compact unit that includes gas and water management systems in addition to the stack. Therefore, its energy use as a unit depends on the total energy requirements of all its components. The modelling of each component is necessary and is accomplished through laboratory experimental measurements and referring to electrochemical models from literature, as explained below. The PEM electrolyser used in this study is an AC powered unit of one 4-cell stack, manufactured by Proton Onsite (PROTON OnSite, 2012). It is rated at 1.2kW and maximum hydrogen production at 600cc/min, with a permissible current of 0-30A, at stack voltage of 6.5-7.5VDC. The characteristic I-V curve of this electrolyser stack is given in Figure 3.3 of Chapter 3

The numerical model developed in this study is a semi-empirical model developed from basic electrochemical equations of the electrolysis process and experimental data. The model is divided in two main sub-models. The first is an electrochemical sub-model based on experimental analysis of hydrogen generation rates combined with fundamental electrolysis theory resulting in the hydrogen production computation. The experiments examine the hydrogen production rates for pressure set points within the operating range and for a 1 bar interval. The second sub-model deals with the stack voltage calculations and is based on thermal semi-empirical methodologies. The combination of these two sub-models in a complete model for the PEM electrolyser allows for simulation for any user defined electrolyser size and thus unique stack current, size and temperature. Finally, a combination of the stack voltage with the input current to the stack allows for the stack energy use calculation.

The generated hydrogen amount is calculated by the first law of electrolysis of Faraday, as described in Equation (4.1):

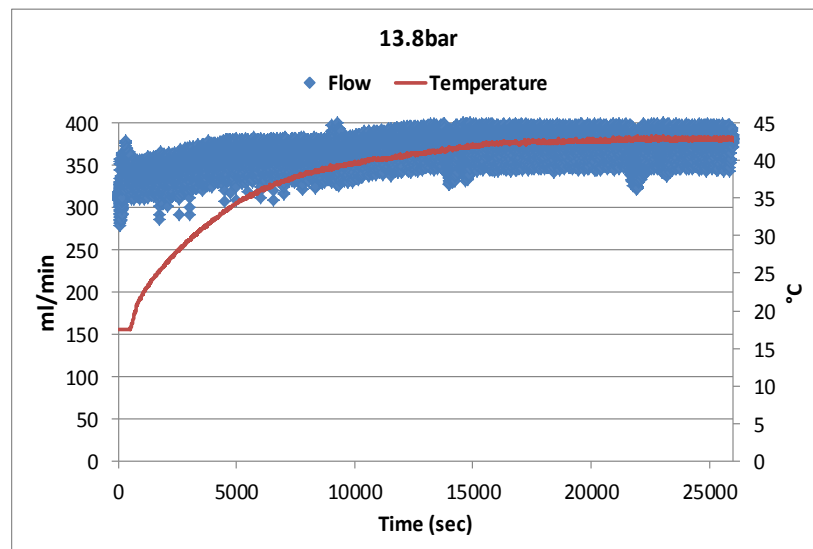
$$V_{H_2} = \int_0^t \frac{\eta_F \times n_c \times R \times I \times T}{F \times p \times n} dt \quad (4.1)$$

The Faraday efficiency in general is assumed to be very high, ~99% (Gorgun, 2006; Garcia-Valverde, et al., 2011). Equation (4.1) has been widely used in reported research to evaluate hydrogen generation rates without taking into consideration any actual losses related to a real system operation.

In a compact hydrogen production system such as the PEM electrolyser used in this study, hydrogen is collected and measured after it passes through gas management modules. The electrolyser includes a drying and purification unit and a hydrogen accumulator that introduce extra inefficiencies in the system. Evaluating the actual effect of these losses on the generated hydrogen flow rates is very important so that the simulation can predict accurate results. These extra losses are evaluated through the experimental process described below. The effect of the losses and inefficiencies on the generated hydrogen changes according to the generation pressure. Additionally the range of the hydrogen production rates also varies with the production pressure and modelling was based on these flow rates.

The PEM electrolyser used operates for hydrogen production pressures in the range of 3 to 13.8 bar, and the amount of the generated hydrogen is different at each pressure set point. The generation rates depend on the set pressure and the stack produces at the adequate rate so as to achieve the necessary pressure at the outlet. Moreover, as the stack presents different operational behaviour at each pressure set point, the energy use is also different. Experiments were conducted and the hydrogen production flow rates, the energy use and temperature of the stack were recorded for pressures between 5 to 13.8 bar with a 1 bar step. The temperature of the electrolyser stack is assumed to be uniform. The pressure at the output was kept constant for each test with back pressure regulation. The tests were repeated 3 times each to reassure data logging accuracy and confirm the uncertainty, see Appendix C for uncertainty analysis.

A measurement of the hydrogen generation flow at the maximum operating pressure of 13.8bar is presented at Figure 4.1. The data logging is performed for a time interval of 1 second. The generated hydrogen, before it flows to the output is first accumulated in a small tank in the interior of the electrolyser. From there, hydrogen that does not satisfy the purity requirements is vented out through an alternative outlet. This causes a small pressure drop that leads to hydrogen generation fluctuation that can be seen in the measured flow. The detailed measurements of the hydrogen flow at each pressure step are presented in Appendix D. From the experiments, it is observed that as the operating pressure increases the flow rates increase proportionally.



Figures 4.1, Hydrogen flow at the generating pressure of 13.8bar

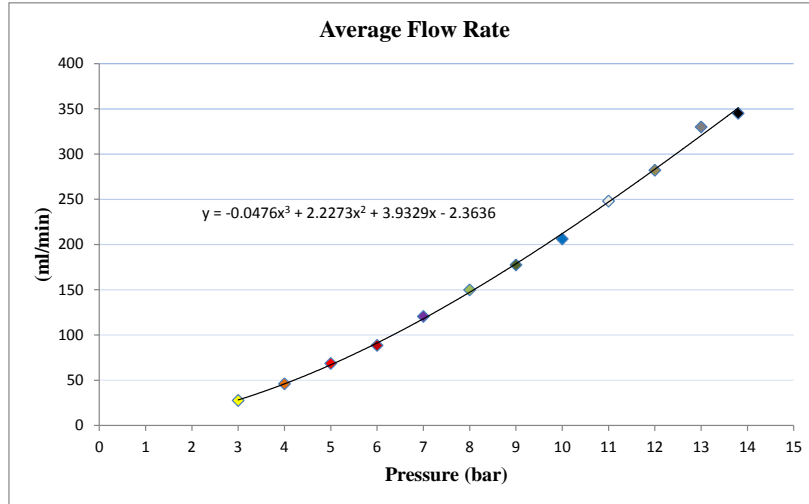


Figure 4.2, Average hydrogen flow rates curve for the complete pressure range of the electrolyser, 3 to 13.8bar

The hydrogen generation curve that is developed through polynomial interpolation of the experimental data as shown in Figure 4.2 is given by Equation (4.2).

$$H_2 = \begin{cases} -4.76 \times 10^{-2} p_{H_2}^3 + 2.23 p_{H_2}^2 + 3.93 p_{H_2} - 2.36 & \text{for } 3 \leq p_{H_2} \leq 13.8 \\ 0 & \text{for } p_{H_2} \leq 3 \text{ or } p_{H_2} \geq 13.8 \end{cases} \quad (4.2)$$

The flow rates correspond directly to the pressure set point and thus, the higher the pressure the greater the hydrogen generation. Therefore, the stack operates at a more frequent rate to produce the necessary hydrogen and the temperature and energy use increase accordingly, as shown in Figures 4.3 and 4.4.

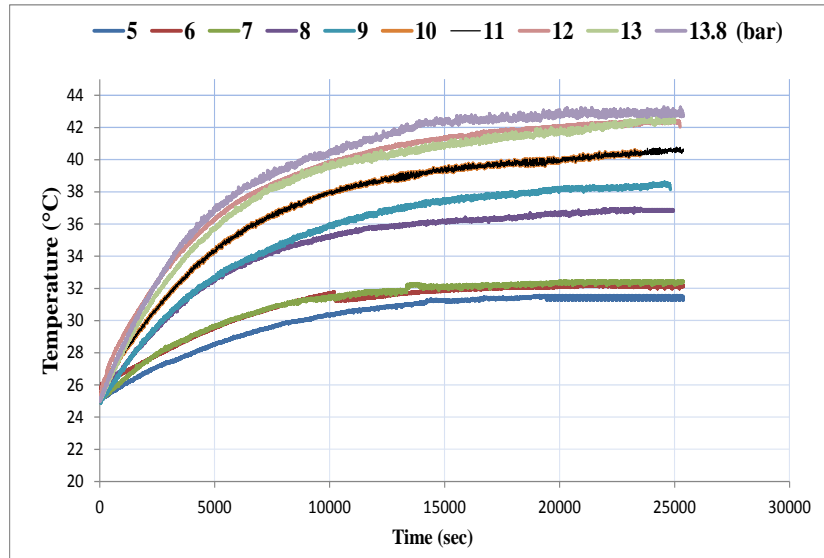


Figure 4.3, Experimental temperature measurements for pressures of 5 to 13.8 bar

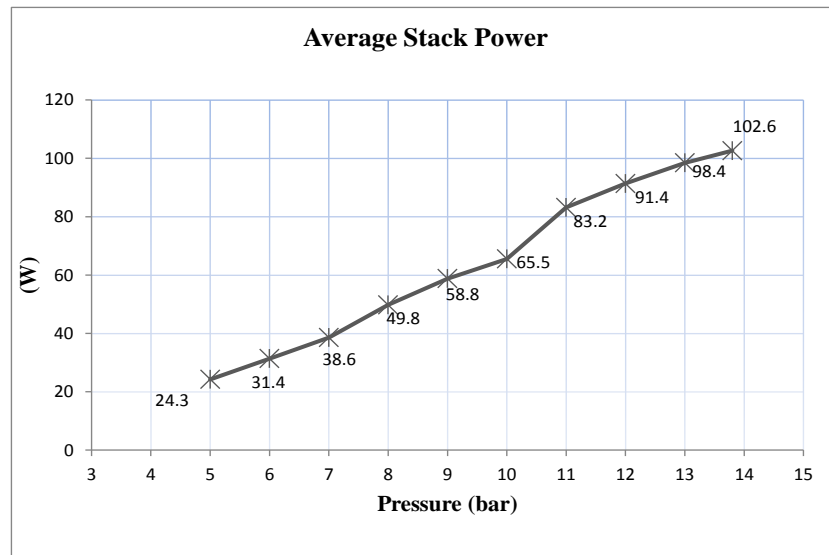


Figure 4.4, Experimentally measured energy use of the stack for pressures of 5 to 13.8bar

Figures 4.2 and 4.3 show that hydrogen flow rates and stack temperature are higher at higher pressure set-points. The stack temperature shows a greater increase as the flow rates increase, as the stack operates at a more frequent basis in order to produce sufficient hydrogen to maintain the pressure. At pressures up to 9 bar, the stack temperature is less than 40°C. For pressures within the range of 10 to 13.8 bar the stack temperature rises above 40°C and also increases at a higher rate. This is explained by the fact that the stack operation at this pressure range is more frequent and thus the stack reaches high temperatures faster. Moreover, this increase in the stack temperature causes an increase in the hydrogen production that leads to higher efficiencies. Between pressures of 10 and

13.8 bar, which is the maximum production pressure, highest efficiencies are observed, see Table 4.1. In particular, the most efficient performance is at the maximum production pressure, which corresponds also to the highest hydrogen production rates.

Table 4.1 Average flow rates, maximum temperature and stack efficiency

Pressure Set-point (bar)	Average Flow Rate (ml/min)	Maximum Temperature (°C)	Stack Efficiency (%)
5	68.53	31.56	53.81
6	88.52	32.22	55.3
7	120.50	32.44	57.63
8	149.89	36.97	57.76
9	177.48	38.57	57.94
10	206.17	40.46	58.43
11	248.03	40.84	58.46
12	282.12	42.44	60.56
13	330.62	42.59	63.5
13.8	345.04	43.25	63.6

The specific energy use of the stack per mass and per volume can be seen in Table 4.2. The smallest specific energy use is observed at 13.8 bar and it corresponds to 5.1 kWh/Nm³ and 60.8 kWh/kg. It can thus be concluded that the optimum performance of the electrolyser is when the stack operates at maximum rates at the maximum operating pressure.

Table 4.2: Specific energy use of the stack per mass and per volume

Pressure(bar)	KWh/Nm ³	kWh/kg
5	6.1	72.8
6	5.9	70.8
7	5.7	68.0
8	5.7	67.8
9	5.6	67.6
10	5.6	67.0
11	5.6	67.0
12	5.4	64.7
13	5.1	61.0
13.8	5.1	60.8

4.3 Electrical Characteristics Measurements for the Start Up

The start-up process of the electrolyser is separated into two main phases:

1. The heating period, where the heating element of the palladium purification membrane is heated to the operating temperature of 273°C
2. The stack generation phase where hydrogen is firstly produced and it is combined with the second phase of the heating period.

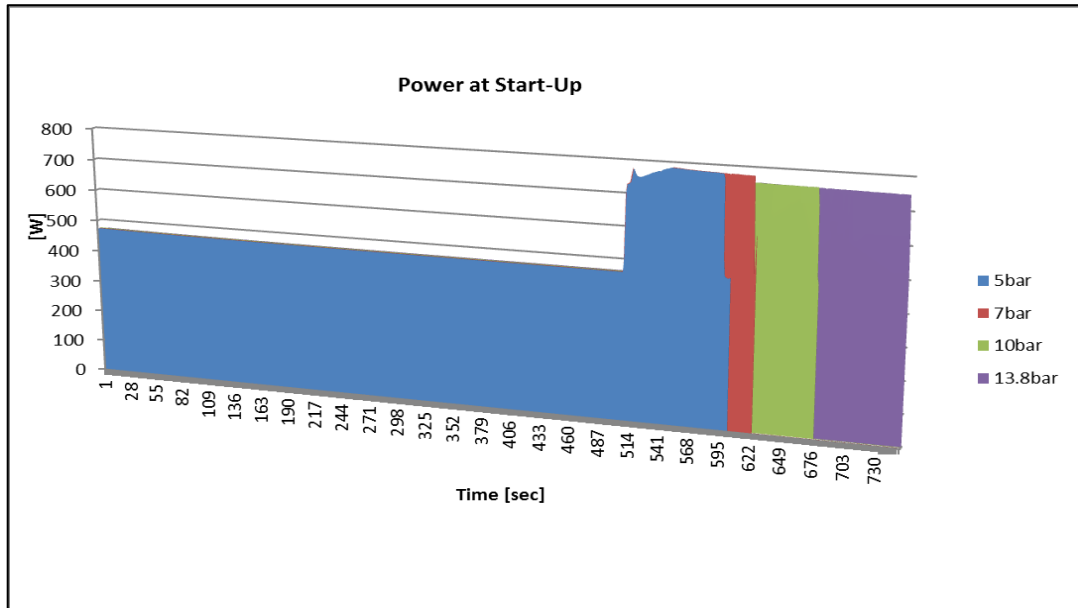


Figure 4.5, power of the electrolyser during start-up for the distinct pressures set-points of 5bar, 7bar, 10bar and 13.8bar

The stack produces according to the pressure set point; therefore the duration of this period is different for each pressure set point, see Figure 4.5. The higher the operating pressures the higher the duration of the stack generation at the beginning. This is explained by the fact that the flow rates correspond directly to the pressure set-point and thus, the higher the pressure the greater the hydrogen generation has to be to reach the set-point.

The durations of the two phases are:

- 8.5 minutes average for the heating period, at 474W
- 1.55 minutes for the stack generation at 5bar
- 1.92 minutes for the stack generation at 7bar
- 2.7 minutes for stack generation at 10bar
- 3.68 minutes for stack generation at 13.8bar

The heater works during the start-up of the electrolyser and at certain points during operation that are dependent on the amount of generated hydrogen. Its operation is simulated by a model that introduces the periods where the heater is ON and extra 474W are added to the electrolyser energy demands. It is observed that there is a linear relation between the generation times and the pressure set-point, and thus at any pressure this can be calculated.

4.4 Stack Direct Measurements

The stack polarisation curve as provided by the manufacturer is shown in Figure 3.3. Through direct measurements to the stack (see indicatively Figure 4.11); the polarisation curve was found to be the one shown in Figure 4.6.

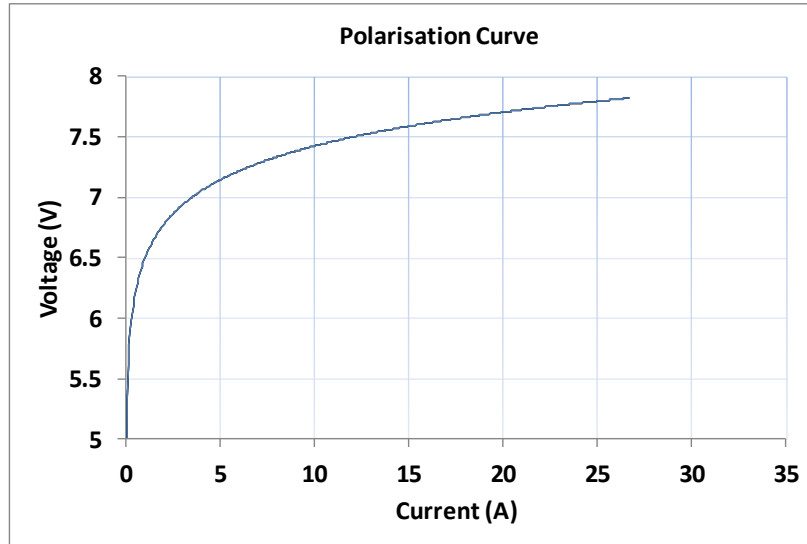


Figure 4.6, Experimental stack polarisation curve

The direct current to the stack is measured to have a maximum value of approximately 27A (a value slightly smaller than the manufacturer specifications), when the stack operates at maximum rate. The stack operates at two observed modes according to the electrolyser operation. The current varies between 0-27A and the variation depends on the hydrogen that should be produced, which in turn depends on the demanded pressure. The higher the pressure set point, the stack has to operate at a higher rate to produce the necessary hydrogen amount to reach this pressure. Thus the current to the stack is higher in this case and takes the maximum value of 27A for longer periods.

Figures 4.7 and 4.8 present the characteristic stack current, voltage and power values for the operations at 13.8bar. The stack current, voltage and power values for the operations 5bar and 10bar are presented in the Appendix D. The operation at 5bar is characterised by current values between 0 to 12A for the greatest period of time. For the operation at 10bar, current takes values between 3A and 18A for the greatest period and for the 13.8bar operation the current has the maximum value of 27A for almost all the time.

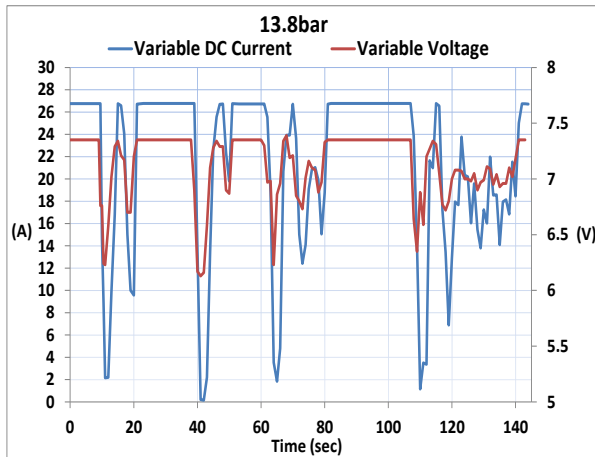


Figure 4.7, Variable DC current and voltage to the stack while producing constant hydrogen at 13.8bar

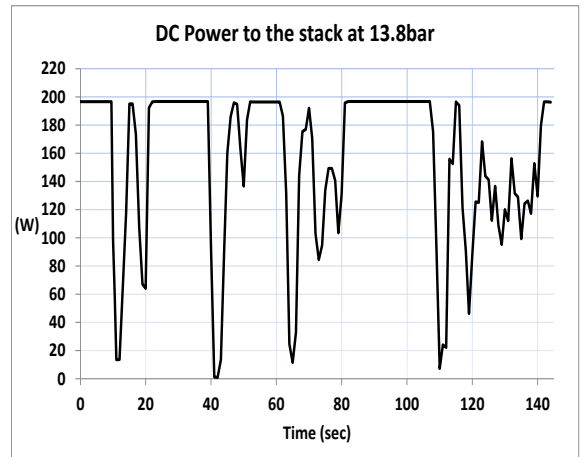


Figure 4.8, Variable DC power to the stack while producing constant hydrogen at 13.8bar

Figures 4.9 and 4.10 are indicative of the operation at periods when the stack operates constantly at the maximum rate. The stack voltage reduces with time as the stack temperature rises (Carmo, et al., 2013), (Larminie & Dicks, 2003), (Lympelopoulous & Zoulias, 2008), which leads to a reduction of stack power with time. Within 22 minutes the stack voltage reduced from 8.02V to 7.5V, and the stack power from 209W to 202W. The stack current on the contrary, remains constant at 27A.

The stack operates at a constant maximum rate at periods when the production pressure never reaches the set pressure. For example, if the generated hydrogen is sent to ambient at atmospheric pressure the stack will always operate at maximum rate as it will always try to reach the set pressure, regardless the set point. This operation cannot be tested for a long period of time as the electrolyser control systems identify this operation as erroneous and the production stops. This parameter is not taken into consideration in the numerical model development where the electrolyser operates efficiently at maximum rate until the necessary pressure is reached.

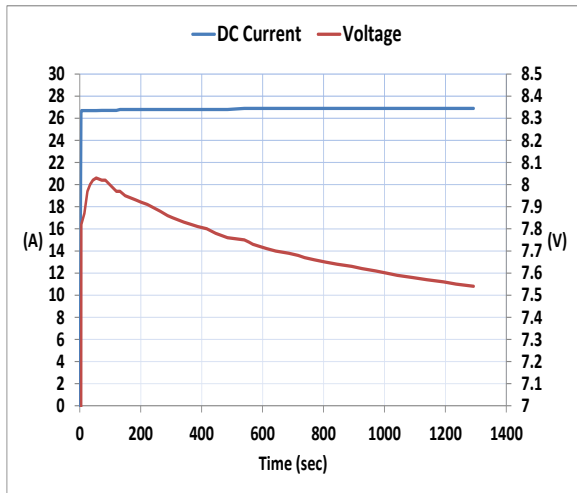


Figure 4.9, Maximum DC current and voltage to the stack for maximum stack operation

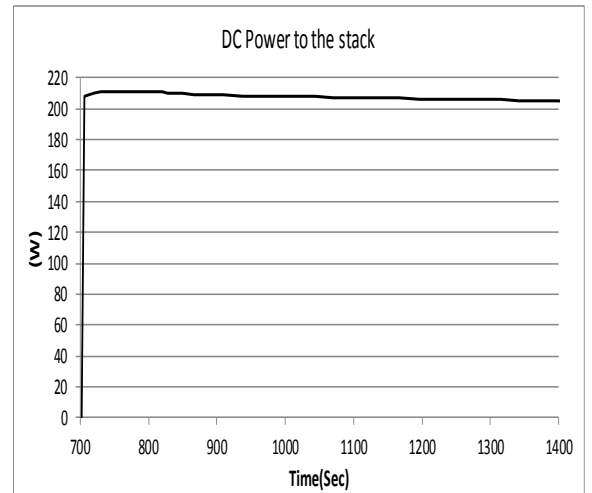


Figure 4.10, Maximum DC power to the stack for maximum stack operation



Figure 4.11, Stack measurements

4.5 Metal Hydride Storage Experiment

The metal hydride storage tank used in these tests consists of LaNi_5 powder form storage alloy. The metal alloy absorbs hydrogen when compressed at certain pressure, called the plateau pressure. The desorption process depends mainly on the heat transfer to the material as well as the pressure difference. The thermochemical equilibrium of the system is characterised by the pressure composition isotherms (PCI) of Figure 4.12. The PCI describes the hydrogen dissociation process for the absorption and desorption phases, as a function for hydrogen concentration.

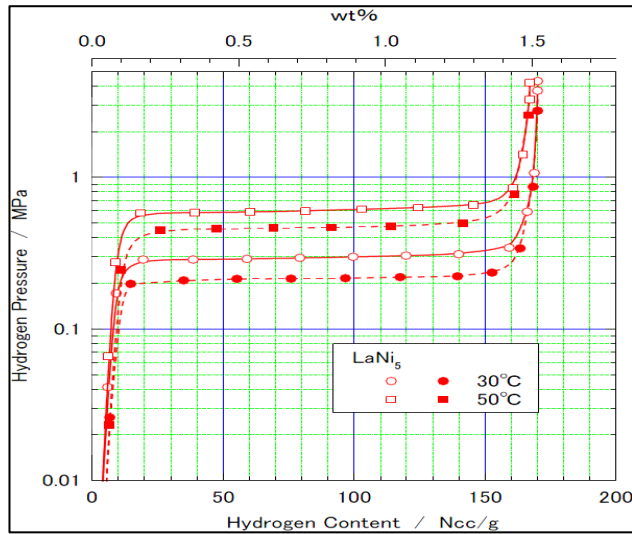


Figure 4.12, PCI of LaNi₅, source: (Nasir, et al., 2014)

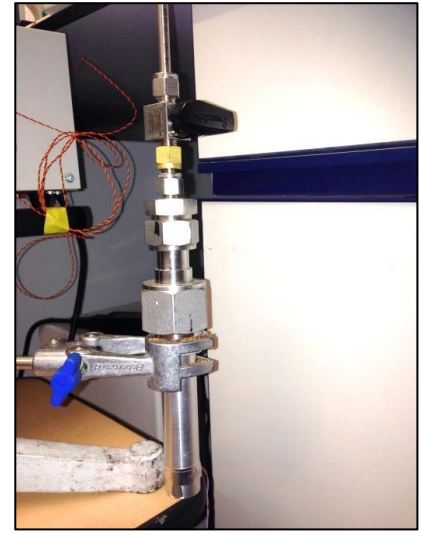


Figure 4.13, The experimental Metal Hydride Tank

The metal hydride storage tank used in the experiments is made of aluminium and all the fittings, valves, nuts gland and gasket are stainless steel from Swagelok, see Figure 4.13. Aluminium was chosen because it presents higher thermal conductivity ($205 \text{ Wm}^{-1}\text{K}^{-1}$) in comparison to stainless steel ($50.2 \text{ Wm}^{-1}\text{K}^{-1}$) (Hyper Physics, 2014).

One of the most crucial parameters in the experimental testing of metal hydrides is to ensure that the container is clean, chemically inert and no moisture is present. Additionally, it has to be ensured that there are no leaks from the tank, as hydrogen is colourless and odourless and any leak can impose a risk. This was ensured by performing pressure tests in the lab; vacuuming the tank and keeping it in vacuum for 60 hours. Also, the pressure was kept at 10 bar for 24 hours; 20 bar and 60 bar for 1 hour, and again no leaks were detected.

LaNi₅ can hold 150cc of hydrogen per gr, and 40gr of it are contained in the tank. So the amount of hydrogen that can be stored in the tank can be calculated as shown in Equation (4.3):

$$\begin{aligned}
 H2_{\text{stored}} &= 150 \left(\frac{\text{ml}}{\text{gr}} \right) * 40 \text{gr} = 6000 \text{ml} = 6 \text{Nl} = 0.006 \text{Nm}^3 \\
 H2_{\text{stored}} &= 0.006 (\text{Nm}^3) * 0.0899 \left(\frac{\text{kg}}{\text{Nm}^3} \right) = 5.394 * 10^{-4} \text{kg} = 0.5394 \text{gr}
 \end{aligned}
 \tag{4.3}$$

4.5.1 Metal Hydride Experimental Description and Results

Experiments are performed with an aim to fill the tank with hydrogen at different absorption pressures, so that the interaction between the electrolyser and the storage is examined (Satya Sekhar, et al., 2012; Souahlia, et al., 2014). The absorption pressures are determined by the electrolyser pressure range of 3-13.8 bar, and tests were performed for pressures from 5 bar to 13.8 bar at 1 bar intervals. For each test, it was important to ensure the same initial conditions of the tank as possible, in terms of temperature and tank pressure. After completion of each test and each desorption the minimum pressure that was achieved in the tank was 1 bar.

The metal hydride tank was fixed to the setup so that the produced hydrogen from the PEM electrolyser could flow directly to the tank. In the beginning the valve of the tank is kept closed. The generated hydrogen flows through the line up until the valve, and is accumulated until it reaches the set pressure. At this point, the valve of the metal hydride tank is switched to ON and the absorption phase starts and is continued until no hydrogen flow is observed. During this phase, hydrogen flow rates, temperatures and pressures are recorded every 1sec. For the complete test setup see Figure 4.14.

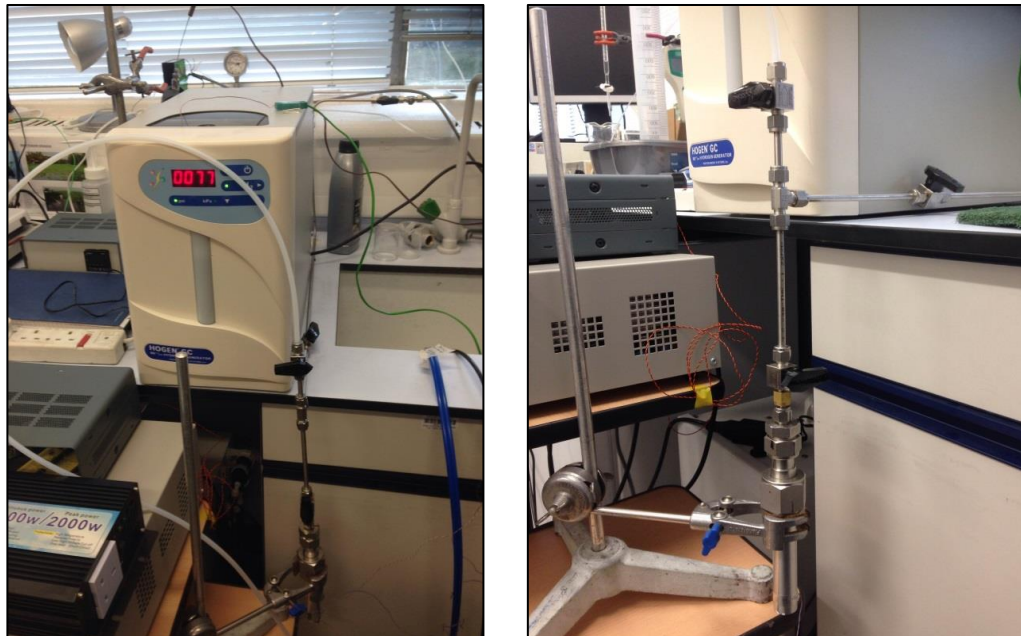


Figure 4.14, The experimental setup for the metal hydride experiment

The flow rates of all the tests, for the pressure set points, from the electrolyser to the metal hydride tank can be seen in Figure 4.15.

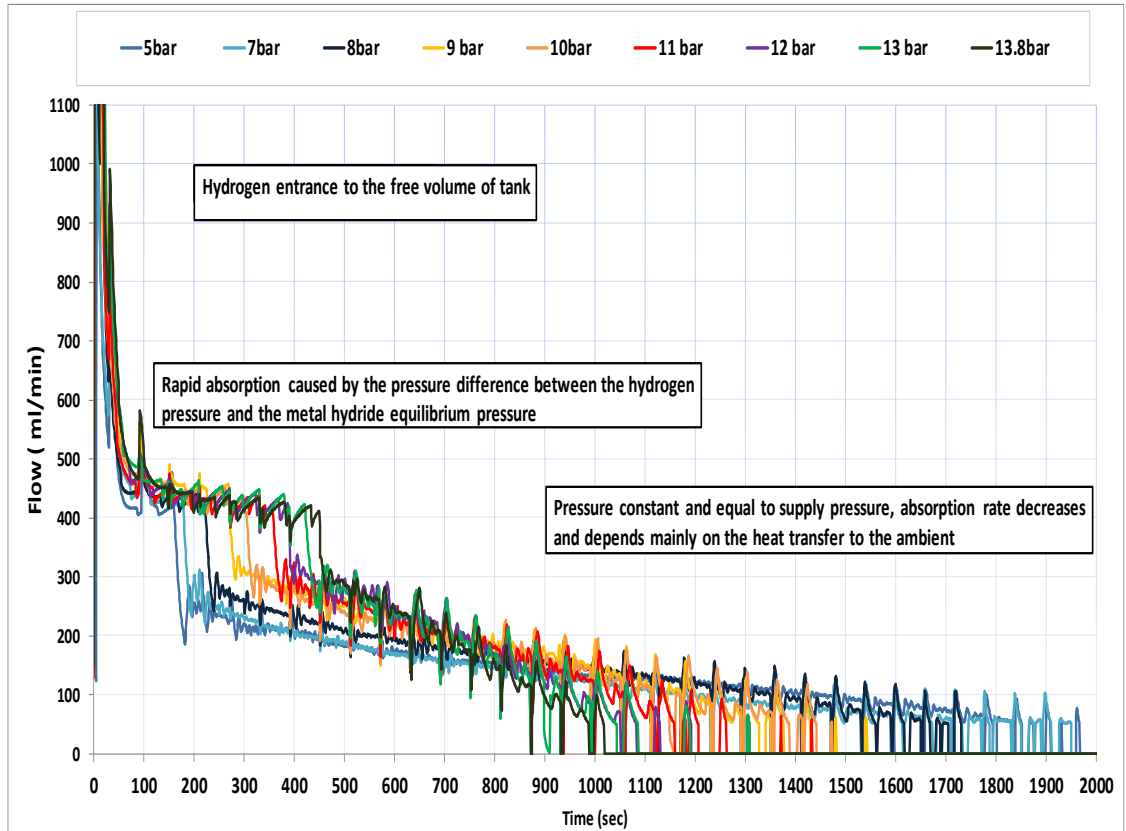


Figure 4.15, Hydrogen flow rates to the metal hydride tank from the electrolyser during absorption phase

The temperature of the metal hydride tank during the absorption phase at each different hydrogen supply pressure can be seen in Figure 4.16. For each pressure set point the maximum temperature is reached at a different time point, as the rate of the absorption evolution is different. Table 4.3 shows the maximum temperatures reached at each test and the equivalent time point.

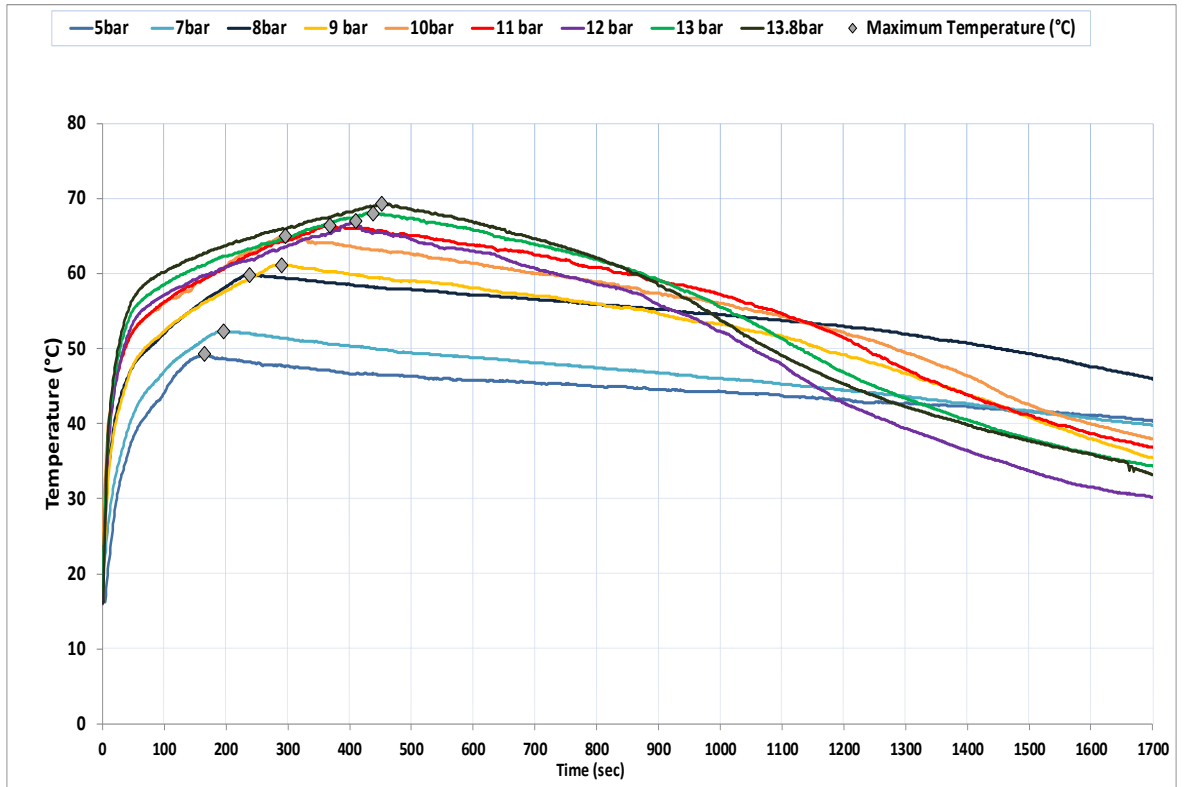


Figure 4.16, Temperatures of the metal hydride tank from the electrolyser during absorption phase

Table 4.3, Maximum temperatures during absorption phases and the time to reach it, for each hydrogen supply pressure

Pressure (bar)	Maximum Temperature (°C)	Time to reach Maximum Temperature (sec)
5	49.3	165
7	52.3	196
8	59.8	238
9	61.1	290
10	65.0	296
11	66.4	368
12	67.0	410
13	68.0	438
13.8	69.3	452

4.5.1.a General Observations

The metal hydride tank is not completely full of the alloy powder, as the metal alloys expand during absorption. Thus the internal volume of the tank is divided in two parts, the free volume one and the volume occupied by the metal alloy powder. As observed in the experimental results curves of the hydrogen flow and temperature increase of the tank of Figures 4.15 and 4.16, the total absorption time can be assumed to consist of two periods. During the first period of the absorption phase, hydrogen is absorbed rapidly and the highest peaks are observed at the flow rates. Likewise, the tank temperature increases sharply during this first period, it reaches the maximum point and then reduces slowly and gradually to ambient as desorption slows down and eventually stops.

The peaks of the hydrogen flow rates that are observed during the first period of the absorption are caused by two main facts: the entrance of hydrogen into the free volume of the tank and the rapid absorption caused by the pressure difference between the hydrogen pressure and the metal hydride equilibrium pressure (Souahlia, et al., 2014). The entrance into the free volume of the tank causes the first high peaks of flow higher than 1000ml/min, which is out of the flow meter range.

Over the second period of absorption, the pressure inside the tank has reached equilibrium and is constant and equal to the supply pressure. At this stage absorption becomes slower and depends mainly on the heat transfer rates between the tank and the environment, as shown in Figure 4.15. Temperature as well, follows a similar pattern with the fastest increase rate taking place during first phase of absorption and reaching the highest values, as shown in Figure 4.16. This is due to the fact that during this phase the flow rates are higher and more hydrogen molecules enter the tank to react with the hydride alloy. Therefore, as the reaction rate is a high, temperatures increase rapidly. When the pressure inside the tank reaches equilibrium the temperature has the maximum value as after that point the flow of hydrogen to the tank happens at a slower rate and therefore reaction also becomes slower. During the second stage of absorption temperatures present a decreasing tendency.

4.5.1.b Observations in Relation to the Pressure Difference Effect

The experiments indicate that the storage process is different at each pressure set point, as the hydrogen flow, the temperatures and the filling time are altered. The general observation is that as the pressure rises, the filling time is faster as the hydrogen flow becomes higher and the temperature reaches higher points, as shown in Tables 4.3 and 4.4. Higher hydrogen supply pressures lead to higher absorption masses and higher temperatures. This is due to the fact that at higher pressures, the hydrogen flow to the tank is higher and a greater number of alloy particles absorb hydrogen. This is also the reason why the temperatures are higher the higher the pressure, as the reaction is more intense. The decrease in temperature after the peak is more intense in the higher pressures, as the higher the temperature difference between the tank and the environment the more enhanced the heat transfer process.

The mass of hydrogen that is stored in the metal hydride tank increases with the increase in the pressure, and also hydrogen is absorbed with a faster rate. Figure 4.18 shows this increase in the mass absorption as pressure increases, with the inclination angle becoming bigger. The stored mass varies between 0.4361gr at 5bar to 0.4718gr at 13.8bar, as shown in Figure 4.19. The volume of the stored gas on the contrary decreases with the pressure increase, as the density of hydrogen increases with pressure, as shown in Figure 4.20. In addition to the mass calculation through the hydrogen flow rates, the metal hydride tank was measured twice at each experiment. Once after the completion of the absorption process, and once after desorption process. In this way, the added hydrogen was calculated through direct weighting on a scientific scale, as presented in Figure 4.17.

Table 4.4, Time to complete storage process in relation to hydrogen supply pressure

Pressure (bar)	Time to charge (min)
5	32.7
7	26.9
8	26
9	22.1
10	21.9
11	21.02
12	19.85
13	18.1
13.8	16.93



Figure 4.17, measurement of the weight of the Metal Hydride tank at the beginning and at the end of the experiment

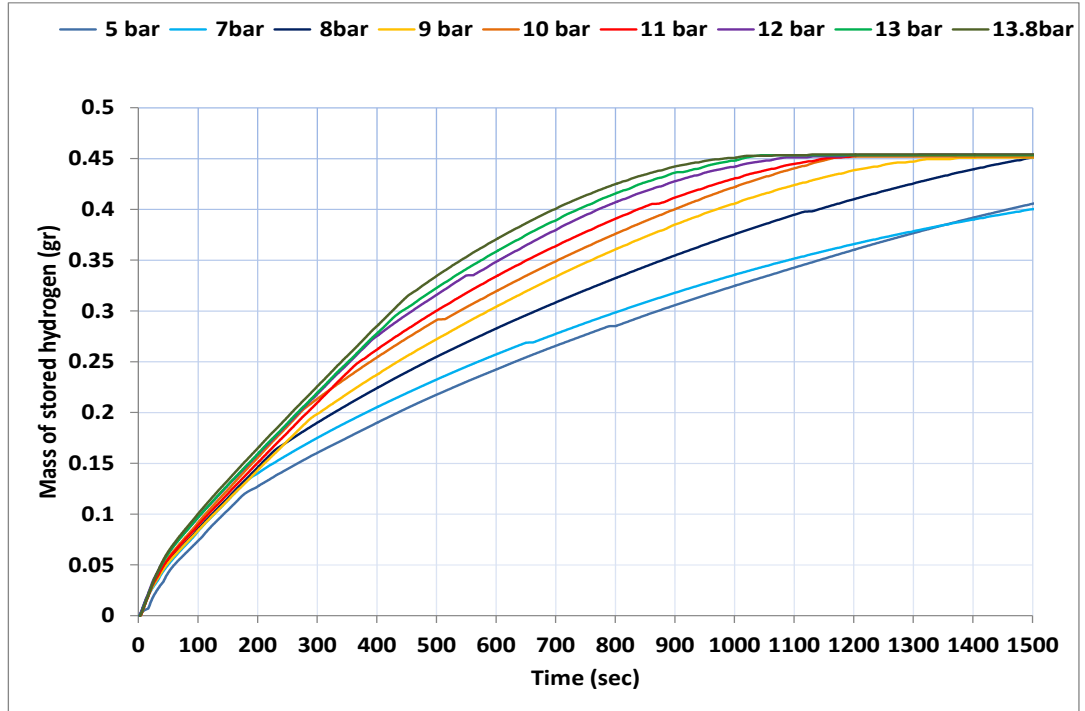


Figure 4.18, Mass of hydrogen stored in the metal hydride tank in relation to the supply pressure

An extra significant parameter regarding the performance of the electrolyser and metal hydride storage system is the hydrogen storage capacity. This is expressed as the amount of hydrogen stored per kg of the metal hydride alloy, see Equation (4.4):

$$\text{Hydroden_Storage_Capacity} = \frac{\text{Weight_of_the_hydrogen_absorbed}}{\text{Weight_of_the_metal_hydride}} \times 100 \quad (4.4)$$

In our case the mass of the metal hydride is 40gr and the mass of absorbed hydrogen is measured during each experiment. Table 4.5 shows the hydrogen storage capacity values for each distinct hydrogen supply pressure. As with the stored mass, the hydrogen storage capacity increases with pressure, and achieves its maximum value at 13.8 bar. These values are in relation to the maximum hydrogen storage capacity of LaNi_5 , which is 1.4wt% (Souahlia, et al., 2014). It should be here noted that the maximum hydrogen storage capacity observed was 1.180wt% which is 15.7% less than the maximum. This could be due to the material and also due to the fact that the hydrogen that enters the metal hydride tank during the initial peaks is out of the flow meter range.

Table 4.5, Hydrogen storage capacity (wt%) for each test

Pressure (bar)	Hydrogen Storage Capacity
5	1.090
7	1.092
8	1.127
9	1.130
10	1.132
11	1.134
12	1.135
13	1.145
13.8	1.180

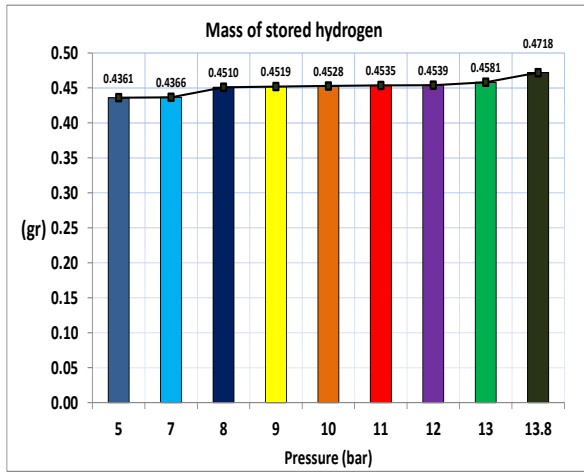


Figure 4.19, Mass of stored hydrogen in the metal hydride tank in relation to the supply pressure

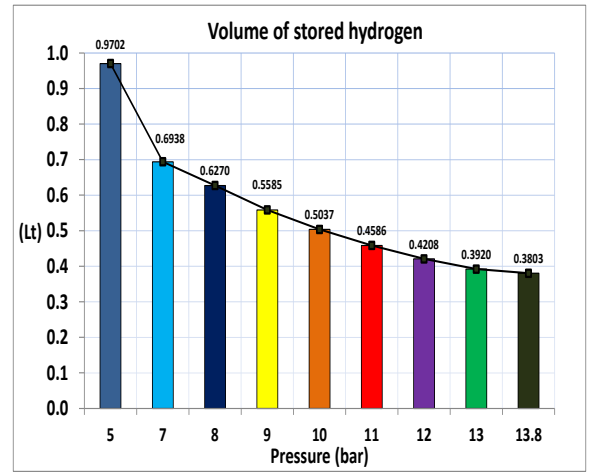


Figure 4.20, Volume of stored hydrogen in the metal hydride tank in relation to the supply pressure

Regarding the operating pressure, the experimental recordings are shown in Figure 4.21. As hydrogen supply pressure becomes higher, time to reach pressure equilibrium is longer.

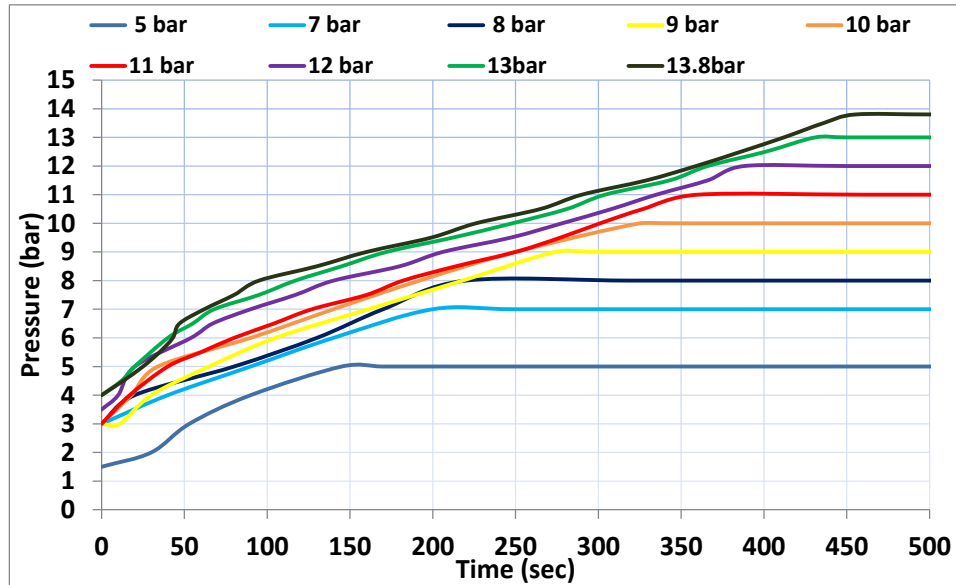


Figure 4.21, Pressure increase over time in the metal hydride tank in relation to the hydrogen supply pressure
 An interesting point to show here is the relation between the hydrogen mass accumulated in the tank at pressure equilibrium point over the maximum mass, see Table 4.6 and Figure 4.22.

Table 4.6, Hydrogen mass accumulated in the tank at pressure equilibrium point over the maximum mass

Pressure (bar)	Tmax(°C)	mTMAX(gr)	mTOTAL(gr)	mTMAX/mTOTAL(gr)
5	49.29	0.114	0.436	0.262
7	52.3	0.141	0.437	0.323
8	59.81	0.167	0.451	0.371
9	61.12	0.215	0.452	0.475
10	64.97	0.223	0.453	0.492
11	66.39	0.250	0.454	0.552
12	65.9	0.275	0.454	0.606
13	68.05	0.300	0.457	0.656
13.8	69.29	0.316	0.472	0.67

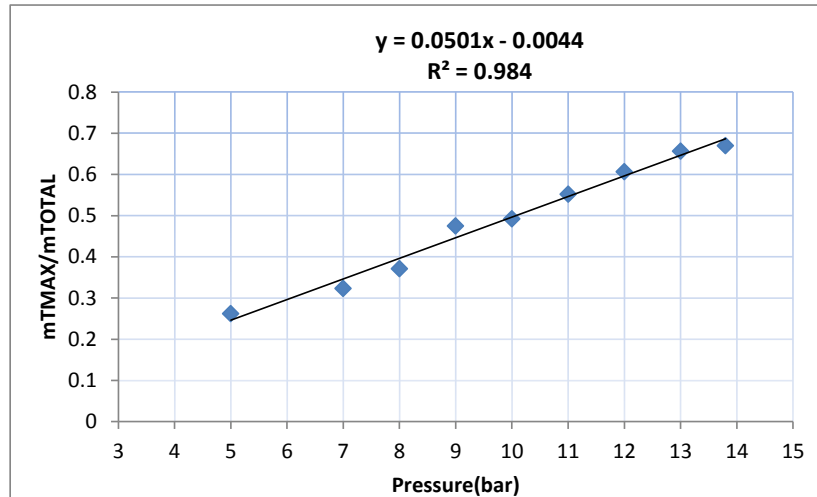


Figure 4.22, Hydrogen mass accumulated in the tank at pressure equilibrium point over the maximum mass

4.5.2 Metal Hydride Experimental Results Discussion

In this part the interaction between the electrolyser and a metal hydride storage cylinder of 40gr of LaNi₅ was examined, for hydrogen generation pressures 3-13.8 bar. Tests were conducted for 9 pressure set points of 1bar difference. The initial tests at pressures of 5 bar, 10 bar and 13.8 bar were repeated 4 to 5 times each to reassure the data logging accuracy and confirm the uncertainty, see Appendix C. The main observations of the test results are:

- Charging time varies from 16.93mins to 32.7mins, inverse to pressure increase. The maximum absorption time is observed at pressure of 5 bar
- Absorption temperature rises with pressure rise
- The flow rates from the electrolyser present a peak during first stage of absorption characteristic for each pressure
- This peak flow is caused from the pressure drop in the beginning of the absorption phase and presents greatest values at high pressures which become smoother at lower pressures. This is due to the electrolyser operation that tends to increase flow rates until the set pressure is reached

After this first absorption period the flow presents a more stabilised reducing behaviour until the MH cylinder is full, which again is distinct for each pressure point.

4.6 Alkaline Solid Polymeric Membrane (ASPM) Electrolyser Experimental Measurements

Additional experimental measurements were carried out with an Alkaline Solid Polymeric Membrane (ASPM) Electrolyser from ActaSpa (ACTA, 2014). This electrolyser comprises of a 9-cell stack and the separation of gases is done through a novel solid polymeric membrane that is immersed in an alkaline aqueous solution of deionised water and potassium carbonate (K_2CO_3). The experiments with an electrolyser of different technology than the Proton Exchange Membrane Technology offer the possibility to compare the efficiencies and performances and reach beneficial conclusions on the integration of each of the electrolyser in the solar hydrogen system.

The polarisation curve measurements for the ASPM stack were performed for various temperature set points within the range of 25°C to 46°C, as shown in Figures 4.23 and 4.24.

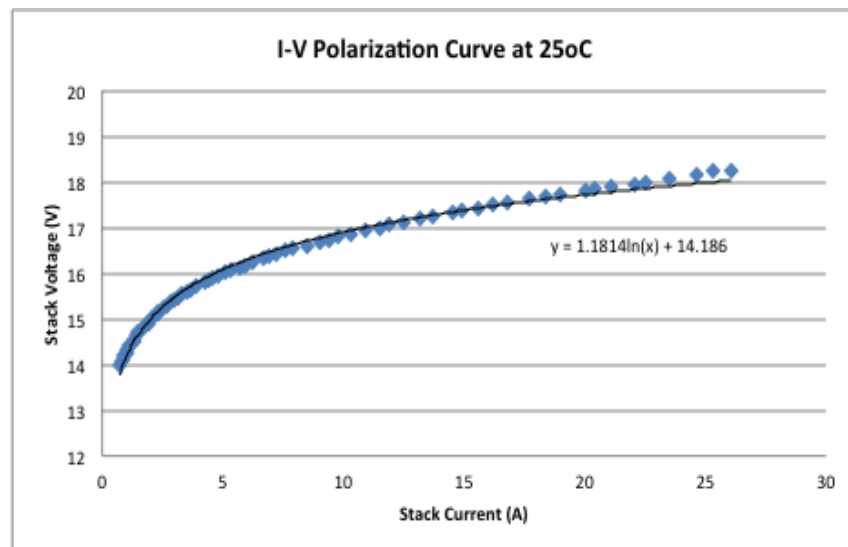


Figure 4.23, I-V Polarisation curve for the ASPM Stack at 25°C

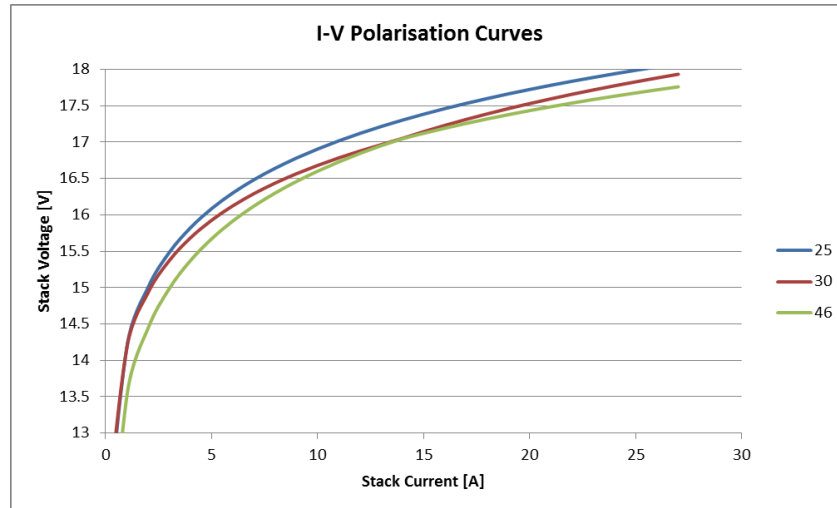


Figure 4.24, I-V Polarisation curve for the ASPM Stack at 25°C, 29°C and 30°C

The results indicate that the I-V curves are highly affected by the temperature, and as the operating temperature increases for the same current the stack voltage drops. At higher temperatures the energy consumption of the stack is reduced, as the increase in temperature causes a decrease in the activation and the ohmic losses. Reduction in power use and increase in hydrogen flow rates can be seen in Figure 4.25 and Table 4.7.

Table 4.7, Reduction in the energy consumption of the stack with the increase in operating temperature

Temperature (°C)	Stack Current (A)	Stack Voltage (V)	Power (W)
25	27	18.08	488.16
30	27	17.93	484.11
46	27	17.76	479.52

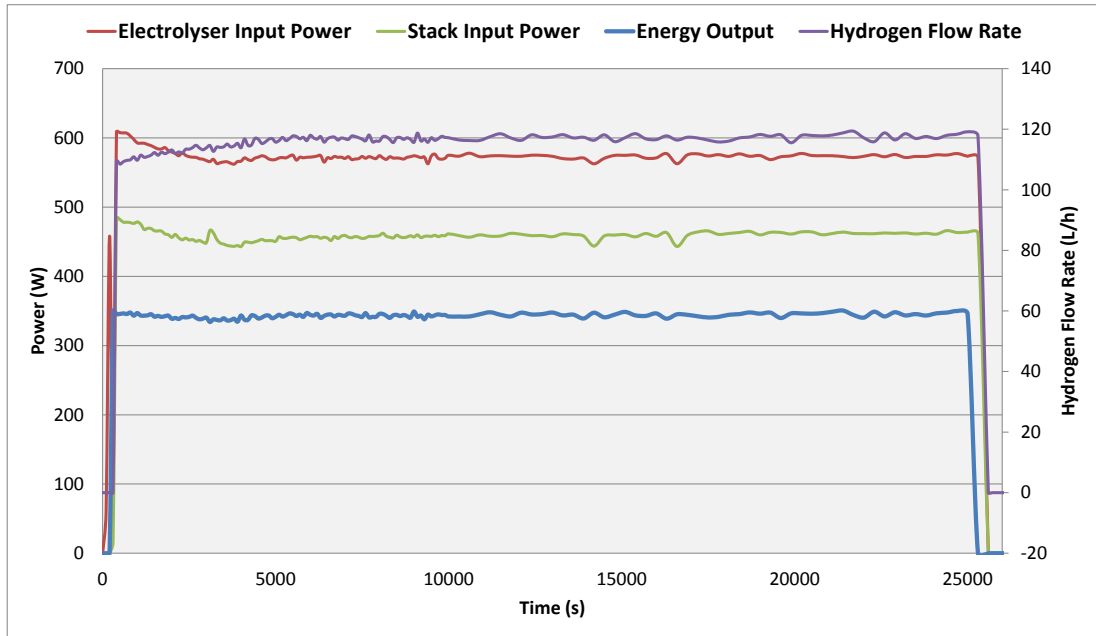


Figure 4.25, ASPM Electrolyser hydrogen flow rate and stack input power over time

It is observed that as the stack generates over time the hydrogen flow rates increase and the stack power decreases. This is due to the fact that with time, the stack temperature increases, stack voltage decreases as shown in Figure 4.26 and the hydrogen generation increases according to Faraday's first law of electrolysis, shown in Equation (4.5).

$$v_H = v_M(l) \times \left(\frac{10^3 \text{ ml}}{l} \right) \times \left(\frac{60 \text{ sec}}{\text{min}} \right) \left(\frac{I \left(\frac{C}{\text{sec}} \right)}{2 \times F(C)} \right) = \frac{R \times (273.15 + T)}{p} (10^3) (60) \frac{I}{2 \times F} \text{ ml min}^{-1} \quad (4.5)$$

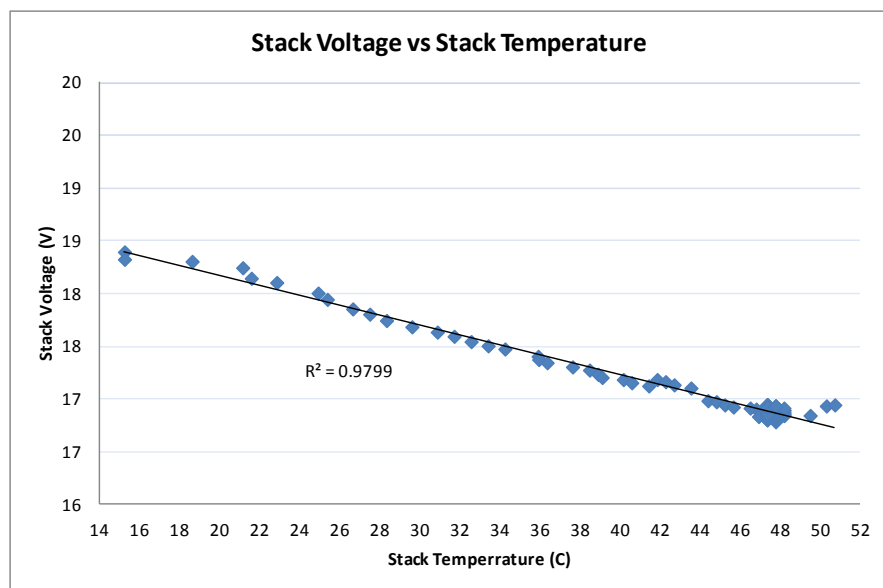


Figure 4.26, Stack Voltage over Stack temperature

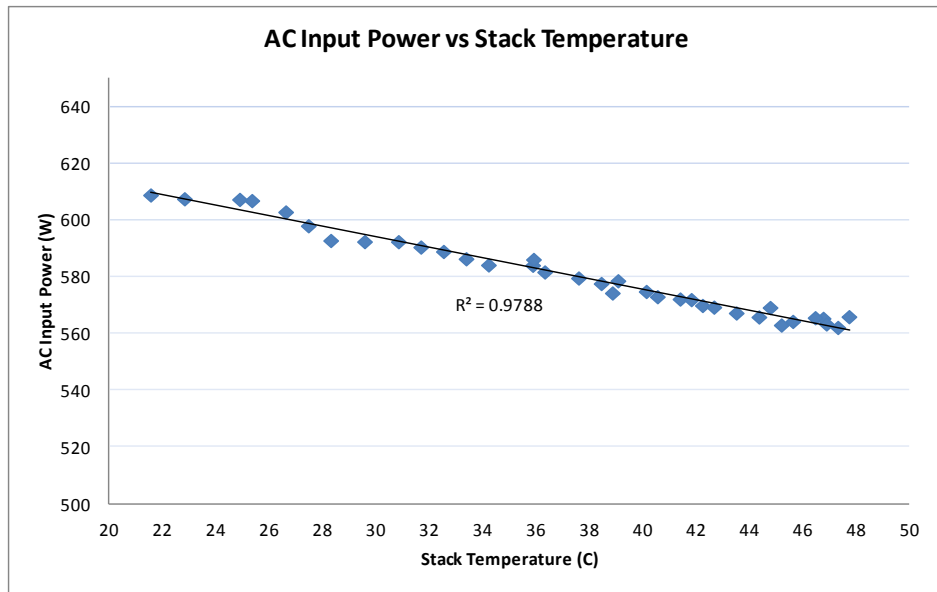


Figure 4.27, Stack input power over stack temperature for the ASPM electrolyser

Figure 4.28 shows the increase in the hydrogen flow rates and stack efficiency as the stack temperature increases. In total, since the beginning of generation hydrogen flow rates increase from an average of 110l/h to an average of 118l/h (a 7.3% increase), and the stack temperature increases from 21.56°C to 47.77°C (a 121.56% increase). Additionally, the stack power decreases as the temperature increases, as can be seen in Figure 4.27.

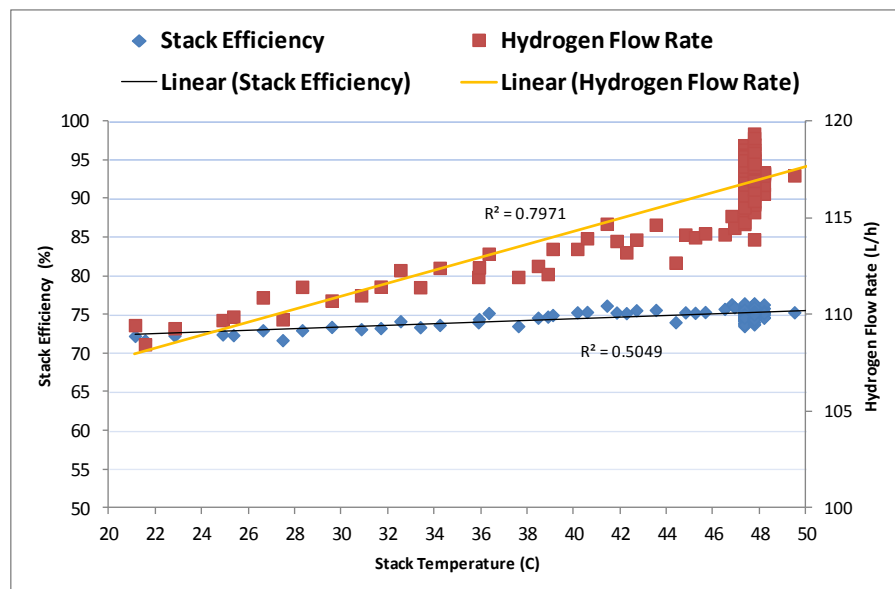


Figure 4.28, Hydrogen flow rates over stack temperature for the ASPM electrolyser

4.6.1 ASPM electrolyser Experimental Results Discussion

The ASPM electrolyser is more efficient than the PEM electrolyser in terms of stack efficiency. It is a bigger unit, as it consists of 9 cells, of 54cm² cell area, whereas the PEM consists of 4 cells of 28 cm² cell area. In terms of energy use in the stacks, the PEM stack at maximum production rates uses 300W, whereas the ASPM stack uses 457.8W averagely. The ASPM electrolyse presents a more efficient operation as it does not employ a heating element for the purification of hydrogen, but instead it uses amine membranes. This has a great effect on the total energy efficiency of the unit, and could act as a guide for future improvements in the PEM unit, that can lead to total energy use reduction.

Moreover, the ASPM electrolyser is more cost effective than the PEM electrolyser, because no noble and expensive metals are used for the electrodes (as iridium and platinum for the PEM electrolyser). However, it employs an alkaline solution, of potassium carbonate that contains a greater environmental risk than the proton exchange membrane.

4.7 Summary

This chapter presented results of the tests carried out during the experimental part of this research. The primary set of experiments with the PEM electrolyser which lead to the development of the numerical model regarding the PEM electrolyser operation, its controls and the metal hydride storage have been presented. Information about the efficiency of the hydrogen generation process in terms of stack and complete electrolyser unit, losses due to the hydrogen management systems, hydrogen temperature, for different hydrogen generation pressure have been presented.

Furthermore, experimental tests on an alternative electrolyser unit containing an Alkaline Solid Polymeric Membrane have been performed and presented in this part of the research. The results are evaluated in comparison to the PEM electrolyser tests results and act as an indication for potential performance improvement.

In the following chapter, the numerical model development is presented based on the results of the experiments of this chapter and furthermore the model is validated through a second set of experimental tests.

Chapter 5. Numerical Model Development

5.1 Introduction

This chapter presents the development steps of the solar hydrogen system numerical model. The main components developed are the PEM electrolyser, the controls and gas management and the metal hydride storage. These act as a system in the simulation to model a compact electrolyser unit. These novel components are created based on FORTRAN programming and are integrated into the libraries of TRNSYS software. FORTRAN programming language was selected as it is the core programming language of the TRNSYS computational kernel and components.

5.2 Introduction to TRNSYS

TRNSYS (TRaNsient SYstem Simulation) is a simulation software that allows evaluation and simulation of behaviour of various transient energy systems, such as electrical and mechanical systems, building thermal performance and renewable energy systems.

It consists of two parts, the main engine which is called the kernel and a component library. TRNSYS combines these parts in a graphical user interface, where the kernel reads and processes the input file (deck file, *.dck file) and the information of the components.

In more detail, the kernel solves the system in an iterative way, determines the convergence, and plots system variables. It also provides utilities that determine thermophysical properties, invert matrices, perform linear regressions, and interpolate external data files.

The library of components models the performance of parts of the system. The standard library includes approximately 150 models, such as renewable energy systems, pumps, multizone buildings, alkaline electrolysers, weather data processors, economics routines, and basic HVAC equipment. Models are constructed in such a way that users can modify existing components or write their own. The TRNSYS components can be written in programming languages such as FORTRAN, C or C++ which allow the creation of a Windows Dynamic Link Library, *.dll. The DLL refers to a shared library between the TRNSYS kernel and the component, and the new components can be flexibly incorporated into the simulation without the need for recompiling the entire TRNSYS software (Solar Energy Laboratory, University of Wisconsin-Madison, 2014). This facilitates the creation

of simulation components that do not exist in the default library of TRNSYS (Solar Energy Laboratory, University of Wisconsin-Madison, 2014).

The components of TRNSYS include programming subroutines that describe their function and are interlinked in the graphical interface. The solving of the system is achieved through the successive substitution method or the Powell's method (Solar Energy Laboratory, University of Wisconsin-Madison, 2014). In the successive substitution method the outputs of a component are used as inputs to other components. A component is called only if its inputs change during a timestep and convergence is reached only when the outputs vary within the tolerance limits defined in the deck file. The successive substitution method calls a component as many times as required in a timestep and proceeds to the next timestep after convergence. Timestep is constant during simulation and in this study it is one minute, and the successive method is followed.

For the case of the solar hydrogen system simulations TRNSYS is considered as the most appropriate software for three main reasons, that are also supported by existing literature (Ulleberg & Morner, 1997; Ulleberg, 1998; Behzadi & Niasati, 2014):

- a) It makes it possible to create the new components that are developed in this research, into one of the standard programming languages and integrate these components in the standard libraries. In this research FORTRAN is used.
- b) it offers the possibility to interconnect the hydrogen components with the standard components of the electrical, the weather data and control libraries
- c) the developed model is particularly useful and suitable for design and optimization of the control strategies and the system sizing through multiple iterations

5.3 Model Development Strategy

Before the simulation of the integrated system the modelling of each component is necessary. This is accomplished through the results of the laboratory experimental measurements described in Chapter 4 and also referring to electrochemical models from the literature. The basic components of the system that are developed for the purposes of this study are:

- The PEM electrolyser hydrogen generation process
- The controls and gas management
- The metal hydride storage components

These components act as a combination in the simulation in order to offer the modelling of the compact solar hydrogen system. A second experimental study of the system was conducted to validate the developed numerical model and is described in sections 5.4 to 5.9 of this chapter.

5.3.1 PEM electrolyser hydrogen generation process

From Equations (4.1) and (4.2) of Chapter 4 an operation coefficient is derived through the division of the actual hydrogen generation to the maximum theoretical. This operation coefficient is characteristic for the operation at certain pressures within the working range, as given in Table 5.1. It takes into consideration the losses caused by the gas management systems as described above and is an index of the actual hydrogen generation in comparison to the maximum theoretical one, which in this case is for $I=27A$, 4 cells and 1 stack. The user can model any size of this electrolyser based on this coefficient in order to get the equivalent hydrogen production results. By inputting stack current, stack temperature and number of cells to the model, the model calculates the volumetric flow rates as given in Equation (5.1). It is observed that the losses are reduced for operation at higher production pressures.

$$V_{H_2Actual} = \int_0^t \frac{\eta_F \times n_c \times CO \times R \times I \times T}{F \times p \times n} dt \quad (5.1)$$

Table 5.1, Coefficient of performance of the PEM electrolyser operation

Pressure Set Point (bar)	Operation Coefficient (co)
3	0.034
4	0.055
5	0.080
6	0.110
7	0.140
8	0.172
9	0.208
10	0.246
11	0.286
12	0.326
13	0.370
13.8	0.403

A factor taken into consideration in the PEM electrolyser model is the connection to the metal hydride storage. This affects the flow rates of the electrolyser as the pressure at the output during the first stage of the absorption is not kept constant, as described in section 4.5.1 of Chapter 4. Therefore, the effect of the accumulated hydrogen mass in the metal hydride tank is inputted in the model of the PEM electrolyser, as a factor resulted from the following comparison: the accumulated mass is compared at each timestep to the maximum mass that has been recorded during the experiments when the metal hydride tank reached equilibrium pressure, for each distinct pressure set point. The result of this comparison has an effect on the operational coefficient, and while the accumulated mass is still smaller than the maximum mass at equilibrium, the co is higher than the one presented in Table 5.1, and takes the value of 0.4825. At the timestep that the accumulated mass becomes equal with the mass at pressure equilibrium the co takes the value of Table 5.1, according to the pressure set point.

5.3.2 Cell Voltage and Power

The cell voltage of a PEM electrolyser stack has been described and studied by many researchers. Among them are, Larminie and Dicks (Larminie & Dicks, 2003), Dursun et al. (Dursun, et al., 2012), Marangio et al. (Marangio, et al., 2009). The model used in this study for the stack voltage submodel of the PEM electrolyser model is the one suggested by the North Dakota University team (Dale, et al., 2008; Biaku, et al., 2008) and is described by Equation (5.2).

$$V_{tot} = V_{Nernst} + V_{Activation} + V_{Ohmic} \Rightarrow$$

$$V_{tot} = \left[V_{rev}^0 + \frac{RT}{nF} \ln\left(\frac{p_{H_2} p_{O_2}^{1/2}}{p_{H_2O}} \right) \right] + \left[\frac{RT_{an}}{a_{an} F} \operatorname{arcsinh}\left(\frac{j}{2j_{0,an}} \right) + \frac{RT_{cat}}{a_{cat} F} \operatorname{arcsinh}\left(\frac{j}{2j_{0,cat}} \right) \right] + \left[\left(\frac{\phi}{\sigma} \right) j \right] \quad (5.2)$$

Equation (5.2) shows that the cell voltage is a combination of three different voltages. The first term is the Nernst voltage, where the reversible cell voltage and the partial pressures at the anode and cathode are taken into account. This is the theoretical voltage that is necessary for the electrolysis without taking into consideration any losses (Carmo, et al., 2013; Dale, et al., 2008). The second part is called activation overvoltage and represents the overvoltage that the electrochemical reaction has to overcome in order to initiate. The electrochemical model used to describe this part of the reaction is based on the Butler-Volmer equation (Carmo, et al., 2013). The last term, the ohmic resistance overvoltage is connected to the ohmic losses. The flow of electrons through the current collectors and separators plates faces a resistance, and this is the cause of the ohmic overvoltage. Similarly part of the ohmic resistance is imposed by the conduction of protons through the membrane (Dale, et al., 2008). The conductivity of the membrane is given by Equation (5.4) and it depends only on the stack temperature as the membrane is assumed to be fully saturated with water (Garcia-Valverde, et al., 2011).

The reversible cell voltage of the PEM Electrolyser cell is calculated in more detail according to the suggested temperature dependent model of Dale et al. (Dale, et al., 2008), by Equation (5.3). The standard value of 1.23V for the reversible cell voltage has been widely used by many researchers. Nevertheless, taking into consideration the effect of temperature on the reversible cell voltage enhances the accuracy of the model, as the reversible cell voltage decreases with temperature (Dale, et al., 2008). The membrane

thickness and type, conductivity and exchange current densities that are used in this work are based on the experimental analysis of (Dale, et al., 2008) and (Biaku, et al., 2008) on a larger scale PEM electrolyser by the same manufacturer; information regarding these values is not available from the manufacturers. The temperature is inputted to the model after it was measured experimentally, as shown in Figure 4.3 of Chapter 4.

$$V_{rev} = 1.5241 - 1.2261 \times 10^{-3} T + 1.1858 \times 10^{-5} T \ln(T) + 5.6692 \times 10^{-7} T^2 \quad (5.3)$$

$$\sigma = 0.048026 + 8.15178 \times 10^{-4} T + 5.11692 \times 10^{-7} T^2 \quad (5.4)$$

The power related to the hydrogen production rate of each cell is calculated by Equation (5.5). The operation coefficient results in the accurate calculation of the average power as the current to the stack varies significantly according to the pressure and consequently the flow rates.

$$P_{H_2} (W) = I \times V_{tot} \times CO \quad (5.5)$$

The energy content of the generated hydrogen is calculated by Equation (5.6).

$$E_{H_2} (kWh) = \int_0^t H_2 (ml/min) \times 60 (min/h) \times 10^{-6} (m^3/ml) \times 141.1 (MJ/kg) \times \rho (kg/m^3) \times \frac{1}{3.6} (kWh/MJ) dt \quad (5.6)$$

The complete TRNSYS component includes the above computational processes and offers the user the possibility to calculate information regarding: (a) hydrogen generation rates, (b) cell and stack voltage, (c) energy use of the stack that corresponds to the generation rates and (d) energy content of the generated hydrogen for HHV (141.1MJ/kg) (Gupta, 2009). The necessary inputs to the model are: (a) stack current, (b) stack temperature, (c) operational pressure, (d) number and size of cells and (e) number of stacks from which the hydrogen flow rates are calculated accordingly. The PEM electrolyser component is named type2627, and its parameters, inputs and outputs can be seen in Figure 5.1. The code of the component in FORTRAN can be found in Appendix D.

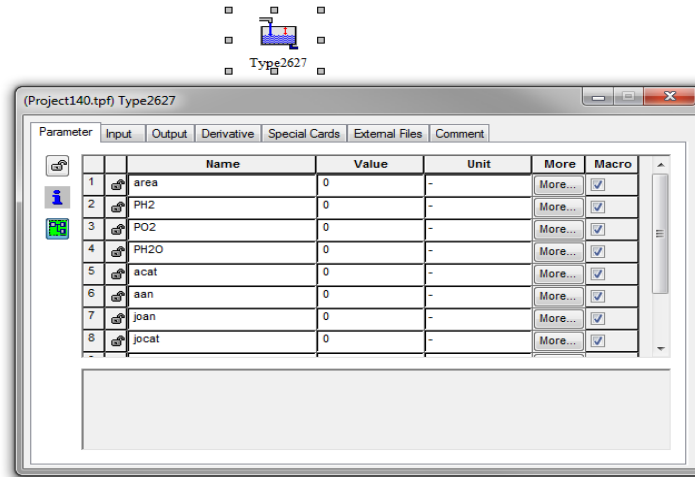


Figure 5.1, TRNSYS PEM electrolyser component parameters

5.3.3 Electrolyser controls component

The electrolyser controls are introduced as a separate component; in this way the model offers flexibility to the user to examine stack operation alone or compact electrolyser unit operation. The controls component combines the energy demand and operational profile of the palladium purifier/ heater operation (as described in section 4.3) with the electrolyser operation and performs at each step an iterative comparison to the available energy supplied by the PV array and the inverter. The basic equation that describes the operation of the component is Equation (5.7).

$$if \text{ } _{P_{PV}} > (P_{(purifier)} + P_{(Aux)}) \text{ } _{AND} \text{ } _{P_{PV}} > ((I_{Electrolyser} \times V_{Stack} \times CO) + P_{(Aux)}) \quad (5.7)$$

$$\text{Then } P_{Available} = P_{PV}$$

$$\text{Else } P_{Available} = 0$$

Additionally, it offers the possibility to examine different solutions for the operation of the hydrogen purification system. The PEM electrolyser controls component is named type2628, and its parameters, inputs and outputs can be seen in Figure 5.2. The code of the component in FORTRAN can be found in Appendix D.

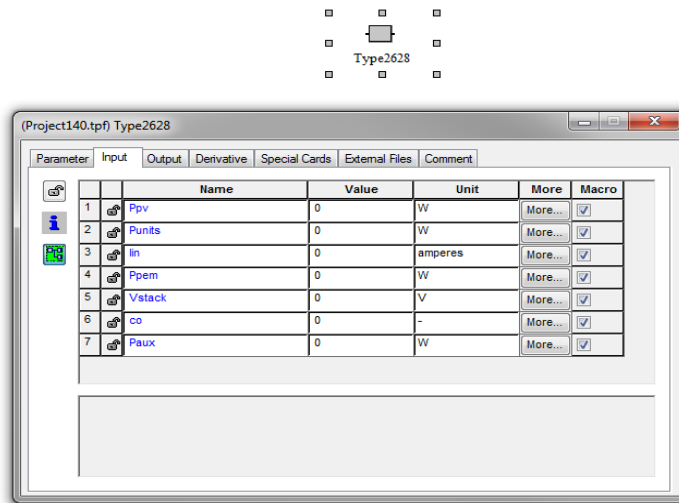


Figure 5.2, TRNSYS PEM electrolyser controls component inputs

5.3.4 Metal Hydride Storage Component

The storage tank used in this study is a metal hydride storage tank developed in the Hydrogen Laboratory of Brunel University. The metal hydride alloy employed is LaNi₅ and 40 gr are contained in the tank. Based on this storage tank, a numerical component was developed that models the absorption process and is used as a suggested storage method for the case study application. The absorbed mass and charging time are described by the basic Equations (5.8) and (5.9):

$$H_{2\text{stored}} = \int_0^{\text{ChargingTime}} \text{Flow} \left(\frac{\text{kg}}{\text{min}} \right) dt \quad (5.8)$$

$$\text{ChargingTime} = \frac{H_{2\text{Max}}}{\text{Flow} \left(\frac{\text{Nm}^3}{\text{min}} \right)} = \frac{150 \left(\frac{\text{ml}}{\text{gr}} \right) * 40 \text{gr} * 10^{-6} \left(\frac{\text{Nm}^3}{\text{ml}} \right)}{\text{Flow} \left(\frac{\text{Nm}^3}{\text{min}} \right)} = \frac{6 * 10^{-3} \text{Nm}^3}{\text{Flow} \left(\frac{\text{Nm}^3}{\text{min}} \right)} \quad (5.9)$$

The created component can be used to simulate any size of metal hydride storage tank that employs LaNi₅ hydride alloy of 150 (ml/gr) hydrogen absorption ability. The user needs to input the alloy content and the average hydrogen flow input for the suitable pressure. Additionally, the model offers the possibility to calculate the heat transfer losses of the tank based on the fundamental thermodynamical principals for convective and radiative

heat losses, if the user inputs the tank area and heat transfer coefficients for the tank material by Equations (5.10) to (5.12):

$$Q_{total} = Q_{radiation} + Q_{convection} \quad (5.10)$$

$$Q_{convection} = h_c \times tank_area \times (T_{tank} - T_{ambient}) \quad (5.11)$$

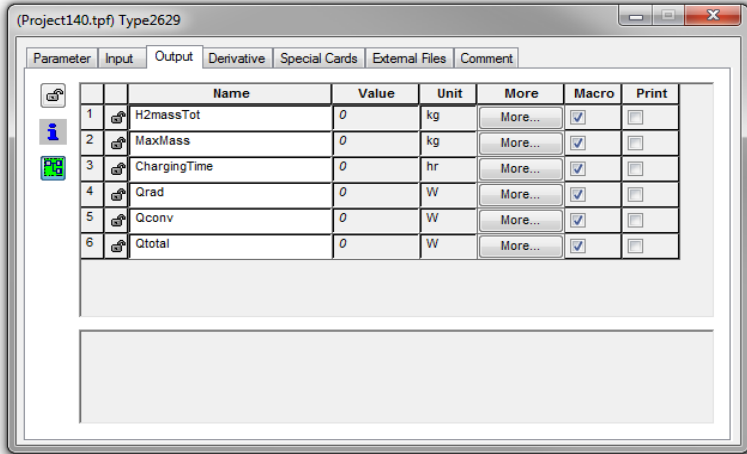
$$Q_{radiation} = h_r \times tank_area \times (T_{tank} - T_{ambient}) \quad (5.12)$$

Where, $h_c=205 \text{ W/m}^2\text{K}$ and $h_r=308 \text{ W/m}^2\text{K}$ for aluminium

The metal hydride component is named type2629, and its parameters, inputs and outputs can be seen in Figures 5.3. The code of the component in FORTRAN can be found in Appendix D.



Type2629



Parameter	Input	Output	Derivative	Special Cards	External Files	Comment
		Name	Value	Unit	More...	Macro <input checked="" type="checkbox"/> Print <input type="checkbox"/>
1	<input type="checkbox"/>	H2massTot	0	kg	More...	<input checked="" type="checkbox"/> <input type="checkbox"/>
2	<input type="checkbox"/>	MaxMass	0	kg	More...	<input checked="" type="checkbox"/> <input type="checkbox"/>
3	<input type="checkbox"/>	ChargingTime	0	hr	More...	<input checked="" type="checkbox"/> <input type="checkbox"/>
4	<input type="checkbox"/>	Qrad	0	W	More...	<input checked="" type="checkbox"/> <input type="checkbox"/>
5	<input type="checkbox"/>	Qconv	0	W	More...	<input checked="" type="checkbox"/> <input type="checkbox"/>
6	<input type="checkbox"/>	Qtotal	0	W	More...	<input checked="" type="checkbox"/> <input type="checkbox"/>

Figure 5.3, TRNSYS metal hydride component outputs

5.3.5 Photovoltaic System

The photovoltaic panels were simulated using standard TRNSYS components for mono-crystalline panels. The TRNSYS component used to simulate the PV panels used is type 194 that determines the electrical performance of crystalline panels based on the 5 parameter model presented by DeSoto et al. (University of Wisconsin - Madison, 2014).

The component that was used is based on the five-parameter equivalent circuit model by Duffie and Beckman [1991], and reliably extrapolates performance information provided

by the manufacturer at standard rating conditions (1,000 W/m², 25°C) to other operating conditions (TRNSYS 17, 2012). The panel's current and voltage relation depends on insolation and temperature and is calculated by Equation (5.13).

$$I = I_L - I_o \left[\exp\left(\frac{V + I \times R_s}{\alpha} \right) - 1 \right] - \frac{V + I \times R_s}{R_{sh}} \quad (5.13)$$

Where, $\alpha = \frac{N_s \times n_i \times k \times T_c}{q}$

The panels are connected to the electrolyser through an inverter that supplies AC voltage at 230V. The losses of the system are computed and the inverter efficiency corresponds to the actual one of the inverter used in the experiments, which has a measured efficiency varying between 86% to 93%, depending on the fraction of power that goes through, and the AC power.

5.4 Model validation - Experimental Weather and PV Power Input Data

A second experimental study of the system was conducted to validate the developed numerical model. The experiments had a focus on validating the model for the operation of the electrolyser and the balance-of-plant when it is coupled to a PV system. The electrolyser operates on a direct coupling with the PV panels and it is important that the model accurately represents the reality and takes into consideration the effect of the available PV power.

Two sets of laboratory tests were performed for the numerical model validation. The first set of experiments was performed for conditions characteristic for the United Kingdom as the information regarding the PV panels refer to an array installed in Brunel University. The second set of experiments was performed for conditions characteristic to Jamaica. Two sets of PV power data are used as input data to the experiments:

1. Power output data of a PV array installed in Brunel University for the first week of June 2013 in UK and
2. Power output data for a PV array installed in Jamaica for days in May 2013 and December 2013

The UK data is retrieved from an online monitoring system that is installed to monitor the PV array: <http://www.sunnyportal.com/Templates/Start.aspx?ReturnUrl=%2f> (SMA Solar

Technology AG, 2013). The PV data that refer to Jamaica are retrieved from an online monitoring system that is installed in the University of Technology in Kingston, Jamaica: <https://shrp.utech.edu.jm/login.html> (Conext ComBox Login, 2014). Additionally the weather data for the Jamaica experiment periods are retrieved from a weather station that is installed in the University of Technology.

Information regarding the PV panel power output and the related weather data are available for the period between 2011-2013. The period selected for the conduction of the experiments for the UK (London) conditions is the first week of June 2013. June is the month with the highest irradiance rates in the UK and thus offers the period that is mostly suitable for the tests. Additionally the selected period includes clear sky days with constantly high irradiance and days with variable cloud coverage where the irradiance output is quite variable. The PV array at Brunel University consist of two types of PV panels, Monocrystalline (MonoSi) panels manufactured by Sharp with 14.1% efficiency and Heterojunction with Intrinsic Thin Layer (HIT) panels from Sanyo with 16.8% efficiency. 4 Sanyo HIT 210W modules and 5 Sharp monoSi 185W modules compose the array. The characteristics of the modules are presented in Table 5.2. For the Jamaica case, a PV array installed in the University of Technology in Kingston that supplies the PEM electrolyser in Jamaica is used. The PV array consists of 6 Trina Solar TSM-180DA01 panels rated at 180W and 14.1% efficiency. The characteristics of the modules are gathered in Table 5.2 and their detailed specifications can be found in the Appendix D.

Table 5.2, Electrical and Thermal characteristics of the PV modules of the experimental PV emulator

PV Type	Sanyo Heterojunction with Intrinsic Thin Layer (HIP)-210NHE1	Sharp MonoSi NUS5E3E/NU185E1	Trina Solar TSM-180DA01
Nominal Power Output P_{MP}	210	185	180
V_{MP} [V]	41.3	24	36.8
I_{MP} [A]	5.09	7.71	4.90
V_{OC} [V]	50.9	30.2	44.20
I_{SC} [A]	5.57	8.54	5.35
Temperature Coefficient of Power [%/°C]	-0.30	-0.485	-0.45

The data of the UK case include:

- Irradiance [W/m^2]
- Temperature [$^{\circ}\text{C}$]
- Relative Humidity [%]
- Power Output [W] of the two sets of panels

The time interval of the data is 5 minutes, and a representation of the power and irradiance can be seen in Figure 5.4. A representation of the data set can be found in Appendix D.

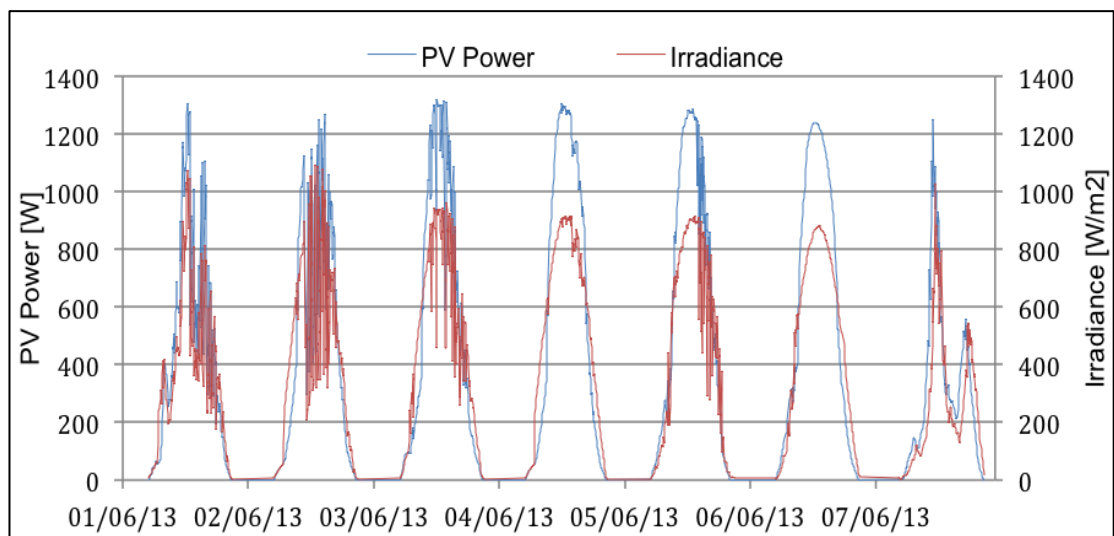


Figure 5.4, Power output data of the PV array for the first week of June 2013 in United Kingdom

For the Jamaica conditions two periods were selected that represent periods of maximum and minimum irradiance levels in Jamaica, May 2013 and December 2013. Again, the selected data offer days with clear sky and therefore high irradiance throughout the day as well as days with unstable cloud coverage, where the output of the PV panels varies significantly in both periods, see Figures 5.5 and 5.6. Irradiance data for Jamaica is available for the period 2011-2013 and the available data has a time interval of 15 minutes. In this case, the PV output power has been generated through simulating the PV array for the selected period in TRNSYS. A typical example can be seen in Appendix D.

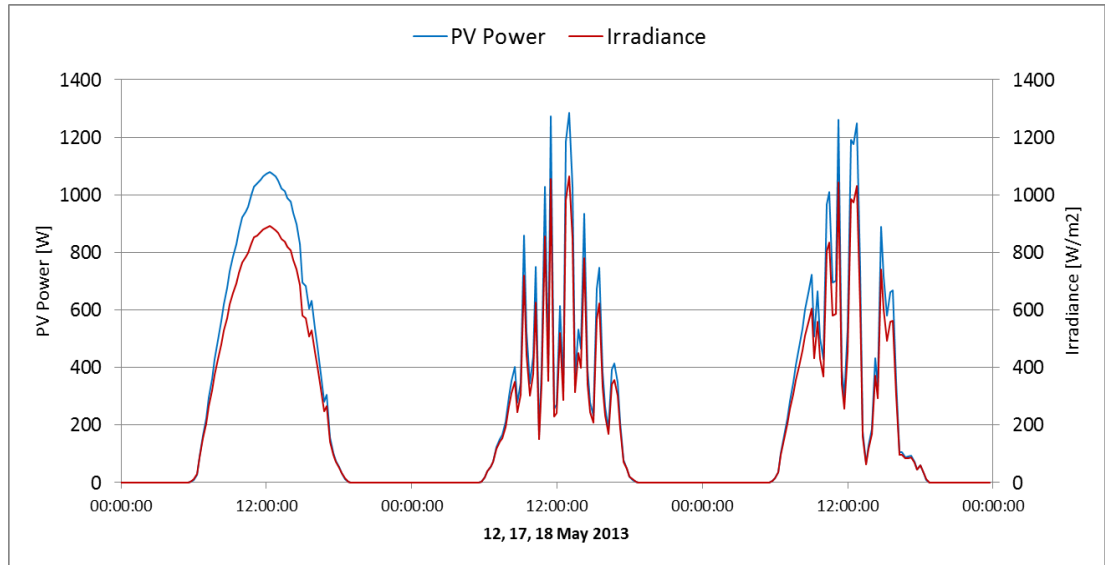


Figure 5.5, Power output and irradiance data of the PV array installed in University of Technology in Kingston for days in May 2013

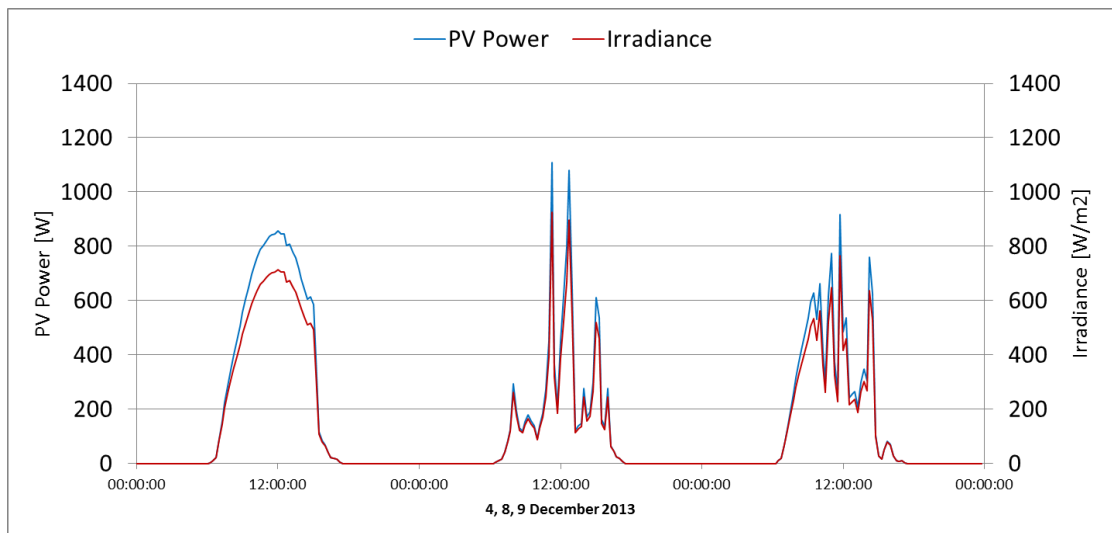


Figure 5.6, Power output and irradiance data of the PV array installed in University of Technology in Kingston for days in December 2013

As explained in Chapter 3, for the performance of the validation experiments a PV data emulator is assembled and used. The PV emulator uses the PV power output data from the installed arrays and generates the same power output profile. The use of the PV emulator offers the flexibility to test for many different sets of irradiance in the laboratory and also to repeat the experiments under the same conditions.

5.5 Experiments for the Numerical Model Validation

The purpose of the tests is to

- Validate the numerical model
- Evaluate the periods during the day that the electrolyser stops operating due to deficient power
- Evaluate the effect of the electrolyser operation and efficiency being subject to the variable irradiance and power and therefore to stops and start ups

For the validation experiments four distinctive pressure set points were selected:

- 5 bar
- 7 bar
- 10 bar
- 13.8 bar

5.6 Experiments for the UK (London) Conditions

Figures 5.7 and 5.8 show the recordings of the tests under the conditions of the UK, under volatile irradiance for Day 1 and constantly high irradiance for Day 4. The rest of the validation experiments are presented in graphs in the Appendix D.

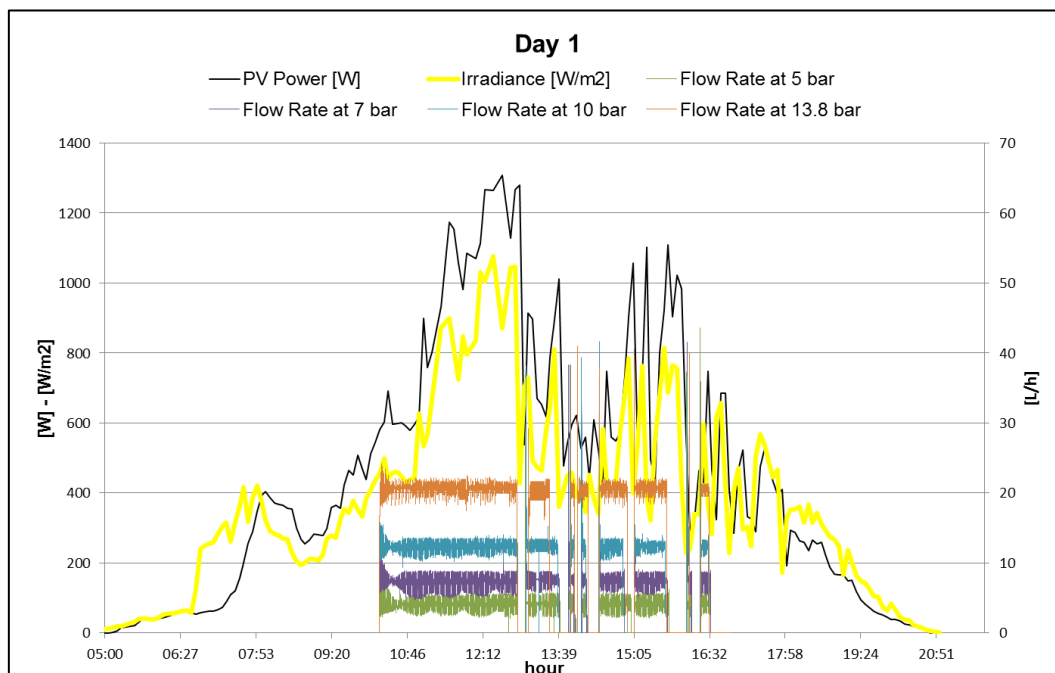


Figure 5.7, Hydrogen production rate in L/h at 5bar, 7bar,10bar,13.8bar pressure set points during day 1 that presents unstable irradiance levels

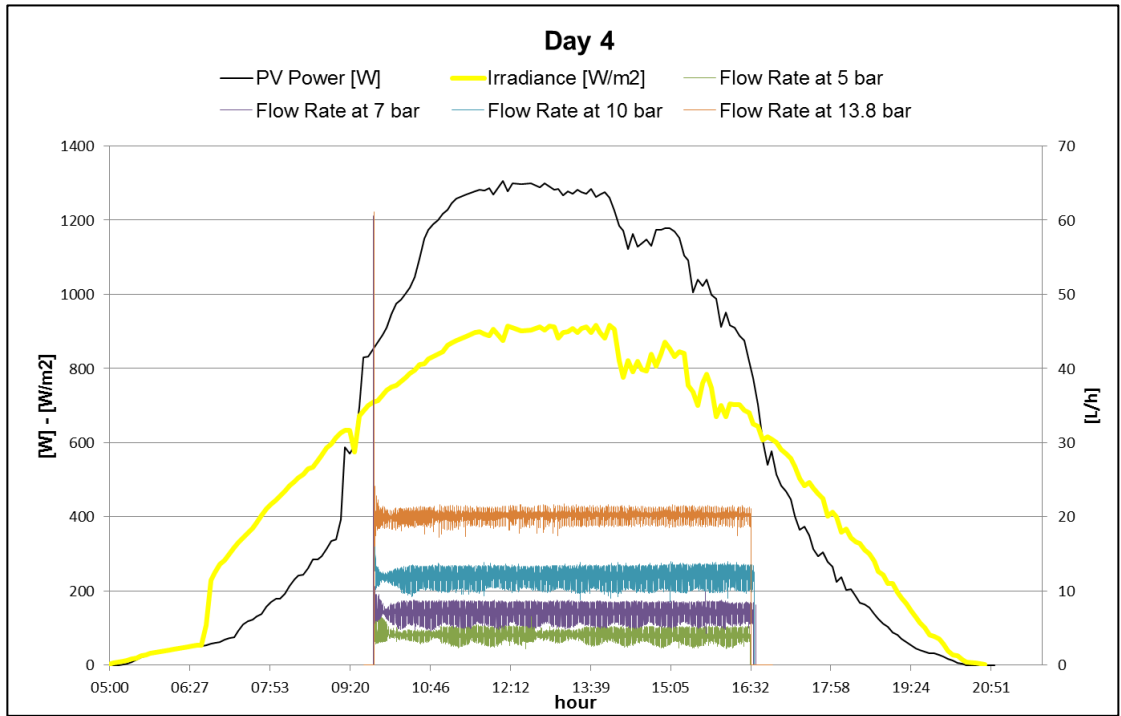


Figure 5.8, Hydrogen production rate in L/h at 5bar, 7bar,10bar,13.8bar pressure set points during day 4 that presents consistently high irradiance levels

Operating the electrolyser under this direct connection to the available PV power output sets it subject to stops and start-ups, which in turn affect the efficiency and the specific energy use, see Figures 5.9 to 5.11.

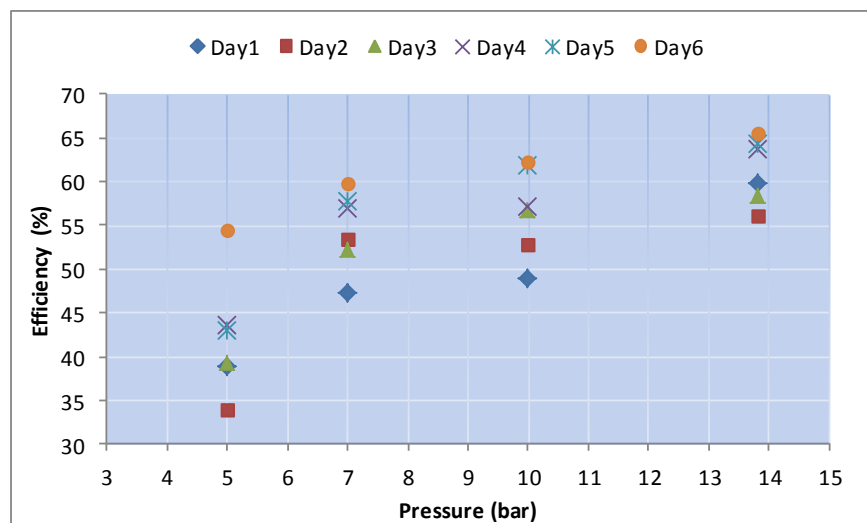


Figure 5.9, Efficiency vs pressure set point for each day of the United Kingdom experimental days

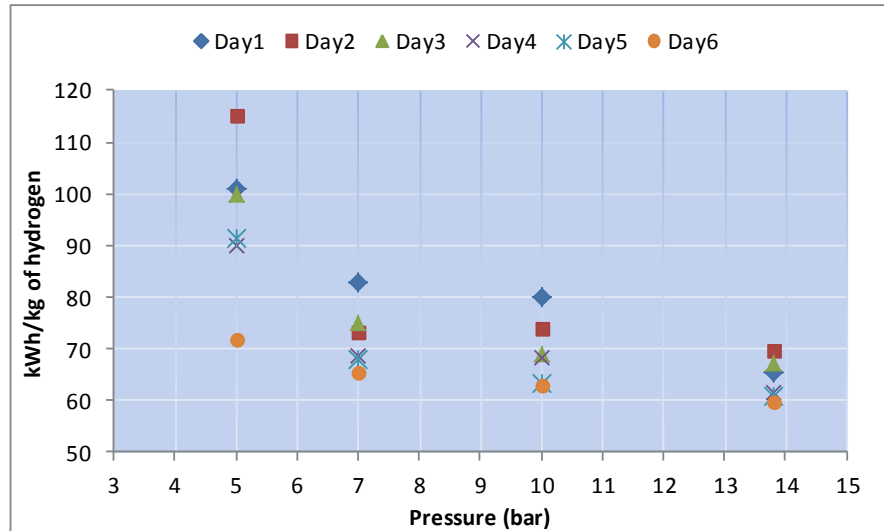


Figure 5.10, kWh/kg of H₂ vs pressure set point for each day of the United Kingdom experimental days

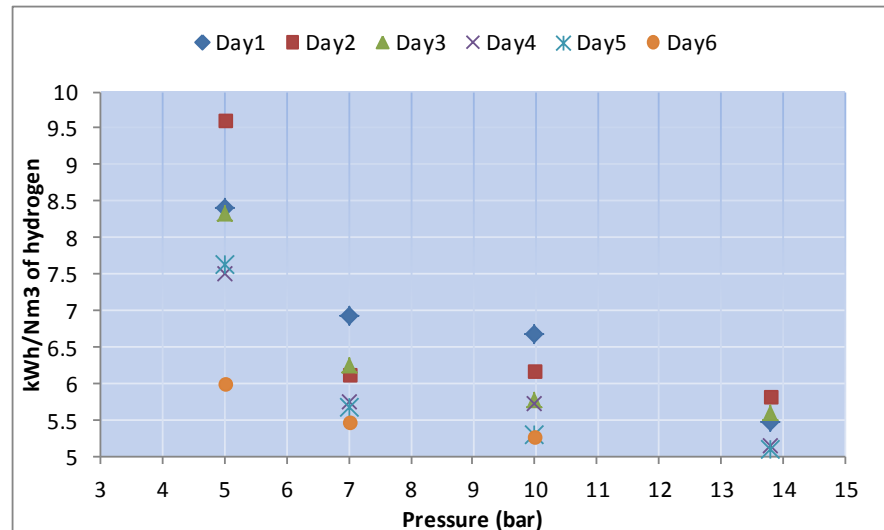


Figure 5.11, kWh/Nm³ of H₂ vs pressure set point for each day of the United Kingdom experimental days

The variability of the operating conditions on the days with unstable and variable irradiance levels has a negative impact on the electrolyser performance. The electrolyser is highly affected by the different operating conditions. Being subject to the variable PV power output sets the system subject to stops and start-ups and thus the operation of the stack is not continuous. This affects the stack efficiency that in this case is reduced. Between Day1 of the tests that is a day with extreme variability in irradiance and Day 6 that is a day with constantly high irradiances a 16% average difference is noted.

When the stack stops operating, the temperature drops. This affects the activation overpotential losses and the amount of energy that is necessary to start the electrolysis process is bigger than the energy required maintaining it. Additionally, when the stack

remains non-operational for a period long enough to reduce the temperature significantly then the activation overpotential is higher than at higher temperatures and thus the activation losses and the energy required increase:

- The ohmic losses of the stack increase at lower temperatures
- Every time the electrolyser goes to idle state and the electrolysis process stops, the stack needs to be fully hydrated again to become operational. This also requires extra energy supply
- The pressurisation of the produced hydrogen occurs through electrochemical compression, as hydrogen is produced, accumulated and released at the selected pressure set-point. Every time after a stop in the operation of the stack, hydrogen has to be produced at a rate to reach the selected pressure level, and this is more energy demanding than maintaining a constant flow at the selected pressure.

Additionally, the efficiency is affected by the selected pressure set-point and thus the produced hydrogen flow rate. At higher production pressures the efficiency is higher. A characteristic example is the efficiency improvement as the pressure is higher during Day 1 that is highly volatile and Day 6 that has constant operation, as can be seen in Table 5.3.

Table 5.3, Stack efficiency improvement with pressure and irradiance profile

	Stack Efficiency (%)					
Pressure	Day1	Day2	Day3	Day4	Day5	Day6
5	38.8	34.0	39.2	43.6	42.9	54.5
7	47.3	53.5	52.2	57.0	57.8	59.9
10	48.9	52.9	56.8	57.2	61.8	62.2
13.8	59.7	56.2	58.4	63.6	63.6	63.6

Thus, in order to improve the efficiency of the system and reassure a stabilised operation it is important to optimise the power supply to the electrolyser. An improved PV power output management is required and this will be examined in the simulation of the system.

5.7 Experiments for the Jamaica Conditions

Figures 5.12 and 5.13 show the recordings of the tests under the conditions in Jamaica under constantly high irradiance for the 12th of May and volatile irradiance for the 17th of May. The rest of the validation experiments are presented in graphs in the Appendix D.

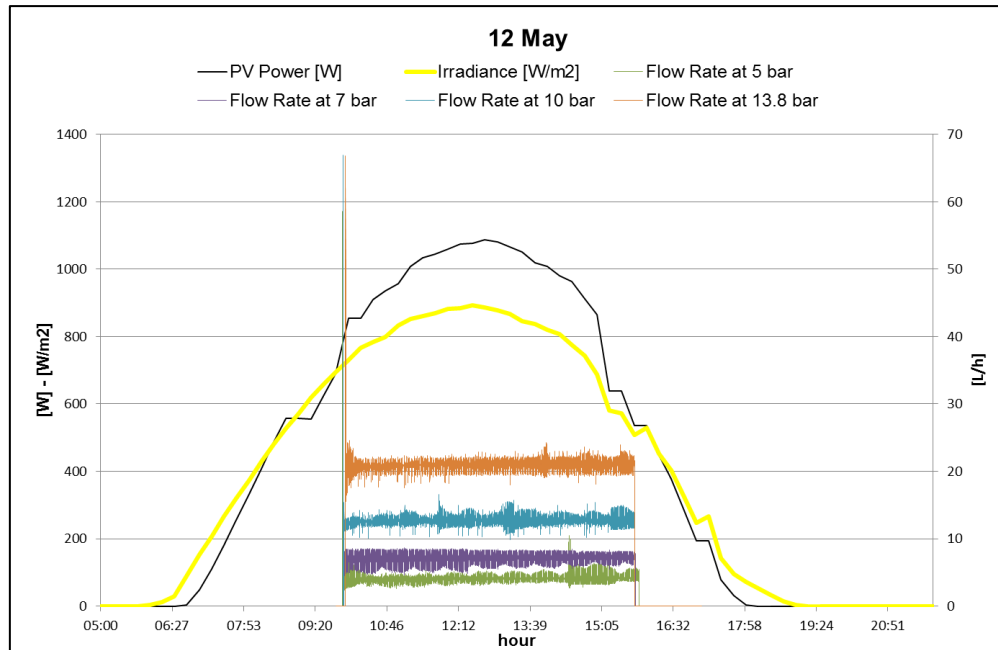


Figure 5.12, Hydrogen production rate in L/h at 5bar, 7bar, 10bar, 13.8bar pressure set points during 12th of May in Jamaica, that presents consistently high irradiance levels

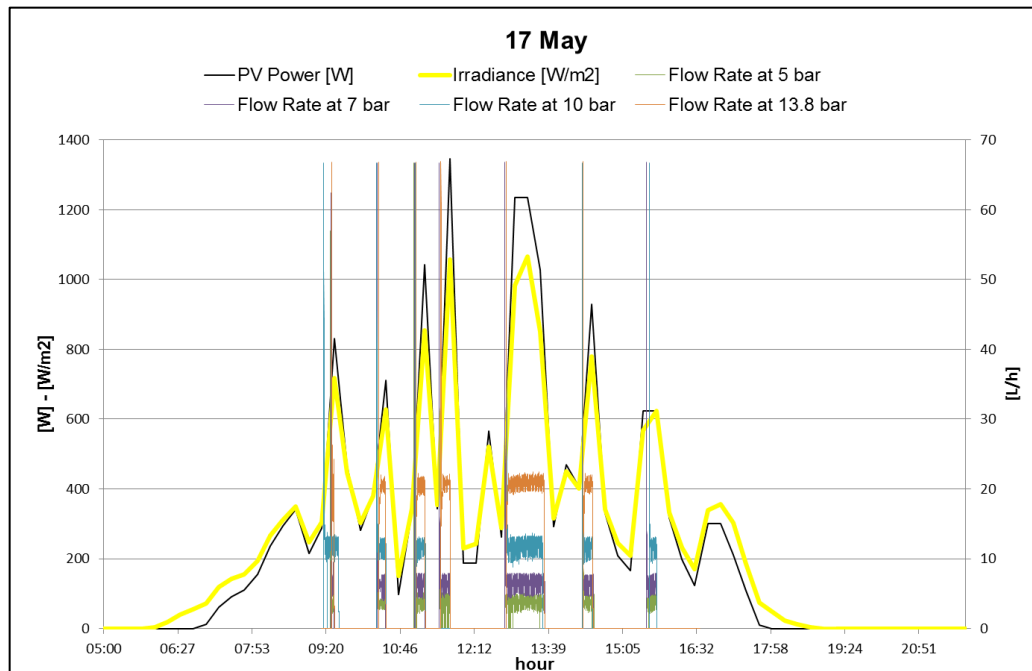


Figure 5.13, Hydrogen production rate in L/h at 5bar, 7bar, 10bar, 13.8bar pressure set points during 17th of May in Jamaica, that presents unstable irradiance levels

Operating the electrolyser under this direct connection to the available PV power output sets it subject to stops and start-ups, which in turn affect the efficiency and the specific energy use that can be seen in Figures 5.14 to 5.16.

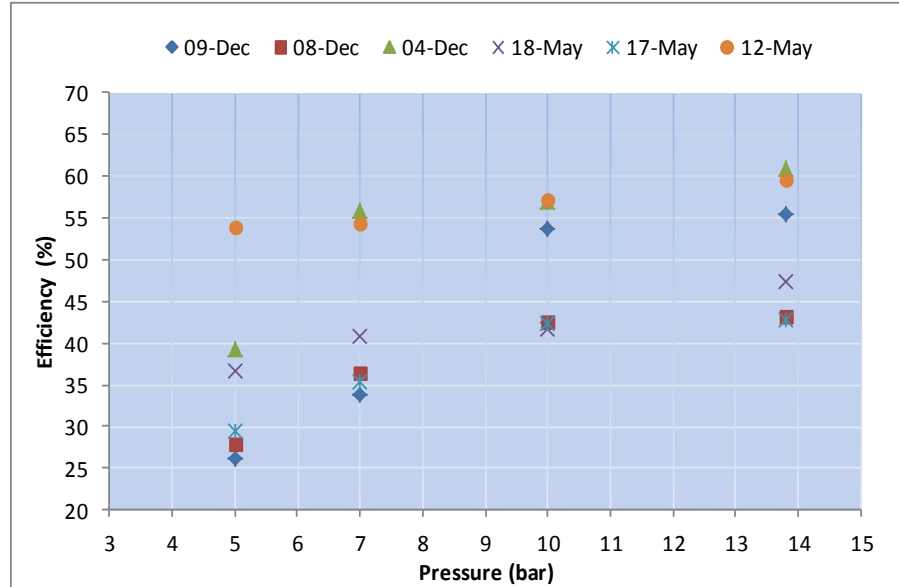


Figure 5.14, Efficiency vs pressure set point for each day of the Jamaica experimental days

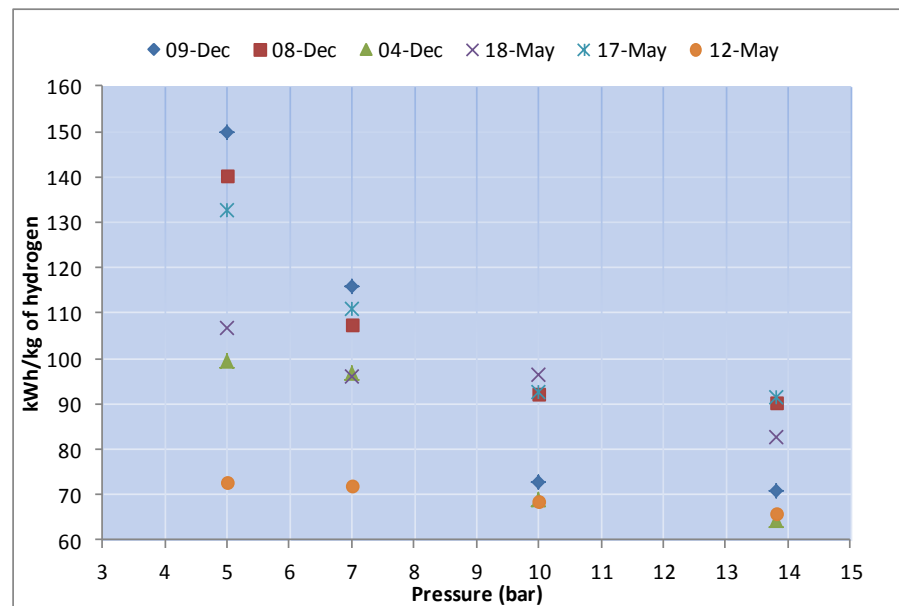


Figure 5.15, kWh/kg of H₂ vs pressure set point for each day of the Jamaica experimental days

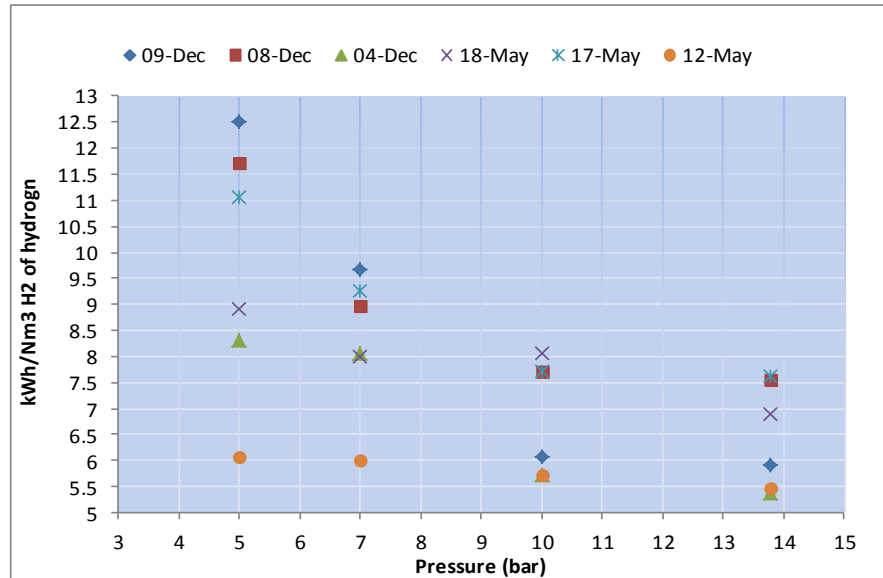


Figure 5.16, kWh/Nm³ of H₂ vs pressure set point for each day of the Jamaica experimental day

5.8 Effect of the irradiance input on the efficiency of the electrolyser

The operation and energy utilisation and efficiency of the system is highly affected by the irradiance levels and subsequently the available PV power output. The electrolyser is a commercial unit comprised of supplementary components that manage its operation and for that reason it requires a minimum energy supply. This depends mainly on the heater function that is variable, and when it is on it adds approximately 450W to the system. In combination with the stack that requires at maximum 300W a total 750W demand is reached. The integrated system operation is a combination of the available irradiance – PV power output and the energy requirements of the electrolyser. Thus, there are occasions that even though the PV output drops below 500W the system keeps operating as the electrolyser energy requirements at that occasion consist only of the energy for the stack operation and the valves and pump. In contrast, if at these occasions the total system requirements are a combination of the heater and stack operation, the total energy requirements rise to 700-750W and the electrolyser stops producing and goes to idle state. This is observed in Figures 5.7, 5.8, 5.12 and 5.13 where there are periods of zero flow rates and periods of hydrogen production. It is observed that at the beginning of production periods there are flow rates that reach up to more than 1000ml/min. This is due to the fact that at the beginning of operation and hydrogen generation, hydrogen is produced and accumulated in the electrolyser. When the selected pressure set point is

reached, hydrogen is released and the flow rates are regulated according to the pressure set point. The lower the flow rates the faster they are regulated. Measurements for the four selected pressure set points for small periods of operation with 1 second interval of data logging can be seen in the Appendix D.

Hence, operating the electrolyser under this direct connection to the available PV power output sets it subject to stops and start-ups, which in turn affect the efficiency. A comparison between the efficiency of the electrolyser for the same operational pressure indicates that on the days with stable operation the system performs better.

Additionally, the efficiency is affected by the selected pressure set-point and thus the produced hydrogen flow rate. At higher production pressures the efficiency is higher, as the stack operates at a higher rate and higher temperatures. The most efficient operation of the system (5.1kWh for the production of 1Nm³ of hydrogen in Day 5 of the experiments for UK conditions) is when the electrolyser is not subject to the intermittency of the power supply, but operates stabilised at the highest hydrogen generation pressure. On the contrary, operating the electrolyser at low operating pressures is always the least efficient way. These results are evaluated in combination with the energy use of the stack in section 4.2 of Chapter 4.

The stack energy demand increases as the operating pressure increases but it is proved that even though operation at highest pressures is more energy demanding the energy content of the produced hydrogen results in more efficient operation. The total hydrogen production is indicated in Tables 5.4 and 5.5. The increase in the hydrogen generation is averagely 70.8% for these pressure set points and is proportionally higher than the increase of the stack energy demand which is averagely 61.7%, from one pressure set point to the next, as shown in Figure 4.4. This is indicative of the improved performance of the stack in higher operating pressures. Thus sizing the PV system adequately so that high pressure constant operation is assured is the optimisation strategy for the simulation and the case study application.

Table 5.4, Total generated hydrogen (L) for the UK representative experimental days

Pressure Set-point(bar)	June 1 st	June 2 nd	June 3 rd	June 4 th	June 5 th	June 6 th
5	20.56	25.6	27.9	27.6	27.64	27.97
7	35.66	42.9	47.85	47.3	49.42	48.53
10	59.64	77.7	80.52	84.4	81.76	84.32
13.8	97.2	118.5	140.1	137	137.5	142

Table 5.5, Total generated hydrogen (L) for the Jamaica representative experimental days

Pressure Set-point (bar)	May12 th	May17 th	May18 th	Dec4 th	Dec8 th	Dec9 th
5	24.37	8.03	8.23	17.78	2.82	1.71
7	42.93	12.96	13.84	33.5	4.29	2.02
10	78.05	21.42	23.1	61.5	7.17	3.79
13.8	127.52	37.88	51.75	101.5	11.44	6.03

5.9 Numerical model validation

The experimental results described in sections 5.6 and 5.7 act as a validation of the developed electrolyser numerical model. The TRNSYS model that represents the experimental setup and includes the developed components can be seen in Figure 5.17. The model consists of data readers for generic data files components (TRNSYS types 9a) for the irradiance data (1) and the temperature data (2). Type 16a solar radiation processor component (3) interpolates radiation data, calculates several quantities related to the position of the sun, and estimates solar insolation on a number of surfaces of either fixed or variable orientation, type 194 component simulates crystalline photovoltaic array (4), type 175a component simulates the DC/AC inverter (5), type 2628 simulates the controls of the electrolyser (6), type 2627 simulates the PEM electrolyser (7), and type 2729 simulates the metal hydride storage (9). The components 2627, 2628, and 2629 are the user written components described in sections 5.3.1 to 5.3.4. Type 14h is the component used to simulate the pattern of the heater operation (8) and acts with combination to the

controls component. For the validation of the PEM electrolyser operation the metal hydride storage component is not connected to the hydrogen output.

The temperature and irradiance data of the UK and Jamaica locations that correspond to the experimental periods are inputted to the generic data readers and the solar radiation processor. The temperature and the computed irradiance data are used for the calculation of the PV panels' power output which represents the power output of the tests. The electrolyser is supplied through the power inverter and the recorded data are: flow rates, response to the intermittent power supply and electrochemical characteristics of the stack. Type 65d and 25c components are used for the graphical representation of the simulation results and the export of the results in a format that can be analysed (excel files).

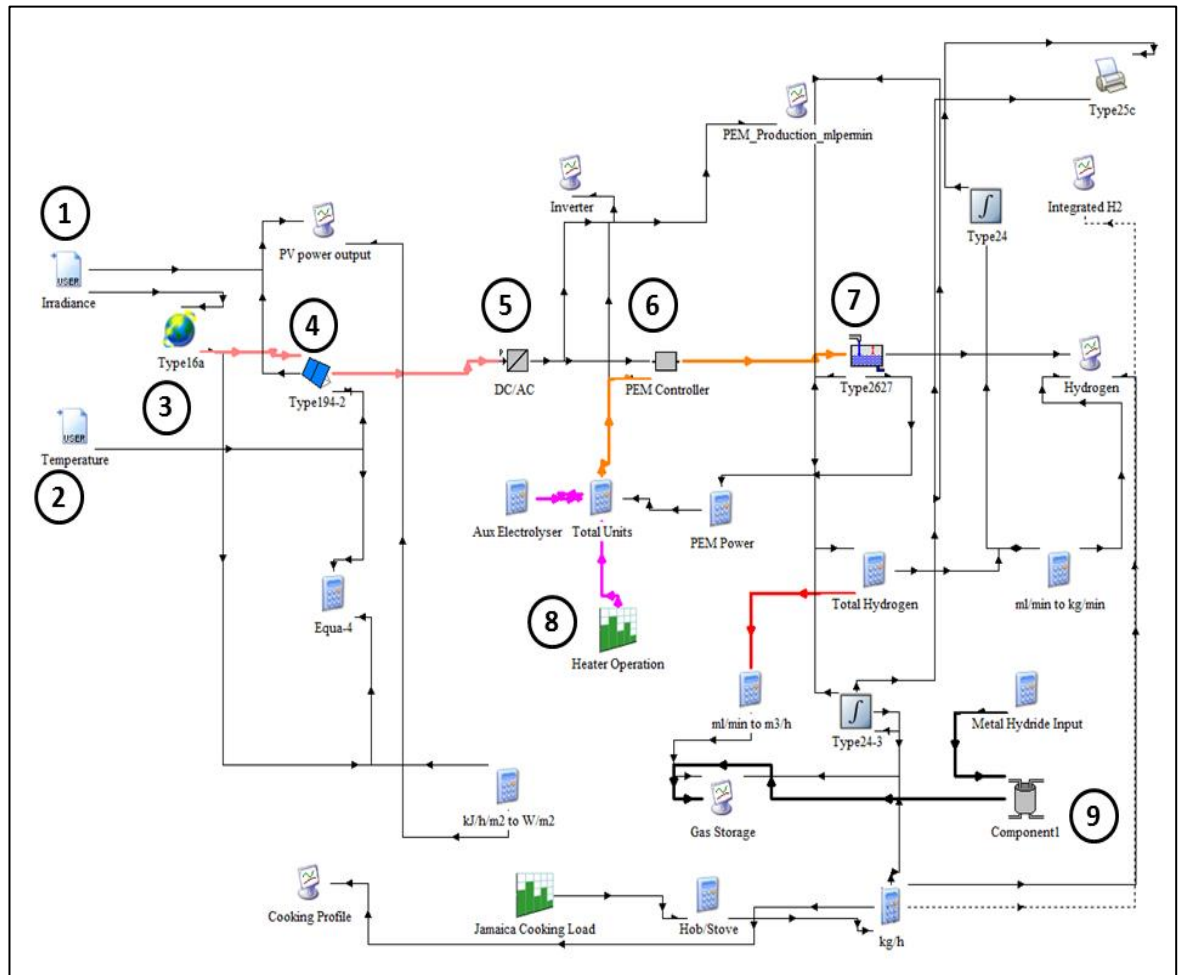


Figure 5.17, TRNSYS model of the experimental setup for the validation

Figures 5.18 to 5.21 show the experimental and simulation hydrogen flow rates for 5bar, 7bar, 10bar and 13.8bar for operation during the second of June for the UK experimental data. The figures show a good agreement between the actual production trend and the simulated. At the beginning of the operation and at every restart the hydrogen flow rates present a peak which in a few seconds starts to reduce. This is because at the start of the generation process hydrogen is accumulated in the electrolyser until the necessary production pressure levels are achieved. Thus the accumulated gas exits at a high rate and when the pressure is stabilised the flow is stabilised too. Comparison between all the results of the UK and Jamaica experimental sets and the simulation results is performed and the average difference is 6.22% for 5bar, 6.12% for 7bar, 4.46% for 10bar and 3.70% for 13.8bar. The similarity between the experimental and simulation results increases at higher operating pressures as at higher flow rates the effect of the peaks is less prominent. Thus it is concluded that the model can be used with confidence for the simulation of the solar hydrogen system and to enhance this further, statistical validation of the model is performed in section 5.10 of this Chapter.

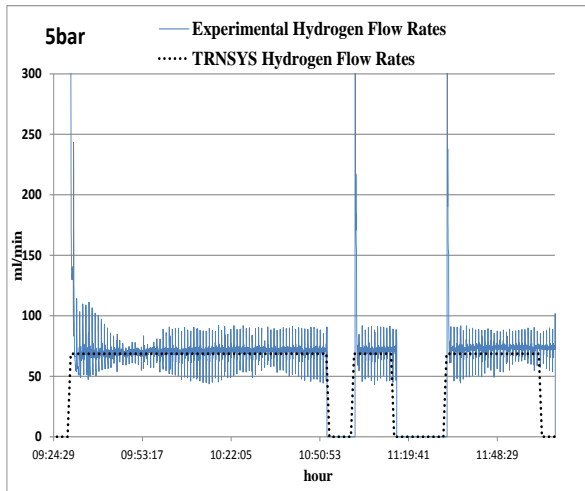


Figure 5.18, Comparison between TRNSYS and experimental results of produced hydrogen flow rates at 5bar

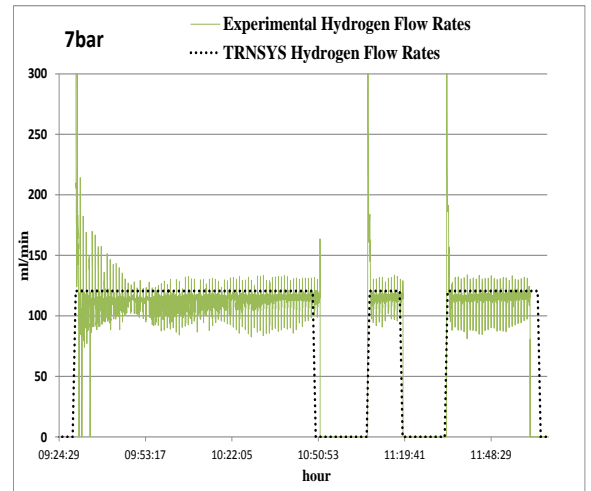


Figure 5.19, Comparison between TRNSYS and experimental results of produced hydrogen flow rates at 7bar

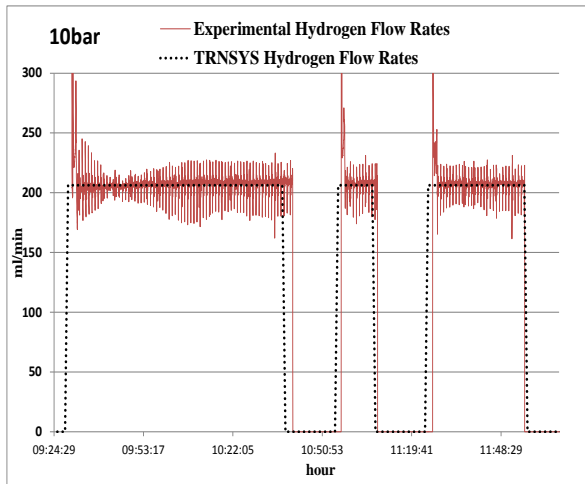


Figure 5.20, Comparison between TRNSYS and experimental results of produced hydrogen flow rates at 10bar

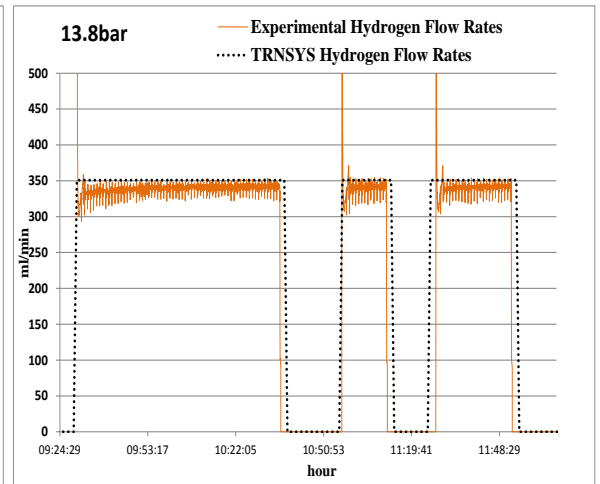


Figure 5.21, Comparison between TRNSYS and experimental results of produced hydrogen flow rates at 13.8bar

5.10 Statistical Validation of Models

The developed model in TRNSYS is used as a mean to evaluate the performance of an actual solar hydrogen system of any scale. Thus it has to be validated as a reliable tool for this purpose and this is done here through the statistical validation of the numerical model and the experimental results. The null hypothesis is used, and the first step is the F-test that will show whether the variances of the data samples are equal or unequal.

F-Test Two-Sample for Variances

	<i>Variable 1</i>	<i>Variable 2</i>
Mean	64.4	66.638
Variance	811.784	775.393
Observations	10	10
df	9	9
F	1.047	
P(F<=f) one-tail	0.473	
F Critical one-tail	3.179	

There are two options for the F-test:

- If $P > 0.05$, the variances are not unequal and the null hypothesis cannot be rejected. Therefore, the variances are equal
- If $P < 0.05$, the variances are unequal and the null hypothesis is rejected

Here, for the stack power results it is observed that the $P=0.473$, therefore the variances are equal and the null hypothesis confirmed. The second step is to execute the t-test, to confirm whether the means of the two data sets are equal.

t-Test: Two-Sample Assuming Equal Variances

	<i>Variable 1</i>	<i>Variable 2</i>
Mean	66.638	64.4
Variance	775.393	811.784
Observations	10	10
Pooled Variance	793.589	
Hypothesized Mean Difference	0	
df	18	
t Stat	0.178	
P(T<=t) one-tail	0.430	
t Critical one-tail	1.734	
P(T<=t) two-tail	0.861	
t Critical two-tail	2.101	

In the case that there is no indication which data set has the greater mean, the value that is important is the $P(T \leq t)$ two-tail. Again the P is compared according to the 0.05 value and the options are:

- If $P(T \leq t)$ two-tail < 0.05 , the means are different and the null hypothesis is rejected
- If $P(T \leq t)$ two-tail > 0.05 , the means are equal and the null hypothesis is confirmed

Here $P=0.861$. Alternatively, the value t Stat is compared to the value t Critical two-tail and if it is smaller, then the means are equal and the model data and the experimental data are equivalent. Here $t \text{ Stat}=0.183 < t \text{ Critical two-tail}=2.101$.

Figure 5.22 shows additionally how close the experimental and the numerical model results are.

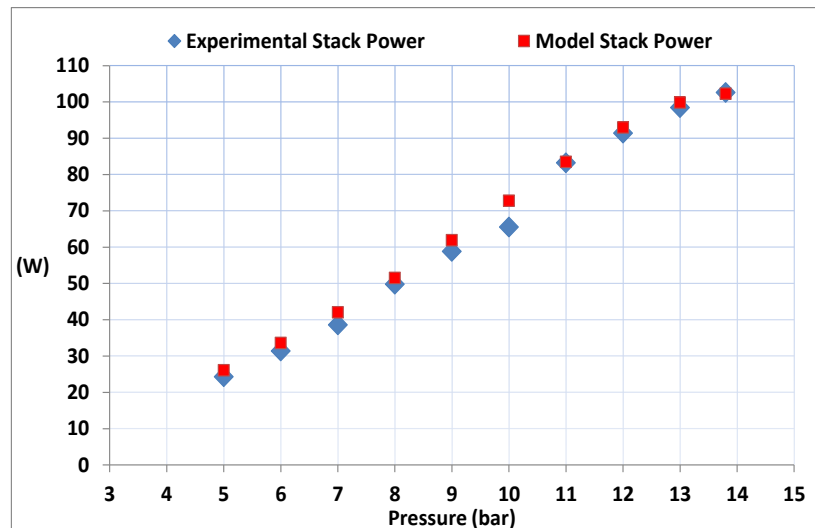


Figure 5.22, Experimental and numerical model stack power results

The statistical validation of the numerical model results is also performed for the hydrogen generation calculations, the stack voltage, stack temperature and metal hydride storage charging times. The results of the F-test for the null hypothesis and of the t-test for can be seen in Table 5.6. It is observed from the F-tests results that for all the parameters the variances are equal and the null hypothesis confirmed. Furthermore, the t-test shows that the means are equal and the model data and the experimental data are equivalent. The details of the statistical analyses and graphical representation of the experimental and numerical model results is given in the Appendix D.

Table 5.6, Results of F-test and t-test for the model calculated parameters

Model calculated parameter	P(F<=f) one-tail	P(T<=t) two-tail
Hydrogen generation	0.5	1
Stack voltage	0.427	0.2
Stack temperature	0.475	0.999
Metal hydride storage charging times	0.321	0.429

5.11 Sensitivity Parametric Tests on the Hydrogen Generation Flow Rates of the PEM Electrolyser Model

Having assured that the model is statistically confirmed, sensitivity tests were executed on the critical parameters of the model. The parameters that affect the hydrogen generation rates are examined and these are the stack current, the stack temperature and the hydrogen generation pressure. The sensitivity of the hydrogen generation to these variables can be seen in Figures 5.23 to 5.25.

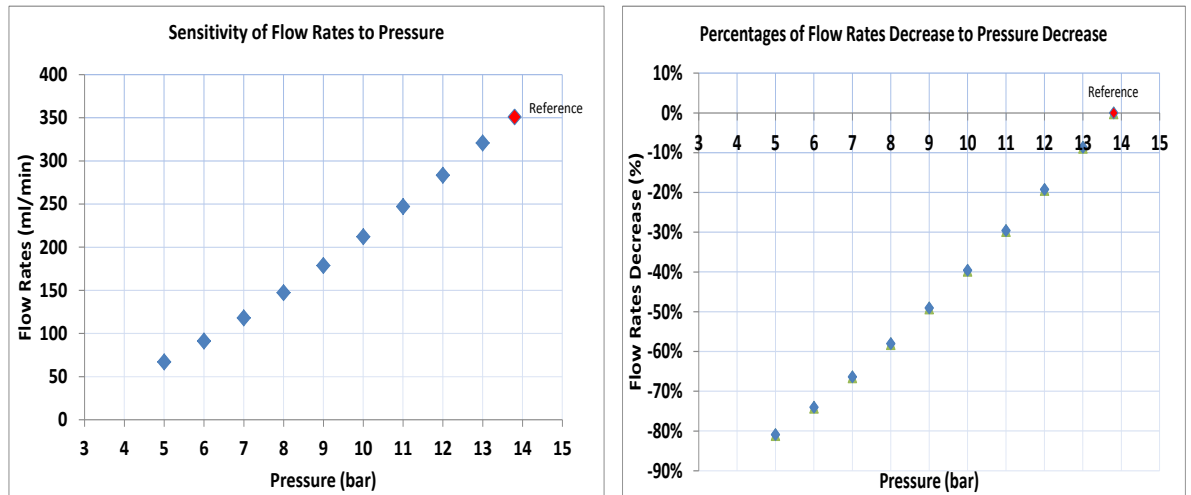


Figure 5.23, Sensitivity of hydrogen flow rates to hydrogen generation pressure

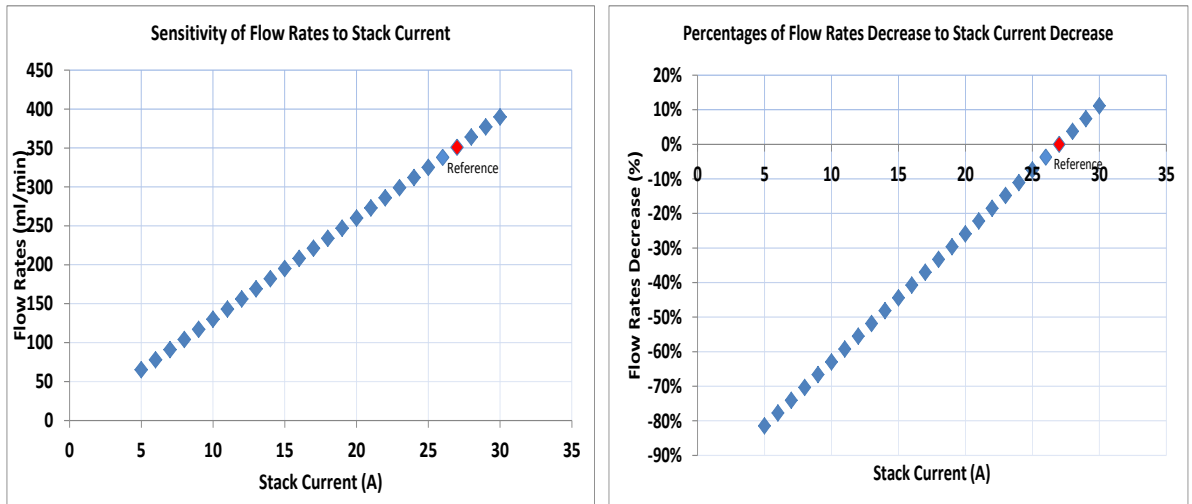


Figure 5.24, Sensitivity of hydrogen flow rates to stack current

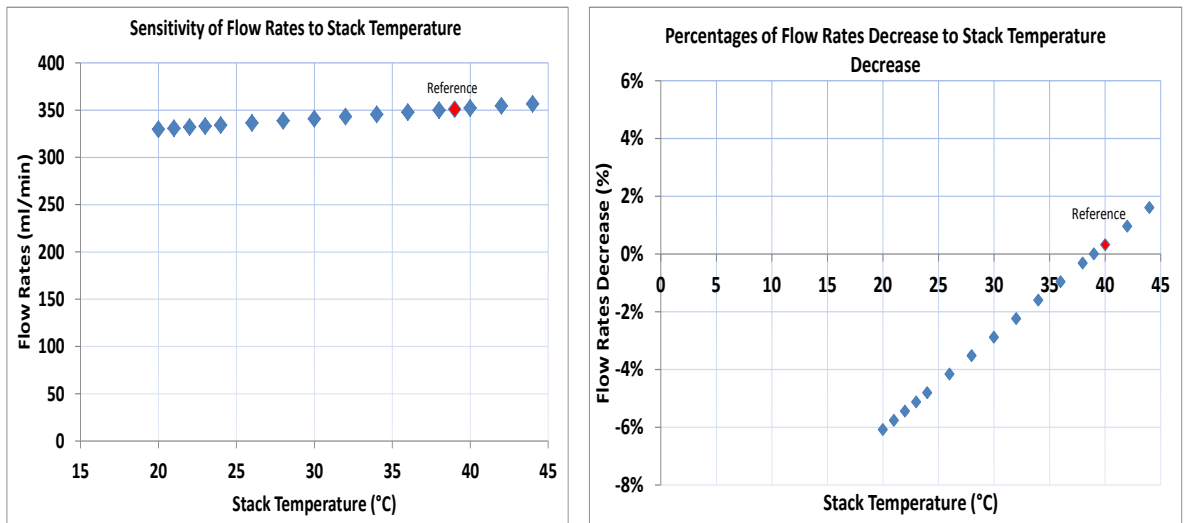


Figure 5.25, Sensitivity of hydrogen flow rates to stack temperature

Figure 5.23 shows that the hydrogen generation decreases with a decrease in the hydrogen generation pressure. For each one bar of pressure drop the hydrogen flow rates reduce by an average of 31.55 ml/min. In total a pressure drop from 13.8 to 5bar causes an 80.9% drop in the flow rates. In relation to the stack current, Figure 5.24 shows that one ampere decrease in the stack current causes a 13ml/min reduction in the flow rates. In total a stack current decrease from 27 to 5A causes the flow rates to reduce by 81.5%. Finally, the temperature has the least effect on the hydrogen generation rates, as every one degree of increase causes 1.12ml/min increase. Figure 5.25 shows that a rise of temperature from 39°C to 44°C causes only a 1.6% increase in the flow rates. Therefore, in the case of this PEM electrolyser model, it is concluded that the parameter with the greatest impact factor

on the system is the hydrogen generation pressure. This is reasonable and is explained by the fact that the higher the desired generation pressure the higher are the flow rates. When pressure is increased the maximum stack current remains the same, 27A, but the stack generates at a much higher rate. In terms of sensitivity, the system is more sensitive to pressure difference, followed by stack current and finally it is least sensitive to stack temperature.

5.12 ASPM Electrolyser day tests

The experimental tests emulating daily conditions for the UK have been performed with the Alkaline Solid Polymeric Membrane (ASPM) Electrolyser from ActaSpa (ACTA, 2014) for comparison purposes. The results can be seen in Figures 5.26 to 5.31. The efficiencies of the electrolyser for each operational day can be seen in Table 5.7.

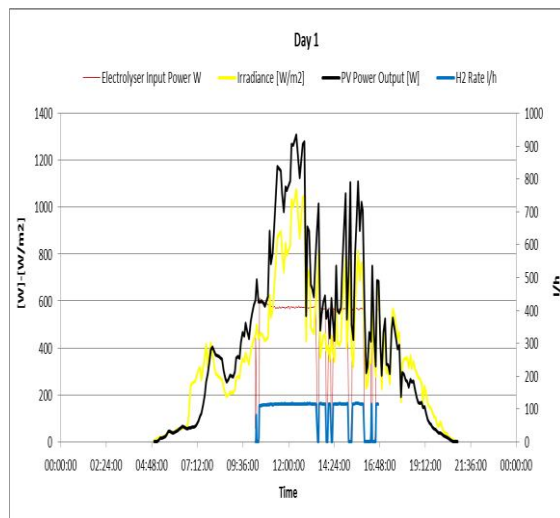


Figure 5.26, Hydrogen production rate in L/h Day 1 of the UK data, that presents unstable irradiance levels

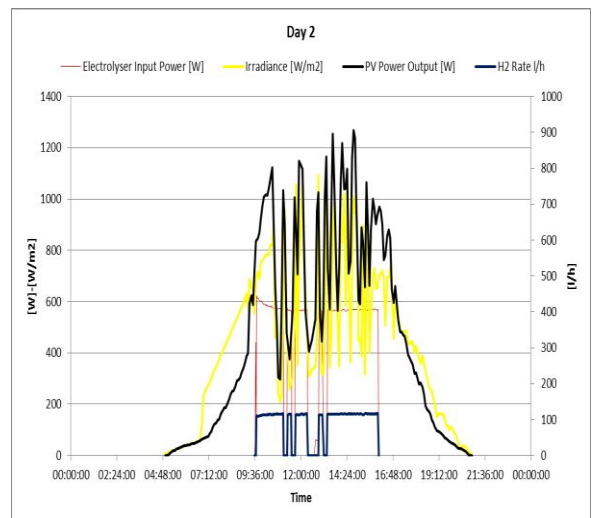


Figure 5.27, Hydrogen production rate in L/h Day 2 of the UK data, that presents unstable irradiance levels

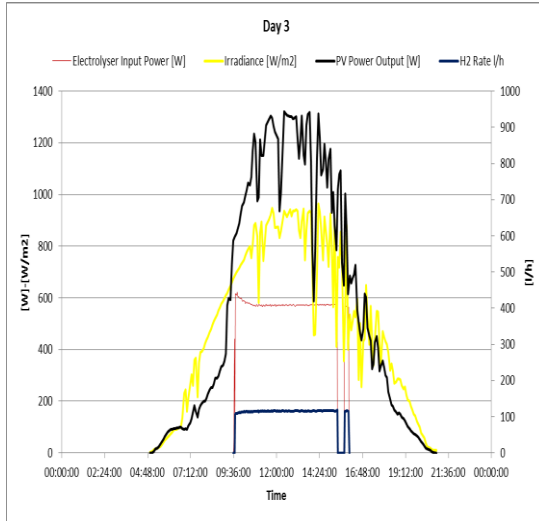


Figure 5.28, Hydrogen production rate in L/h Day 3 of the UK data, that presents unstable irradiance levels

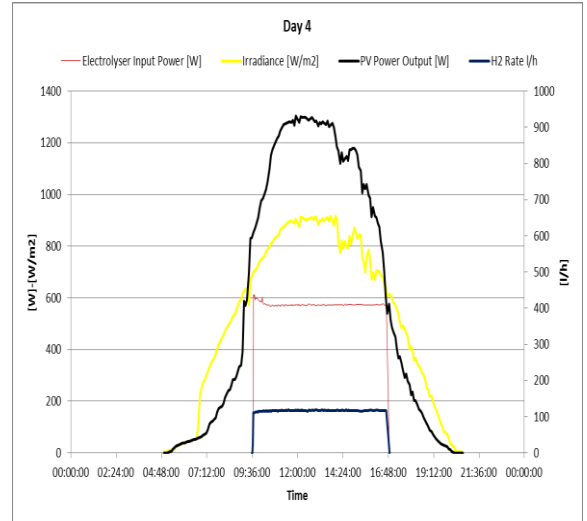


Figure 5.29, Hydrogen production rate in L/h Day 4 of the UK data, that presents constantly high irradiance levels

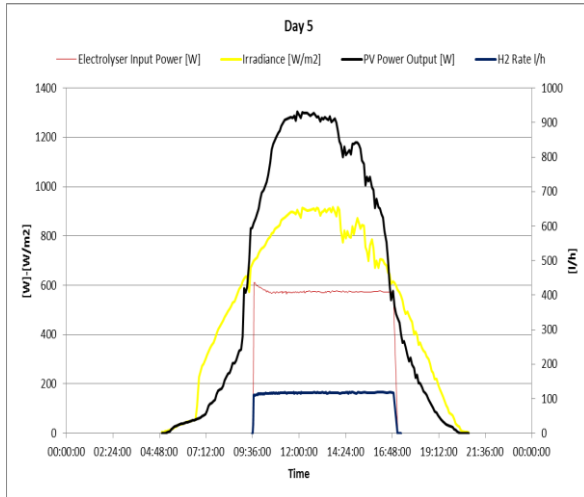


Figure 5.30, Hydrogen production rate in L/h Day 5 of the UK data, that presents constantly high irradiance levels

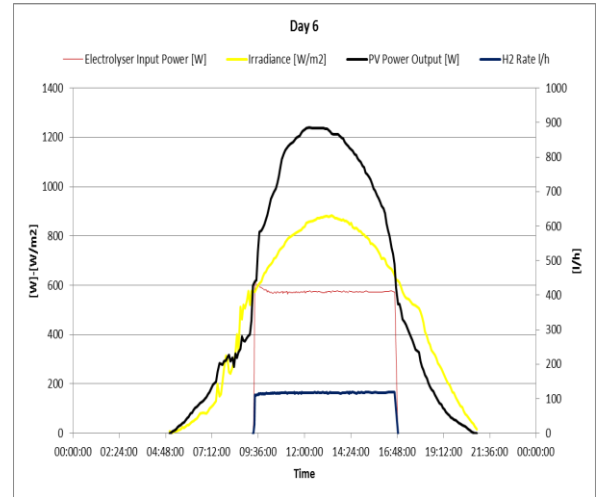


Figure 5.31, Hydrogen production rate in L/h Day 6 of the UK data, that presents constantly high irradiance levels

Table 5.7, ASPM electrolyser efficiencies for each experimental day

	Hydrogen Flow Rate [l/h]	Stack Efficiency[%]
Day1	115.25	63.63
Day2	115.75	64.98
Day3	115.94	72.17
Day4	117.26	77.2
Day5	117.04	77.2
Day6	117.04	77.74

5.13 Summary

Chapter 5 presented the process of the development of the numerical model components of the solar powered electrolyser. The numerical model components are developed and incorporated into the standard libraries of TRNSYS components, where the simulation of the system is performed.

The numerical components are based on results of the experiments described in Chapter 4 regarding the operation of the PEM electrolyser of this research, its controls and the metal hydride storage used. Furthermore, validation experiments regarding the operation of the system under various weather conditions, characteristic of the UK (London) and Jamaica indicate that the model accurately represents the reality. Finally, the numerical model results were additionally validated through statistical analyses.

The scope of the numerical model is to simulate the operation of the solar hydrogen system to satisfy domestic cooking demand. As a main motivation for this research, Jamaica is the country examined as one case study for the application of the system. The following chapter presents three country cases including Jamaica that are used as case studies for the model simulation. The motivation, the country current domestic cooking conditions and the domestic cooking demand profiles are presented through data mining and one specific quantitative study.

**Chapter 6. Case Study Countries
Presentation and Cooking Demand
Calculation**

6.1 Introduction

Three countries were selected as case studies for the evaluation of the application of the solar hydrogen system; Ghana, Jamaica and Indonesia. All three countries have developing economies (The International Statistic Institute, 2015) and geographically belong to the near equatorial region. In addition, a high proportion of domestic energy demand is for cooking and is dominated by fossil fuels, mainly firewood, charcoal and petroleum by-products (World Health Organisation, 2014). Poor ventilation and out-dated cooking methods result in numerous deaths every year directly related to the emissions of these cooking fuels (IEA, 2006). Moreover, these countries can experience financial instabilities because of their dependence on imports of petroleum products for their energy needs.

In this chapter statistical analyses are performed and the domestic cooking demand profile is created for the three countries. For Jamaica and Indonesia, this is based on available data from the literature, but for Ghana a specific quantitative study is conducted due to lack of available data. The cooking demand profile is used to size solar hydrogen plant for rural communities in the three countries (presented in Chapter 7).

6.2 Ghana Case Study

Ghana was selected as it is a typical example of a developing economy faced with challenges and problems in the cooking sector. Ghana has a GDP growth rate of 6% per year (Seth & Essandoh, 2011) is rich in renewable energy sources, but has nevertheless a high dependency on solid and fossil fuels, especially in the cooking sector.

With an aim to create a cooking demand profile for a Ghanaian household and due to lack of available data in the literature, a questionnaire survey was developed for the collection of data. Data collection and analysis methodology are presented in this section together with results. The main drive was to calculate the average daily cooking demand for a typical Ghanaian household to be used as an input in the simulation. Additional original outcomes are presented in relation to the current energy use, socio- economic status of the households and fuel use.

6.2.1 Motivation and Research Questions

Ghana, as shown in Figure 6.1, is a west African country with tropical climate, total land area of 238,500km² and a population of 27 million (Ghana Statistical Service, 2014). It is positioned in the gulf of Guinea and is a country well-endowed with water resources. Two rainy seasons take place, one from April to July and one from September to November. In the north of the country, the rain period is slightly different and the rainy season begins in April and lasts until September. Annual rainfall ranges from about 1,100 mm (about 43 in) in the north to about 2,100 mm (about 83 in) in the southeast. In relation to temperatures, the minimum yearly average is 20.5°C and the yearly maximum is 26°C. A dry desert northeast wind called “harmattan”, blows from December to March, reducing the humidity and causing hot days and cool nights in the north. In the south the effects of the harmattan happen in January. In most areas of the country, the highest temperatures are recorded in March whereas the lowest in August (Ghana Web, 2014).

The Volta river system basin covers 70% of the country area and another 22% of Ghana is covered by the south-western river system. The coastal river system covers the remaining 8% of the country (Food and Agriculture Organisation of the United Nations, 2014). Furthermore the Volta Lake, with a surface of 8,500 km², is one of the world's largest artificial lakes (Britannica, 2014). Altogether, the renewable water of the country resources is estimated to be 53.2 billion m³ per year. The solar energy potential of the country is also very high, ranging from 4-6 kWh/m² providing excellent conditions for photovoltaic panel applications (Seth & Essandoh, 2011).



Figure 6.1, Ghana location in Africa and country map, source: (Goffs School, 2014)

Renewable energy plays a big part of the energy generation in the country, with 60% of the electricity generated from hydropower (Seth & Essandoh, 2011). The greatest percentage of final energy use corresponds to the residential sector, see Figure 6.2.

Additionally, the country's energy share is directly affected by the residential sector and is dominated by solid fuels, see Figure 6.3.

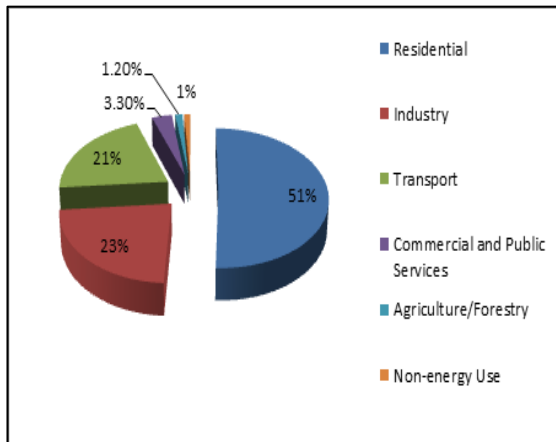


Figure 6.2, Ghana Final Energy Consumption, source: (Seth & Essandoh, 2011)

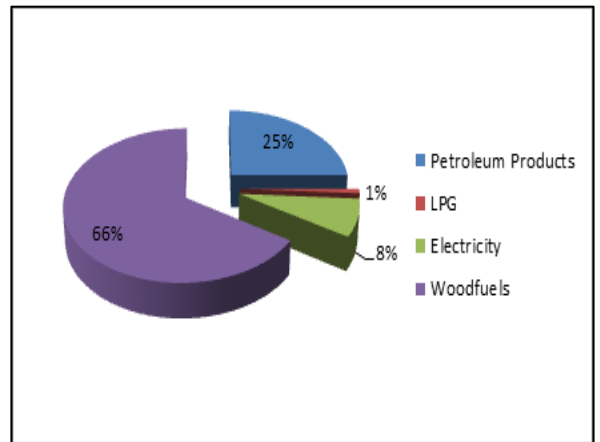


Figure 6.3, Ghana Energy Share by Type in 2012, source: (Seth & Essandoh, 2011)

In the residential sector, the prime proportion of energy needs originates from cooking, and it accounts for almost 95% of the household energy use (Abavana, 2004). The majority of the population-57%-lives in rural areas and statistics show that most Ghanaians rely completely on the use of biomass for cooking (firewood, coal, and dung) as well as a small percentage on LPG. (International Network on Gender and Sustainable Energy, 2006). Table 6.1 and Figure 6.4 show that almost 75% of cooking energy comes from solid fuels with firewood being the predominant. Within the 2000-2010 decade there has been a shift from firewood to gas and charcoal use. Rural households mainly depend on firewood whereas urban households on charcoal which needs three times as much wood to produce the same amount of energy output. Urbanisation has therefore a highly negative impact on deforestation. Electricity is almost never an option as cooking energy, and in particular for the poor rural households (Abavana, 2004). The promotion of the use of LPG has also been part of the government policy.

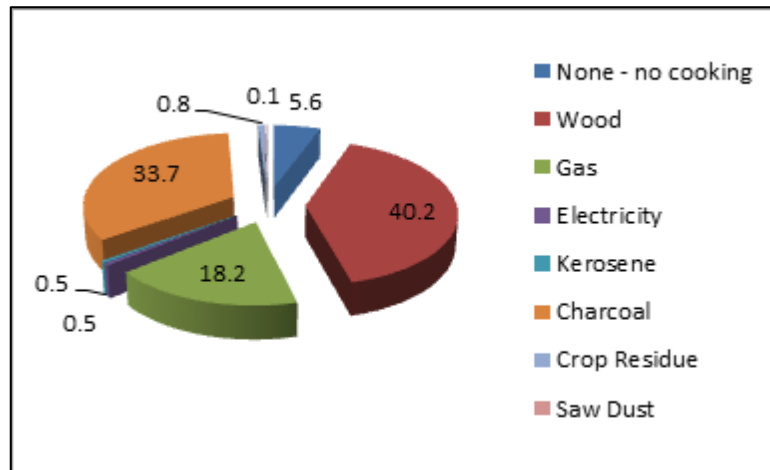


Figure 6.4, Fuel Used for Cooking as percentage in Households in Ghana in 2010, source: (Ghana Statistical Service, 2013)

Table 6.1, Fuel Used for Cooking as percentage in households in Ghana, 2000 and 2010, source: (Ghana Statistical Service, 2013)

Main Fuel used for Cooking	(% of households) in 2000	(% of households) in 2010
None - no cooking	3.5	5.6
Wood	55.8	40.2
LPG	6.2	18.2
Electricity	1.1	0.5
Kerosene	2	0.5
Charcoal	30	33.7
Crop Residue	*	0.8
Saw Dust	*	0.1
Animal Waste	*	0
Other	1.1	0.1
Total	100	100

LPG represents 18.2% of the cooking energy share in the residential sector; setting is as the first step into a cleaner use of energy for cooking (Ministry of Energy, 2010), see Figures 6.5 and 6.6. Nevertheless, Ghana relies on imports for Petroleum and LPG, in the

form of crude oil from Middle East and Nigeria, with the oil imports being 3,419ktoe in 2007 (Energy Commission Ghana, 2006). Predicting the future of the LPG cost and import rate is not an easy task, as it is highly affected by geopolitics and petroleum demand and supply.

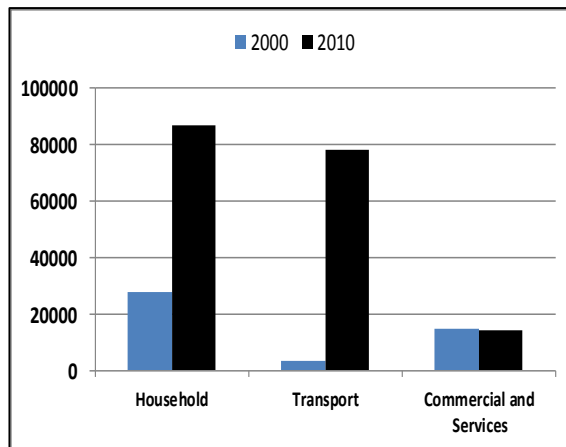


Figure 6.5, LPG consumption Share in Ghana, source: (Energy Commission Ghana, 2013)

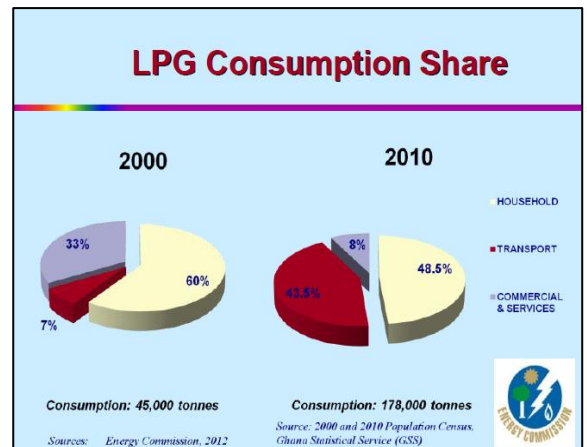


Figure 6.6, LPG consumption Share in Ghana, source: (Energy Commission Ghana, 2013)

The recent increase in the LPG prices has forced the local population to turn once more to the use of charcoal as the next cleanest cooking fuel. In turn this has intensified even further deforestation and desertification rates, indoor air pollution and hazardous health impacts, and poses also an extra threat to energy security as the amplified demand in charcoal and firewood cannot be satisfied by the production (Ahiataku-Togobo, 2013).

With a view to enhance the energy stability and the promotion of sustainability, the country has introduced national renewable energy policy plans to promote a shift to cleaner fuels and to improve the environmental status of the country (Strategic National Energy Plan 2006-2020 Annex 1, 2006). Among these are:

- The Ministry of Energy targets to increase the use of renewable energy : 10% of electricity generation from renewables by 2020 (excluding hydro)
- Subsidies/ incentives for renewable energy
- Reduction of firewood use in urban households by 30% by 2015 and 50% by 2050
- Reduction of the firewood in rural households by 10% by 2020
- Improved efficiency cook stove penetration of 5% by 2015 and 10% by 2020 (in the commercial sector)

-
- 1% penetration of biogas for cooking in hotels, restaurants, and institutional kitchens by 2015 and 2% by 2020
 - Firewood plantation projects
 - LPG subsidies

(Ghana Energy Ministry, 2014)

These targets aim to reduce the wood requirements for the production of charcoal by 50% by 2020, and thus contribute effectively to the reduction of GHG emissions and deforestation (Strategic National Energy Plan 2006-2020 Annex 1, 2006, p. 78). Additionally, there was a success in promoting the use of LPG, as a cleaner and safest cooking fuel. The percentage of the households that use LPG has been reported to increase from 4% in 1998 to 9.5% in 2006 (Akpalu, et al., 2011).

Furthermore, the ‘Ahibenso’ and the ‘Gyapa’ improved charcoal cooking stoves programmes were promoted by the government and the “Enterprise World” NGO (PDD Ghana Improved Stoves, 2009). This could result in great savings in term of fuel usage and energy cost, with numbers indicating that there could be even 20% annual savings in the cost of coal. Of these two programmes only Gyapa had some success with over 54,000 Gyapa stoves being sold from November 2002 to December 2003 and another 124,000 stoves from January 2004 to December 2006 (Strategic National Energy Plan 2006-2020 Annex 1, 2006, pp. 60-61)

Hence, the cooking energy sector in Ghana presents a challenge and a potential for the implementation of renewable energy projects that will enhance the sustainability and energy security.

With a view to quantify the current daily cooking demand, fuels used and attitudes towards solar hydrogen as new fuel, the following research questions were formulated:

- What is the daily cooking demand of an average Ghanaian household?
- What is the actual situation in terms of cooking fuels use in the Ghanaian household? (With a focus on rural households that represent the poorest and less developed part of the country).
- What are the actual consequences of the use of solid fuels on the people
- What is the socio-economic context of the fuel use and purchase; how do the fuel prices affect the household cooking; what is the actual increase on the fuel prices?

-
- Is there a willingness of the local people to switch to a hydrogen based cooking system and what are the reasons?

6.2.2 Sources and Methods of Data Collection

The aim of this section is to create a cooking demand profile for a Ghanaian household. Within this broad aim other general topics are examined:

- Cost of fuels
- Socio – economical relation of household and fuel use
- Potential of introducing a solar hydrogen system in Ghana

A questionnaire survey was conducted with a quantitative approach, with the help of Dr Divine Novieto, of Ho Polytechnic in the Ghana Volta region, who carried out the questionnaire survey. Local people from three communities were selected for the field study: Akatsi, Keta and Sogakope. The profiles of the communities are the following:

I. Akatsi: Tatorme Community

Akatsi is the administrative capital of the Akatsi South District Assembly; the total surface area is 960.445 km² (Ghana Volta Region Akatsi, 2014). The total population is 93,477. Akatsi has a dam (caterpillar) which served as a source of water for the community before the coming of the pipe water from the government. The dam is still in use and can serve as a source of water for the project. The community involved is Tatorme which is closer to the dam.

II. Keta: Kedzi community

Keta is the administrative capital of Keta Municipal Assembly. It has a total surface area of 1086km² but 30% of it is covered by water bodies (Ghana Volta Region Keta, 2006).The town is sandwiched between the sea and the fresh water lagoon. The community involved in the data collection is Kedzi, which also situated between the sea and Keta Lagoon.

III. Sogakope: Gbornor community

Sogakope is the administrative capital of south Tongu district assembly. It is located on the banks of the Volta lake one of the largest manmade lakes in the world (Tongu, 2006). The selected community is Gbornor, which is located on the banks of the Volta Lake and the inhabitants depend on the lake for their livelihood.

These communities are located in the south of the country, in the Volta region, one of Ghana's 10 administrative regions, see Figure 6.7. The region is located in the south-east part of Ghana, bordering with the Republic of Togo at the east and contains 8.6% of the country's population according to the national statistical service of Ghana (Ghana, 2012).

Volta region is dominated by the river Volta and Lake Volta on its western part (Ghana Tourism, 2009). The majority of the population in the area are occupied in the agriculture, forestry, fishing, hunting industries, wholesale and retail trade. The percentage of the females is higher in the wholesale and retail trade while that of the males is much higher in the fishing industry. Educational attainment in the region is comparable to the national levels. (Government of Ghana, 2014).

The majority of the population in Ghana inhabits in rural areas where most of the traditional cooking takes place and it is based mainly on charcoal and firewood (Ahiataku-Togobo, 2013). These communities were selected as they represent the typical rural households of Ghana. In addition to that they have abundant water resources which are a basic requirement for the operation of a solar electrolytic hydrogen generation plant.



Figure 6.7, Ghana map, location in Africa and the selected fieldwork locations, source: (Ezilon maps, 2009)

In total 155 participants of age 18 years and above from various rural backgrounds that represent social groups of Ghana took part in the survey. Raw data were collected through interviews and standardised questionnaires (Toprisk, et al., 2015), and a sample can be found in Appendix E. 53 questionnaires were selected from the Akatsi community, 64

questionnaires from the Keta community and 38 questionnaires from the Sogakope community. A camera was also used to take characteristic pictures of the current fuel supply and usage as well as the cooking devices and cooking conditions in the households. The fieldwork was conducted in September 2014.

The questionnaires include factual questions with pre-determined answers and opinion based questions with an open-ended form where the participants had the liberty to give their own answers. The structure of the questionnaires and each question position was chosen so as to promote the flow of questions. The main subjects that are addressed are:

- Sources of energy for cooking
- Socio-economic background of the households
- Cooking behaviour

For the factual questions a multiple response approach was followed and for the opinion based questions the answers were categorised and coded (The University of Reading Statistical Services Centre, 2001). For the data collection purposes two local interviewers were selected. Both were of Ghanaian origins and familiar to the region, the local people and the dialects spoken. In this manner the response and the engagement of the participants was maximised, as in this way the research achieves the best results (Arber, 1991).

6.2.3 Interview plan design

The methodology of the data collection consisted in the following four main steps:

Step 1:

The main interviewer conducted a first visit to the selected communities with a purpose to introduce himself and explain the purpose of the survey. The people were in this way informed of the cause of the study and were interested in their contribution to it; this was proved by the eagerness to participate. This step assisted in gaining a broad understanding of the communities and helped design the next steps with a more focused approach.

Step 2:

After the original meetings the survey dates were arranged and the questionnaires were prepared. The interviewers visited the three communities within a period of three weeks in September and October 2014 for the data collection. The participants were proved willing to provide the requested data and also stated a series of their own questions and arguments regarding the application of a new cooking fuel, which proves that the research indeed pursues a real social issue.

Step 3:

The raw data were collected, sent to Brunel University London, and the analysis process started.

Step 4:

The fourth and final step consisted of the outputs of the data analysis that resulted in two parts. The first one is the creation of the cooking demand profile of a typical rural Ghanaian household. The second part includes general conclusions regarding the fuel use in relation to the socio-economic profile and the energy and environmental factors that are involved.

6.2.4 Target Population and Research Constraints

The survey sample constitutes of participants that vary according to their profession and area, see Table 6.2. The majority of the population forming the sample is engaged in trading and owning their own business (in total 63.87%).

Table 6.2, Categories and numbers of stakeholders that participated in the Survey

Category	Number of People in Akatsi	Number of People in Keta	Number of People in Sogakope	Total Number of People	Percentage in Relation to the Total Population
Bank Worker	1	1	0	2	1.29%
Business Woman	6	8	8	22	14.19%
Clerk/ Secretary	6	5	1	12	7.74%
Farmer	0	0	4	4	2.58%
Fisherman/ Fishmonger	0	4	0	4	2.58%
Hairdresser/ Seamstress	5	5	0	10	6.45%
Nurse	1	2	0	3	1.94%
Teacher	8	12	0	20	12.90%
Trader	25	27	25	77	49.68%
Pensioner	1	0	0	1	0.65%
Total	53	64	38	155	100%

The third largest category is teachers, followed by clerks/ secretaries, hairdressers/ seamstresses, farmers and fishermen/ fishmongers, nurses, bank workers and pensioners. Additionally, the majority of the sample population, 94%, is female. This is normal as household cooking in Ghana is still a woman dominated task. Traditionally, women are responsible for household tasks as fetching water, collecting firewood, cleaning, taking care of the children and cooking (International Network on Gender and Sustainable Energy, 2010). Women are responsible for the cooking fuel supply to the household and were naturally more interested in the survey but also more easily accessible. The local fuel markets were the meeting point during the first visits to the communities as can be seen in Figures 6.8 and 6.9. Finding the adequate participants for the research was a challenge and

especially in an environment like rural Ghana where the collection of fuel and cooking process consumes a big part of their day. In addition to that, Ghana is still a male dominated country so interaction with the female participants had to be careful and keeping always the necessary formalities. Bawakyillenuo (Bawakyillenuo, 2007) quoting Valentine (Valentine, 2005) says characteristically “interviewing in different cultural contexts, particularly in less developed countries, requires heightened sensitivity...”



Figure 6.8, The Charcoal market in Akatsi



Figure 6.9, The firewood market in Keta

6.2.5 Main Fuel Use

In order to calculate the average cooking demand per household, the participants are clustered according to their main cooking fuel use. Each participant represented one household and a total of 155 participants took part in the survey. Of the total 155 participants, 67 use LPG as their main cooking fuel, 60 use charcoal and 28 use firewood, see Figure 6.10. In total, 56.77% of the participants use solid fuels as main source for cooking and 43.23% use LPG.

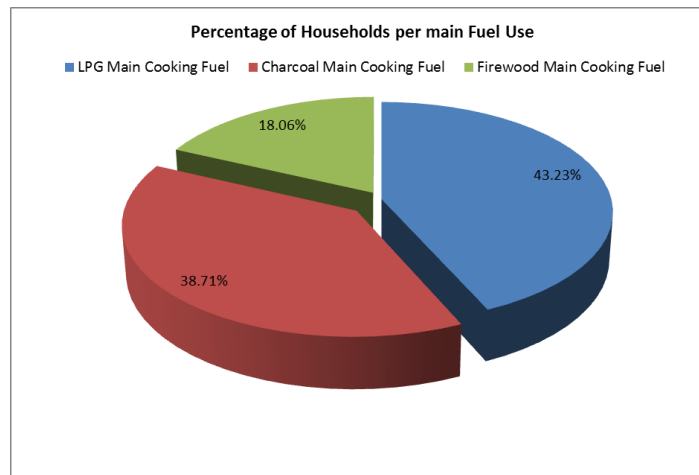


Figure 6.10, Percentage of households per main fuel use

The fieldwork results indicate that LPG is mostly used by the participants (43.23%), followed by charcoal (38.71%) and firewood (18.06%). This is in contrast to the national statistics indicating firewood as the main cooking fuel (40.2%), followed by charcoal (33.7%) and LPG (18.2%) (Ghana Statistical Service, 2013). However, a research study by Akpalu et al. (Akpalu, et al., 2011) shows evidence that LPG is now the preferred fuel, followed by charcoal and then firewood similarly to our survey. This might be caused by two main facts discussed below.

6.2.6 Locality and diversity of the sample population

The majority of the participants come from Akatsi (53 participants) and from Keta (64 participants) and their influence on the data is significant. The majority of the Akatsi and Keta sample population has higher education, in contrast to the Sogakope population, as shown in Figures 6.11 to 6.13.

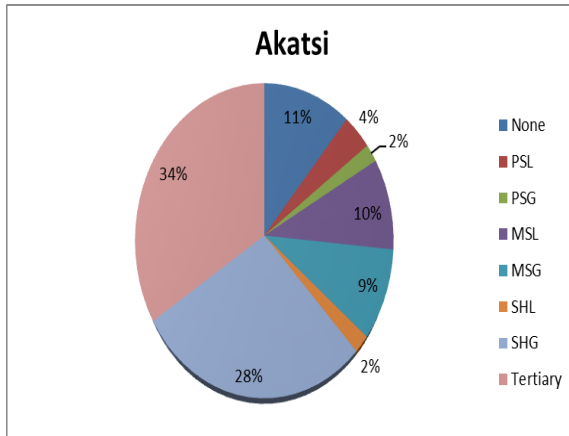


Figure 6.11, Akatsi participants' educational attainment*

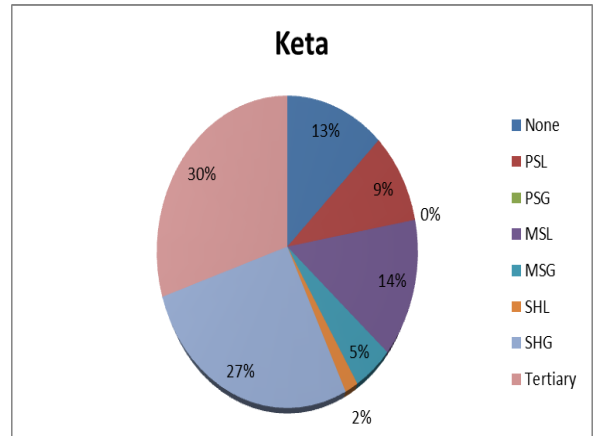


Figure 6.12, Keta participants' educational attainment*

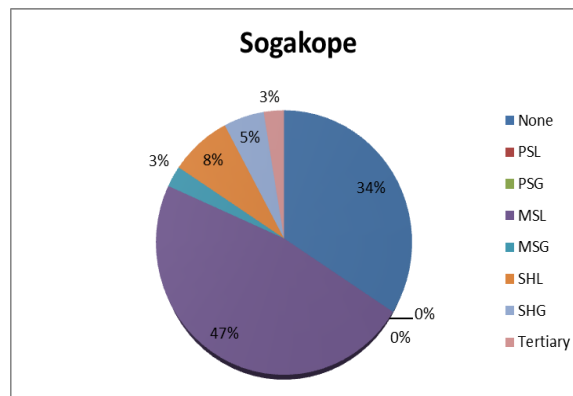


Figure 6.13, Sogakope participants' educational attainment*

**PSL: Primary School Leaver, PSG: Primary School Graduate, MSL: Middle School Leaver, MSG: Middle School Graduate, SHL: Secondary High School Leaver, SHG: Secondary High School Graduate*

The choice of the cooking fuel presents trends that are associated to the area, the educational attainment and the profession. Figure 6.14 and Table 6.3 present the relation between the main cooking fuel and the educational degrees of the participants. The tendency observed is that the use of LPG is more frequent among the participants with secondary school and university degree. The fuel use trend varies according to the area, the profession and income in a similar way to the educational attainment. Figure 6.15 shows that in the Sogakope population, which consists mainly of traders and has the lowest income of the sample, the use of firewood dominates, in contrast to Akatsi and Keta where LPG and charcoal are predominantly used.

Table 6.3, Percentage of the population in relation to their educational attainment and main fuel use

	Charcoal	Firewood	LPG	Grand Total
None	20.0%	50.0%	3.0%	18.1%
PS	10.0%	0.0%	4.5%	5.8%
MS	40.0%	46.4%	6.0%	26.5%
SH	25.0%	3.6%	34.3%	25.2%
Tertiary	5.0%	0.0%	52.2%	24.5%

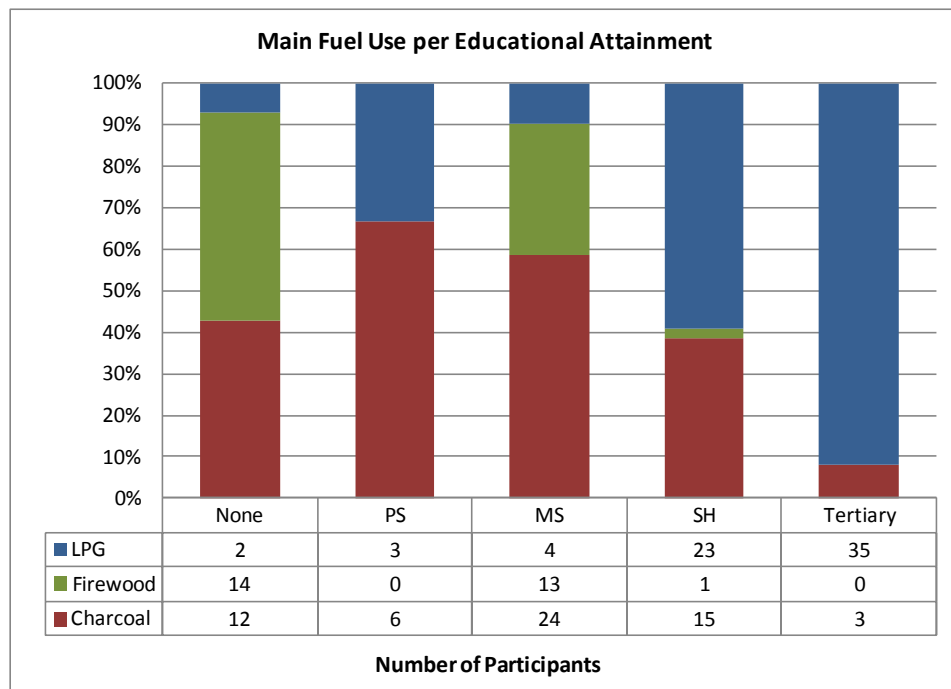


Figure 6.14, Main fuel use according to the educational attainment

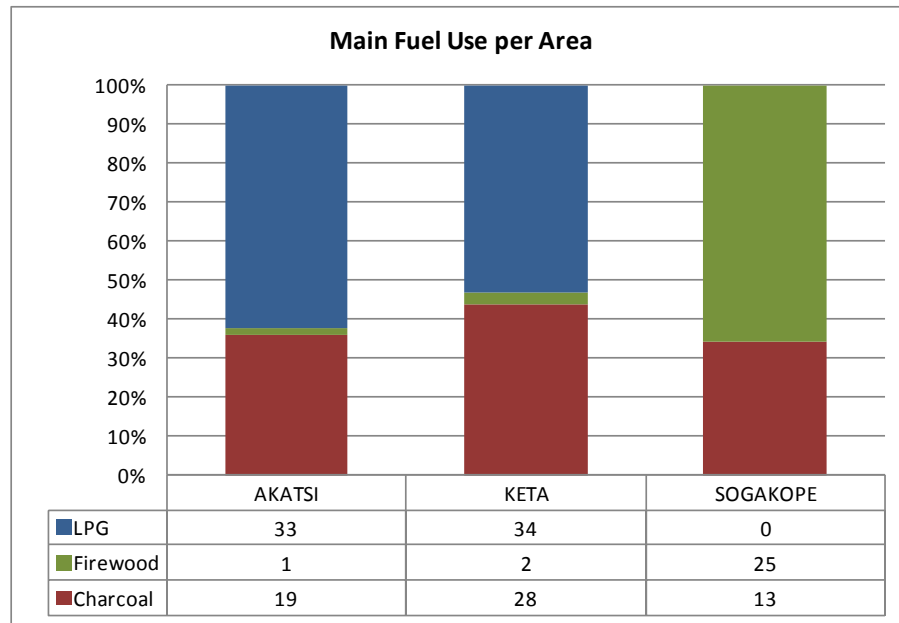


Figure 6.15, Main fuel use per area

6.2.7 Total Fuel Use

The households tend to use more than one cooking fuels to satisfy their daily needs. These additional fuels, act as a backup in case the main one finishes, or they are used for the cooking of particular dishes. Where charcoal is used as a back up to firewood or LPG, it is the fuel used specifically for the following:

- Preparation (grilling) of fresh fish, because the oil from the fish gets into the burners so people prefer using the grill on the charcoal pot.
- For the cooking of black-eyed beans since it takes a long time to cook so use of LPG is considered a waste by them.

In other cases there is a parallel use of the cooking fuels. In some instances it was observed by the local interviews, when soup is cooked on the charcoal pot to a point, it is transferred to the local stove (using firewood) and then the main meal is prepared on the charcoal pot. And once the local stove is lit for example in the evening, all the soups are heated on it and earlier grilled fish or meat is warmed on it before it is turned off. In these homes they rely on food warming first thing in the morning and last thing in the evening. Further to this, rural Ghana is an area where fuel supply is not guaranteed at all times, and there are periods where there can be shortages (Ahiataku-Togobo, 2013) . The use of two fuels and consequently two cooking devices enhances the energy security of the households. Charcoal is the fuel mostly used by the majority of the households (65.15%),

as indicated in Figure 6.16. This percentage includes use as main and additional cooking fuel. Second to that, 52.90% of the households use LPG as main or additional cooking fuel and last is firewood, with total use of 36.77% of the households. To include the use of both main and additional fuels in each household the term *total fuel use* is facilitated, and the detailed percentages can be seen in Tables 6.4 to 6.6.

Table 6.4, LPG use and additional fuels

	Participants	Percentages for the LPG use
LPG only	35	52.2%
LPG main and Charcoal additional	31	46.3%
LPG main and Firewood additional	1	1.5%
Total	67	100%

Table 6.5, Charcoal use and additional fuels

	Participants	Percentages for the Charcoal use
Charcoal only	17	28.3%
Charcoal main and LPG additional	15	25.0%
Charcoal main and Firewood additional	28	46.7%
Total	60	100%

Table 6.6, Firewood use and additional fuels

	Participants	Percentages for the Firewood use
Firewood only	19	67.9%
Firewood main and Charcoal additional	9	32.1%
Firewood main and LPG additional	0	0.0%
Total	28	100%

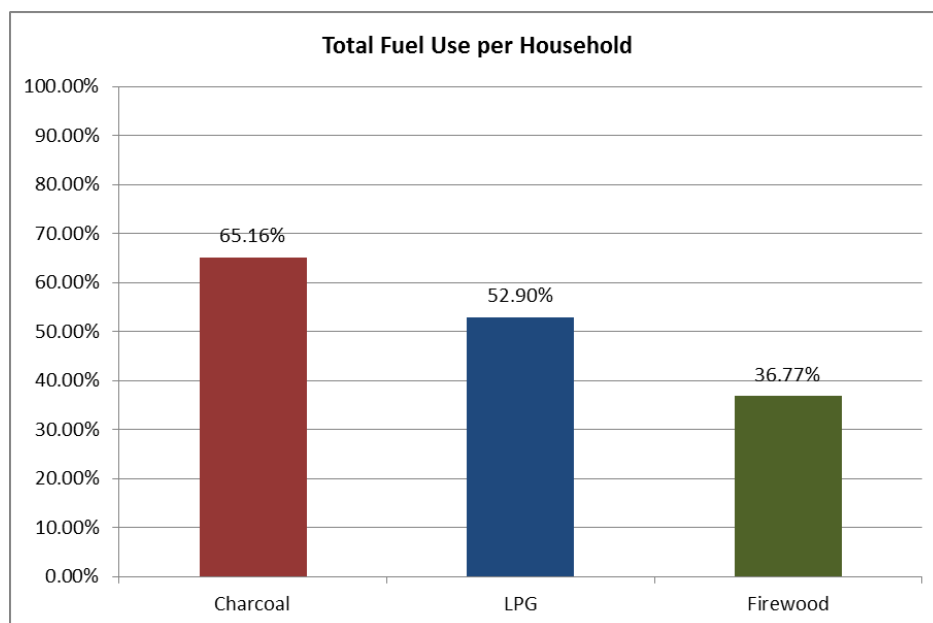


Figure 6.16, Total fuel use per household

As the educational attainment becomes higher a similar trend to the main fuel use is observed and the total fuel use is mainly represented by LPG and charcoal. In general, charcoal presents an almost equal usage trend by all educational categories, whereas LPG and firewood present almost equally opposite trends, with LPG increasing as the educational attainment advances and firewood use reduces; as shown in Figure 6.17 and Table 6.7.

The total fuel use of each area is also presented in Figure 6.18 and Table 6.8. A very similar trend to the main fuel use is observed. In Akatsi, charcoal is used in the majority of the households, almost 75%, followed very closely by LPG and lastly firewood. In Keta, LPG is present in most of the households, followed by charcoal and then firewood. In Sogakope, the use of LPG is completely non-existent, and firewood is again used in most households.

Table 6.7, Percentage of the population in relation to their educational attainment and total fuel use

	Charcoal	Firewood	LPG	Grand Total
None	14.2%	13.5%	3.2%	18.1%
PS	5.8%	1.9%	2.6%	5.8%
MS	18.1%	15.5%	6.5%	26.5%
SH	20.6%	5.2%	17.4%	25.2%
Tertiary	6.5%	0.6%	23.2%	24.5%

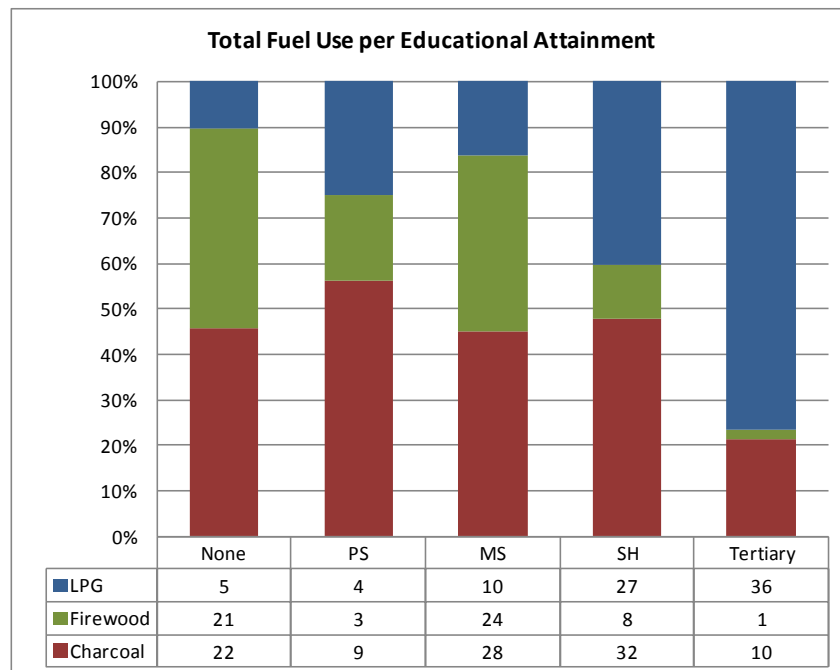


Figure 6.17, Total fuel use per educational attainment

Table 6.8, Percentages of total fuel use in relation to each area and its population

	Charcoal	Firewood	LPG
AKATSI	75.5%	17.0%	69.8%
KETA	64.1%	28.1%	70.3%
SOGAKOPE	52.6%	84.2%	0.0%

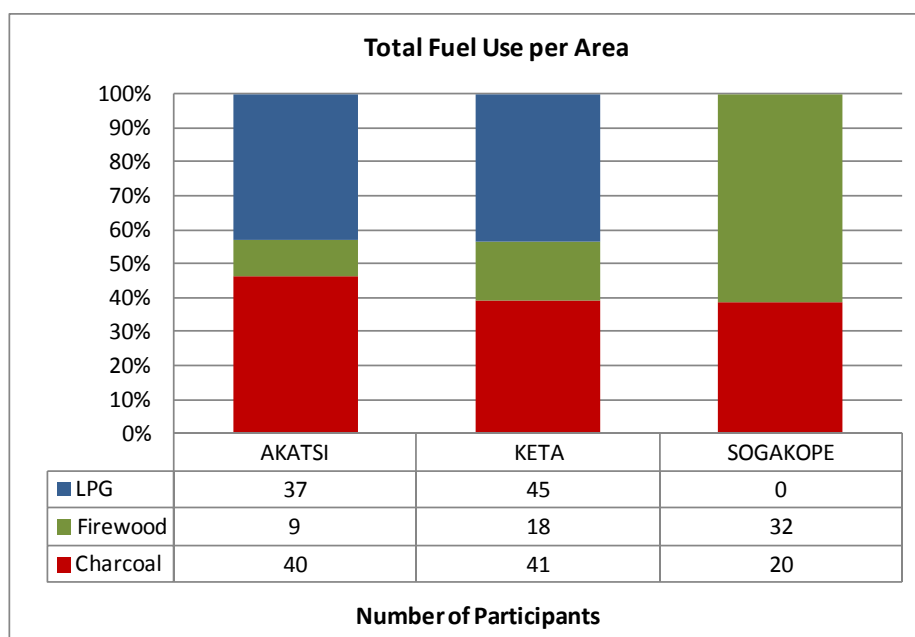


Figure 6.18, Total fuel use per area

6.2.8 Cooking Devices Use

The main types of cooking devices used in Ghana, and in agreement also to the participants' responses are:

- Gas burner
- Charcoal pot
- Local stove

A combination or individual use of the above is observed, and this is always in relation to the fuel use of the household, see Table 6.9 and Figures 6.19 to 6.23. Most of the households have gas burner and charcoal pot followed by charcoal pot and local stove.

Table 6.9, Cooking device use per fuel use

	LPG	Charcoal	Firewood	Percentage of the use of the cooking devices (%)
Gas Burner	36	0	0	23
Charcoal pot	0	17	0	11
Local stove	0	0	19	12
Charcoal pot & gas burner	41	39	0	26
Charcoal pot & local stove	0	38	38	25
Charcoal pot & gas burner & local stove	4	4	6	3



Figure 6.19, Cooking with local firewood stove



Figure 6.20, Charcoal pot



Figure 6.21, Firewood local stove



Figure 6.22, Firewood local stove



Figure 6.23, Firewood local stove

6.2.9 Daily cooking demand calculation for Ghanaian households

The above analysis provides data for the calculation of the average daily cooking demand of a typical household. The data for the total fuel use per household have been provided by the participants in different units, sizes and periods of supply. In most instances the participants gave information of the used fuels in kg according to the period of supply, which varied from a few days to 3 months. These values were averaged per month, year, and day, and the daily values were used for the calculation of the daily cooking demand. For each fuel, the adequate calorific value was used in order to convert the kg of each fuel to the common base of kWhs. Further to this, for each fuel and therefore cooking device used, the cooking efficiency differs, and what is important is to evaluate the total kWhs related to the end use. Equation (6.1) is used to calculate the cooking demand and is based

on the daily amount of each fuel used by each household. For each participant, the daily amount of each of the three fuels is multiplied with the fuel calorific value and the related fuel stove efficiency. The results of these calculations are summed for all the participants and averaged for their size, which is 155, to result to a number that represents the average cooking demand.

$$AverageCookingDemand = \frac{1}{155} \sum_{i=1}^{155} \{ [LPGDaily(kg) \times 13(kWh/kg) \times 0.45] + [CharcoalDaily(kg) \times 8.5(kWh/kg) \times 0.18] + [FirewoodDaily(kg) \times 3.9(kWh/kg) \times 0.14] \} \quad (6.1)$$

From the application of Equation (6.1), the average daily cooking demand of a typical Ghanaian household is found to be **2.50kWh**. The average size of the survey households is 5 people, consisting of children, adults and elderly, with the majority being young population. 90% of the occupants of the households in the survey are under 60 years old, as shown in Figure 6.24. Populations with youthful structure are very common in developing economies, as is the case of Ghana, with 93.3% of the population being under 59 years old and 58.3% of the population under 24 years old, according to the census of 2010 (Ghana Statistical Service, 2013).

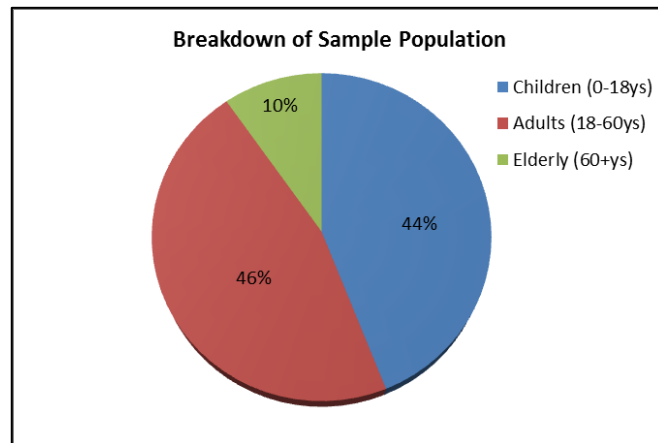


Figure 6.24, Age breakdown of the sample population

Table 6.10 shows the calculated yearly amounts of cooking fuels and the equivalent energy contents, based on the calculated cooking demand and the assumption that each fuel would be used as the only fuel for the satisfaction of the cooking demand.

Table 6.10, Average yearly fuel consumption for a typical Ghanaian household, if the demand was satisfied only by one cooking fuel

Fuel	Stove Efficiency (%) [*]	Calorific Value of Fuel (kWh/kg) [*]	Consumption (kg/year)	Consumption (kWh/year)
Firewood	14	3.9	1671.3	6518
Charcoal	18	8.5	596.5	5070
LPG	45	13	156	2028

^{*} Source: (Afrane & Ntiamoah, 2012)

6.2.10 Costs Analysis

According to the questionnaires responses the cost per kg of each fuel is shown in Table 6.11. Fuels are purchased in standard forms and sizes.

Table 6.11, Type and costs of standard fuel purchased units

Fuel	Purchase Unit	Weight (kg)	Cost of Purchase Unit (GHS)	Average Cost of Purchase Unit (£)	Average Cost per kg (GHS per kg)
Charcoal	Small Bag	10	12,15,17	3.63	1.70
	Medium Bag	20	20,25,26	5.55	1.30
	Large (No.4) Bag	50	50,60,65	13.87	1.30
LPG	Small cylinder	6	20	4.26	3.33
	Medium cylinder	13	45	9.60	3.45
	Large cylinder	15	50	10.67	3.33
Firewood	1 tie	18	5	1.07	0.28

According to the Energy Outlook of the country for 2013, the average price per small and large charcoal bag in the Volta Region was 12.75GHS/bag (£2.3/bag) and 24GHS/bag (£4.3/bag) (Energy Commission Ghana, 2013). The fieldwork data indicate that these prices are now 12-17GHS/bag (£2.2 - £3/bag) and 50-65GHS/bag (£8.95 – £11.6/bag)

according to the area, with a maximum increase of 33.33% for the small bag and 170.83% for the large bag. To provide a comparison basis, the cost in US cents and UK pennies per kWh for each fuel is calculated by Equation (6.2) and is given in Table 6.12.

$$AverageCostperFuel = \frac{1}{155} \sum_{i=1}^{155} \left\{ \frac{(GHS/month) \times (Conversion_Rate(\$cents / GHS))}{Fuel(kg/month) \times CalorificValueofFuel(kWh/kg)} \right\} \quad (6.2)$$

Table 6.12, Comparison between the fuel costs of the field study and reported 2005 data, *Source: (Ahiataku-Togobo, 2007)

Fuel	Cost (\$cents/kWh) 2014 Case Study Data	Cost UK pennies /kWh) 2014 Case Study Data	Cost (\$cents/kWh) 2005*	% Increase
Firewood	2.49	1.74	1.2	107.5%
Charcoal	4.37	3.06	1.9	130%
LPG	7.94	5.56	5.5	44.4%

In comparison to the data provided by Ahiataku & Togobo (Ahiataku-Togobo, 2007) these fuel prices are increased since the 2005 levels. The reasons are mainly the volatility and increase in oil prices that have an effect on imported LPG, and the deforestation that led to scarcity of the produced firewood and charcoal (Energy Commission Ghana, 2013).

According to the field data LPG is the most costly fuel on a cost per kWh basis, as demonstrated in Table 6.13. However, to evaluate the actual expenses of the fuel use, the annual demand for cooking by each fuel is calculated. In this case charcoal is the most expensive followed by LPG and firewood. Regardless of this fact though, lower income households insist on using firewood and charcoal. 42.37% of the charcoal users base their selection on habit of using this particular fuel but mainly because they perceive it as low-cost. This percentage is even higher for the people that use firewood, 92.6%.

Table 6.13, Fuel costs per kWh for the total fuel use of each main fuel and total cost for the average household

Fuel	Cost of fuel (GHS/kWh) Case Study Data	Cooking fuel consumption to satisfy demand(kWh/year)	Cooking fuel consumption to satisfy demand(kg/year)	Annual cost per household (GHS)	Annual cost per household (£)
Firewood	0.08	6518	1671.3	521.4	95.5
Charcoal	0.14	5070	596.5	709.8	130
LPG	0.26	2028	156	527.3	96.60

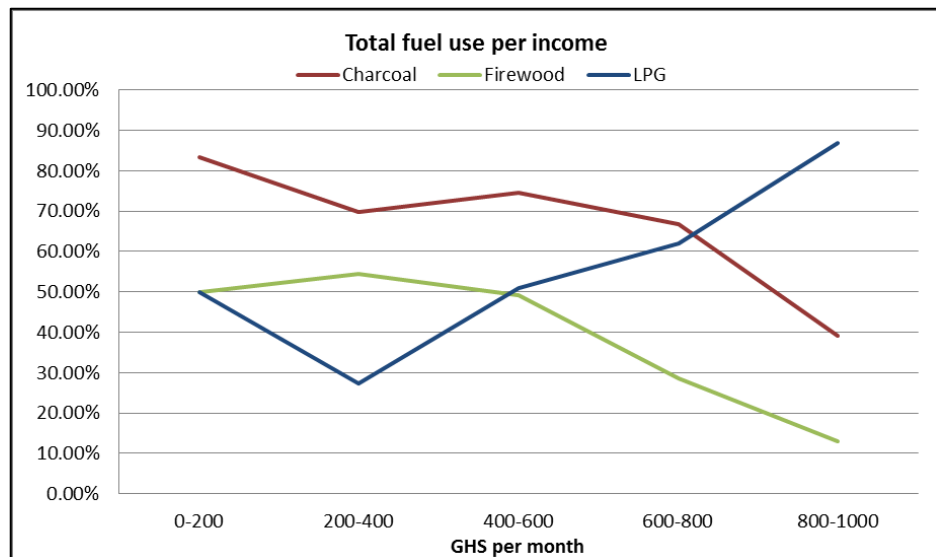


Figure 6.25, Trends in fuel use according to the household income

Figure 6.25 shows the trend between the fuel use and the household income. It is shown clearly that the use of LPG increases as the income increases whereas the use of charcoal and firewood decrease. In Figures 6.27 and 6.28 the detailed data are provided regarding main and total fuel use and income. Therefore the poor population of the sample depends mainly on solid fuels, which has an effect on their health and wellbeing. As Boadi and Kuitunen report, (Boadi & Kuitunen, 2006), the socioeconomic status of local population in Ghana has a significant impact on the respiratory health and the use of firewood and charcoal is highly associated. More particularly, they highlight that poor households are more susceptible to respiratory health problems because of their dependence on solid fuels. This is also evident in this research with 70% of the charcoal and firewood users

stating that they prefer to cook in the outside areas of the house, due to the smoke and the dirt emitted by the combustion of these fuels.

6.2.11 Percentage of cooking expenses

According to the field data the average household spends an average of 50GHS per month for the supply of cooking fuel. This corresponds to 9.12% of the average income, which is 547.6GHS per month.

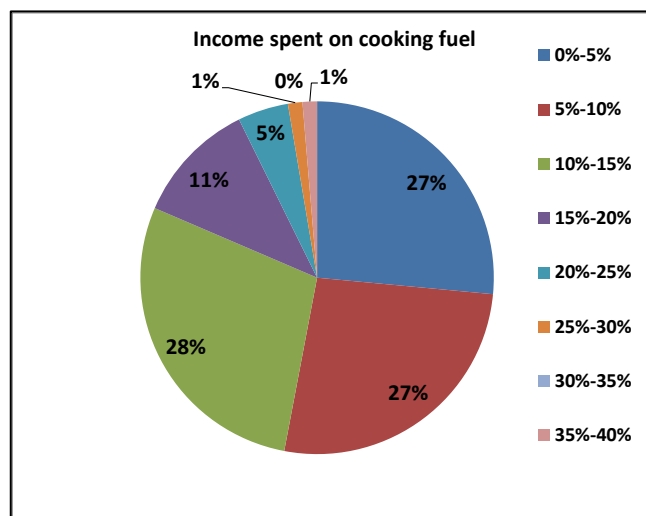


Figure 6.26, Representation of income percentages spent on cooking fuel for the total sample

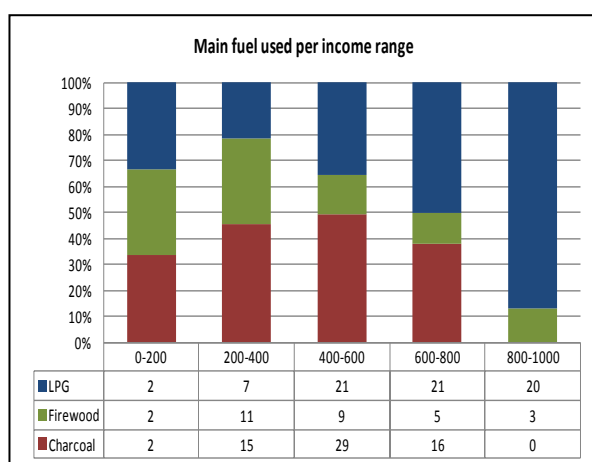


Figure 6.27, Main fuel use according to the household income

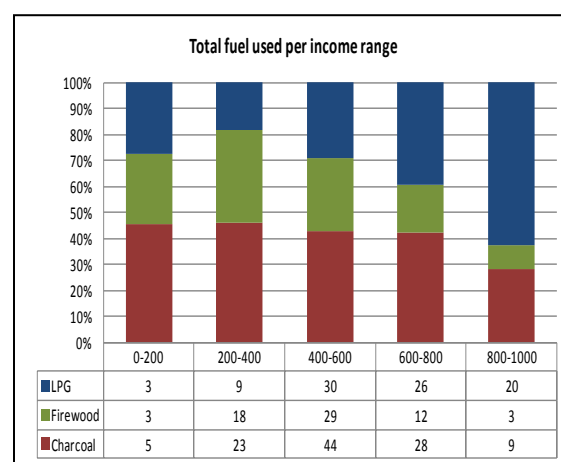


Figure 6.28, Total fuel use according to the household income

82% of the participants spent a maximum 15% of their income to purchase cooking fuel, as shown in Figure 6.26. In this percentage the extra costs for the fuel supply are also considered, which consist in the travelling costs to the fuel market. The different modes of transport to convey the fuel and the charges vary; these include motorcycle, taxi, bus and head porters. The average transport cost is 4GHS as seen in Table 6.14.

Table 6.14, Extra costs spent for the acquisition of cooking fuel

Extra costs related to the energy needs for cooking (GHS per month)								
	0	2	3	4	5	6	7	8
Percentage of the total sample (%)	11.6	3.8	10.3	48.4	7.1	12.3	0.7	5.8

6.2.12 Reasons for the main fuel selection

The key reasons for the selection of each main fuel are seen in Figure 6.29. 37.29% of the people that use charcoal and 70.37% of the people that use firewood base their selection on habit of using this particular fuel. On the contrary, the majority- 87.88%- of the people that use LPG as their main cooking fuel, prefer it as its use is neat and fast. The use of charcoal and LPG is also preferred as many participants indicate that there is reduced smoke emission of these fuels in comparison to firewood.

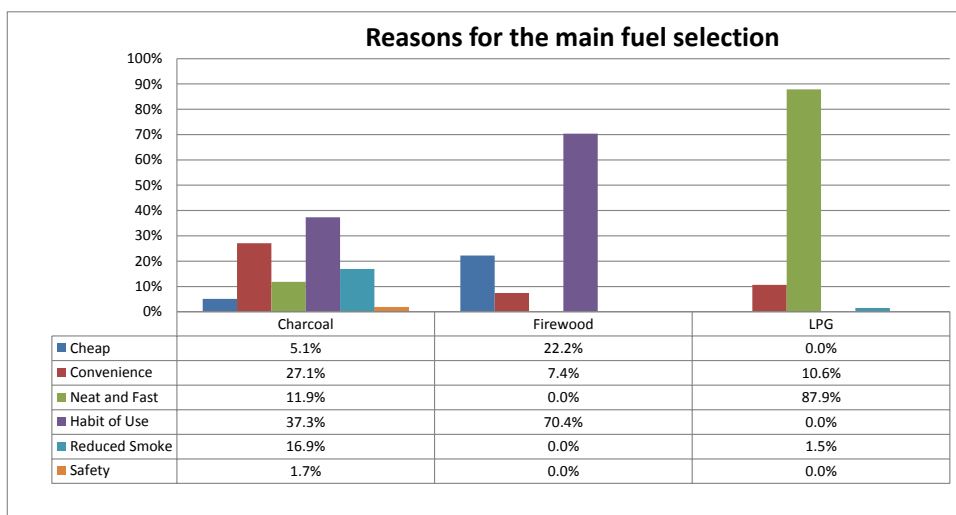


Figure 6.29, Percentages of the reason for the main fuel selection accordance to the use of each fuel

6.2.13 Would you change to a new fuel?

99.4% of the participants of the field study showed willingness to change the currently used cooking fuels, to hydrogen cooking gas. The main reasons for the switch would be if it was cheaper and safer in use than the current cooking fuels, and especially for the users of firewood and charcoal, as shown in Figure 6.30. More particular, many participants have reported problems related to smoke and dirt, linked to the use of firewood. Specifically, participants from Sogakope stated that firewood produces a lot of dirt and smoke when burned, and especially when it is not properly dried and that charcoal produces a lot of dirt. It should be noted that all participants show interest in the hydrogen technology as something new and innovative.

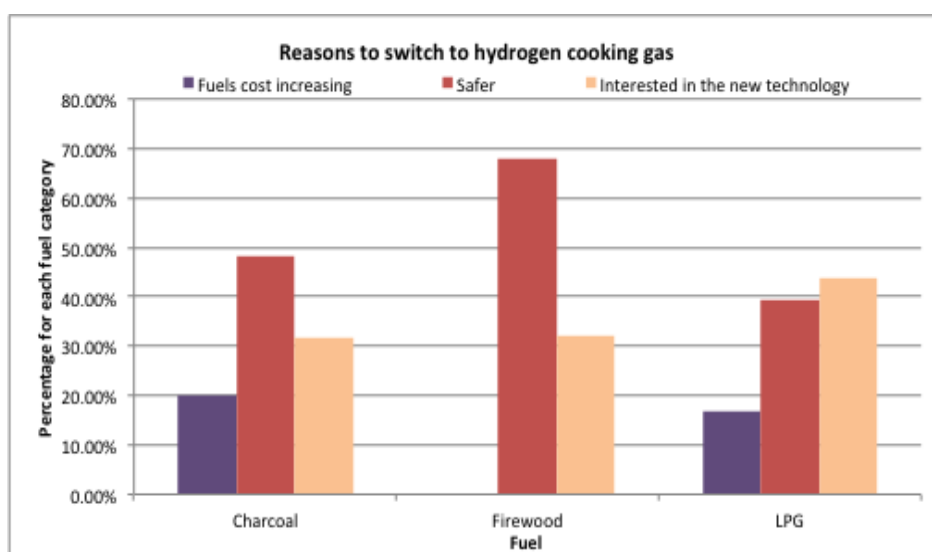


Figure 6.30, Reasons to switch to hydrogen cooking gas

6.2.14 Emissions Related to the use of the Cooking Fuels

The fuel use for the generation of cooking energy in the residential sector, firewood in particular, is the main contributor to the emissions of the country. 68% of carbon monoxide (CO), more than 50% of methane, over 70% of sulphur oxides (SO_x) and almost 70% of nitrous oxide (NO₂) emissions result from the use of solid fuels for cooking. Carbon Dioxide (CO₂) accounted for 15% of the country's emissions, as presented in Table 6.15 (Strategic National Energy Plan 2006-2020 Annex 1, 2006, p. 53).

Table 6.15, Ghana percentage share of gaseous emissions to the environment, 2000 – 2004, source (Strategic National Energy Plan 2006-2020 Annex 1, 2006, p. 53):

SECTOR	AVERAGE PERCENTAGE SHARE OF EMISSIONS 2000 - 2004							
	Greenhouse Gases				Pollutant Gases			
	CO ₂	CH ₄	N ₂ O	CO	*SO _x	*NO _x	*VOC	PM
Residential	14.5	53.0	68.6	68.5	72.2	11.6	19.6	22.4
Commercial/Services	0.2	negligible	negligible	negligible	0.1	0.3	negligible	negligible
Transport	61.6	0.4	19.1	8.0	12.4	51.8	6.4	0.7
Industry	21.5	7.0	9.3	9.0	12.5	5.6	3.0	3.4
Agriculture & Fisheries	1.4	2.4	2.4	2.5	2.5	2.4	1.0	1.2

The high economic growth of Ghana is expected to contribute to the rise of the GHG emissions by 200% by the year 2020, in comparison to the 2000 levels, see Table 6.16.

Table 6.16, GHG Emission forecast for 2015 and 2020 in CO₂ equivalent, source (Strategic National Energy Plan 2006-2020 Annex 1, 2006, p. 54):

Greenhouse Gases	2000		2004		2015		2020	
	Million Tonnes	%						
CO ₂	7	39	9	39	16	58	33	70
Methane	9	59	10	59	11	41	14	29
Nitrous Oxide	0.2	2	0.2	2	0.4	1	0.5	1
Total	16.2	100	19.2	100	27.4	100	48	100

Table 6.17, Inventory data for cook-stove emissions (kg/MJ fuel), source: (Afrane & Ntiamoah, 2012)

Item	Charcoal Stove	Biogas Stove	LPG Stove	Firewood Stove	Kerosene Stove
CO₂	5.20E-01	1.47E-01	1.20E-01	9.59E-01	1.40E-01
CO	6.00E-02	2.03E-04	1.00E-03	8.00E-02	1.23E-02
NO _x	5.19E-05	9.15E-06	5.74E-06	1.04E-04	7.17E-05
N ₂ O	0.00E+00	0.00E+00	0.00E+00	1.00E-05	1.00E-06
SO ₂	0.00E+00	1.02E-05	0.00E+00	2.10E-05	9.30E-05
NMVOC	2.00E-03	6.10E-05	1.00E-03	3.00E-03	1.43E-04
CH ₄	2.00E-03	1.02E-04	1.91E-06	3.04E-03	1.34E-05
PM	1.00E-03	4.82E-06	0.00E+00	3.00E-02	9.00E-06

Table 6.18, Annual CO₂ emissions that correspond to the used fuels of the field study

Fuel	Annual tonnes of fuel	Annual Emissions (tonnes of CO₂)	Annual Emissions (tonnes of CO)
LPG	6.07	34.1	0.3
Charcoal	29.72	472.9	54.6
Firewood	109.88	1479.5	123.4
Total	145.67	1986.5	178.3

Firewood is the fuel responsible for the greatest part of the CO₂ emissions of all the cooking fuels of the case study. Most of the firewood emissions occur during the cooking stage whereas the majority of charcoal emissions occur during production stage. This is in accordance to the study of Afrane & Ntiamoah (Afrane & Ntiamoah, 2012), who resulted amongst other that firewood contributes most to the Global Warming Potential of all the cooking fuels in Ghana. Firewood thus, is the fuel that affects the most the environment and the health of the people involved in cooking with it. This is due to the fact that

firewood not only has a high CO₂ emissions factor, as shown in Table 6.17, but it is the fuel with the biggest consumption in the field study. Taking into consideration these emission factors, the annual emission of the fuels used in the field study are calculated and correspond to 34.1tn of CO₂ from the use of LPG, 474.9tn from the use of charcoal and 1427.3tn from the use of firewood, see Table 6.18 and Figure 6.31.

Thus, replacing the use of the currently used fuels with hydrogen as a cooking fuel for the 155 households of the participants could lead to the reduction of 1986.5 tonnes of CO₂/year. This corresponds to 12.8 tonnes of CO₂/year/household. As a comparison, the CO₂ emission of the average UK household is approximately 6 tonnes of CO₂/year to include all energy use (Palmer & Cooper, 2012). According to the World Bank Data, the total CO₂ emissions of the country for 2011 were 9.9Mtonnes of tonnes of CO₂. Reducing the cooking related emissions of the Ghanaian population can thus lead to a significant CO₂ reduction of the country's and worldwide emissions.

Carbon Monoxide is also an important aspect of the emissions as it has a significantly negative impact on human health, and can even prove lethal in high concentrations (United Nations, 2014). Charcoal and firewood combustion especially, lead to high carbon monoxide emissions, as shown in Figure 6.32, and as it is odourless it can prove very hazardous. The emissions of CO of the field study fuels can be seen in Table 6.18.

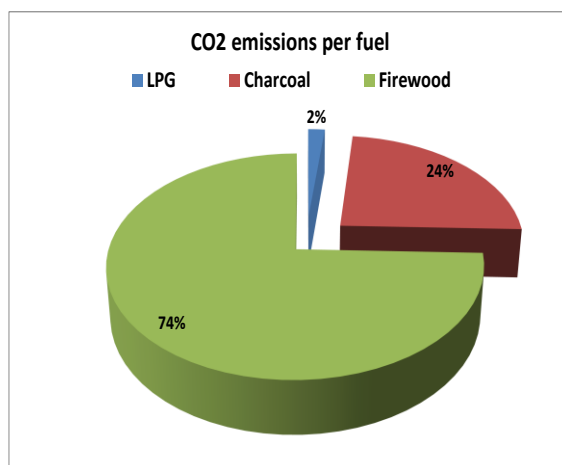


Figure 6.31, Percentage of the CO₂ emissions for each fuel

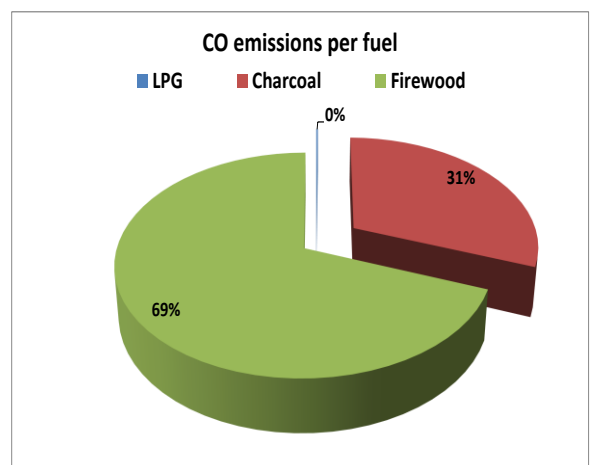


Figure 6.32, Percentage of the CO emissions for each fuel

6.3 Jamaica Case Study

6.3.1 Motivation

Jamaica is an island country of the Great Antilles in the Caribbean Sea of a population of almost 3 million people and its capital is Kingston. It has annual average solar irradiance values of 4.1-5.6 kWh/m²/day, as shown in Figure 6.33 (Loy & Coviello, 2005), and is a country well-endowed with natural resources. Nevertheless, it remains dependant on imports of petroleum products, which account for 90% of its energy mix (Planning Institute and Statistical Institute of Jamaica, 2007). The remaining 10% is covered by firewood, solar, wind, hydro, coal and bagasse, as shown in Figure 6.34 (Ministry of Energy and Mining, 2010). This situation results in high-energy import bills and cost of energy generation and distribution. The oil refinery stations use aged technology and they are at the stage of maintenance or replacement. The energy security of the country is subject to the global oil prices and availability and in the past Jamaica has suffered greatly at periods of oil crisis.

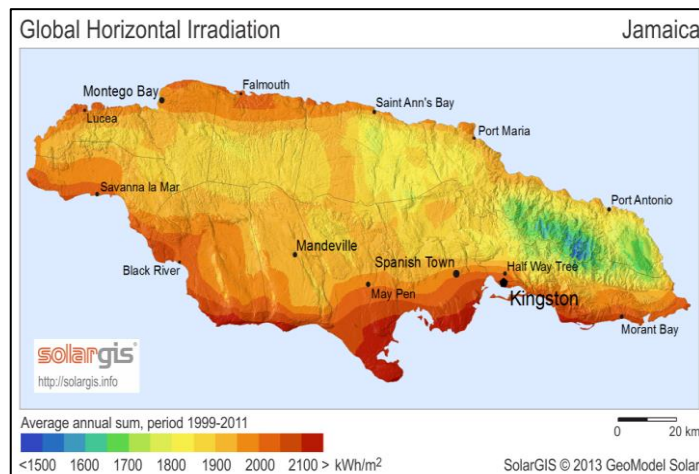


Figure 6.33, Jamaica Global Horizontal Irradiation, source: (Solar GIS, 2013)

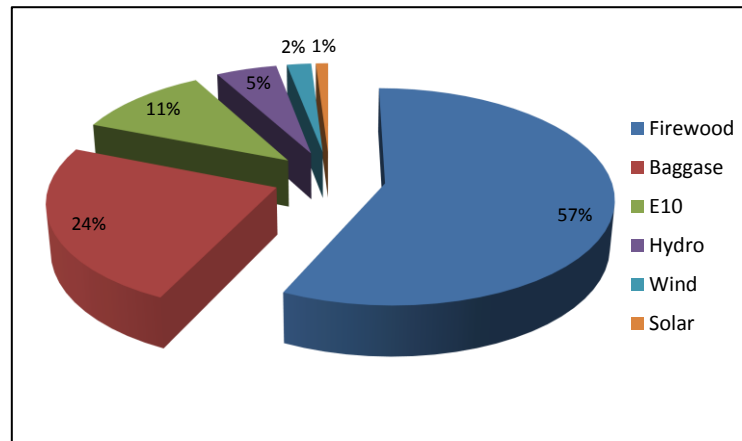


Figure 6.34, Breakdown of Energy Sources other than Oil, source: (Ministry of Energy and Mining, 2010)

The import of oil represents more than 30% of the value of all imports, and more than 100% of export earnings (Planning Institute and Statistical Institute of Jamaica, 2007). Cooking is one of the activities that are highly affected by the instability of the energy supply, as it mainly depends on LPG. As seen in Table 6.19, 86% of the overall Jamaican households use LPG for cooking, with firewood and charcoal being the second most popular. There are many rural houses that use only firewood and charcoal.

Deforestation is of particular concern in Jamaica because of the frequency of extreme climate-related events like droughts, flooding, tropical storms, and hurricanes that the Caribbean region has experienced in recent times. These events cause environmental impacts such as loss of soil in agricultural areas, silting of the oceans, and loss of biodiversity. Charcoal is produced from cutting and burning of trees. This is a non-managed process, as the trees cut by charcoal burners are not replanted, resulting in high rates of deforestation. The past 20 years the forest area in Jamaica has steadily declined by almost 0.1% per year, leading to a 2.5% reduction which corresponds to a total of over 250 km² forest area (Owen & Camirand, 2000). The wood is usually converted to charcoal in out-dated, inefficient charcoal furnaces, which visibly pollute the atmosphere, with smoke, particulates, CO₂ and other gases. Figure 6.35 shows that there is a trend between CO₂ emissions and fossil fuel consumption. This condition intensifies further in periods of economic crisis and in periods of high volatilities in oil prices.

Within this context, the Government of Jamaica engaged into the National Energy Policy 2009-2030, which seeks to create an efficient, diversified, and environmentally sustainable energy sector (Ministry of Energy and Mining, Jamaica, 2010). Producing electrolytic hydrogen using solar energy is a sustainable process within the scope of this energy policy.

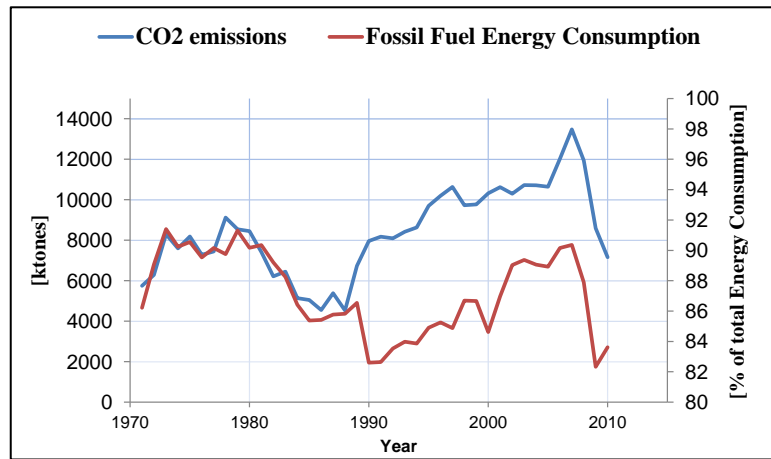


Figure 6.35, CO₂ emissions in relation to fossil fuel consumption in Jamaica, source: (The World Bank, 2014)

Table 6.19, Distribution of households by source and use of energy for cooking, source (Planning Institute and Statistical Institute of Jamaica, 2007)

	Electricity	Kerosene	LPG	Charcoal	Firewood	Solar	Total
% of Households	1.3	0.4	86	5.2	7.1	0	100

6.3.2 Daily cooking demand calculation for Jamaican households

The cooking profile of a typical Jamaican household is calculated through the use of Equation (6.3) based on data provided by the Planning and Statistical Institute of Jamaica (The Planning Institute and the Statistical Institute of Jamaica, 2007), as seen in Table 6.20. The average size of the LPG cylinders is multiplied to the LPG calorific value and the LPG stove efficiency, and averaged over the period of supply.

Table 6.20, Size, Price and Durability of LPG Cylinders in Jamaica, source: (The Planning Institute and the Statistical Institute of Jamaica, 2007)

Cylinder Size	Means					
	Urban		Rural		All	
	Unit Price (JM\$)	Weeks Lasted	Unit Price (JM\$)	Weeks Lasted	Unit Price (JM\$)	Weeks Lasted
20lb	949.5	6.85	1101.82	6.90	1003.55	6.87
25lb	1144.66	7.71	1154.54	7.56	1149.27	7.64
30lb	1236.92	8.74	1297.89	7.31	1268.06	8.01
100lb	3744.17	22.97	3911.78	21.64	3802.64	22.53

$$CD_j = \frac{LPG_{cyl_j} (kg) \times CVLPG (kWh / kg) \times LPG_{eff}}{(days)} \quad (6.3)$$

The average daily cooking demand of a typical Jamaican household is found to be **1.98kWh**.

6.4 Indonesia Case Study

6.4.1 Motivation

A third case study for the application of the solar hydrogen system is selected to be Indonesia, see Figure 6.36. Indonesia is a country in Southeast Asia and Oceania, with a population of approximately 250 million. It is the fourth most populated country on the planet and consists of 17,508 islands, about 6,000 of which are inhabited. The largest are Java, Sumatra, Borneo (shared with Brunei and Malaysia), New Guinea (shared with Papua New Guinea), and Sulawesi. The capital, Jakarta, is on Java and is the nation's largest city.



Figure 6.36, Indonesia in the globe, source: (International Energy Agency, 2008)

In terms of weather conditions, Indonesia is characterized by a monsoonal climate, with a wet (December – March) and a dry period (June – September). Average annual rainfall in the lowlands varies from 1,780–3,175 millimetres and up to 6,100 millimetres in mountainous regions. Mountains receive the highest rainfall. Humidity is generally high, averaging about 80%. Temperatures vary little throughout the year; the average daily temperature range of Jakarta is 26–30°C (Weather Online, 2015).

Deforestation and the destruction of peat lands make Indonesia the world's third largest emitter of greenhouse gases. Indonesia is a major consumer of traditional biomass in the domestic sector, especially in the remote rural areas. As can be seen in Figure 6.37, the household sector is the second most energy demanding, with 31% of the total demand in 2012. 72.1% of the household energy demand in 2012 was satisfied by firewood, followed

by LPG and electricity, as shown in Figure 6.38. Firewood is predicted to have a continuous major presence in the energy mix, with almost 45% at 2035 (BBPT, 2014). 69% of the people that live in rural areas and 19% of the urban inhabitants use firewood to cook (Huboyo, et al., 2013) Energy poverty is a major social issue in the country as the poor are forced to use pollutant and time demanding energy sources to cook in inefficient traditional cooking devices (Gunningham, 2012). According to the International Energy Agency, 72% of the total population of Indonesia depends on fossil based fuels for cooking, i.e. almost 170 million. This percentage is even higher in the rural population, at 95% (IEA, 2006).

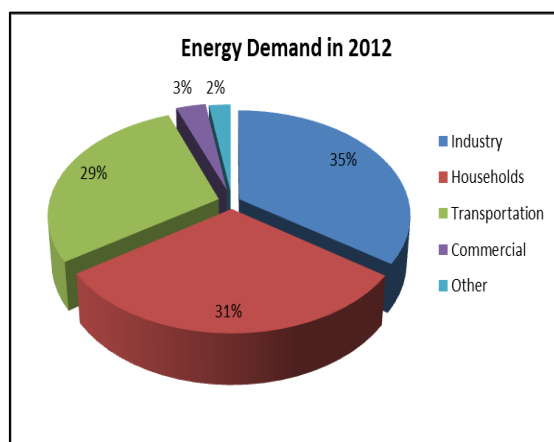


Figure 6.37 Indonesia energy demand by sector in 2012, source: (BBPT, 2014)

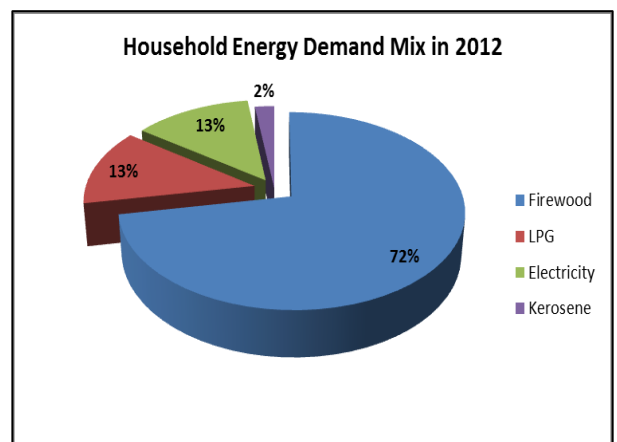


Figure 6.38, Indonesia primary energy demand mix in 2012, source: (International Energy Agency, 2013); (Hasan, et al., 2012)

The fuel mostly used for cooking has traditionally been kerosene, which was subsidised by the Indonesian government. This subsidy was a major cost burden for the state as it reached the equivalent of 18% of the state expenditures and 57% of the total petroleum products subsidy in 2008 (Pertamina, 2008). Subsidised fuels in Indonesia are amongst the cheapest in Asia, and are rated at around 30% of world prices. The prospect to reduce this subsidy was a risk in terms of social implications but at the same time the subsidy was not reaching its final target due to misuse and fuel smuggling in the oil supply industry (Pertamina, 2008). Due to the increase in oil prices the subsidy presented an increasing tendency too, and therefore it became imperative for the government to find a solution to replace kerosene with a cheaper fuel. Further to this, the use of firewood and charcoal is also widespread in Indonesia especially in areas where kerosene supply was not

guaranteed at all periods due to bad weather and unapproachable areas. In this spirit, the programme to replace kerosene with LPG was launched. The LPG subsidy is much smaller, as the end user energy equivalent of LPG is much higher. In addition to the financial benefits the replacement of kerosene with LPG had multiple targets:

- To improve indoor air quality and the health of the people (mainly women and children) that was seriously impaired by the use of kerosene and the other solid fuels
- To reduce greenhouse gas emissions and deforestation
- To eliminate time and labour to gather biomass for cooking
- To improve cleanness and convenience in cooking

This programme was implemented by the Indonesian government and Pertamina (Pertamina, 2008), which is the national oil and gas company and is indicative of the willingness to introduce alternative cooking fuels. Additional programs of fuel and stove replacement are implemented, through the introduction of more efficient firewood, biofuel and biogas stoves (EEP, 2013)

Furthermore, with a total of over 400Mtonnes of energy related CO₂ emissions in 2011, and a prediction that they will rise to above 800 Mt in 2035; Indonesia has adopted emission reduction targets, according to the Copenhagen Accord (International Energy Agency, 2013). The country has introduced various renewable energy enhancement plans such as the reduction of the oil, gas and coal in the energy mix, as indicated in Figure 6.39.

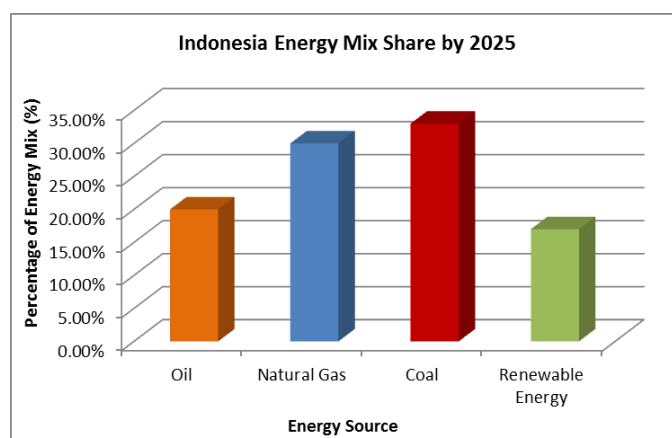


Figure 6.39, Indonesia energy mix share by 2015, source: (Mujiyanto & Tiess, 2013)

With a population rise to almost 302 million by 2035, and the increasing energy demand, Indonesia will become a net importer of energy. This condition that poses a risk on energy

security in combination with the commitment to reduce emissions, lead to an increase in renewable energy investments (Mujiyanto & Tiess, 2013). The country already includes in its renewable energy policy the investment and creation of small hydro power plants, as well as biofuel, palm fuel and solar energy industry (Winrock International, 2007). This policy and the abundant natural resources of the country (75.67GW hydro and 4.8kWh/m²/day solar), (MEMR, 2011), can act as a support to the evaluation of the application of the solar hydrogen system to produce hydrogen as an alternative cooking fuel. So far solar energy has been used for rural electrification in off grid applications and solar thermal applications. A solar hydrogen plant can promote even further the solar power applications and also provide with an alternative fuel much cleaner and sustainable than biofuels, or palm oil which causes extreme deforestation for the growth of palm tree plantations (Rainforest Action Network, 2014).

6.4.2 Daily cooking demand calculation for Indonesian households

The average daily cooking profile of a typical Indonesian household is calculated through the use of Equation (6.4) based on the data provided by the kerosene to LPG gas conversion programme in Indonesia, (Pertamina, 2008), as shown in Table 6.21 and is found to be **2kWh**.

Table 6.21, Size and durability of LPG and kerosene cylinders in Indonesia, source: (Pertamina, 2008)

	Size (kg)	Days lasted
LPG cylinder	3	10.6
Kerosene cylinder	3.4	7

$$CD_I = \frac{1}{2} \sum \left\{ \frac{LPGcyl_I (kg) \times CVLPG (kWh/kg) \times LPG_{eff}}{(days)} + \frac{Kcyl (kg) \times CVK (kWh/kg) \times K_{eff}}{(days)} \right\} \quad (6.4)$$

6.5 Summary

Energy use with a focus on domestic cooking and its fuels in rural Ghana, Jamaica and Indonesia was examined in this Chapter 6. The domestic daily cooking demand profile was calculated as 2.5kWh/day for Ghana, 1.98kWh/day for Jamaica and 2kWh/day for Indonesia.

A quantitative survey in the form of questionnaires and on site interviews of 155 participants was carried out in Ghana. The collected data and analysis indicated that even though charcoal and firewood still dominate as cooking fuels especially in the low income and low educational attainment households, there is a preference towards LPG as a main cooking fuel, with 43.23% of the participants using it as their main fuel.

In addition to that firewood and charcoal are responsible for 98% of the CO₂ and 100% of the CO emissions from cooking. Indoor air pollution that is related to the use of these fuels and their combustion in open flames and traditional cooking devices is reported to be a problem in all three case study countries.

People driven from the rising cost of the current fuels and the problems related to their use are willing to try a new fuel, as indicated by the positive response of 99.35% of the participants in Ghana case study.

Therefore, the application of the solar hydrogen system as a means of providing a new, clean, cost effective and safe cooking fuel in the case study countries will be examined in the Chapter 7.

**Chapter 7. Case Studies Numerical Model
Development and Weather Data Effect on
Simulation**

7.1 Introduction

Based on the daily average cooking demand profiles for Ghana, Jamaica and Indonesia calculated in Chapter 6, case studies for the selected countries are developed in this chapter. The cooking demand profile is used to size solar hydrogen plant case studies for rural communities based on the TRNSYS numerical model developed and presented in Chapter 4. The optimised system and its effectiveness are analysed through multiple sets of simulations in TRNSYS.

Case studies are developed for small communities of 20 households in each country. The design consists of a central plant, where the electrolysis process is powered by PV panels. Hydrogen is generated at low pressure (13.8bar), directly stored in metal hydride cylinders and distributed to the households on a monthly basis. Different PV system and timeframe scenarios are examined; direct connection of the PV array and the electrolyser and connection through a PV-battery system. These two variations are examined for current conditions and after a 20 year timeframe, which takes into consideration the PV panel degradation period. The systems are designed and optimised as autonomous in order to meet the hydrogen demand at the minimum cost of energy.

7.2 Design and Optimisation Methodology of the Solar Hydrogen system

The design and optimisation of the solar hydrogen system plant is the most critical stage in the simulation process. The challenge of the system design is to satisfy the cooking demand by sizing the system power components in the optimum cost effective way. Many researchers have reported work on the optimisation of similar systems. Degiorgis et al. (Degiorgis, et al., 2007) have presented a techno-economic analysis and optimisation strategy of a renewable hydrogen based power system. Guinot et al., (Guinot, et al., 2014), Behzadi and Niasati, (Behzadi & Niasati, 2014) and Zhou et al. (Zhou, et al., 2007), describe optimisation techniques for power management strategy in solar hydrogen systems. The importance in control and design strategies in PV powered hydrogen systems is also highlighted in the work of Ulleberg (Ulleberg, 1998; Ulleberg, 2004). This work followed the methodology described by Zoulias and Lymeropoulos (Zoulias & Lymeropoulos, 2008) and the basic steps are described in sections 7.2.1 to 7.2.6 and Figure 7.1.

7.2.1 Identification of cooking loads

As mentioned before, the cooking demand is the most critical factor for the sizing of the solar hydrogen system. For this work this has been calculated as described in chapter 6. The cooking profile variation was also defined, and all possible fluctuations were taken into consideration. The hourly profile presents the same trend every day and it is shown in Appendix E. The cooking profile defines suitable storage size and type while seasonal and annual storage are typical options. In this case storage is monthly defined by current practice; the Ghana survey and the Jamaica review, indicate that the most common frequency of fuel supply is once a month.

7.2.2 Decision of the appropriate renewable energy sources

The second step in the design process is to decide the renewable energy type. In this decision two main factors are taken into consideration:

- i. The availability of renewable energy sources for the location examined, e.g. solar, wind, hydro etc.
- ii. The available space for the installation
- iii. The costs related to the installation

In this study, solar energy was selected, as defined by the main aims of this project demonstrated in Chapter 1 of this thesis.

7.2.3 Identification of the weather data to be used in the simulation

In order to evaluate the performance of the system, weather data related to the selected renewable energy source as well as the location are necessary. These can either be actual data for a set of many years or data from a Typical Meteorological Year (TMY) file, which represent the typical weather conditions for a location. Solar irradiance, temperature, wind speed and relative humidity are typical values included in these data. In this study, Typical Meteorological Year files were used, from Meteonorm 7 (Meteotest, 2014). Furthermore, for the Jamaica case, recent weather data for the period 2010-2013 were available from a weather station installed in the University of Technology. These data were also used in simulation runs to compare with TMY weather file simulations (presented in Chapter 8).

7.2.4 Identification of the major power components of the system and the control strategy

All the major power components of the solar hydrogen system included in the simulation were identified as:

- i. PV array
- ii. Inverter
- iii. Battery
- iv. PEM electrolyser
- v. Controls
- vi. Hydrogen storage
- vii. Hydrogen stove

The components that could be used directly through the data base of the TRNSYS software were identified, and these were the PV panels, the inverter and the battery. For the simulation of the PEM electrolyser, its controls, the metal hydride storage cylinders and the hydrogen stove, user defined components were developed. More specifically, the novel components based on FORTRAN programming, as presented in Chapters 4 and 5, were used for the PEM electrolyser, the controls unit and the metal hydride storage cylinders.

In this step the management strategy is also defined. As mentioned in 7.2.1, a monthly supply strategy is adopted. The total monthly hydrogen production should be able to provide enough hydrogen for the following month. The monthly demands are constant, depending on the month period (30, 31 or 28 days for February).

After the basic major components were selected and created and the supply strategy decided, preliminary tests were run to define the best technical component configuration. The efficiencies, life span and load curves are taken into consideration as well as technical parameters of the system components. All combinations of the equipment sizes and power ranges were evaluated and multiple iterations were run until the most suitable designs were achieved.

7.2.5 Cost analysis of the different feasible power component configuration and sensitivity analysis of the impact of different equipment costs on the total cost

A cost analysis of the system configurations is carried out. Cost data from the equipment manufacturers are gathered or additional cost data from available relevant data bases. A comparison between the costs of the different components is carried out and is critical for the various sizing options and optimisation of the system configuration; e.g. selecting a bigger PV array could be more cost effective than a bigger battery bank. An overall cost analysis, taking into account capital and O&M costs is conducted and the net present value of each configuration is presented in Chapter 9.

A sensitivity analysis is also a significant part of the cost analysis process, as it presents the impact of the cost of each component on the total cost of the energy generated by the system. In the case of the solar hydrogen system, this is very important as the prices of the electrolysers are currently still high, but are predicted to drop in the future and this has an effect on the total costs of the system.

7.2.6 Evaluation and interpretation of the results analysis

The combination of steps 7.2.4 and 7.2.5, results in the optimum design decision for the system. The equilibrium between demand satisfaction and costs has been analysed and determines the final decision of the system size and configuration. Demand satisfaction is always the first priority but over dimensioning a power system should be avoided in such cases where the shortage effect is minimal but the cost implications are significant. The system is designed so that the extra hydrogen production acts supplementary for the months that there is shortage, and a regulated operation and fuel supply is guaranteed for both scenarios. A small annual shortage results in costs savings in comparison to oversizing a system.

Based on the above, the design and optimisation methodology for this research was developed. The strategy can be also summarised in the block decision diagram of Figure 7.1.

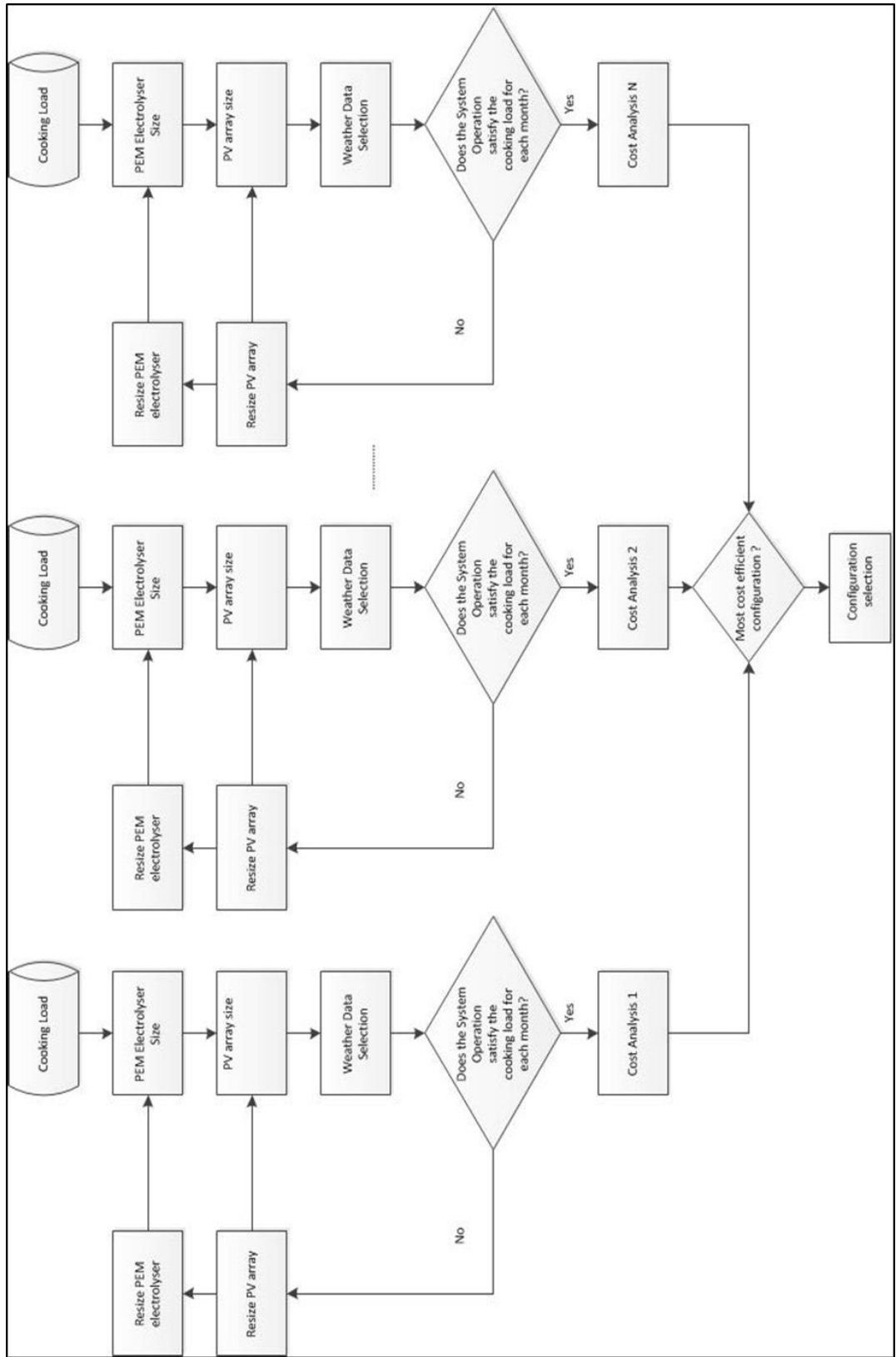


Figure 7.1, Flowchart of the system design decision making

7.3 Case Studies Development

In this part the application of a large scale solar hydrogen system based on the developed numerical model is presented. The analysis performed is based on, sizing the components and their parameters adequately to satisfy small communities of 20 households each, and the methodology is described in section 7.2 of this chapter.

3 case studies are developed, one for each community:

- Jamaica rural community of 20 households
- Ghana rural community of 20 households
- Indonesia rural community of 20 households

The systems are designed and optimised as autonomous systems to meet the hydrogen demand at the minimum cost of energy. In each system there are parameters that change such as meteorological data and cooking load profiles. This will affect the size of plant components such as photovoltaic panels, inverter, the PEM electrolyser, controls and hydrogen storage. The timestep for the simulations is one minute and the error tolerance is set at 0.01 (University of Wisconsin - Madison, 2012). Two technological and two timeframe scenarios are examined for each case study: Direct connection of the PV array to the electrolyser and connection through a battery bank, for current application and after a 20 year panel degradation period.

The photovoltaic panels characteristics used for all the systems are the TrinaSolar TSM-180DA01, with a rated power of 180W (Civic Solar, 2015) . These panels were selected as they are used as the actual power source in the existing small scale solar hydrogen system in the University of Technology, in Kingston, Jamaica. Additionally, they present a low cost and efficient solution for application in developing economies where cost has a significant impact factor on energy projects.

7.3.1 Ghana Case Study

Direct Connection of PV array and Electrolysers

The TRNSYS model for the simulation of the Ghana case study for direct connection of PV array and electrolyser is shown in Figure 7.2. The electrolyser is supplied through the PV, according to their yield which depends on the weather data.

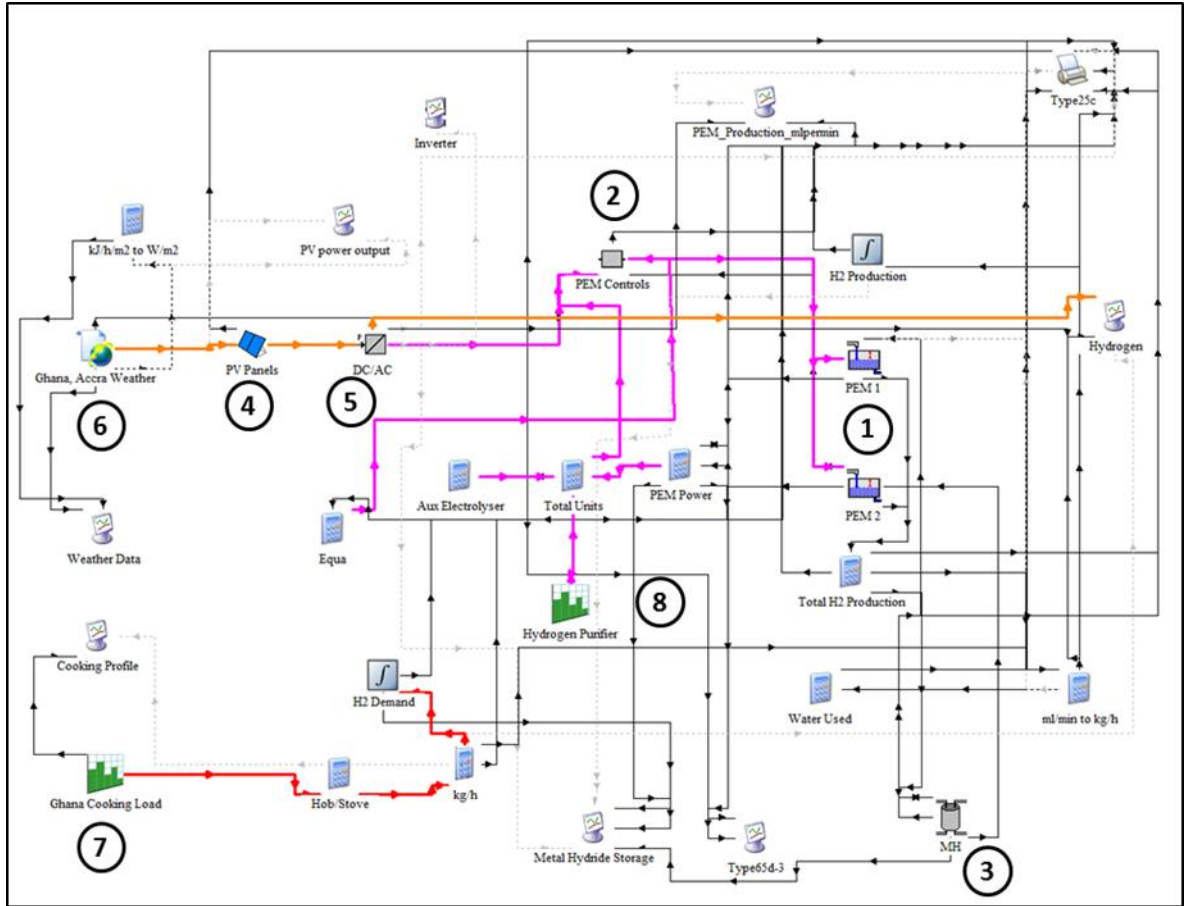


Figure 7.2, Ghana direct connection case study TRNSYS print screen

The model's main parts consist of the PV array (4) that supplies the PEM electrolyser (1) through an inverter (5), the electrolyser auxiliary components (controls (2), and gas management parts (8)), and the metal hydride storage components (3). It also includes the necessary weather data (6) for the simulation, the cooking load profile for the application (7) and other computational components.

The cooking load for each household is the factor that determines the hydrogen demand and thus the size of the electrolyser and the photovoltaic array. From the field data presented in Chapter 6, the cooking demand was estimated as 2.5kWh/day, for the average household, which consists of 5 occupants. With hydrogen stove efficiency of 60%, this is equivalent to 4.20kWh/day of hydrogen or 0.1072kg of hydrogen per day, according to Equation (7.1):

$$\frac{4.2\left(\frac{kWh}{day}\right)}{141.1\left(\frac{MJ}{kg}\right)} = \frac{4.2\left(\frac{kWh}{day}\right)}{39.19\left(\frac{kWh}{kg}\right)} = 0.1072\left(\frac{kg}{day}\right) \quad (7.1)$$

$$3.6\left(\frac{MJ}{kWh}\right)$$

Therefore, for the 20 households 2.15kg of hydrogen per day are necessary, and depending on the days of each month, the monthly demand varies slightly from 60.2 kg/month in February to 66.7 kg/month with an annual requirement of 785 kg.

Thus, the numerical model system needs to be of adequate size so as to satisfy each monthly demand.

PV array

For the system sizing, the performance degradation of the PV panels over time has to be taken into consideration (Zhou, et al., 2007; Guinot, et al., 2014). The panels will not perform as efficiently after a decade but the amount of produced hydrogen has to be the same. Therefore, the panel degradation rate is taken into account for the sizing. According to NREL, (NREL, 2012), the degradation rate for monocrystalline panels, for installations after 2000, is 0.36%. Therefore, for the Trina Solar panels the annual degradation rates are calculated resulting to 167.47 kW at the end of year 20 with a corresponding 93.04% of the initial rated power. This means that the photovoltaic array should be oversized by 6.96% of the required initial size that satisfies the demand. The photovoltaic panels array consists of 430 panels, of maximum rated power 77.4kW requiring 546m². The experiments indicated that the electrolyser works more efficiently when it operates continuously and is not subject to stops and start-ups. Therefore, the purpose of the photovoltaic system size is to ensure this operation. The TRNSYS component used to simulate the PV panels is type 194 that determines the electrical performance of crystalline panels based on the 5 parameter model presented by DeSoto et al. (University of Wisconsin - Madison, 2014).

Metal Hydride Storage

For the metal hydride storage it is assumed that each household will have a storage tank able to satisfy the monthly demand which will be replaced with a full one for the following month. Therefore, the tank size should be 67kg for 20 houses or 3.35kg for each house.

The amount of the metal hydride alloy of each tank is calculated according to the hydrogen absorption ability of the selected alloy. In this case LaNi₅ is chosen, as it is the metallic alloy of the experimental part and the numerical model component. The hydrogen absorption ability of LaNi₅ is 150ml/gr, therefore for each household Equation (7.2) gives the quantity of the alloy necessary in each tank:

$$LaNi_5 \text{ _content} = \frac{3.35(kg)}{150\left(\frac{ml}{gr}\right) \times 10^{-6} \left(\frac{Nm^3}{ml}\right) \times 0.0899\left(\frac{kg}{Nm^3}\right)} = 248.4kg \quad (7.2)$$

The electrolyser is connected directly to the metal hydride storage, and the hydrogen is stored and distributed to the households at the generated pressure, which is 13.8bar.

PEM Electrolysers

Two electrolysers are selected for the Ghana case study, based on the developed PEM numerical model presented in Chapter 5. They are designed and sized in order to satisfy the demand, based also on market parameters and actual technology sizes (Proton Onsite, 2014). The parameters of each one are shown in Table 7.1.

Table 7.1, Each PEM electrolysers' parameters in the Ghana case study

Maximum Hydrogen Production rate (Nm ³ /h)	2
Number of stacks	4
Number of cells	20
Cell area (cm ²)	92
Stack current (A)	110
Maximum Stack Power (kW)	10.25
Hydrogen generation pressure (bar)	13.8
Stack efficiency	63.6%

Weather data

The weather data used in the simulation for the Ghana case study is composite TMY data from Meteonorm 7.0 database from the weather station in Accra (Accra, id: 3888, WMO id: 654720) (Meteotest, 2014). The weather station includes radiation measurements and the data of the TMY refer to a radiation period from 1991 - 2010 and a temperature period from 2000 - 2009. The weather processor is simulated by type 15-6 component for Meteonorm files weather data processor, form the standard weather data processors library of TRNSYS (University of Wisconsin - Madison, 2014). The annual global horizontal irradiance and temperature values are shown in Figure 7.3. The minimum yearly average temperature is 20.5°C and the yearly maximum is 26°C. The irradiance and temperatures in Ghana present a period of minimum values during the summer months, June, July, August and September. This is the irradiance profile of near equatorial regions, such as Ghana, that is only a few degrees north of the equator. This period corresponds partly to the rain season in Ghana, (World Weather and Climate Information, 2013).

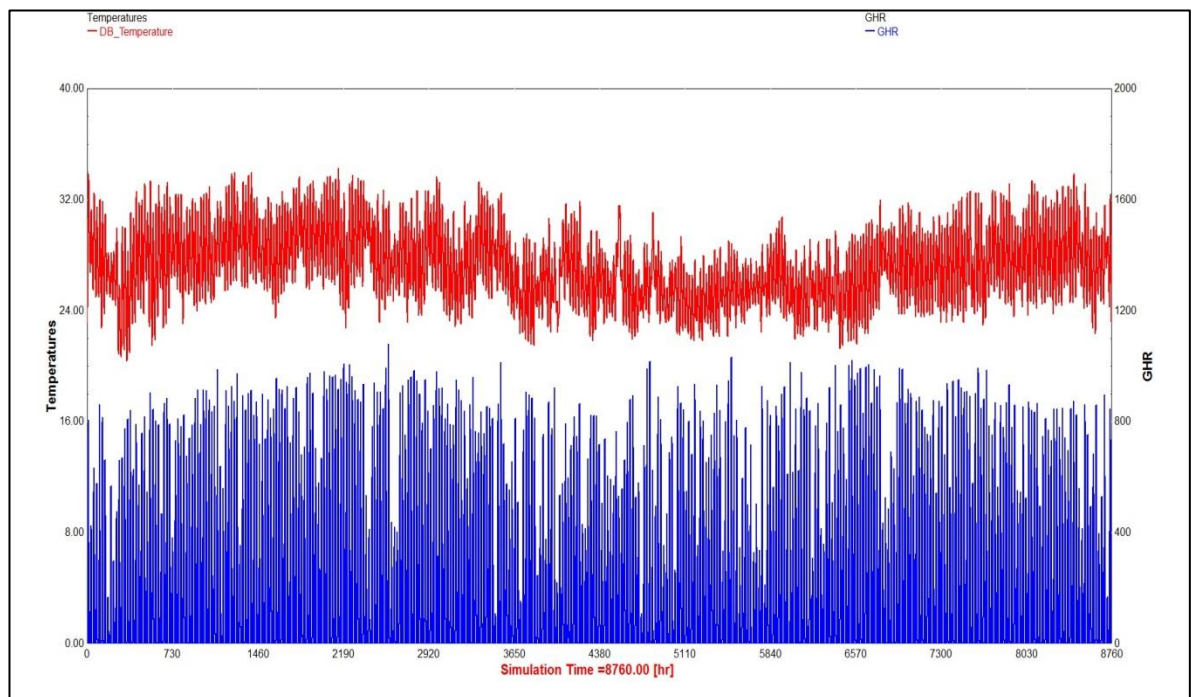


Figure 7.3, Ghana annual global horizontal irradiance and temperature values from Meteonorm file

Inverter Characteristics

The inverter is necessary to convert the photovoltaic DC power to AC power for the electrolyzers. In this case study the inverter's size is 78kW maximum power, based on market parameters and actual technology sizes (SMA Solar Technology AG, 2013). The TRNSYS component used is the 48.b type with maximum inverter efficiency of 96% and a high limit of fractional state of charge of 0.95 (University of Wisconsin - Madison, 2014).

System Operation

Figure 7.4 shows the TRNSYS simulations results, for the month of May of the Meteorological Typical Weather Year as an indicative month of the annual simulation. It can be observed that the maximum amount stored for distribution (purple line) follows the hydrogen generation (light blue line) until it reaches the maximum point. The results of the simulation are in accordance to the numerical model, and when the metal hydride tank reaches the peak point of the charging phase (see Chapter 5, section 5.2.1) the charging flow rate from the electrolyser and thus the power demand is reduced. This is observed at 3314hs in Figure 7.4 where the hydrogen flow rate is reduced from 342634ml/min to 28997ml/min, and stack power demand is reduced from 20.5 kW to 17.4 kW. Figure 7.5 shows the monthly hydrogen demand and equivalent production in kg for the current conditions and after the 20 year period. The production, of the preceding month has to satisfy the demand of the following month, as the purpose is to supply the consumers on a monthly basis. The system is designed so that the extra hydrogen production acts supplementary for the months there is shortage, and a regulated operation and fuel supply is guaranteed for current and future scenarios. There are eight months in the year where the production is over satisfying the demand. This extra hydrogen acts as a balance in the months where production is less.

To provide with a system that the production would be higher than the demand in the months that present shortages (July, August and September) would mean oversizing significantly and this would also have an effect on the cost. The designed system provides with 815kg of hydrogen at current conditions, and 783.4kg of hydrogen after the 20 year period and satisfies the demand by 30kg extra of hydrogen per year at current conditions.

Table 7.2 shows the generation rates of the system and also the performance degradation on the PV array output.

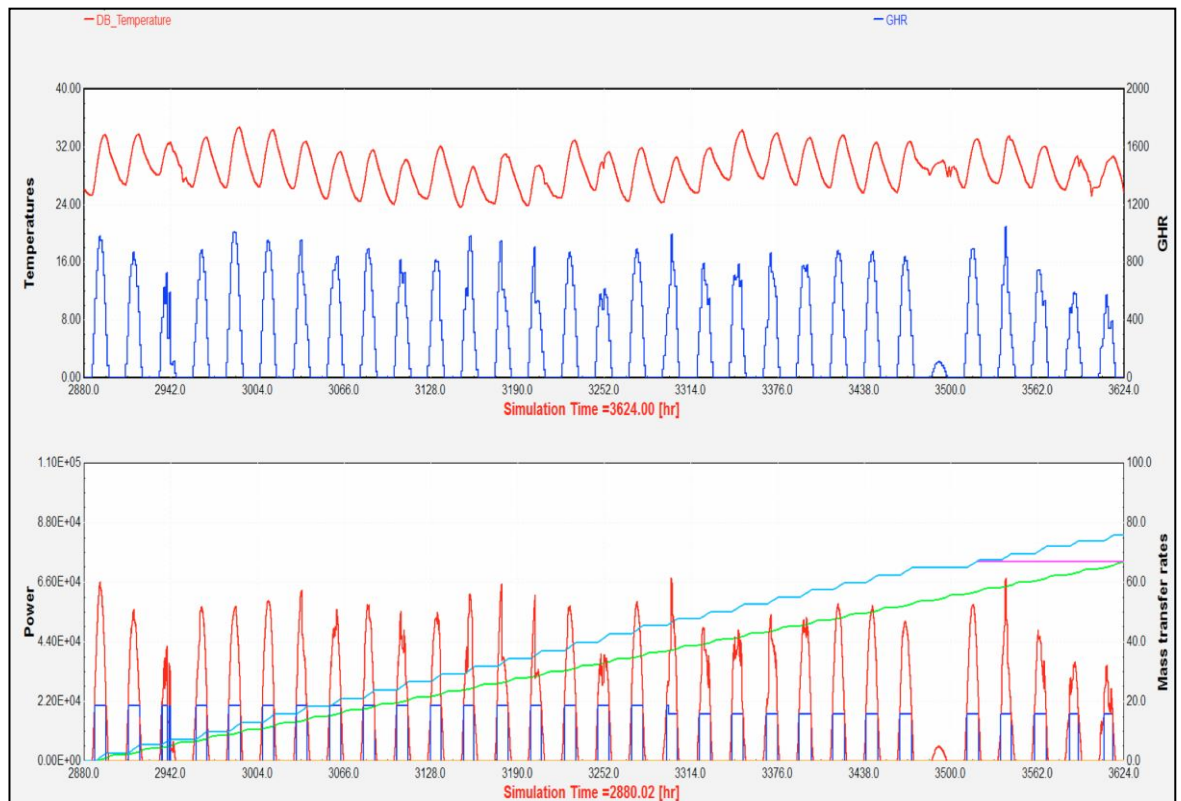


Figure 7.4, TRNSYS simulation results for the Ghana direct connection case study for the month of May

Upper graph: red line is temperature and blue is the global horizontal irradiance.

Lower graph: red line is PV array production, blue is power to electrolyser, green is monthly accumulated cooking demand, light blue is hydrogen generated for distribution and purple is maximum amount stored.

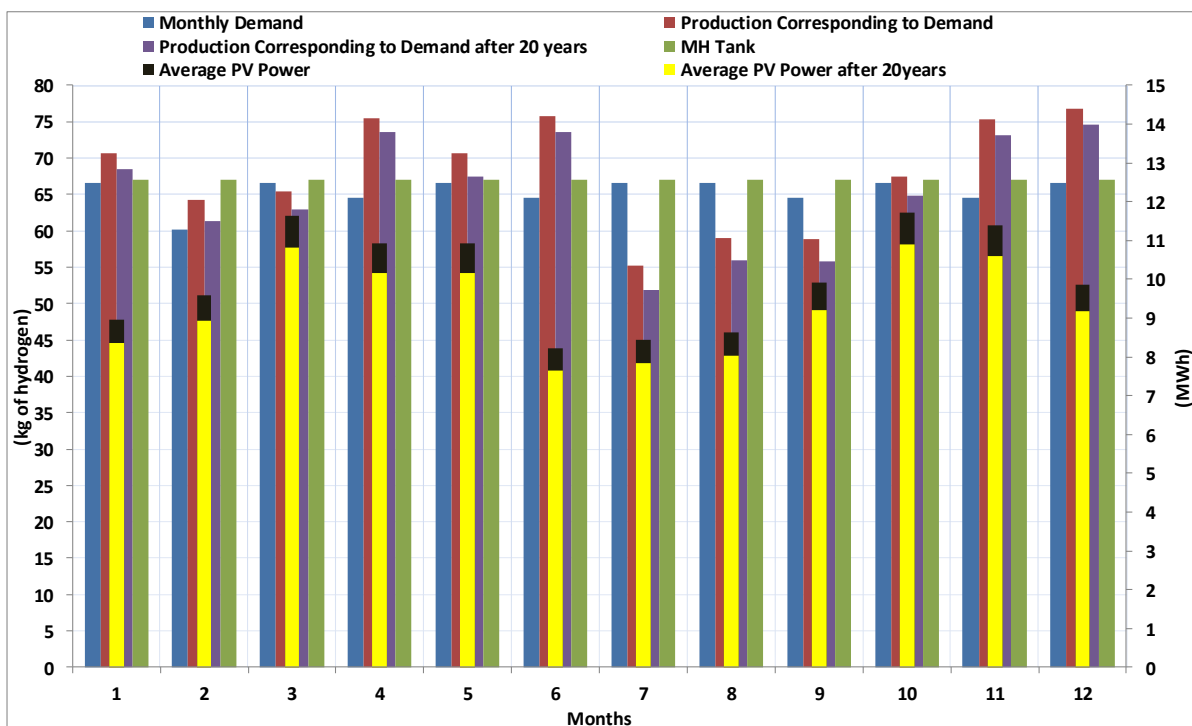


Figure 7.5, Monthly demand and production of hydrogen and PV yield for the current conditions and after the panel degradation period for the Ghana case study

Table 7.2, Ghana case study hydrogen production and PV yield at current and future conditions

Annual Hydrogen Demand (kg)	785
Annual Hydrogen Production (kg) at current conditions	815
Annual Hydrogen Production (kg) at the end of 20 years	783.4
Monthly Average PV Energy (MWh) at current conditions	10.02
Monthly Average PV Energy (MWh) at the end of 20 years	9.32

7.3.2 Jamaica and Indonesia Case Studies

A similar procedure as described for the Ghana case study is followed for the case studies of Jamaica and Indonesia. Direct connection of the PV array to the electrolyser and connection through a battery bank, for current application and after a 20 year panel degradation period are examined. The results of the hydrogen generation and the PV panel energy output for the case studies are shown in tables 7.3 to 7.7. Detailed presentation of the case studies model development and graphic results simulation can be found in Appendix F.

Table 7.3, Ghana battery case study hydrogen production and PV yield at current and future conditions

Annual Hydrogen Demand (kg)	785
Annual Hydrogen Production (kg) at current conditions	800
Annual Hydrogen Production (kg) at the end of 20 years	783.4
Monthly Average PV Energy (MWh) at current conditions	7.25
Monthly Average PV Energy (MWh) at the end of 20 years	6.79

Table 7.4, Jamaica case study hydrogen production and PV yield at current and future conditions

Annual Hydrogen Demand (kg)	621.6
Annual Hydrogen Production (kg) at current conditions	653
Annual Hydrogen Production (kg) at the end of 20 years	620
Monthly Average PV Energy (MWh) at current conditions	7.8
Monthly Average PV Energy (MWh) at the end of 20 years	7.3

Table 7.5 Jamaica battery case study hydrogen production and PV yield at current and future conditions

Annual Hydrogen Demand (kg)	621.6
Annual Hydrogen Production (kg) at current conditions	627.6
Annual Hydrogen Production (kg) at the end of 20 years	621.2
Monthly Average PV Energy (MWh) at current conditions	6.3
Monthly Average PV Energy (MWh) at the end of 20 years	5.9

Table 7.6, Indonesia case study hydrogen production and PV yield at current and future conditions

Annual Hydrogen Demand (kg)	631.0
Annual Hydrogen Production (kg) at current conditions	670.0
Annual Hydrogen Production (kg) at the end of 20 years	635.4
Monthly Average PV Energy (MWh) at current conditions	7.5
Monthly Average PV Energy (MWh) at the end of 20 years	7

Table 7.7, Indonesia battery case study hydrogen production and PV yield at current and future conditions

Annual Hydrogen Demand (kg)	631
Annual Hydrogen Production (kg) at current conditions	652
Annual Hydrogen Production (kg) at the end of 20 years	632
Monthly Average PV Energy (MWh) at current conditions	5.2
Monthly Average PV Energy (MWh) at the end of 20 years	4.8

7.4 Weather Data Effect on the Simulation

Weather data and in particular air temperature and solar irradiance are an important input for the system sizing. The following sections present an analysis of weather data sources and their suitability as inputs for the solar hydrogen system in TRNSYS. Recent weather data for Jamaica and weather data available from the Meteonorm database are analysed and compared through the use of Finkelstein-Schafer Statistics. Moreover, the effect of the future weather data on the numerical model is evaluated. The potential to establish solar hydrogen plants in the case study countries is further evaluated through the creation of novel solar hydrogen potential maps.

Weather data is a significant factor for the simulation of energy systems. Suitable weather data allow the simulation to give solid results and thus understanding of the energy system's behaviour (Rahman & Dewsbury, 2007). The ideal case would be to use many years of weather data to perform the simulation. This however would require time consuming processes with data not available in many cases. In order to overcome this, simulation based on one year weather data that represents typical weather conditions of a location is the most appropriate solution (Rahman & Dewsbury, 2007).

Weather data selection should be based mainly on their impact on the simulation results. This is not always easy since the evaluation of the data quality implies that there is data available for the desired location. Countries with established weather stations offer the possibility of recent and accurate weather data but in countries with no weather stations, or with weather stations that record few weather parameters, an extra effort is needed to acquire this data. In this case the user has to consider carefully data quality before proceeding to the simulation. For example single year weather data do not provide the same quality and representation of climatic conditions as synthetic data resulting from decades of observations. Energy consumption estimation, energy costs analysis, solar systems simulation in the long-term should be based on synthetic weather data (US Department of Energy, 2013).

7.5 Weather Data Types

Several organisations have developed weather data sets of specific format for various locations. The most common and widely used are the TMY (Typical Meteorological Year) format and WYEC2 (Weather Year for Energy Calculations) format, produced by NREL

(National Renewable Energy Laboratory) and ASHRAE (the American Society of Heating, Refrigerating and Air-Conditioning Engineers). These data sets contain synthesised hourly data of one year (8,760 hours) that represent long-term statistical tendencies and weather patterns (Crawley, 1998). Therefore WYEC2 and TMY weather files represent typical weather patterns with TMY data updated to become more suitable for work requiring solar radiation data. A description of the various weather data sets types follows is presented in Appendix G.

7.6 Meteonorm Weather Data

Meteonorm is a software that offers access to weather data for many locations. It contains global weather data that can be retrieved in 36 different formats (e.g. TMY, TMY2, .epw, and user defined format) and can be used as an input to many energy and building simulation softwares. The standard output files contain global radiation, diffuse radiation, global and diffuse inclined radiation, direct normal radiation and air temperature. In Meteonorm a variety of global and regional databases are examined and combined to create the weather data sets, with the most important sources being the Global Energy Balance Archive (GEBA) and the World Meteorological Organisation Climatological Normals (WMO/OMM) 1961-1990 (Meteonorm Version 7, 2014). Data for temperature, humidity, wind speed and precipitation is available for the climatological periods 1961-1990 and 2000-2009. Solar radiation data is available for the climatological periods 1981-1990 and 1986-2005 and 1991-2010, depending on the software version that is used. In more detail the monthly average values that are provided by Meteonorm database are:

- Global radiation
- Ambient air temperature
- Humidity
- Precipitation, days with precipitation
- Wind speed and direction
- Sunshine duration

The available stations of Meteonorm and the parameters they measure can be seen in Figure 7.6.



Figure 7.6, Meteorological Stations Map, source: (Meteotest, 2014). Red dots indicate availability of radiation data.

Monthly data are calculated from the weather stations of the selected area or the nearest available weather stations. For radiation, in the case of low density of available ground data (distance between the weather station and the selected location greater than 30km (10km for Europe) and altitude difference more than 100m) satellite images are used in combination with ground data. In case that no measured radiation data is available for a distance greater than 200km (for Europe 50km) only satellite data is used. The daily values are then generated through a stochastic weather generator that creates the typical mean year of data (8760 values per parameter) (Meteonorm Version 7, 2014). The daily values generation process can be seen schematically in Figure 7.7.

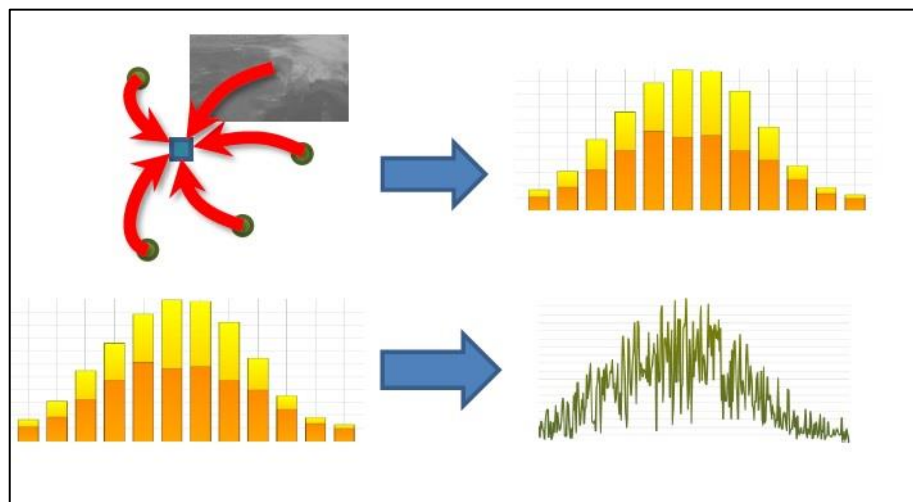


Figure 7.7, Meteonorm Typical Meteorological Year data generation process, source: (Meteonorm Version 7, 2014)

The stochastic method is based on models that generate intermediate data with the same statistical properties as the measured data (average, variance, autocorrelation) (Gansler, et

al., 1994). As a first step daily values are derived from monthly values and then the hourly values are generated. For global horizontal radiation the methodology by Aguiar et al. is followed (Aguiar & Collares-Pereira, 1988). Temperature hourly values are generated by a methodology developed within the framework of the European Union IST project SoDa. Detailed information of the stochastic generation processes can be found in the *Meteonorm Handbook part 2: Theory* (Meteonorm, 2014).

7.7 Suitable Weather Data Type for the Solar Hydrogen System Simulation

Song & Haberl (2013) suggest that TMY2 format is the most suitable for energy systems simulations where solar variation is critical for the results (Song & Haberl, 2013). Crawly (1998) also adds that the TMY2 method shows good results and provides users with energy simulation results that most closely represent weather patterns (Crawley, 1998). Therefore the TMY2 weather data format is the most suitable for the simulation of the solar hydrogen system in TRNSYS software.

Weather data for Jamaica available in TRNSYS is derived from *Meteonorm 7.0* database. The typical weather year for Jamaica consists of data measured on weather stations of the island; one in Kingston and one in Montego Bay, see Table 7.8.

Table 7.8, Jamaica Weather Station Information, source: (Meteotest, 2014)

Weather Station Name	id	WMO id	Longitude	Latitude	Altitude	Station Type
Norman Manley/ Kingston	5997	783970	-76.78	17.93	3	10
Sangster/ Montego	5996	783880	-77.92	18.5	1	10

The weather stations of Jamaica record temperature, wind speed and relative humidity but not irradiance. The irradiance data is GOES satellite data of the years 2010 - 2013 with a resolution of 8km on the horizontal, adopted to regional stations (Cuba, Puerto Rico and Central America) for the period 1971-1990 (*Meteonorm Version 7*, 2014). Three hourly satellite pictures of the geostationary satellites have been used. These satellite pictures are processed to daily means and summed up to monthly values. These monthly values are interpolated with mean ground measurements. The difference between the ground

measurements and satellite information is interpolated spatially with the inverse distance method. This gives a result which includes the values at the ground stations and the variation of the satellite pictures (Meteonorm Version 7, 2014).

The composite weather data of Meteonorm is compared to recent weather data of Jamaica from a weather station installed in University of Technology in Kingston in December 2010, and can be seen in Figure 7.8 (University of Technology, Jamaica, 2010).

The recent weather data sets include:

- Global horizontal radiation
- Dry bulb temperature
- Wind speed and
- Relative humidity data



Figure 7.8 ,Weather Station in the University of Technology, Jamaica, source: (University of Technology, Jamaica, 2010)

7.8 Comparison of the Meteonorm Weather Data with the Recent Weather Data for Kingston

The comparison between the recent weather data of Kingston with the composite Meteonorm weather data provides useful results in terms of identification of variations and possible differences in certain periods. In the case of the solar hydrogen system big variations in the irradiance data can result in oversizing or under sizing the PV array. Hence, identifying the periods that there are differences between the two data sets is critical, and the effect of the dissimilarities between the two data sets is proven through simulations that are based on these weather data sets.

The analysis is based on the Finkelstein-Schafer (FS) Statistics which constitute in the generation and comparison of Cumulative Distribution Functions (CDF). The FS statistical method has been greatly used in the TMY generation process. Wilcox and Marion (Wilcox & Marion, 2008), Levenmore and Chow (Levenmore & Chow, 2006), Lee, Woo and Levenmore (Lee, et al., 2009) are some of the researchers that present the method and discuss the technical advantages of the FS statistics in the TMY generation process. Furthermore, the FS statistical method has been the main assessment method in the process of comparing different sets of weather data and generating TMY for various locations around the world. Kalogirou (Kalogirou, 2003) and Argiriou et al. (Argiriou, et

al., 1999), examine the methodologies and describe the process for the generation of TMY in south east Europe. Rahman and Dewsbury (Rahman & Dewsbury, 2007), Zang et al. (Zang, et al., 2012) and Chan et al. (Chan, et al., 2006) present work regarding the generation of TMY files in locations in Asia. Similarly, Fagbenle (Fagbenle, 1995) and Ohunakin et al. (Ohunakin, et al., 2013) report the process of creating TMY in Africa.

The Finkelstein-Schafer (FS) Statistical method is applied as a mean of comparing two sets of distributions and indicating their similarities or dissimilarities. The smaller the FS the more similar the two distribution sets, and in the case the FS statistic is zero the two sets are identical. In the case of Typical Meteorological Year generation the FS statistic is used to compare the distribution of a selected weather parameter in a month to the long-term distribution in that month. If the FS statistic is small then the mean, median, mode, standard deviation, percentiles of the actual data will be similar to these statistics of the long-term data.

The FS statistic between two data sets is calculated by the equations 7.3 to 7.5:

$$FS_x(y, m) = \frac{1}{N} \sum_{i=1}^N |CDF_m(x_i) - CDF_{y,m}(x_i)| \quad (7.3)$$

$$FS_{weighted}(y, m) = \frac{1}{M} \sum_{x=1}^M WF_x \times FS_x(y, m) \quad (7.4)$$

$$\sum_{x=1}^M WF_x = 1 \quad (7.5)$$

(Finkelstein & Schafer, 1971)

The FS statistic for a month is calculated as the weighted sum of all the FS statistics of separate weather parameters. The month with the smallest FS statistic is chosen as the typical to represent this month in the Typical Meteorological Year. The FS statistic tends not to consider periods of extremities in the weather conditions, i.e. heat wave periods or extremely cold ones (Rahman & Dewsbury, 2007). These periods are important for the design of energy systems and the FS statistics for each parameter separately will be more indicative of these periods, than the total weighted one.

7.8.1 Comparison Steps

The recent weather data come from the weather station that is located at the University of Technology in Kingston. Quarterly values for 36 parameters for a three year period (2011, 2012, and 2013) are available. From these parameters, dry bulb temperature, global horizontal radiation, wind speed and relative humidity will be used for the analysis. From these quarterly values the daily average values are generated. The hourly average values for dry bulb temperature, global horizontal radiation, wind speed and relative humidity are available in the Meteororm weather data set for Jamaica. From these hourly values the daily average values are generated.

In order to compare these sets of weather data the FS statistical method is used and adapted so as to make three comparison processes:

- 2011 weather data set and the Meteororm typical year data
- 2012 weather data set and the Meteororm typical year data
- 2013 weather data set and the Meteororm typical year data

The CDF curves for the Meteororm weather data set for Kingston, Jamaica and for the recent weather data sets are generated for the daily average values of the following parameters:

- Global Horizontal Radiation
- Dry Bulb Temperature
- Relative Humidity
- Wind Speed

The CDF curves for the above parameters are generated for every month for the three year period of the recent data and for every month of the Meteororm file. These CDF curves are compared and the similarities of the distribution sets are measured by Finkelstein-Schafer (FS) Statistics, as per the adjusted equations 7.6 to 7.8:

$$FS_x = \frac{1}{N} \sum_{i=1}^N |CDF_{MeteorormDataSet}(x_i) - CDF_{RecentDataSet}(x_i)| \quad (7.6)$$

$$FS_{weighted} = \frac{1}{M} \sum_{x=1}^M WF_x \times FS_x \quad (7.7)$$

$$\sum_{x=1}^M WF_x = 1 \quad (7.8)$$

In more detail, the steps that are followed are:

- The CDF curves of each weather parameter for the recent weather data set are generated for each month. The CDF comprises of a table of values of cumulative frequency (%) versus the weather parameter values
- The CDF curves for each weather parameter for each month of the Meteonorm file are generated
- The FS statistic for each parameter is evaluated by calculating the absolute difference between the CDF values of the Meteonorm weather data set and the CDF values of the recent weather data sets. The absolute difference values are summed and divided by the total number of occurrences in each month, i.e. to number of days of every month, as the CDFs for every month are generated.
- The CDF curves for the whole year of each of the three years of the recent weather data sets are generated and the CDF curves for the Meteonorm year as well
- The FS statistics for each weather parameter for each of the three recent years and the Meteonorm data are calculated
- The total weighted FS statistics for each month and for each year are calculated by multiplying the FS of each parameter to the weighted factor and summing them
- The weighting factors are considered equal for each weather parameter, and are taken as 0.25 so that equal importance is given on the impact of each parameter (Argiriou, et al., 1999).
- Months with missing values are limited from the analysis. These are January and December 2011.
- For the calculations regarding Global Horizontal Radiation, the night-time zeroes are not taken into consideration, according to Levenmore (Levenmore & Chow, 2006)

7.8.2 CDF Curves and Results

The CDF curves of Global Horizontal Radiation for each of the three years of recent data in comparison to the CDF curves for Meteoronorm typical year are given in Figures 7.9 to 7.12. The CDF curves for Dry Bulb Temperature, Relative Humidity and Wind Speed are presented in Appendix G. The calculated FS statistics of each weather parameter for each month and each of the total years of the three years are given in the Appendix G. Total FS statistics of recent weather data compared with Meteoronorm weather data are given in Table 7.9. In addition to the FS statistics the minimum, maximum and average daily values of the weather parameters are calculated so as to enhance the understanding of the similarities and variations between the data sets. Tables G.1 to G.13 of Appendix G contain the comparison between the averages, minimum and maximum values of each weather parameter for each month of each of the three years of the recent data set and each month of the Meteoronorm year. Furthermore, the values of each weather parameter for 2011, 2012 and 2013 and the Meteoronorm year can be seen graphically in Appendix G.

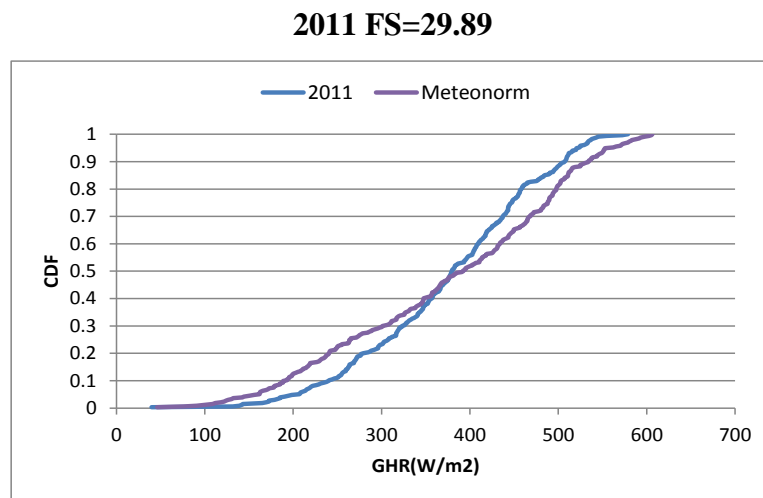


Figure 7.9, Comparison between the CDF curves for Global Horizontal Radiation for 2011

2012 FS=40.46

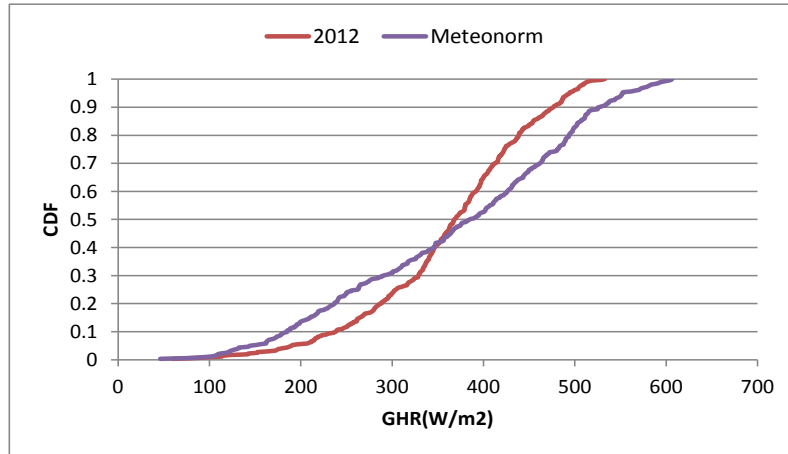


Figure 7.10, Comparison between the CDF curves for Global Horizontal Radiation for 2012

2013 FS=43.18

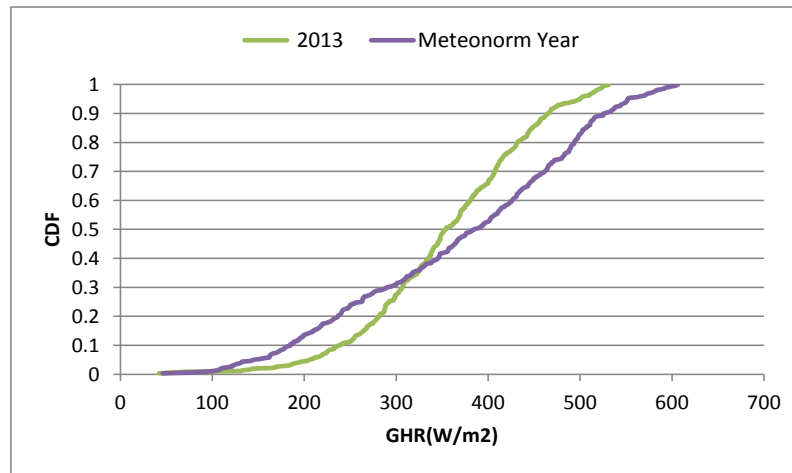


Figure 7.11, Comparison between the CDF curves for Global Horizontal Radiation for 2013

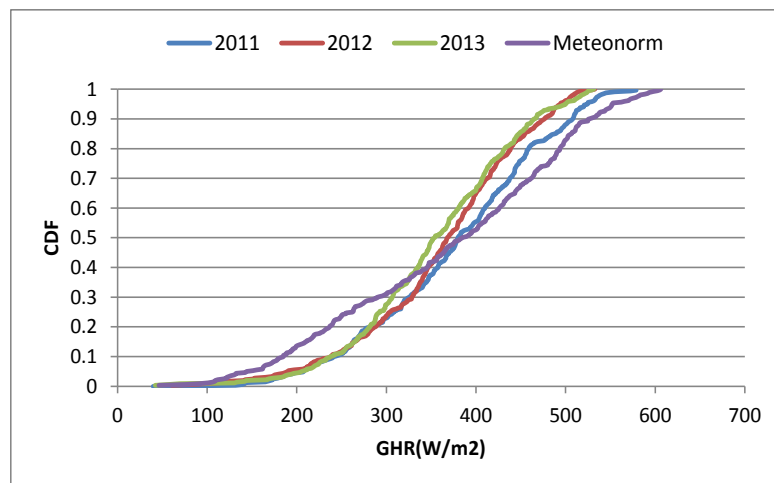


Figure 7.12, Comparison between the CDF curves for Global Horizontal Radiation for all the years

Table 7.9, Total FS Statistics of Recent Weather Data of Kingston compared with Meteonorm Weather Data

	GHR (W/m²)	T(°C)	RH(%)	WS(m/s)	Weighting Factor for Each Parameter	TOTAL Weighted FS
2011	29.89	2.31	5.32	0.89	0.25	9.60
2012	40.46	1.95	5.33	0.69	0.25	12.11
2013	43.18	1.46	4.75	0.65	0.25	12.51

From the comparison of the results of the FS analysis and the average, minimum and maximum values of the weather parameters the following is concluded:

- For Global Horizontal Radiation, the CDF curve of 2011 is more similar to the Meteonorm CDF curve than the 2012 and 2013 curves. This is also obvious from the FS value that for 2011 is the smallest of the three. In general, the three years have similar CDF curves and are more similar to each other than to the Meteonorm year. The average yearly Global Horizontal Radiation value of Meteonorm is 1.55% smaller than the average of 2011, 2.26% bigger than 2012 and 4.14% bigger than 2013, which also indicates that 2011 is more similar to Meteonorm than the other years. Also the maximum Global Horizontal Radiation value for Meteonorm is greater than the maximum values for all the three recent years by 4.6% for 2011, 12.15% for 2012 and 12.34% for 2013. Therefore, Meteonorm overestimates the Global Horizontal Radiation and the calculated numbers are close to the 10% that is the overestimation of the hourly model that calculates the total radiation for Meteonorm for individual months and 6% for yearly sums (Meteonorm Version 7, 2014). Global Horizontal Radiation is the weather parameter mostly affecting the operation of the solar hydrogen system, as the PV panels yield depends mainly on that. Therefore, overestimation of the radiation values could possibly lead to underestimation of the panels yield and consequently hydrogen production. Nevertheless, this will be examined thoroughly through simulations which will indicate if there is an effect and how significant it is.
- For Dry Bulb Temperature the CDF curve of 2013 is closer to the CDF for Meteonorm than 2012 and 2011. The FS statistic for 2013 is 1.46 whereas for 2011 it is 2.31 and for 2012 it is 1.95. 2011 and 2012 have similar average yearly temperatures, 25.82 °C and 25.76 °C each, whereas 2013 has an average

temperature of 26.25°C which is closer to the Meteonorm average of 27.72 °C. Therefore, Meteonorm average yearly temperature is 6.85% higher than 2011, 7.07% higher than 2012 and 5.3% higher than 2013. Moreover, Meteonorm minimum and maximum values for all months are consistently higher by average 1.16 °C than the minimum and by 2.4 °C than the maximum values for all months of all the three years. According to Meteonorm, the root mean square error in generating the daily values from the monthly values is 1.2 °C (Meteonorm Version 7, 2014). As with Global Horizontal Radiation, Dry Bulb Temperature has an effect on the operation of PV panels. High temperatures affect the panels' voltage and cause it to drop, thus causing a consequent reduction in the power output. Again, this effect of the Meteonorm temperature overestimation will be examined through simulations.

- For Relative Humidity the CDF curves for all three years are almost similar and the one closest to the Meteonorm CDF curve is for 2013. The FS statistic for 2013 is 4.75, for 2011 is 5.32 and for 2012 is 5.33. Therefore, it is concluded that the three years differ in a similar way from the Meteonorm year and specifically 2011 and 2012 can be considered as similar. This is highlighted even more from the average yearly values that are 74.30% for 2011, 74.91% for 2012 and 74.05% for 2013. The average value for the Meteonorm year is 69.61%, which is 6.74% smaller than 2011, 7.61% smaller than 2012 and 6.38% smaller than 2013. Additionally, the minimum and maximum values of Meteonorm are smaller by 4.47% average than the minimum and by 1.09% by the maximum of each of the three years. It can be thus concluded that Meteonorm underestimates the relative humidity values.
- For Wind Speed the CDF curve for 2013 is the closest one to the Meteonorm CDF. Again all three years have similar CDF curves, and in particular 2012 and 2013 are more similar. The FS for 2013 which is the most similar year is 0.65 and for 2012 is 0.69 and 2011 is 0.89. The average yearly wind speed of Meteonorm is by average 25% greater than the average yearly values for all three years. The minimum value of Meteonorm year is smaller than the minimum value for each of the three years by 54.84% and the maximum value is greater by 54.26%.
- The weighted FS statistics between the recent weather data and the Meteonorm data indicate that the year that is most similar to the Meteonorm year is 2011, with FS=9.38. 2012 has FS=12.11, and 2013 FS=12.51.

7.9 Comparison of the Effect of the Composite and the Recent Weather Data on the Simulation Results

This section examines the effect of the composite and recent weather data on the simulation through the comparison of the results. The Meteonorm irradiance data for Jamaica is GOES satellite data of the years 2010 - 2013 with a resolution of 8km on the horizontal, adopted to regional stations (Cuba, Puerto Rico and Central America) for the period 1971-1990 (Meteonorm Version 7, 2014), and for all other parameters the data refers to the period 2000 – 2009. Therefore, especially for the case of the irradiance data, there is a possibility of an inaccuracy in the data. Section 7.8 concluded that Meteonorm overestimates global horizontal irradiance, temperature and wind speed and underestimates humidity.

More specifically, the FS between Meteonorm and 2013 weather data is the largest of the three recent years (2011, 2012, and 2013). Thus, the comparison of the hydrogen generation will be done through simulations that employ the Meteonorm and the 2013 weather data set. The monthly and annual hydrogen generation simulation results for the direct connection system for the Jamaica case study with Meteonorm and with the 2013 weather data sets are presented in Figure 7.13 and Table 7.10. It can be seen that the annual hydrogen generation is higher when using Meteonorm than the 2013 weather data by 5.81kg. This corresponds to a 0.9% smaller annual hydrogen generation resulting from the use of the recent weather data. This confirms the difference indicated by the FS of 12.5 between the 2013 and Meteonorm weather data.

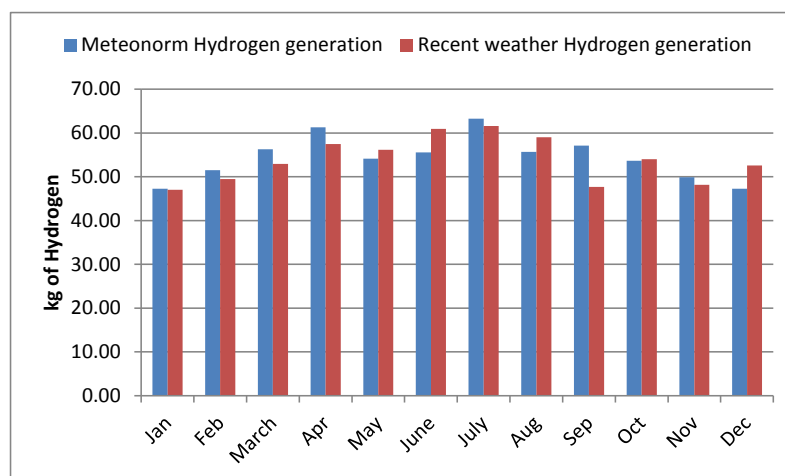


Figure 7.13, Comparison of the hydrogen generation results of the simulation with the Meteonorm and the 2013 recent weather data

Table 7.10, Hydrogen generation results of the simulation with the Meteonorm and the 2013 recent weather data

	Meteonorm Hydrogen generation (kg)	Recent weather Hydrogen generation (kg)
January	47.27	47.01
February	51.50	49.49
March	56.28	52.93
April	61.27	57.50
May	54.16	56.14
June	55.57	60.92
July	63.25	61.58
August	55.67	59.01
September	57.12	47.71
October	53.65	54.01
November	49.89	48.17
December	47.27	52.61
Complete Year	652.89	647.08

The overestimation of the global horizontal radiation in Meteonorm, leads to a smaller size of PV array than if sizing would be based on the recent weather data. Nevertheless, this difference is very small and even though the recent weather data simulation gives a smaller result in terms of hydrogen generation, the demand is still covered.

Therefore, it can be concluded that even though the FS statistics between the Meteonorm weather data set and the 2013 recent weather data set indicate a difference, the simulation results between the two data sets are very similar. It is thus considered suitable to use the Meteonorm file for simulation, as the inaccuracy of the irradiance data which are GOES satellite data is proved to have a negligible effect.

7.10 Comparison of the effect of the Future Weather Files on the Simulation Results

The generation of future weather files has been studied by many researchers (Belcher, et al., 2005; Jentsch, et al., 2008; Jentsch, et al., 2013; Eames, et al., 2012). Four are the main methodologies according to the literature for the generation of future weather data:

- The Extrapolating Statistical Method,
- The Morphing Procedure based on the imposed offset method,
- The Stochastic Weather Model and
- The Global and Regional Climate Change Models.

According to the literature and the comparison between these four methods, the morphing method is proved to be the most reliable as the future climate data are generated based on present day weather data (Belcher, et al., 2005; Guan, 2008). It has to be noted though, that the variability and character of the present-day files is transferred to the future files too. The basic methodology of the morphing method is developed by Belcher et al, (Belcher, et al., 2005). It is published by the Chartered Institution of Building Services Engineers (CIBSE) and is utilised as a baseline for transforming current CIBSE Test Reference Years (TRY) and Design Summer Years (DSY) into future climate projection weather years (Jentsch, et al., 2008). As described in the literature, ‘Morphing involves shifting and stretching the climatic variables in the present –day weather time series to produce new weather time series that encapsulate the average climate change while preserving the physically realistic weather sequences of the source data’ (Belcher, et al., 2005; Guan, 2008). The algorithms that comprise the basis of the morphing method are described by the following equations (Belcher, et al., 2005):

$$x = x_o + \Delta_{xm} \tag{7.9}$$

(Shift by Δ_{xm} is applied to the present day climate variable x_o for each month m)

$$x = a_m \times x_o \tag{7.10}$$

(Linear stretch to the present day climate variable x_o)

$$x = x_o + \Delta_{xm} + a_m \times (x_o - (x_o)_m) \tag{7.11}$$

(Combination of shift and stretch)

Where:

- x_o : the existing hourly climatic data,
- Δ_{xm} : the absolute change in monthly-mean climatic variable for month m ,
- α_m : the fractional change in monthly –mean climatic variable for month m and
- $(x_o)_m$: the climatic variable x_o average over month m .

The weather files from Meteornorm used for the simulations so far set the basis for the generation of future climatic files. The CCWorldWeather Generator tool developed by Southampton University, (University of Sounthampton, 2012), is used to perform the ‘morphing’ procedure. This is a tool specialised for the generation of future climatic files to be used in energy simulation programs. It is excel-based and takes as input ‘present-day’ epw files (Jentsch, et al., 2008; University of Sounthampton, 2012). The weather files for the case studies in epw format are morphed using the HadCM3 A2 experiment data for the 2050 scenario ensemble timeframe. The results of the process are the future weather files for the 2050 scenario, which covers the years 2041-2070 and therefore is the most suitable to be used for simulation results after the 20 year period. The emissions scenario covered by the CCWorldWeather Generator tool is the medium – high one, (Jentsch, et al., 2013). The irradiance of the future morphed file is reduced in comparison to the typical Meteornorm weather file as shown in Figure 7.14. In average, monthly irradiance is reduced by approximately 11 kJ/h/m², or 1.45%.

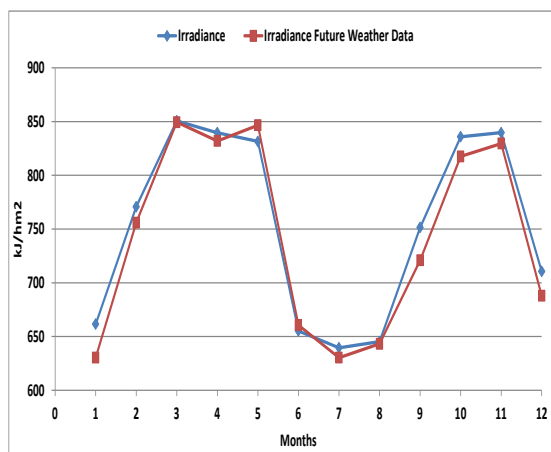


Figure 7.14, Comparison of the Irradiance with the Meteornorm weather file and the morphed weather file

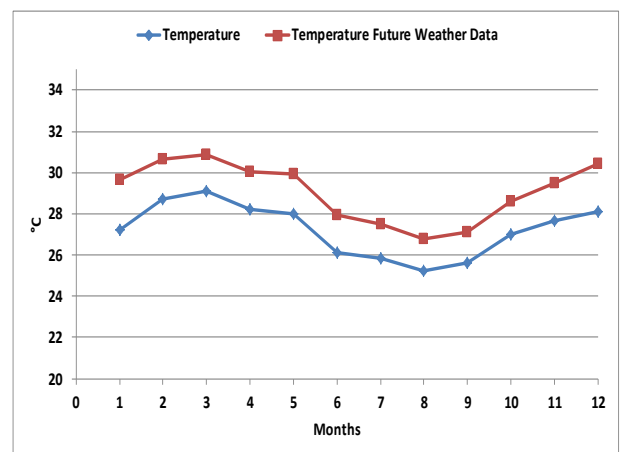


Figure 7.15, Comparison of the temperature with the Meteornorm weather file and the morphed weather file

The monthly PV yield for the future weather file is smaller than the PV yield for the typical Meteonorm weather file. In average the monthly PV yield is reduced by 12.61MWh or 2.3% for the future weather file. Future temperatures are predicted to arise (Jentsch, et al., 2008), and this is obvious in Figure 7.15, where it shows that the future temperatures are increased in relation to the typical Meteonorm weather file. All the monthly averages are approximately 6.72% or 1.83 °C.

7.10.1 CDF comparison

The weather data of Meteonorm for Ghana are compared with the weather data of the morphed future weather file for Ghana, in order to estimate the significance of the difference, through the use of Finkelstein-Schafer statistics. The procedure that is followed is the same as it is described in section 8.5.

The CDF curves of Global Horizontal Radiation (Wh/m^2) and Dry Bulb Temperature ($^{\circ}\text{C}$) for each of the Meteonorm typical weather data file are compared to the CDF curves for the morphed future Meteonorm typical year. The comparison is shown in Figures 7.16 and 7.17. The calculated FS statistic for the Dry Bulb Temperature is 1.83 °C and for the Global Horizontal Irradiance it is 5.89 kJ/m^2 for the comparison between the typical weather file and the morphed weather file. The difference between the Global Horizontal Irradiance between the typical and the morphed file is very small and this can be also observed in Figure 7.16, where the two irradiance profiles are almost similar, with the morphed one presenting marginally smaller values. In the case of Dry Bulb Temperature the difference between the two weather files is bigger than in the case of irradiance, as indicated in Figure 7.17. Approximately, there is a 1.83 °C increase in the temperature values, from the typical to the morphed weather file. Therefore, it can be concluded that the morphed file overestimates the temperature increase.

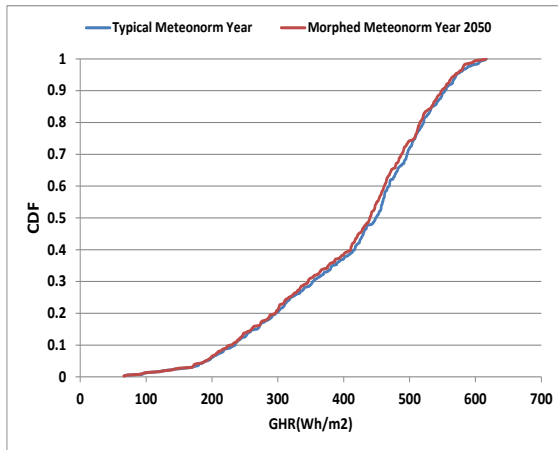


Figure 7.16, Comparison between the CDF curves for Global Horizontal Irradiance for Typical Meteorology Year and Morphed Meteorology Year

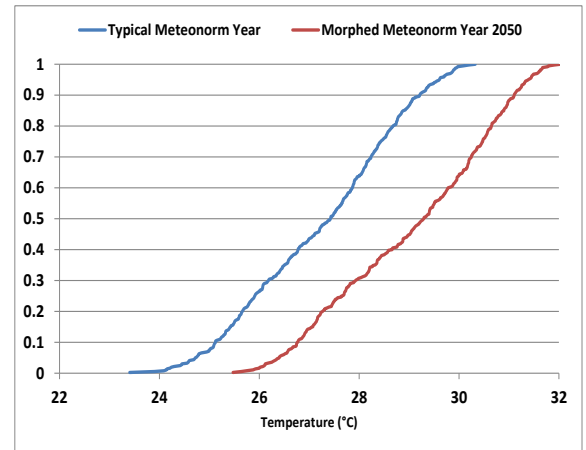


Figure 7.17, Comparison between the CDF curves for Temperature for Typical Meteorology Year and Morphed Meteorology Year

It should be noted here that there is a cause of inaccuracy in the weather data generated through the morphing process and this is the difference between the time base of HadCM3 and the typical Meteorology data. In theory, the epw files used for morphing should be formed of weather data derived from measured parameters of the years 1961-1990, in order to correspond to the HadCM3 reference timeframe. If the relative change of the HadCM3 data to the 1961-1990 baseline is superimposed on data from other periods (1971-1990), which according to observed climate trends, have already experienced higher temperature levels than the 1961-1990 baseline, then extra inaccuracies are caused. This can result in the morphed weather file that is generated using such an epw file to overestimate the effects of climate change for the given location (Jentsch, et al., 2013). In the case of the Ghana .epw weather file, the data correspond to a radiation period from 1991 - 2010 and for a temperature period from 2000 - 2009.

In order to evaluate further the difference between the values of the two files, a comparison between the simulation results of the future weather files and the TMY file for Ghana is conducted, for the direct PV electrolyser connection case study. The results indicate that the hydrogen generation for one year with the morphed files is smaller by 11.6kg or 1.5%, as shown in Figure 7.18. Therefore, it can be concluded that the effect of the climate change on the weather data and the future predicted files does affect the simulation.

Considering that morphing uncertainties add to the already existing uncertainties of the weather files used (Metetest, 2014), it is more accurate to use the current weather files for

the prediction of the hydrogen yield for any future conditions, such as the 20year panel degradation period. The same conclusion applies for Jamaica and Indonesia.

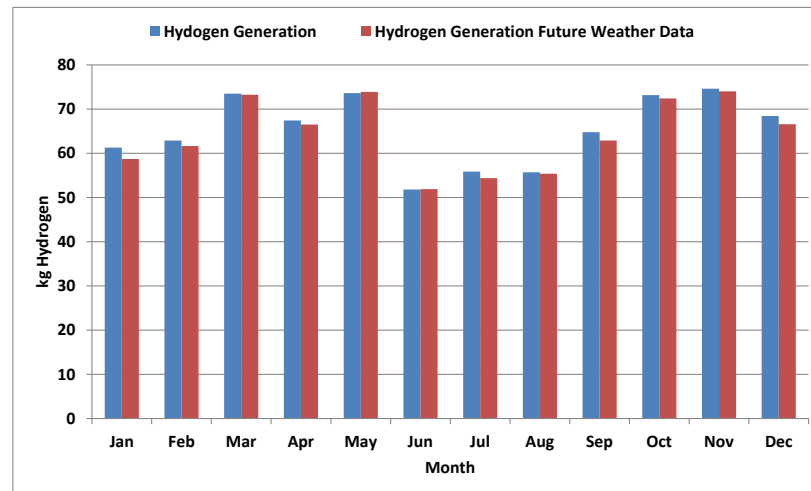


Figure 7.18, Comparison of the hydrogen generation with the Meteorom weather file and the morphed weather file

7.11 Generation of Solar Hydrogen Potential Maps

A step further to the analysis of the solar hydrogen system in the case study countries is the evaluation of the country potential of solar hydrogen generation through the creation of solar hydrogen potential maps. The generation procedure is partly based on the methodology of the National Renewable Energy Laboratory (NREL) for the estimation of the potential for hydrogen production from key renewable resources in the United States (Milbrandt & Mann, 2007) :

1. The country is separated in specific areas. In this research, the areas are represented by the administrative areas.
2. The solar potential for each country in kWh/m²/day is evaluated for each administrative area
3. In each area 10% of the land is assumed to be used for solar panel installation, and only 30% of this area to be actually covered with solar panels (Milbrandt & Mann, 2007).
4. The solar panels utilised are assumed to have an efficiency of 15%.
5. The electricity demand of the electrolysis process is 61kWh/kg of hydrogen, for the PEM electrolyzers used (see Chapter 5).

The above steps are combined in the Equation (7.12) that calculates the normalised hydrogen potential in (thousand kg/km²/year).

$$SHpotential = \frac{0.1 \times 0.3 \times 0.15 \times 10^3 \times Solar \left(\frac{kWh}{m^2 day} \right) \times \left(365 \frac{day}{year} \right)}{61 \left(\frac{kWh}{kg} \right)} \quad (7.12)$$

The above calculations were followed for Ghana, Jamaica and Indonesia. In order to create the solar hydrogen potential maps the results of these calculations were used as input to the ArcMap software which is a professional Geographic Information Software (GIS) for the generation of maps (ESRI, 2015). The software receives the information (numbers) from the inputted database and lays it on the country map as features. A GIS system is the most appropriate way to generate maps as it is designed to analyse, manage and present any type of spatial or geographical data. Rumbayan et al. describe how using this software can prove to be a very effective in the generation of solar energy potential maps and present an application study in Indonesia (Rumbayan, et al., 2012). The steps of the map generation process are presented in Appendix G.

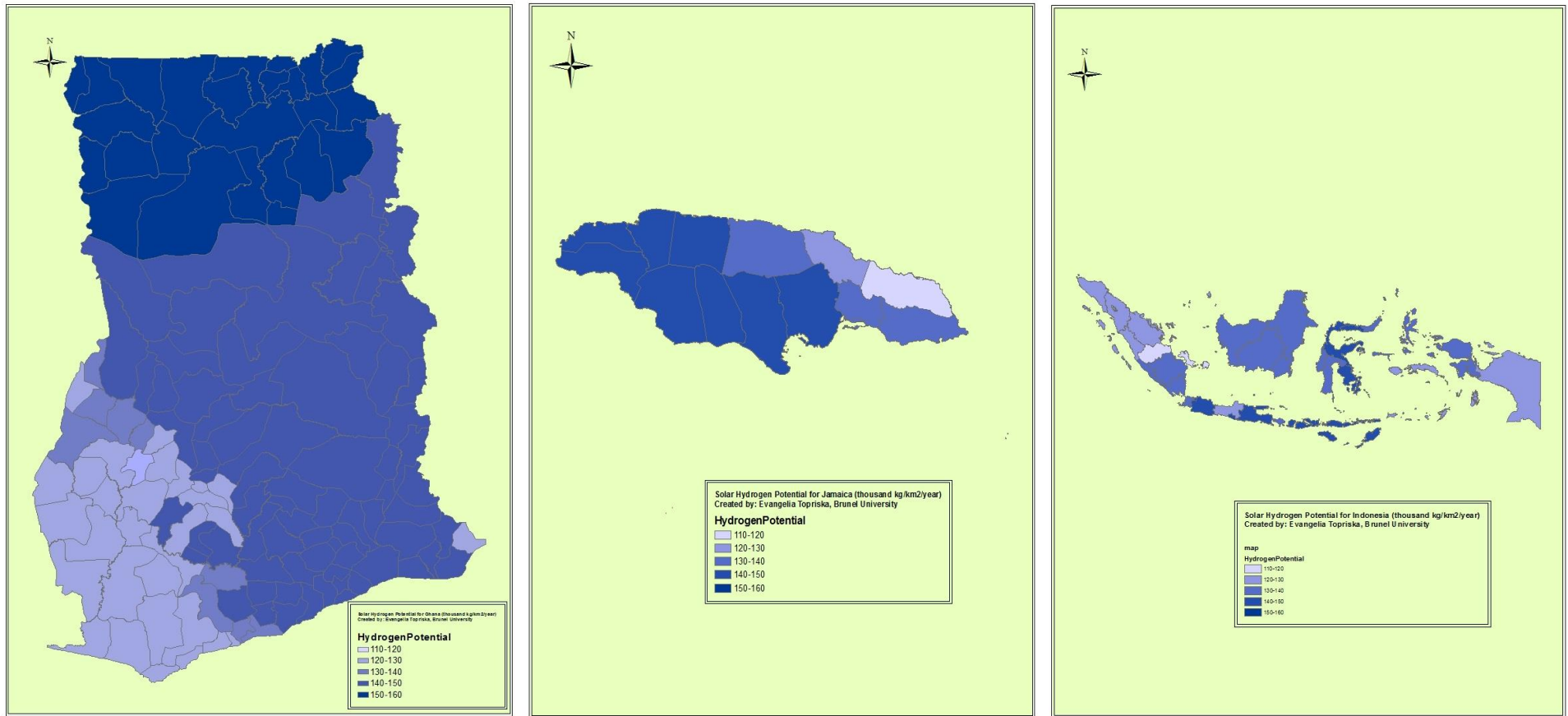


Figure 7.19, Solar hydrogen potential maps for Ghana, Jamaica and Indonesia

7.12 Discussion of the Solar Hydrogen Potential Maps

Figure 7.19 presents the solar hydrogen generation potential in Ghana, Jamaica and Indonesia. The map sizes appear in auto-zoom scale to show the variations within the countries clearly, but in reality Indonesia is the biggest country, followed by Ghana and last Jamaica. Each administrative area is characterised by a specific range of hydrogen potential in the normalised unit of *thousands of kg of hydrogen per km² per year*. The solar hydrogen potential values are grouped into five classifications: 110-120, 120-130, 130-140, 140-150 and 150-160. The darkest colours on the maps indicate the higher solar hydrogen potential. It is observed that Ghana includes areas with higher solar hydrogen potential than Jamaica and Indonesia, and this is due to the higher global horizontal radiation in Ghana (4-6 kWh/m²/day). In total country area indicators, Table 7.11 shows that Ghana has the greatest solar hydrogen potential per area unit of the three countries. However in total country area, Indonesia presents by far the greatest potential as it is the biggest country of the three, followed by Ghana and last Jamaica. These results and the generated maps can act as an indicator of the most appropriate areas for the solar hydrogen system application and can be used as a mean to assess the replacement of the currently used fossil fuels by hydrogen.

Table 7.11, Total country solar hydrogen potential indicators

Country	Ghana	Jamaica	Indonesia
Average (thousand kg/km ² /year)	140.5	139.2	133.5
Total area (km ²)	238,535	10,991	1,904,569
Country Annual Solar Hydrogen Potential (million.kg/year)	33,514	1,530	254,260

7.13 Summary

This Chapter presented the application of the numerical model of the solar hydrogen cooking system in developing economies. Three countries were examined for the application, Ghana, Jamaica and Indonesia. The calculation of the domestic daily cooking demand profile resulted in 2.5kWh/day for Ghana, 1.98kWh/day for Jamaica and 2kWh/day for Indonesia. These values were inputted in the numerical model developed in TRNSYS which is used for the design and sizing of a solar hydrogen plant. Hydrogen generation rates were calculated according to the available PV output for the weather conditions of each country, for a direct connection of the PV array to the electrolyser plant and a connection through battery bank. The results are presented for two scenarios, the current conditions and the conditions after the 20 year period, which takes into consideration the panel degradation. The system is designed so that the extra hydrogen production acts supplementary for the months that there is shortage, and a regulated operation and fuel supply is guaranteed for both scenarios.

Furthermore, the effect of the weather data on the simulation was evaluated through comparison of the composite Meteororm weather file used for the simulation, to a recent weather data set of Jamaica. Finkelstein-Schafer statistic indicates a difference between the datasets. Nevertheless, the results of the simulation with the two weather data sets differ only by 0.9% in the annual hydrogen production, thus confirming that the use of the composite weather file is reliable. The climate change effect on the weather data and their influence on the simulation were evaluated through simulations with generated future weather files. The hydrogen generation for one year based on the morphed files is only 1.5% lower than the Meteororm simulation results. Moreover the morphed files introduce further uncertainties to the weather files. Therefore, the future conditions as represented by the future weather files have a negligible effect on the simulation results and it is preferable not to employ them. Finally, the potential of the development of solar hydrogen plants in the case study countries, was estimated through the creation of novel solar hydrogen potential maps, that can be used as a decision making tool for investments.

Chapter 8 presents the cost analysis of the solar hydrogen systems developed for the case studies and evaluates the CO₂ saving potential by the application of the case studies system by calculating the Marginal Abatement Cost curves for the different system configurations.

Chapter 8. Techno-economic Analysis

8.1 Introduction

This chapter presents the financial evaluation of the large scale solar hydrogen systems that were developed and described in Chapter 7 based on the solar hydrogen numerical model of TRNSYS. The analysis is based on actual market prices of the system components, adjusted to the size and requirements of the system. Cost Benefit Analysis (CBA) is performed for six versions of system configuration for each case study country. The two main designs are: (i) direct connection of the PV array to the electrolyser and (ii) supply of the electrolyser through a battery bank. The sub-configurations for each of the main designs depend on the storage option and are: (i) metal hydride storage, (ii) compressed gas storage and (iii) hydrogen distribution through pipelines.

Furthermore, Marginal Abatement Cost (MAC) Curves are calculated and quantitatively present and compare which designs are the most effective in emissions reduction and what is their cost.

8.2 Ghana Case Studies Cost Analysis

8.2.1 Direct connection of PV Array and Electrolyser: Scenario 1

According to the fuel cell and hydrogen joint undertaking of the European Union (Bertuccioli, et al., 2014), the prices of the commercially available electrolyser technologies are shown in Table 8.1.

Table 8.1, Overview of commercially available electrolyser technologies, source: (Bertuccioli, et al., 2014)

		Alkaline	PEM
Development Status		Commercial	Commercial medium and small applications ($\leq 300\text{kW}$)
System Size Range	Nm^3/h	0.25-760	0.01-240
	kW	1.8-5,300	0.2-1150
Hydrogen Purity		99.5%- 99.9998%	99.9%-99.9999%
Indicative System Cost	£/kW	800-960	1520-1840
Indicative System Cost*	€/kW	1,000-1,200	1900-2300
Indicative System Cost- Future Prediction	£/kW	480	800
	€/kW	600	1000

**Including power supply, system control, gas drying (purity above 99.4%), excluding grid connection, external compression and hydrogen storage*

According to the U.S. Solar Market Insight Report, for the second quarter of 2014, the price of the flat-roof non-residential PV systems is \$2.39 per W_{dc} , (Honeyman, et al., 2014) . Additionally, the DOE report of 2012 regarding photovoltaic pricing trend (Feldman, et al., 2012) predicted that in 2013 the average system price would be at the range of \$3. In Europe the Fraunhofer Institute reports prices of 1.35€/ W_{dc} for the end of 2013,(Fraunhofer Institute, 2014). According to recent actual market prices, the total capital costs of a PV system can be seen in Table 8.2, (Ecoenergia, 2014) . Therefore, the PV system price used for the cost analysis of the case studies is £0.91 per W_{dc} . PV system life is assumed to be 20 years for the analysis. The Ghana case studies are sized according to the average daily cooking demand of a typical household, which is 2.5kWh or 2.15kg of hydrogen per month The PV system that is suggested includes the following components:

- PV array of 77.4kW: 430 modules Trina Solar TSM-180DA01
- Inverters : 4 SUNNY TRIPOWER 20000TL-10 Economic Excellence
- PV combiner boxes

- Charge Controller
- DC/AC isolator
- Cables and connectors

Table 8.2, Price apportionment for the PV system installation

PV system part	Cost per unit (€cents/W _{dc})	Cost per unit (£pennies /W _{dc})
PV panels	65	51
Inverter	15	12
PV Panel Mounting	12	9
Electrical Labour: PV panels, DC/AC isolators, PV combiner boxes installation	5	4
Cables, Connectors, Monitors, Central Panel	15	12
Lightning Protection	4	3
Total	116	91

Zoulias and Lymberopoulos conducted detailed techno-economic studies for standalone power systems with an electrolyser capital cost of 8150 € per Nm³/h and a lifetime of 20 years (Zoulias & Lymperopoulos, 2008). The price used for the analysis of the electrolysers in this research is 2,320€ per kW, according to the Development of Water Electrolysis in the European Union final report, (Bertuccioli, et al., 2014), which includes recent data from 17 electrolyser manufacturers. The chosen value is multiplied by the energy input to the electrolyser (kWh/Nm³) and the price in € per Nm³/h is derived. For the 2Nm³/h electrolysers this price is 9591€ per Nm³/h, or £7,673 per Nm³/h. The operation and maintenance costs are assumed to be 2% of the capital expenditure per year. The lifetime of the electrolyser stack is assumed to be 20,000 hours of operation, (Bertuccioli, et al., 2014). In this analysis the life span for the electrolyser is 10 years. Thus, after 10 years the electrolysers should be replaced and the prices are assumed to be 50% reduced of the present ones (Bertuccioli, et al., 2014).

A cost analysis model was developed that estimates the cost of the various suggested PV-electrolyser system combinations. All the costs throughout the lifetime of the system are considered, i.e. capital costs for the purchase and installation, operation and maintenance

(O&M) costs. The total costs are converted to present day values, through the use of Equation (8.1), where:

PC = the present day cost of the investment

C_i = is the Capital and O&M costs in year i of the system

N = the life span of the system

r = the discount rate, that evaluates the effect of time on the money value

$$PC(\pounds) = \sum_{i=0}^N \frac{C_i}{(1+r)^i} \quad (8.1)$$

Through the above process, the unit cost of hydrogen throughout the lifetime of the project is calculated, using Equation (8.2). This is an important parameter in hydrogen generation systems, as it gives a clear view of the cost of energy and can relate it to the targets of the hydrogen cost that the European Union and the US Department of Energy set (Bertuccioli, et al., 2014; NREL, 2014; DOE , 2012).

$$H_2 \text{ cost} (\pounds / kg) = \frac{PC}{N \times m_{H_2 / year}} \quad (8.2)$$

Where $m_{H_2 / year}$ is the annual mass of generated hydrogen.

1a. Metal Hydride Storage

The metal hydride storage cylinders used in this scenario have market prices of £1,000 per Nm^3 , (Pragma Industries, 2014; Hydrogen Components Inc., 2014; chris.bruniau@pragma-industries.com, 2015). Further quotation information of the metal hydride tanks is also available in Appendix H. The prices and cost analysis of this scenario case study can be seen in Tables 8.3 and 8.4. Additionally, the sensitivity analysis of Table 8.5 shows that the metal hydride storage is the system part that contributes the most to the total costs.

Table 8.3, Scenario 1a - Distribution of costs

Component	Sizes	Capital Cost (£)	O&M (% of investment costs)	Lifetime (years)
PV System	77.4kW	70,434	2%	20
PEM Electrolyser	2Nm ³ /h per electrolyser 20 cells, 4 stacks	7,673 per Nm ³ /h	2%	10
MH Storage	20 Tanks	1,000 per Nm ³	2%	20

*£0.91/W_{ac} for the whole system: panels, inverters and installation costs

Table 8.4, Present cost analysis model for the solar hydrogen system, referring to scenario 1a

Life Cycle Cost Evaluation Model for the Different Combinations of the Solar Hydrogen System							
Input Parameters							
PV System Capital Cost (£/kW)	Electrolyser Capital Cost (£ per Nm ³ /h)	PV system Size (kW)	Electrolyser Size (Nm ³ /h)	Electrolysers number	PV System Life (ys)	Electrolyser System Life (ys)	Annual Hydrogen Production of the System (kg)
910	7673	77.4	2	2	20	10	815
Calculated Parameters							
PV System Capital Cost (£)	Capital Cost of Electrolyser System (£)	Capital Cost of Hydrogen Storage System (£)	O&M Costs of the PV System (£)	O&M Costs of the Electrolyser System (£)	O&M Costs of the Hydrogen Storage System (£)	Discount Rate r	Life Cycle (ys)
70434	30692	744500	1408.68	613.84	14890	0.05	20
System Size	Year (i)	PV-Electrolyser Capital Cost (£)	O&M of Total system Cost (£)	Total Costs (£)	Present Value (£)	Annual Hydrogen Production (kg)	Unit Cost of H2 (£/kg)
	0	845626	16912.52	862538.52	862538.52	815	55.66
	1	0	2835.12	2835.12	2700.12		
	2	0	2835.12	2835.12	2571.54		
	3	0	2835.12	2835.12	2449.09		
	4	0	2835.12	2835.12	2332.46		
	5	0	2835.12	2835.12	2221.39		
	6	0	2835.12	2835.12	2115.61		
	7	0	2835.12	2835.12	2014.87		
	8	0	2835.12	2835.12	1918.92		
	9	0	2835.12	2835.12	1827.55		
Electrolyser Replacement	10	15346	2835.12	18181.12	11161.63		
	11	0	2835.12	2835.12	1657.64		
	12	0	2835.12	2835.12	1578.70		
	13	0	2835.12	2835.12	1503.53		
	14	0	2835.12	2835.12	1431.93		
	15	0	2835.12	2835.12	1363.74		
	16	0	2835.12	2835.12	1298.80		
	17	0	2835.12	2835.12	1236.96		
	18	0	2835.12	2835.12	1178.05		
	19	0	2835.12	2835.12	1121.95		
	20	0	2835.12	2835.12	1068.53		
TOTAL					907292		

Table 8.5, Sensitivity analysis of the scenario 1a system

Sensitivity Analysis	
System Part	Percentages (%)
PV system	8.3
Electrolyser	3.6
Metal Hydride Storage	88.1

Therefore, according to the Scenario 1a cost analysis, the total present cost is £907,292 which corresponds to a unit cost of £55.76 per kg of H₂. This high cost is mainly due to the H₂ storage cost in metal hydride tanks. MH storage can be a competitive option only if the prices reduce dramatically. Additionally, there are two important issues related to the use of metal hydride storage tanks, and these are:

- The weight of the tank is very high. Indicatively, the tanks suggested to be used in the study would weight around 200kg each. Thus this sets a problem in the transportation of the tanks to the households.
- The heat necessary for the release of hydrogen

Nonetheless, hydrogen storage in metal hydrides constitutes a much safer option than the storage in high pressure gas cylinders. Especially in the case of domestic applications the stored gas should not exceed much the pressure of 10bar for safety reasons. R&D is progressing actively in this sector and it is expected to improve these issues in the nearby future. Nonetheless, for comparison purposes the cost evaluation of compressed hydrogen storage cylinders is presented in the following section.

1b. Compressed Gas Storage Cylinders

Bu using compressed gas storage, at 13.8bar, which is the maximum hydrogen production pressure of the used PEM electrolyser, the costs would be reduced. This option is not efficient in terms of system dimensions, as in this pressure range and for a monthly supply strategy, almost 2.7Nm³ of hydrogen storage would be required. Therefore, this option is examined for higher pressure, at the range of 100bar, and a cost of 38€/Nm³ –

£27/ Nm³. The prices, the cost and sensitivity analysis of the scenario can be seen in Tables 8.6 to 8.8.

Table 8.6, Scenario 1b - Distribution of costs

Component	Sizes	Capital Cost (£)	O&M(% of investment costs)	Lifetime (years)
PV System	77.4kW	70,434	2%	20
PEM Electrolyser	2Nm ³ /h per electrolyser 20 cells, 4 stacks	7,673 per Nm ³ /h	2%	10
Compressed Gas Storage	20 tanks	£27/ Nm ³	2%	20

Table 8.7, Present cost analysis model for the solar hydrogen system, referring to scenario 1b

Life Cycle Cost Evaluation Model for the Different Combinations of the Solar Hydrogen System							
Input Parameters							
PV System Capital Cost (£/kW)	Electrolyser Capital Cost (£ per Nm ³ /h)	PV system Size (kW)	Electrolyser Size (Nm ³ /h)	Electrolysers number	PV System Life (ys)	Electrolyser System Life (ys)	Annual Hydrogen Production of the System (kg)
910	7673	77.4	2	2	20	10	815
Calculated Parameters							
PV System Capital Cost (£)	Capital Cost of Electrolyser System (£)	Capital Cost of Hydrogen Storage System (£)	O&M Costs of the PV System (£)	O&M Costs of the Electrolyser System (£)	O&M Costs of the Hydrogen Storage System (£)	Discount Rate r	Life Cycle (ys)
70434	30692	20326	1409	614	407	0.05	20
System Size	Year (i)	PV-Electrolyser Capital Cost (£)	O&M of Total system Cost (£)	Total Costs (£)	Present Value (£)	Annual Hydrogen Production (kg)	Unit Cost of H2 (£/kg)
	0	121452	2429.04	123880.88	123880.88	815	10.35
	1	0	2835.12	2835.12	2700.12		
	2	0	2835.12	2835.12	2571.54		
	3	0	2835.12	2835.12	2449.09		
	4	0	2835.12	2835.12	2332.46		
	5	0	2835.12	2835.12	2221.39		
	6	0	2835.12	2835.12	2115.61		
	7	0	2835.12	2835.12	2014.87		
	8	0	2835.12	2835.12	1918.92		
	9	0	2835.12	2835.12	1827.55		
Electrolyser Replacement	10	15346	2835.12	18181.12	11161.63		
	11	0	2835.12	2835.12	1657.64		
	12	0	2835.12	2835.12	1578.70		
	13	0	2835.12	2835.12	1503.53		
	14	0	2835.12	2835.12	1431.93		
	15	0	2835.12	2835.12	1363.74		
	16	0	2835.12	2835.12	1298.80		
	17	0	2835.12	2835.12	1236.96		
	18	0	2835.12	2835.12	1178.05		
	19	0	2835.12	2835.12	1121.95		
	20	0	2835.12	2835.12	1068.53		
TOTAL					168634		

Table 8.8, Sensitivity analysis of the scenario 1b system

Sensitivity Analysis	
System Part	Percentages (%)
PV system	58.0
Electrolyser	25.3
Compressed Gas Storage	14.6

Therefore, according to the Scenario 1b cost analysis, the total present cost is £168,634 which corresponds to a unit cost of £10.35 per kg of H₂. The cost is radically reduced in this case, as compressed gas storage is a much cheaper option than the metal hydride storage, including the compressor costs. From the sensitivity analysis, the PV array is the component contributing most to the total cost.

1c. Distribution of Hydrogen through a Piping system

A solution to the above problem could be the design of a piping system from the solar hydrogen plant to the households that would carry hydrogen in low pressures, in a similar way to the natural gas network. Almost 1500km of H₂ pipelines have been constructed in Europe and another 900km in the USA (Roads 2HyCom Project, 2009). Transporting hydrogen through high pressure steel pipelines is a challenging task as hydrogen causes embrittlement in pipe materials. Nevertheless, low pressure hydrogen pipelines are more flexible in the selection of the pipe material. For the case of a central solar hydrogen generation plant, for the distribution of the hydrogen gas to the households, two types of pipelines are considered necessary:

1. Low-pressure distribution system from the plant to the community
2. Service pipelines, that link the households to the low-pressure distribution system (Dodds & McDowall, 2012)

Prices and costs of this scenario can be seen in Tables 8.9 to 8.11.

Table 8.9, Scenario 1c - Distribution of costs

Component	Sizes	Capital Cost (£)	O&M(% of investment costs)	Lifetime (years)
PV System	77.4kW	70,434	2%	20
PEM Electrolyser	2Nm ³ /h per electrolyser 20 cells, 4 stacks	7,673 per Nm ³ /h	2%	10
Hydrogen Pipeline		650000	2%	20

Table 8.10, Present cost analysis model for the solar hydrogen system, referring to scenario 1c

Life Cycle Cost Evaluation Model for the Different Combinations of the Solar Hydrogen System							
Input Parameters							
PV System Capital Cost (£/kW)	Electrolyser Capital Cost (£ per Nm ³ /h)	PV system Size (kW)	Electrolyser Size (Nm ³ /h)	Electrolysers number	PV System Life (ys)	Electrolyser System Life (ys)	Annual Hydrogen Production of the System (kg)
910	7673	77.4	2	2	20	10	815
Calculated Parameters							
PV System Capital Cost (£)	Capital Cost of Electrolyser System (£)	Capital Cost of Hydrogen Distribution System (£)	O&M Costs of the PV System (£)	O&M Costs of the Electrolyser System (£)	O&M Costs of the Hydrogen Storage System (£)	Discount Rate r	Life Cycle (ys)
70434	30692	650000	1409	614	32500	0.05	20
System Size	Year (i)	PV-Electrolyser Capital Cost (£)	O&M of Total system Cost (£)	Total Costs (£)	Present Value (£)	Annual Hydrogen Production (kg)	Unit Cost of H2 (£/kg)
	0	751126	34522.52	785648.52	785648.52	815	50.94
	1	0	2835.12	2835.12	2700.12		
	2	0	2835.12	2835.12	2571.54		
	3	0	2835.12	2835.12	2449.09		
	4	0	2835.12	2835.12	2332.46		
	5	0	2835.12	2835.12	2221.39		
	6	0	2835.12	2835.12	2115.61		
	7	0	2835.12	2835.12	2014.87		
	8	0	2835.12	2835.12	1918.92		
	9	0	2835.12	2835.12	1827.55		
Electrolyser Replacemen	10	15346	2835.12	18181.12	11161.63		
	11	0	2835.12	2835.12	1657.64		
	12	0	2835.12	2835.12	1578.70		
	13	0	2835.12	2835.12	1503.53		
	14	0	2835.12	2835.12	1431.93		
	15	0	2835.12	2835.12	1363.74		
	16	0	2835.12	2835.12	1298.80		
	17	0	2835.12	2835.12	1236.96		
	18	0	2835.12	2835.12	1178.05		
	19	0	2835.12	2835.12	1121.95		
	20	0	2835.12	2835.12	1068.53		
TOTAL					830402		

Table 8.11, Sensitivity analysis of the scenario 1c system

Sensitivity Analysis	
System Part	Percentages (%)
PV system	9.1
Electrolyser	4.0
Hydrogen Pipeline	86.9

The total present cost is £830,402 which corresponds to a unit cost of £50.94 per kg of H₂. The sensitivity analysis shows that the pipeline infrastructure is responsible for the biggest part of the costs.

8.2.2 Connection of the PV Array to the Electrolyser through a Battery Bank Scenario 2

The second scenario for the Ghana case study includes battery storage in the PV system. Using battery as a means of storing the energy supplied to the electrolyser system, presents certain advantages:

- Provides constant energy supply to the hydrogen generation system
- The size of the installed PV array is reduced, as the abundant energy is stored and used in periods of low PV power output
- The cost of the PV system is reduced

The costs of the PV part and the different storage configurations of the system are presented in Table 8.12. In the PV part, the costs of the battery are added which are 0.1£ /kWh. Prices and hydrogen unit costs of the three scenarios are presented in Table 8.13. Detailed presentation of the present cost analysis model for the solar hydrogen system for scenarios 2a (battery – metal hydride storage), 2b (battery – compressed gas storage) and 2c (battery – hydrogen pipeline system) can be found in Appendix H.

Table 8.12, Distribution of costs

Component	Sizes	Capital Cost (£)	O&M(% of investment costs)	Lifetime (years)
PV System	54kW	49,140	2%	20
Battery bank (Lead Acid)	48V/3500Ah	22,000	2%	10
PEM Electrolyser	2Nm ³ /h per electrolyser 20 cells, 4 stacks	7,673 per Nm ³ /h	2%	10
MH Storage		1,000 per Nm ³	2%	20
Compressed Gas Storage	20 tanks	£27/ Nm ³	2%	20
Hydrogen Pipeline		650000	2%	20

Table 8.13, Hydrogen unit costs referring to the battery system configurations

Ghana	Unit Cost (£/kg of Hydrogen)
Battery – MH	57.17
Battery – CGS	11.01
Battery – H2 Pipeline	51.15

8.3 Jamaica and Indonesia Case Studies Cost Analysis

The Jamaica case studies are sized according to the average daily cooking demand of a typical Jamaican household, which is 1.98kWh or 1.68kg of hydrogen per month, as showed in section 7.3.2, Chapter 7. According to this demand the system is sized as: 63kW PV array the no-battery case, and 50kW PV array and 150kWh battery, the battery case. The Indonesia case studies are sized according to the local household cooking demand, which is 2kWh or 2.7kg of hydrogen per month. According to this demand the system is sized as: 54kW PV array the no-battery case, and 36kW PV array and 150kWh battery, the battery case. The unit prices of the system components are the ones presented in section 8.2. The detailed tables presenting the cost benefit analysis of Jamaica and Indonesia case studies are presented in Appendix H.

8.4 Cost Benefit Analysis Results Discussion

Table 8.14 presents comparatively the results of the cost of hydrogen generation per kg of hydrogen for all the case study scenarios. Based on the results of the economic analysis, Table 8.14 shows that the most cost effective solution is the one with no battery and with compressed gas storage.

PV panels are still cheaper than the electrolyzers. Therefore, it is most cost efficient to install a bigger size of PV array to supply smaller size electrolyzers.

Table 8.14, Comparison of the scenarios of each case study country

Ghana	Unit Cost (£/kg of Hydrogen)
No battery –MH	55.66
No battery – CGS	10.35
No battery – H2 Pipeline	50.94
Battery – MH	57.17
Battery – CGS	11.01
Battery – H2 Pipeline	51.15
Jamaica	
No battery –MH	56.35
No battery – CGS	11.56
No battery – H2 Pipeline	62.56
Battery – MH	59.26
Battery – CGS	12.65
Battery – H2 Pipeline	64.16
Indonesia	
No battery –MH	55.09
No battery – CGS	10.65
No battery – H2 Pipeline	60.35
Battery – MH	56.25
Battery – CGS	10.59
Battery – H2 Pipeline	60.17

By selecting two electrolyzers of 20 cells and 4 stacks each, (apart from the Indonesia battery case study where the electrolyzers have 3 stacks) the production can satisfy the demand according to the monthly supply strategy.

Using compressed gas storage is an option that presents disadvantages in terms of safety for stationary domestic applications. One suggestion could be the cascade gas storage option, which uses the high pressure compressed gas cylinder situated at a location outside the household, connected to a low pressure cylinder inside the household that would provide the hydrogen gas to the stove at a low controlled pressure (Wilson, 2009). However, this option is considered complicated for a household application, and also involves certain risk as the high pressure compressed gas cylinders would be stored in the vicinity of the houses, in neighbourhoods that can be densely populated.

For the Jamaica and Indonesia case studies, the second most cost effective option is the metal hydride storage system without batteries. For Ghana, pipeline costs without batteries are less than the metal hydride case as the storage required is bigger than in Jamaica and Indonesia. The pipeline option is a well-established technology in Europe, USA and Japan and can be safely applied in the case studies. However, the implications and requirements to construct this system have been only theoretically evaluated; as it is not within the scope of this research to technically examine hydrogen pipelines. The metal hydride option is tested within the scope of this research and can be safely proposed as a storage system.

In terms of costs, the suggested system is still far from the European and DOE hydrogen costs targets (Bertuccioli, et al., 2014; NREL, 2014; DOE , 2012). The prices of the electrolyser and especially the metal hydride storage are still high in comparison to the traditional fuel generation and storage techniques. Nevertheless, the capital costs taken into consideration in this analysis are expected to be reduced in the nearby future thanks to higher production rates of electrolysers and reduced costs of the catalysts and metal hydride materials. An analogy can be made with PV cells costs, that as shown in Figure 8.1, their price reduced by 99.6% in a 35year period. As is projected by the IEA report on hydrogen production and storage, (IEA, 2006), the future potential costs of electrolytic hydrogen production are predicted to reduce by more than 50%.

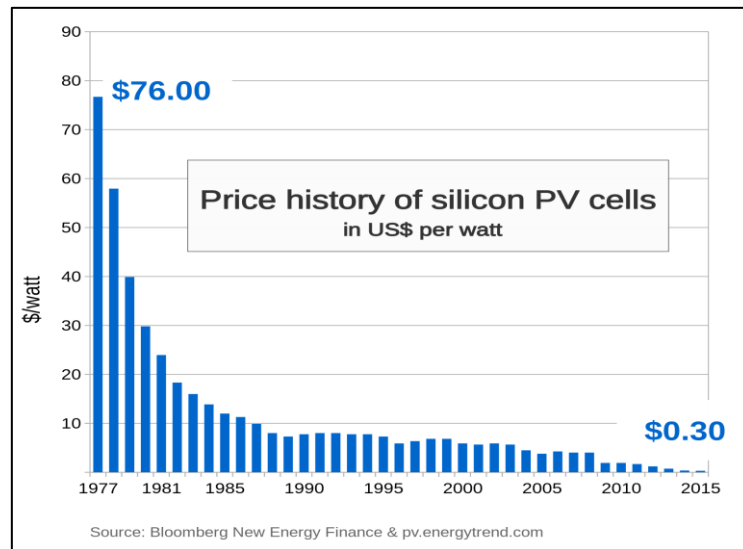


Figure 8.1, Price history of silicon PV cells, source: (Bloomberg New Energy Finance, 2015; Energy Trend PV, 2015)

8.5 Marginal Abatement Cost Curves

Marginal Abatement Cost (MAC) Curves consist of a popular method to quantitatively present and compare which actions are most effective in emissions reduction and what is their cost (McKinsley & Company, 2009). It is a visual method to evaluate carbon-reducing capital projects by ranking them in terms of carbon reduction and relative costs.

The marginal abatement cost is plotted on the y-axis, and the suggested technologies are hierarchically categorised from lowest to highest (left to right). The width of the column is equivalent to the amount of CO₂ emissions saved by the project, and the area of each column is equal to the cost or benefit of the project. Negative MAC values represent the self-financing projects. Oppositely, positive MAC curves require further financial consideration with respect to their costs. A MAC curve is a straightforward way to show proposed options that may be part of a sustainable development pathway, and what the costs and impacts of these alternatives could be. A MAC curve presents the extra (or ‘marginal’) costs and carbon reduction (or ‘abatement’) potential of these options in relation to a baseline. Figures 8.2, 8.3 and 8.4, show the calculated curves for each option for the Ghana, Jamaica and Indonesia case studies in relation to the CO₂ reduction target (indicated with the black dotted line), which represents the emissions from the cooking fuel use. The discount rate for these investments is assumed to be 3.5% as it is based on a societal perspective (Kesicki, 2011; HM Treasury, 2011).

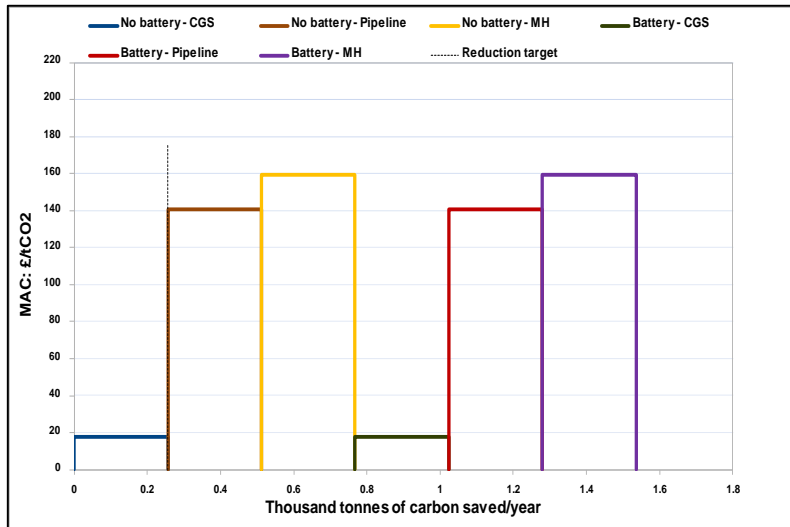


Figure 8.2, Ghana case studies options MAC curves

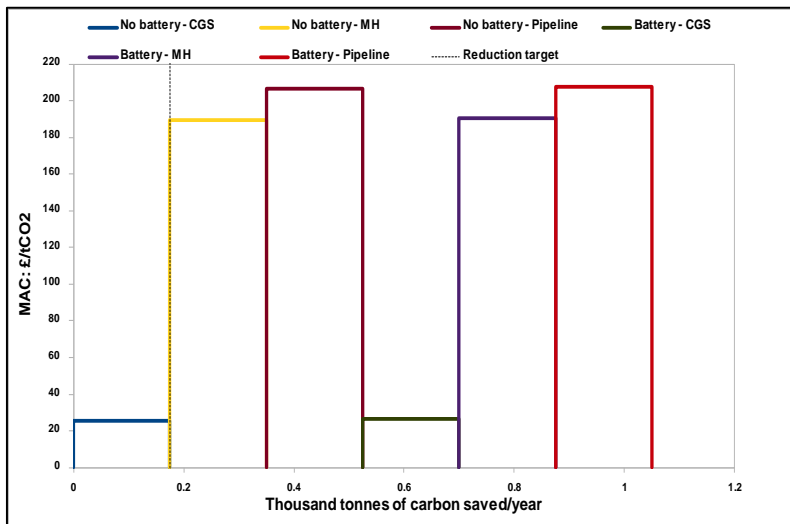


Figure 8.3, Jamaica case studies options MAC curves

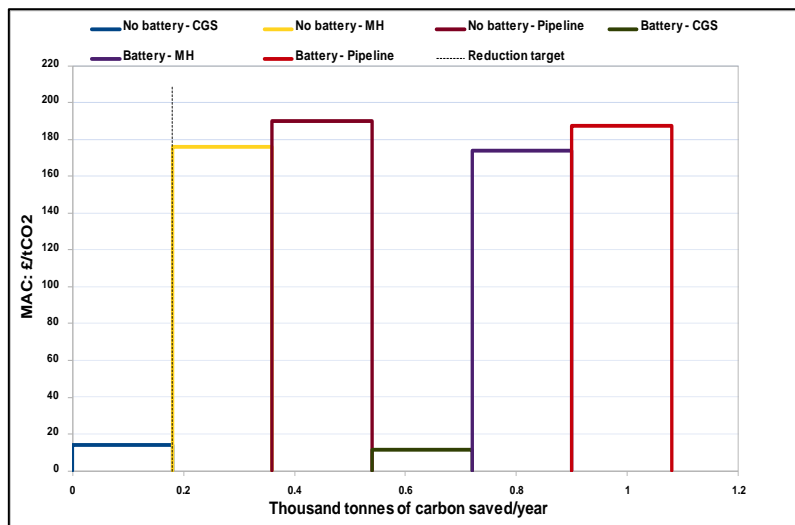


Figure 8.4, Indonesia case studies options MAC curves

As can be seen from the above MAC curves, all the suggested solutions can result in the CO₂ emissions reduction target, which is 175tn for the Jamaica case study, 256tn for the Ghana case study and 180tn for the Indonesia case study (EIA, 2012). These emissions correspond to the cooking fuel emissions of the 20 houses in each case, as explained in more detail in Chapter 7.

For the Ghana case study the most expensive solution is the battery with metal hydride storage case with 159.4£/tonne of CO₂, whereas the most cost effective one is the no-battery case with compressed gas storage with 17.8£/tonne of CO₂. Assuming that the investment capital cost would be covered by a state subsidy and the annual costs would be waved off, each year £2,140 would be saved from the 20 households, which contributes to the annual benefit of the project.

Contrariwise, for the Jamaica case study the most expensive solution is the battery with the hydrogen pipeline system case with 207.7£/tonne of CO₂, whereas the most cost effective one is the no-battery case with compressed gas storage with 26.7£/tonne of CO₂. For Jamaica, the compressed gas and metal hydride storage systems are smaller than the Ghana case, but the hydrogen pipeline system has the same size as it supplies the same amount of households. Therefore, the pipeline system results in higher costs in this case. Again assuming that the investment capital cost would be covered by a state subsidy and the annual costs would be waved off, each year £1000 would be saved from the 20 households which contributes to the annual benefit of the project.

Finally, for the Indonesia case study the most expensive solution is the no battery with the hydrogen pipeline system case with 190£/tonne of CO₂, whereas the most cost effective one is the battery compressed gas storage with 11.54£/tonne of CO₂. Each year £3200 would be waved off households assuming capital investment and annual O&M costs are covered by state subsidy.

The MAC curves information of the case studies can be found in Appendix H.

8.6 Summary

Chapter 8 examined the financial evaluation of large scale solar hydrogen systems case studies. Six configurations of the system are examined based on the two main designs of direct connection of the PV array to the electrolyser and supply of the electrolyser through a battery bank. Cost benefit analyses of the sub-configurations of the main designs are performed for the storage and distribution options of metal hydride tanks, compressed gas cylinders and hydrogen pipelines.

In all cases the direct connection systems are most cost efficient than the battery systems. Moreover, the results of the analyses indicate that the different configurations have a different effect on the generated hydrogen unit cost for each country, as they depend on the size of the hydrogen demand. For Ghana the system with the highest cost is the metal hydride storage with 57.17£/kg, whereas for Jamaica and Indonesia is the hydrogen pipeline network with 64.16£/kg and 60.17£/kg.

The replacement of the conventional cooking systems in the case studies with the solar hydrogen system has a significant capital cost at the present, that is however projected to decrease. Furthermore, the operational costs are minimal. The proposed systems can have a significant impact in CO₂ emissions reduction; 175tn of CO₂/year can be saved for the Jamaica case study, 256tn of CO₂/year for the Ghana case study and 180tn of CO₂/year for the Indonesia case study. The carbon reduction achieved in relation to the costs is further evaluated through Marginal Abatement Cost curves.

The proposed system provides improved health conditions, enhanced energy security and reduces environmental impact in terms of CO₂ emissions and reduced deforestation. The communities can benefit from the provision of a clean fuel which can be locally produced.

Chapter 9 will summarise the results and findings obtained from this study, and provide recommendations for future research.

Chapter 9. Conclusions and Future Recommendations

9.1 Overview

The main objective of the project was to investigate the application of a novel stand-alone solar-powered PEM electrolyser plant to produce hydrogen gas at a scale suitable for storage and distribution to multiple households for cooking. The main components of the system are a PV panel array which powers a PEM electrolyser plant, low pressure metal hydride storage systems and hydrogen stoves.

This thesis described the experimental and numerical process to evaluate the system's operation related to the PV array, the electrolytic hydrogen generation and the storage of the gas. It was centered around the development of a model that will simulate a solar powered PEM electrolyser plant for the generation of hydrogen to be used as a cooking fuel.

A numerical model was developed in TRNSYS based on experimental results of a purpose -built experimental rig. The model includes two new components developed based on this project for the simulation of the PEM electrolyser and hydrogen storage system. After validation of the components, large scale case studies were developed for application in Jamaica, Ghana and Indonesia.

This thesis includes (a) an extensive examination of solar hydrogen systems with a focus on location specific production of hydrogen for cooking (b) develops a model with two new components that can be used to simulate the system and examine the impact of technical parameters and (c) considers and analyses social and cultural factors that affect the system application.

Objectives set in the beginning of this research project were achieved as follows:

- A comprehensive literature review of solar hydrogen system applications with an overview of each component of the system is presented in Chapter 2
- The design and construction of the experimental setup, components and measuring equipment, are presented in Chapter 3. The objective of the experiments, along with the tests processes, is thoroughly explained.
- The results of experiments for the electrical characterisation of the proton exchange membrane (PEM) electrolyser unit, the electrochemical operation of the stack, the storage of hydrogen in metal hydride and the interaction between the metal hydride tank and the electrolyser are presented in Chapter 4. Experiments

with an alkaline solid polymeric membrane (ASPM) electrolyser were conducted and comparatively demonstrated.

- A numerical model of the solar hydrogen system in TRNSYS software was developed and presented in Chapter 5. The model includes novel components for the operation of the PEM stack, the PEM electrolyser controls and the metal hydride storage. The creation of the components in FORTRAN programming language and their integration in the TRNSYS libraries is presented. The validation process of the numerical model through a second set of experimental tests is demonstrated in this chapter.
- Ghana, Jamaica and Indonesia are the countries selected as case studies for the evaluation of the application of the solar hydrogen system and an overview of their energy sector with a focus on cooking is presented in Chapter 6. Statistical analyses are performed, and a specific quantitative study for Ghana and the domestic cooking demand profile is created for the three countries.
- The developed numerical model is employed and case studies for small communities of 20 households in the selected countries are developed in Chapter 7 with an aim to satisfy the cooking demands of the communities with the solar hydrogen system. A detailed description regarding the sizing of the system and its components is presented along with the simulation results.
- The impact of the weather data on the simulation is also explored in Chapter 7. Recent weather data for Jamaica and weather data available from the Meteorom database are analysed and compared through the use of Finkelstein-Schafer Statistics and simulations with the different weather data sets. The effect of the future weather data on the numerical model is evaluated following a similar methodology. Novel solar hydrogen potential maps are generated in this part that can act as initial decision making tool for solar hydrogen investments in the case study countries.
- Techno economic, analysis of the systems, with a comparison of different hydrogen distribution methods and marginal abatement cost (MAC) curves of the solar hydrogen system in Jamaica, Ghana and Indonesia are presented in Chapter 8.

9.2 Main Findings

- The literature review revealed that the use of cooking fuels is a major issue in developing economies for three main factors; impact on health, environmental impact (deforestation and CO₂ emissions) and energy security. It was shown through literature review that:
 - There is a shift towards introducing cleaner and renewable energy based cooking systems in developing economies. The projects that have been successful and mostly accepted by the local societies are those that are easily adopted and do not cause disruption of the daily habits and cooking schedule of local residents that traditionally cook in stoves
 - A solar powered electrolysis system has been proposed as a suitable option to generate hydrogen as an alternative cooking fuel
 - Hydrogen's high energy content of 140.4 MJ/kg on a weight basis, its fast diffusion and the fact that its combustion has no harmful gas by-products are advantageous characteristics for an energy carrier
 - Electrolytic hydrogen's costs are predicted to decrease in the near future
 - PEM electrolysis is advantageous over alkaline electrolysis as it provides greater safety since no caustic electrolyte is used and better efficiency in preventing gas mixing
 - Safety in domestic applications is of key importance in the project and the safety aspects that have to be addressed are highlighted as colour addition to the hydrogen gas flame and gas odorisation. In terms of hydrogen storage and distribution, the literature survey showed that the metal hydrides present a safety advantage as they operate in low pressures (2-25 bar) and have present higher energy density than compressed hydrogen gas and liquid hydrogen. Thus metal hydride was selected as the preferred storage method evaluated in this research work.

- The numerical model is developed based on the experimental tests results. The main components developed in this research are the PEM electrolyser, the controls and gas management and the metal hydride storage. The experiments provided information regarding: hydrogen generation rates, efficiency of the hydrogen

generation process in terms of stack and the complete electrolyser unit, losses due to the hydrogen management systems, hydrogen temperature and interaction between electrolyser and metal hydride storage, all for different hydrogen generation pressure. The main results of the experiments showed that:

- Hydrogen flow rates and stack temperature are higher at higher pressure set-points
- The stack temperature shows a greater increase as the flow rates increase, as the stack operates at a more frequent basis in order to produce sufficient hydrogen to maintain the pressure. At pressures up to 9 bar, the stack temperature is less than 40°C. For pressures within the range of 9 to 13.8 bar the stack temperature rises above 40°C and also increases at a higher rate
- This increase in the stack temperature causes an increase in the hydrogen production that leads to higher efficiencies. Between pressures of 10 and 13.8 bar, which is the maximum production pressure, highest efficiencies are observed
- The most efficient operation is at 13.8 bar and it corresponds to 5.1 kWh/Nm³ and 60.8 kWh/kg
- The direct current to the stack is measured to have a maximum value of approximately 27A when the stack operates at maximum rate. The current varies between 0-27A and the variation depends on the hydrogen that should be produced, which in turn depends on the demanded pressure.
- The stack voltage reduces with time as the stack temperature rises, which leads to a reduction of stack power with time.
- Additional tests with an ASPM electrolyse suggest that the replacement of the heating element for the purification of hydrogen, could lead to total energy use reduction
- As the pressure rises, the filling time of the metal hydride tank is faster as the hydrogen flow becomes higher and the temperature reaches higher points.

-
- Higher hydrogen supply pressures lead to higher absorption masses and higher temperatures. The stored mass varies between 0.4361gr at 5 bar to 0.4718gr at 13.8 bar
 - The maximum hydrogen storage capacity observed was 1.180wt% which is 15.7% less than the maximum for LaNi_5
- A numerical model was developed based on the above experimental results. TRNSYS was selected as the simulation software as it offers the possibility to add new components that are developed in this research, in one of the standard programming languages and integrate these components in the standard libraries; in this research FORTRAN is used. Furthermore, it allows interconnection of the hydrogen components with the standard components of the electrical, the weather data and control libraries which is essential for the optimization of the control strategies and the system sizing through multiple iterations. The main outcomes of the model development are:
- Creation of the PEM electrolyser component in TRNSYS that calculates information regarding: (a) hydrogen generation rates, (b) cell and stack voltage, (c) energy use of the stack that corresponds to the generation rates and (d) energy content of the generated hydrogen. The PEM electrolyser component is named type2627
 - Creation of the PEM electrolyser controls component is named type2628
 - Creation of the metal hydride storage tank which is named type2629 and models the absorption process
 - Comparison between all the validation experimental sets and the simulation results is performed and the average difference is 6.22% for 5bar, 6.12% for 7bar, 4.46% for 10bar and 3.70% for 13.8bar
- Statistical analyses are performed and the domestic cooking demand profile is created for the three case study countries. For Jamaica and Indonesia, this is based on available data from the literature, but for Ghana a specific quantitative study is conducted. The average daily cooking demands of typical households were found

to be 1.98 kWh for Jamaica, 2.50kWh for Ghana and 2 kWh for Indonesia. The main findings of the Ghana quantitative study are:

- The fuel use trend varies according to the area, the profession, the income and the educational attainment
 - Charcoal, firewood and LPG are the currently used cooking fuels
 - The poor population of the sample depends mainly on solid fuels, which has an effect on their health and wellbeing. 70% of the charcoal and firewood users stated that they suffer from the smoke and the dirt emitted by the combustion of these fuels
 - 99.4% of the participants showed willingness to change the currently used cooking fuels, to hydrogen cooking gas if it was cheaper and safer in use than the current cooking fuels
 - Replacing the use of the currently used fuels with hydrogen as a cooking fuel could lead to the annual reduction of 1986.5 tonnes of CO₂ and 178.3 tonnes of CO
- Based on the TRNSYS numerical model case studies are developed for small communities of 20 households in each country. In each case hydrogen is produced in a central plant, where the electrolysis process is powered by PV panels for a direct connection of the PV array to the electrolyser plant and a connection through battery bank. Hydrogen is generated at low pressure (13.8bar), directly stored in metal hydride cylinders and distributed to the households on a monthly basis.
- The system is designed so that the extra hydrogen production acts supplementary for the months that there is shortage, for two scenarios, the current conditions and the conditions after the 20 year period and a regulated operation and fuel supply is guaranteed for both scenarios
- Recent weather data for Jamaica and weather data available from the Meteonorm database are analysed and compared through the use of Finkelstein-Schafer Statistics in order to examine the suitability of the composite weather data.

Moreover, the effect of the future weather data on the numerical model is evaluated. The main results can be summarised as:

- Finkelstein-Schafer statistic indicates a difference between the recent and composite weather datasets. Nevertheless, the results of the simulation with the two weather data sets were found to differ only by 0.9% in the annual hydrogen production, thus confirming that the use of the composite weather file is reliable
 - The hydrogen generation for one year based on the morphed files is only 1.5% smaller than the Meteornorm simulation results. Moreover the morphed files introduce further uncertainties to the weather files. Therefore, the future conditions as represented by the future weather files have a negligible effect on the simulation results and it is thus preferable not to employ them
 - Solar hydrogen potential maps are created for the three case study countries and Ghana is proved to have the greatest solar hydrogen potential per area unit of the three countries, with 140.5 thousand kg/km²/year
- Cost benefit analyses of six configurations of the system are examined based on the two main designs of direct connection of the PV array to the electrolyser and supply of the electrolyser through a battery bank. Sub-configurations of the main designs are performed for the storage and distribution options of metal hydride tanks, compressed gas cylinders and hydrogen pipeline. The main conclusions of the economic analysis are:
- Direct connection systems are most cost efficient than the battery systems
 - The proposed systems can have a significant impact in CO₂ emissions reduction; 175tn of CO₂/year can be saved for the Jamaica case study, 256tn of CO₂/year for the Ghana case study and 180tn of CO₂/year for the Indonesia case study. This corresponds to an average 10tn of CO₂/year savings per household.
 - For Ghana the system with the highest cost is the metal hydride storage, whereas for Jamaica and Indonesia is the hydrogen pipeline network, which is further confirmed through Marginal Abatement Cost curves.

9.3 Recommendations for Further Work

The following are suggested as further work related to this research:

- The additional tests with the ASPM electrolyser indicated that the replacement of the heating element for the purification of hydrogen, could act as a future improvement in the PEM unit that can lead to energy use reduction. Therefore, it is recommended that the electrolysers employed in the future implementations of this research project be altered to include a different purification system than the current one. An alternative version of the purification system could be integrated in the TRNSYS model developed in this research as now the stack operation is modelled separately than the gas management components.
- It is suggested that a Life Cycle Analysis (LCA) should be conducted to assess the environmental impacts associated with the solar-powered PEM electrolyser plant. LCA can act as a complementary study to this research by evaluating the life cycle environmental performance of the system, and giving the comparison with the current situation of the conventional cooking systems.
- Further experimental test are required on the safety aspect of the hydrogen stove. With a preliminary basis the suggestions that are included in Appendix I for the addition of flame colour and odour to the gas, tests could be carried out in order to identify the most suitable and durable option. Interaction with the hydrogen gas, with the metal hydride storage and toxicity are some of the factors that are recommended to be studied.
- Quantitative surveys have been proved to provide good detail of information and also additional valuable data related to the main topic of quantifying the average daily cooking demand. Therefore, similar surveys in Jamaica and Indonesia would supplement the data and offer an evaluation the social and cultural implementations of this study.
- The weather data analysis could be expanded to compare the composite weather data of Meteonorm for Jamaica with longer term recent weather data, i.e. more than the three year period that is studied in this research. This would require the availability of the recent weather data, which is challenging. Furthermore, a similar analysis could be expanded to Ghana and Indonesia.

References

- Aim & Thurlby Thandar Instruments, 2014. *QPX1200S and QPX1200SP - 60 volts, 50 amps, 1200 watts.* [Online] Available at: <http://www.tti-test.com/products-tti/psu/qpx-series.htm> [Accessed 2014].
- Energy Commission Ghana, 2013. *Energy Outlook for Ghana 2013*, Accra: Energy Commission.
- International Energy Agency, 2013. *Southeast Asia Energy Outlook*, France: IEA.
- PDD Ghana Improved Stoves, 2009. *THE GOLD STANDARD: Project Design Document for Gold Standard Voluntary Offset Project Improved Household Charcoal Stoves in Ghana*, s.l.: The Gold Standard: Premium Quality Carbon Credits.
- University of Wisconsin - Madison, 2012. *TRNSYS 17 Mathematical Reference*, Madison: Solar Energy Laboratory, University of Wisconsin.
- Aalborg , 2014. *Aalborg High Quality Flow Instrumentation.* [Online] Available at: <http://www.aalborg.com/> [Accessed 2014].
- Abavana, C. G., 2004. *Ghana: Energy and Poverty Reduction Strategy*, Ouagadougou, Burkina Faso: Government of Ghana.
- Acar, C. & Dincer, I., 2013. Comparative Assessment of Hydrogen Production Methods from Renewable and Non-Renewable Sources. *International Journal of Hydrogen Energy*, p. 12.
- ACP Science and Technology Programme, 2015. *The application of solar-powered Polymer Electrolyte Membrane (PEM) electrolyzers for the sustainable production of hydrogen gas as fuel for domestic cooking.* [Online] Available at: <http://www.acp-st.eu/content/application-solar-powered-polymer-electrolyte-membrane-pem-electrolyzers-sustainable-product> [Accessed November 2015].
- ACTA, 2014. *ACTA Powered by Nature.* [Online] Available at: <http://www.actaspa.com/> [Accessed May 2014].
- Afrane, G. & Ntiamoah, A., 2012. Analysis of the Life-Cycle Costs and Environmental Impacts of Cooking Fuels used in Ghana. *Applied Energy*, Volume 98, pp. 301-306.
- Aguiar, R. & Collares-Pereira, M., 1988. A Simple Procedure for Generating Sequences of Daily Radiation Values Using a Library of Markov Transition Matrices. *Solar Energy*, 40(3), pp. 269-279.
- Ahiataku-Togobo, W., 2007. *Ghana Household Energy Project* , Abuja: s.n.
- Ahiataku-Togobo, W., 2013. *National Cooking Energy Strategies-Lessons from Ghana*, Ouagadougou: Ministry of Energy Ghana.
- Akpalu, W., Dasmani, I. & Aglobitse, P. B., 2011. Demand for Cooking Fuels in a Developing Country: To What Extend do Taste and Preferences Matter. *Energy Policy*, 39(2011), pp. 6525-6531.

-
- Alfrane, G. & Ntiamoah, A., 2012. Analysis of the Life-Cycle Costs and Environmental Impacts of Cooking Fuels Used in Ghana. *Applied Energy*, p. 6.
- Analog Devices, 2007-2013. *Quad, 12-/14-/16-Bit nanoDACs with 5 ppm/°C On-Chip Reference, I2C Interface.* [Online] Available at: http://www.analog.com/static/imported-files/data_sheets/AD5625R_5645R_5665R_5625_5665.pdf [Accessed July 2014].
- Arber, S., 1991. The Research Process. In: G. N., ed. *Researching Social Life*. London: SAGE Publications.
- Argiriou, A. et al., 1999. Comparison of Methodologies for Generation Using 20 Years Data for Athens, Greece. *Solar Energy*, 66(1), pp. 33-45.
- Ayers, K. et al., 2010. Research Advances towards Low Cost High Efficiency PEM Electrolysis. *ECS Transactions*, p. 12.
- Barbir, F., 2005. PEM Electrolysis for production of hydrogen from renewable energy sources. *Elsevier*, p. 9.
- BBPT, 2014. *Indonesia Energy Outlook 2014*. Jakarta, Agency for the Assessment and Application of Technology.
- Behzadi, M. S. & Niasati, M., 2014. Comparative performance analysis of a hybrid PV/FC/battery stand-alone system using different power management strategies and sizing approaches. *International Journal of Hydrogen Energy*, 40(2015), pp. 538-548.
- Belcher, S. E., Hacker, J. N. & Powell, D. A., 2005. Constructing Design Weather Data for Future Climates. *Building Services Eng. Res. Technol.*, 26(1), pp. 49-61.
- Bertuccioli, L. et al., 2014. *Development of Water Electrolysis in the European Union*, s.l.: Fuel Cells and Hydrogen Joint Undertaking.
- Biaku, C. Y. et al., 2008. A semiempirical Study of the Temperature Dependence of the Anode Charge Transfer Coefficient of a 6kW PEM Electrolyser. *International Journal of Hydrogen Energy*, 33(2008), pp. 4247-4254.
- Bloomberg New Energy Finance, 2015. *Bloomberg New Energy Finance*. [Online] Available at: <http://about.bnef.com/> [Accessed December 2015].
- Boadi, K. O. & Kuitunen, M., 2006. Factors Affecting the Choice of Cooking Fuel, Cooking Place and Respiratory Health in the Accra Metropolitan Area, Ghana. *Journal of Biosocial Science*, 38(2006), pp. 403-412.
- Britannica, E., 2014. *Lake Volta*. [Online] Available at: <http://www.britannica.com/EBchecked/topic/632445/Lake-Volta> [Accessed November 2014].
- Carmo, M., Fritz, D. L., Mergel, J. & Stolten, D., 2013. A Comprehensive Review on PEM Water Electrolysis. *International Journal of Hydrogen Energy*, Volume 38, pp. 4901-4934.
- Carmo, M., Fritz, D., Mergel, J. & Stolten, D., 2013. A comprehensive Review on PEM Water Electrolysis. *International Journal of Hydrogen Energy*, p. 34.

Chan, A. L., Chow, T. T., Fong, S. K. & Lin, J. Z., 2006. Generation of Typical Meteorological Year for Hong Kong. *Energy Conversion and Management*, Volume 47, pp. 87-96.

Chen, G., Chen, X. & Yue, P., 2002. Electrochemical Behavior of Novel Ti/IrO_x-Sb₂O₅-SnO₂ Anodes. *Journal of Physical Chemistry*, p. 6.

chris.bruniau@pragma-industries.com, 2015. *Metal hydride tank - pragma industries quate*, s.l.: s.n.

Civic Solar, 2015. *Trina Solar TSM-180DA01 180 Watts Solar Panel*. [Online] Available at: <http://www.civicsolar.com/product/trina-solar-tsm-180da01-solar-panel> [Accessed May 2015].

Clarke, R. E., Giddey, S. & Badwal, S., 2009. Stand-Alone PEM Water Electrolysis System for Fail Safe Operation with Renewable Energy Source. *International Journal of Hydrogen Energy*, p. 8.

Conext ComBox Login, 2014. *Conext ComBox Login*. [Online] Available at: <https://shrp.utech.edu.jm/login.html> [Accessed July 2014].

Crawley, D. B., 1998. *Which Weather Data Should You Use for Energy Simulations of Commercial Buildings?*, Washington D.C.: ASHRAE.

Cuce, E. & Cuce, P. M., 2012. A comprehensive review on solar cookers. *Applied Energy*, Volume 103, pp. 1399-1421.

Dale, N., Mann, M. & Salehfar, H., 2008. Semiempirical model based on thermodynamic principles for determining 6kW proton exchange membrane electrolyser stack characteristics. *Journal of Power Sources*, p. 6.

de Oliveira-Souza, A. et al., 2000. influence of the Preparation Method on the Morphological and Electrochemical Properties of Ti/IrO₂ coated Electrodes. *Electrochimica Acta*, p. 7.

Degiorgis, L., Santarelli, M. & Cali, M., 2007. Hydrogen from Renewable Energy: A Pilot Plan for Thermal Production and Mobility. *Journal of Power Sources*, Volume 171, pp. 237-246.

Dehouche, Z., Savard, M., Laurencelle, F. & Goyette, J., 2005. Ti-V-Mn Based Alloys for Hydrogen Compression System. *Journal of Alloys and Compounds*, 400(2005), pp. 276-280.

Dodds, P. E. & McDowall, W., 2012. *A review of hydrogen delivery technologies for energy system models*, London: UCL Energy Institute, University College London.

DOE, 2012. *Technical Plan - Production*. [Online] Available at: <http://www1.eere.energy.gov/hydrogenandfuelcells/mypp/pdfs/production.pdf> [Accessed August 2015].

DOE, 2013. *Hydrogen Production*. [Online] Available at: http://www1.eere.energy.gov/hydrogenandfuelcells/production/natural_gas.html [Accessed NOVEMBER 2013].

DuPont, 2013. *DuPont Nafion membranes and dispersions*. [Online] Available at: http://www2.dupont.com/FuelCells/en_US/products/nafion.html [Accessed March 2013].

DuPont, 2013. *DuPont™ Nafion® XL Membrane*. [Online] Available at: http://www2.dupont.com/FuelCells/en_US/products/nafion_xl_membrane.html [Accessed July 2014].

Dursun, E., Acarkan, B. & Kilic, O., 2012. Modeling of Hydrogen Production with a Stand-Alone Renewable Hybrid Power System. *International Journal of Hydrogen Energy*, 37(2012), pp. 3098-3107.

Eames, M., Kershaw, T. & Coley, D., 2012. A Comparison of Future Weather Created from Morphed Observed Weather and Created by a Weather Generator. *Building and Environment*, 56(2012), pp. 252-264.

Ecoenergia, 2015, *Renewable Energy Sources / Photovoltaic Projects Construction* [Online] Available at: <http://ecoenergia.gr/en/>

EEP, 2013. *Reducing Deforestation and GHG Emission with Biomass Stove and Fuel as Alternative Energy for a Community*, s.l.: Energy and Environmental Partnership with Indonesia.

EIA, 2012. *Total Carbon Dioxide Emissions from the Consumption of Energy 2012*. [Online] Available at: http://www.eia.gov/beta/international/data/browser/#?cy=2012&start=1980&end=2012&ord=SA&vs=INTL.44-8-GHA-MMTCD.A~INTL.44-8-IDN-MMTCD.A~INTL.44-8-JAM-MMTCD.A&v=H&vo=0&so=0&io=0&c=00000000000000001000102&pa=00000000000000000000000003&f=A&ug=g&ct=0&tl_type=p [Accessed May 2015].

Electronics Hub, 2015. *Solar Energy Power Generation*. [Online] Available at: <http://www.electronicshub.org/solar-energy-power-generation/> [Accessed December 2015].

Encyclopaedia Britannica, 2014. *Photovoltaic effect*. [Online] Available at: <http://www.britannica.com/science/photovoltaic-effect> [Accessed January 2014].

Energy Commission Ghana, 2006. *Woodfuels and Renewables*, Accra: Energy Commission.

Energy Commission Ghana, 2013. *2013 Energy Outlook for Ghana*, Accra: Energy Commission Ghana.

Energy Trend PV, 2015. *PV Spot Price*. [Online] Available at: <http://pv.energytrend.com/pricequotes.html> [Accessed December 2015].

-
- ESRI, 2015. *ArcGIS for Desktop*. [Online] Available at: <http://www.esri.com/software/arcgis/arcgis-for-desktop> [Accessed April 2015].
- European Photovoltaic Industry Association, 2013. *Global Market Outlook for Photovoltaic 2013-2017*. [Online] Available at: http://www.epia.org/index.php?eID=tx_nawsecuredl&u=0&file=/uploads/tx_epiapublications/GMO_2013_-_Final_PDF_01.pdf&t=1389623464&hash=74ca4c6a2243eea77607bf007a02c5368138e768 [Accessed January 2014].
- Ezilon maps, 2009. *Ghana Map - Political Map of Ghana*. [Online] Available at: <http://www.ezilon.com/maps/africa/ghana-maps.html> [Accessed November 2014].
- Fagbenle, R. L., 1995. Generation of a Test Reference Year for Ibadan, Nigeria. *Energy Conversion and Management*, Volume 36, pp. 61-63.
- Farnell, 2014. *TENMA - 72-7224 - CLAMP METER, DIG, HAND HELD, 3999*. [Online] Available at: <http://uk.farnell.com/tenma/72-7224/clamp-meter-dig-hand-held-3999/dp/1283640> [Accessed July 2014].
- Finkelstein, J. M. & Schafer, R. E., 1971. Improved Goodness of Fit-Tests. *Biometrika*, 58(3), pp. 641-645.
- Foell, W., Pachauri, S., Spreng, D. & Zerriffi, H., 2011. Household cooking fuels and technologies in developing economies. *Energy Policy*, 39(2011), pp. 7487-7496.
- Food and Agriculture Organisation of the United Nations, 2014. *Ghana Water resources*. [Online] Available at: http://www.fao.org/nr/water/aquastat/countries_regions/gha/index.stm [Accessed November 2014].
- Fraunhofer Institute, 2014, *Photovoltaics Report*. [Online] Available at: <https://www.ise.fraunhofer.de/de/downloads/pdf-files/aktuelles/photovoltaics-report-in-englischer-sprache.pdf>
- Gansler, R. A., Klein, S. A. & Beckman, W. A., 1994. Assessment of the Accuracy of Generated Meteorological Data for use in Solar Energy Simulation Studies. *Solar Energy*, 53(3), pp. 279-287.
- Garcia-Valverde, R., Espinosa, N. & Urbina, A., 2011. Simple PEM Water Electrolyser Model and Experimental Validation. *International Journal of Hydrogen Energy*, 37(2012), pp. 1927-1938.
- Gas Sense, 2014. *GasSense*. [Online] Available at: <http://www.gassense.eu/en/c/239-gas-sensors> [Accessed July 2014].
- Ghana Energy Ministry, 2014. *Ministry of Energy and Petroleum (MoEP), Ghana*. [Online]
-

Available at: <http://www.energymin.gov.gh/>
[Accessed November 2014].

Ghana Statistical Service, 2013. *Population and Housing Census 2010*, Accra: Ghana Statistical Service.

Ghana Statistical Service, 2013. *Population and Housing Census 2010*, Accra: Ghana Statistical Service.

Ghana Statistical Service, 2013. *Population and Housing Census 2010*, Accra: Ghana Statistical Service.

Ghana Statistical Service, 2014. *2010 Population and Housing Census*. [Online] Available at: <http://www.statsghana.gov.gh/docfiles/2010phc/National%20Population%20Projection%20010%20to%202014.pdf>
[Accessed November 2014].

Ghana Tourism, 2009. *Ghana Tourism*. [Online] Available at: http://www.touringghana.com/regions/volta_region.asp
[Accessed November 2014].

Ghana Volta Region Akatsi, 2014. *Akatsi South District*. [Online] Available at: <http://akatsi.ghanadistricts.gov.gh/>
[Accessed November 2014].

Ghana Volta Region Keta, 2006. *Ghana Volta Region Keta*. [Online] Available at: <http://keta.ghanadistricts.gov.gh/>
[Accessed November 2014].

Ghana Web, 2014. *Climate*. [Online] Available at: <http://www.ghanaweb.com/GhanaHomePage/geography/climate.php>
[Accessed November 2014].

Ghana, N. S. S. o., 2012. *Population by region, district, locality of residence, age groups and sex, 2010*. [Online] Available at: http://www.statsghana.gov.gh/docfiles/population_by_region_district_locality_of_residence_age_groups_and_sex_2010.pdf
[Accessed November 2014].

Global Alliance for Clean Cooking, 2015. *Cookstoves2015*. [Online] Available at: <https://www.cleancooking2015.org>
[Accessed November 2015].

Goffs School, 2014. *Goffs to Ghana*. [Online] Available at: <http://www.goffs.herts.sch.uk/enrichment/goffstoghana.shtml>
[Accessed November 2014].

Gorgun, H., 2006. Dynamic Modelling of a Proton Exchange Membrane Electrolyser. *International Journal of Hydrogen Energy*, 31(2006), pp. 29-38.

Government of Ghana, 2014. *Volta*. [Online] Available at: <http://www.ghana.gov.gh/index.php/about-ghana/regions/volta>
[Accessed November 2014].

-
- Guan, L., 2008. Preparation of Future Weather Data to Study the Impact of Climate Change on Buildings. *Building and Environment*, 44(2009), pp. 793-800.
- Guinot, B. et al., 2014. Techno-Economic Study of PV-Hydrogen-Battery Hydrogen System for Off-Grid Power Supply: Impact of Performances' Ageing on Optimal System Sizing and Competitiveness. *International Journal of Hydrogen Energy*, 2015(40), pp. 623-632.
- Gunningham, N., 2012. Managing the Energy Trilemma: The Case of Indonesia. *Energy Policy*, Volume 54, pp. 184-193.
- Gupta, R. B., 2009. *Hydrogen Fuel: Production, Transport and Storage*. Boca Raton: Taylor&Francis Group, LLC.
- Gupta, R. B., 2009. *Hydrogen Fuel-Production, Transport and Storage*. Boca Raton, Florida: Taylor & Francis Group LLC.
- Gupta, R. B., 2009. *Hydrogen Fuel-Production, Transport and Storage*. Boca Raton, Florida: Taylor & Francis Group LLC.
- H2FC European Infrastructure Project, 2013. *The European Technical School on Hydrogen and Fuel Cells 2013*. [Online] Available at: <http://h2fc.eu/technicalschool/46> [Accessed November 2015].
- Hamdan, M., 2011. *PEM Electrolyzer Incorporating an Advanced Low Cost Membrane*. [Online] Available at: http://www.hydrogen.energy.gov/pdfs/review11/pd030_hamdan_2011_o [Accessed January 2014].
- Hasan, M. H., Mahlia, T. I. & Nur, H., 2012. A Review on Energy Scenario and Sustainable Energy in Indonesia. *Renewable and Sustainable Energy Reviews*, 16(2012), pp. 2316-2328.
- Hinnemann, B. et al., 2005. Biornimetric Hydrogen Evolution: MoS₂ nanoparticles grown on graphene: an Advanced Catalyst for the Hydrogen evolution Reaction. *Journal of the American Chemical Society*.
- HM Treasury, 2011. *The Green Book - Appraisal and Evaluation in Central Government*, London: HM Treasury.
- Huboyo, H. S. et al., 2013. Characteristics of Indoor Air Pollution in Rural Mountainous and Rural Coastal Communities in Indonesia. *Atmospheric Environment*, Volume 82#, pp. 343-350.
- Hydrogen Components Inc., 2014. *Metal Hydrides*. [Online] Available at: <http://www.hydrogencomponents.com/hydride.html> [Accessed June 2015].
- Hyper Physics, 2014. *Thermal Conductivity*. [Online] Available at: <http://hyperphysics.phy-astr.gsu.edu/hbase/tables/thrcn.html> [Accessed 2014].
- IEA, 2006. *Energy For Cooking in Developing Countries*. [Online] Available at: <http://www.iea.org/publications/freepublications/publication/cooking.pdf> [Accessed November 2013].
-

-
- IEA, 2006. *Energy For Cooking in Developing Countries*. [Online] Available at: <http://www.iea.org/publications/freepublications/publication/cooking.pdf> [Accessed November 2013].
- IEA, 2006. *Hydrogen Production and Storage*, Paris: International Energy Agency.
- International Association for Hydrogen Energy, 2014. *International Association for Hydrogen Energy*. [Online] Available at: <http://www.iahe.org/> [Accessed July 2015].
- International Energy Agency, 2006. *Hydrogen Production and Storage-Hydrogen Implementing Agreement*, Paris: International Energy Agency.
- International Energy Agency, 2008. *Energy Policy Review of Indonesia*, France: IEA.
- International Energy Agency, 2011. *World Energy Outlook 2011*, s.l.: International Energy Agency.
- International Network on Gender and Sustainable Energy, 2006. *Gender Assessment of the Ghana Energy Sector*, s.l.: International Network on Gender and Sustainable Energy.
- International Network on Gender and Sustainable Energy, 2010. *Gender Assessment of the Ghana Energy Sector*, Ghana: Ministry of Energy.
- Inventors, 2015. *Definition of a Solar Cell - History of Solar Cells*. [Online] Available at: http://inventors.about.com/od/sstartinventions/a/solar_cell.htm [Accessed August 2015].
- Jentsch, M. F., Bahaj, A. S. & James, P. A., 2008. Climate Change Future Proofing of Buildings - Generation and Assessment of Building Simulation Weather Files. *Energy and Buildings*, 40(2008), pp. 2148-2168.
- Jentsch, M. F., James, P. A., Bourikas, L. & Bahaj, A. S., 2013. Transforming Existing Weather Data for Worldwide Locations to Enable Energy and Building Performance Simulation under Future Climates. *Renewable Energy*, 55(2013), pp. 514-524.
- Johnson , E., 2012. *Substituting LP Gas for Wood: Carbon and Deforestation Impacts*, s.l.: World LP Gas Association.
- Kalogirou, S. A., 2003. Generation of Typical Meteorological Year (TMY-2) for Nicosia, Cyprus. *Renewable Energy*, Volume 28, pp. 2317-2334.
- Kaygusuz, K., 2011. Energy for Sustainable Development: A Case of Developing Countries. *Renewable and Sustainable Energy Reviews*, p. 11.
- Kesicki, F., 2011. *Marginal Abatement Cost Curves for Policy Making - Expert-based vs..* Rio de Janeiro, 33rd IAEE International Conference.
- Kirk-Othmer Encyclopedia of Chemical Technology, 1992. *Fundamentals and Use of Hydrogen as a Fuel..* New York: Wiley.
- Larminie, J. & Dicks, A., 2003. *Fuel Cell Systems Explained*. Chichester, England: John Wiley & Sons.
- Larminie, J. & Dicks, A., 2003. *Fuel Cells Systems Explained*. Second ed. Chichester, England : John Wiley and Sons Ltd.

-
- Larsen, H., Feidenhans, R. & Sonderberg Petersen, L., 2004. *Hydrogen and its Competitors*, Iceland: Riso National Laboratory.
- Lee, K., Yoo, H. & Levenmore, G. J., 2009. Generation of Typical Weather Data Using the ISO Test Reference Year (TRY) Method for Major Cities of South Korea. *Building and Environment*, Volume 45, pp. 956-963.
- Levenmore, G. J. & Chow, D. H., 2006. *Solar Irradiation and Coincident Dry-bulb Temperature Selection for Load Calculations*, USA: ASHRAE.
- Loy, D. & Coviello, M., 2005. *Renewable Energies Potential in Jamaica*, Santiago: Ministry of Commerce Science & Technology Government of Jamaica.
- Lymperopoulos, N. & Zoulias, E., 2008. *Hydrogen-based Autonomous Power Systems: Techno-economic Analysis of the Integration of Hydrogen in Autonomous Power Systems*. s.l.:Springer.
- Manabe, A. et al., 2013. Basic study of alkaline water electrolysis. *Electrochimica Acta*, p. 7.
- Marangio, F., Santarelli, M. & Cali, M., 2009. Theoretical Model and Experimental Analysis of a High Pressure PEM Water Electrolyser for Hydrogen Production. *International Journal of Hydrogen Energy*, 34(2009), pp. 1143-1158.
- Massachusetts Academy of Math and Science, 2013. Cooking in Developing Countries. In: *Got Food? Recent advances in Food Science and Technology*. Massachusetts: Massachusetts Academy of Math and Science, p. 173.
- McKinsley & Company, 2009. *Pathways to a Low-Carbon Economy, Version 2 of the Global Greenhouse Gas Abatement Cost Curve*, s.l.: McKinsley & Company.
- MEMR, 2011. *Directorate General of Mineral and Coal, Indonesian Coal Resources Development and Future Direction of Coal Export*. Japan, International Symposium Clean Coal Day, Japan.
- Meteonorm Version 7, 2014. *Handbook Part1: Review and Software*, Bern: Meteonorm.
- Meteonorm, 2014. *Meteonorm Global Meteorological database*. [Online] Available at: http://meteonorm.com/images/uploads/downloads/mn71_software.pdf [Accessed June 2014].
- Meteotest, 2014. *Measurement Stations*. [Online] Available at: <http://meteonorm.com/products/meteonorm/stations/> [Accessed July 2014].
- Meteotest, 2014. *Meteonorm*. [Online] Available at: <http://meteonorm.com/> [Accessed November 2014].
- Meteotest, 2014. *Weather Stations in Meteonorm*. [Online] Available at: <http://meteonorm.com/en/> [Accessed July 2014].
- Milbrandt, A. & Mann, M., 2007. *Potential for Hydrogen Production from Key Renewable Resources in the United States*, Springfield , USA: NREL.
- Ministry of Energy and Mining, Jamaica, 2010. *National Renewable Energy Policy, 2009-2030*, Kingston: Ministry of Energy and Mining, Jamaica.
-

-
- Ministry of Energy and Mining, 2010. *National Renewable Energy Policy 2009-2030*, Kingston: Ministry of Energy and Mining.
- Ministry of Energy and Mining, 2010. *National Renewable Energy Policy 2009-2030*, Kingston: Ministry of Energy and Mining.
- Ministry of Energy, 2010. *National Energy Policy*, Ghana: Ministry of Energy.
- Mocoteguy, P. & Brisse, A., 2013. A Review and Comprehensive Analysis of Degradation Mechanisms of Solid Oxide Electrolysis Cells. *International Journal of Hydrogen Energy*, p. 6.
- Momirlan, M. & Veziroglou, V., 2002. Current Status of Hydrogen Energy. *Renewable and Sustainable Energy Reviews*, p. 39.
- Mujiyanto, S. & Tiess, G., 2013. Secure Energy Supply in 2025 : Indonesia's Need for an Energy Policy Strategy. *Energy Policy*, Volume 61, pp. 31-41.
- Murata Power Solutions, 2014. *ACM20 Series Four-Function AC Power Meters*. [Online] Available at: <http://www.murata-ps.com/datasheet?http://www.murata-ps.com/data/meters/acm20.pdf> [Accessed July 2014].
- Nasir, A., Fashe, J., Freeman, B. & Benamaisia, E., 2014. *Design and Dynamic Integration of Fuel cell and Solid State Hydrogen Storage Container for Low Carbon Combined Heat and Power Supply*, Uxbridge: Brunel University.
- NREL, 2012. *Photovoltaic Degradation Rates- An analytical Review*, Springfield: NREL.
- NREL, 2014. *Hydrogen Station Compression, Storage and Dispensing Technical Status and Costs*, Denver USA: NREL.
- Ohunakin, O. S., Adaramola, M. S., Oyewola, O. M. & Fagbenle, R. O., 2013. Generation of Typical Meteorological Year for North-East Nigeria. *Applied Energy*, Volume 112, pp. 152-159.
- Ojong, E., Smolinka, T., Guillet, N. & Mayousse, E., 2012. *A New Highly Efficient PEM Electrolysis Stack without Flow Channels Operating at High Pressure*. s.l., s.n.
- Owen, E. B. & Camirand, R., 2000. *Forest Cover and Deforestation in Jamaica-An Analysis of Forest Cover Estimates over Time*, Kingston: Forestry Department.
- Palmer, J. & Cooper, I., 2012. *United Kingdom Housing Energy Fact File*, s.l.: Department of Energy and Climate Change.
- Paterson Instruments, 2014. *Gas Sensors Approved for Industrial and Commercial use*. [Online] Available at: <http://www.gas-measuring-instrument.com/gas-sensors-approved-for-industrial-and-commercial-use-1-c.asp> [Accessed September 2014].
- Pavel, C. et al., 2013. Highly Efficient Platinum Group Metal Free Based Membrane-Electrode Assembly for Anion Exchange Membrane Water Electrolysis. *Angewandte Chemie*, Volume 52, pp. 1-5.
- Pertamina, 2008. *Kerosene to LP Gas Conversion Programme in Indonesia*, France: World LP Gas Association.
-

-
- Piroschka Otte, P., 2013. Solar cookers in developing countries—What is their key to success. *Energy Policy*, 63(2013), pp. 375-381.
- Planning Institute and Statistical Institute of Jamaica, 2007. *Residential Consumer End Use Survey Volume 1*, Kingston, Jamaica: Planning Institute and Statistical Institute of Jamaica.
- Pragma Industries, 2014. *Metal Hydride Hydrogen Storage Vessels*. [Online] Available at: <http://www.pragma-industries.com/products/hydrogen-storage/> [Accessed June 2015].
- Programme, U. N. D., 2015. *The Mekhe Solar Cooker Project*. [Online] Available at: http://www.undp.org/content/undp/en/home/librarypage/environment-energy/climate_change/the_mekhe_solar_cookerproject.html [Accessed November 2015].
- PROTON OnSite, 2012. *Technology*. [Online] Available at: <http://www.protononsite.com/resources/white-papers.html> [Accessed December 2012].
- Proton Onsite, 2014. *Proton Onsite*. [Online] Available at: <http://protononsite.com/> [Accessed May 2014].
- PVEducation.org, 2013. *Photovoltaic Effect*. [Online] Available at: <http://www.pveducation.org/pvcdrom/solar-cell-operation/photovoltaic-effect> [Accessed January 2014].
- Rabady, I. R., 2013. Optimized multi-junction photovoltaic solar cells for terrestrial applications. *Solar Energy*, p. 10.
- Rahman, I. A. & Dewsbury, J., 2007. Selection of Typical Weather Data for Subang, Malaysia. *Building and Environment*, Issue 42, pp. 3636-3641.
- Rainforest Action Network, 2014. *Indonesia Climate Change and Rainforests*, San Francisco: Rainforest Action Network.
- Raspberry Pi, 2014. *Raspberry Pi org Model B*. [Online] Available at: <http://www.raspberrypi.org/product/model-b/> [Accessed May 2014].
- Roads 2HyCom Project, 2009. *Fuel Cells and Hydrogen in a Sustainable Energy Economy*, s.l.: Roads 2HyCom Project.
- Rumbayan, M., Abudureyimu, A. & Nagasaka, K., 2012. Mapping of Solar Energy Potential in Indonesia using artificial neural network and geographical information system. *Renewable and Sustainable Energy Reviews*, 16(2016), pp. 1437-1449.
- Sakintuna, B., Lamari-Darkrim, F. & Hirscher, M., 2007. Metal Hydride Materials for Solid Hydrogen Storage: A Review. *International Journal of Hydrogen Energy*, pp. 1121-1140.
- Satya Sekhar, B., Suresh, P. & Muthukumar, P., 2012. Performance Tests on Metal Hydride Based Hydrogen Storage Devices. *International Journal of Hydrogen Energy*, 2013(38), pp. 9570-9577.
-

-
- Seth, M. & Essandoh, O., 2011. *Ghana Country Report*, s.l.: Ministry of Energy Ghana.
- Simon, G. L., Bumpus, A. G. & Mann, P., 2011. Win-win scenarios at the climate–development interface: Challenges and opportunities for stove replacement programs through carbon finance. *Global Environmental Change*, 22(2012), pp. 275-287.
- SMA Solar Technology AG, 2013. *Sunny Portal*. [Online] Available at: <http://www.sunnyportal.com/Templates/Start.aspx?ReturnUrl=%2f> [Accessed July 2014].
- Solar cooker, 2015. *Solar Cookers: Pros and Cons of the Different Types*. [Online] Available at: <http://www.solarcooker-at-cantinawest.com/solarcookers-prosandcons.html> [Accessed November].
- Solar Cookers International, 2015. *How Many Solar Cookers?*. [Online] Available at: <http://www.solarcookers.org/our-work/solar-cooker-distribution/> [Accessed November 2015].
- Solar Energy Laboratory, University of Wisconsin-Madison, 2014. *TRNSYS 1 Programmer's Guide*, Wisconsin-Madison: University of Wisconsin-Madison.
- Solar GIS, 2013. *Free Download of Solar Radiation Maps: Global Horizontal Irradiation (GHI)*. [Online] Available at: <http://solargis.info/doc/71> [Accessed November 2013].
- Song, S. & Haberl, J. S., 2013. Analysis of the Impact of Using Synthetic Data Correlated with Measured Data on the Calibrated as-built Simulation of Commercial Building. *Energy and Buildings*, p. 11.
- Sontay, 2012. *PM-CTR 4-20mA, 0-5Vdc & 0-10Vd*. [Online] Available at: <https://www.sontay.com/media/specs/PM-CTR.pdf> [Accessed 2014].
- Souahlia, A. et al., 2014. Experimental Study of Metal Hydride-Based Hydrogen Storage Tank at Constant Supply Pressure. *International Journal of Hydrogen Energy*, 2014(39), pp. 7365-7372.
- Spath, P. L. & Mann, M. K., 2001. *Life Cycle Assessment of Hydrogen Production via Natural Gas Steam Reforming*, Colorado: NREL.
- Strategic National Energy Plan 2006-2020 Annex 1, 2006. *Strategic National Energy Plan 2006-2020 Annex 1*, Accra: Energy Commission Ghana.
- SunPower, 2014. *Most Efficient Solar*. [Online] Available at: <http://us.sunpower.com/about/sunpower-technology/most-efficient-solar/> [Accessed January 2014].
- Terezo, A., Bisquert, J., Pereira, E. & Garcia-Belmonte, G., 2001. Separation of Transport, Charge Storage and Reaction Processes of Porous Electrochemical IrO₂ and IrO₂/Nb₂O₅ Electrodes. *Journal of Electroanalytical Chemistry*, p. 11.
- The International Statistical Institute, 2015. *Developing Countries*. [Online] Available at: <http://www.isi-web.org/component/content/article/5-root/root/81-developing> [Accessed May 2015].
-

-
- The Planning Institute and the Statistical Institute of Jamaica, 2007. *Residential Consumer End Use Survey*, Kingston: The Planning Institute and the Statistical Institute of Jamaica.
- The UN Refugee Agency, 2004. *Solar cooker offers ray of hope for refugee environment*. [Online]
Available at: <http://www.unhcr.org/40c08d4b4.html>
[Accessed November 2015].
- The University of Reading Statistical Services Centre, 2001. *Approaches to the Analysis of Survey Data*, Reading: The University of Reading.
- The World Bank, 2014. *Jamaica Development Indicators, Latin America and Caribbean, (developing only)*. [Online]
Available at: <http://data.worldbank.org/country/jamaica?display=default>
[Accessed May 2014].
- Thomson, D. E., 2005. *Verification, Validation and Solution Quality in Computational Physics*, Moffett Field, CA: NASA Ames Research Centre.
- Tongu, G. V. R. S., 2006. *South Tongu District*. [Online]
Available at: <http://southtongu.ghanadistricts.gov.gh/>
[Accessed November 2014].
- Topriska, E. et al., 2015. *Analysis of domestic cooking fuels demand in Ghana: field work and case study application of solar hydrogen cooking system*. Bucharest, s.n.
- TRNSYS 17, 2012. *Mathematical Reference*, Madison: Solar Energy Laboratory, University of Wisconsin.
- Ulleberg, O., 1998. *HYDROGEMS*, Kjeller: s.n.
- Ulleberg, O., 1998. *Stand-Alone Power Systems for the Future: Optimal Design, Operation & Control of Solar Hydrogen Energy Systems*. Trondheim: Department of Thermal Energy and Hydropower, Norwegian University of Science and Technology.
- Ulleberg, O., 2004. The Importance of Control Strategies in PV-Hydrogen Systems. *Solar Energy*, 76(2004), pp. 323-329.
- Ulleberg, O. & Morner, S. O., 1997. TRNSYS Simulation Models for Solar-Hydrogen Systems. *Pergamon*, p. 9.
- United Nations in India, 2015. *Sustainable Energy for all*. [Online]
Available at: <http://in.one.un.org/task-teams/sustainable-energy-for-all>
[Accessed November 2015].
- United Nations, 2006. *UN Millenium Project Goals, Targets and Indicators*. [Online]
Available at: <http://www.unmillenniumproject.org/goals/gti.htm#goal1>
[Accessed November 2013].
- United Nations, 2014. *Global Alliance for Clean Cookstoves*. [Online]
Available at: <http://www.cleancookstoves.org/our-work/the-solutions/cookstove-fuels.html>
[Accessed November 2014].
-

-
- United Nations, 2015. *A cooking stove improves lives in Kenya*. [Online] Available at: http://www.un.org/en/sustainablefuture/stories_kenya_cooking_stove.shtml [Accessed November 2015].
- United Nations, 2015. *Goal 7: Ensure access to affordable, reliable, sustainable and modern energy for all*. [Online] Available at: <http://www.un.org/sustainabledevelopment/energy/> [Accessed November 2015].
- University of Southampton, 2012. *Climate Change World Weather File Generator for World-Wide Weather Data – CCWorldWeatherGen*. [Online] Available at: <http://www.energy.soton.ac.uk/ccworldweathergen/> [Accessed March 2015].
- University of Technology Jamaica, 2014. *Sustainable Hydrogen Cooking Gas*. [Online] Available at: <http://www.solarhydrogen.utechsapna.com/> [Accessed May 2014].
- University of Technology, Jamaica, 2010. *Faculty of Engineering & Computing Receives Portable Weather Station for Solar Energy Research*. [Online] Available at: <http://www.utechjamaica.edu.jm/news/vol14iss11/> [Accessed July 2014].
- University of Technology, Jamaica, 2015. *Sustainable Hydrogen Cooking Gas Project*. [Online] Available at: <http://www.solarhydrogen.utechsapna.com/> [Accessed November 2015].
- University of Wisconsin - Madison, 2014. *TRNSYS Standard Component Library Overview*, Madison: University of Wisconsin - Madison.
- Ursua, A., Martin, I. A., Barrios, E. & Sanchis, P., 2013. Stand-alone operation of an alkaline water electrolyser fed by wind and photovoltaic systems. *International Journal of Hydrogen Energy*, p. 16.
- US Department of Energy, 2013. *Energy Plus Simulation Software - Weather Data for Simulation*. [Online] Available at: http://apps1.eere.energy.gov/buildings/energyplus/weatherdata_simulation.cfm [Accessed July 2014].
- Veziroglou, N. & Sahin, S., 2008. 21st Century Energy:Hydrogen Energy System. *Energy Conversion and Management*, p. 12.
- Weather Online, 2015. *Weather Online- Indonesia*. [Online] Available at: <http://www.weatheronline.co.uk/reports/climate/Indonesia.htm> [Accessed February 2015].
- Welaya, Y. M., El Gohary, M. M. & Ammar, N. R., 2012. Steam and Partial Oxidation Reforming Options for Hydrogen Production from Fossil Fuels for PEM Fuel Cells. *Alexandria Engineering Journal*, p. 6.
- Wenham, S. R., Green, M. A., Watt, M. E. & Corkish, R., 2007. *Applied Photovoltaics*. Padstow, Cornwall: TJ International Ltd.
-

-
- Wilcox, S. & Marion, W., 2008. *User's Manual for TMY3 Data Sets*. [Online] Available at: <http://www.nrel.gov/docs/fy08osti/43156.pdf> [Accessed July 2014].
- Wilson, E. A., 2009. *Investigation of Renewable, Coupled Solar-Hydrogen Fuel Generation with Thermal Management Systems Suitable for Equatorial Regions*. Uxbridge: Brunel University.
- Winrock International, 2007. *Indonesia Overview of the National Energy Policy*, s.l.: Winrock International.
- World Health Organisation, 2006. *Fuel for Life : Household Energy and Health*. [Online] Available at: <http://www.who.int/indoorair/publications/fuelforlife.pdf> [Accessed November 2013].
- World Health Organisation, 2006. *World Health Organisation*. [Online] Available at: <http://www.who.int/mediacentre/news/releases/2006/pr22/en/> [Accessed November 2013].
- World Health Organisation, 2014. *Household air pollution and health*. [Online] Available at: <http://www.who.int/mediacentre/factsheets/fs292/en/> [Accessed November 2015].
- World Nuclear Association, 2014. *World Nuclear Association*. [Online] Available at: <http://www.world-nuclear.org/info/Current-and-Future-Generation/World-Energy-Needs-and-Nuclear-Power/> [Accessed March 2014].
- World Weather and Climate Information, 2013. *Average weather in Accra, Ghana*. [Online] Available at: <http://www.weather-and-climate.com/average-monthly-Rainfall-Temperature-Sunshine,Accra,Ghana> [Accessed November 2014].
- Zang, H., Xu, Q., Pengwei, D. & Ichiyanagi, K., 2012. A Modified Method to Generate Typical Meteorological Years from Long-Term Weather Database. *International Journal of Photoenergy*, Volume 2012, p. 9.
- Zeng, K. & Zhang, D., 2014. Evaluating the effect of surface modifications on Ni based electrodes for alkaline water electrolysis. *Fuel*, p. 7.
- Zhou, K., Ferreira, J. A. & de Hann, S., 2007. Optimal Energy Management Strategy and System Sizing Method for Stand-Alone Photovoltaic-Hydrogen Systems. *International Journal of Hydrogen Energy*, 2008(33), pp. 477-489.
- Zini, G. & Tartarini, P., 2012. *Solar Hydrogen Energy Systems*. s.l.:Springer.
- Zini, G. & Tartarini, P., 2012. *Solar Hydrogen Energy Systems*. Italy: Springer.
- Zoulias, E. I. & Lympelopoulos, N., 2008. *Hydrogen-Based Autonomous Power Systems*. 1 ed. London: Springer.
- Zoulias, E. et al., 2005. *A Review on Water Electrolysis*, Nicosia, Cyprus: Frederick Research Centre (FRC), Centre for Renewable Sources (CRES).
- Zuttel, A., 2003. Materials for Hydrogen Storage. *Materials Today*, 6(9), pp. 24-33.

**Experimental and computational study of a solar
powered hydrogen production system for domestic
cooking applications in developing economies**

Appendices

A thesis submitted for the degree of

Doctor of Philosophy (PhD)

by

Evangelia Vasiliki Topriská

College of Engineering, Design, and Physical Sciences

Brunel University London



Contents

Appendix A. Pioneer Demonstration Solar Hydrogen System Projects	15
Appendix B. Analysis and Market Research of individual PEM electrolyzers characteristics.....	18
Appendix C. Experimental Setup.....	30
C.1 Python Code for the programming of the Raspberry Pi.	33
C.2 Python Code Example	34
C.3 Uncertainty Analysis	35
Appendix D. Numerical Model Development and Validation.....	40
D.1 TRNSYS Codes.....	47
D.2 Data of Validation Experiments	74
Appendix E. Ghana Quantitative Survey.....	94
E.1 Additional Information of the Field Study.....	100
Appendix F. Jamaica and Indonesia Case Studies Jamaica Case Study.....	105
F.1 Jamaica Case Studies	108
F.2 Indonesia Case Study	119
Appendix G. Weather Data Analysis	128
G.1 Weather Data Types	128
Appendix H. Economic Analysis of Case Studies	152
H.1 Connection of the PV Array to the Electrolyser through a Battery Bank for Ghana Case Studies	152
H.2 Jamaica Case Studies Cost Analysis	156
H.3 Indonesia Case Studies Cost Analysis.....	163
H.4 Marginal Abatement Curves Calculation Methodology.....	170
H.5 Quotation of the metal hydride tanks	171
Appendix I. Hydrogen Safety Report	172

Appendix J. Risk Assessment for Hydrogen Lab Work	183
References	187

List of figures

Figure B.1, Quotation of the HOGEN GC600 electrolyser from Proton OnSite.....	27
Figure B.2, Quotation of the H-Tec Electrolyser	28
Figure B.3, Quotation of the Hydrogenics electrolyser	29
Figure C.1, % Error vs. Device Flow	38
Figure D.1, Hydrogen flow at the generating pressure of 5bar.....	40
Figure D.2, Hydrogen flow at the generating pressure of 6bar.....	40
Figure D.3, Hydrogen flow at the generating pressure of 7bar.....	40
Figure D.4, Hydrogen flow at the generating pressure of 8bar.....	40
Figure D.5, Hydrogen flow at the generating pressure of 9bar.....	41
Figure D.6, Hydrogen flow at the generating pressure of 10bar.....	41
Figure D.7, Hydrogen flow at the generating pressure of 11bar.....	41
Figure D.8, Hydrogen flow at the generating pressure of 12bar.....	41
Figure D.9, Hydrogen flow at the generating pressure of 13bar.....	41
Figure D.10, Variable DC current and voltage to the stack while producing constant hydrogen at 5bar.....	42
Figure D.11, Variable DC power to the stack while producing constant hydrogen at 5bar	42
Figure D.12, Variable DC current and voltage to the stack while producing constant hydrogen at 10bar.....	42
Figure D.13, Variable DC power to the stack while producing constant hydrogen at 10bar	42
Figure D.14, Hydrogen production rate in L/h at 5bar, 7bar,10bar,13.8bar pressure set points during day 2 that presents unstable irradiance levels	43
Figure D.15, Hydrogen production rate in L/h at 5bar, 7bar,10bar,13.8bar pressure set points during day 3 that presents unstable irradiance levels	43
Figure D.16, Hydrogen production rate in L/h at 5bar, 7bar, 10bar, 13.8bar pressure set points during day 5 that presents consistently high irradiance levels	44

Figure D.17, Hydrogen production rate in L/h at 5bar, 7bar,10bar,13.8bar pressure set points during day 6 that presents consistently high irradiance levels	44
Figure D.18, Hydrogen production rate in L/h at 5bar, 7bar,10bar,13.8bar pressure set points during 18 th of May in Jamaica, that presents unstable irradiance levels	45
Figure D.19, Hydrogen production rate in L/h at 5bar, 7bar,10bar,13.8bar pressure set points during 4 th of December in Jamaica, that presents consistently high irradiance levels	45
Figure D.20, Hydrogen production rate in L/h at 5bar, 7bar,10bar,13.8bar pressure set points during 8 th of Deceber in Jamaica, that presents unstable irradiance level.....	46
Figure D.21, Hydrogen production rate in L/h at 5bar, 7bar,10bar,13.8bar pressure set points during 9 th of December in Jamaica, that presents unstable irradiance levels	46
Figure D.22, Experimental and numerical model hydrogen flow rates results.....	75
Figure D.23, Stack voltage results from the IV curve and the model at 39°C.....	75
Figure D.24, Experimental and numerical model stack temperature data	78
Figure D.25, Experimental and numerical model metal hydride tank filling times.....	78
Figure D.26, Trina Solar panels characteristics	80
Figure D.27, Sanyo HIT panels characteristics.....	81
Figure D.28, Sharp panels characteristics	82
Figure E.1, Questionnaire sample of the Ghana survey.....	94
Figure E.2, Questionnaire sample of the Ghana survey.....	95
Figure E.3, Questionnaire sample of the Ghana survey.....	96
Figure E.4, Questionnaire sample of the Ghana survey.....	97
Figure E.5, Questionnaire sample of the Ghana survey.....	98
Figure E.6, Questionnaire sample of the Ghana survey.....	99
Figure E.7, Household area where cooking takes place in relation to the used main fuel	100
Figure E.8, Time of the day that cooking takes place	101

Figure E.9, Time of the day that cooking takes place in relation to the main cooking fuel	102
Figure E.10, Time of the day that cooking takes place according to the profession	102
Figure E.11 , Percentage of LPG cylinders’ sizes preferred by the participants	104
Figure E.12, Percentage of charcoal bags’ sizes preferred by the participants.....	104
Figure E.13, Percentage of firewood ties number preferred by the participants.....	104
Figure F.1, Ghana battery case study TRNSYS print screen.....	106
Figure F.2, TRNSYS simulation results for the Ghana battery case study for the month of May	107
Figure F.3, Monthly demand and production of hydrogen and PV yield for the current conditions and after the panel degradation period for the Ghana battery case study.....	108
Figure F.4, Jamaica direct connection case study TRNSYS print screen.....	110
Figure F.5, Jamaica annual global horizontal irradiance and temperature values from Meteonorm file.....	112
Figure F.6, TRNSYS simulation results for the Jamaica direct connection case study for the month of April.....	113
Figure F.7, TRNSYS simulation results for the Jamaica direct connection case study for the month of May.....	114
Figure F.8, Monthly demand and production of hydrogen and PV yield for the current conditions and after the panel degradation period for the Jamaica case study	115
Figure F.9, Jamaica battery case study TRNSYS print screen	116
Figure F.10, TRNSYS simulation results for the Jamaica battery case study for the month of April.....	117
Figure F.11, TRNSYS simulation results for the Jamaica battery case study for the month of May	118
Figure F.12, Monthly demand and production of hydrogen and PV yield for the current conditions and after the panel degradation period for the Jamaica battery case study	118
Figure F.13, Indonesia direct connection case study TRNSYS print screen	120

Figure F.14, Indonesia annual global horizontal irradiance and temperature values from Meteorom file.....	122
Figure F.15, TRNSYS simulation results for the Indonesia direct connection case study for the month of May	123
Figure F.16, Monthly demand and production of hydrogen and PV yield for the current conditions and after the panel degradation period for the Indonesia case study.....	124
Figure F.17 Indonesia battery case study TRNSYS print screen.....	125
Figure F.18, TRNSYS simulation results for the Indonesia battery case study for the month of May.....	126
Figure F.19, Monthly demand and production of hydrogen and PV yield for the current conditions and after the panel degradation period for the Indonesia battery case study...	127
Figure G.1, Comparison between the CDF curves for Temperature for 2011.....	132
Figure G.2, Comparison between the CDF curves for Temperature for 2012.....	132
Figure G.3, Comparison between the CDF curves for Temperature for 2013.....	132
Figure G.4, Comparison between the CDF curves for Temperature for all years	133
Figure G.5, Comparison between the CDF curves for Relative Humidity for 2011	133
Figure G.6, Comparison between the CDF curves for Relative Humidity for 2012	133
Figure G.7, Comparison between the CDF curves for Relative Humidity for 2013	134
Figure G.8, Comparison between the CDF curves for Relative Humidity all years.....	134
Figure G.9, Comparison between the CDF curves for Wind Speed for 2011	134
Figure G.10, Comparison between the CDF curves for Wind Speed for 2012	135
Figure G.11, Comparison between the CDF curves for Wind Speed for 2013	135
Figure G.12, Comparison between the CDF curves for Wind Speed for all years	135
Figure G.13, CDF Comparison of global horizontal radiation for February 2011	136
Figure G.14, CDF Comparison of global horizontal radiation for March 2011	136
Figure G.15, CDF Comparison of global horizontal radiation for April 2011	136
Figure G.16, CDF Comparison of global horizontal radiation for May 2011	137

Figure G.17, CDF Comparison of global horizontal radiation for June 2011	137
Figure G.18, CDF Comparison of global horizontal radiation for July 2011	137
Figure G.19, CDF Comparison of global horizontal radiation for August 2011	138
Figure G.20, CDF Comparison of global horizontal radiation for September 2011.....	138
Figure G.21, CDF Comparison of global horizontal radiation for October 2011	138
Figure G.22, CDF Comparison of global horizontal radiation for November 2011.....	139
Figure G.23, Global Horizontal Radiation in Kingston, Jamaica for 2011.....	145
Figure G.24, Dry Bulb Temperature in Kingston, Jamaica for 2011.....	146
Figure G.25, Relative Humidity in Kingston, Jamaica for 2011	146
Figure G.26, Wind Speed in Kingston, Jamaica for 2011	146
Figure G.27, Global Horizontal Radiation in Kingston, Jamaica for 2012.....	147
Figure G.28, Dry Bulb Temperature in Kingston, Jamaica for 2012.....	147
Figure G.29, Relative Humidity in Kingston, Jamaica for 2012	147
Figure G.30, Wind Speed in Kingston, Jamaica for 2012	148
Figure G.31, Global Horizontal Radiation in Kingston, Jamaica for 2013.....	148
Figure G.32, Dry Bulb Temperature in Kingston, Jamaica for 2013.....	148
Figure G.33, Relative Humidity in Kingston, Jamaica for 2013	149
Figure G.34, Wind Speed in Kingston, Jamaica for 2013	149
Figure G.35, Global Horizontal Radiation in Kingston, Jamaica from Meteonorm Typical Meteorological Year.....	149
Figure G.36, Dry Bulb Temperature in Kingston, Jamaica from Meteonorm Typical Meteorological Year.....	150
Figure G.37, Relative Humidity in Kingston, Jamaica from Meteonorm Typical Meteorological Year.....	150
Figure G.38, Wind Speed in Kingston, Jamaica from Meteonorm Typical Meteorological Year.....	150
Figure G.39, Solar hydrogen potential map generation steps	151

Figure H.1, Marginal Abatement Curves Calculation for Ghana	170
Figure H.2, Marginal Abatement Curves Calculation for Jamaica	170
Figure H.3, Marginal Abatement Curves Calculation for Indonesia	171
Figure H.4, Quotation from Pragma Industries regarding the price of the metal hydride tanks	171
Figure I.1 chemical structure of TBM	174
Figure I.2, chemical structure of DMS.....	174
Figure I.3, Wick odorizer, adjustable and non-adjustable	178
Figure I.4, By-pass odorizer.....	178
Figure I.5, Space shuttle launch, blue colour for H ₂ -O ₂ fuelled engines.....	179

List of Tables

Table.A.1, Milestone Project on Solar Hydrogen Systems.....	17
Table B.1, Comparison between the technical characteristics of the electrolyzers	24
Table B.2, Basic criteria for the selection of the three final manufacturers.....	26
Table C.1, Experimental Equipment Costs	30
Table C.2, Laboratory equipment for the experimental setup	32
Table C.3, Digital mass flow meter characteristics.....	37
Table C.4, Measurements uncertainties of the flow meter.....	39
Table D.1, Summary of types of Experiments and the total number of days of experimental work	83
Table D.2, Example of weather and PV Power Output Data used in the Experiments, for the 1 st of June 2013	84
Table D.3, Example of weather and PV Power Output Data used in the Experiments, for the 1 st of June 2013	85
Table D.4, Typical example of current values used in the Jamaica conditions experiments	85
Table D.5, Example of measured data of the experimental test at 5 bar for day 6 of the UK data set.....	86
Table D.6, Example of measured data of the experimental test at 7 bar for day 6 of the UK data set.....	87
Table D.7, Example of measured data of the experimental test at 10 bar for day 6 of the UK data set.....	88
Table D.8, Example of measured data of the experimental test at 13.8 bar for day 6 of the UK data set.....	89
Table D.9, Example of measured data of the experimental test at 5 bar for day 1 of the UK data set.....	90
Table D.10, Example of measured data of the experimental test at 7 bar for day 1 of the UK data set.....	91

Table D.11, Example of measured data of the experimental test at 10 bar for day 1 of the UK data set.....	92
Table D.12, Example of measured data of the experimental test at 13.8 bar for day 1 of the UK data set.....	93
Table E.1, Household area where cooking takes place in relation to the used main fuel .	100
Table F.1, Ghana battery case study hydrogen production and PV yield at current and future conditions.....	108
Table F.2, monthly and annual demand in kg of hydrogen for the Ghanaian case study .	109
Table F.3, Jamaica case study hydrogen production and PV yield at current and future conditions	115
Table F.4 Jamaica battery case study hydrogen production and PV yield at current and future conditions.....	119
Table F.5, monthly and annual demand in kg of hydrogen for the Indonesian case study	120
Table F.6, Indonesia case study hydrogen production and PV yield at current and future conditions	124
Table F.7 Each PEM electrolysers’ parameters in the Indonesia battery case study	125
Table F.8, Indonesia battery case study hydrogen production and PV yield at current and future conditions.....	127
Table G.1, FS Statistics for each month of each of the three recent yearly weather data sets compared to the Meteonorm Weather Data for Global Horizontal Radiation	139
Table G.2, FS Statistics for each month of each of the three recent yearly weather data sets compared to the Meteonorm Weather Data for Dry bulb temperature	139
Table G.3, FS Statistics for each month of each of the three recent yearly weather data sets compared to the Meteonorm Weather Data for Relative Humidity	140
Table G.4, FS Statistics for each month of each of the three recent yearly weather data sets compared to the Meteonorm Weather Data for Wind Speed.....	140
Table G.5, Weighted FS Statistics for each month	141

Table G.6, Minimum and Maximum Daily Values of Global Horizontal Radiation for the recent and Meteorological data.....	141
Table G.7, Minimum and Maximum Daily Values of Temperature for the recent and Meteorological data	142
Table G.8, Minimum and Maximum Daily Values of Relative Humidity for the recent and Meteorological data	142
Table G.9, Minimum and Maximum Daily Values of Wind Speed for the recent and Meteorological data	143
Table G.10, Average Values of Global Horizontal Radiation for the recent and Meteorological data	143
Table G.11, Average Values of Temperature for the recent and Meteorological data.....	144
Table G.12, Average Values of Relative Humidity for the recent and Meteorological data..	144
Table G.13, Average Values of Wind Speed for the recent and Meteorological data.....	145
Table H.1, Scenario 2a - Distribution of costs	152
Table H.2, Present cost analysis model for the solar hydrogen system, referring to scenario 2a.....	153
Table H.3, Sensitivity analysis of the scenario 2a system	153
Table H.4, Present cost analysis model for the solar hydrogen system, referring to scenario 2b.....	154
Table H.5, Sensitivity analysis of the scenario 2b system	154
Table H.6, Present cost analysis model for the solar hydrogen system, referring to scenario 2c.....	155
Table H.7, Sensitivity analysis of the scenario 2b system	155
Table H.8, Present cost analysis model for the solar hydrogen system, referring to Jamaica scenario 1a.....	157
Table H.9, Sensitivity analysis of the Jamaica scenario 1a system	157
Table H.10, Present cost analysis model for the solar hydrogen system, referring to Jamaica scenario 1b.....	158

Table H.11, Sensitivity analysis of the Jamaica scenario 1b system	158
Table H.12, Present cost analysis model for the solar hydrogen system, referring to Jamaica scenario 1c.....	159
Table H.13, Sensitivity analysis of the Jamaica scenario 1c system	159
Table H.14, Present cost analysis model for the solar hydrogen system, referring to Jamaica scenario 2a.....	160
Table H.15, Sensitivity analysis of the Jamaica scenario 2a system	160
Table H.16, Present cost analysis model for the solar hydrogen system, referring to Jamaica scenario 2b.....	161
Table H.17, Sensitivity analysis of the Jamaica scenario 2b system	161
Table H.18, Present cost analysis model for the solar hydrogen system, referring to Jamaica scenario 2c.....	162
Table H.19, Sensitivity analysis of the Jamaica scenario 2c system	162
Table H.20 , Present cost analysis model for the solar hydrogen system, referring to Indonesia scenario 1a	164
Table H.21, Sensitivity analysis of the Indonesia scenario 1a system.....	164
Table H.22, Present cost analysis model for the solar hydrogen system, referring to Indonesia scenario 1b.....	165
Table H.23, Sensitivity analysis of the Indonesia scenario 1b system.....	165
Table H.24, Present cost analysis model for the solar hydrogen system, referring to Indonesia scenario 1c	166
Table H.25, Sensitivity analysis of the Indonesia scenario 1c system.....	166
Table H.26, Present cost analysis model for the solar hydrogen system, referring to Indonesia scenario 2a	167
Table H.27, Sensitivity analysis of the Indonesia scenario 2a system.....	167
Table H.28, Present cost analysis model for the solar hydrogen system, referring to Indonesia scenario 2b.....	168
Table H.29, Sensitivity analysis of the Indonesia scenario 2b system.....	168

Table H.30, Present cost analysis model for the solar hydrogen system, referring to Indonesia scenario 2c	169
Table H.31, Sensitivity analysis of the Indonesia scenario 2c system.....	169
Table I.1, typical flame colorants, source: (Kosanke, et al., 2004).....	180

Appendix A. Pioneer Demonstration Solar Hydrogen System Projects

This appendix and Table A.1 provide literature information regarding the pioneer projects of solar hydrogen systems.

The ground breaking solar hydrogen project started in 1993 in Julich, Germany. The PHOEBUS project (“Photovoltaik, Elektrolyse, Brennstoffzelle and Systemtechnik”- Photovoltaic, Electrolysis, Fuel Cells and System Engineering) was meant to be an independent renewables energy system that would supply the Central Library of Forschungszentrum Julich (FZJ) (Meurer, et al., 1999). The goal of the PHOEBUS project was to integrate hydrogen storage into an autonomous energy production system based on photovoltaic panels. The system consisted of a photovoltaic panels generator that supplied an alkaline electrolyser through an MPP tracker and a DC/DC converter. It also included a lead-acid battery that served as a day-by-day buffer. What is very important regarding the PHOEBUS project is that the operation and the efficiency of the system and its parts were carefully examined. The contribution of this project to the solar hydrogen sector is major and it is worth mentioned that it was the “pioneer solar hydrogen project”.

The “Solar-Hydrogen Cycle Project- SAPHYS” was a project introduced by the Italian National Agency for New Technology, Energy and Environment in 1994. The plant was comprised of photovoltaic panels that were directly coupled to an alkaline electrolyser and the produced hydrogen was stored in metal hydride alloys and standard gas cylinders (Galli & Stefanoni, 1997)

Another promising project that expands the renewable part of the hydrogen production is the design and construction of a pilot hydrogen plant for thermal production and mobility in a small village in the area of Valle d’Aosta in Italy. This project consisted of a PEM electrolyser that was supplied by a combination of photovoltaic panels and hydroelectricity, taking advantage of the natural resources of the area (Degiorgis, et al., 2007). This work proved that renewable hydrogen systems could prove to be a very efficient and cost effective way to produce and distribute energy locally.

In the recent years, the European Union countries have demonstrated a great interest towards the research and the development of solar hydrogen production systems. This is proved by a series of projects that have advanced throughout Europe in the decades 1991-2000, 2001-2010. The FIRST Project was an off-grid photovoltaic panel hydrogen production project in Madrid, Spain. The project was introduced by a telecommunication

company and consisted of two main designs; a solar hydrogen fuel cell system, where the fuel cell was mainly used as a backup system for the batteries, and a fully autonomous PEM electrolyser system with metal hydride storage and a fuel cell (Yilanci, et al., 2008).

The HARI Project in the United Kingdom introduced the integration of an alkaline electrolyser and fuel cell system into an already existing renewable energy production scheme, consisting of photovoltaic panels and wind turbines. In the same way, the HRI Project in Canada introduced a solar-wind hydrogen production project that mainly examined the possibilities of long-term hydrogen storage.

The INTA project in Spain, 1989, investigated the solar hydrogen production with a target to explore the storage possibilities and the applications in the space sector. Different possible ways to power the alkaline electrolyser were examined: the direct coupling with the photovoltaic panels through and MPP tracker and the connection through a DC/AC inverter.

The Schatz Project was one of the numerous in Germany and consisted of a directly coupled alkaline electrolyser with photovoltaic panels and a PEM fuel cell. During the operation of this system, problems regarding the matching of the photovoltaic panels with the electrolyser during cold and hot weather conditions were reported as well as malfunction of the fuel cell. In a similar way the Solar-Wasserstoff-Bayern project, was an industrial scale programme that utilised photovoltaic panels to supply via a DC/DC connection an alkaline electrolyser and a fuel cell.

Germany has been one of the European countries that have been most advanced in the sector of solar hydrogen research. This is mostly indicative from the self-sufficient Solar House Project, in Freiburg, Germany constructed by the Freinhofer Institute for Solar Energy Systems. This house was energy autonomous, and covered all the needs in electricity, heating, domestic hot water and cooking by photovoltaic panels. Hydrogen is used as a medium to store energy and a fuel cell is used for the conversion of the energy to electricity. What is very significant in this project is that for the first time the use of catalytic combustion for the combustion of hydrogen for domestic cooking is introduced (Yilanci, et al., 2008) (Goetzberger, et al., 1993).

Outside Europe, there has been a steady growth of interest towards solar hydrogen systems from the Middle East, and especially Saudi Arabia and the Gulf countries. These countries being the main producers and exporters of oil begin to change their energy policies as the

world proceeds further in renewable energy policies. The oil reserves are limited, and as scientifically proven they will be depleted within the following 5 decades. Thus, the major oil exporters keeping an eye in the future want to limit their internal oil consumption and instead sell (Rifkin, 2003). This can be achieved by switching their national energy systems and adapting renewable energy sources and solar hydrogen systems as this has been showed by the HYSOLAR Project. In this project, the Kingdom of Saudi Arabia has collaborated with German institutes and universities in order to promote the solar hydrogen technology and educate the local scientists (Grasse, et al., 1991) (Abaoud & Hartmut, 1998)

Table.A.1, Milestone Project on Solar Hydrogen Systems

Project Name	Author Name	Country	Electrolyser Type	Type of Connection between PV and Electrolyser	Purpose	Year
Solar Hydrogen Cycle Project-SAPHYS	Galli, Stefanoni	Italy	Alkaline-Alyser 0100, by Metkon Alyser, Switzerland	Direct	Fuel Cell-electricity	1997
PHOEBUS	(Meurer, et al., 1999)	Germany	7 bar Alkaline, by Alyser, Switzerland	DC/DC Conversion	Fuel Cell-electricity	1993
Valle d'Aosta	Degiorgis, Santarelli, & Cali	Italy	PEM	DC/AC conversion	Thermal production & mobility	2007
FIRST		Spain	PEM	Direct	Fuel Cell-electricity	2000
HARI		United Kingdom	Alkaline	DC/AC conversion	PEM Fuel Cell-electricity	2002
HRI		Canada	Alkaline	DC/AC conversion	PEM Fuel Cell-electricity	2001
INTA		Spain	Alkaline	DC/AC conversion	PAFC/PEM-electricity	1989-1997
Schatz		Germany	Alkaline	Direct	PEM Fuel Cell-electricity	1989
Solar-Wasserstoff-Bayern		Germany	Alkaline	DC/DC	PAFC-electricity	1989
Freiburg Solar House		Germany	Alkaline	DC/AC conversion	PAFC-electricity	1992

Appendix B. Analysis and Market Research of individual PEM electrolyser characteristics

This appendix presents the information related to the market research for the electrolyser selection. The market analysis is presented in the form of a deliverable report of the ACP/EU PROJECT 2012-2015.

The application of Solar-Powered Polymer Electrolyte Membrane (PEM) Electrolysers for the Sustainable Production of Hydrogen Gas as Fuel for Domestic Cooking - ACP/EU PROJECT 2012-2015

Activity (Year 1): Acquisition of Equipment

Prepared by Brunel University

Evangelia Topriská, Zahir Dehouche and Maria Kolokotroni

Introduction

This Report deals with the presentation of the procedure done in order to specify the Electrolyser models that are appropriate for the project. A thorough market research was conducted and the most prominent Electrolyser Manufacturers in the global market were detected and contacted. In more details the steps followed to complete the search were:

- Specification of the requirements for the Electrolyser (*see table 1*) (membrane type, hydrogen production flow rate, hydrogen delivery pressure etc.)
- Detailed and in-depth research so that the best Electrolyser manufacturers of the English, European and Global market were found. This was a tedious process where each manufacturer was contacted in order to retrieve information. Numerous emails have been sent to the companies and phone calls were made in order to collect the required technical information for the Electrolyser products and their cost. This was a time consuming procedure since some of them are based in countries outside Europe or do not have representative branches in the United Kingdom. In the end, it was not possible to get feedback from all manufactures contacted. Therefore, some were rejected for the reason that they didn't participate in the correspondence. On the other hand, a regular communication was developed between Brunel University and the manufacturers that were eager to make a business deal with us. In this way quotes were gathered and prices for the products that are presented in this report (<GVerkoeyen@hydrogenics.com>, 2012)

(<Piers.Capper@boc.com> Capper, 2012) (<TSkoczylas@protononsite.com>, 2012) (<F.Salusti@acta-nanotech.com>, 2012), (<steveh@itm-power.com> Steve Hallett, 2012) (<b.hempel@h-tec.com> Björn Hempel, 2012) (<pascal.pewinski@ceth.fr>, 2012), (<b.hempel@h-tec.com> Björn Hempel, 2012).

The research, which lasted for almost a month, resulted in seven manufacturers that have products that could be adequate. These are described in detail in the next section.

Originally selected manufacturers

As already stated seven manufacturers were initially considered as possible Electrolyser suppliers. All the Electrolyser models fulfil the requirements of minimum hydrogen gas production rate of 600 cc/min (which roughly corresponds to 1 lt/min), at a discharge pressure of 10-30 bar. In relation to the Nafion membrane, NO Electrolyser manufacturer will provide any kind of information regarding the brand of the internal components. No information is provided regarding the I-V curve of the Electrolyser either. Nevertheless, specifications about the performance and the stability of the membrane are given in detail.

Companies and technologies are here briefly presented. Detailed information of the electrolyser characteristics and comparison process that led to the selection is given in Tables B.1 and B.2.

1. PROTON
2. ACTASPA
3. LINDE
4. ITM
5. HTEC
6. HYDROGENICS
7. CETH2

1.Proton

Three Proton models were originally taken into consideration:

HOGEN GC 600 Series Hydrogen Generator

- i. **HOGEN S10 (13.8 bar)**
- ii. **HOGEN HP10 (same as the S10, only the pressure changes, ~165 bar)**

The HOGEN® hydrogen generators use AC electric power and deionized water to produce a continuous stream of pressurized scientific grade (99.9999 %) hydrogen gas and automatically maintain a user-selected downstream pressure. They are suitable for use in laboratories and light industrial environments. HOGEN® GC series hydrogen generators serve applications requiring up to 2 lt/min of scientific grade (99.9999+%) hydrogen at pressure up to 13.7 bar. Low Maintenance is required and replacement of water quality resin bags every six months.

2. ActaSpa

ActaSpa has a unique technology called AES that combines the advantages of the PEM and Alkaline electrolyzers. There is no need of the noble metals at the electrodes that the PEM electrolyzers require and this reduces the purchase and maintenance costs radically. In addition to this the input power is not required to be constant and the Electrolyser can be directly connected to Off-grid power systems such as Photovoltaic Panels.

Another important advantage is that the hydrogen at the output is already compressed and dry enough for direct use for most applications. For laboratory use a vapour trap is required. Rain water can also be used with the proper filter and in general the purity of the water is not at the levels that a PEM Electrolyser requires which makes this model even more cost effective.

3. Linde

It is a company that offers Laboratory gas generators with low maintenance requirements. They offer a big variety of laboratory Electrolyzers and among them there are models that produce exactly the amount of hydrogen that we require. Its advanced dual-column drying system automatically removes residual moisture from the hydrogen produced. (Gas, 2012)

4. ITM

ITM is a British company that offer some of the most advanced Electrolyser technologies in the global market. Two ITM models were originally taken into consideration:

i. Hbox Solar

This Electrolyser can follow the variable power generation of the PV panels and produce hydrogen at a high efficiency to an energy store. The delivery pressure is 14 bar, with a minimum system efficiency of 78%. It has a rated power of 1.3kWp and hydrogen output

rate up to 3lt/min. This company offers a unique Passive stack design that maximises the efficiency by instantaneously following the characteristic maximum power point locus of a solar cell.

This system has the great advantage that has a DC input and can fluctuate the production according to the input. i.e. the hydrogen production will be in accordance to the production of the PV panels. Plus it causes very low parasitic loads. It has an integrated thermal management system for maximizing the hydrogen gas production rate after periods of darkness or bad weather.

ii. **HBox 3000**

It is similar to HBox Solar but has an AC input

5. H-Tec

This company is also one of the most prominent companies in the Electrolyser market. In fact, their products have been used in similar projects before (Paul, 2009). The product that was considered to be most appropriate for our case was the EL30, in terms of hydrogen production rate and discharge pressure (H-TEC Systems, 2012).

6. Hydrogenics

It is a company situated in Belgium that has the advantage of experience in big projects. This product was attractive because it offered the smallest consumption per kWh (4.9 kWh/Nm³ of H₂ at full load) (Hydrogenics, 2012; <GVerkoeyen@hydrogenics.com>, 2012)

7. CETH2

This is a French company whose products offered the advantage of small hydrogen production. But, the consumption per kWh (5.2 kWh/Nm³ of H₂) is greater than the other manufacturers and its size and weight are also prohibitive (1800x600x2200 mm, 300 kg). (CETH2, 2012)

To conclude to those seven manufacturers, more were examined during this month:

Hydro, is a company from Norway that was also considered a possible supplier. This company was rejected because their electrolyser products are only of very large scale (Power Production Plants) (Hydro, 2012).

Air Liquide, is a French company that was also taken into consideration, since they offer solutions for on-site hydrogen production and hydrogen cylinders for laboratory use. Unfortunately, communication with this company has proved to be impossible in order to request more information about whether they provide Hydrogen Electrolysers (*Air Liquide*, 2011).

Another company that was examined as a possible suitable manufacturer was *Intelligent Energy*, which is the company that enabled the fuel cell use in vehicles and more specifically in taxis, during the 2012 London Olympic Games. As proved, after research this company manufactures only fuel cells and not electrolysers (*Intelligent Energy*, 2012).

Another manufacturer that was considered and rejected was *Air Products*, since the solution they offer is only large scale (*Air Products*, 2012).

Finally, the products of *McPhy Energy* were examined. *McPhy* is a French company that offers complete solutions for hydrogen production and storage. They mainly produce large scale systems as well, but they do offer the possibility of renewable as a supply for the electrolyser. Nonetheless, this complete solution would not be appropriate for the project, since it limits the degree of freedom to design the system (*McPhy Energy*, 2012).

Recommendation of the three manufacturers

Of the above manufacturers after a detailed comparison, four were rejected and three are recommended as most appropriate for the project's requirements. These are the ones that offer the best combination of the price and technical requirements satisfaction (*see table 2*).

They are thus prioritised as:

- 1. ACTA SPA**
- 2. PROTON**
- 3. LINDE**

The products that were considered to be the mostly adequate for our project were the HOGEN® GC600 of Proton, the EL100 of ActaSpa and the NMH2 of Linde.

The HOGEN® GC600 satisfies the requirements of the project and comes at a good price. In addition to this The HOGEN GC 600 is a very reliable product; there are over 1000 systems in the field worldwide and maintain fleet uptime of greater than 99% (<TSkoczylas@protononsite.com>, 2012). Experimentally, it has been used before for laboratory use by Barbir F, Strathclyde University and others. (*Papagiannakis*, 2005;

Barbir, 2005). Also, a Proton Electrolyser was successfully used in a solar hydrogen system in Mexico in 2006 by Arriaga et al (Arriaga, et al., 2006). The Linde Electrolyser has a user friendly digital display that informs the user about the operating status and diagnostic data. The greatest advantage of this company is that it is a local manufacturer and supplier, located in Surrey that is not far from Brunel University. Finally, the EL100 has the great advantage that it fulfils our requirements and at the same time has a flexible power input and the best price.

In this part the reasons for the rejection of the rest of the manufacturers have to be mentioned:

The products of ITM are considered to be the most technologically developed and advanced in comparison to the rest. What is even more important is the HBox Solar fulfils the DC input requirement and plus offers a unique management system that automatically regulates the hydrogen production according to the power input. Nevertheless, their price was far exceeding our criteria and this complete solution that they offer limits the possibilities of experimental investigation from Brunel University's part.

For the H-Tec Electrolyser the delivery time is approximately 7 months after receipt of initial payment (H-TEC quote). The company is currently working on the CE certification of their electrolysers. Until the final CE certification their electrolysers must be used only for evaluation purposes, and as they state in their quote "*It is not admissible to pass on the units to third parties or to market them before final granting of CE certification*" (<b.hempel@h-tec.com> Björn Hempel, 2012).

The size of the system and also the price was the main reason that the Hydrogenics Electrolyser was declined since in this case it was extremely out of our budget.

The CETH2 even though contacted many times by our part never replied or sent any feedback. Finally, they responded informing us that they do not any more produce small scale electrolyser systems (<pascal.pewinski@ceth.fr>, 2012).

The comparison between the technical characteristics of the electrolysers can be found in the tables accompanying this document, where it can be seen more clearly the dominance of the three recommended models over the rest.

Table B.1, Comparison between the technical characteristics of the electrolyzers

Characteristics	HOKEN GC 600 (Proton)	HOKEN S10 (Proton)	HBox Solar (ITM)	Hbox 3000	Linde NMH2 generator	Acta EL100	Hydro genics	CETH 2	HTEC
Purchase Cost (€)	11,396		32,594	23,819	12,927	4,300	85,000		52,717
Maintenace Period and Cost (€)	Expected life over 10 years. Replace water quality resin bag every six months				Expected life over 10 years. H2 cell standard costs 1,484€. Deionisation bag extra cost				
Membrane Type	Proton Exchange Membrane (PEM) solid electrolyte, maintenance and caustic-free	Proton Exchange Membrane (PEM) - caustic-free	PEM		Solid polymer membrane				
Net Hydrogen Production Rate	600 cc/min→1 SLPM (actually is 0.6 SLPM)	4.7 SLPM	20 – 40 kg H ₂ /Year		1 SLPM	1.66 SLPM	166 SLPM	83.33 SLPM	5.5 SLPM
Delivery Pressure	3 - 13.8 bar	13.8 bar	14 bar		0.1-10.5 bar	15-30 bar	10	14 bar	30 bar
Purity	99.99990%	99.99950%	99.99%		99.99950%	99.94% at 30 bar without purification system, 99.99% with purification system	99.99 %	99.99 %	
Manual Fill Water Capacity	1.9 liters		8 litres			5 lt			
Water Requirement Rate at Max Consumption Rate	0.9 lt per 24 hours of operation	0.47 L/hr	150 cc/h→0.0025 SLPM			0.08 lt per hour	60 lt per hour	<10 lt per hour	

Table B.1 continued

Input Water Quality	ASTM Type II Reagent Grade DI Water	ASTM Type II Reagent Grade DI Water	Deionised ASTM Type 2 DI water	Deionised ASTM Type 2 DI water	Deionized or distilled	Supermarket grade, demineralized water		tap water	tap water
Electrical Specification	110-220 VAC, 1ph, 50/60 Hz	205-240 VAC, 1ph, 50/60 Hz	DC	AC	AC	AC/ DC 20-80 V	400 V , 3ph	400 V , 3ph	35-250 VAC
Rated power	<1200 watts	8 kVA	1.3 kW	700 W			100kV A	40 kVA	1.8 kW
Control Systems	LED high visibility display; Adjustable pressure output; Remote alarm terminal; Switchable psi/kPa pressure reading	Fully automated, push button start/stop. On-board H2 Leak detection. Automatic fault detection system depressurization.	Intelligent control for MPPT tracking the available input from the PV	No MPPT or Thermal management	Auto shut-off and low internal volume (< 40ml)	Alarm LED, Low water level alarm, automatic pressure release, Self-diagnostics			
Dimensions	58 x 71 x 41 cm	97 x 114 x 132 cm	67.5 x 126 x 92 cm	52 x 49 x 85 cm	23 x 35 x 43 cm	25.2 x 46.1 x 50 cm	170 x 185 x 260cm	2400 x 180 x 220 cm	120 x 56 x 60 cm
Weight	30 kg	295 kg			18 kg	27 kg	1000kg	1500kg	120kg
Operating Environment	Laboratory, indoor, temperature-controlled & well ventilated	Indoor	Indoors, well ventilated	Indoors, well ventilated		Laboratory, Indoor and Off Grid			
Environmental Conditions (temperature, RH)		5-40°C, 0 to 90% RH non-condensing, Non-hazardous/non-classified environment, ventilation needed	15 – 25°C	15 – 25°C		5-40 °C and 20-95% RH	5-40 °C and 20-95% RH	3-40 °C and 0-95% RH	5-40 °C and 0-90% RH
Warranty	2 years parts factory labor				2years parts, factory labor				2 years parts factory labour
Training	None	None	None	None	None	None	Yes	Yes	Yes

Table B.2, Basic criteria for the selection of the three final manufacturers

Basic Choice Criteria*	Limits	ACTASPA EL100	PROTON-HOGEN GC600	LINDE NMH2 generator	ITM-Hbox Solar	ITM-Hbox 3000	Hydrogenics	CETH2	HTEC EL30
Price €		4,300	11,396	12,927	32,593.85	23,818.58	85,000	...	52,717
PEM Membrane	<i>It should have PEM membrane . Does it?</i>	yes	yes	yes	yes	yes	yes	yes	yes
Minimum Hydrogen Production Rate of 600 cc/min	<i>Is the Minimum Production Rate 600 cc/min?</i>	yes	yes	yes	yes	yes	yes	yes	yes
Hydrogen Discharge Pressure 10-30 bar	<i>Is the Hydrogen delivered at 10-30 bar?</i>	yes	yes	yes	yes	yes	yes	yes	yes
DC input	<i>Is the supply DC?</i>	yes	no	no	yes	no	no	no	yes
Maintenance Cost €	<i>low-big ?</i>	low	low	low	low	low	big	big	big
Rated Power	<i><1000</i>	700 W	<1200 watts	...	1.3 kW	700 W	100 kVA	40 kVA	1.8 kW
Dimensions	<i>As small as possible for lab use</i>	25.2 x 46.1 x 50 cm	58 x 71 x 41 cm		67.5 x 126 x 92 cm	52 x 49 x 85 cm	170 x 185 x 260cm	2400 x 180 x 220 cm	120 x 56 x 60 cm
Weight	<i>As light as possible for lab use</i>	27 kg	30 kg				>1000kg	1500kg	120kg
Choice Output		YES	YES	YES	NO	NO	NO	NO	NO

The quotation of the HOGEN GC600 can be seen in Figure B.1

Proton Energy Systems, Inc d/b/a Proton OnSite 10 Technology Drive Wallingford CT 06492 USA Phone: 203-878-2000 Fax: 203-949-8016		 THE LEADER IN ON SITE GAS GENERATION.		Quote Number: 104177 Page: 1 of 4		
Sold To: Brunel University School of Engineering and Design Howell Building, Room 128 Kingston Lane Uxbridge UB8 3PH UK			Date: 2/20/2013 Expires: 4/21/2013 Reference: England Terms & Conditions: See attached Warranty: See attached Sales Person: Lesley Thomson			
1 Required						
Line	Part Number	Rev	Description	Qty	Unit Price	Net Price
1	GC201102000	G	HOGEN GC 600 Hydrogen Generator	1.00	11,843.00	11,843.00
Production Rate: Up to 600 cc/min, 45 to 200 psig (13.8 bar) Complete package unit including PEM cell stack, power supply, maintenance free palladium purification, auto fill water supply, and operation and maintenance manual. 110 to 220 vac, single phase, 50 or 60 HZ Features: 99.9999+% Pure hydrogen Auto fill water level control Compact size and quiet operation Water monitoring system including purity monitor Automatic production control; system senses demand and adjusts production rate Purge airflow monitoring system assures safe operation Automatic leak detection system CE (ex); TUV US; TUV Canada product certifications Shipping Weight 65 lbs Shipping Dimensions: 23"W X 28"L X 16" H Includes Resin Bag, 1 Each (P/N KT-0200-0003)						
				Lead Time	4 Weeks ARO	
2	04-0400-0001		DI Water System, Type 2, H-01-C	1.00	1,593.00	1,593.00
Aqua Solutions Model H-01-C Type II DI System is specifically custom designed to support the HOGEN Hydrogen Generator. It connects directly to the hydrogen generator water inlet and includes a spare cartridge. The capacity is one gallon per day (4 liters). The system dimensions are 12" wide by 12" deep by 18" high and weighs approximately 25 lbs.						
3	KT-0200-0003	E	Kit, Replacement, Resin Bags (2)	1.00	95.00	95.00
For use with deionized water tank. Includes two each (1 Set) of the ION exchange resin bags and one material safety data sheet. Proton Energy Systems recommends replacing the resin bags every six months.						
4	02-2402-0000		Regulator, UHP, Line, Brass	1.00	573.00	573.00
Externally mounted. Brass Line Pressure Regulator is designed to reduce distribution system line pressure to workable levels. Will make the HOGEN® unit run more efficiently if low process pressure is required. NOTE: Not needed if Backup Manifold Auto-Crossover Kit is purchased. Request data sheet P/N PD-0600-0025.						
Shipping Charges To Uxbridge, Middlesex:						\$1,548.00

Figure B.1, Quotation of the HOGEN GC600 electrolyser from Proton OnSite

The quotation of the H-Tec Electrolyser can be seen in Figure B.2



School of engineering and design
 Dr. Zahir Dehouche
 Brunel University
 Howell Building Room 128
 Kingston Lane, Uxbridge, UB8 3PH, UK

Email: Zahir.dehouche@brunel.ac.uk

30.10.2012

Quotation

Dear Dr.Dehouche,

Thank you for your inquiry. We herewith quote as follows:

No.	Description	Qty	Unit price (net)	Total (net)
	Electrolyser EL30/13-3-1-1-0-1 <ul style="list-style-type: none"> • PEM-stack with 13 cells • Hydrogen production 0.3 m³/h (STP) • Hydrogen pressure up to 3.0 MPa • Dew point < -60°C • Nominal power (begin of life, 25°C ambient temperature) 1.8 kW • Grid supply 230 VAC • Water preparation (tap water connection) • Dimensions (H x W x D) 1200 x 560 x 600 mm • Weight approx. 120 kg 	1	44,300.00€	44,300.00€
	Delivery ex works, shipping costs in addition on request	1		
Total (net):				44,300.00€
VAT 19%:				8,417.00€
Total:				52,717.00€

Figure B.2, Quotation of the H-Tec Electrolyser

The quotation of the Hydrogenics electrolyser can be seen in Figure B.3

CONFIDENTIAL		HYDROGENICS	
Quotation N° 124327 from 17.10.2012		Advanced Hydrogen Solutions	
2. PRICE OVERVIEW			
	QTY	UNIT PRICE (€)	TOTAL PRICE (€)
STANDARD OFFER CONSISTING OF:			
HySTAT® 10/10 (10Nm ³ /h, 10 barg) water electrolyser	1	198.000,00	198.000,00
- Power Racks	1		
- Control Panel (Including Exler monitoring system)	1		
- Standard FAT	1		
- Packaging and packaging add-ons	1		
- HTO measurement	1		
- HTA measurement	1		
- Set of documentation	1		
- Standard Toolkit	1		
- Transport EXW, Cevel (Incoterms 2010)	1		
Startup & Commissioning HySTAT®	1		
OPTIONS:			
ATEX Enclosures for Process Part	1	8.000,00	8.000,00
Closed Loop cooling system (Electrolyte Cooling)	1	11.000,00	11.000,00
Chiller (Gas cooling)	1	6.900,00	6.900,00
Hydrogen Purification System (HPS)	1	35.200,00	35.200,00
HPS Nitrogen purge (Automatic)	1	3.400,00	3.400,00
HPS Automatic Restart from Stand-by	1	1.700,00	1.700,00
Online purity measurement (OTH and Dew Point)	1	12.500,00	12.500,00
Blowoff Logic	1	1.800,00	1.800,00
Advanced Toolkit	1	4.800,00	4.800,00
Set of recommended spare parts CE (EPS + HPS Remote IO)	1	8.000,00	8.000,00
1 Year Consumable Parts (HySTAT + Deoxo Dryer + ROS)	1	2.300,00	2.300,00
1. NET TOTAL			
NET TOTAL			293.600,00

Figure B.3, Quotation of the Hydrogenics electrolyser

Appendix C. Experimental Setup

This appendix presents the equipment that was purchased as parts of the experimental setup. The Python code developed for the validation experiments is presented in detail. Furthermore, the uncertainty analysis of the logging equipment that is used is described. Tables C.1 and C.2 present the purchased equipment.

Table C.1, Experimental Equipment Costs

Equipment	Manufacturer	Parts	Cost per part (£)	Total Cost (£)
Model XMF17A-VA16-B5 , XMF-010153 Aalborg Stainless steel body digital mass flow meter	Aalborg	1	£807	£807.00
Polypropylene Tubing 3/32" * 2/8" , 100' / WZ-95875-01	Cole Parmer	1	£24.37	£24.37
Reducing Union, 1/4" * 1/8", Stainless Steel / WZ-30486-08	Cole Parmer	1	£23.15	£23.15
Straight, 1/4", 316 ss fitting, WZ-30620-04	Cole Parmer	1	£15.99	£15.99
Compression Fitting, Reducing Union, 316 ss, 1/4" * 1/8" OD - WZ-31406-01	Cole Parmer	1	£12.40	£12.40
Compression Union , 1/4" * 1/4", Stainless steel - WZ-30486-01	Cole Parmer	1	£20.20	£20.20
PTFE Tubing, 1/16" * 1/8", 25 ft/pack - WZ-06605-27	Cole Parmer	1	£22.28	£22.28
PTFE Tubing 1/8" * 1/4", 25 ft/pack - WZ-06605-30	Cole Parmer	1	£59.00	£59.00
Pressure Gauge	Omega	1	£66.84	£66.84
316 L stainless steel tube, 250 mm G1/8 thread / 4929062	RS	1	£36.09	£36.09
Stainless steel instrumentation tube, 1/4in OD / 4324580	RS	1	£29.37	£29.37
PFA-420-1-2 Swagelok Fitting	Swagelok	1	£12.70	£12.70
PFA-420-1-4 Swagelok Fitting	Swagelok	1	£12.70	£12.70
PFA-220-1-2 Swagelok Fitting	Swagelok	1	£12.40	£12.40
SS-400-3-4TTF SS Swagelok Tube Fitting, Female	Swagelok	1	20.33	£20.33
SS-400-3 SS Swagelok Tube Fitting,	Swagelok	1	14.08	£14.08
SS-4CA-3 SS Poppet Check Valve	Swagelok	1	43.8	£43.80
SS-400-61BT SS Swagelok Tube Fitting	Swagelok	1	12.46	£12.46
PFA-420-1-4 PFA Swagelok Tube Fitting	Swagelok	2	11.8	£23.60
SS-400-P 16 Stainless Steel Plug for 1/4 in	Swagelok	4	3.48	£13.92

Table C.1 continued

SS-400-R-2 SS Swagelok Tube Fitting, Reducer	Swagelok	2	7.6	£15.20
SS-4-TA-7-4RT SS Swagelok Tube Fitting, Female Tube Adapter,	Swagelok	1	6.46	£6.46
SS-42GXS4-1466 SS 1-Piece 40 Series 3-Way Ball Valve	Swagelok	1	72.56	£72.56
SS-400-6-1ZV S Swagelok Tube Fitting, Zero Volume Reducing Union,	Swagelok	1	13.58	£13.58
SS-4P4T-BK SS Quarter-Turn Instrument Plug Valve,	Swagelok	2	39.48	£78.96
SS-1RS4 Integral Bonnet Needle Valve	Swagelok	1	48.45	£48.45
Current Transducer	Sontay	1	30	£30.00
Power Analyser	Murata	1	46.37	£46.37
1500 Watt 24V DC to AC 230V 240V Pure Sine Wave Power Inverter	LiveLife	1	£179.86	£179.86
Raspberry Pi Type B and 8GB SD card	Raspberry Pi	1	£27.40	£27.40
2Ux178Dx203W Electronic Enclosure	RS	1	£18.25	£18.25
USB to RS485 / RS422 Converter, PRO	RS	1	£22.76	£22.76
DC Power Supply Unit with calibration certificate	AIM & THURLBY THANDAR Instruments	1	£1,062.00	£1,062.00
TOTAL COSTS				£2,904.53

Table C.2, Laboratory equipment for the experimental setup

	Part Number	Part Description	Material	Number of items	Maximum Pressure (psig)	Figure
¼" outside diameter	304L-T4-S-035-20	304/304L SS Seamless Tubing, ¼"	Stainless Steel	2	5100	
¼" Tee fitting	SS-400-3	SS Swagelok Tube Fitting, Union Tee, ¼" Tube OD	Stainless Steel	1	5100	
¼" to 1/16" Tee adapter	SS-400-6-1	SS Swagelok Tube Fitting, Reducing Union, ¼" x 1/16" Tube OD	Stainless Steel	1	5100	
¼" straight fitting	SS-400-6	SS Swagelok Tube Fitting, Union, ¼" Tube OD	Stainless Steel	2	5100	
¼" shut off valve	SS-4P4T-BK	SS Quarter-Turn Instrument Plug Valve, ¼" Swagelok Tube Fitting, 1.6 Cv,	Stainless Steel	2	3000	
¼" three way valve	SS-42GXS4-1466	SS 1-Piece 40 Series 3-Way Ball Valve, 0.35 Cv, ¼" Swagelok Tube Fitting	Stainless Steel	1	500	
¼" needle valve	SS-1RS4	SS Integral Bonnet Needle Valve, 0.37 Cv, ¼" Swagelok Tube Fitting, Regulating Stem	Stainless Steel	1	5000	
¼" check valve	SS-4CA-3	SS Poppet Check Valve, Adjustable Pressure, ¼" Swagelok Tube Fitting	Stainless Steel	1	3000	
¼" plug	SS-400-P	316 Stainless Steel Plug for ¼" Swagelok Tube Fitting	Stainless Steel	6	5100	

C.1 Python Code for the programming of the Raspberry Pi.

In order to calculate the current values to be used as an input to the PV emulator for the UK conditions experiments it is necessary to calculate the DC power output of the panels. What is known is the AC power output of the PV array and the inverter efficiency, and thus the following process is performed:

Known parameters

- The values of the AC power output, P_{AC} of the Brunel University PV system are known
- The value of the inverter efficiency, η_{REAL} of the Brunel University PV system is known
- The value of the emulator inverter efficiency, η_{EMUL} is known

Calculated parameters

- DC power output of the Brunel University PV system, P_{DCemul}
- DC current as an input to the PV emulator, I_{DCemul}

The calculations can be seen in Equations (C.1) and (C.2):

$$\begin{aligned} P_{ACreal} &= P_{ACemul} \quad \text{D} \\ \frac{P_{DCreal}}{h_{real}} &= \frac{P_{DCemul}}{h_{emul}} \quad \text{D} \\ P_{DCemul} &= \frac{P_{DCreal} \cdot h_{emul}}{h_{real}} \quad \text{D} \\ P_{DCemul} &= \frac{P_{ACreal} \cdot h_{emul}}{h_{real}^2} \quad \text{D} \\ P_{DCemul} &= \frac{P_{ACreal} \cdot 0.92}{0.885^2} \quad \text{D} \\ P_{DCemul} &= \frac{P_{ACreal}}{0.85} \end{aligned} \quad (C.1)$$

$$I_{DCemul} = \frac{P_{DCemul}}{24} \quad (C.2)$$

C.2 Python Code Example

This example refers to Day2 of the UK experimental set. The current signals change every 5 minutes, i.e.300 seconds, as can be seen in the `time.sleep()` function.

```
import
smbus
import time
bus = smbus.SMBus(1)
#
IC is DAC7578
def out(x):

Vref=5
Vo=x
Dm=4096
D=Dm*Vo/Vref
DMSB=int(D/16)
DLSB=int(16*(D-DMSB*16))#
DAC channel

bus.write_block_data(0x48, 0x00100000, [0x00, DMSB, DLSB])

Io=[0,0,0.3,0.7,0.9,1.2,1.6,2,2.5,3,3.5,3.8,4.2,4.5,4.5,4.6,4.7,4.7,4.8,4.9,4.5]

for z in range(0,21):
zz=Io[z]*0.10
out(zz)
print zz*10
time.sleep(300)

Io=[4.5,4.6,4.5,5,5.7,6.5,7.7,9,8,7,8.3,9,9.3,9.8,9.8,10.3,11.2,12,12.35,12.35,13,14,14.2,
```

14.6,15,16.3,16.6,17,18.7,28,29,29,36,40,41,41,42,43,45,47,47.5,48.7,49,50,50,50,50,50,
50,47,48,50,50,50,50,50,50,50,50,50,50,46,49,50,50,50,50,50,50,50,50,50,50,50,
50,50,50,38,29,38,50,50,50,50,50,50,50,50,50,45.5,49,43,38,50,50,50,36,32,49,42,30,3
3,32,33,34,35.6,27,25,23,21.4,23.5,30.2,29.5,23.7,22.3,21.3,16,16.9,21,22,20,15.5,16.5,
17.5,16.2,14.7,14.36,12,10.3,9,9,8.2,8,7.5,7.6,7.4,7,7,6,6,5,4.6,4.2,4,3.6,3.5,3.3,3,3,
2,2,1.5,1,1,0.5,0.5,0.2,0,0,0,0]

for z in range(0,165):

*zz=Io[z]*0.10*

out(zz)

*print zz*10*

time.sleep(300)

C.3 Uncertainty Analysis

Experimental results involve some degree of uncertainty that is related to various reasons such as the inaccuracy of the measuring equipment, random errors in the measurements and approximations in data reduction relations. These distinct uncertainties eventually form a combined uncertainty in the final result. This is called propagation of uncertainty and it is a crucial factor to determine in the experiments (Coleman & Steele, 1999). In order to use the experimental data to derive useful conclusions and to determine analytical solutions for the numerical model it is necessary to evaluate how “good” the experimental information is.

In most cases the result R is not measured directly but through other measured quantities Q_1, Q_2, \dots, Q_N . The experimental result is a function of the measured quantities through a specified mathematical Equation (C.3):

$$R=f(Q_1, Q_2, \dots, Q_N) \tag{C.3}$$

The uncertainty in the result is given by the positive square root of the combined standard uncertainty $U^2_{(R)}$, which is calculated from the estimated standard deviation of each input.

(Wheeler & Ganji, 1996; Coleman & Steele, 1999)

1. Accuracy of electrolyser input power calculation

The accuracy of the electrolyser input power calculation can be estimated from the Equations (C.4) to (C.9):

$$P = I \times V \times PF \quad (C.4)$$

$$\frac{qP}{qV} = I \times PF \quad (C.5)$$

$$\frac{qP}{qI} = V \times PF \quad (C.6)$$

$$\frac{qP}{qPF} = V \times I \quad (C.7)$$

$$u = \sum_{i=1}^N \sqrt{\frac{\theta f}{\theta x_i}} u^2(x_i) = \sum_{i=1}^3 \left\{ \sqrt{\left[\frac{\theta P}{\theta V} \right]^2 u_V^2 + \left[\frac{\theta P}{\theta I} \right]^2 u_I^2 + \left[\frac{\theta P}{\theta PF} \right]^2 u_{PF}^2} \right\} \quad (C.8)$$

$$\frac{\partial U_P}{\partial P} \dot{\theta}^2 = \frac{\partial U_V}{\partial V} \dot{\theta}^2 + \frac{\partial U_I}{\partial I} \dot{\theta}^2 + \frac{\partial U_{PF}}{\partial PF} \dot{\theta}^2 = \quad (C.9)$$

$$\frac{\partial U_P}{\partial P} \dot{\theta}^2 = (0.01)^2 + (0.036)^2 + (0.03)^2 = 2.296 * 10^{-3}$$

$$\frac{\partial U_P}{\partial P} \dot{\theta} = 0.0479$$

Therefore the uncertainty of the calculated power is approximately 4.79%.

2. Accuracy of electrolyser hydrogen flow measurements

The digital mass flow meter is calibrated against Manufacturing Procedures according to ISO9000-2000 and ANSI/ISO17025. Passing Nitrogen as a simulation gas performs the calibration. The characteristics of the flowmeter can be seen in Table C.3.

Table C.3, Digital mass flow meter characteristics

Digital Mass Flow Meter Model	XFM 17
Serial Number	348433-1
Flow Sensor	Thermal
Flow Range	0 to 1000 sccm@70F
Output Range	0.004 to 0.020A
Device Tolerance	1% Span
Operating Fluid	H ₂
Operating Pressure	14.69psi_abs
Operating Temperature	70F
Flow Attitude	Horizontal

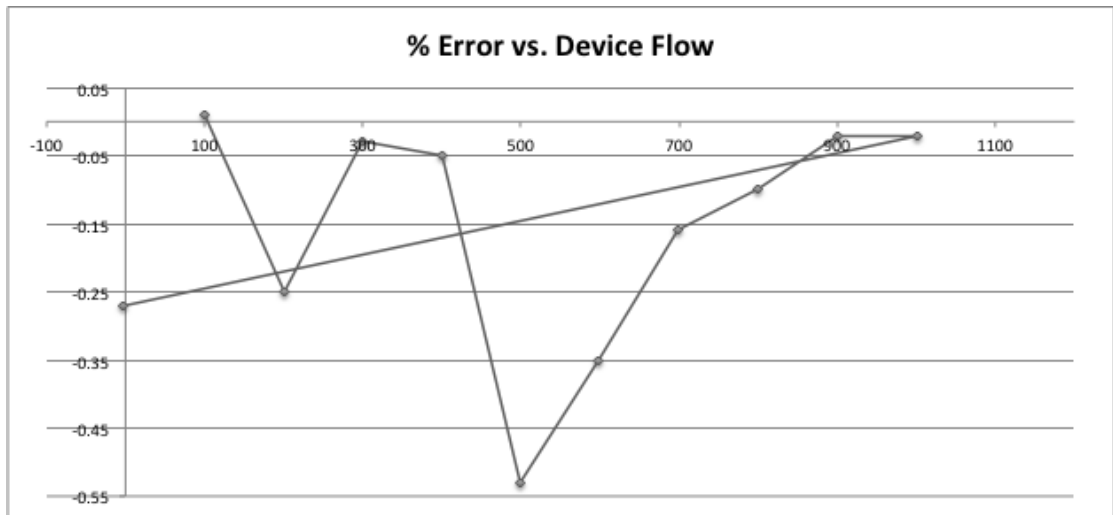


Figure C.1, % Error vs. Device Flow

The error in the experimental measurements according to the flow meter calibration certificate and the flow as seen in Figure C.1 is:

- 0.01% for flow less or equal than 101ccm
- -0.25% for flow less or equal than 200ccm
- -0.03% for flow less or equal to 300ccm
- -0.05% flow less or equal than 400ccm

The XFM flow meter provides reading at STD conditions (70 degree F and 14.7 psia – 21.1 °C and 1 atm) regardless of the gas actual conditions.

The accuracy of the reading will be affected since the actual conditions are different from calibration conditions. The XFM flow meter has pressure coefficient, which is 0.01% of full scale per each PSI difference between actual, and calibration conditions. Since calibration conditions are 14.7 psia the difference with the experimental installation conditions is calculated as bellow:

A typical example is the tests at 13.8 bar, which is 200.152 psi. The difference between this experimental condition and the calibration condition is: 200.152-14.7=188.16 psi. Therefore the estimated additional calibration uncertainty will be: 0.01 * 188.16 = 1.88% of full scale. That number represents additional pressure related uncertainty of the XFM reading. So, for the measurements of each pressure set point are calculated by the bellow Equation (C.10), and can be seen in Table C.4:

$$\frac{U}{p} = \sqrt{(\text{Standard_error})^2 + (\text{Additional_error})^2} \quad (\text{C.10})$$

Table C.4, Measurements uncertainties of the flow meter

Pressure Set Point (bar)	Additional Uncertainty (%)	Standard Uncertainty (%)	Total Uncertainty (%)
5 bar	0.603	-0.0783	0.608
7 bar	0.853	0.01	0.853
10 bar	1.303	-0.25	1.326
13.8 bar	1.880	-0.038	1.88

3. Accuracy of hydrogen temperature measurements

The temperature measurements are taken through a T type thermocouple and a Pico USB TC-08 Thermocouple Data Logger that has a temperature accuracy of $\pm 0.2\%$ of reading.

5. Accuracy of electrolyser energy efficiency calculations

The energy efficiency of the electrolyser can be calculated by the Equation (C.11):

$$h_E = \frac{m_{H_2(\text{exp})} \cdot HHV_{H_2}}{V \cdot I \cdot t} \quad (\text{C.11})$$

Therefore, the combined standard uncertainty for the energy efficiency is given by Equation (C.12):

$$u_{(h_E)} = \sqrt{\left[\frac{Jh_E}{Jm_{H_2(\text{exp})}} \right]^2 u^2(m_{H_2(\text{exp})}) + \left[\frac{Jh_E}{JHHV_{H_2}} \right]^2 u^2(HHV_{H_2}) + \left[\frac{Jh_E}{JV} \right]^2 u^2(V) + \left[\frac{Jh_E}{JI} \right]^2 u^2(I) + \left[\frac{Jh_E}{Jt} \right]^2 u^2(t)} \quad (\text{C.12})$$

$$u_{(h_E)} = \sqrt{\left[\frac{HHV_{H_2}}{V \cdot I \cdot t} \right]^2 u^2(m_{H_2(\text{exp})}) + 0 \cdot u^2(HHV_{H_2}) + \left[-\frac{HHV_{H_2} \cdot m_{H_2(\text{exp})}}{V^2 \cdot I \cdot t} \right]^2 u^2(V) + \left[-\frac{HHV_{H_2} \cdot m_{H_2(\text{exp})}}{V \cdot I^2 \cdot t} \right]^2 u^2(I) + 0 \cdot u^2(t)}$$

Appendix D. Numerical Model Development and Validation

The detailed measurements of the hydrogen flow at each pressure step between 5 to 13 bar are presented in Figures D.1 to D.9.

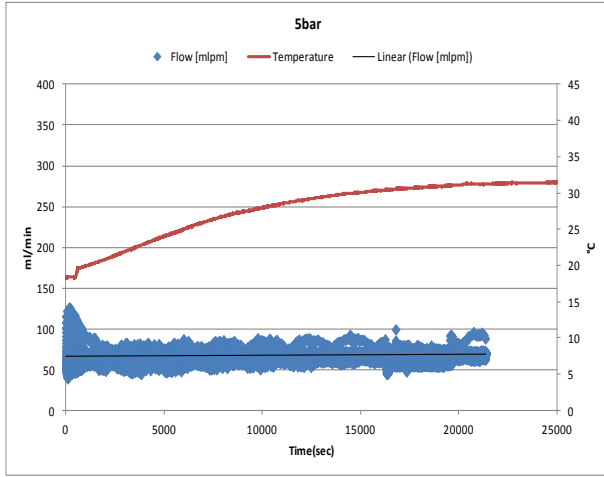


Figure D.1, Hydrogen flow at the generating pressure of 5bar

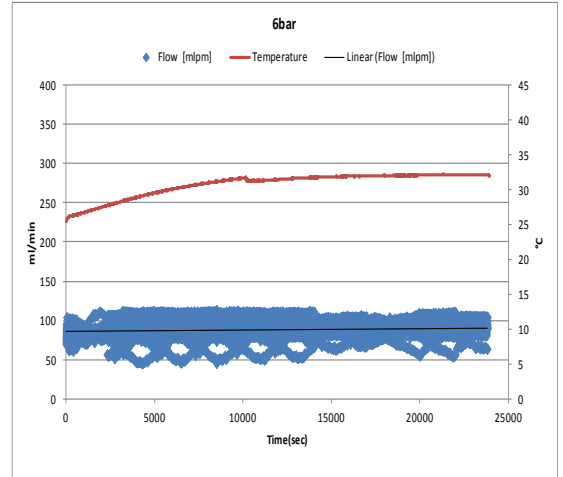


Figure D.2, Hydrogen flow at the generating pressure of 6bar

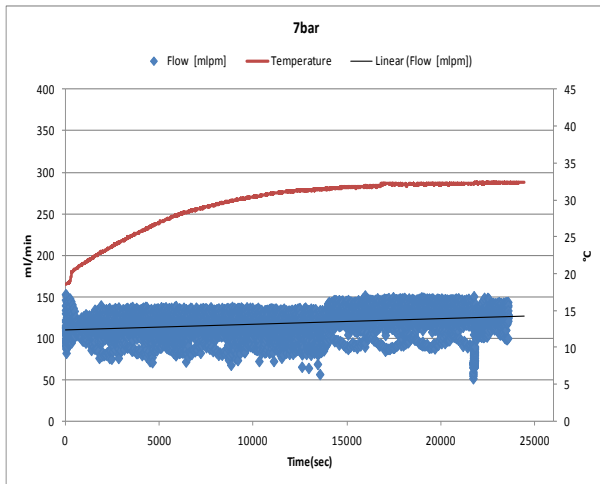


Figure D.3, Hydrogen flow at the generating pressure of 7bar

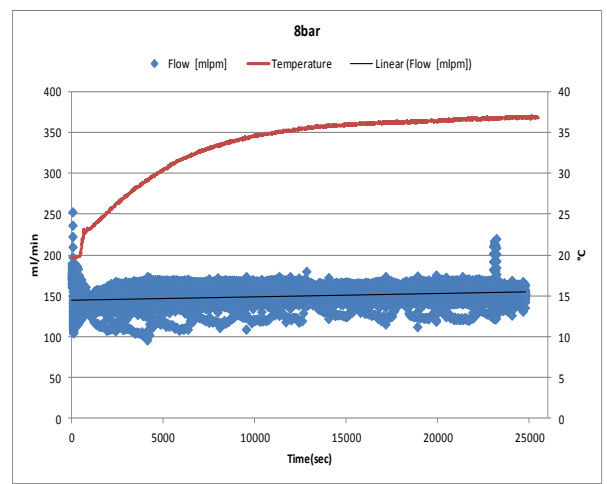


Figure D.4, Hydrogen flow at the generating pressure of 8bar

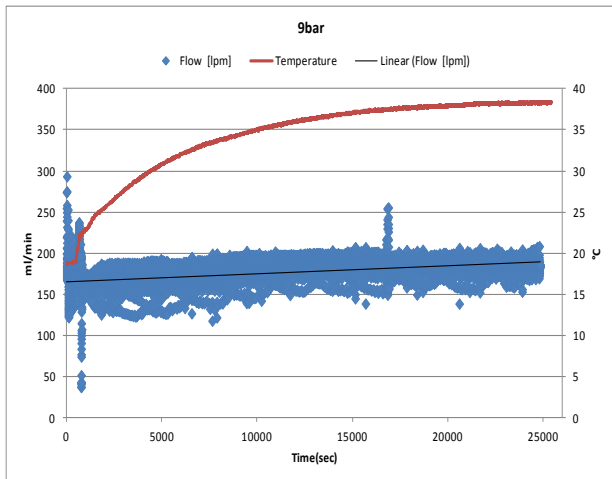


Figure D.5, Hydrogen flow at the generating pressure of 9bar

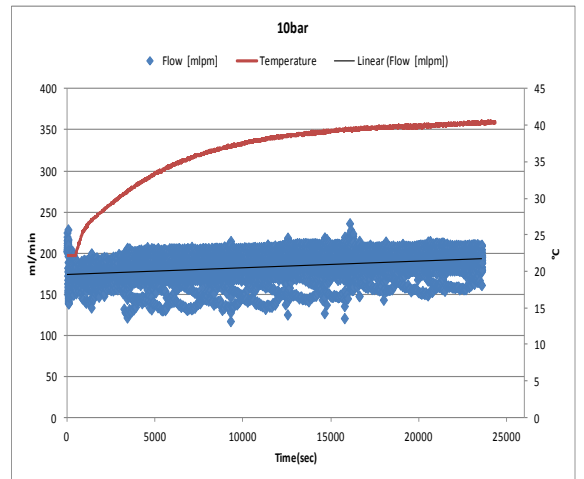


Figure D.6, Hydrogen flow at the generating pressure of 10bar

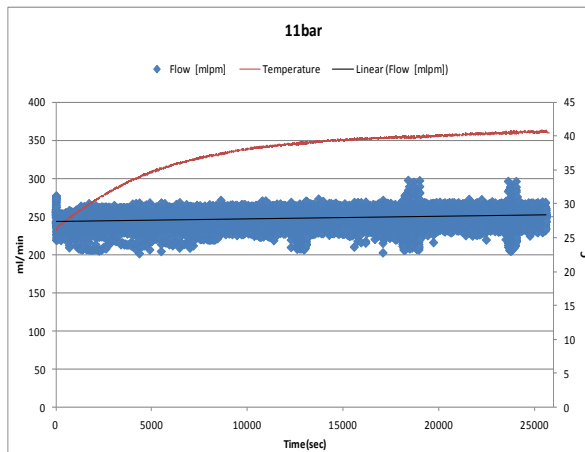


Figure D.7, Hydrogen flow at the generating pressure of 11bar

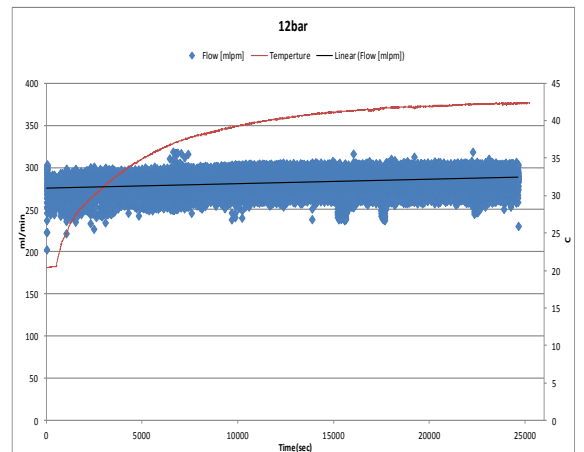


Figure D.8, Hydrogen flow at the generating pressure of 12bar

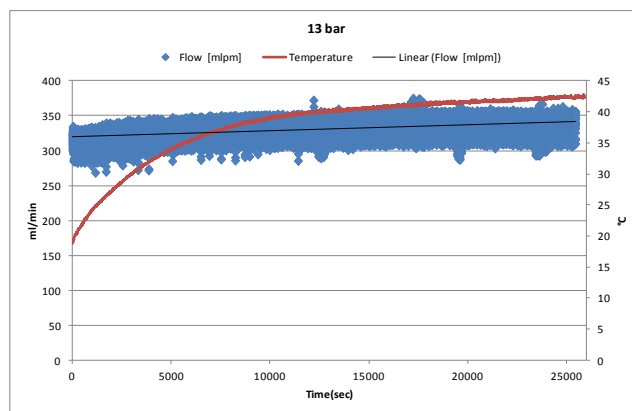


Figure D.9, Hydrogen flow at the generating pressure of 13bar

The stack current, voltage and power values for the operations 5bar and 10bar are presented in Figures D.10 to D13.

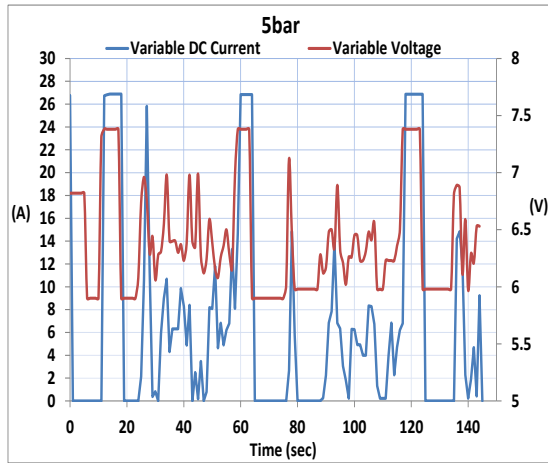


Figure D.10, Variable DC current and voltage to the stack while producing constant hydrogen at 5bar

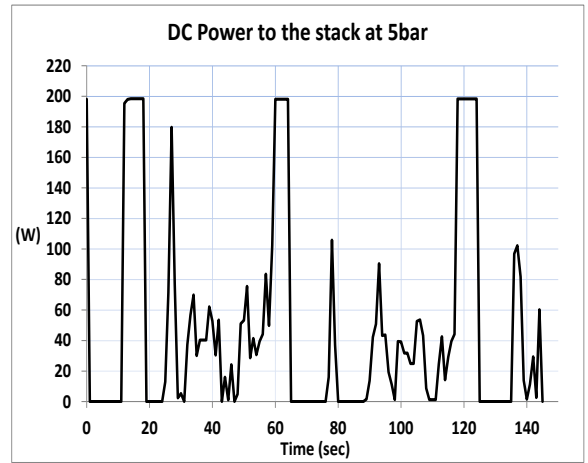


Figure D.11, Variable DC power to the stack while producing constant hydrogen at 5bar

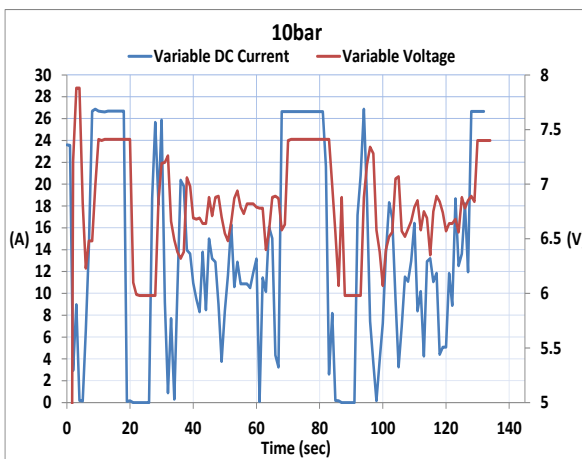


Figure D.12, Variable DC current and voltage to the stack while producing constant hydrogen at 10bar

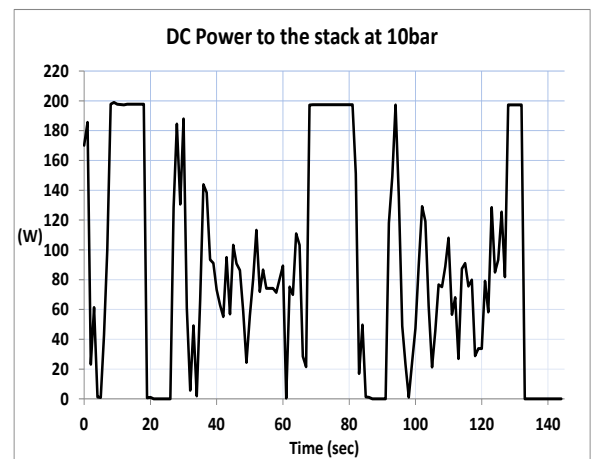


Figure D.13, Variable DC power to the stack while producing constant hydrogen at 10bar

The validation experiments for the UK and Jamaica conditions are presented in Figures D.14 to D.21.

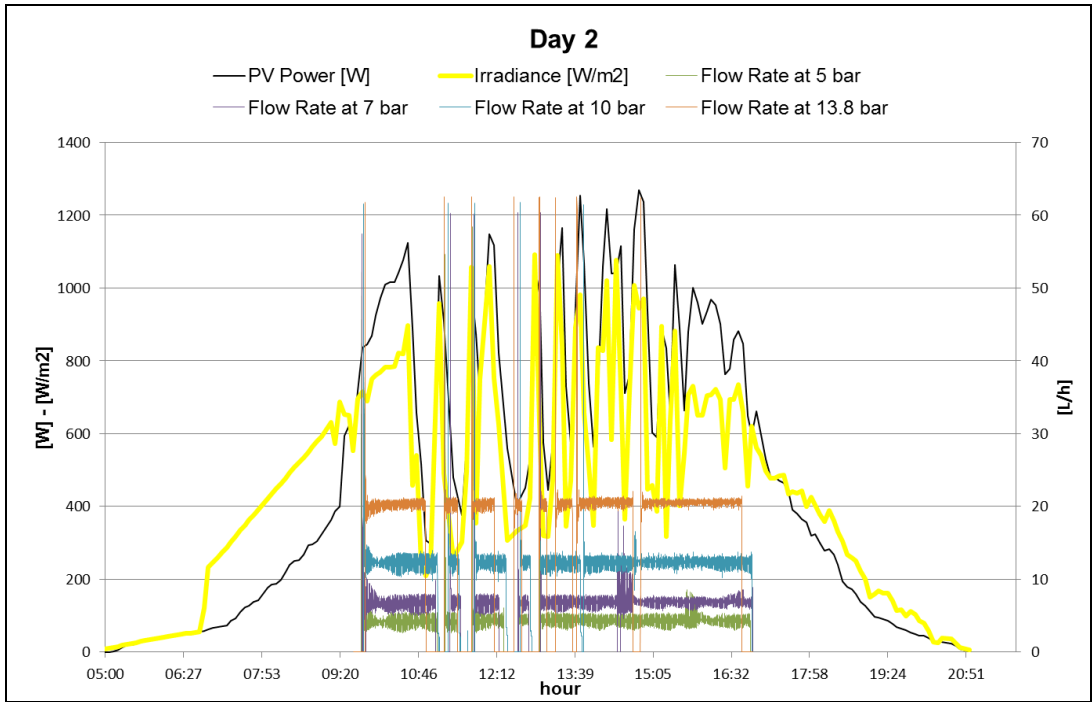


Figure D.14, Hydrogen production rate in L/h at 5bar, 7bar,10bar,13.8bar pressure set points during day 2 that presents unstable irradiance levels

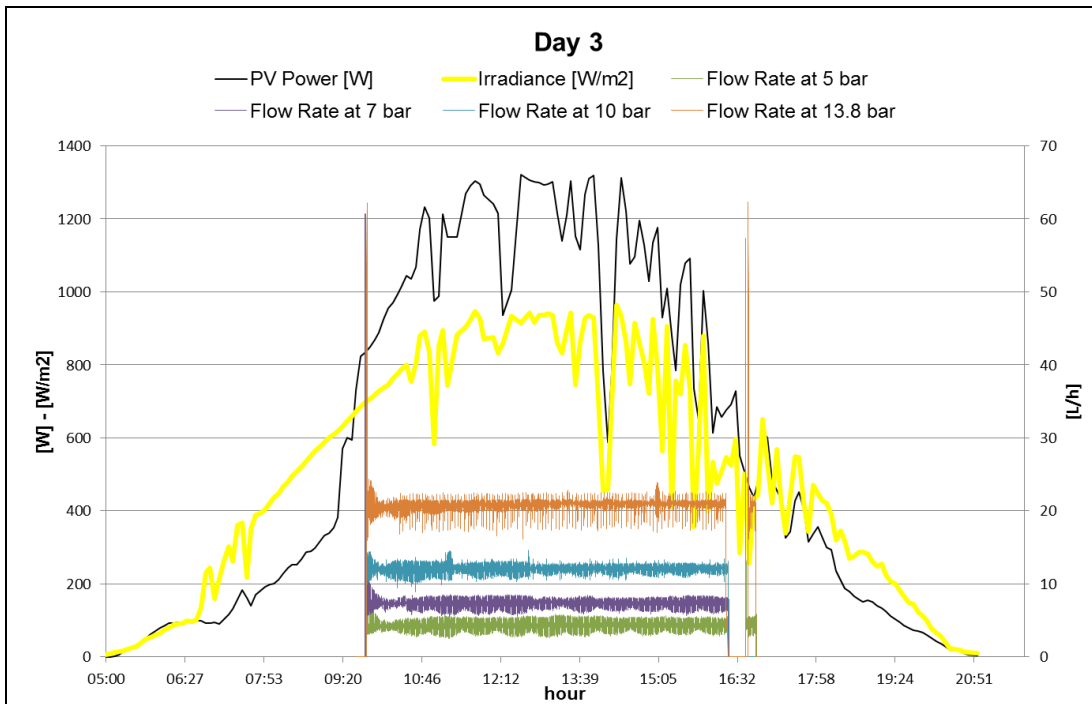


Figure D.15, Hydrogen production rate in L/h at 5bar, 7bar,10bar,13.8bar pressure set points during day 3 that presents unstable irradiance levels

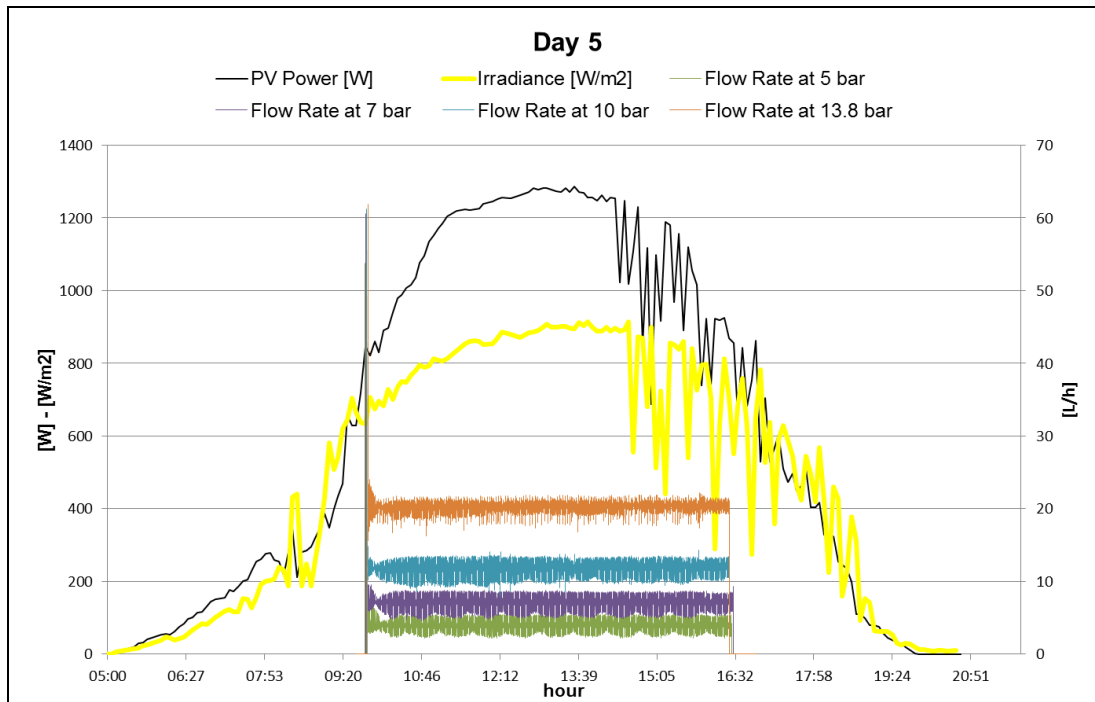


Figure D.16, Hydrogen production rate in L/h at 5bar, 7bar, 10bar, 13.8bar pressure set points during day 5 that presents consistently high irradiance levels

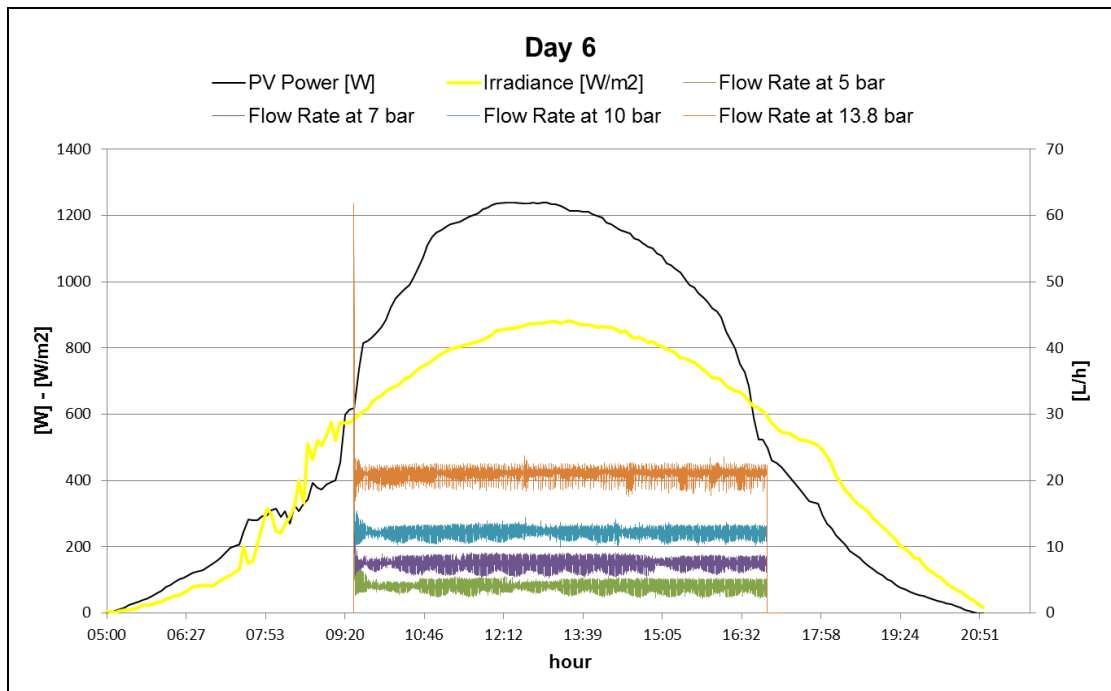


Figure D.17, Hydrogen production rate in L/h at 5bar, 7bar, 10bar, 13.8bar pressure set points during day 6 that presents consistently high irradiance levels

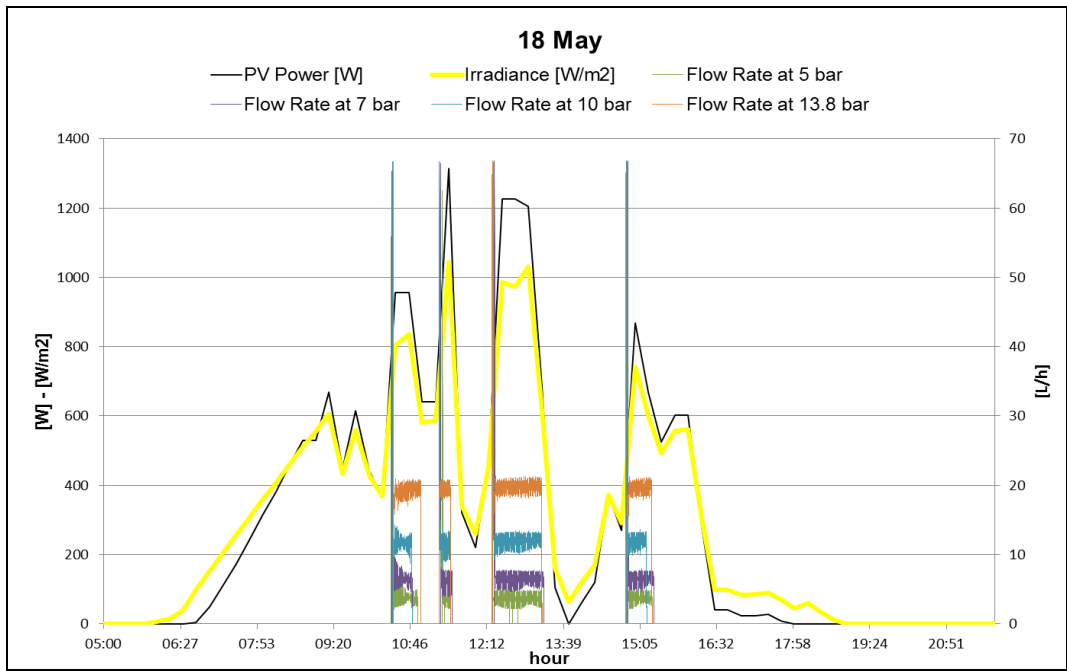


Figure D.18, Hydrogen production rate in L/h at 5bar, 7bar,10bar,13.8bar pressure set points during 18th of May in Jamaica, that presents unstable irradiance levels

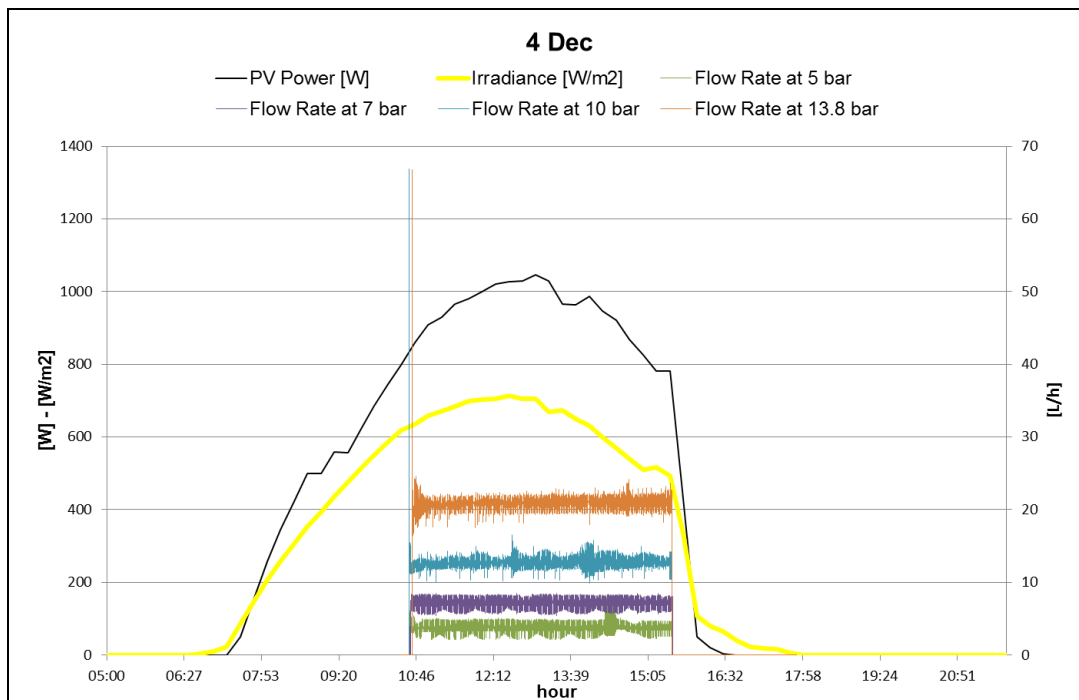


Figure D.19, Hydrogen production rate in L/h at 5bar, 7bar,10bar,13.8bar pressure set points during 4th of December in Jamaica, that presents consistently high irradiance levels

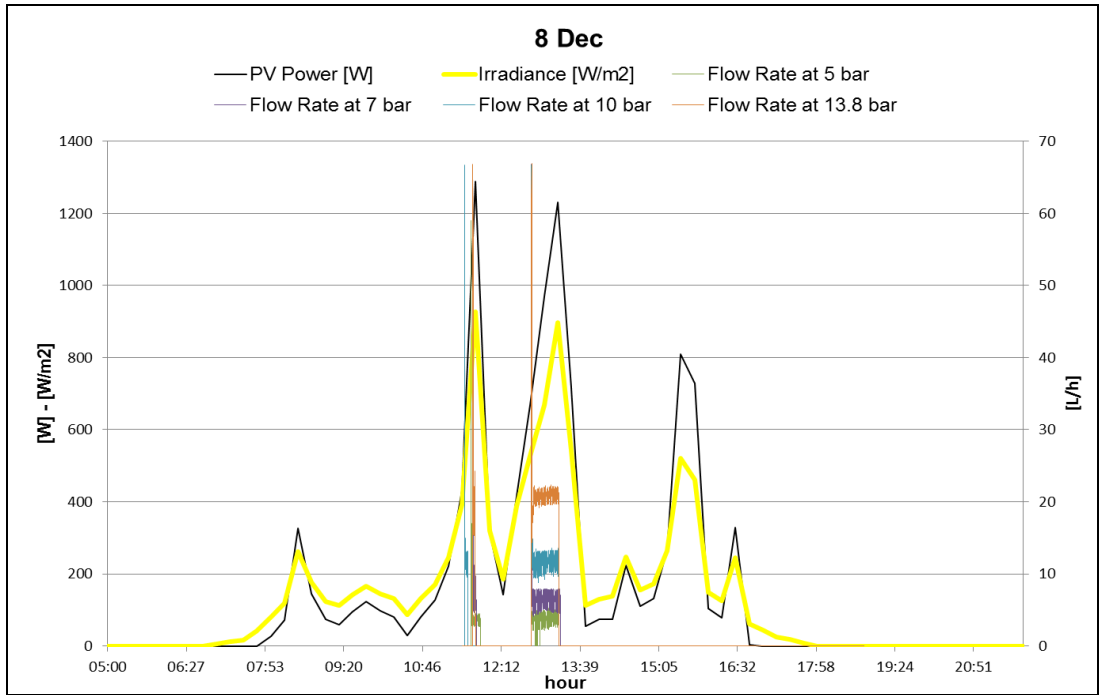


Figure D.20, Hydrogen production rate in L/h at 5bar, 7bar,10bar,13.8bar pressure set points during 8th of Deceber in Jamaica, that presents unstable irradiance level

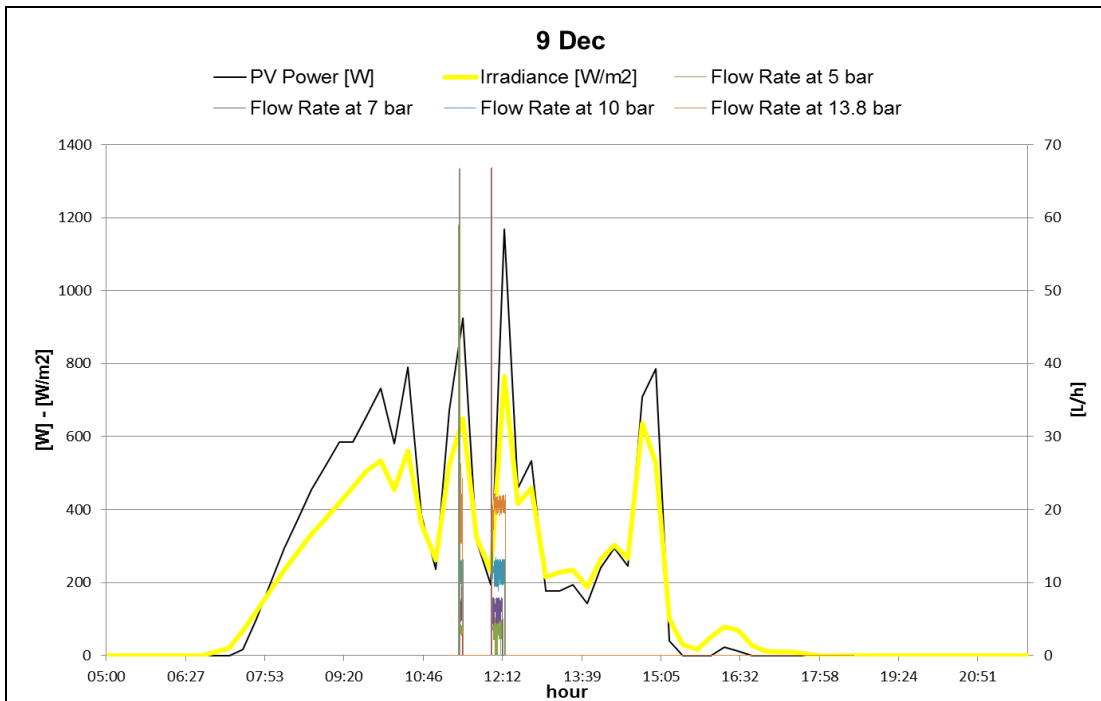


Figure D.21, Hydrogen production rate in L/h at 5bar, 7bar,10bar,13.8bar pressure set points during 9th of December in Jamaica, that presents unstable irradiance levels

The FORTRAN code of the components is given in the bellow section D.1.

D.1 TRNSYS Codes

PEM Electrolyser Component

Subroutine Type2627

! Object: PEM Electrolyser Model

! Simulation Studio Model: Type2627

!

! Author: Evangelia Topriska

! Editor: Evangelia Topriska

! Date: May 02, 2014

! last modified: May 02, 2014

!

!

! ***

! *** Model Parameters

! ***

! area - [-Inf;+Inf]

! PH2 - [-Inf;+Inf]

! PO2 - [-Inf;+Inf]

! PH2O - [-Inf;+Inf]

! acat - [-Inf;+Inf]

! aan - [-Inf;+Inf]

! joan - [-Inf;+Inf]

! jocat - [-Inf;+Inf]

! fi - [-Inf;+Inf]

! ncells - [-Inf;+Inf]

! nstacks - [-Inf;+Inf]

! ***

! *** Model Inputs

! ***

! Tely - [-Inf;+Inf]

! Iely - [-Inf;+Inf]

```

!      Poperational - [-Inf;+Inf]

! ***
! *** Model Outputs
! ***
!
!      H2prod - [-Inf;+Inf]
!
!      O2prod - [-Inf;+Inf]
!
!      Vcell  - [-Inf;+Inf]
!
!      Vely   - [-Inf;+Inf]
!
!      Voc    - [-Inf;+Inf]
!
!      Vact   - [-Inf;+Inf]
!
!      Vohmic- [-Inf;+Inf]
!
!      V      - [-Inf;+Inf]
!
!      sigma  - [-Inf;+Inf]
!
!      co     - [-Inf;+Inf]
!
!      Idens  - [-Inf;+Inf]
!
!      Phydrogen - [-Inf;+Inf]
!
!      nelec  - [-Inf;+Inf]
!
!      ntot   - [-Inf;+Inf]
!
!      I      - [-Inf;+Inf]
!
!      Pstack - [-Inf;+Inf]
!
!
!
!Subroutines:
!MH_ON: it is the model that takes into consideration that a Metal Hydride Storage is conected to
the electrolyser. In this case the electrolyser has a different operation
!MH_OFF: No Metal Hydride Storage exists in the model
! ***
! *** Model Derivatives
! ***

! (Comments and routine interface generated by TRNSYS Studio)
!*****
!-----
! This TRNSYS component skeleton was generated from the TRNSYS studio based on the user-
supplied parameters, inputs,
! outputs, and derivatives. The user should check the component formulation carefully and add the
content to transform

```

! the parameters, inputs and derivatives into outputs. Remember, outputs should be the average value over the timestep

! and not the value at the end of the timestep; although in many models these are exactly the same values. Refer to

! existing types for examples of using advanced features inside the model (Formats, Labels etc.)

!-----

Use TrnsysConstants

Use TrnsysFunctions

!-----

!DEC\$Attributes DLLexport :: Type2627

!-----

!Trnsys Declarations

Implicit None

Double Precision Timestep,Time

Integer CurrentUnit,CurrentType

! PARAMETERS

DOUBLE PRECISION area

DOUBLE PRECISION PH2

DOUBLE PRECISION PO2

DOUBLE PRECISION PH2O

DOUBLE PRECISION acat

DOUBLE PRECISION aan

DOUBLE PRECISION joan

DOUBLE PRECISION jocat

DOUBLE PRECISION fi

DOUBLE PRECISION ncells

DOUBLE PRECISION nstacks

DOUBLE PRECISION temp

! INPUTS

DOUBLE PRECISION Tely

DOUBLE PRECISION Iely

DOUBLE PRECISION Poperational

DOUBLE PRECISION mMh

DOUBLE PRECISION MaxMassMH

! OUTPUTS

DOUBLE PRECISION H2prod
DOUBLE PRECISION O2prod
DOUBLE PRECISION Vcell
DOUBLE PRECISION Vely
DOUBLE PRECISION Voc
DOUBLE PRECISION Vact
DOUBLE PRECISION Vohmic
DOUBLE PRECISION V
DOUBLE PRECISION sigma
DOUBLE PRECISION co
DOUBLE PRECISION Idens
DOUBLE PRECISION Phydrogen
DOUBLE PRECISION nelec
DOUBLE PRECISION ntot
DOUBLE PRECISION I
DOUBLE PRECISION Pstack
DOUBLE PRECISION T

!-----

!Get the Global Trnsys Simulation Variables

Time=getSimulationTime()
Timestep=getSimulationTimeStep()
CurrentUnit = getCurrentUnit()
CurrentType = getCurrentType()

!-----

!-----

!Set the Version Number for This Type

If(getIsVersionSigningTime()) Then
 Call SetTypeVersion(17)
 Return
EndIf

!-----

!-----

!Do Any Last Call Manipulations Here

If(getIsLastCallofSimulation()) Then

```

                Return
    EndIf
!-----
!-----
!Perform Any "After Convergence" Manipulations That May Be Required at the End of Each
Timestep
    If(getIsEndOfTimestep()) Then
        Return
    EndIf
!-----
!-----
!Do All of the "Very First Call of the Simulation Manipulations" Here
    If(getIsFirstCallofSimulation()) Then

        !Tell the TRNSYS Engine How This Type Works
        Call SetNumberOfParameters(11)      !The number of parameters that the the
model wants
        Call SetNumberOfInputs(5)          !The number of inputs that the the model
wants
        Call SetNumberOfDerivatives(0)     !The number of derivatives that the the
model wants
        Call SetNumberOfOutputs(17)       !The number of outputs that the the
model produces
        Call SetIterationMode(1)           !An indicator for the iteration mode
(default=1). Refer to section 8.4.3.5 of the documentation for more details.
        Call SetNumberStoredVariables(0,0) !The number of static variables
that the model wants stored in the global storage array and the number of dynamic variables that
the model wants stored in the global storage array
        Call SetNumberOfDiscreteControls(0) !The number of discrete control
functions set by this model (a value greater than zero requires the user to use Solver 1: Powell's
method)

        Call SetInputUnits(1,'TE1')
            Call SetInputUnits(2,'CU1')
            Call SetInputUnits(3,'PR1')
            Call SetInputUnits(4,'MA1')
            Call SetInputUnits(5,'MA1')

    !

```

```
Call SetOutputUnits(1,'VF1')
Call SetOutputUnits(2,'VF1')
    Call SetOutputUnits(3,'VO1')
Call SetOutputUnits(4,'VO1')
Call SetOutputUnits(5,'VO1')
    Call SetOutputUnits(6,'VO1')
Call SetOutputUnits(7,'VO1')
Call SetOutputUnits(8,'VO1')
Call SetOutputUnits(9,'DM1')
Call SetOutputUnits(10,'DM1')
    Call SetOutputUnits(11,'CD2')
Call SetOutputUnits(12,'PW2')
Call SetOutputUnits(13,'DM1')
    Call SetOutputUnits(14,'DM1')
    Call SetOutputUnits(15,'CU1')
    Call SetOutputUnits(16,'PW2')
    Call SetOutputUnits(16,'TE1')
```

```
Return
```

```
EndIf
```

```
!-----
!-----
```

```
!Do All of the First Timestep Manipulations Here - There Are No Iterations at the Intial Time
```

```
  If (getIsStartTime()) Then
    area = getParameterValue(1)
    PH2 = getParameterValue(2)
    PO2 = getParameterValue(3)
    PH2O = getParameterValue(4)
    acat = getParameterValue(5)
    aan = getParameterValue(6)
    joan = getParameterValue(7)
    jocat = getParameterValue(8)
    fi = getParameterValue(9)
    ncells = getParameterValue(10)
    nstacks = getParameterValue(11)
```

Tely = GetInputValue(1)
Iely = GetInputValue(2)
Poperational=GetInputValue(3)
mMH=GetInputValue(4)
MaxMassMH=GetInputValue(5)

!Check the Parameters for Problems (#,ErrorType,Text)
!Sample Code: If(PAR1 <= 0.) Call FoundBadParameter(1,'Fatal','The first parameter provided to this model is not acceptable.')

!Set the Initial Values of the Outputs (#,Value)
 Call SetOutputValue(1, 0) ! H2prod
 Call SetOutputValue(2, 0) ! O2prod
 Call SetOutputValue(3, 0) ! Vcell
 Call SetOutputValue(4, 0) ! Vely
 Call SetOutputValue(5, 0) ! Voc
 Call SetOutputValue(6, 0) ! Vact
 Call SetOutputValue(7, 0) ! Vohmic
 Call SetOutputValue(8, 0) ! V
 Call SetOutputValue(9, 0) ! sigma
 Call SetOutputValue(10, 0) ! co
 Call SetOutputValue(11, 0) ! Idens
 Call SetOutputValue(12, 0) ! Phydrogen
 Call SetOutputValue(13, 0) ! nelec
 Call SetOutputValue(14, 0) ! ntot
 Call SetOutputValue(15, 0) ! I
 Call SetOutputValue(16, 0) ! P
 Call SetOutputValue(17, 0) ! T

!If Needed, Set the Initial Values of the Static Storage Variables (#,Value)
!Sample Code: SetStaticArrayValue(1,0.d0)

!If Needed, Set the Initial Values of the Dynamic Storage Variables (#,Value)
!Sample Code: Call SetDynamicArrayValueThisIteration(1,20.d0)

!If Needed, Set the Initial Values of the Discrete Controllers (#,Value)

```

!Sample Code for Controller 1 Set to Off: Call SetDesiredDiscreteControlState(1,0)

        Return

    EndIf
!-----
!-----
-
!ReRead the Parameters if Another Unit of This Type Has Been Called Last
    If(getIsReReadParameters()) Then
        !Read in the Values of the Parameters from the Input File
        area = getParameterValue(1)
        PH2 = getParameterValue(2)
        PO2 = getParameterValue(3)
        PH2O = getParameterValue(4)
        acat = getParameterValue(5)
        aan = getParameterValue(6)
        joan = getParameterValue(7)
        jocat = getParameterValue(8)
        fi = getParameterValue(9)
        ncells = getParameterValue(10)
        nstacks = getParameterValue(11)

    EndIf
!-----
!Read the Inputs
    Tely = GetInputValue(1)
    Iely = GetInputValue(2)
    Poperational=GetInputValue(3)
        mMh=GetInputValue(4)
        MaxMassMH=GetInputValue(5)

    !Check the Inputs for Problems (#,ErrorType,Text)
    !Sample Code: If( IN1 <= 0.) Call FoundBadInput(1,'Fatal','The first input provided to this
model is not acceptable.')
        if(Poperational<3) Call FoundBadInput(3,'Fatal','The operational pressure input provided
to this model is not acceptable')

```

if(Poperational>13.8) Call FoundBadInput(3,'Fatal','The operational pressure input provided to this model is not acceptable')

If(ErrorFound()) Return

!-----
!-----

! *** PERFORM ALL THE CALCULATION HERE FOR THIS MODEL. ***

temp=-0.0976*Poperational**2+3.3153*Poperational+16.188

if (mMH<(0.0501*Poperational*MaxMassMH-0.0044*MaxMassMH)) then

co=0.4825

else

co=(-0.0476*Poperational**3+2.2273*Poperational**2+3.9329*Poperational-2.3636)/(0.082*4*(39+273.15)*1000*60*27/(2*96485))

end if

! Hydrogen Production Rates

H2prod =(nstacks*co*0.082*ncells*(temp+273.15)*1000*60*Iely)/(2*96485) ! IN ML/MIN

! Oxygen Production Rates

O2prod=0.5*H2prod

! Current density of the cell

Idens=Iely/area

!

! Cell voltage of a PEM electrolyser cell according to temperature dependance model

! Vrev=1.5241-1.2262/10³*T+1.1858/10⁵*T*ln(T)+5.6692/10⁷*T²

! Voc=Vrev+((Ri*T)/2*F)*ln((pH2*pO2^{0.5})/pH2O)

! Vact=((Ri*Tan)/(aan*F)*arcsinh(j/j0an))+((Ri*Tcat)/(acat*F)*arcsinh(j/j0cat)) Tan=Tcat=T

! fi=178*10⁽⁻⁶⁾micrometer

! sigma=0.0480257+8.15178*(10⁻⁴)*T+5.11692*(10⁻⁷)*T²

```

! Vohmic=j*(fi/sigma)
! Vcell=Voc+Vact+Vohmic

sigma=(0.0480257+8.15178*0.0001*temp)+(5.11692*0.0000001*temp*temp)
Voc=(1.5241-1.2261*10**(-3)*temp)+(1.1858*10**(-5)*temp*log(temp))+(5.6692*10**(-7)*temp**2)+(((8.314*temp)/(2*96485))*log((PH2*sqrt(PO2))/PH2O))

Vact=(((8.314*temp)/(2*aan*96485))*asinh(Idens/(2*joan)))+(((8.314*temp)/(2*acat*96485))*asinh(Idens/(2*jocat)))
Vohmic= Idens*(fi/sigma)
Vcell=Voc+Vact+Vohmic

! Total Stack Voltage
Vely=nstacks*ncells*Vcell
!
! Vtn=1.4759+3.6553*10**(-4)*Tely+3.8037*10**(-7)*Tely**2
! EffElec=Vtn/Vcell

nelec=(1.4759+3.6553*10**(-4)*temp+3.8037*10**(-7)*temp**2) /Vcell

! "Cell Voltage(V) calculation according to the Polarisation curve"
! V=Stack*(ns*0.012*I+1.55*ns/np)
V=nstacks*((ncells*0.012*Iely)+1.55*ncells)
!

! Power of the Stack
Pstack=Iely*Vely*co*((-0.0017*Poperational**3)+(0.0465*Poperational**2)-(0.4323*Poperational)+2.7798)

! Phydrogen=H2prod[m3/h]*141.1[MJ/kg]*0.08344[kg/m3]*0.277778[kWh/MJ] it is in W
Phydrogen=H2prod*60*0.001*141.1*0.08344*0.277778

! Current in the Electrolyser Stack
I=Iely*co

! Total Efficiency
ntot=Phydrogen/Pstack

```

```

T=temp
!-----
!-----
-
!If Needed, Get the Previous Control States if Discrete Controllers are Being Used (#)
!Sample Code: CONTROL_LAST=getPreviousControlState(1)
!-----
-
!-----
!If Needed, Get the Values from the Global Storage Array for the Static Variables (#)
!Sample Code: STATIC1=getStaticArrayValue(1)
!-----
-
!-----
!If Needed, Get the Initial Values of the Dynamic Variables from the Global Storage Array
(#)
!Sample Code: T_INITIAL_1=getDynamicArrayValueLastTimestep(1)
!-----
-
!-----
!Perform All of the Calculations Here to Set the Outputs from the Model Based on the
Inputs

!Sample Code: OUT1=IN1+PAR1

!If the model requires the solution of numerical derivatives, set these derivatives and get
the current solution
!Sample Code: T1=getNumericalSolution(1)
!Sample Code: T2=getNumericalSolution(2)
!Sample Code: DTDT1=3.*T2+7.*T1-15.
!Sample Code: DTDT2=-2.*T1+11.*T2+21.
!Sample Code: Call SetNumericalDerivative(1,DTDT1)
!Sample Code: Call SetNumericalDerivative(2,DTDT2)
!-----

```

```

!-----
!Set the Outputs from this Model (#,Value)
    Call SetOutputValue(1, H2prod) ! H2prod
    Call SetOutputValue(2, O2prod) ! O2prod
    Call SetOutputValue(3, Vcell) ! Vcell
    Call SetOutputValue(4, Vely) ! Vely
    Call SetOutputValue(5, Voc) ! Voc
    Call SetOutputValue(6, Vact) ! Vact
    Call SetOutputValue(7, Vohmic) ! Vohmic
    Call SetOutputValue(8, V) ! V
    Call SetOutputValue(9, sigma) ! sigma
    Call SetOutputValue(10, co) ! co
    Call SetOutputValue(11, Idens) ! Idens
    Call SetOutputValue(12, Phydrogen) ! Phydrogen
    Call SetOutputValue(13, nelec) ! nelec
    Call SetOutputValue(14, ntot) ! ntot
    Call SetOutputValue(15, I) ! I
    Call SetOutputValue(16, Pstack) ! Pstack
    Call SetOutputValue(17, T) ! T

!-----
!-----
!If Needed, Store the Desired Discret Control Signal Values for this Iteration (#,State)
!Sample Code: Call SetDesiredDiscreteControlState(1,1)
!-----
!-----
!If Needed, Store the Final value of the Dynamic Variables in the Global Storage Array (#,Value)
!Sample Code: Call SetValueThisIteration(1,T_FINAL_1)
!-----
    Return
    End
!-----

```

PEM Electrolyser Controls

Subroutine Type2628

! Object: Controller

! Simulation Studio Model: Component1

!

! Author: Evangelia Topriska

! Editor:

! Date: July 10, 2014

! last modified: July 10, 2014

!

!

! ***

! *** Model Parameters

! ***

! ***

! *** Model Inputs

! ***

! Ppv W [-Inf;+Inf]

! Punits W [-Inf;+Inf]

! Iin A [-Inf;+Inf]

! Vstack V [-Inf;+Inf]

! co [-Inf;+Inf]

! Paux W [-Inf;+Inf]

! ***

! *** Model Outputs

! ***

! Pavailable W [-Inf;+Inf]

! Iout A [-Inf;+Inf]

! ***

! *** Model Derivatives

! ***

! (Comments and routine interface generated by TRNSYS Studio)

!*****

!-----
! This TRNSYS component skeleton was generated from the TRNSYS studio based on the user-supplied parameters, inputs,
! outputs, and derivatives. The user should check the component formulation carefully and add the content to transform
! the parameters, inputs and derivatives into outputs. Remember, outputs should be the average value over the timestep
! and not the value at the end of the timestep; although in many models these are exactly the same values. Refer to
! existing types for examples of using advanced features inside the model (Formats, Labels etc.)

!-----
 Use TrnsysConstants
 Use TrnsysFunctions

!-----
!DEC\$Attributes DLLexport :: Type2628

!-----
!Trnsys Declarations
 Implicit None

 Double Precision Timestep,Time
 Integer CurrentUnit,CurrentType,Iteration

! PARAMETERS

! INPUTS
 DOUBLE PRECISION Ppv
 DOUBLE PRECISION Punits
 DOUBLE PRECISION Iin
 DOUBLE PRECISION Ppem
 DOUBLE PRECISION Vstack
 DOUBLE PRECISION co
 DOUBLE PRECISION Paux

! OUTPUTS

DOUBLE PRECISION Pavailable

DOUBLE PRECISION Iout

!-----

!-----

!Get the Global Trnsys Simulation Variables

Time=getSimulationTime()

Timestep=getSimulationTimeStep()

CurrentUnit = getCurrentUnit()

CurrentType = getCurrentType()

!-----

-

!-----

!Set the Version Number for This Type

If(getIsVersionSigningTime()) Then

Call SetTypeVersion(17)

Return

EndIf

!-----

!-----

!Do Any Last Call Manipulations Here

If(getIsLastCallofSimulation()) Then

Return

EndIf

!-----

!-----

!Perform Any "After Convergence" Manipulations That May Be Required at the End of Each Timestep

If(getIsEndOfTimestep()) Then

Return

EndIf

!-----

!-----

!Do All of the "Very First Call of the Simulation Manipulations" Here

 If(getIsFirstCallofSimulation()) Then

 !Tell the TRNSYS Engine How This Type Works

 Call SetNumberofParameters(0) !The number of parameters that the the
model wants

 Call SetNumberofInputs(7) !The number of inputs that the the model
wants

 Call SetNumberofDerivatives(0) !The number of derivatives that the the
model wants

 Call SetNumberofOutputs(2) !The number of outputs that the the model
produces

 Call SetIterationMode(1) !An indicator for the iteration mode
(default=1). Refer to section 8.4.3.5 of the documentation for more details.

 Call SetNumberStoredVariables(0,0) !The number of static variables
that the model wants stored in the global storage array and the number of dynamic variables that
the model wants stored in the global storage array

 Call SetNumberofDiscreteControls(0) !The number of discrete control
functions set by this model (a value greater than zero requires the user to use Solver 1: Powell's
method)

 Call SetInputUnits(1,'PW2')

 Call SetInputUnits(2,'PW2')

 Call SetInputUnits(3,'CU1')

 Call SetInputUnits(4,'PW2')

 Call SetInputUnits(5,'VO1')

 Call SetInputUnits(7,'PW2')

 !

 Call SetOutputUnits(1,'PW2')

 Call SetOutputUnits(2, 'CU1')

 Return

 EndIf

!-----

!-----

!Do All of the First Timestep Manipulations Here - There Are No Iterations at the Intial Time

 If (getIsStartTime()) Then

 Ppv = GetInputValue(1)

```

Punits = GetInputValue(2)
Iin=GetInputValue(3)
Ppem=GetInputValue(4)
Vstack=GetInputValue(5)
co=GetInputValue(6)
Paux=GetInputValue(7)

!Check the Parameters for Problems (#,ErrorType,Text)
!Sample Code: If( PAR1 <= 0.) Call FoundBadParameter(1,'Fatal','The first parameter provided
to this model is not acceptable.')

!Set the Initial Values of the Outputs (#,Value)
    Call SetOutputValue(1, 0) ! Pavailable
    Call SetOutputValue(2, 0) ! Iout

!If Needed, Set the Initial Values of the Static Storage Variables (#,Value)
!Sample Code: SetStaticArrayValue(1,0.d0)

!If Needed, Set the Initial Values of the Dynamic Storage Variables (#,Value)
!Sample Code: Call SetDynamicArrayValueThisIteration(1,20.d0)

!If Needed, Set the Initial Values of the Discrete Controllers (#,Value)
!Sample Code for Controller 1 Set to Off: Call SetDesiredDiscreteControlState(1,0)

    Return

EndIf
!-----
!-----
-
!ReRead the Parameters if Another Unit of This Type Has Been Called Last
    If(getIsReReadParameters()) Then
        !Read in the Values of the Parameters from the Input File
    EndIf
!-----

!Read the Inputs
    Ppv = GetInputValue(1)

```

Punits = GetInputValue(2)
Iin=GetInputValue(3)
Ppem=GetInputValue(4)
Vstack=GetInputValue(5)
co=GetInputValue(6)
Paux=GetInputValue(7)

!Check the Inputs for Problems (#,ErrorType,Text)

!Sample Code: If(IN1 <= 0.) Call FoundBadInput(1,'Fatal','The first input provided to this model is not acceptable.')

If(NotFound()) Return

!-----
!-----
! *** PERFORM ALL THE CALCULATION HERE FOR THIS MODEL. ***
!-----

!-----

!If Needed, Get the Previous Control States if Discrete Controllers are Being Used (#)

!Sample Code: CONTROL_LAST=getPreviousControlState(1)

!-----

!-----

!If Needed, Get the Values from the Global Storage Array for the Static Variables (#)

!Sample Code: STATIC1=getStaticArrayValue(1)

!-----

!-----

!If Needed, Get the Initial Values of the Dynamic Variables from the Global Storage Array (#)

!Sample Code: T_INITIAL_1=getDynamicArrayValueLastTimestep(1)

!-----

!-----

!Perform All of the Calculations Here to Set the Outputs from the Model Based on the Inputs

!Sample Code: OUT1=IN1+PAR1

!If the model requires the solution of numerical derivatives, set these derivatives and get the current solution

!Sample Code: T1=getNumericalSolution(1)

!Sample Code: T2=getNumericalSolution(2)

!Sample Code: DTDT1=3.*T2+7.*T1-15.

!Sample Code: DTDT2=-2.*T1+11.*T2+21.

!Sample Code: Call SetNumericalDerivative(1,DTDT1)

!Sample Code: Call SetNumericalDerivative(2,DTDT2)

!-----

IF ((Ppv-Punits) < 0) THEN

 Pavailable=0

 Iout=0.d0

ELSE IF (((Ppv-Punits)) > 0 .AND. Ppv > ((Iin*Vstack*co)+Paux))THEN

 Pavailable=Ppv

 Iout=Iin

END IF

!-----

!Set the Outputs from this Model (#,Value)

 Call SetOutputValue(1, Pavailable) ! Pavailable

 Call SetOutputValue(2, Iout) ! Iout

!-----

!-----

--

!If Needed, Store the Desired Discret Control Signal Values for this Iteration (#,State)

!Sample Code: Call SetDesiredDiscreteControlState(1,1)

!-----

!-----

!If Needed, Store the Final value of the Dynamic Variables in the Global Storage Array (#,Value)

!Sample Code: Call SetValueThisIteration(1,T_FINAL_1)

!-----

 Return

 End

!-----

```

!-----
-
! This TRNSYS component skeleton was generated from the TRNSYS studio based on the user-
supplied parameters, inputs,
! outputs, and derivatives. The user should check the component formulation carefully and add the
content to transform
! the parameters, inputs and derivatives into outputs. Remember, outputs should be the average
value over the timestep
! and not the value at the end of the timestep; although in many models these are exactly the same
values. Refer to
! existing types for examples of using advanced features inside the model (Formats, Labels etc.)
!-----
    Use TrnsysConstants
    Use TrnsysFunctions

!-----

!DEC$Attributes DLLexport :: Type2629
!-----

!Trnsys Declarations
    Implicit None

    Double Precision Timestep,Time
    Integer CurrentUnit,CurrentType

! PARAMETERS
    DOUBLE PRECISION MatH2Content

! INPUTS
    DOUBLE PRECISION MatSize
    DOUBLE PRECISION H2Flow
    DOUBLE PRECISION Tambient
    DOUBLE PRECISION Ttank
    DOUBLE PRECISION Area
    DOUBLE PRECISION Pin
! output
    DOUBLE PRECISION H2massTot

```

```
DOUBLE PRECISION ChargingTime
DOUBLE PRECISION Qrad
DOUBLE PRECISION Qconv
DOUBLE PRECISION Qtotal
```

```
! VARIABLE DECLARATIONS
```

```
DOUBLE PRECISION H2mas
DOUBLE PRECISION MaxMass
```

```
!-----
!-----
-
```

```
!Get the Global Trnsys Simulation Variables
```

```
Time=getSimulationTime()
Timestep=getSimulationTimeStep()
CurrentUnit = getCurrentUnit()
CurrentType = getCurrentType()
```

```
!-----
!-----
```

```
!Set the Version Number for This Type
```

```
  If(getIsVersionSigningTime()) Then
    Call SetTypeVersion(17)
    Return
  EndIf
```

```
!-----
!-----
```

```
!Do Any Last Call Manipulations Here
```

```
  If(getIsLastCallofSimulation()) Then
    Return
  EndIf
```

```
!-----
```

```
!-----
```

```
!Perform Any "After Convergence" Manipulations That May Be Required at the End of Each Timestep
```

```
  If(getIsEndOfTimestep()) Then
```

```

        Return
    EndIf
!-----
!-----
!Do All of the "Very First Call of the Simulation Manipulations" Here
    If(getIsFirstCallofSimulation()) Then

        !Tell the TRNSYS Engine How This Type Works
        Call SetNumberOfParameters(1)      !The number of parameters that the the
model wants
        Call SetNumberOfInputs(6)         !The number of inputs that the the model
wants
        Call SetNumberOfDerivatives(0)    !The number of derivatives that the the
model wants
        Call SetNumberOfOutputs(6)       !The number of outputs that the the model
produces

        Call SetIterationMode(1)          !An indicator for the iteration mode
(default=1). Refer to section 8.4.3.5 of the documentation for more details.

        Call SetNumberStoredVariables(0,1) !The number of static variables
that the model wants stored in the global storage array and the number of dynamic variables that
the model wants stored in the global storage array

        Call SetNumberOfDiscreteControls(0) !The number of discrete control
functions set by this model (a value greater than zero requires the user to use Solver 1: Powell's
method)

        Call SetInputUnits(1,'MA2')
        Call SetInputUnits(2,'VF1')
        Call SetInputUnits(3,'TE1')
        Call SetInputUnits(4,'TE1')
        Call SetInputUnits(5,'AR1')
        Call SetInputUnits(6,'PR1')

    !

        Call SetOutputUnits(1,'MA1')
        Call SetOutputUnits(2,'MA1')
        Call SetOutputUnits(3,'TD1')
        Call SetOutputUnits(1,'PW2')
        Call SetOutputUnits(2,'PW2')
        Call SetOutputUnits(3,'PW2')

```

Return

EndIf

!-----
!-----

!Do All of the First Timestep Manipulations Here - There Are No Iterations at the Initial Time

If (getIsStartTime()) Then

MatH2Content = getParameterValue(1)

MatSize = GetInputValue(1)

H2Flow = GetInputValue(2)

Tambient=GetInputValue(3)

Ttank=GetInputValue(4)

Area=GetInputValue(5)

Pin=GetInputValue(6)

!Check the Parameters for Problems (#,ErrorType,Text)

!Sample Code: If(PAR1 <= 0.) Call FoundBadParameter(1,'Fatal','The first parameter provided to this model is not acceptable.')

!If Needed, Set the Initial Values of the Static Storage Variables (#,Value)

!Sample Code: SetStaticArrayValue(1,0.d0)

!If Needed, Set the Initial Values of the Dynamic Storage Variables (#,Value)

!Sample Code: Call SetDynamicArrayValueThisIteration(1,20.d0)

Call SetDynamicArrayValueThisIteration(1,H2mas)

!Set the Initial Values of the Outputs (#,Value)

Call SetOutputValue(1, 0.d0) ! H2massTot<-----

Call SetOutputValue(2, 0.d0) ! MaxMas

Call SetOutputValue(3, 0.d0)

Call SetOutputValue(4, 0.d0)

Call SetOutputValue(5,0.d0)

Call SetOutputValue(6,0.d0)

```

!If Needed, Set the Initial Values of the Discrete Controllers (#,Value)
!Sample Code for Controller 1 Set to Off: Call SetDesiredDiscreteControlState(1,0)

        Return

    EndIf

!-----
!-----
!ReRead the Parameters if Another Unit of This Type Has Been Called Last
    If(getIsReReadParameters()) Then
        !Read in the Values of the Parameters from the Input File
        MatH2Content = getParameterValue(1)

    EndIf

!-----

!Read the Inputs
    MatSize = GetInputValue(1)
    H2Flow = GetInputValue(2)
    Tambient=GetInputValue(3)
    Ttank=GetInputValue(4)
    Area=GetInputValue(5)
    Pin=GetInputValue(6)
        !Check the Inputs for Problems (#,ErrorType,Text)
        !Sample Code: If( IN1 <= 0.) Call FoundBadInput(1,'Fatal','The first input provided to this
model is not acceptable.')

    If(ErrorFound()) Return

!-----
!-----
!   *** PERFORM ALL THE CALCULATION HERE FOR THIS MODEL. ***
!-----
!-----
-

!If Needed, Get the Previous Control States if Discrete Controllers are Being Used (#)
!Sample Code: CONTROL_LAST=getPreviousControlState(1)

```

```

!-----
-
!-----
-
!If Needed, Get the Values from the Global Storage Array for the Static Variables (#)
!Sample Code: STATIC1=getStaticArrayValue(1)
!-----
-
!-----
-
!If Needed, Get the Initial Values of the Dynamic Variables from the Global Storage Array
(#)
!Sample Code: T_INITIAL_1=getDynamicArrayValueLastTimestep(1)
             H2mas=getDynamicArrayValueLastTimestep(1)+(H2Flow*0.000001*0.08348)
!-----
-
!-----
-
!Perform All of the Calculations Here to Set the Outputs from the Model Based on the
Inputs

!Mass Trasfer, Absorption Calculations-----
MaxMass=MatSize*MatH2Content*0.000001*0.0899
if (H2mas<=MaxMass)then
H2massTot=H2mas
else
H2massTot=MaxMass
ChargingTime=Time
end if

! Heat Transfer Calculations-----
! Qtotal=Qrad+Qconv---the heat losses form the MHTank are radiative and convective losses
! Qconv=hc*Area*(Ttank-Tambient)
! Qrad=hr*Area*(Ttank-Tambient)
! Qtotal=Qrad+Qconv
! hc=205W/mK and hr=0.308W/mK for Aluminium

Qrad=205*Area*(Ttank-Tambient)
Qconv=0.308*Area*(Ttank-Tambient)
Qtotal=Qrad+Qconv

```

!Sample Code: OUT1=IN1+PAR1

!If the model requires the solution of numerical derivatives, set these derivatives and get the current solution

!Sample Code: T1=getNumericalSolution(1)

!Sample Code: T2=getNumericalSolution(2)

!Sample Code: DTDT1=3.*T2+7.*T1-15.

!Sample Code: DTDT2=-2.*T1+11.*T2+21.

!Sample Code: Call SetNumericalDerivative(1,DTDT1)

!Sample Code: Call SetNumericalDerivative(2,DTDT2)

!-----
-
!-----
-

!Set the Outputs from this Model (#,Value)

Call SetOutputValue(1, H2massTot)

Call SetOutputValue(2, MaxMass)

Call SetOutputValue(3, ChargingTime)

Call SetOutputValue(4, Qrad)

Call SetOutputValue(5, Qconv)

Call SetOutputValue(6, Qtotal)

!-----
!-----

!If Needed, Store the Desired Discret Control Signal Values for this Iteration (#,State)

!Sample Code: Call SetDesiredDiscreteControlState(1,1)

!-----
!-----

!If Needed, Store the Final value of the Dynamic Variables in the Global Storage Array (#,Value)

!Sample Code: Call SetValueThisIteration(1,T_FINAL_1)

Call SetDynamicArrayValueThisIteration(1,H2mas)

!-----

Return

End

!-----

D.2 Statistical Validation of Numerical Model

The details of the statistical analyses and graphical representation of the experimental and numerical model results is given in the bellow sections.

Hydrogen Generation

F-Test Two-Sample for Variances

	<i>Variable 1</i>	<i>Variable 2</i>
Mean	201.628	201.620
Variance	9561.034	9567.199
Observations	10	10
df	9	9
F	0.999	
P(F<=f) one-tail	0.500	
F Critical one-tail	0.315	

Here, for the hydrogen flow rates results it is observed that the $P=0.5 > 0.05$, therefore the variances are equal and the null hypothesis confirmed. The second step is to execute the t-test, to confirm whether the means of the two data sets are equal.

t-Test: Two-Sample Assuming Equal Variances

	<i>Variable 1</i>	<i>Variable 2</i>
Mean	201.628	201.620
Variance	9561.034	9567.199
Observations	10	10
Pooled Variance	9564.116	
Hypothesized Mean Difference	0	
df	18	
t Stat	0.000	
P(T<=t) one-tail	0.500	
t Critical one-tail	1.734	
P(T<=t) two-tail	1.000	
t Critical two-tail	2.101	

Here $P(T \leq t)$ two-tail = $1 > 0.05$. Alternatively, the value t Stat is compared to the value t Critical two-tail and if it is smaller, then the means are equal and the model data and the experimental data are equivalent. Here t Stat = $0 < t$ Critical two-tail = 2.101 . Figure D.22 shows how close the experimental and the numerical model results are.

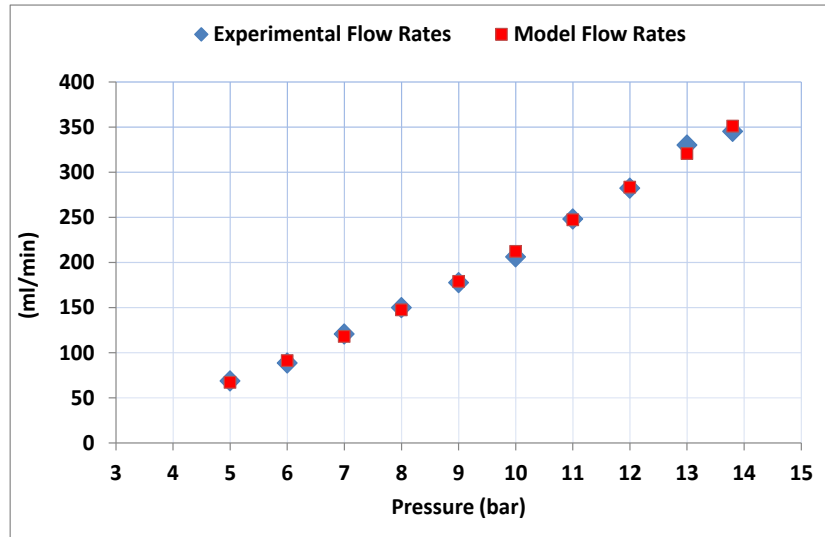


Figure D.22, Experimental and numerical model hydrogen flow rates results

Stack Voltage

The stack voltage is compared in relation to the IV curve data, at 39 °C. Figure D.23 shows that there is no significant difference between the results of the model and the actual experimental.

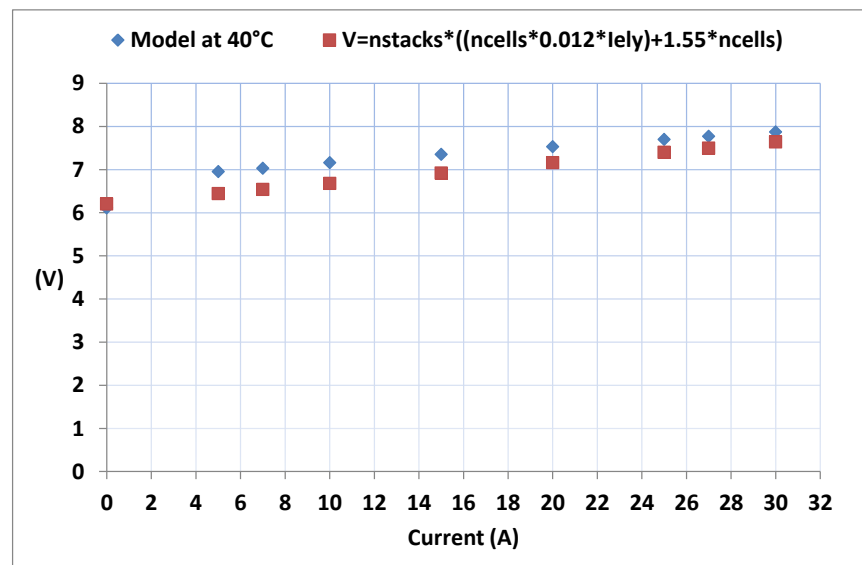


Figure D.23, Stack voltage results from the IV curve and the model at 39°C

F-Test Two-Sample for Variances

	<i>Variable 1</i>	<i>Variable 2</i>
Mean	6.941	7.274
Variance	0.261	0.298
Observations	9	9
df	8	8
F	0.875	
P(F<=f) one-tail	0.427	
F Critical one-tail	0.291	

$P=0.427 > 0.05$, therefore the variances are equal and the null hypothesis confirmed. The second step is to execute the t-test, to confirm whether the means of the two data sets are equal.

In the t-test $P(T \leq t) \text{ two-tail} = 0.2 > 0.05$. Also the value t Stat is compared to the value t Critical two-tail and $t \text{ Stat} = 1.336 < t \text{ Critical two-tail} = 2.121$. Therefore, the means of the two data sets are equal.

t-Test: Two-Sample Assuming Equal Variances

	<i>Variable</i>	
	<i>1</i>	<i>Variable 2</i>
Mean	7.274	6.941
Variance	0.298	0.261
Observations	9	9
Pooled Variance	0.280	
Hypothesized Mean Difference	0	
df	16	
t Stat	1.336	
P(T<=t) one-tail	0.100	
t Critical one-tail	1.746	
P(T<=t) two-tail	0.200	
t Critical two-tail	2.120	

Therefore, the model can replace experimentation and used confidently for the study of applications within the limitations of the developed solar hydrogen model.

Stack Temperature

F-Test Two-Sample for Variances

	<i>Variable 1</i>	<i>Variable 2</i>
Mean	38.055	38.058
Variance	20.866	19.979
Observations	10	10
df	9	9
F	1.044	
P(F<=f) one-tail	0.475	
F Critical one-tail	3.179	

$P=0.475 > 0.05$, therefore the variances are equal and the null hypothesis confirmed. The second step is to execute the t-test, to confirm whether the means of the two data sets are equal.

t-Test: Two-Sample Assuming Equal Variances

	<i>Variable 1</i>	<i>Variable 2</i>
Mean	38.058	38.055
Variance	19.979	20.866
Observations	10	10
Pooled Variance	20.423	
Hypothesized Mean Difference	0	
df	18	
t Stat	0.001	
P(T<=t) one-tail	0.499	
t Critical one-tail	1.734	
P(T<=t) two-tail	0.999	
t Critical two-tail	2.101	

In the t-test $P(T \leq t) \text{ two-tail} = 0.999 > 0.05$. Also the value t Stat is compared to the value t Critical two-tail and $t \text{ Stat} = 0.001 < t \text{ Critical two-tail} = 2.101$. Therefore, the means of the

two data sets are equal. Figure D.24 shows the similarity between the experimentally measured temperature data and the temperatures calculated by the numerical model.

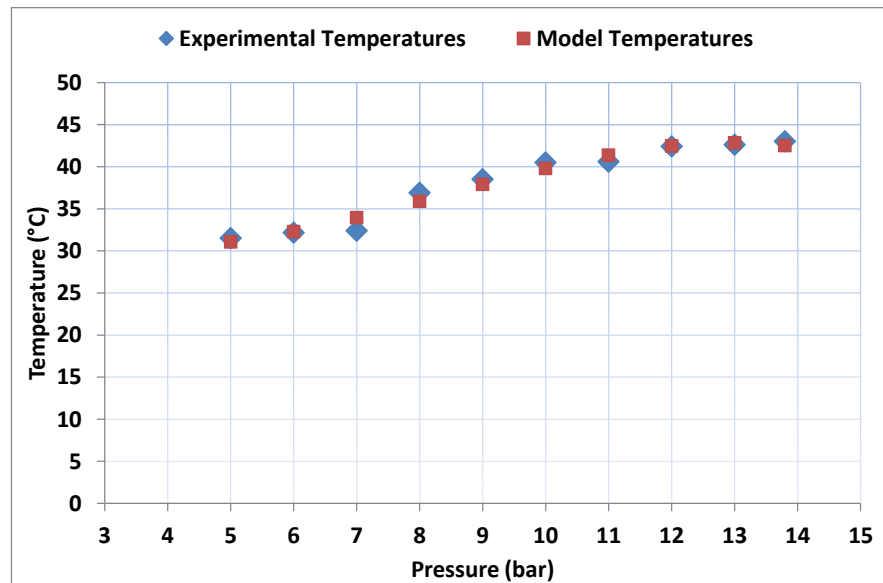


Figure D.24, Experimental and numerical model stack temperature data

Metal Hydride Storage Charging Times

The model calculates the metal hydride tank charging times in relation to the hydrogen inlet pressure and flow rates. A feedback loop sends the information regarding the filling status and accordingly controls the electrolyser hydrogen generation rates.

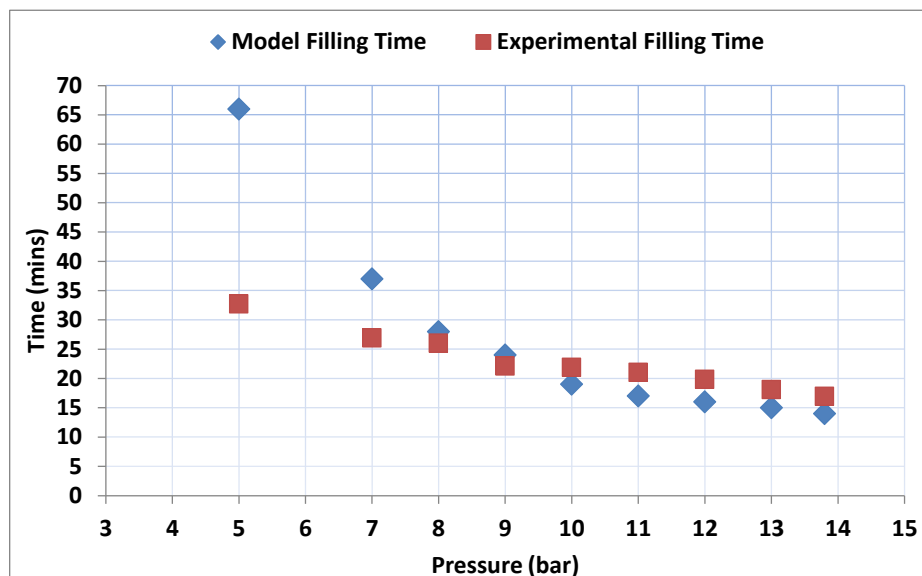


Figure D.25, Experimental and numerical model metal hydride tank filling times

Figure D.25 shows that there is a greater similarity between the experimental and the numerical model results for pressures greater than 8bar. The robustness of the model is additionally corroborated through the results of the statistical analysis.

F-Test Two-Sample for Variances

	<i>Variable 1</i>	<i>Variable 2</i>
Mean	17.500	20.843
Variance	13.100	8.857
Observations	6	7
df	5	6
F	1.479	
P(F<=f) one-tail	0.321	
F Critical one-tail	4.387	

$P=0.321 > 0.05$, therefore the variances are equal, and the t-Test for equal variances can be performed.

t-Test: Two-Sample Assuming Equal Variances

	<i>Variable 1</i>	<i>Variable 2</i>
Mean	20.843	19.000
Variance	8.857	26.667
Observations	7	7
Pooled Variance	17.762	
Hypothesized Mean Difference	0	
df	12	
t Stat	0.818	
P(T<=t) one-tail	0.215	
t Critical one-tail	1.782	
P(T<=t) two-tail	0.429	
t Critical two-tail	2.179	

$P(T<=t) \text{ two-tail} = 0.429 > 0.05$. Also the value t Stat is compared to the value t Critical two-tail and $t \text{ Stat} = 0.818 < t \text{ Critical two-tail} = 2.179$. Therefore, the means of the two data sets are equal. This means that the charging times calculated by the model can be used confidently as an accurate representation of reality for the estimation of the hydrogen storage in the metal hydride cylinders.

D.3 Data of Validation Experiments

The characteristics of the Trina Solar panels that have been used in the experimental part of this research and also for the development of the case studies can be seen in Figure D.26.

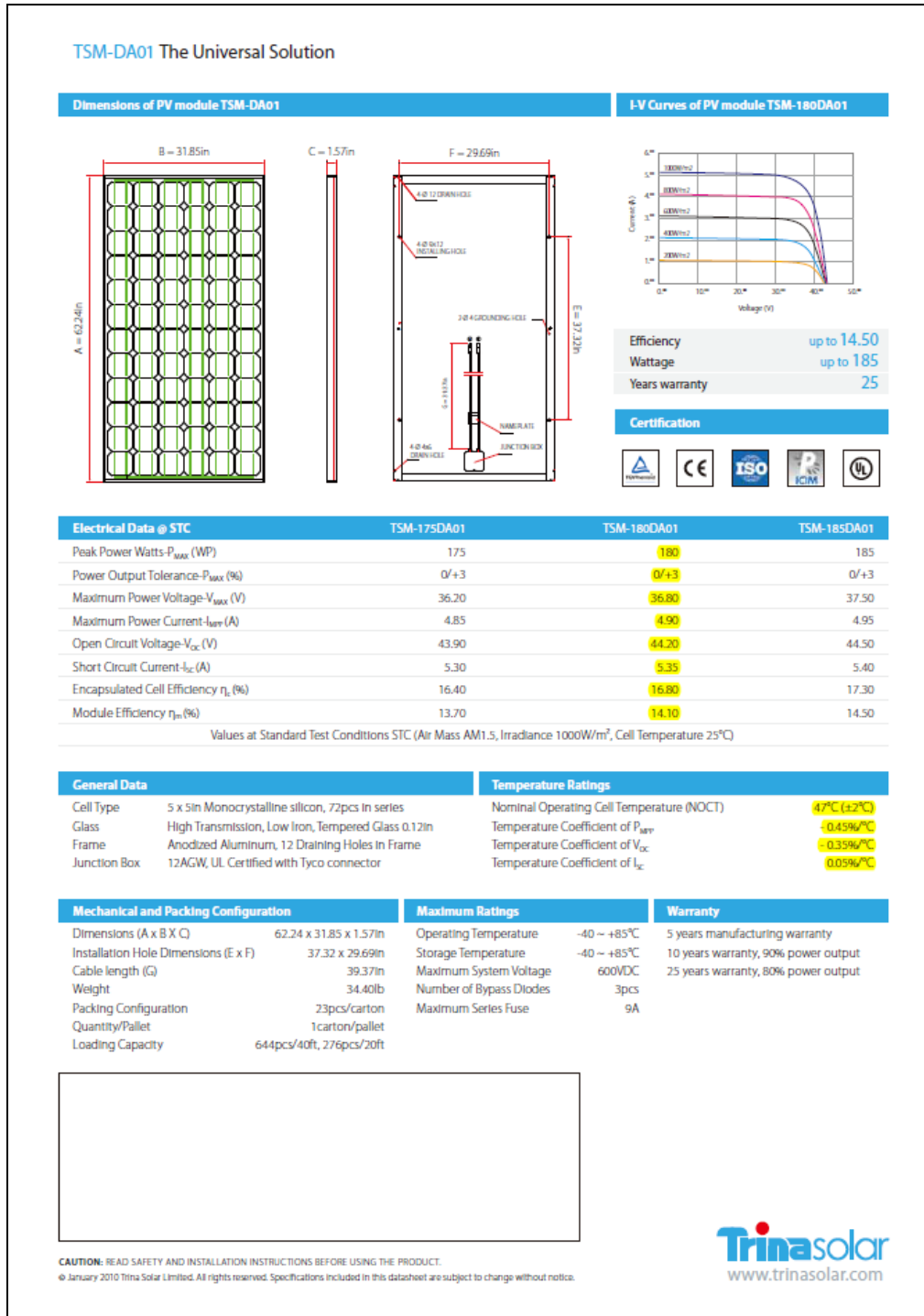


Figure D.26, Trina Solar panels characteristics

The characteristics of the Sanyo HIT and the Sharp panels that have been used in the experimental part of this research and also for the development of the case studies can be seen in Figures D.27 and D.28.

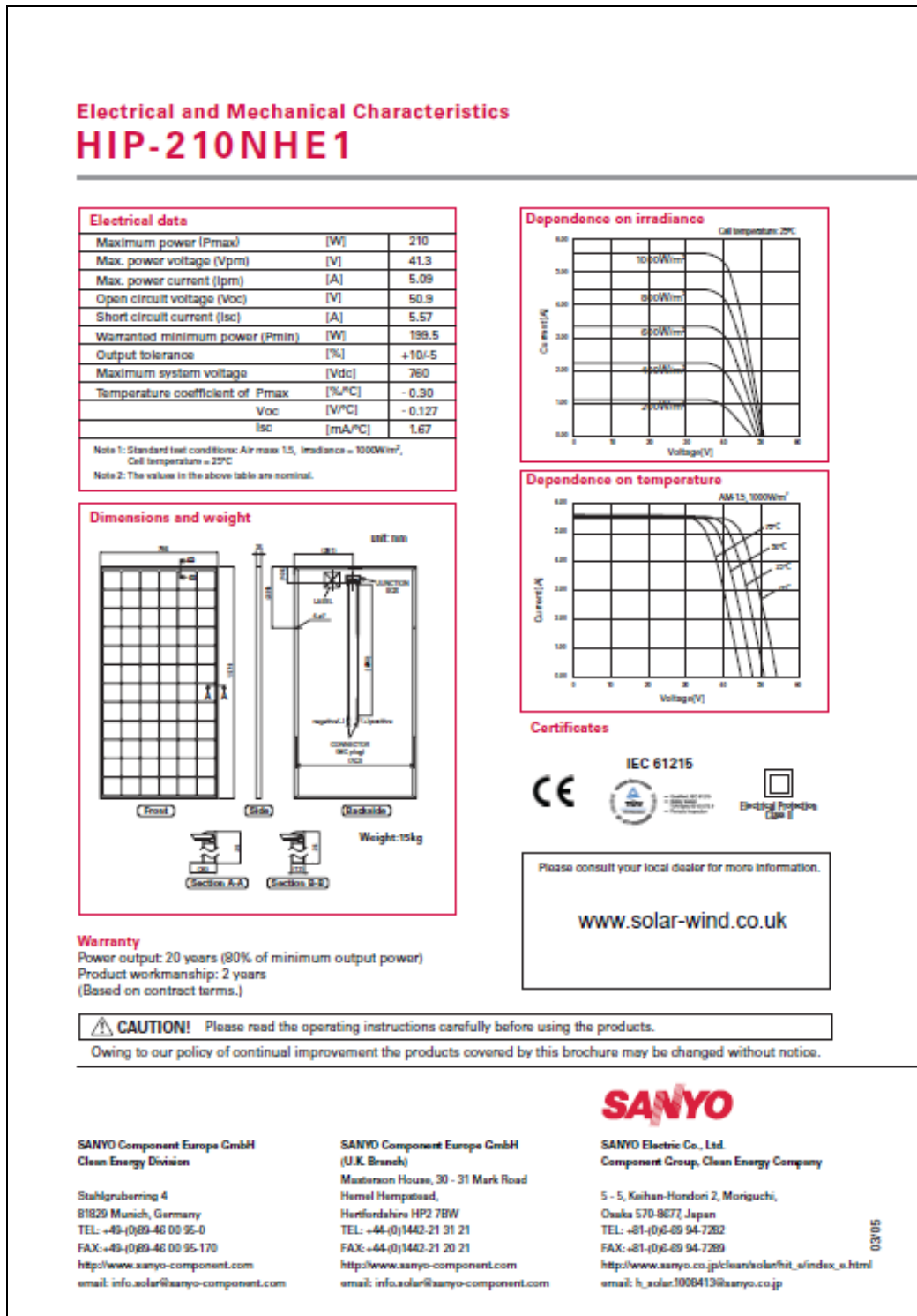


Figure D.27, Sanyo HIT panels characteristics

Specifications NUSSE3E / NU18E1

Cell	Monocrystalline silicon solar cells, 155.5 mm square
No. of cells and connections	48 in series
Maximum system voltage	1,000 V DC
Nominal power	185 W
Dimensions	1,318 x 994 x 46 mm
Weight	16.0 kg
Type of output terminal	Lead wire with connector

Ambient conditions

Parameters	Rating	Unit
Operating temperature	-40 to +90	°C
Storage temperature	-40 to +90	°C
Storage humidity	up to 90	%

Temperature coefficients

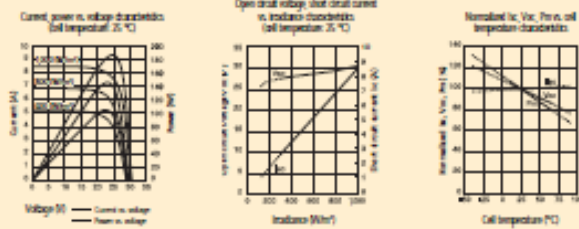
α_{Pm}	-0.485% / °C
α_{Voc}	+0.053% / °C
α_{Voc}	-104 mV / °C

Electrical data

Parameters	Symbol	Min.	Typ.	Unit
Open circuit voltage	V_{oc}	—	30.2	V
Maximum power voltage	V_{Pm}	—	24.0	V
Short circuit current	I_{sc}	—	8.54	A
Maximum power current	I_{Pm}	—	7.71	A
Nominal power	P_m	175.8	185.0	W
Module efficiency	η_m	—	14.1	%

The electrical data applies under Standard Test Conditions (STC): Radiation 1,000 W/m² with a spectrum of AM 1.5 and at a cell temperature of 25 °C.

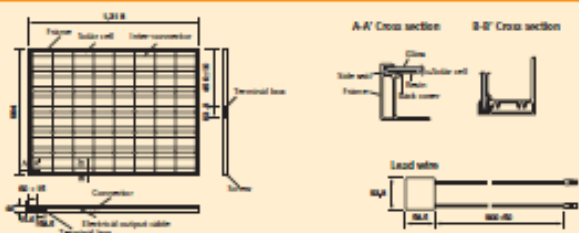
Characteristics



Application options

- Grid connected residential systems
- Office buildings
- Solar power stations
- Solar villages
- Villas, mountain cottages
- Lighting equipment
- Traffic signs
- Radio relay stations
- Beacons
- Telemetry systems
- Telecommunication systems

Outline dimensions



This module should not be connected to any direct load. In the absence of confirmation by specification sheets, Sharp takes no responsibility for any defects that may occur in equipment using any Sharp products shown in catalogs, data books, etc. Contact Sharp in order to obtain the latest specification sheets before using any Sharp products. Specifications are subject to change without notice.

SHARP

Central & Eastern Europe
Tel: +43-021-72 71 90 - Fax: +43-021-72 71 91 41
www.sharp-coe.com

France
Tel: +33-01-49 90 34 00 - Fax: +33-01-48 63 26 21
www.sharp.fr

Germany & Austria
Tel. Germany: +49-0218 05-01 52 22 (ger)
Tel. Austria: +49-0218 25-43 06 40 (aue)
www.sharp.de/ger | www.sharp.at/aue

Italy
Tel: +39-02-89 59 51 - Fax: +39-02-89 53 08 95
www.sharp.it

Spain & Portugal
Tel: +34-0213-5 01 97 00 - Fax: +34-0213-6 75 46 11
www.sharp.es

Nordic countries
Tel: +46-028-6 34 36 00 - Fax: +46-028-4 34 36 10
www.sharp.se

Switzerland
Tel: +41-021-8 46 61 11 - Fax: +41-021-8 46 62 25
www.sharp.ch

BeneLux
Tel: +31-020-6 35 95 00 - Fax: +31-020-6 35 95 95
www.sharp.nl | www.sharp.be

United Kingdom
Tel: +44-017 61-2 05 23 33 - Fax: +44-017 61-2 05 70 76
www.sharp.co.uk/hol

The reference image on the front side shows a 400 Wp PV system from Sharp in Palermo.

Solar/120513_2_118

Figure D.28, Sharp panels characteristics

D.4 UK and Jamaica Experimental Conditions for Model Validation

Table D1 shows the type and number of the total experiments conducted.

Table D.1, Summary of types of Experiments and the total number of days of experimental work

Experiment	Outcomes of experiment	Number of tests	Days
PEM Electrolyser Hydrogen Pressure Effect on the Hydrogen Production and Energy Use	<ul style="list-style-type: none"> Hydrogen production pattern according to the production pressure Energy use pattern according to the production pressure 	24	24
		24	24
PEM Electrolyser Hydrogen Production under UK Conditions	<ul style="list-style-type: none"> PV power effect on the produced hydrogen flow rates Effect of the different production pressure on the hydrogen production Efficiency of the stack Efficiency of the system 	28	28
		28	28
		28	28
		28	28
PEM Electrolyser Hydrogen Production under Jamaican Conditions	<ul style="list-style-type: none"> PV power effect on the produced hydrogen flow rates Effect of the different production pressure on the hydrogen production Efficiency of the stack Efficiency of the system 	24	24
		24	24
		24	24
		24	24
ASPM Electrolyser Hydrogen Production	<ul style="list-style-type: none"> PV power effect on the produced hydrogen flow rates Efficiency of the stack Efficiency of the system 	10	10
		10	10
		10	10
PEM Electrolyser Direct Stack Measurements	<ul style="list-style-type: none"> Stack Current Measurement Stack Voltage Measurement I-V polarisation curve creation 	12	12
		12	12
		5	5
ASPM Electrolyser Direct Stack Measurements	<ul style="list-style-type: none"> Stack Current Measurement Stack Voltage Measurement I-V polarisation curve creation 	3	3
Metal Hydride Storage of Hydrogen Gas	<ul style="list-style-type: none"> Charge period Discharge period Volume/ mass of hydrogen stored 	25	25
		25	25
		25	25

Tables D.2 and D.3 show indicative values of the weather and PV power data that are used as input of the experimental conditions for the numerical model validation. Table D.4 shows typical example of current values used in the Jamaica conditions experiments

Table D.2, Example of weather and PV Power Output Data used in the Experiments, for the 1st of June 2013

Date	Time [hh:mm:ss]	Sanyo Power [W]	Sharp Power [W]	Total Power [W]	GHI [W/m ²]	RH [%]	Te mp [°C]
Sat, 1 June	12:55:00	272	266	538	427.7	35.5	17.8
Sat, 1 June	13:00:00	456	459	915	703.1	35.6	17.7
Sat, 1 June	13:05:00	442	456	898	730.4	36.0	17.4
Sat, 1 June	13:10:00	332	337	669	492.4	36.8	17.3
Sat, 1 June	13:15:00	323	330	653	473.6	38.0	17.0
Sat, 1 June	13:20:00	304	313	617	463.6	38.6	16.7
Sat, 1 June	13:25:00	391	397	788	581.1	39.3	16.7
Sat, 1 June	13:30:00	442	452	894	644.1	38.2	16.8
Sat, 1 June	13:35:00	502	510	1012	810.0	37.2	16.9
Sat, 1 June	13:40:00	240	238	478	360.3	37.1	17.1
Sat, 1 June	13:45:00	267	275	542	409.0	37.0	17.1
Sat, 1 June	13:50:00	294	302	596	449.7	37.0	17.0
Sat, 1 June	13:55:00	309	314	623	458.5	37.0	17.0
Sat, 1 June	14:00:00	262	265	527	389.2	35.7	17.0

Table D.3, Example of weather and PV Power Output Data used in the Experiments, for the 1st of June 2013

Date	Time [hh:mm:ss]	Sanyo Power [W]	Sharp Power [W]	Total Power [W]	GHI [W/m ²]	RH [%]	Temp [°C]
Sat, 1 June	14:10:00	221	222	443	344.6	36.3	17.1
Sat, 1 June	14:15:00	301	309	610	450.5	36.1	17.1
Sat, 1 June	14:20:00	259	263	522	383.5	36.0	17.1
Sat, 1 June	14:25:00	215	218	433	340.8	36.5	17.1
Sat, 1 June	14:30:00	368	379	747	584.1	36.1	17.0
Sat, 1 June	14:35:00	276	284	560	423.6	34.6	17.1
Sat, 1 June	14:40:00	271	277	548	412.4	33.9	17.3
Sat, 1 June	14:45:00	284	288	572	430.8	34.7	17.4
Sat, 1 June	14:50:00	365	372	737	579.1	33.7	17.4
Sat, 1 June	14:55:00	449	455	904	680.0	33.1	17.5
Sat, 1 June	15:00:00	525	533	1058	785.4	32.4	17.9

Table D.4, Typical example of current values used in the Jamaica conditions experiments

Date	Time	Irradiance [W/m ²]	DC Power [W]	Inverter Voltage [V]	Current [A]
18 May	10:15:00	803	968.3	24	40.35
18 May	10:30:00	835	1008.37	24	42.02
18 May	10:45:00	581	694.26	24	28.93
18 May	11:00:00	587	702.11	24	29.25
18 May	11:15:00	1044	1261.89	24	52.58
18 May	11:30:00	340	396.14	24	16.51
18 May	11:45:00	258	295.24	24	12.30
18 May	12:00:00	452	533.64	24	22.24
18 May	12:15:00	985	1191.59	24	49.65

Tables D.5 to D.12 show measurements for the four selected pressure set points for small periods of operation. The data logging is performed for a time interval of 1 second

Table D.5, Example of measured data of the experimental test at 5 bar for day 6 of the UK data set

Date:	Time [09:45]	Sanyo Power [W]	Sharp Power [W]	Total Power [W]	Irradiance [W/m²]	Electrolyser Power [W]	Stack Power [W]	Hydrogen Flow Rate [ml/min]
						Error 4.79%	Error 4.79%	Uncertainty 0.608 %
Thursday, 6 June 13	09:45:01	475	348	823	615.94	660.99	130.99	68.28
Thursday, 6 June 13	09:45:02	475	348	823	615.94	574.94	44.94	71.47
Thursday, 6 June 13	09:45:03	475	348	823	615.94	538.1	8.1	67.76
Thursday, 6 June 13	09:45:04	475	348	823	615.94	534.66	4.66	64.46
Thursday, 6 June 13	09:45:05	475	348	823	615.94	561.9	31.9	63.78
Thursday, 6 June 13	09:45:06	475	348	823	615.94	580.21	50.21	65.48
Thursday, 6 June 13	09:45:07	475	348	823	615.94	581.46	51.46	66.84
Thursday, 6 June 13	09:45:08	475	348	823	615.94	576.4	46.4	67.47
Thursday, 6 June 13	09:45:09	475	348	823	615.94	565.97	35.97	67.26
Thursday, 6 June 13	09:45:10	475	348	823	615.94	570.14	40.14	67.13
Thursday, 6 June 13	09:45:11	475	348	823	615.94	548.02	18.02	66.58
Thursday, 6 June 13	09:45:12	475	348	823	615.94	559.03	29.03	65.38
Thursday, 6 June 13	09:45:13	475	348	823	615.94	562.42	32.42	65.3
Thursday, 6 June 13	09:45:14	475	348	823	615.94	578.07	48.07	64.38
Thursday, 6 June 13	09:45:15	475	348	823	615.94	582.19	52.19	66.37
Thursday, 6 June 13	09:45:16	475	348	823	615.94	559.55	29.55	68.1
Thursday, 6 June 13	09:45:17	475	348	823	615.94	564.45	34.45	67.55
Thursday, 6 June 13	09:45:18	475	348	823	615.94	562.57	32.57	66.79

Table D.6, Example of measured data of the experimental test at 7 bar for day 6 of the UK data set

Date: Thursday, 6 June 13	Time [09:45]	Sanyo Power [W]	Sharp Power [W]	Total Power [W]	Irradiance [W/m ²]	Electrolyser Power [W]	Stack Power [W]	Hydrogen Flow Rate [ml/min]
						Error 4.79%	Error 4.79%	Uncertainty 0.853%
Thursday, 6 June 13	09:45:01	475	348	823	615.94	183.14	153.14	118.25
Thursday, 6 June 13	09:45:02	475	348	823	615.94	159.32	129.32	115.03
Thursday, 6 June 13	09:45:03	475	348	823	615.94	53.45	23.45	111.68
Thursday, 6 June 13	09:45:04	475	348	823	615.94	24.01	0.00	110.32
Thursday, 6 June 13	09:45:05	475	348	823	615.94	20.65	0.00	108.59
Thursday, 6 June 13	09:45:06	475	348	823	615.94	39.71	9.71	107.16
Thursday, 6 June 13	09:45:07	475	348	823	615.94	95.59	65.59	106.14
Thursday, 6 June 13	09:45:08	475	348	823	615.94	111.43	81.43	104.54
Thursday, 6 June 13	09:45:09	475	348	823	615.94	93.54	63.54	103.62
Thursday, 6 June 13	09:45:10	475	348	823	615.94	69.28	39.28	106.00
Thursday, 6 June 13	09:45:11	475	348	823	615.94	44.91	14.91	113.54
Thursday, 6 June 13	09:45:12	475	348	823	615.94	40.98	10.98	123.11
Thursday, 6 June 13	09:45:13	475	348	823	615.94	51.64	21.64	128.40
Thursday, 6 June 13	09:45:14	475	348	823	615.94	94.02	64.02	132.77
Thursday, 6 June 13	09:45:15	475	348	823	615.94	88.37	58.37	130.02
Thursday, 6 June 13	09:45:16	475	348	823	615.94	79.94	49.94	124.81

Table D.7, Example of measured data of the experimental test at 10 bar for day 6 of the UK data set

Date: Thursday, 6 June 13	Time [09:45]	Sanyo Power [W]	Sharp Power [W]	Total Power [W]	Irradiance [W/m²]	Electrolyser Power [W]	Stack Power [W]	Hydrogen Flow Rate [ml/min]
						Error 4.79%	Error 4.79%	Uncertainty 1.326 %
Thursday, 6 June 13	09:45:01	475	348	823	615.94	713.04	183.04	202.22
Thursday, 6 June 13	09:45:02	475	348	823	615.94	713.72	183.72	205.62
Thursday, 6 June 13	09:45:03	475	348	823	615.94	713.58	183.58	208.21
Thursday, 6 June 13	09:45:04	475	348	823	615.94	713.04	183.04	210.83
Thursday, 6 June 13	09:45:05	475	348	823	615.94	703.23	173.23	213.00
Thursday, 6 June 13	09:45:06	475	348	823	615.94	573.41	43.41	211.51
Thursday, 6 June 13	09:45:07	475	348	823	615.94	502.23	0.00	203.19
Thursday, 6 June 13	09:45:08	475	348	823	615.94	494.97	0.00	197.12
Thursday, 6 June 13	09:45:09	475	348	823	615.94	499.38	0.00	192.86
Thursday, 6 June 13	09:45:10	475	348	823	615.94	527.35	0.00	188.88
Thursday, 6 June 13	09:45:11	475	348	823	615.94	631.70	101.70	189.33
Thursday, 6 June 13	09:45:12	475	348	823	615.94	689.05	159.05	195.76
Thursday, 6 June 13	09:45:13	475	348	823	615.94	698.32	168.32	202.82
Thursday, 6 June 13	09:45:14	475	348	823	615.94	686.50	156.50	204.39
Thursday, 6 June 13	09:45:15	475	348	823	615.94	604.96	74.96	204.66
Thursday, 6 June 13	09:45:16	475	348	823	615.94	533.97	0.00	202.07

Table D.8, Example of measured data of the experimental test at 13.8 bar for day 6 of the UK data set

Date: Thursday, 6 June 13	Time [09:45]	Sanyo Power [W]	Sharp Power [W]	Total Power [W]	Irradiance [W/m²]	Electrolyser Power [W]	Stack Power [W]	Hydrogen Flow Rate [ml/min]
						Error 4.79%	Error 4.79%	Uncertainty 1.88 %
Thursday, 6 June 13	09:45:01	475	348	823	615.94	192.61	162.61	335.54
Thursday, 6 June 13	09:45:02	475	348	823	615.94	191.26	161.26	338.00
Thursday, 6 June 13	09:45:03	475	348	823	615.94	191.53	161.53	339.62
Thursday, 6 June 13	09:45:04	475	348	823	615.94	191.30	161.30	342.84
Thursday, 6 June 13	09:45:05	475	348	823	615.94	192.50	162.50	345.22
Thursday, 6 June 13	09:45:06	475	348	823	615.94	192.54	162.54	347.57
Thursday, 6 June 13	09:45:07	475	348	823	615.94	192.65	162.65	349.74
Thursday, 6 June 13	09:45:08	475	348	823	615.94	190.93	160.93	351.68
Thursday, 6 June 13	09:45:09	475	348	823	615.94	190.55	160.55	335.64
Thursday, 6 June 13	09:45:10	475	348	823	615.94	190.59	160.59	317.93
Thursday, 6 June 13	09:45:11	475	348	823	615.94	191.98	161.98	321.07
Thursday, 6 June 13	09:45:12	475	348	823	615.94	193.47	163.47	324.60
Thursday, 6 June 13	09:45:13	475	348	823	615.94	195.76	165.76	326.75
Thursday, 6 June 13	09:45:14	475	348	823	615.94	195.91	165.91	329.31
Thursday, 6 June 13	09:45:15	475	348	823	615.94	195.50	165.50	332.87
Thursday, 6 June 13	09:45:16	475	348	823	615.94	195.42	165.42	336.61

Tables D.9 to D.12 show the measurements of the operation of the electrolyser for variable irradiance conditions.

Table D.9, Example of measured data of the experimental test at 5 bar for day 1 of the UK data set

Date:	Time [hh:mm:ss]	Sanyo Power [W]	Sharp Power [W]	Total Power [W]	Irradiance [W/m ²]	Electrolyser Power [W]	Stack Power [W]	Hydrogen Flow Rate [ml/min]
Thursday, 1 June 13					Error 4.79%	Error 4.79%		Uncertainty 0.608 %
Saturday, 1 June 13	12:50:52	638	642	1280	1046.25	508.75	0.00	70.74
Saturday, 1 June 13	12:50:53	638	642	1280	1046.25	510.42	0.00	68.49
Saturday, 1 June 13	12:50:54	638	642	1280	1046.25	510.03	0.00	68.15
Saturday, 1 June 13	12:50:55	638	642	1280	1046.25	510.37	0.00	69.90
Saturday, 1 June 13	12:50:56	638	642	1280	1046.25	508.07	0.00	70.66
Saturday, 1 June 13	12:50:57	638	642	1280	1046.25	486.43	0.00	74.35
Saturday, 1 June 13	12:50:58	638	642	1280	1046.25	54.68	0.00	47.85
Saturday, 1 June 13	12:50:59	638	642	1280	1046.25	3.28	0.00	58.52
Saturday, 1 June 13	12:55:00	272	266	538	427.72	44.72	0.00	0.00
Saturday, 1 June 13	12:55:01	272	266	538	427.72	17.31	0.00	0.00
Saturday, 1 June 13	12:55:02	272	266	538	427.72	14.12	0.00	0.00
Saturday, 1 June 13	12:55:03	272	266	538	427.72	13.78	0.00	0.00
Saturday, 1 June 13	12:55:04	272	266	538	427.72	14.18	0.00	0.00
Saturday, 1 June 13	12:55:05	272	266	538	427.72	14.21	0.00	0.00
Saturday, 1 June 13	12:55:06	272	266	538	427.72	14.21	0.00	0.00
Saturday, 1 June 13	12:55:07	272	266	538	427.72	14.15	0.00	0.00
Saturday, 1 June 13	12:55:08	272	266	538	427.72	14.15	0.00	0.00

Table D.10, Example of measured data of the experimental test at 7 bar for day 1 of the UK data set

Date: Thursday, 1 June 13	Time [hh:mm:ss]	Sanyo Power [W]	Sharp Power [W]	Total Power [W]	Irradiance [W/m ²]	Electrolyser Power [W]	Stack Power [W]	Hydrogen Flow Rate [ml/min]
					Error 4.79%	Error 4.79%		Uncertainty 0.853 %
Saturday, 1 June 13	12:50:52	638	642	1280	1046.25	532.60	2.60	125.68
Saturday, 1 June 13	12:50:53	638	642	1280	1046.25	567.04	37.04	123.98
Saturday, 1 June 13	12:50:54	638	642	1280	1046.25	589.50	59.50	127.12
Saturday, 1 June 13	12:50:55	638	642	1280	1046.25	569.98	39.98	129.63
Saturday, 1 June 13	12:50:56	638	642	1280	1046.25	563.26	33.26	125.99
Saturday, 1 June 13	12:50:57	638	642	1280	1046.25	119.82	89.82	91.30
Saturday, 1 June 13	12:50:58	638	642	1280	1046.25	8.96	13.57	81.36
Saturday, 1 June 13	12:50:59	638	642	1280	1046.25	43.57	0.00	0.00
Saturday, 1 June 13	12:55:00	272	266	538	427.72	21.07	0.00	0.00
Saturday, 1 June 13	12:55:01	272	266	538	427.72	17.11	0.00	0.00
Saturday, 1 June 13	12:55:02	272	266	538	427.72	15.94	0.00	0.00
Saturday, 1 June 13	12:55:03	272	266	538	427.72	16.43	0.00	0.00
Saturday, 1 June 13	12:55:04	272	266	538	427.72	16.54	0.00	0.00
Saturday, 1 June 13	12:55:05	272	266	538	427.72	16.54	0.00	0.00
Saturday, 1 June 13	12:55:06	272	266	538	427.72	16.54	0.00	0.00
Saturday, 1 June 13	12:55:07	272	266	538	427.72	16.51	0.00	0.00

Table D.11, Example of measured data of the experimental test at 10 bar for day 1 of the UK data set

Date:	Time	Sanyo Power	Sharp Power	Total Power	Irradiance	Electrolyser Power	Stack Power	Hydrogen Flow Rate
Thursday, 1 June 13	[hh:mm:ss]	[W]	[W]	[W]	[W/m ²]	[W]	[W]	[ml/min]
					Error 4.79%	Error 4.79%		Uncertainty 1.326%
Saturday, 1 June 13	12:50:52	638	642	1280	1046.25	100.01	70.01	214.60
Saturday, 1 June 13	12:50:53	638	642	1280	1046.25	116.90	86.90	197.30
Saturday, 1 June 13	12:50:54	638	642	1280	1046.25	195.12	165.12	193.17
Saturday, 1 June 13	12:50:55	638	642	1280	1046.25	183.18	153.18	204.45
Saturday, 1 June 13	12:50:56	638	642	1280	1046.25	15.90	0.00	97.08
Saturday, 1 June 13	12:50:57	638	642	1280	1046.25	26.42	0.00	86.91
Saturday, 1 June 13	12:50:58	638	642	1280	1046.25	28.90	0.00	65.90
Saturday, 1 June 13	12:50:59	638	642	1280	1046.25	18.63	0.00	66.89
Saturday, 1 June 13	12:55:00	272	266	538	427.72	15.94	0.00	0.00
Saturday, 1 June 13	12:55:01	272	266	538	427.72	16.15	0.00	0.00
Saturday, 1 June 13	12:55:02	272	266	538	427.72	16.36	0.00	0.00
Saturday, 1 June 13	12:55:03	272	266	538	427.72	16.33	0.00	0.00
Saturday, 1 June 13	12:55:04	272	266	538	427.72	16.36	0.00	0.00
Saturday, 1 June 13	12:55:05	272	266	538	427.72	16.36	0.00	0.00
Saturday, 1 June 13	12:55:06	272	266	538	427.72	16.36	0.00	0.00
Saturday, 1 June 13	12:55:07	272	266	538	427.72	16.33	0.00	0.00
Saturday, 1 June 13	12:55:08	272	266	538	427.72	16.29	0.00	0.00
Saturday, 1 June 13	12:55:09	272	266	538	427.72	16.33	0.00	0.00
Saturday, 1 June 13	12:55:10	272	266	538	427.72	16.29	0.00	0.00
Saturday, 1 June 13	12:55:11	272	266	538	427.72	16.33	0.00	0.00

Table D.12, Example of measured data of the experimental test at 13.8 bar for day 1 of the UK data set

Date: Thursday, 1 June 13	Time [hh:mm:ss]	Sanyo Power [W]	Sharp Power [W]	Total Power [W]	Irradiance [W/m ²]	Electrolyser Power [W]	Stack Power [W]	Hydrogen Flow Rate [ml/min]
					Error 4.79%	Error 4.79%		Uncertainty 1.88 %
Saturday, 1 June 13	12:50:52	638	642	1280	1046.25	19.44	0.00	342.15
Saturday, 1 June 13	12:50:53	638	642	1280	1046.25	214.83	184.83	335.17
Saturday, 1 June 13	12:50:54	638	642	1280	1046.25	556.57	26.57	330.72
Saturday, 1 June 13	12:50:55	638	642	1280	1046.25	261.14	231.14	302.81
Saturday, 1 June 13	12:50:56	638	642	1280	1046.25	21.17	0.00	139.99
Saturday, 1 June 13	12:50:57	638	642	1280	1046.25	27.80	0.00	117.41
Saturday, 1 June 13	12:50:58	638	642	1280	1046.25	20.61	0.00	91.59
Saturday, 1 June 13	12:50:59	638	642	1280	1046.25	5.01	0.00	0.00
Saturday, 1 June 13	12:55:00	272	266	538	427.72	2.45	0.00	0.00
Saturday, 1 June 13	12:55:01	272	266	538	427.72	1.02	0.00	0.00
Saturday, 1 June 13	12:55:02	272	266	538	427.72	5.84	0.00	0.00
Saturday, 1 June 13	12:55:03	272	266	538	427.72	6.37	0.00	0.00
Saturday, 1 June 13	12:55:04	272	266	538	427.72	8.40	0.00	0.00
Saturday, 1 June 13	12:55:05	272	266	538	427.72	4.78	0.00	0.00
Saturday, 1 June 13	12:55:06	272	266	538	427.72	2.79	0.00	0.00
Saturday, 1 June 13	12:55:07	272	266	538	427.72	3.54	0.00	0.00

Appendix E. Ghana Quantitative Survey

This appendix presents examples of the questionnaires of the Ghana quantitative survey in Figures E.1 to E.6.

①

**Sustainable Production of Hydrogen Gas as Fuel for Domestic Cooking Data
collection Questionnaire for Ghana**

Identification – Town and Household ID Akatsi 1
 Interviewee Name: Ellea Age: 63 Gender: F Occupation: Teacher (Retired)
 Educational attainment: Teacher training

Questions

- What types of fuel do you use for cooking in your household?
 - Charcoal
 - Fire wood
 - LPG
 - Others
- Which of the listed fuel types do you use most and why?
 - LPG
 - Reasons clean and quick to use.
- What types of cooking devices do you use in your household?
 - Charcoal pot
 - Gas burner 2 burners
 - Local stove
 - Others.....

LPG ⇒ 15kg.
Cost = 50 GH₵.
weight = 15kg.
Duration = 1 month.
- In which part of the house does the household do its cooking?
 - Kitchen
 - Backyard
 - Veranda
 - Else..

Charcoal medium bag
Cost = 20 GH₵
weight = 20 kg.
Duration = 2 months
- State the cooking fuel consumed per cooking (kg).
 - Morning (4am-9am)
 - Afternoon (11am – 2pm)
 - Evening (5pm – 9pm)
- Total fuel used per month (kg)
 -
- What is the cost of the cooking fuel? (per week or per month, as is more suitable)
- What is the income level of your household? 900 GH₵.
- What is the percentage of household income used on cooking fuel?
- What is the breakdown of occupancy of your household?
 - Children (0 – 18yrs) X
 - Adult (18 - 60yrs) 2
 - Elderly (60+) 1
- Do you have Electricity in your house? Yes
- If yes do you use it for cooking? Yes
- Do you have solar energy in use in your house? Yes
- Would you be willing to change to a new clean energy source for cooking and a better cooking stove? Yes

Solar lantern.

- Give reasons for your answer in question 14 (respiratory problems caused by current cooking system..)
 - I want to try the new gas
 -
 -
- Are there any extra costs related to the energy needs for cooking? (e.g. travelling to obtain fuel supplies)
 - 40 GH₵

Date: 29/09/14
 Interviewer: Dijine.

Figure E.1, Questionnaire sample of the Ghana survey

Sustainable Production of Hydrogen Gas as Fuel for Domestic Cooking Data
collection Questionnaire for Ghana

Identification – Town and Household ID Akatsi 53
Interviewee Name: Roselyn Age 37 Gender F Occupation Teacher
Educational attainment Diploma

Questions

1. What types of fuel do you use for cooking in your household?
 - i. Charcoal
 - ii. Fire wood
 - iii. LPG
 - iv. Others
2. Which of the listed fuel types do you use most and why?
 - i. LPG
 - ii. Reasons Neat and Fast
3. What types of cooking devices do you use in your household?
 - i. Charcoal pot
 - ii. Gas burner
 - iii. Local stove
 - iv. Others.....

LPG. Large weight = 15kg. Cost = 50 GHS. Duration = 2 months.
4. In which part of the house does the household do its cooking?
 - i. Kitchen
 - ii. Backyard
 - iii. Veranta
 - iv. Else..
5. State the cooking fuel consumed per cooking (kg).
 - i. Morning (4am-9am)
 - ii. Afternoon (11am – 2pm)
 - iii. Evening (5pm – 9pm)
6. Total fuel used per month (kg)
 - i.
7. What is the cost of the cooking fuel? (per week or per month, as is more suitable)
8. What is the income level of your household? 900 GHS.
9. What is the percentage of household income used on cooking fuel?
10. What is the breakdown of occupancy of your household?
 - i. Children (0 – 18yrs) 2
 - ii. Adult (18 - 60yrs) 2
 - iii. Elderly (60+) 1
11. Do you have Electricity in your house? Yes No
12. If yes do you use it for cooking? Yes No
13. Do you have solar energy in use in your house? Yes No
14. Would you be willing to change to a new clean energy source for cooking and a better cooking stove? Yes No
15. Give reasons for your answer in question 14 (respiratory problems caused by current cooking system..)
 - i. I will try new fuel (hydrogen gas)
 - ii.
 - iii.
16. Are there any extra costs related to the energy needs for cooking? (e.g. travelling to obtain fuel supplies)
 - i. 4 GHS.

Date 5/10/14
Interviewer Divine

Figure E.2, Questionnaire sample of the Ghana survey

①

Sustainable Production of Hydrogen Gas as Fuel for Domestic Cooking Data
collection Questionnaire for Ghana

Identification – Town and Household ID Keda-K1
Interviewee Name: Chashe Age 62 Gender F Occupation trader
Educational attainment None

Questions

1. What types of fuel do you use for cooking in your household?
 - i. Charcoal
 - ii. Fire wood
 - iii. LPG
 - iv. Others
2. Which of the listed fuel types do you use most and why?
 - i. Charcoal
 - ii. Reasons Less smoke
3. What types of cooking devices do you use in your household?
 - i. Charcoal pot
 - ii. Gas burner
 - iii. Local stove
 - iv. Others

Charcoal large No 4 bag.
weight = 50kg.
Cost = 65 GHS
Duration = 1.5 months
4. In which part of the house does the household do its cooking?
 - i. Kitchen
 - ii. Backyard
 - iii. Veranta
 - iv. Else..

Firewood 1 tie.
weight = 18kg
Cost = 5 GHS.
Duration = 1.5 days.
5. State the cooking fuel consumed per cooking (kg).
 - i. Morning (4am-9am)
 - ii. Afternoon (11am – 2pm)
 - iii. Evening (5pm – 9pm)
6. Total fuel used per month (kg)
7. What is the cost of the cooking fuel? (per week or per month, as is more suitable)
8. What is the income level of your household? 500 GHS
9. What is the percentage of household income used on cooking fuel?
10. What is the breakdown of occupancy of your household?
 - i. Children (0 – 18yrs) 9
 - ii. Adult (18 - 60yrs) 2
 - iii. Elderly (60+) 1
11. Do you have Electricity in your house? Yes No
12. If yes do you use it for cooking? Yes No
13. Do you have solar energy in use in your house? Yes No
14. Would you be willing to change to a new clean energy source for cooking and a better cooking stove? Yes No
15. Give reasons for your answer in question 14 (respiratory problems caused by current cooking system..)
 - i. If it is safe I will try it
 - ii.
 - iii.
16. Are there any extra costs related to the energy needs for cooking? (e.g. travelling to obtain fuel supplies)
 - i. 6 GHS

Date 25/09/14
Interviewer Diana

Figure E.3, Questionnaire sample of the Ghana survey

GH

Sustainable Production of Hydrogen Gas as Fuel for Domestic Cooking Data

collection Questionnaire for Ghana

Identification – Town and Household ID Kedua - K64
 Interviewee Name: Emily Age 39 Gender F Occupation Clerk
 Educational attainment Diploma

Questions

1. What types of fuel do you use for cooking in your household?
 - i. Charcoal
 - ii. Fire wood
 - iii. LPG
 - iv. Others
2. Which of the listed fuel types do you use most and why?
 - i. LPG
 - ii. Reasons Fast and neat
3. What types of cooking devices do you use in your household?
 - i. Charcoal pot
 - ii. Gas burner
 - iii. Local stove
 - iv. Others.....

LPG. Large.
Duration → 2.5 months
4. In which part of the house does the household do its cooking?
 - i. Kitchen
 - ii. Backyard
 - iii. Veranda
 - iv. Else..
5. State the cooking fuel consumed per cooking (kg).
 - i. Morning (4am-9am)
 - ii. Afternoon (11am – 2pm)
 - iii. Evening (5pm – 9pm)
6. Total fuel used per month (kg)
 - i.
7. What is the cost of the cooking fuel? (per week or per month, as is more suitable)
8. What is the income level of your household? 700GHS
9. What is the percentage of household income used on cooking fuel?
10. What is the breakdown of occupancy of your household?
 - i. Children (0 – 18yrs) 2
 - ii. Adult (18 - 60yrs) 2
 - iii. Elderly (60+) X
11. Do you have Electricity in your house? Yes No
12. If yes do you use it for cooking? Yes No
13. Do you have solar energy in use in your house? Yes No
14. Would you be willing to change to a new clean energy source for cooking and a better cooking stove?
 Yes No
15. Give reasons for your answer in question 14 (respiratory problems caused by current cooking system..)
 - i. If it is cheaper.
 - ii.
 - iii.
16. Are there any extra costs related to the energy needs for cooking? (e.g. travelling to obtain fuel supplies)
 - i. 4 GH

Date 29/9/14
 Interviewer Diana/Eric

Figure E.4, Questionnaire sample of the Ghana survey

①

Sustainable Production of Hydrogen Gas as Fuel for Domestic Cooking Data
collection Questionnaire for Ghana

Identification – Town and Household ID Soga G1
Interviewee Name: Christiana Age 52 Gender F Occupation trader
Educational attainment Middle Sch. Leaver

Questions

1. What types of fuel do you use for cooking in your household?
 - i. Charcoal
 - ii. Fire wood ✓
 - iii. LPG
 - iv. Others
2. Which of the listed fuel types do you use most and why?
 - i.
 - ii. Reasons
3. What types of cooking devices do you use in your household?
 - i. Charcoal pot
 - ii. Gas burner
 - iii. Local stove ✓
 - iv. Others.....
4. In which part of the house does the household do its cooking?
 - i. Kitchen
 - ii. Backyard ✓
 - iii. Veranta
 - iv. Else..

*1 tie of firewood = 18kg
cost = 5GHS
Duration - 5 days
Per day - 18/5 = 3.6kg.
∴ Per month - 3.6 x 31 days
= 111.6kg.*
5. State the cooking fuel consumed per cooking (kg).
 - 20% i. Morning (4am-9am) ✓ 0.72kg
 - 40% ii. Afternoon (11am - 2pm) ✓ 1.44kg
 - 40% iii. Evening (5pm - 9pm) ✓ 1.44kg

*Cost = 5GHS/5 = 1GHS Per day
∴ 1 month = 31 GHS.*
6. Total fuel used per month (kg)
 - i. 111.6kg
7. What is the cost of the cooking fuel? (per week or per month, as is more suitable) 31+4 = 35GHS
8. What is the income level of your household? 420 GHS
9. What is the percentage of household income used on cooking fuel? 8.3%
10. What is the breakdown of occupancy of your household?
 - i. Children (0 - 18yrs) 2
 - ii. Adult (18 - 60yrs) 3
 - iii. Elderly (60+) 1
11. Do you have Electricity in your house? Yes No
12. If yes do you use it for cooking? Yes No
13. Do you have solar energy in use in your house? Yes No
14. Would you be willing to change to a new clean energy source for cooking and a better cooking stove? Yes No
15. Give reasons for your answer in question 14 (respiratory problems caused by current cooking system..).
 - i. New technology, I want to try it and see
 - ii. its performance.
 - iii.
16. Are there any extra costs related to the energy needs for cooking? (e.g. travelling to obtain fuel supplies)
 - i. 4GHS 4GHS

Date 30/9/14
Interviewer Divine

Figure E.5, Questionnaire sample of the Ghana survey

Sustainable Production of Hydrogen Gas as Fuel for Domestic Cooking Data
collection Questionnaire for Ghana

Identification – Town and Household ID Soja G. 38
Interviewee Name: Happy Age 40 Gender F Occupation Trader/Famer
Educational attainment: Middle sch.

Questions

1. What types of fuel do you use for cooking in your household?
 - i. Charcoal
 - ii. Fire wood
 - iii. LPG
 - iv. Others
2. Which of the listed fuel types do you use most and why?
 - i. Firewood
 - ii. Reasons I am used to it
3. What types of cooking devices do you use in your household?
 - i. Charcoal pot
 - ii. Gas burner
 - iii. Local stove
 - iv. Others..... Firewood, 1 fire, can 5 gas weight = 18 kg,
4. In which part of the house does the household do its cooking?
 - i. Kitchen
 - ii. Backyard
 - iii. Veranda
 - iv. Else.. Duration = 4 days.
5. State the cooking fuel consumed per cooking (kg).
 - i. Morning (4am-9am)
 - ii. Afternoon (11am – 2pm)
 - iii. Evening (5pm – 9pm)
6. Total fuel used per month (kg)
 - i.
7. What is the cost of the cooking fuel? (per week or per month, as is more suitable)
8. What is the income level of your household? 290 GH\$
9. What is the percentage of household income used on cooking fuel?
10. What is the breakdown of occupancy of your household?
 - i. Children (0 – 18yrs) 2
 - ii. Adult (18 - 60yrs) 2
 - iii. Elderly (60+) X
11. Do you have Electricity in your house? Yes No
12. If yes do you use it for cooking? Yes No
13. Do you have solar energy in use in your house? Yes No
14. Would you be willing to change to a new clean energy source for cooking and a better cooking stove? Yes No
15. Give reasons for your answer in question 14 (respiratory problems caused by current cooking system..)
 - i. I want to try the new gas provided
 - ii. it is safe.
 - iii.
16. Are there any extra costs related to the energy needs for cooking? (e.g. travelling to obtain fuel supplies)
 - i. Delivered.

Date 10/10/14
Interviewer Divine/Thery.

Figure E.6, Questionnaire sample of the Ghana survey

E.1 Additional Information of the Field Study

Household area where cooking takes place

Figure E.7 shows that the place of the house where cooking takes place varies according to the main fuel used. The majority of the people that use charcoal as their main cooking fuel perform their cooking both in the kitchen and external spaces of the household. The users of firewood as their main cooking fuel cook mainly in external spaces, and finally the users of LPG as their main fuel cook almost particularly in the kitchen, see Table E.1.

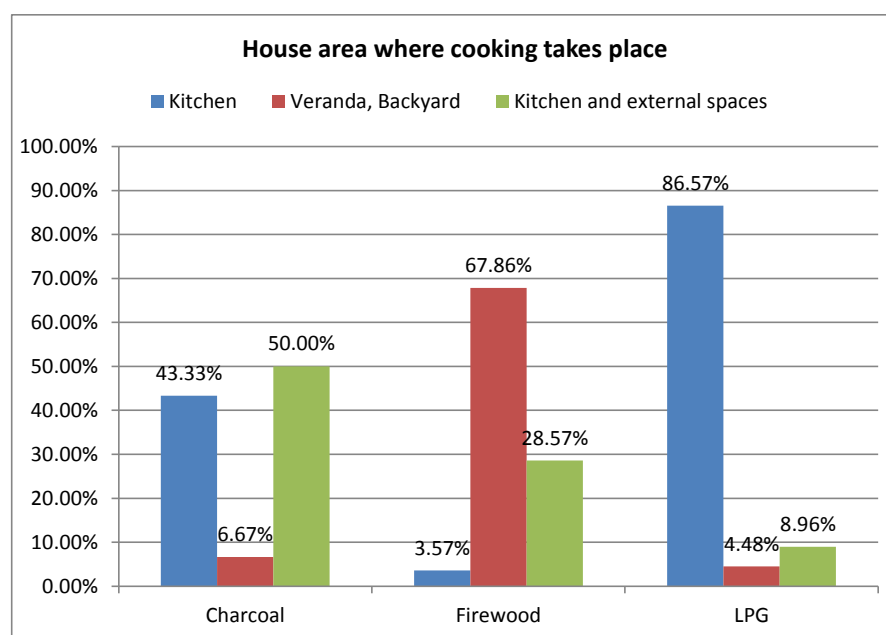


Figure E.7, Household area where cooking takes place in relation to the used main fuel

Table E.1, Household area where cooking takes place in relation to the used main fuel

Row Labels	Kitchen	Veranda, Backyard	Kitchen & external
Charcoal	43.33%	6.67%	50.00%
Firewood	3.57%	67.86%	28.57%
LPG	86.57%	4.48%	8.96%

This is explained by the fact that cooking with solid fuels produces particles, smoke and dirt and open spaces, outdoor cooking is preferred.

Daily Profile of the Cooking Demand

The cooking periods were separated according to the cooking habits of the local population. They were thus defined as:

- Morning (4.00am-9.00am)
- Afternoon (11.00am-2.00pm)
- Evening (5.00pm-9.00pm)

The field data shows that 72.26% of the population cooks throughout the day, during all three cooking periods. 27.10% cooks during morning and afternoon and only 0.65% cooks only in the afternoon, see Figure E.8. Detailed information about the quantity of the fuel used during each cooking time were given only by a small percentage of the participants that indicate that 20% of the daily fuel is used for morning cooking, 40% for afternoon cooking and 40% for evening cooking, in the case that cooking is done throughout the day.

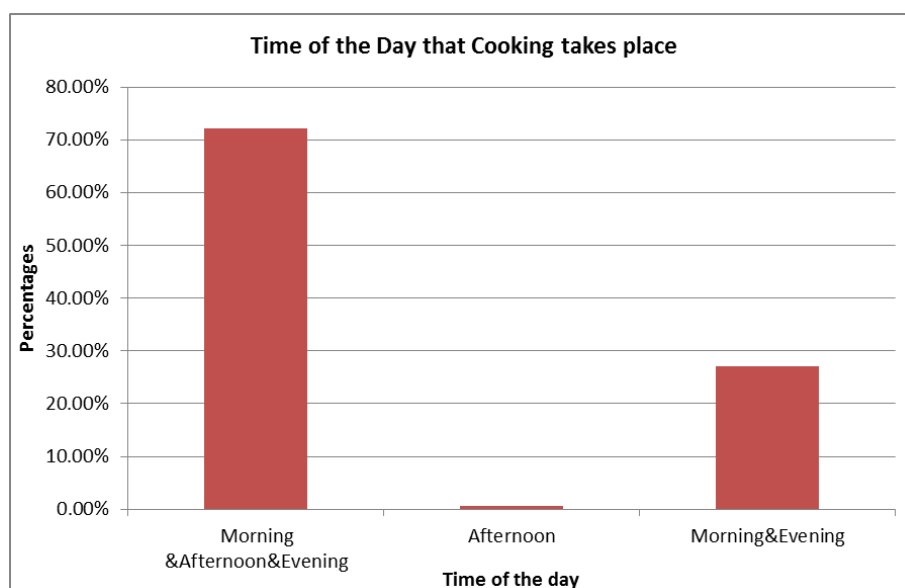


Figure E.8, Time of the day that cooking takes place

Figure E.9 shows the relation between periods of the day that cooking takes place in relation to the main cooking fuel and Figure E.10 deals with the periods of the day that cooking takes place according to the profession.

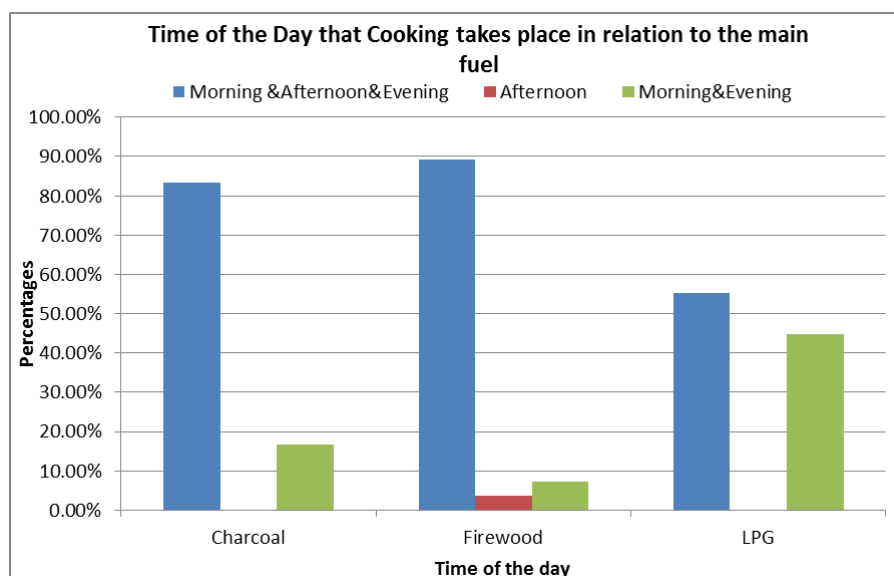


Figure E.9, Time of the day that cooking takes place in relation to the main cooking fuel

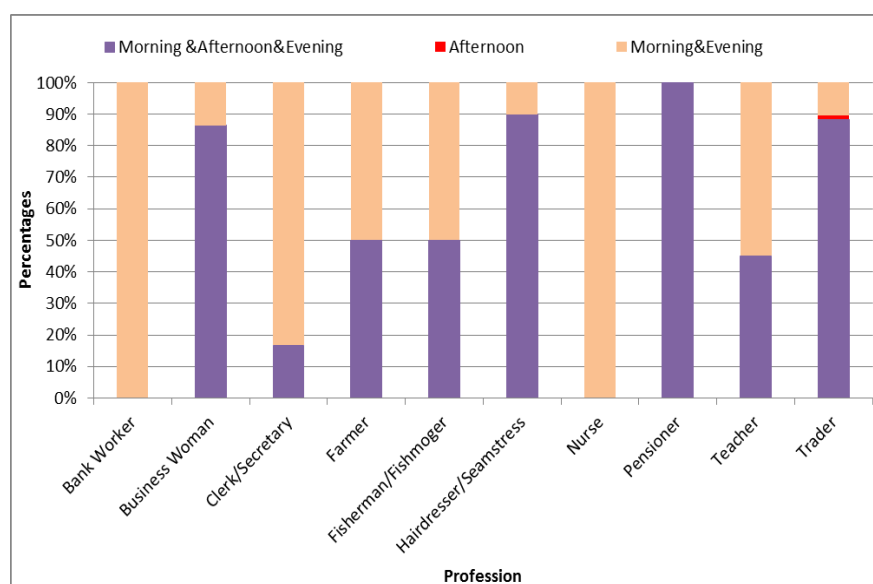


Figure E.10, Time of the day that cooking takes place according to the profession

Bank workers and nurses are the only professions that exclusively cook only in the morning and evening, when all the other professions have a share in afternoon cooking too. It can thus be concluded that the cooking requirements are spread throughout the whole day.

Electricity and Solar Energy Use

Additional socio- economic and energy use data are included in the field study. In this sector, conclusions regarding the use of electricity, solar energy are demonstrated.

Of the total 155 participants, 153 have electricity in their houses, and only 2 do not have. Both come from Keta and use Charcoal as their main cooking fuel and firewood as the additional. None of the participants use electricity for cooking purposes.

Only 2 participants use solar energy in their houses, and again this is not for cooking purposes. Solar lanterns are used by both households, and these are probably through the promotion of this technology from the program (Government of Ghana, 2013) . Both participants work as teachers and have higher education and degrees.

Size of the Fuel Purchase Units

The three cooking fuels of this study come in specific storage units and sizes. LPG is stored in cylinders that according to their size and weight are classified as:

- Small cylinder, 6kg
- Medium cylinder, 13kg
- Large cylinder, 15kg

Charcoal is purchased in bags that according to their size are classified as:

- Mini bag, 10kg
- Medium bag, 20kg
- Large bag (“No. 4 bag”, as called by the locals), 50kg

Firewood is sold in ties, of 18kg each.

Figures E.11 to E.13 show the distribution of the sizes of LPG cylinders, charcoal bags and firewood ties that are purchased by the participants. In the case of LPG, it is shown that the large cylinder (15kg) is preferred by 64.63% of the people who use LPG, followed by 29.27% that prefer medium LPG cylinders (13kg). Small cylinders (6kg) are selected only by 6.1% of the participants. 50% of the people who use charcoal prefer large size bags (50kg), and 44.12% choose the medium size bags of 20kg. Mini charcoal bags are selected only by 5.88% of the charcoal users. Finally, 90% of the firewood users purchase firewood in single ties, and the rest 10% purchase them in double and triple ties.

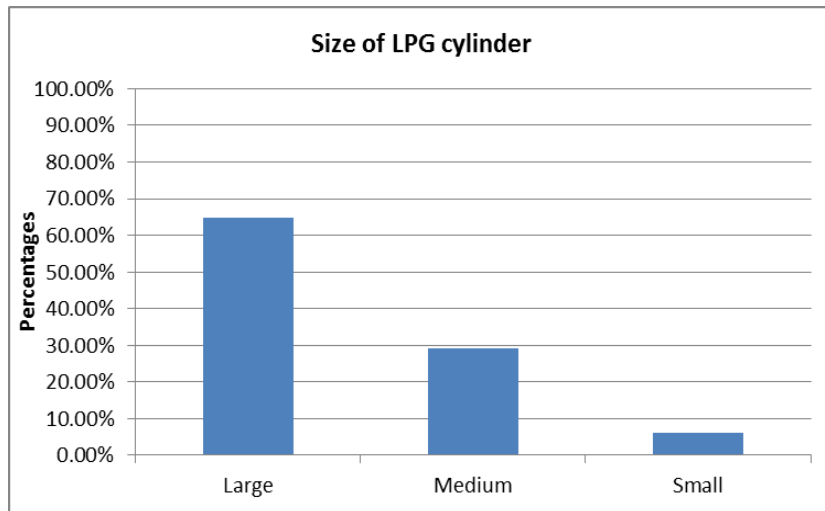


Figure E.11 , Percentage of LPG cylinders' sizes preferred by the participants

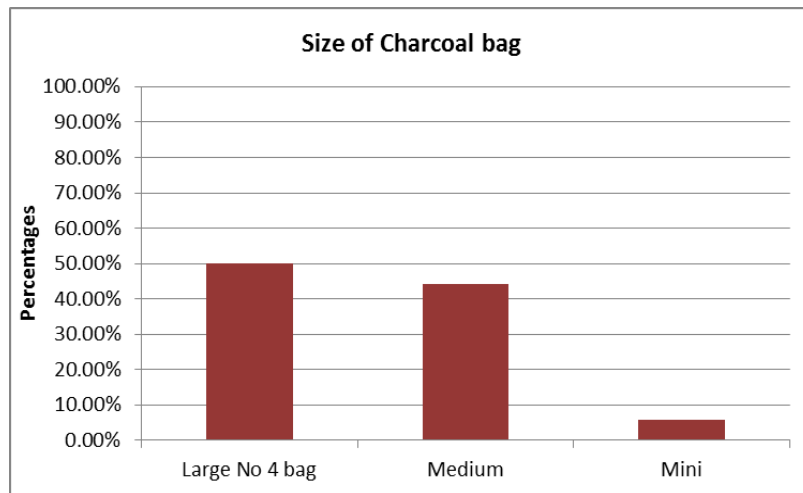


Figure E.12, Percentage of charcoal bags' sizes preferred by the participants

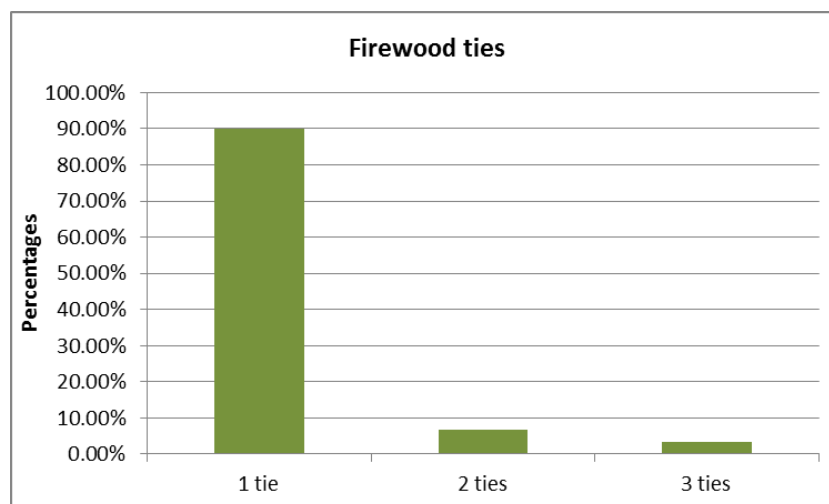


Figure E.13, Percentage of firewood ties number preferred by the participants

Appendix F. Jamaica and Indonesia Case Studies Jamaica Case Study

This appendix presents the case studies model development and graphic results simulation for the Ghana, Jamaica and Indonesia case studies, for the direct connection and the battery systems.

F.1 Ghana Battery Case Study

An optimised option in terms of operation of the case study system is to include a battery, as shown in Figure F.1. This will reduce the need of the oversized PV array. A 220kWh lead-acid storage battery bank is used and a 54kW photovoltaic array. In this case the size of the photovoltaic array is 30% reduced compared to the direct connection (section 7.3.1). The battery has a charging efficiency of 90% and is simulated by the type 47a TRNSYS component (University of Wisconsin - Madison, 2012). The electrolyser and the metal hydride storage component is the same as in the direct connection case study. Weather processor type and input data are also the same.

As before, the 20 year performance degradation period of the photovoltaic array is taken into consideration with 50.5kW predicted power of the 20th year. For the battery case study a different strategy is followed, as the load power is essential to be a known input parameter to the battery. The battery input has to be specified and this is done by inputting the electrolyser power demand. Therefore, the electrolyser is set to operate for specific hours during each day so that the total production satisfies the demand. The electrolyser is set to operate for 7 hours, (10.00 to 17.00) and the system is sized so that it will be able to provide the energy for the electrolyser to operate these 7 hours every day. In TRNSYS when the battery connection is implemented, the supply of the system comes both from the battery and the grid by default. In the case of the solar powered electrolysis system, the hours that the system operates under grid supply are not taken into consideration. This strategy is again followed for cost efficiency purposes, as it is more preferable to have small time periods that the electrolysers do not operate, but the demand is still satisfied, than oversizing the PV battery system.

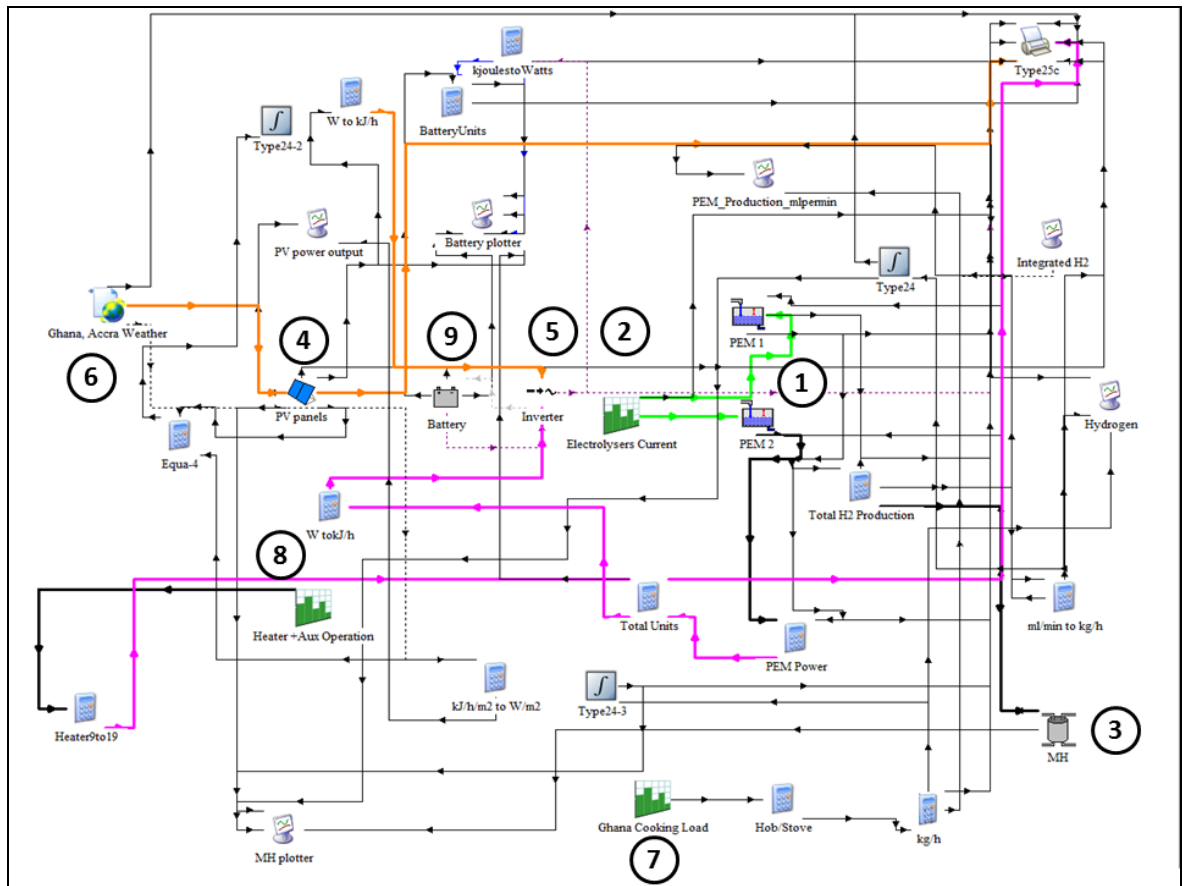


Figure F.1, Ghana battery case study TRNSYS print screen

The model's main parts consist of the PV array (4) that supplies the PEM electrolyser (1) through an inverter (5), the electrolyser auxiliary components (controls (2), and gas management parts (8)), and the metal hydride storage components (3). It also includes the necessary weather data (6) for the simulation, the cooking load profile for the application (7), the battery (9) and other computational components.

Figure F.2 shows the simulation results of the PV- battery case study for the month of May. During periods where the PV array generates excess energy that covers the electrolyser demand, this excess energy is stored in the battery, and this is observed by the battery energy flow that is positive. At moments where the PV power drops, during evening hours or low irradiance times, the energy stored in the battery is used to supply the electrolyser, and the battery energy flow is negative. The lower graph compares the monthly accumulated cooking demand of the community which is indicated with blue and the hydrogen that is generated for distribution to the households and is indicated with purple.

Figure F.3 shows the monthly demand and production of hydrogen and PV yield for the current conditions and after the panel degradation period for the battery case study. The monthly demand remains the same, but the PV yield is now smaller than the no-battery case study, as the battery offers storage and management of the excess PV energy. Furthermore, the hydrogen generation follows a more uniform profile during all months than for the direct connection case. The designed system provides with 800kg of hydrogen at current conditions, over satisfying the demand by 15kg and 783.4kg of hydrogen after the 20 year period. Table F.1 shows the generation rates of the system and also the performance degradation rates on the PV array output.

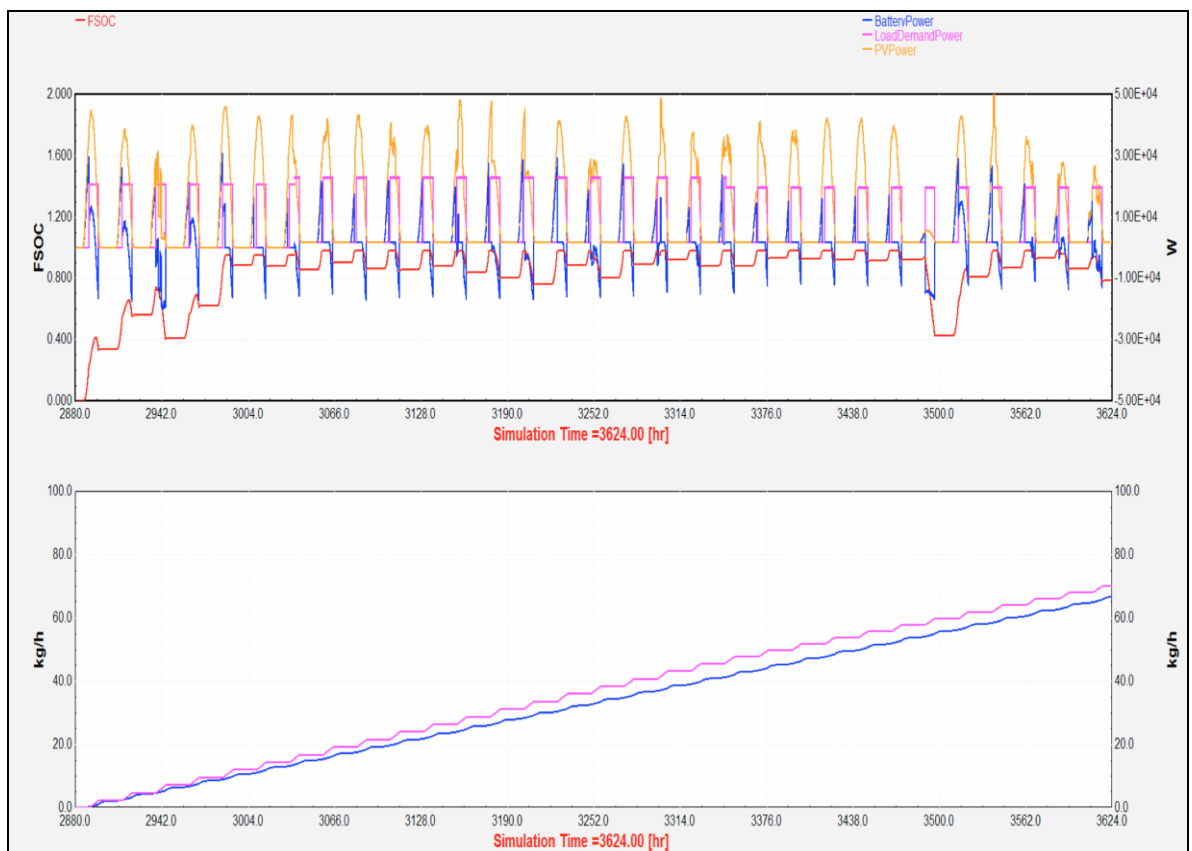


Figure F.2, TRNSYS simulation results for the Ghana battery case study for the month of May

In the upper graph, PV power output is indicated with orange colour, electrolyser power input with purple and battery power flow with blue. The red line shows the fractional state of charge (between 0-1) of the battery.

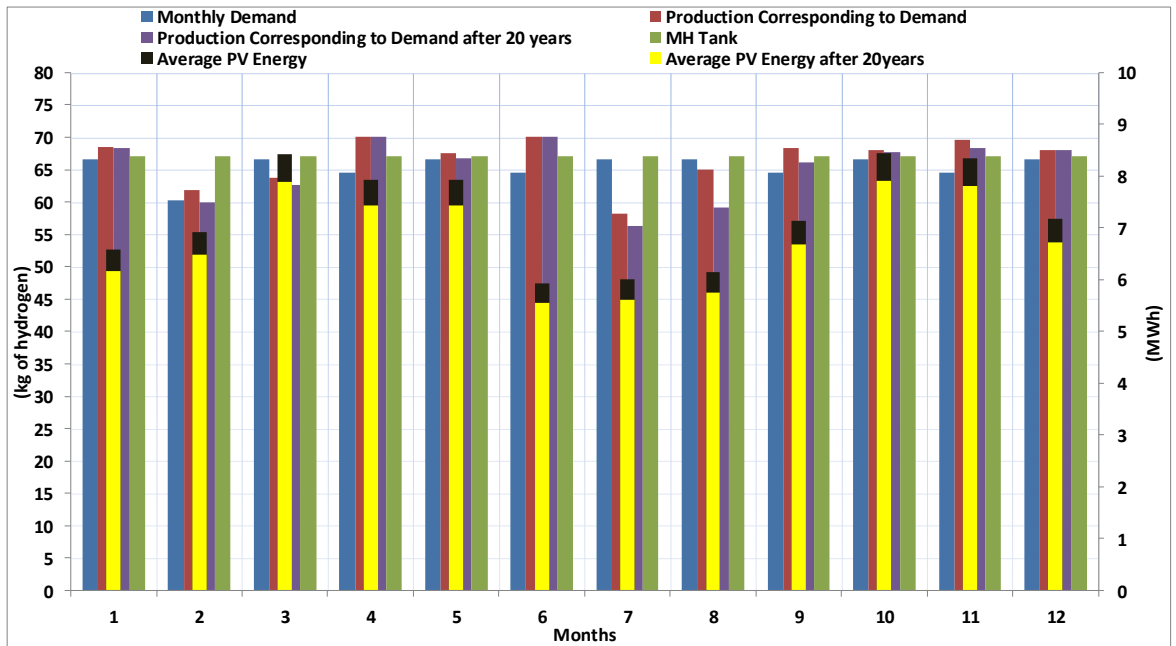


Figure F.3, Monthly demand and production of hydrogen and PV yield for the current conditions and after the panel degradation period for the Ghana battery case study

Table F.1, Ghana battery case study hydrogen production and PV yield at current and future conditions

Annual Hydrogen Demand (kg)	785
Annual Hydrogen Production (kg) at current conditions	800
Annual Hydrogen Production (kg) at the end of 20 years	783.4
Monthly Average PV Energy (MWh) at current conditions	7.25
Monthly Average PV Energy (MWh) at the end of 20 years	6.79

F.2 Jamaica Case Studies

Direct Connection of PV array and Electrolysers

From statistical data, the cooking demand for a typical Jamaican household was estimated as 1.98kWh/day, (The Planning Institute of Jamaica & The Statistical Institute of Jamaica, 2007). With hydrogen stove efficiency of 60%, this is equivalent to 3.3kWh/day of hydrogen or 0.0842kg of hydrogen per day, according to Equation (F.1):

$$\frac{3.3(\frac{kWh}{day})}{141.1(\frac{MJ}{kg})} = \frac{3.3(\frac{kWh}{day})}{39.19(\frac{kWh}{kg})} = 0.0842(\frac{kg}{day}) \quad (F.1)$$

$$3.6(\frac{MJ}{kWh})$$

Therefore, for the 20 households 1.68kg of hydrogen per day is necessary, and depending on the days of each month, the monthly demand can be seen in Table F.2, as derived from the TRNSYS monthly calculations.

Table F.2, monthly and annual demand in kg of hydrogen for the Ghanaian case study

Month	Monthly Cooking Demand of 20 households (kg/month)
January	52.8
February	47.7
March	52.8
April	51.1
May	52.8
June	51.1
July	52.8
August	52.8
September	51.1
October	52.8
November	51.1
December	52.8
Total Annual	52.8

The TRNSYS model of the Jamaica direct connection case study is shown in Figure F.4. The component types used in the Jamaica case studies are the same ones that were described in the Ghana case studies, in sections 7.3.1 of the thesis.

PV array

For the system sizing, again the 20 year performance degradation of the photovoltaic panels is taken into consideration. As discussed in the Ghana case study the power output at the end of the 20th year will be 93.04% of the original rated power. This means that in order to ensure that the photovoltaic array output will be enough to satisfy the demand after 20 years the array should be oversized by 6.96% of the current size that satisfies the demand. Therefore, a 63kW array is examined for the Jamaica case study, which after 20 years will reach the level of 58.9kW and will still be enough to satisfy the annual cooking needs, as seen in Table F.3. The photovoltaic panels array consists of 350 panels, of a total area of 440m².

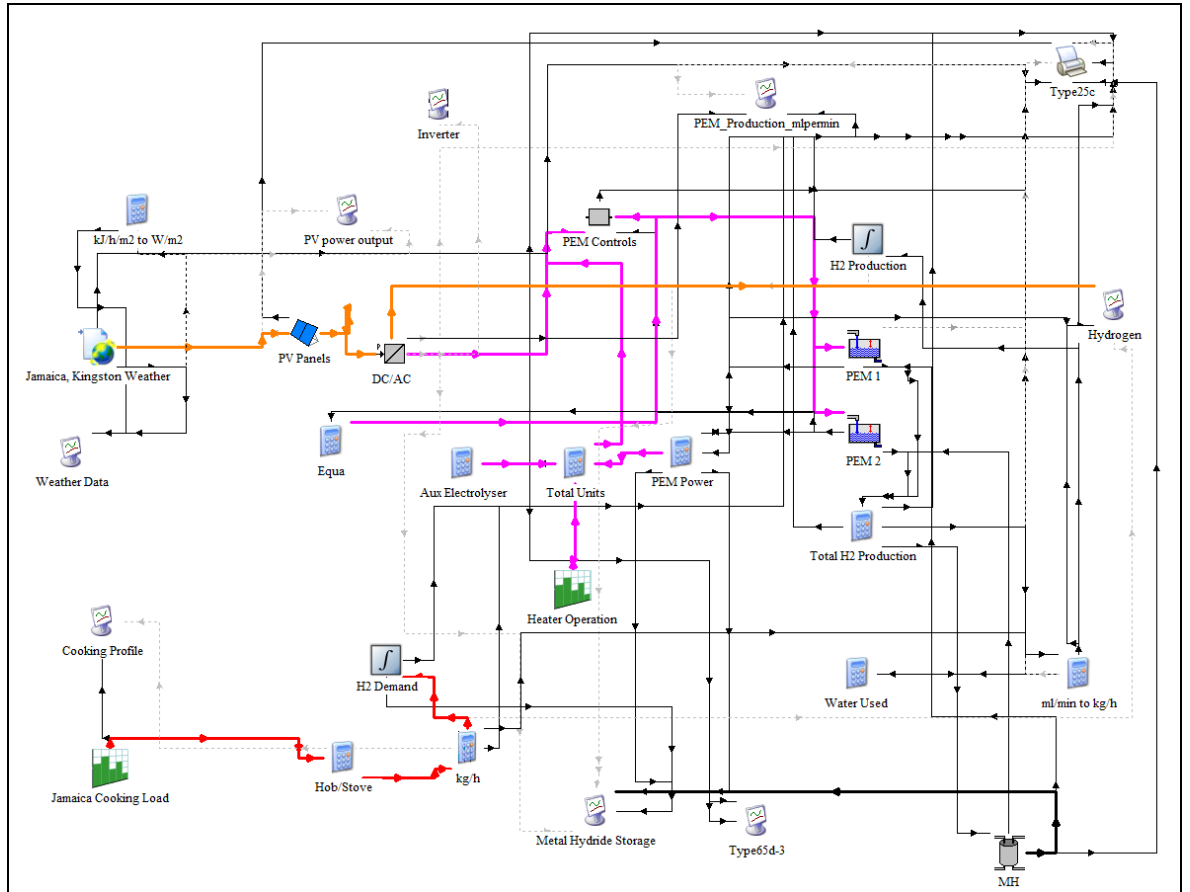


Figure F.4, Jamaica direct connection case study TRNSYS print screen

Metal Hydride Storage

For the metal hydride storage, one storage tank corresponds to each household per month which would be replaced with a full one for the following month. Therefore, the tank size should be able to cover the demand of every month. It is selected to be 53kg for 20 houses or 2.65kg for each house.

The amount of the metal hydride alloy of each tank is calculated according to the hydrogen absorption ability of the selected alloy. In this case LaNi_5 is chosen, as it is the metallic alloy of the experimental part. The hydrogen absorption ability of LaNi_5 is 150ml/gr, therefore for each household Equation (F.2) gives the quantity of the alloy necessary in each tank:

$$LaNi_5 \text{ _content} = \frac{2.65(kg)}{150\left(\frac{ml}{gr}\right) \times 10^{-6} \left(\frac{Nm^3}{ml}\right) \times 0.0899\left(\frac{kg}{Nm^3}\right)} = 196.5kg \quad (F.2)$$

The electrolyser is connected directly to the metal hydride storage, and the hydrogen is stored and distributed to the households at the generated pressure, which is maximum 13.8bar.

PEM Electrolysers

Two electrolysers are selected for the Jamaica case study, based on the developed PEM numerical model presented in Chapter 5. The parameters of each one are shown in Table 7.3.

Weather data

The weather data used in the simulation for the Jamaica case study is composite TMY data from Meteonorm 7.0 database from the weather station in Kingston (Norman Manley/Kings, id: 5997,WMO id: 783970) , (Meteotest, 2014). This weather station does not include radiation recording but the irradiance data comes from GOES satellite measurements of the years 2010 - 2013 with a resolution of 8km on the horizontal, adopted to regional stations (Cuba, Puerto Rico and Central America) for the period 1971-1990 (Meteonorm Version 7, 2014). For all other parameters, the data refers to the period 2000 – 2009. The weather processor is simulated by type 15-6 component for Meteonorm files weather data processor, from the standard weather data processors library of TRNSYS (University of Wisconsin - Madison, 2014). The annual global horizontal irradiance and temperature values are shown in Figure F.5. Monthly mean global horizontal irradiance values in Jamaica vary slightly during the year but present the highest values during the period April to August, remain in very high levels during March and September and have lower values during the rest of the year, October to February (GAISMA, 2014) . Temperatures follow a similar profile and are rather constant throughout the year, with an average of 25°C to 30°C in the lowlands and 15°C to 22°C at higher elevations. In Jamaica there are two types of climates that are defined by the geographic separation of the island from its mountains (the Blue Mountains, and the John Crow Mountains). The windward side of the mountains is characterized by an upland tropical climate, whereas a semiarid climate prevails on the leeward side. Warm eastern and north-eastern winds bring rainfall throughout the year. The rain period is from May to October, with the highest rainfall rates in those two months. The average rainfall is 196 cm/year. Rainfall is much greater in the mountain areas facing the north and east. In the high elevation areas of the John Crow Mountains and the Blue Mountains, rainfall exceeds

508cm per year. The south-western half of the island lies in the rain shadow of the mountains.

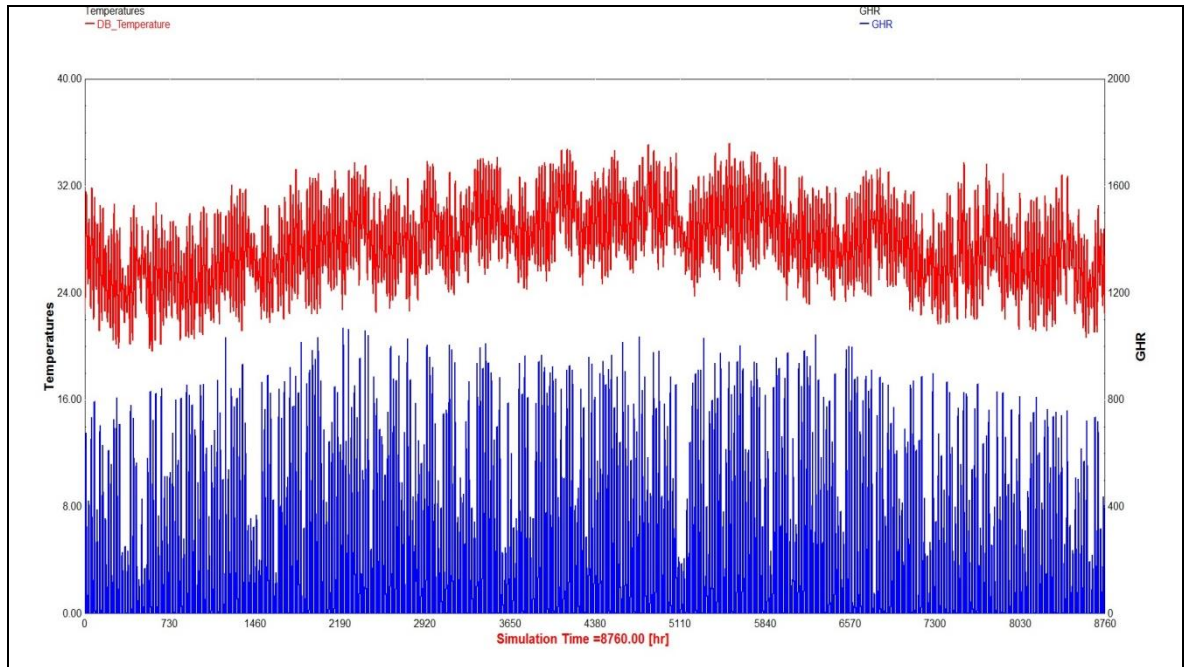


Figure F.5, Jamaica annual global horizontal irradiance and temperature values from Meteornorm file

Inverter Characteristics

In this case study the inverter has size of 63kW maximum power, based again on market parameters and real technology sizes (SMA Solar Technology AG, 2013). The TRNSYS component used is the 48.b type (University of Wisconsin - Madison, 2014).

System Operation

Figure F.6 shows the TRNSYS simulations results, for the month of April of the Meteornorm Typical Weather Year as an indicative month of the annual simulation. The April simulation results are compared to May, in Figure F.7. The total produced hydrogen amount of April is 61.3kg and this satisfies the May demand that is 52.8kg. The results of the simulation are in accordance to the numerical model, and when the metal hydride tank reaches the peak point of the charging phase (as explained in Chapter 5, section 5.2.1) the charging flow rate from the electrolyser and thus the power demand is reduced. This is observed at 2600hs in Figure F.6.

Figure F.8 shows the monthly hydrogen demand and equivalent production in kg for the current conditions and after the 20 year period. The production, of the preceding month has to satisfy the demand of the following month, as the purpose is to supply the consumers on a monthly basis. The system is designed so that the extra hydrogen production acts supplementary for the months there is shortage, and a regulated operation and fuel supply is guaranteed for current and future scenarios. There are eight months in the year where the production is over satisfying the demand. This extra hydrogen acts as a balance in the months where production is less. The designed system provides with 653kg of hydrogen at current conditions, and 620kg of hydrogen after the 20 year period. Table F.3 shows the generation rates of the system and also the performance degradation on the PV array output.

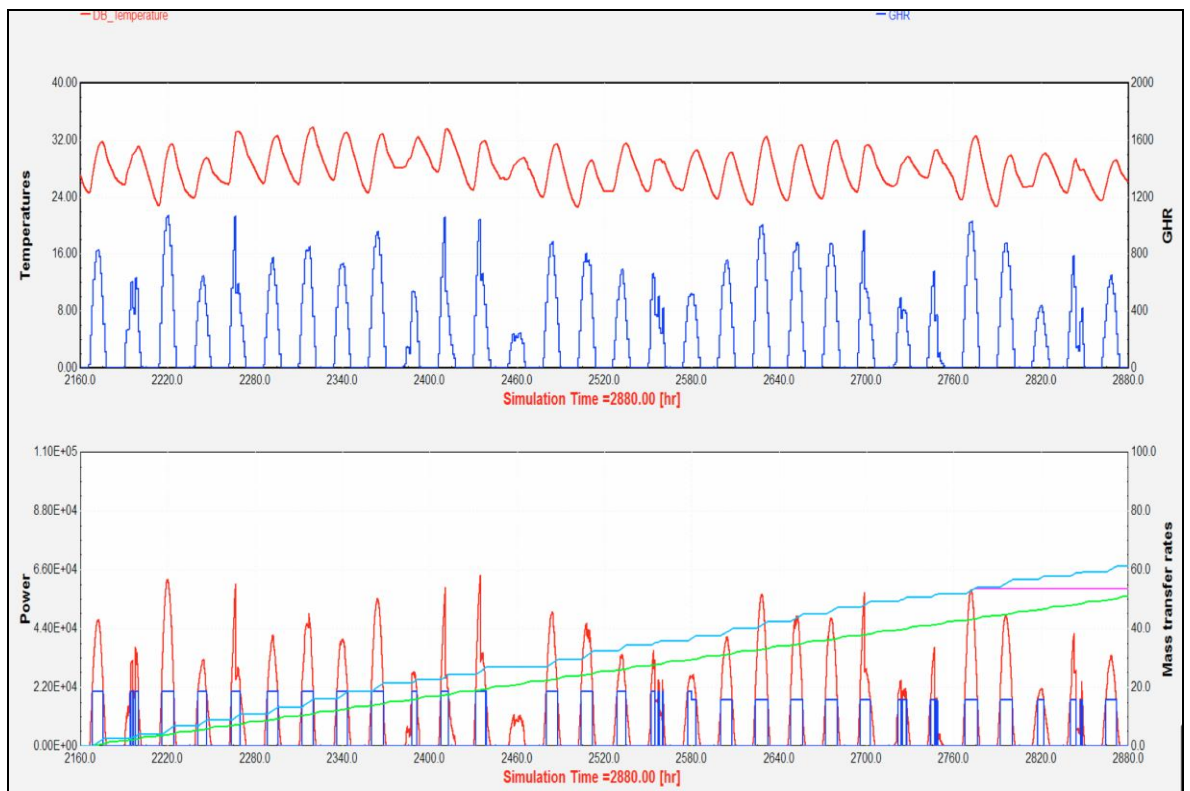


Figure F.6, TRNSYS simulation results for the Jamaica direct connection case study for the month of April

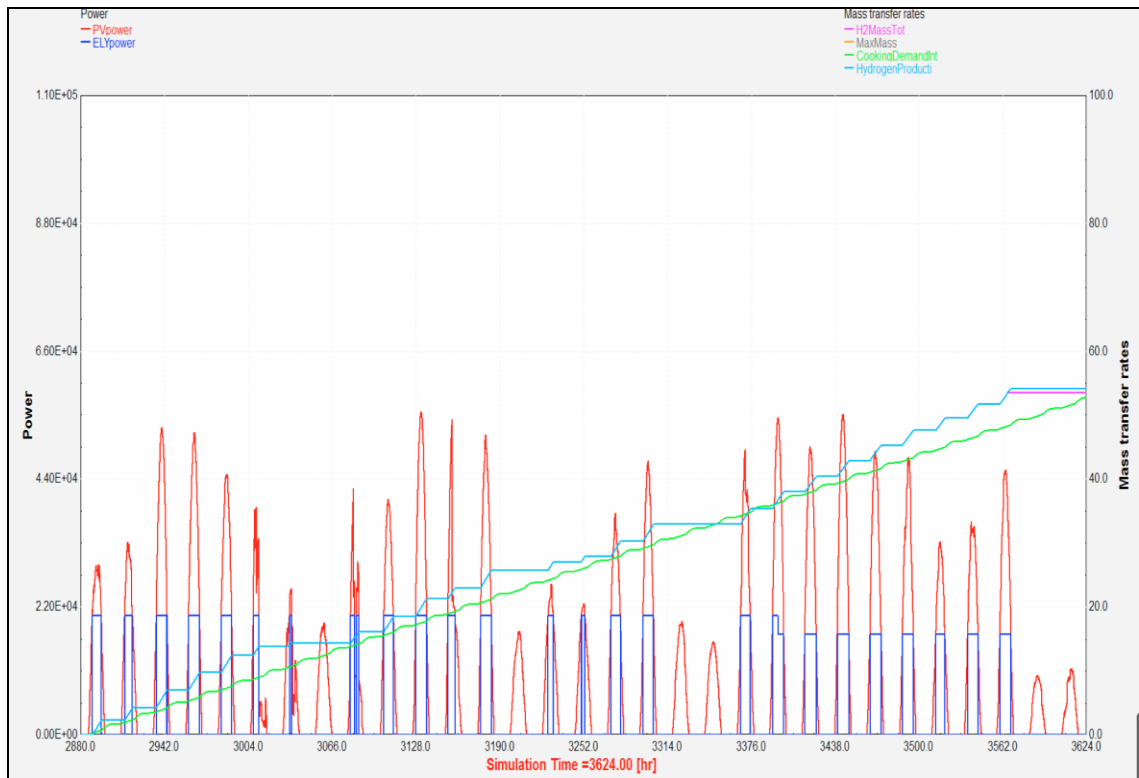


Figure F.7, TRNSYS simulation results for the Jamaica direct connection case study for the month of May

In the upper graph temperature (red) and global horizontal irradiance (blue) are presented. In the lower graph, the production of the PV array is indicated with red and the power to the electrolyser system with blue. The monthly accumulated cooking demand of the community is indicated with green and the hydrogen that is generated for distribution to the households is indicated with light blue. The purple line indicates the maximum amount that can be stored for distribution and until it reaches the maximum point it follows the light blue line.

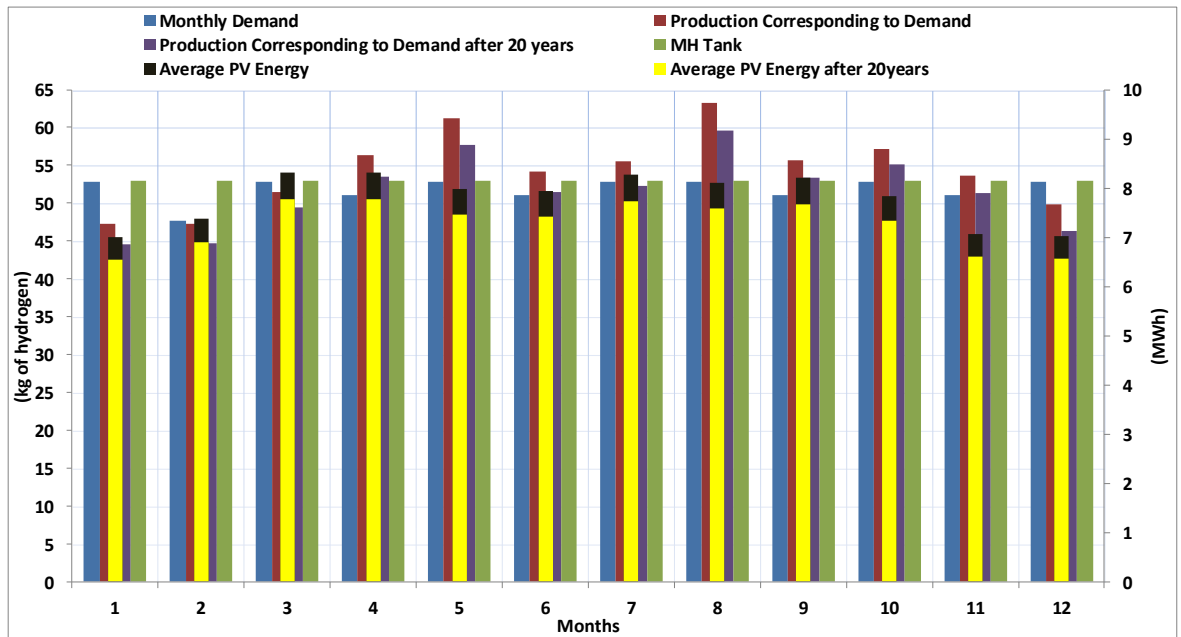


Figure F.8, Monthly demand and production of hydrogen and PV yield for the current conditions and after the panel degradation period for the Jamaica case study

Table F.3, Jamaica case study hydrogen production and PV yield at current and future conditions

Annual Hydrogen Demand (kg)	621.6
Annual Hydrogen Production (kg) at current conditions	653
Annual Hydrogen Production (kg) at the end of 20 years	620
Monthly Average PV Energy (MWh) at current conditions	7.8
Monthly Average PV Energy (MWh) at the end of 20 years	7.3

Battery Case

The TRNSYS model of the PV- battery case study for Jamaica can be seen in Figure F.9. A 150kWh lead-acid storage battery bank is used and a 50kW photovoltaic array for the case study where the electrolyzers are supplied through a battery system. In this case the size of the photovoltaic array is 21% reduced. The battery has a charging efficiency of 90% and is simulated by the type 47a TRNSYS component (University of Wisconsin - Madison, 2012). The electrolyzers and the metal hydride storage component is the same as

in the direct connection case study and have the same size too. Weather processor and input data are also the same.

The electrolyser power demand is inputted as the load demand of the battery and the electrolyser is set to operate for specific hours during each day so that the total production satisfies the cooking demand. The electrolyser is set to operate for 5.5 hours, (10.30 to 16.00) and the system is sized so that it will be able to provide the energy for the electrolyser to operate these 5.5 hours every day. The hours that the system operates under grid supply are not taken into consideration. This strategy is again followed for cost efficiency purposes, as it is more preferable to have small time periods that the electrolyzers do not operate, but the demand is still satisfied, than oversizing the PV battery system.

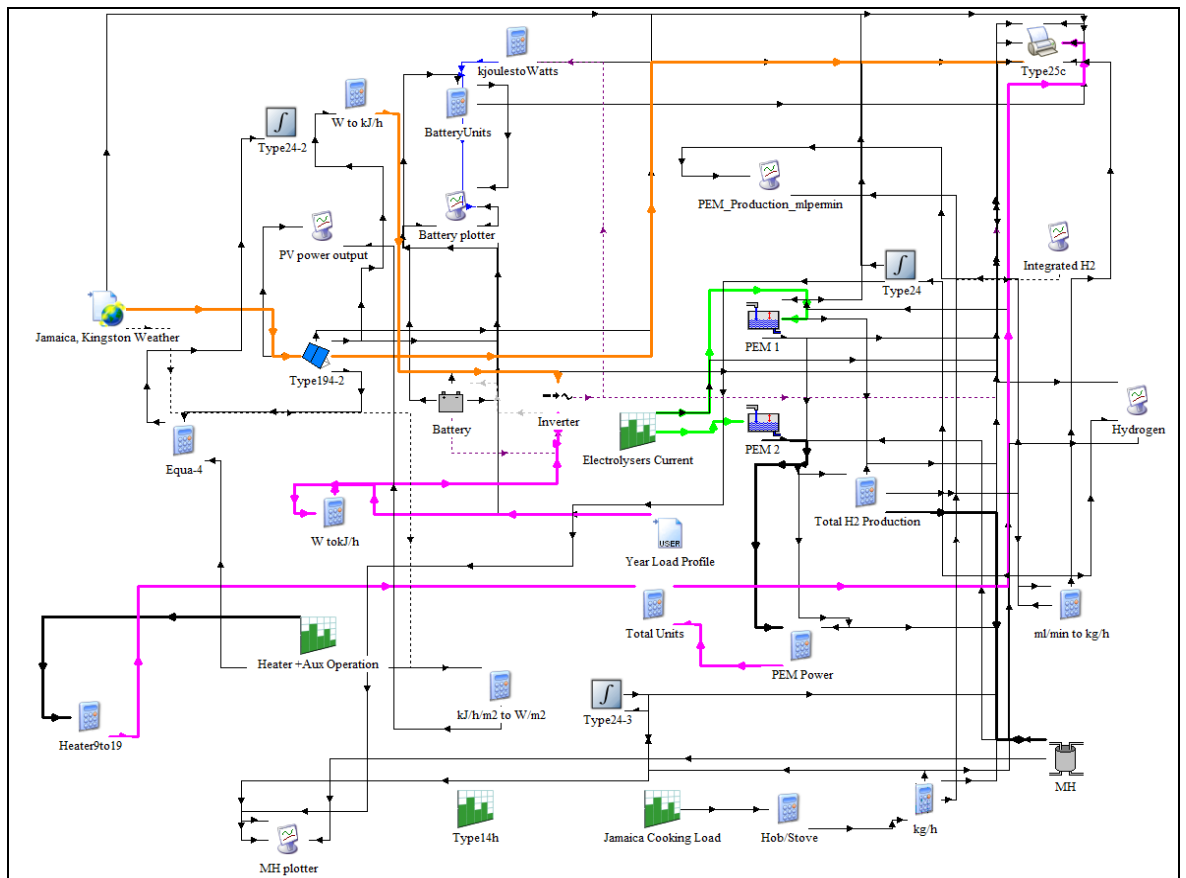


Figure F.9, Jamaica battery case study TRNSYS print screen

Figure F.10 shows the simulation results of the PV- battery case study for the month of April. In The April simulation results are compared to May, in Figure F.11. The total

produced hydrogen amount of April is 53.6kg and this satisfies the May demand that is 52.8kg.

Figure F.12 shows the monthly demand and production of hydrogen and PV yield for the current conditions and after the panel degradation period for the battery case study. The monthly demand remains the same, but the PV yield is now smaller than the no-battery case study, as the battery offers storage and management of the excess PV energy. The designed system provides with 627.6kg of hydrogen at current conditions, over satisfying the demand by 6kg and 621.2kg of hydrogen after the 20 year period. Table F.4 shows the generation rates of the system and also the performance degradation rates on the PV array output.

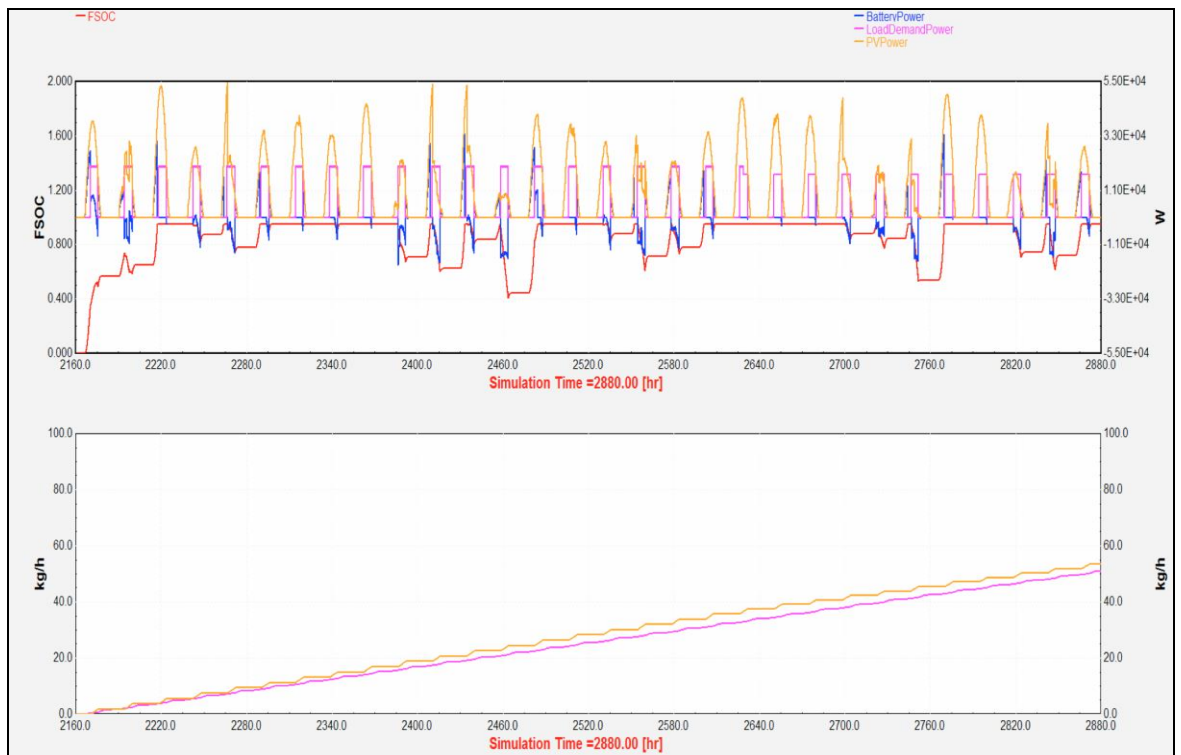


Figure F.10, TRNSYS simulation results for the Jamaica battery case study for the month of April

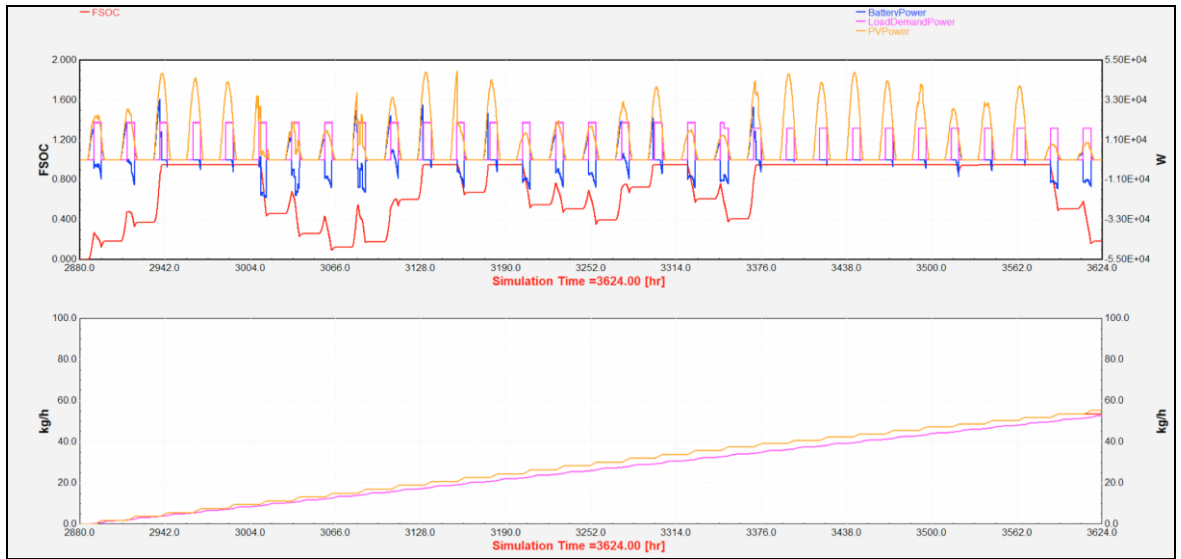


Figure F.11, TRNSYS simulation results for the Jamaica battery case study for the month of May

The upper graph, PV power output is indicated with orange colour, electrolyser power input with purple and battery power flow with blue. The red line shows the fractional state of charge (between 0-1) of the battery. The lower graph compares the monthly accumulated cooking demand of the community which is indicated with purple and the hydrogen that is generated for distribution to the households and is indicated with orange.

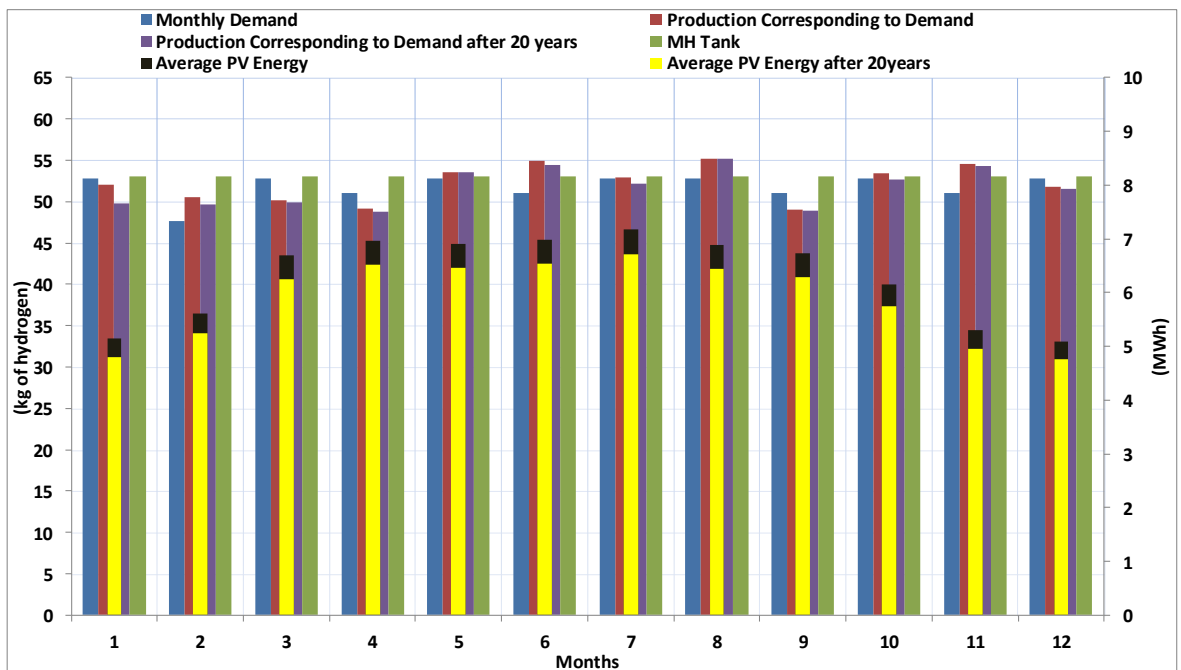


Figure F.12, Monthly demand and production of hydrogen and PV yield for the current conditions and after the panel degradation period for the Jamaica battery case study

Table F.4 Jamaica battery case study hydrogen production and PV yield at current and future conditions

Annual Hydrogen Demand (kg)	621.6
Annual Hydrogen Production (kg) at current conditions	627.6
Annual Hydrogen Production (kg) at the end of 20 years	621.2
Monthly Average PV Energy (MWh) at current conditions	6.3
Monthly Average PV Energy (MWh) at the end of 20 years	5.9

F.3 Indonesia Case Study

Direct Connection of PV array and Electrolysers

From statistical data, the cooking demand for a typical Indonesian household was estimated as 2kWh/day, (Pertamina, 2008). With hydrogen stove efficiency of 60%, this is equivalent to 3.34kWh/day of hydrogen or 0.085kg of hydrogen per day, according to Equation (F.3):

$$\frac{3.34\left(\frac{kWh}{day}\right)}{141.1\left(\frac{MJ}{kg}\right)} = \frac{3.34\left(\frac{kWh}{day}\right)}{39.19\left(\frac{kWh}{kg}\right)} = 0.085\left(\frac{kg}{day}\right) \quad (F.3)$$

$$3.6\left(\frac{MJ}{kWh}\right)$$

Therefore, for the 20 households 1.7kg of hydrogen per day is necessary, and depending on the days of each month, the monthly demand can be seen in Table F.5, as derived from the TRNSYS monthly calculations.

PV array

A 54kW array is examined for the Indonesia case study, which after 20 years will reach the level of 50.4kW and will still be enough to satisfy the annual cooking needs. The photovoltaic panels array consists of 300 panels, of a total area of 378m². The TRNSYS model of the Indonesia direct connection case study is shown in Figure F.13.

Table F.5, monthly and annual demand in kg of hydrogen for the Indonesian case study

Month	Monthly Cooking Demand of 20 households (kg/month)
January	53.6
February	48.4
March	53.6
April	51.9
May	53.6
June	51.9
July	53.6
August	53.6
September	51.9
October	53.6
November	51.9
December	53.6
Total Annual	53.6

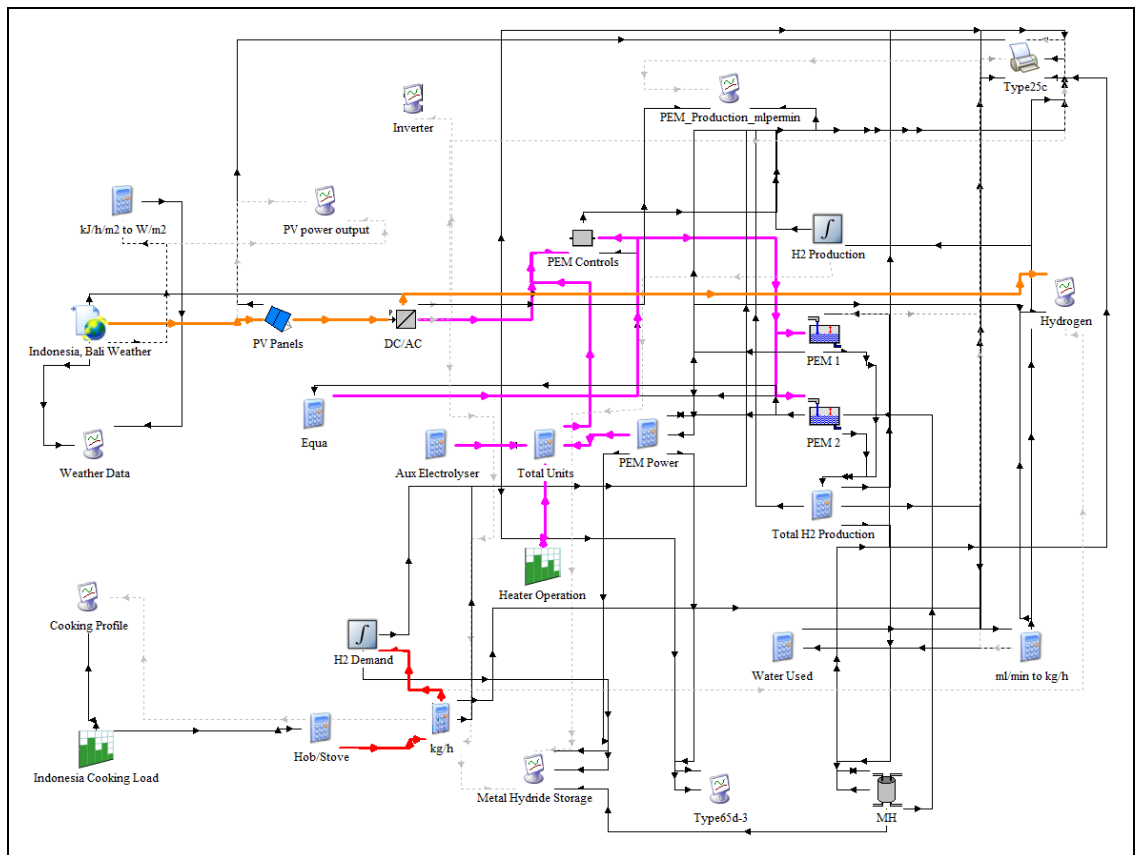


Figure F.13, Indonesia direct connection case study TRNSYS print screen

Metal Hydride Storage

The metal hydride tank size is selected to be 54kg for 20 houses or 2.7kg for each house. Equation (F.4) gives the quantity of the alloy necessary in each tank:

$$LaNi_5 \text{ content} = \frac{2.7(kg)}{150\left(\frac{ml}{gr}\right) \times 10^{-6} \left(\frac{Nm^3}{ml}\right) \times 0.0899\left(\frac{kg}{Nm^3}\right)} = 200kg \quad (F.4)$$

The electrolyser is connected directly to the metal hydride storage, and the hydrogen is stored and distributed to the households at the generated pressure, which is maximum 13.8bar.

PEM Electrolysers

Two electrolysers are selected for the Indonesia case study, based on the developed PEM numerical model presented in Chapter 5. The parameters of each one are shown in Table 7.3.

Weather data

The weather data used in the simulation for the Indonesia case study is composite TMY data from Meteonorm 7.0 database from the weather station in Bali (BALI INTL/NGURAH, id: 7181,WMO id: 972300) . The weather station in Bali, does not record irradiance but the irradiance data are the result of interpolation of irradiance data of nearby stations for a radiation period from 1991 – 2010. For all other parameters data refers to the period 2000 – 2009. The weather processor is simulated by type 15-6 component for Meteonorm files weather data processor, form the standard weather data processors library of TRNSYS (University of Wisconsin - Madison, 2014). The annual global horizontal irradiance and temperature values are shown in Figure F.14.

In terms of weather conditions, Indonesia is characterized by a monsoonal climate, with a wet (December – March) and a dry period (June – September). Average annual rainfall in the lowlands varies from 1,780–3,175 millimetres and up to 6,100 millimetres in mountainous regions. Mountains receive the highest rainfall. Humidity is generally high,

averaging about 80%. Temperatures vary little throughout the year; the average daily temperature range of Jakarta is 26–30°C (Weather Online, 2015). The irradiance and temperatures present a period of minimum values from June to September.

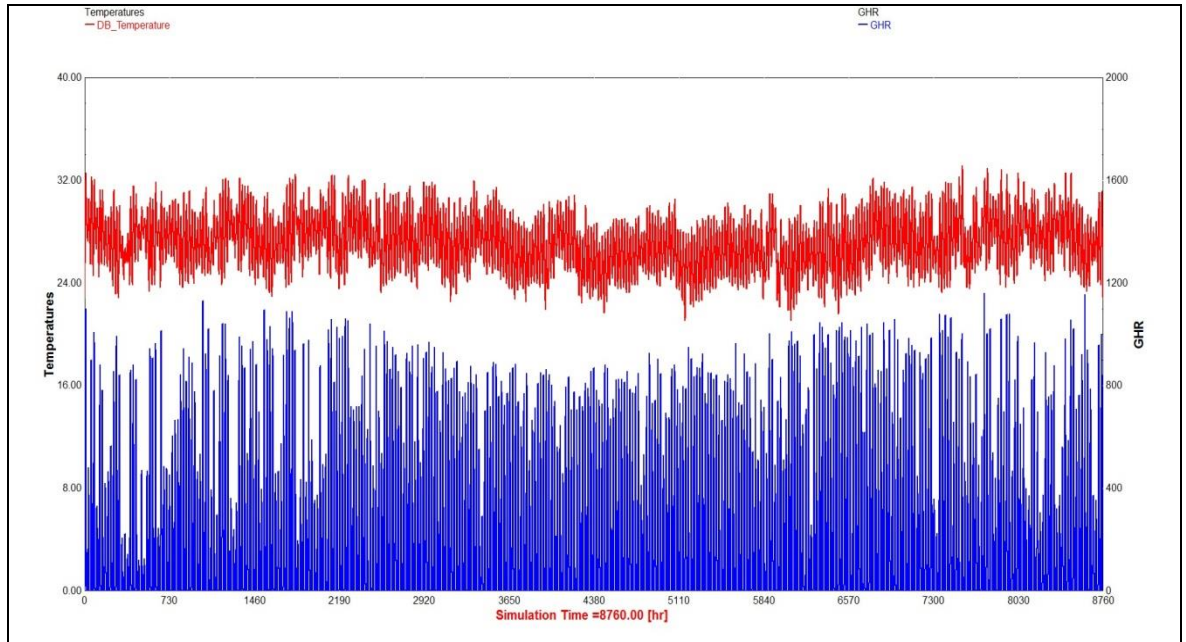


Figure F.14, Indonesia annual global horizontal irradiance and temperature values from Meteonorm file

Inverter Characteristics

The inverter selected for the direct connection of the Indonesia case has size of 54kW maximum power, based again on market parameters and real technology sizes (SMA Solar Technology AG, 2013).

System Operation

Figure F.15 shows the TRNSYS simulations results, for the month of May of the Meteonorm Typical Weather Year as an indicative month of the annual simulation. The results of the simulation are in accordance to the numerical model, and when the metal hydride tank reaches the peak point of the charging phase (as explained in Chapter 5, section 5.2.1) the charging flow rate from the electrolyser and thus the power demand is reduced. This is observed at 3376hs in Figure F.15.

Figure F.16 shows the monthly hydrogen demand and equivalent production in kg for the current conditions and after the 20 year period. There are seven months in the year where

the production is over satisfying the demand. This extra hydrogen acts as a balance in the months where production is less. The designed system provides with 670kg of hydrogen at current conditions, and 635.4kg of hydrogen after the 20 year period. Table F.6 shows the generation rates of the system and also the performance degradation on the PV array output. The current demand is over satisfied by almost 39kg.

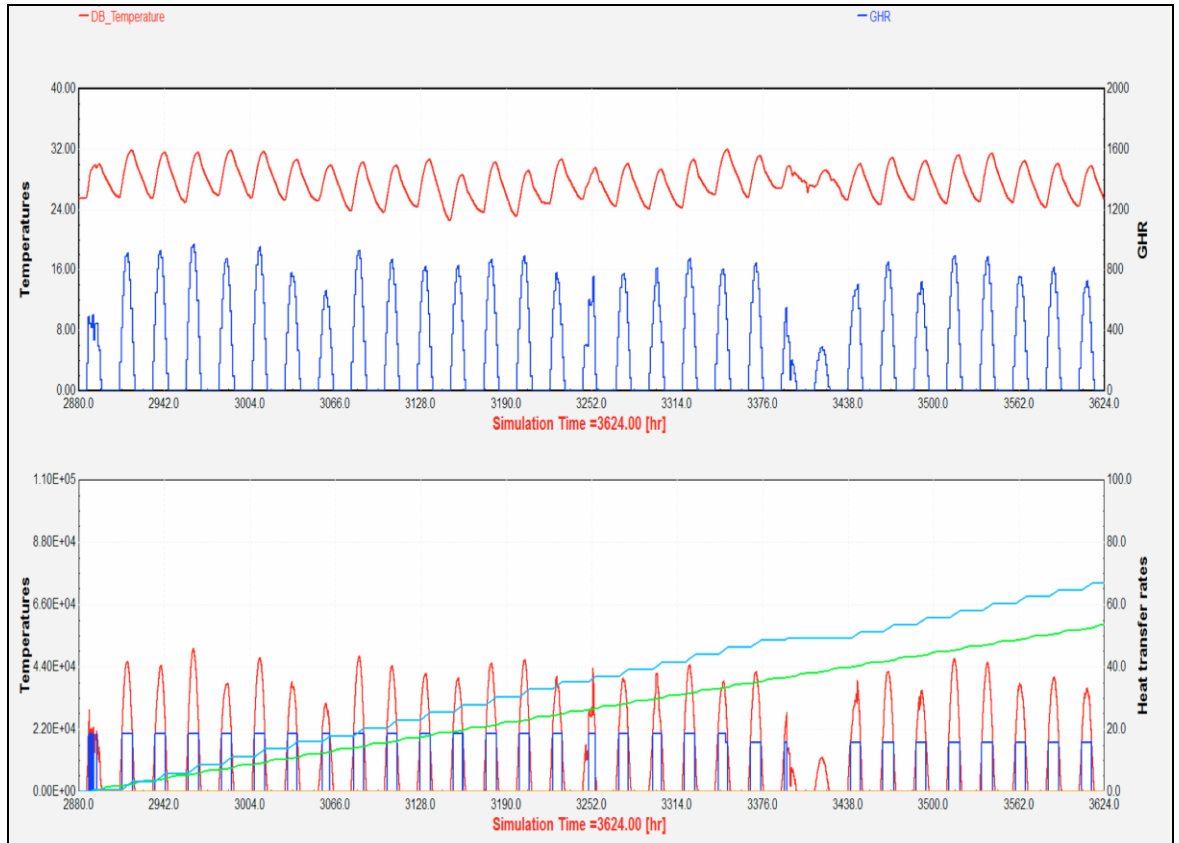


Figure F.15, TRNSYS simulation results for the Indonesia direct connection case study for the month of May

In the upper graph temperature (red) and global horizontal irradiance (blue) are presented. In the lower graph, the production of the PV array is indicated with red and the power to the electrolyser system with blue. The monthly accumulated cooking demand of the community is indicated with green and the hydrogen that is generated for distribution to the households is indicated with light blue. In this case, the purple line that indicates the maximum amount that can be stored for distribution and until it reaches the maximum point cannot be distinguished from the light blue, as the maximum hydrogen amount for storage is not reached

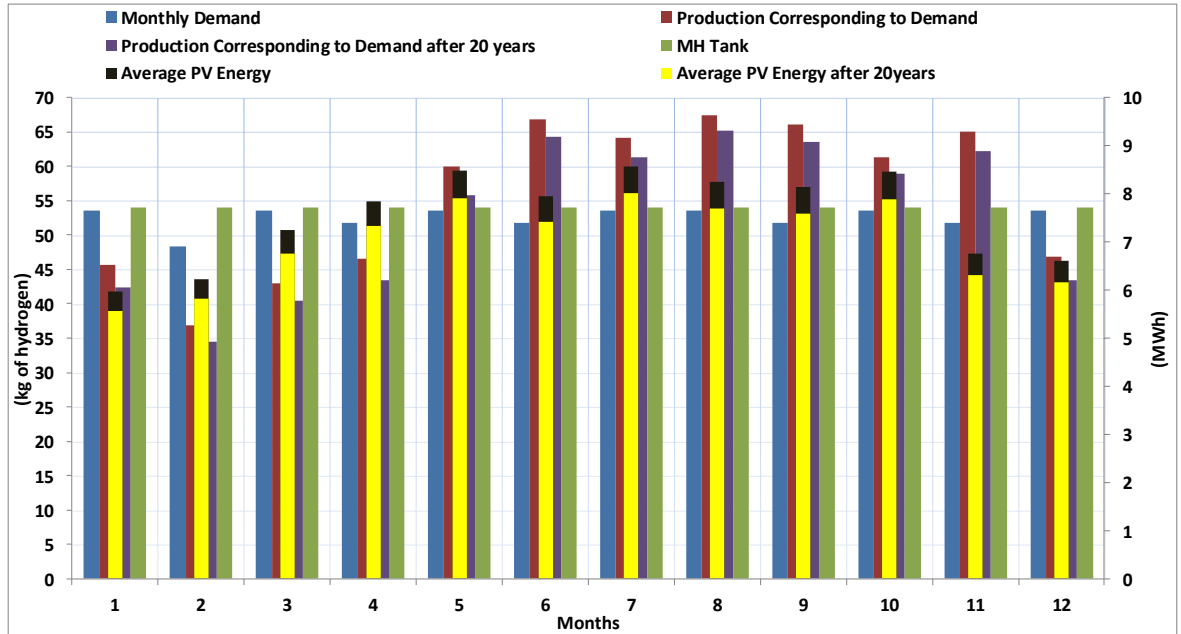


Figure F.16, Monthly demand and production of hydrogen and PV yield for the current conditions and after the panel degradation period for the Indonesia case study

Table F.6, Indonesia case study hydrogen production and PV yield at current and future conditions

Annual Hydrogen Demand (kg)	631.0
Annual Hydrogen Production (kg) at current conditions	670.0
Annual Hydrogen Production (kg) at the end of 20 years	635.4
Monthly Average PV Energy (MWh) at current conditions	7.5
Monthly Average PV Energy (MWh) at the end of 20 years	7

Battery Case

The TRNSYS model of the PV- battery case study for Indonesia can be seen in Figure F.17. A 150kWh lead-acid storage battery bank is used and a 36kW photovoltaic array. The size of the photovoltaic array is reduced by 29% of the direct connection case. The battery has a charging efficiency of 90% and is simulated by the type 47a TRNSYS component (University of Wisconsin - Madison, 2012). The electrolyzers used in this case have the characteristics of Table F.7. The metal hydride storage component is the same as in the direct connection case study and has the same size too. Weather processor and input data are also the same. Again in this case the 20 year performance degradation period of the photovoltaic array is taken into consideration and at the end of the 20th year the power

output is predicted to be approximately 33.5kW and is enough to generate the necessary hydrogen amount to satisfy the demand. The same strategy as in the previous case studies is followed and the electrolyser is set to operate for 8 hours (09.00 to 17.00) and the system is sized so that it will be able to provide the energy for the electrolyser to operate these 8 hours every day.

Table F.7 Each PEM electrolyser's parameters in the Indonesia battery case study

Maximum hydrogen production rate (Nm ³ /h)	1.5
Number of stacks	3
Number of cells	20
Cell area (cm ²)	92
Stack current (A)	110
Maximum Stack Power (kW)	7.7

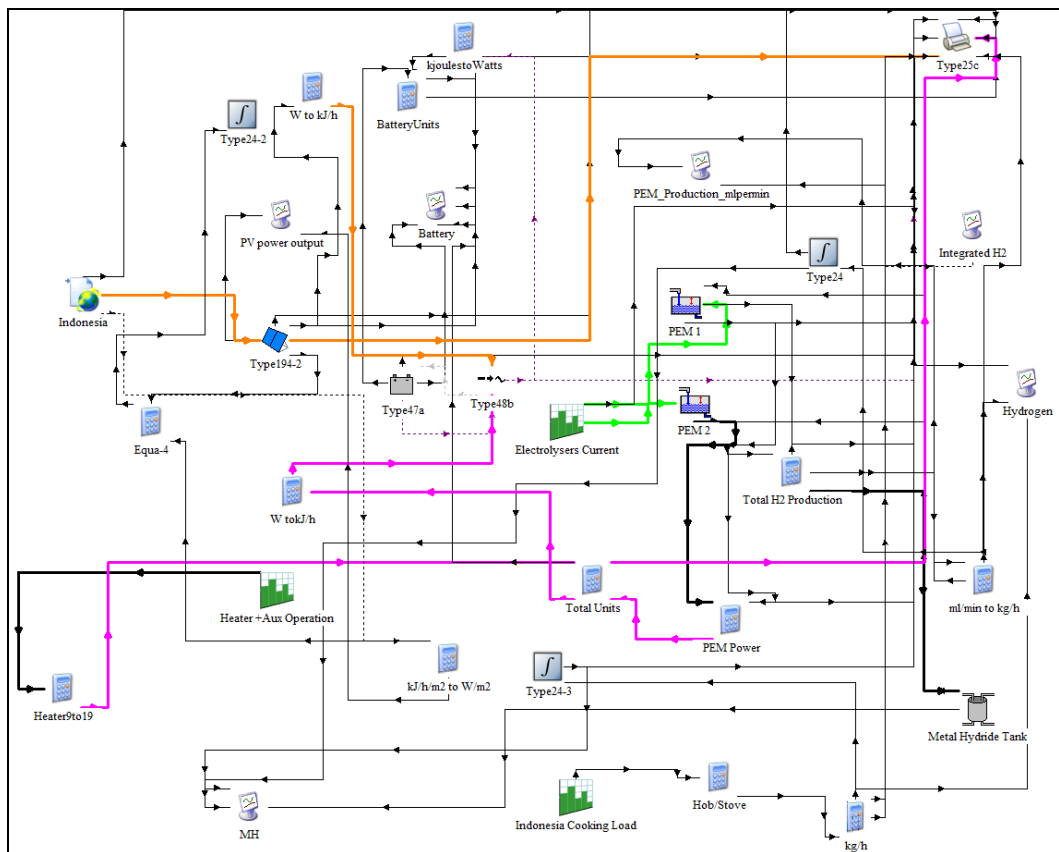


Figure F.17 Indonesia battery case study TRNSYS print screen

Figure F.18 shows the simulation results of the PV- battery case study for the month of May. Figure F.19 shows the monthly demand and production of hydrogen and PV yield

for the current conditions and after the panel degradation period for the battery case study. The monthly demand remains the same, but the PV yield is now smaller than the no-battery case study, as the battery offers storage and management of the excess PV energy. The designed system provides with 652kg of hydrogen at current conditions, over satisfying the demand by 21kg and 632kg of hydrogen after the 20 year period. Table F.8 shows the generation rates of the system and also the performance degradation rates on the PV array output.

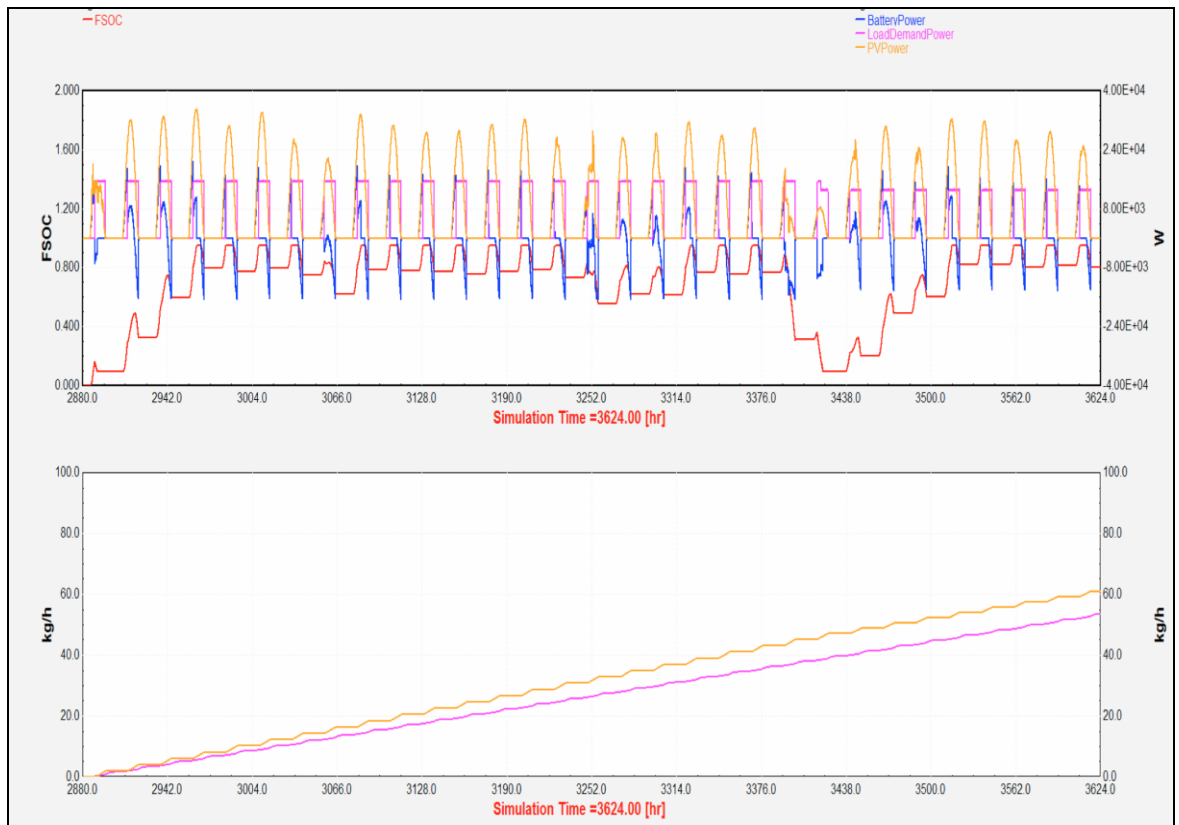


Figure F.18, TRNSYS simulation results for the Indonesia battery case study for the month of May

In the upper graph, PV power output is indicated with orange colour, electrolyser power input with purple and battery power flow with blue. The red line shows the fractional state of charge (between 0-1) of the battery. The lower graph compares the monthly accumulated cooking demand of the community which is indicated with purple and the hydrogen that is generated for distribution to the households and is indicated with orange.

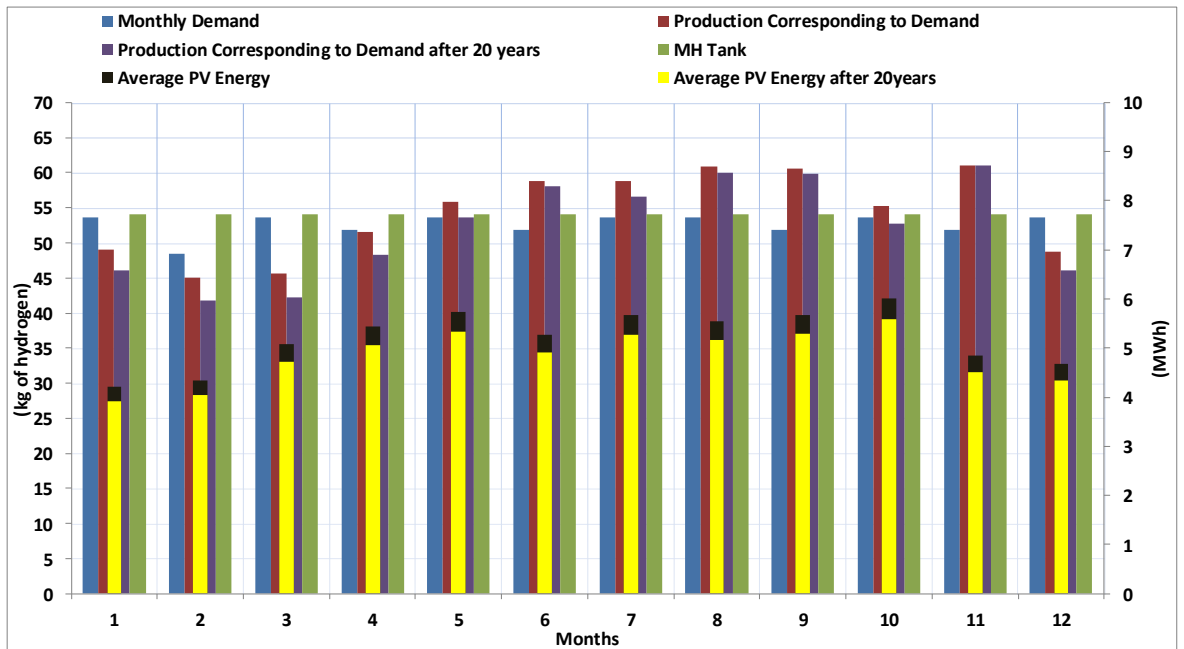


Figure F.19, Monthly demand and production of hydrogen and PV yield for the current conditions and after the panel degradation period for the Indonesia battery case study

Table F.8, Indonesia battery case study hydrogen production and PV yield at current and future conditions

Annual Hydrogen Demand (kg)	631
Annual Hydrogen Production (kg) at current conditions	652
Annual Hydrogen Production (kg) at the end of 20 years	632
Monthly Average PV Energy (MWh) at current conditions	5.2
Monthly Average PV Energy (MWh) at the end of 20 years	4.8

Appendix G. Weather Data Analysis

G.1 Weather Data Types

G.1.1 Test Reference Year – TRY

The initial attempt to create synthetic weather data sets was the Test Reference Year – TRY of the National Climatic Data Centre (NOAA - National Oceanic and Atmospheric Administration, 2014) . TRY data contain dry-bulb temperature, dew point, wind direction and speed, barometric pressure, relative humidity, cloud cover and type and a placeholder for solar radiation. No actual solar data was contained in the TRY files. As a result the building simulation softwares that used them had to calculate the solar radiation based on the cloud cover and cloud type. But the greatest drawback of the TRY data files was the fact that they consisted of an actual historic weather year. The selection method was based on the elimination of years that had months with extremely high or low mean temperatures from a period of almost 30 years (1948-1975). The result was limiting as it provided with an extremely mild year (Crawley, 1998).

G.1.2 Typical Meteorological Year – TMY

In order to overcome these restrictions that were posed by the use of TRY data, NOAA along with the Sandia National Laboratory (Sandia National Laboratories , 2014) created a new data set format, the Typical Meteorological Year – TMY. The data of TMY are derived from the Sandia Method and consist of 12 months that were selected from a 23 year period of record (1952-1975, SOLMET/ERSATZ database) to represent typical months (User's Manual for TMY2, 2013). Individual months were selected based on a monthly composite weighting of solar radiation, dry-bulb temperature, dew point, and wind velocity as compared to the long-term distribution (Crawley, 1998). The result is that TMY files consist of months of different years but that represent the mean average most accurately and they permit performance comparisons of systems for many locations.

G.1.3 Typical Meteorological Year 2 -TMY2

In order to update the TMY files, a new method was proposed in 1978 for the creation of Typical Meteorological Year that resulted in the creation of TMY2 (User's Manual for TMY2, 2013). TMY2 files are based on real data from 239 stations across the USA during the years 1961 and 1990 (30 years). The data comes from two types of stations: primary and secondary. 56 stations are primary stations and they offer the possibility to record

solar radiation data. The secondary stations make no solar radiation measurements but use modelled solar radiation data such as radiation computed from cloud cover. Both primary and secondary stations are National Weather Service stations that collected meteorological data for the period 1961-1990 (User's Manual for TMY2, 2013). The modifications between TMY and TMY2 consist in the methods that calculate time (solar versus local), formats, elements and units. The result is that the new data takes into consideration recent climate changes and offer more precise values of solar radiation for numerous reasons:

- More than 90% of the solar radiation data in both data bases are modelled, thus offering a better model for estimating values
- More measured data, some of which is direct normal radiation
- Enhanced instrument calibration methods
- Rigorous procedures for evaluating data quality

Comparison between the data used to construct the TMY and TMY2 indicate that the differences in the results are not derived from the cloud cover that has almost remained the same for the two periods, but from the differences in the instruments calibration. The computational process has remained the same apart from some differences in the weighting factors. The Sandia Method was used in both cases. This is an empirical approach that chooses individual months from different years from the period of record (Sandia National Laboratories , 2014). For example, in the case of the TMY2, all 30 Januaries of the recorded data are examined, and the one judged most typical is selected to be included in the TMY. The other months of the year are treated similarly, and then the 12 selected typical months are linked together to form a complete year (User's Manual for TMY2, 2013).

The 12 selected typical months for each station were chosen from statistics and five elements were used as a criterion: global horizontal radiation, direct normal radiation, dry bulb temperature, dew point temperature, and wind speed. These are the fundamentals for simulation of solar energy conversion systems and building systems.

G.1.4 Typical Meteorological Year 3 -TMY3

The TMY3 data files include 1020 locations in the USA including Guam, Puerto Rico, and US Virgin Islands, derived from a 1991-2005 period of record. The design of the TMY3 had a purpose to maximise the number of stations and the number of years. For sites where

data were available since 1975 the period of 1975-2005 was kept. Keeping a long record period provides data that represent better the climate characteristics. Again in the case of the TMY3 the Sandia Calculation method was used (Wilcox & Marion, 2008). The most significant difference between the TMY2 and TMY3 is that only modelled solar radiation data was included in the TMY3 data in order to provide more consistent values (Wilcox & Marion, 2008) and that in the TMY2 months with many runs are eliminated immediately whereas in TMY3 only the month with the most runs is eliminated.

What should be noted here is that the format between the TMY, the TMY2 and the TMY3 is different and therefore extra care should be given on the data processors. Furthermore, as TMY data, the TMY3 data provide average conditions and is not suitable for simulations where extreme weather conditions should be taken into consideration, e.g. wind energy systems.

G.1.5 ASHRAE Weather Data (WYEC)

ASHRAE commissioned numerous research projects within the years 1970 to 1983 regarding the creation of weather data. The weather data set that was created is known as Weather Year for Energy Calculations (WYEC). It uses the TRY format with the main difference being that it includes solar radiation data; either measured or calculated from cloud cover and type. The basic method was again to select the month that the mean dry-bulb temperature was closest to the average in the 30 year period of record (Crawley, 1998).

Furthermore, ASHRAE developed the International Weather for Energy Calculations (IWEC) files under the Research Project RP 1015. The IWEC data files are 'typical' weather files suitable for use with building energy simulation programs for 227 locations outside the USA and Canada. The files are derived from up to 18 years of hourly weather data originally archived at the National Climatic Data Centre. The weather data is enhanced by solar radiation estimated on an hourly basis from earth-sun geometry and hourly weather elements, particularly cloud amount information (US Department of Energy, 2013).

More recently, within the auspice of the RP-1477 project ASHRAE developed the IWEC2 weather files. These files stem from meteorological reports of weather stations around the world that are archived in the Integrated Surface Hourly (ISH) data base maintained by the National Climatic Data Center (NOAA - National Oceanic and Atmospheric

Administration, 2014). For the selected locations, the ISH database contains weather observations on average at least four times per day of wind speed and direction, sky cover, visibility, ceiling height, dry-bulb temperature, dew-point temperature, atmospheric pressure, liquid precipitation, and present weather for at least 12 years of record up to 25 years (ASHRAE, 2008).

G.1.6 CIBSE TRY Weather Data

In the United Kingdom, CIBSE Test Reference Years (TRY) have been used for building energy simulation and energy use comparison. Test Reference Years and Design Summer Years (DSY) for 14 UK locations have been produced by CIBSE in association with the (UK) Met Office, for use with building energy simulation softwares. The TRYs are composed of 12 separate months of data, each again selected as the most average month from a 23 year set of data (1983 to 2005). The selection criterion is the cumulative distribution function of the daily mean values of three parameters: dry-bulb temperature, global solar irradiance and wind speed (CIBSE, 2007). Finkelstein-Schafer statistic is used to compare the cumulative distribution function, and the months with the smallest statistic are selected (Univeristy of Exeter, 2013). The DSY creation on the other side is relatively simple in comparison to the TRY creation. The Design Summer Year is a single contiguous year and the method to select it is to calculate the mean average dry-bulb temperature in the period from April to September within the period 1982-2005. The year with the third hottest April to September period is the DSY. The CIBSE TRY/DSY files are based on data from UK weather stations, and this is why they are of limited number (Univeristy of Exeter, 2013)

G.2 CDF curves for Dry Bulb Temperature, Relative Humidity and Wind Speed

The comparison between the averages, minimum and maximum values of each weather parameter for each month of 2011 and of the three years of the recent data set and of the Meteonorm year can be seen in Tables G.1 to G.13. Furthermore, the values of each weather parameter for 2011, 2012 and 2013 and the Meteonorm year can be seen graphically in Figures G.1 to G.22.

2011 FS=2.31

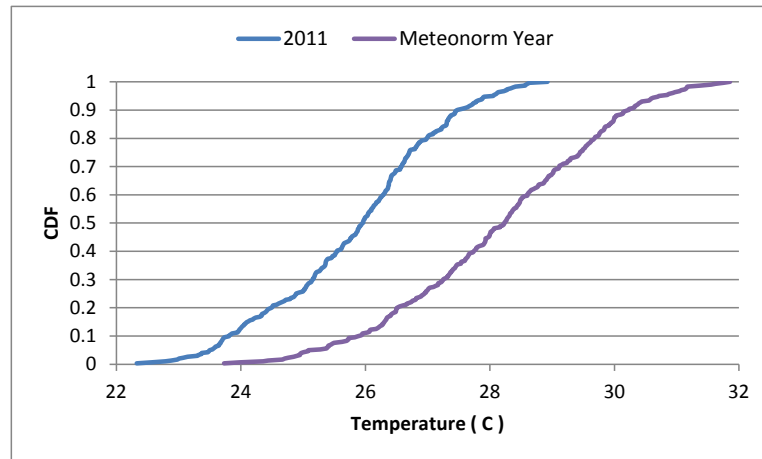


Figure G.1, Comparison between the CDF curves for Temperature for 2011

2012 FS=1.95

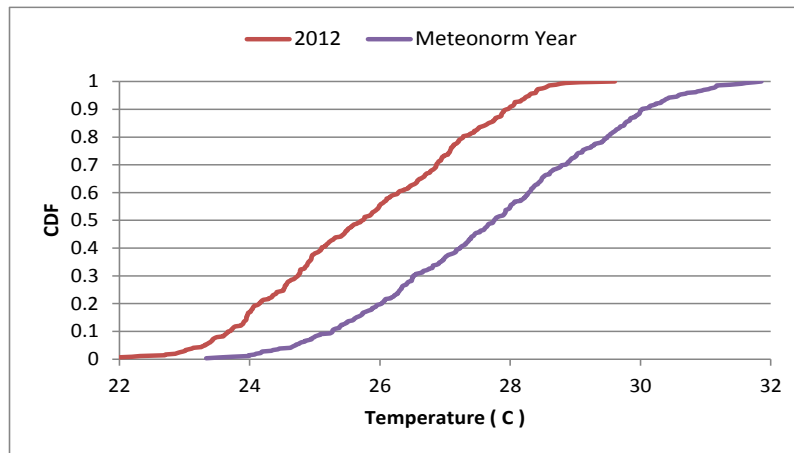


Figure G.2, Comparison between the CDF curves for Temperature for 2012

2013 FS=1.46

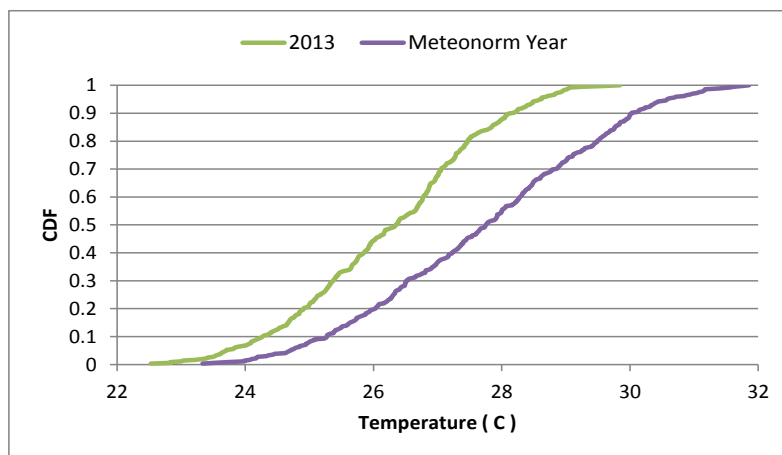


Figure G.3, Comparison between the CDF curves for Temperature for 2013

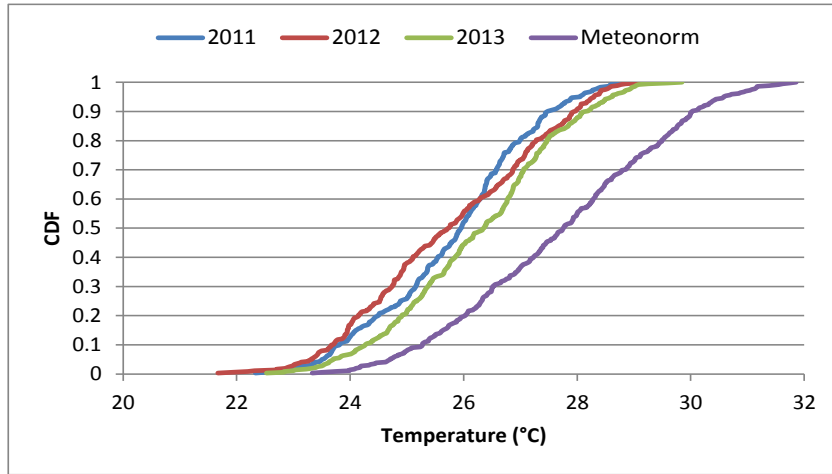


Figure G.4, Comparison between the CDF curves for Temperature for all years

2011 FS=5.32

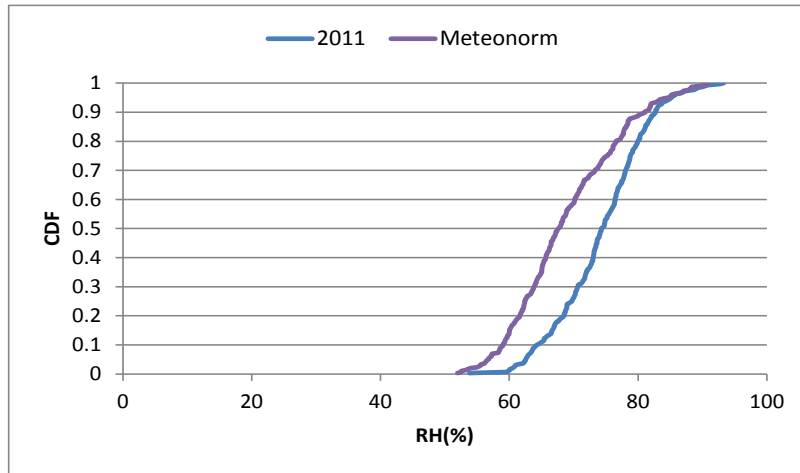


Figure G.5, Comparison between the CDF curves for Relative Humidity for 2011

2012 FS=5.33

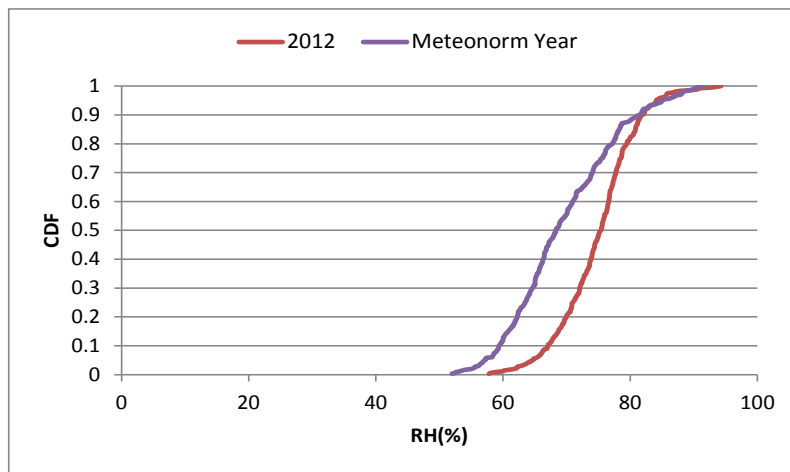


Figure G.6, Comparison between the CDF curves for Relative Humidity for 2012

2013 FS=4.75

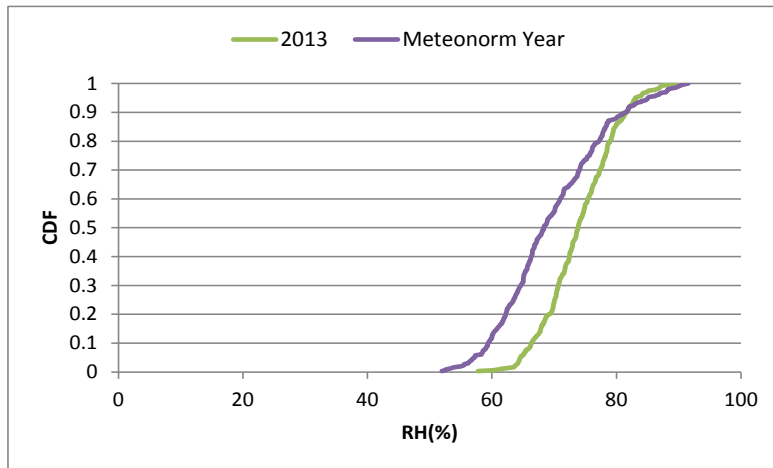


Figure G.7, Comparison between the CDF curves for Relative Humidity for 2013

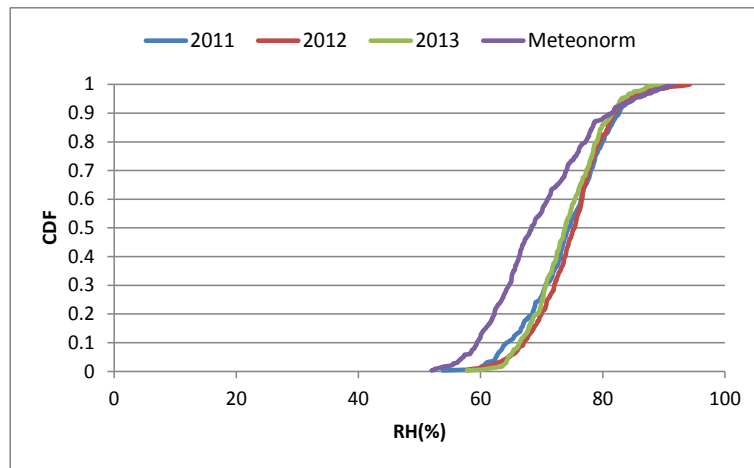


Figure G.8, Comparison between the CDF curves for Relative Humidity all years

2011 FS=0.89

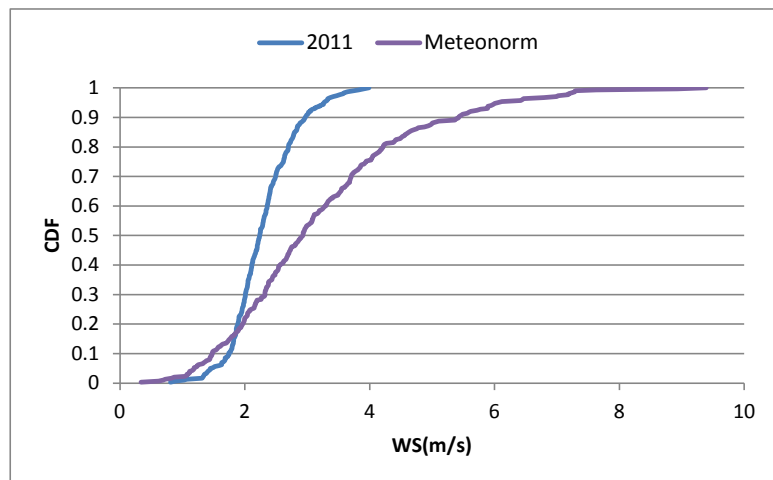


Figure G.9, Comparison between the CDF curves for Wind Speed for 2011

2012 FS=0.69

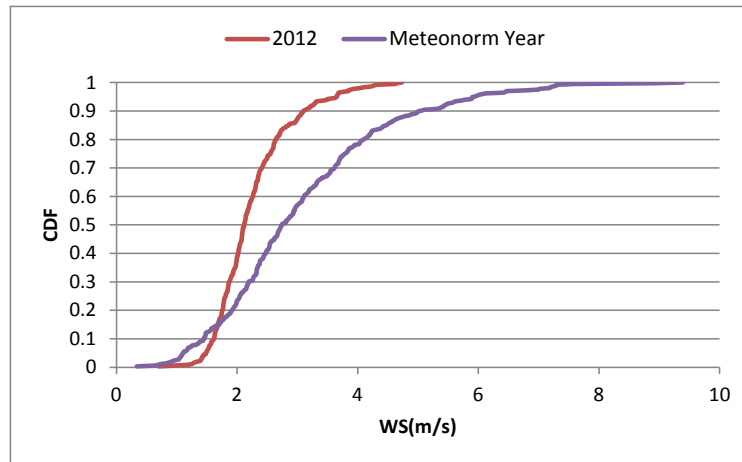


Figure G.10, Comparison between the CDF curves for Wind Speed for 2012

2013 FS=0.65

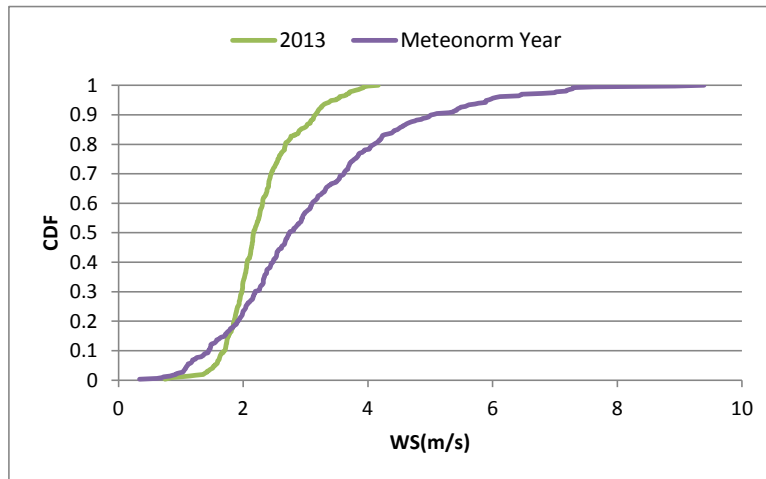


Figure G.11, Comparison between the CDF curves for Wind Speed for 2013

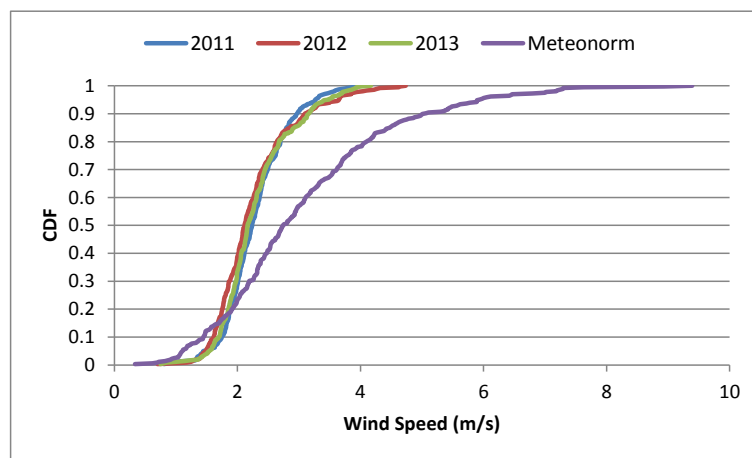


Figure G.12, Comparison between the CDF curves for Wind Speed for all years

G.3 CDF Comparison for each month for the recent weather data for 2011*

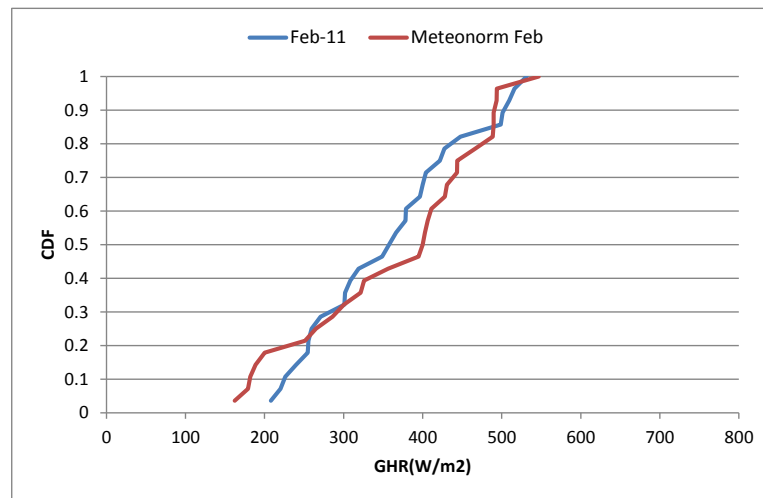


Figure G.13, CDF Comparison of global horizontal radiation for February 2011

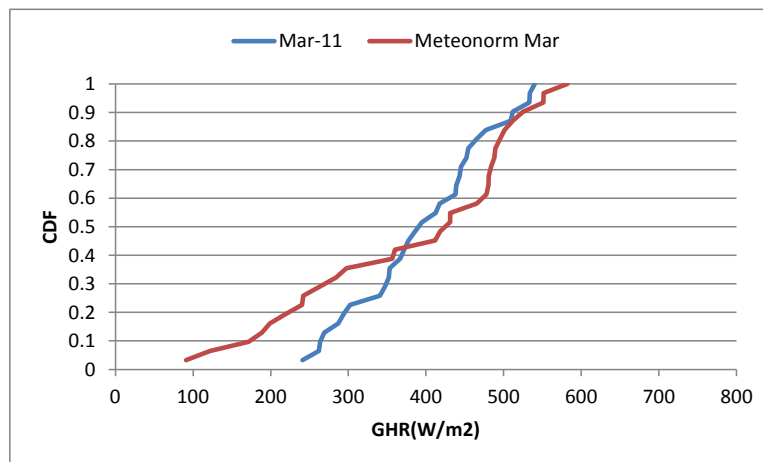


Figure G.14, CDF Comparison of global horizontal radiation for March 2011

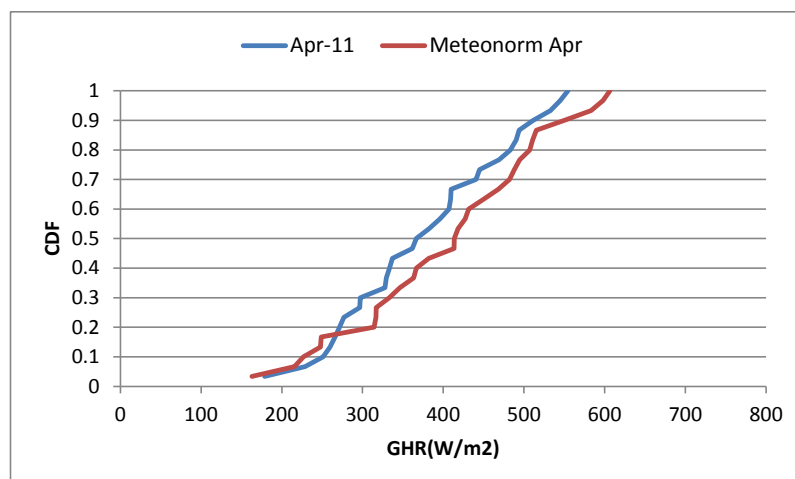


Figure G.15, CDF Comparison of global horizontal radiation for April 2011

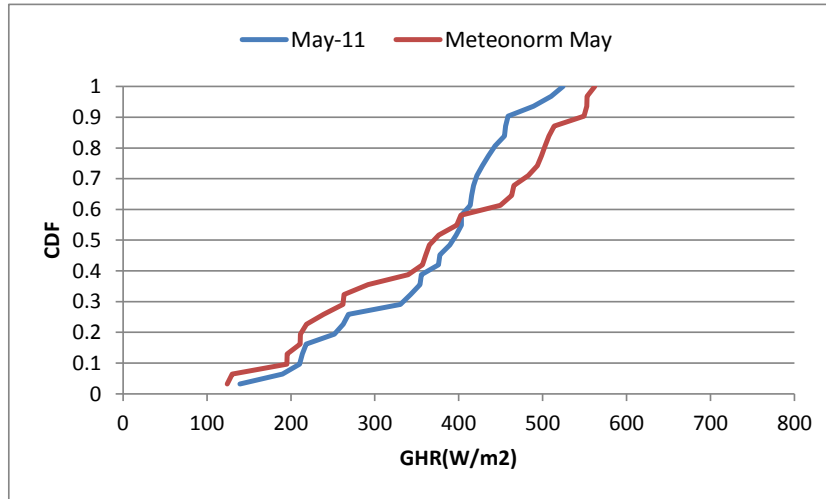


Figure G.16, CDF Comparison of global horizontal radiation for May 2011

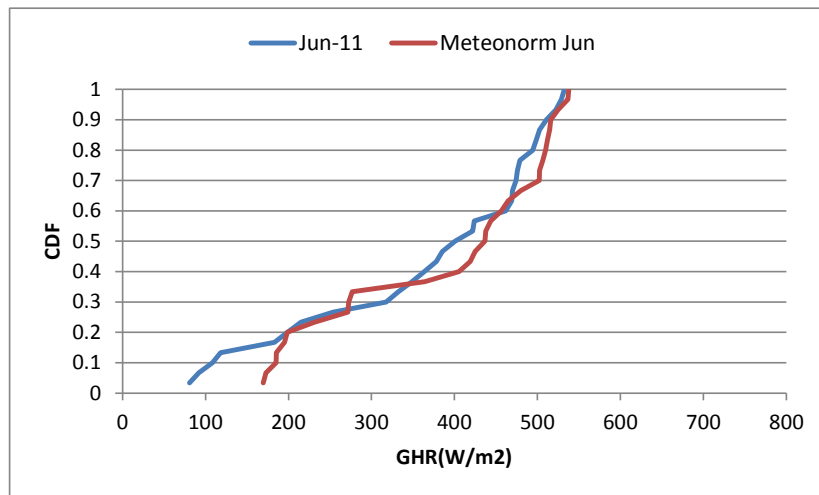


Figure G.17, CDF Comparison of global horizontal radiation for June 2011

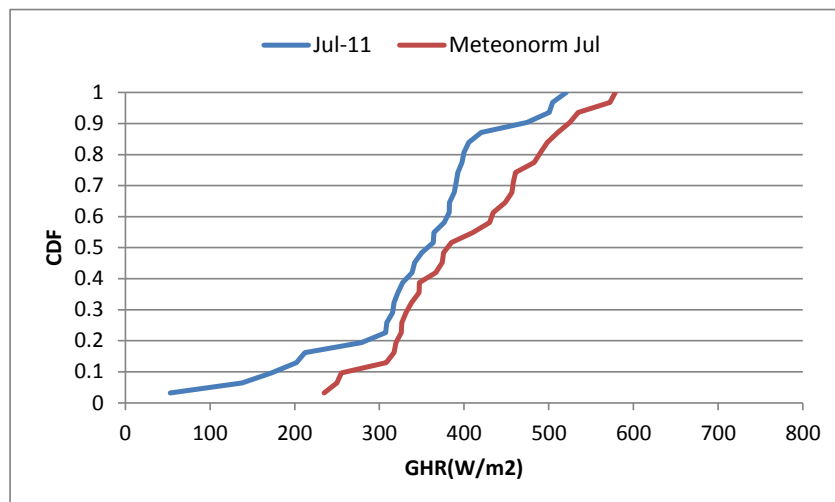


Figure G.18, CDF Comparison of global horizontal radiation for July 2011

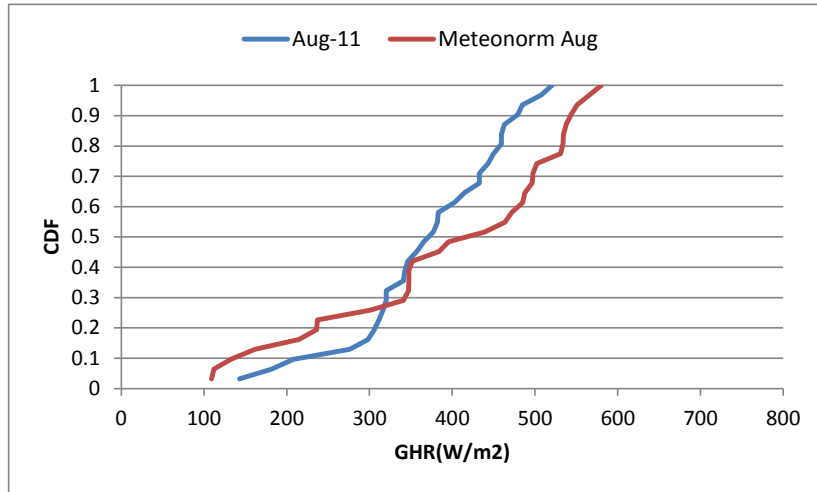


Figure G.19, CDF Comparison of global horizontal radiation for August 2011

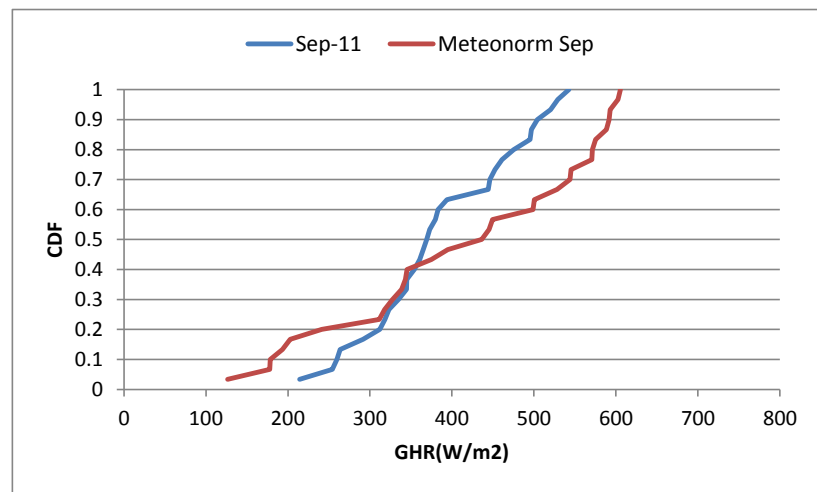


Figure G.20, CDF Comparison of global horizontal radiation for September 2011

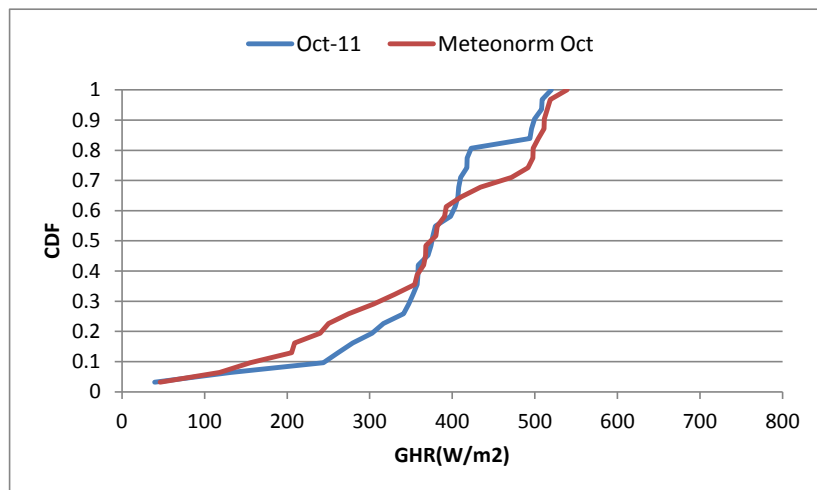


Figure G.21, CDF Comparison of global horizontal radiation for October 2011

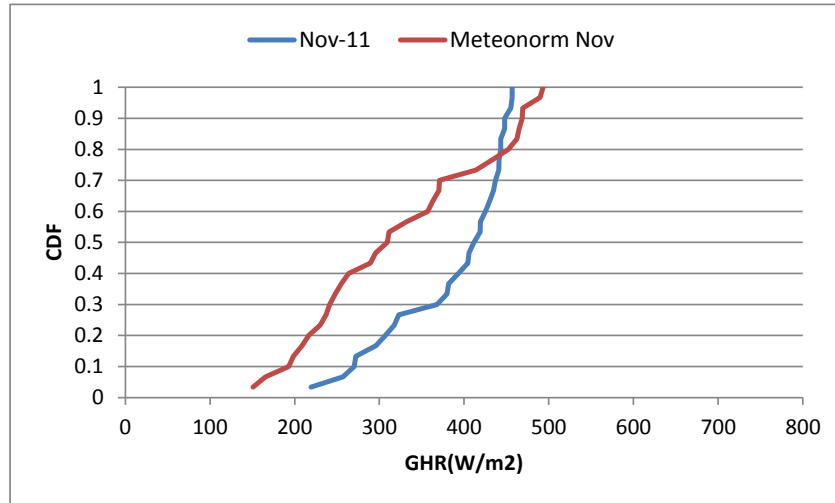


Figure G.22, CDF Comparison of global horizontal radiation for November 2011

*January and December lack data and are excluded from the computation

Table G.1, FS Statistics for each month of each of the three recent yearly weather data sets compared to the Meteonorm Weather Data for Global Horizontal Radiation

GHR(W/m ²) FS			
	2011	2012	2013
January	-	32.2	54.8
February	28.6	51.6	26.6
March	50.4	66.0	42.0
April	33.7	65.9	47.2
May	40.9	59.3	38.0
June	27.8	47.5	62.0
July	59.5	14.6	32.5
August	57.7	69.3	60.7
September	64.5	175.2	94.6
October	30.1	27.3	42.7
November	71.7	45.6	33.5
December	-	51.4	55.6
Complete Year	29.9	40.5	43.2

Table G.2, FS Statistics for each month of each of the three recent yearly weather data sets compared to the Meteonorm Weather Data for Dry bulb temperature

T(°C) FS			
	2011	2012	2013
January	-	1.11	0.66
February	1.56	1.38	0.93
March	2.92	2.80	2.20
April	2.83	3.07	1.73
May	3.33	2.47	2.64
June	2.36	1.57	1.38
July	3.12	2.20	2.13
August	2.56	2.28	1.93
September	1.70	1.83	1.06
October	1.57	1.68	1.04
November	1.11	1.30	0.82
December	-	1.26	1.01
Complete Year	2.32	1.95	1.47

Table G.3, FS Statistics for each month of each of the three recent yearly weather data sets compared to the Meteonorm Weather Data for Relative Humidity

RH(%) FS			
	2011	2012	2013
January	-	1.92	2.51
February	2.23	4.54	2.19
March	3.17	8.28	6.53
April	4.07	11.39	4.87
May	7.03	8.05	7.71
June	7.95	3.53	5.43
July	10.64	4.01	6.50
August	10.94	8.17	7.65
September	6.48	4.59	4.59
October	5.52	5.57	5.79
November	2.95	4.88	6.17
December	-	4.57	4.31
Complete Year	5.32	5.33	4.75

Table G.4, FS Statistics for each month of each of the three recent yearly weather data sets compared to the Meteonorm Weather Data for Wind Speed

WS(m/s) FS			
	2011	2012	2013
January	-	0.76	0.59
February	0.82	0.90	0.64
March	0.73	1.06	0.97
April	0.68	0.80	0.51
May	1.45	1.14	1.49
June	1.98	1.59	1.79
July	1.99	1.86	1.75
August	1.42	1.10	1.33
September	0.56	0.61	0.54
October	0.31	0.31	0.45
November	0.38	0.41	0.30
December	-	0.48	0.42
Complete Year	0.89	0.69	0.65

Table G.5, Weighted FS Statistics for each month

FS weighted			
	2011	2012	2013
January	-	9.00	14.65
February	8.29	14.61	7.58
March	14.30	19.54	12.93
April	10.33	20.28	13.57
May	13.18	17.75	12.44
June	10.02	13.53	17.66
July	18.81	5.66	10.72
August	18.14	20.21	17.89
September	18.30	45.55	25.20
October	9.37	8.72	12.50
November	19.03	13.05	10.18
December	-	14.42	15.34
Total	9.60	12.11	12.51

Table G.6, Minimum and Maximum Daily Values of Global Horizontal Radiation for the recent and Meteorom data

GHR(W/m²)								
	2011		2012		2013		Meteorom	
	min	max	min	max	min	max	min	max
January	-	-	141.9	477.5	189.9	468.1	75.7	472.3
February	208.1	531.6	211.3	449.7	187.0	501.9	162.2	546.8
March	240.9	540.1	173.9	529.2	130.4	523.7	90.9	582.2
April	178.8	554.5	113.5	532.8	217.7	524.6	163.1	606.5
May	139.2	524.2	257.4	515.1	143.2	529.7	124.1	562.1
June	80.6	532.6	121.5	517.9	202.9	510.7	169.4	537.6
July	53.2	520.7	214.8	511.2	69.4	518.2	234.9	578.7
August	142.9	520.6	211.5	512.3	42.2	531.7	108.9	580.2
September	214.5	542.7	97.9	504.8	57.1	516.6	126.5	605.4
October	39.7	520.0	60.4	506.9	167.4	516.3	46.3	539.0
November	219.2	456.8	189.8	466.2	182.6	471.5	150.8	493.4
December	-	-	142.3	436.0	211.2	455.8	106.1	454.3
Complete Year	39.7	578.7	60.4	532.8	42.2	531.7	46.3	606.5

Table G.7, Minimum and Maximum Daily Values of Temperature for the recent and Meteorom data

T(°C)								
	2011		2012		2013		Meteorom	
	min	max	min	max	min	max	min	max
January	-	-	22.61	24.98	22.83	26.34	23.34	27.30
February	22.98	25.02	23.32	25.17	23.63	25.92	23.73	27.78
March	22.33	26.41	21.92	27.05	22.83	26.82	24.91	28.62
April	23.32	26.82	23.01	26.27	24.30	27.39	25.95	30.24
May	24.08	27.31	24.70	28.56	24.75	28.00	26.94	31.16
June	23.65	28.92	24.33	29.08	26.83	29.08	27.27	31.62
July	24.41	28.33	24.75	29.61	24.91	29.85	28.27	31.86
August	24.03	28.27	25.76	28.58	23.62	29.26	27.41	31.15
September	25.36	27.33	23.11	27.73	23.53	28.97	26.37	30.44
October	23.82	27.17	23.41	27.27	25.17	27.96	24.85	30.03
November	24.40	26.72	23.78	26.36	23.83	27.19	24.95	29.45
December	-	-	22.32	26.65	22.53	26.18	23.99	28.19
Complete Year	22.33	28.92	21.67	29.61	22.53	29.85	23.34	31.86

Table G.8, Minimum and Maximum Daily Values of Relative Humidity for the recent and Meteorom data

RH(%)								
	2011		2012		2013		Meteorom	
	min	max	min	max	min	max	min	max
January	-	-	62.26	85.64	63.60	80.41	59.29	88.88
February	59.70	85.73	65.74	80.06	63.77	84.25	52.54	83.00
March	53.82	81.16	63.45	86.79	60.13	84.91	55.33	85.23
April	62.56	81.19	69.17	90.60	61.04	82.43	53.56	83.19
May	62.80	82.40	65.78	82.24	64.27	86.45	51.98	82.73
June	60.09	93.31	57.80	89.71	61.57	78.57	55.54	85.13
July	64.97	87.09	58.71	80.69	57.74	88.17	52.52	77.83
August	68.69	87.59	66.09	85.68	65.86	90.35	57.33	90.50
September	72.51	83.71	67.43	90.85	67.43	90.85	61.88	88.27
October	71.76	90.86	71.95	94.29	72.46	84.18	61.94	91.00
November	62.69	82.89	68.42	82.94	69.86	87.21	57.21	89.58
December	-	-	63.20	87.02	66.08	82.11	61.29	91.56
Complete Year	53.82	93.31	57.80	94.29	57.74	90.35	51.98	91.56

Table G.9, Minimum and Maximum Daily Values of Wind Speed for the recent and Meteorom data

WS(m/s)								
	2011		2012		2013		Meteorom	
	min	max	min	max	min	max	min	max
January	-	-	1.33	3.65	1.83	3.55	0.97	5.30
February	1.34	3.90	1.44	3.28	0.75	3.71	1.07	7.63
March	1.41	3.42	1.56	3.67	0.80	3.40	0.62	5.72
April	1.79	3.82	1.29	3.64	1.42	4.17	0.72	5.89
May	1.39	2.78	1.63	4.73	1.51	3.54	0.83	7.30
June	0.81	3.99	0.94	4.62	1.46	4.00	1.38	9.39
July	1.33	3.52	1.53	3.85	1.64	3.80	1.37	8.93
August	1.43	3.01	1.42	4.64	1.36	3.85	1.11	7.01
September	1.63	3.32	1.25	2.96	1.40	3.15	0.34	5.00
October	0.88	2.11	0.70	3.20	1.37	2.66	0.87	5.06
November	1.63	2.31	1.39	2.35	1.42	3.02	0.69	3.30
December	-	-	1.48	3.23	1.62	3.70	0.92	4.86
Complete Year	0.81	3.99	0.70	4.73	0.75	4.17	0.34	9.39

Table G.10, Average Values of Global Horizontal Radiation for the recent and Meteorom data

GHR(W/m ²)				
	2011	2012	2013	Meteorom
January	-	319.7	330.5	314.4
February	358.9	344.3	357.3	366.0
March	396.2	345.1	348.9	381.0
April	378.4	340.8	372.1	406.7
May	366.2	394.3	372.7	372.1
June	368.1	382.3	357.0	388.5
July	343.6	392.9	378.0	403.1
August	371.8	359.2	371.9	394.8
September	387.0	381.6	330.5	417.3
October	371.1	374.1	358.3	367.6
November	386.9	353.6	338.6	325.2
December	-	346.0	331.9	299.6
Complete Year	372.8	361.2	354.0	369.6

Table G.11, Average Values of Temperature for the recent and Meteoronorm data

T(°C)				
	2011	2012	2013	Meteoronorm
January	-	23.75	24.65	25.31
February	24.11	24.32	24.74	25.67
March	24.03	24.16	24.76	26.95
April	25.11	24.87	26.21	27.95
May	25.88	26.74	26.57	29.20
June	26.99	27.78	27.96	29.35
July	26.78	27.70	27.77	29.90
August	26.88	27.15	27.50	29.43
September	26.52	26.39	27.16	28.22
October	26.12	26.00	26.66	27.69
November	25.61	25.42	25.90	26.72
December	-	24.80	25.04	26.05
Complete Year	25.82	25.76	26.25	27.72

Table G.12, Average Values of Relative Humidity for the recent and Meteoronorm data

RH(%)				
	2011	2012	2013	Meteoronorm
January	-	73.87	71.10	72.66
February	71.20	74.05	71.74	69.60
March	69.12	74.85	73.09	66.58
April	70.55	78.21	71.63	66.82
May	73.35	74.35	74.05	66.34
June	74.54	69.11	70.64	66.59
July	75.46	68.65	71.32	64.82
August	77.96	74.97	74.48	67.73
September	78.49	77.52	76.99	73.45
October	79.70	80.15	79.16	74.75
November	72.31	76.92	79.37	73.36
December	-	76.16	74.88	72.67
Total	74.30	74.91	74.05	69.61

Table G.13, Average Values of Wind Speed for the recent and Meteonorm data

WS(m/s)				
	2011	2012	2013	Meteonorm
January	-	1.95	2.29	2.60
February	2.19	2.13	2.36	3.00
March	2.49	2.15	2.13	3.09
April	2.49	2.19	2.53	2.90
May	2.21	2.55	2.18	3.59
June	2.51	2.90	2.72	4.49
July	2.22	2.36	2.48	4.20
August	2.25	2.53	2.28	3.58
September	2.34	2.25	2.28	2.71
October	2.25	2.17	2.09	2.29
November	2.00	1.82	2.02	2.10
December	-	2.07	2.19	2.30
Total	2.30	2.26	2.29	3.07

G.4 Meteonorm and Recent Weather Data Annual Graphs of GHR, Temperature, RH, Wind Speed

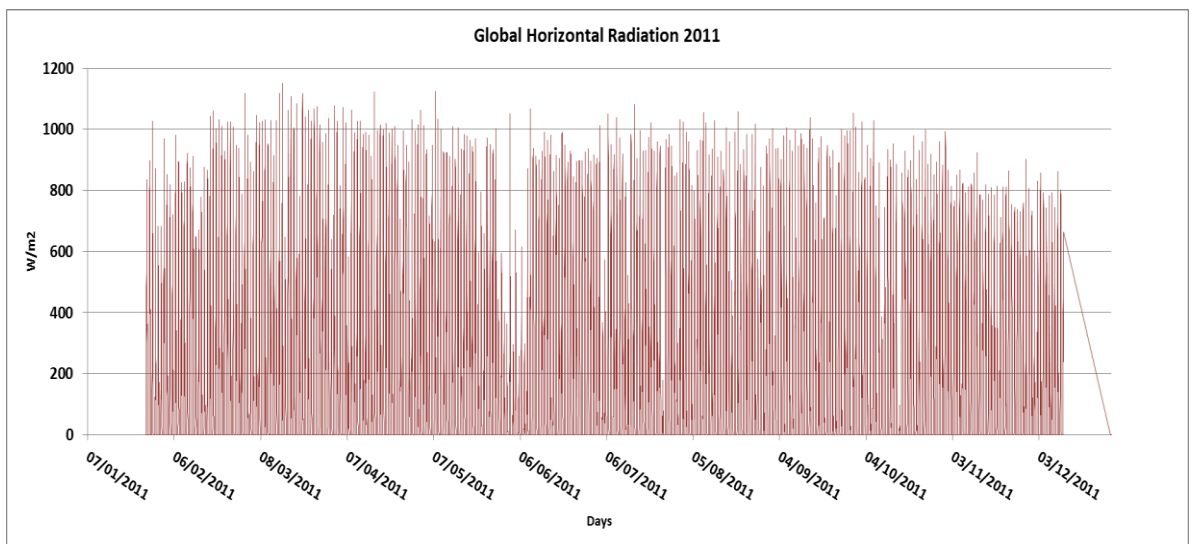


Figure G.23, Global Horizontal Radiation in Kingston, Jamaica for 2011

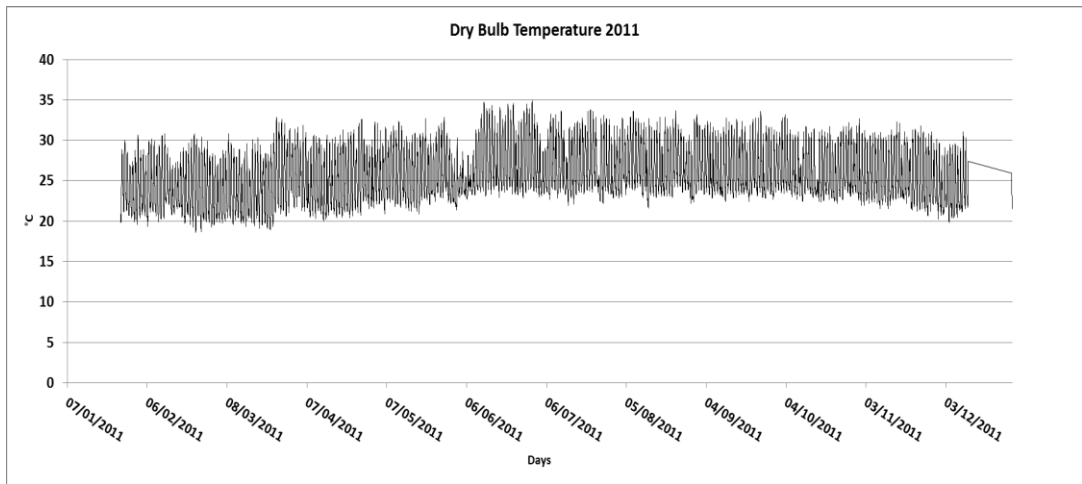


Figure G.24, Dry Bulb Temperature in Kingston, Jamaica for 2011

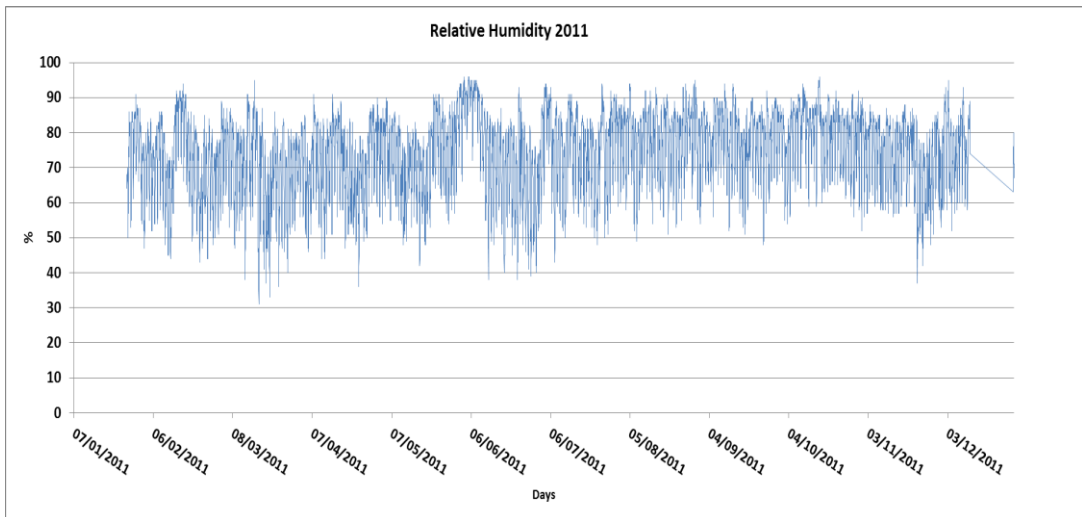


Figure G.25, Relative Humidity in Kingston, Jamaica for 2011

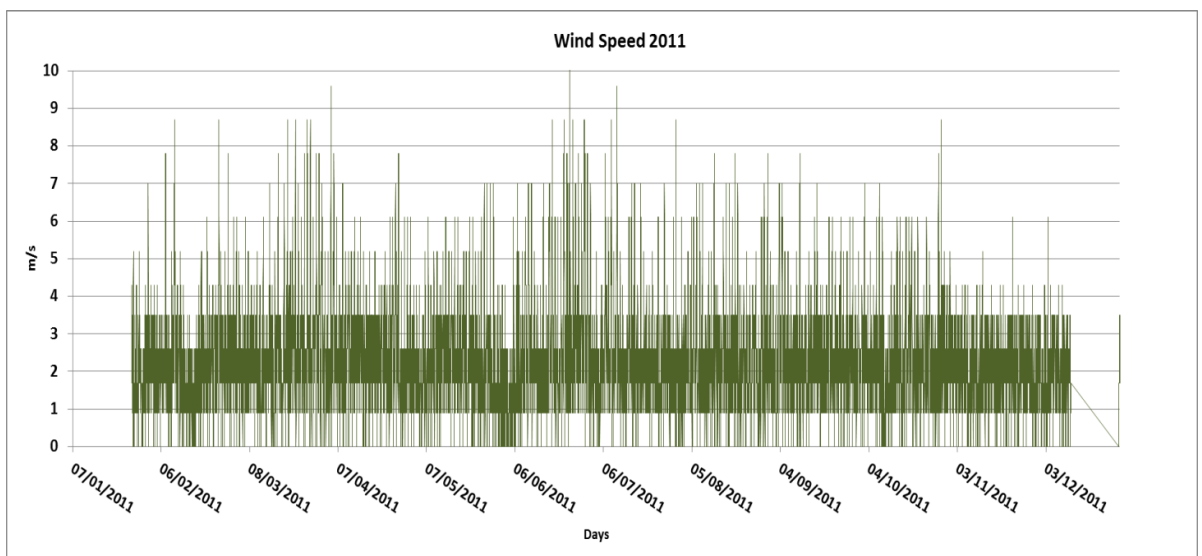


Figure G.26, Wind Speed in Kingston, Jamaica for 2011

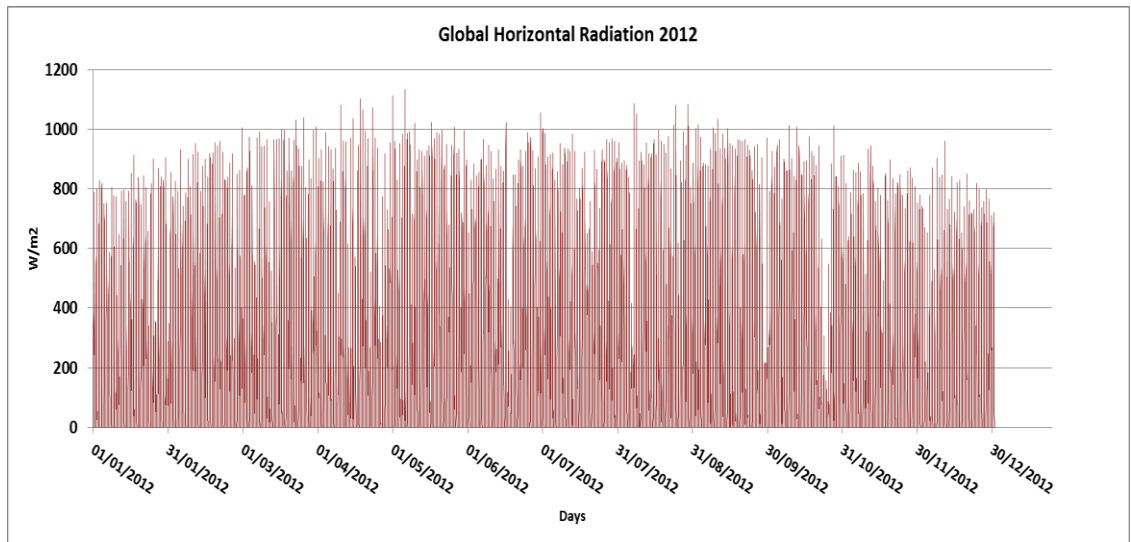


Figure G.27, Global Horizontal Radiation in Kingston, Jamaica for 2012

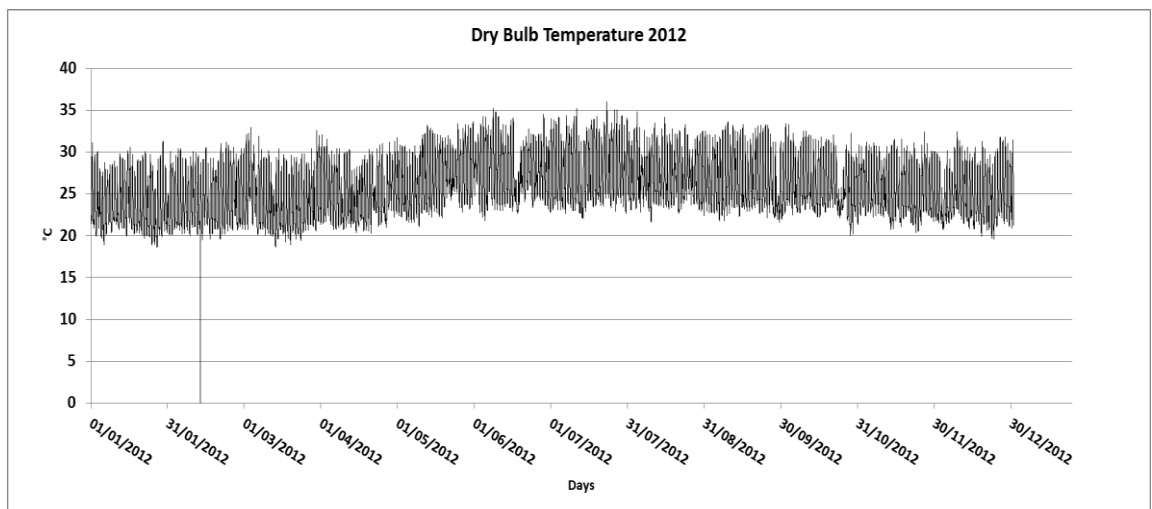


Figure G.28, Dry Bulb Temperature in Kingston, Jamaica for 2012

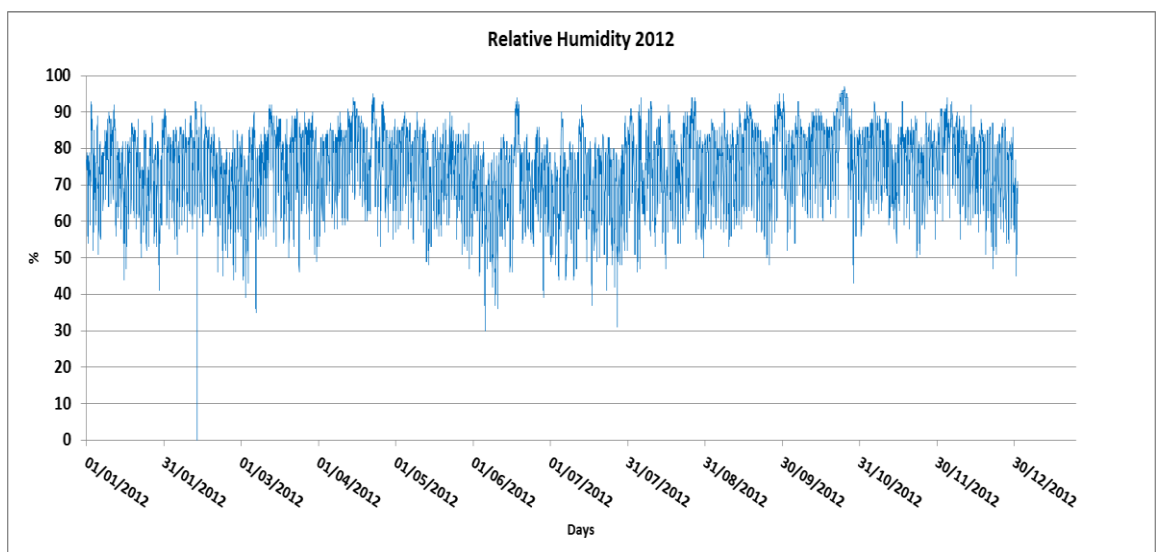


Figure G.29, Relative Humidity in Kingston, Jamaica for 2012

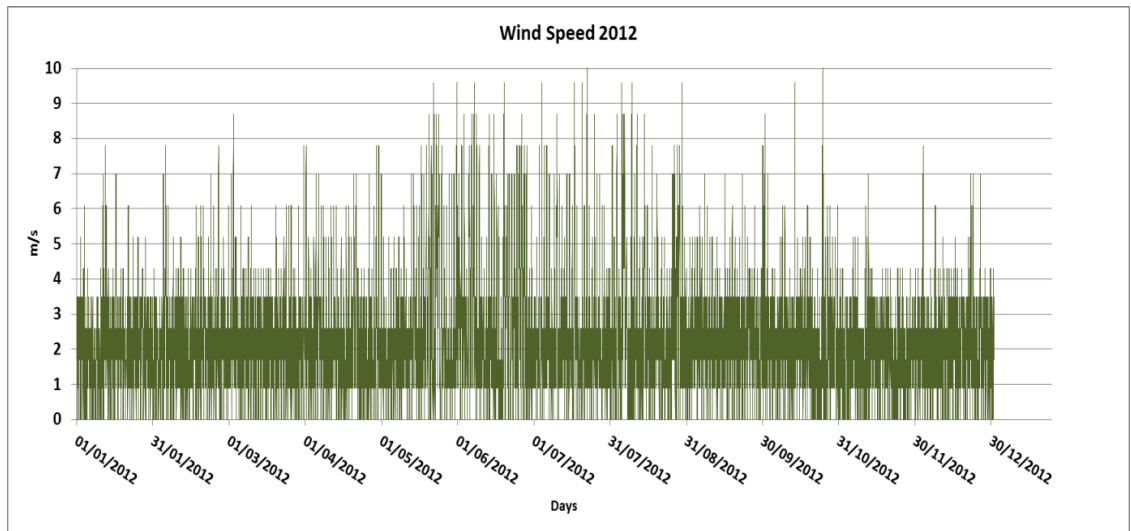


Figure G.30, Wind Speed in Kingston, Jamaica for 2012

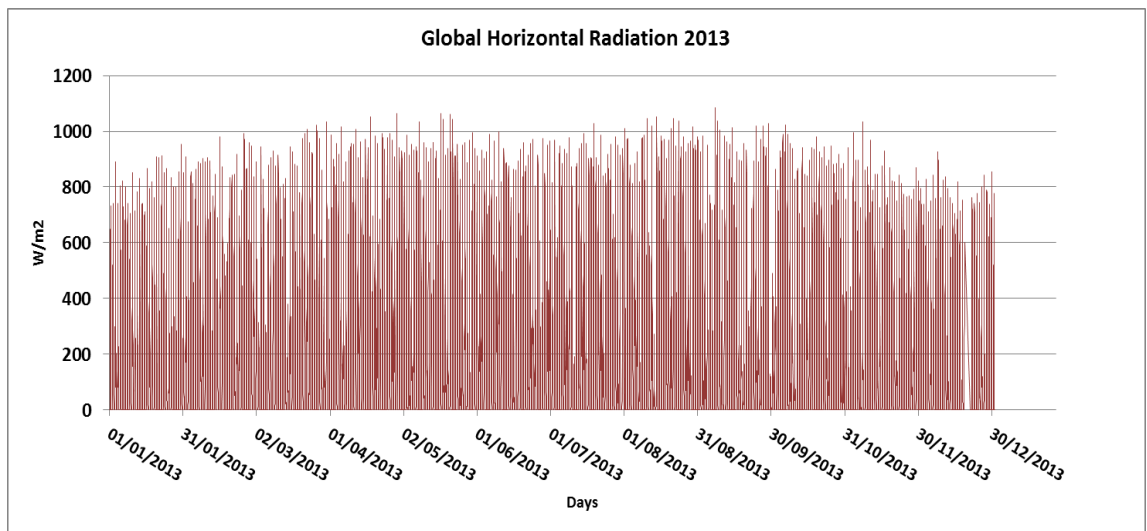


Figure G.31, Global Horizontal Radiation in Kingston, Jamaica for 2013

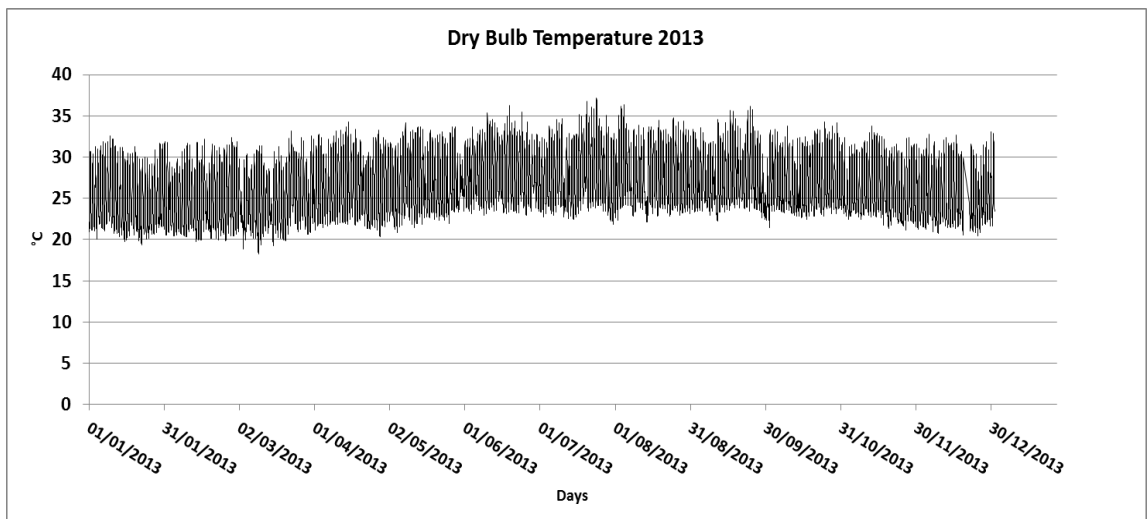


Figure G.32, Dry Bulb Temperature in Kingston, Jamaica for 2013

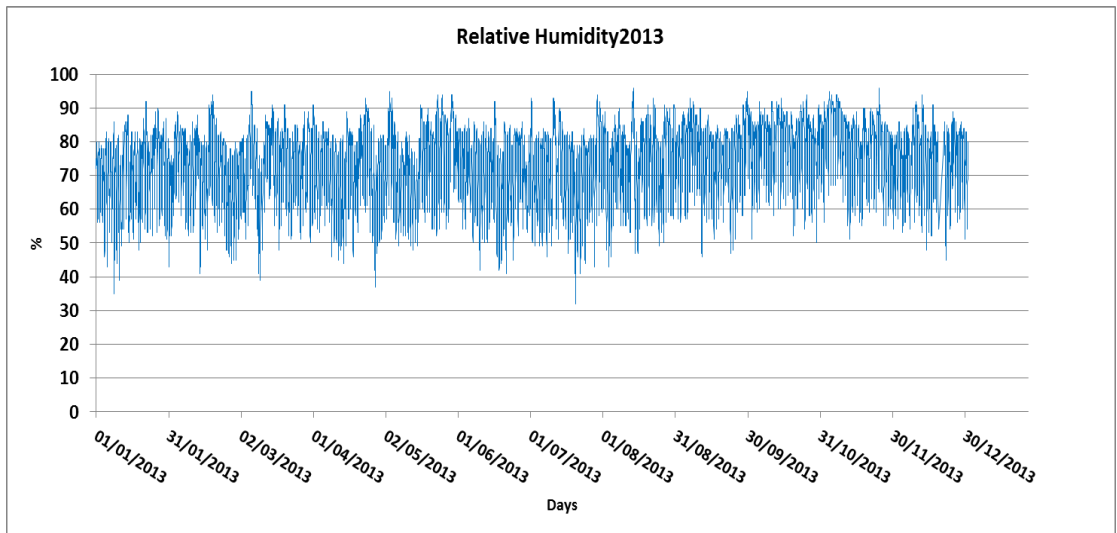


Figure G.33, Relative Humidity in Kingston, Jamaica for 2013

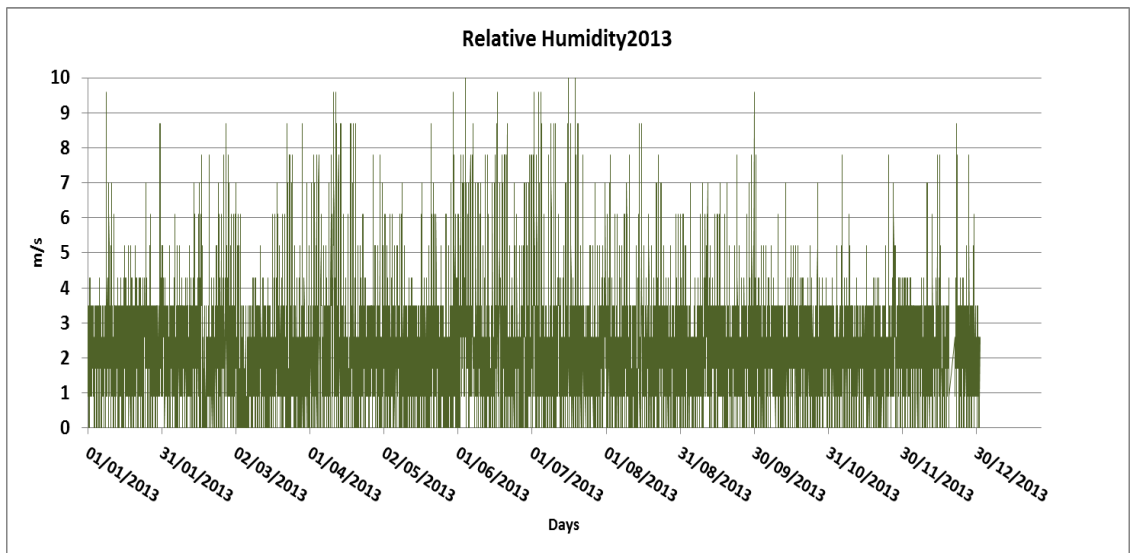


Figure G.34, Wind Speed in Kingston, Jamaica for 2013

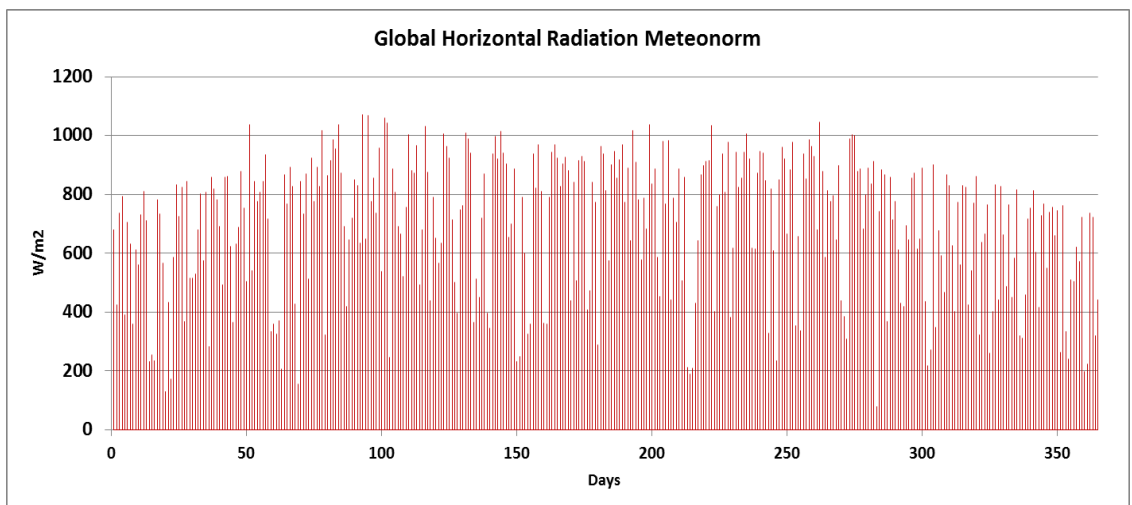


Figure G.35, Global Horizontal Radiation in Kingston, Jamaica from Meteonorm Typical Meteorological Year

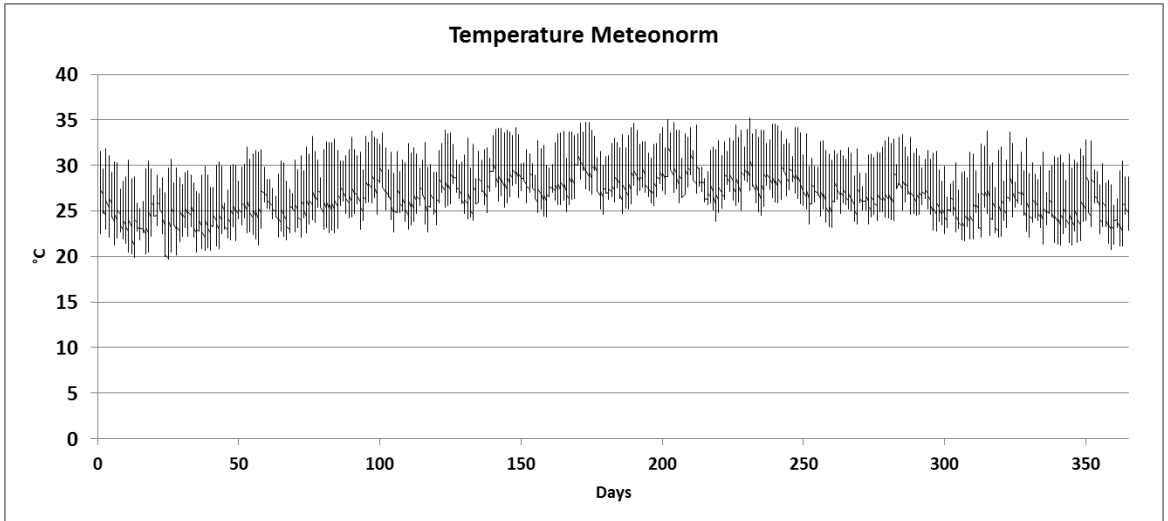


Figure G.36, Dry Bulb Temperature in Kingston, Jamaica from Meteonorm Typical Meteorological Year

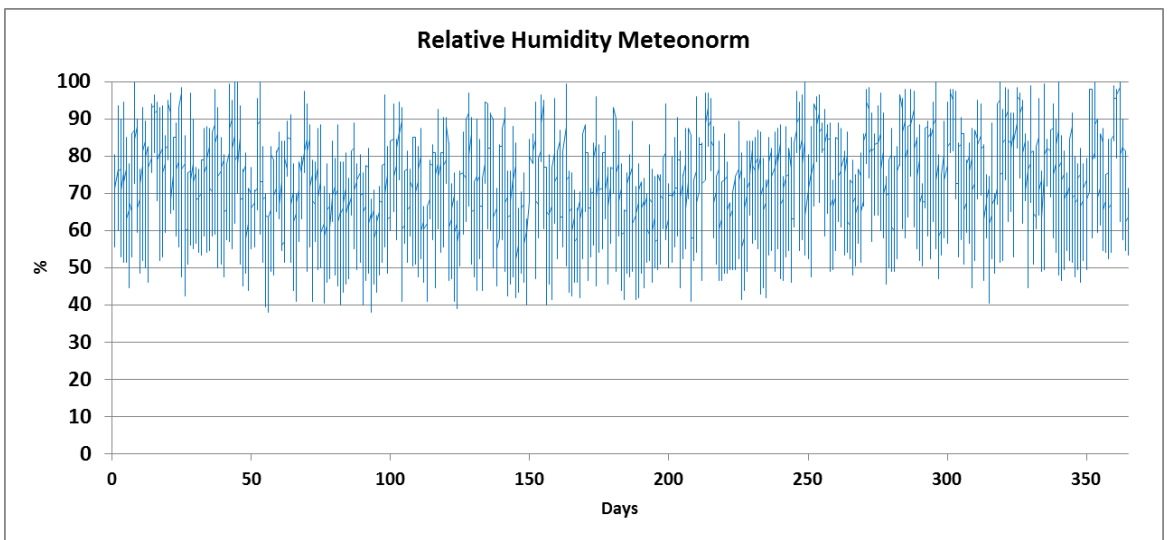


Figure G.37, Relative Humidity in Kingston, Jamaica from Meteonorm Typical Meteorological Year

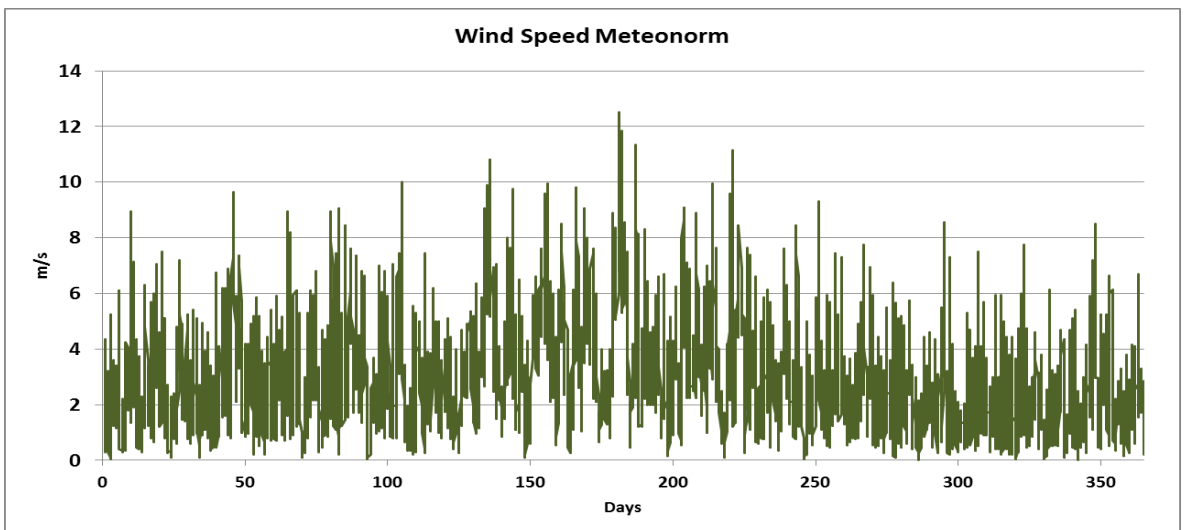


Figure G.38, Wind Speed in Kingston, Jamaica from Meteonorm Typical Meteorological Year

G.5 Steps of the Solar Hydrogen Potential Map Generation Process

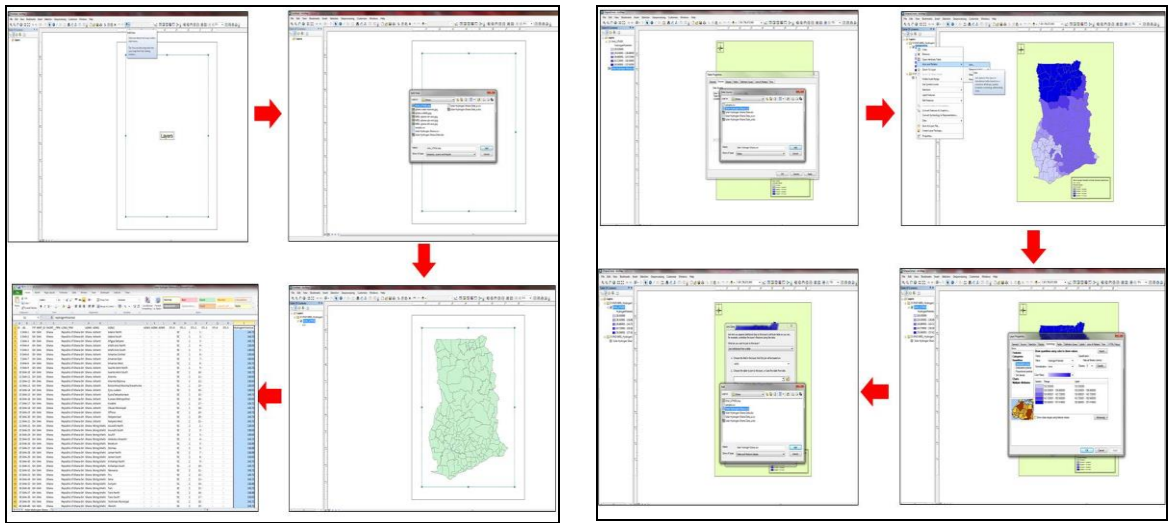


Figure G.39, Solar hydrogen potential map generation steps

The steps of the map generation process are seen schematically in Figure G.39 and are:

1. ArcMap is opened and layer added: file Ghana.shp or Indonesia.shp or Jamaica.shp
2. A data base is created based on the dbf file that contains the information of the country map (the .shp file). The file that is created has the same format as the shp file and a column is added in the end with the calculation of the Solar Hydrogen Potential results.
3. The created database is added to the map through the layer and the map properties.
4. The colours of the maps according to the hydrogen potential range are defined through the layer properties (symbology – quantities – graduated colour – classification – range and colour label)
5. The result is the country's map of solar hydrogen potential in thousands of kg of hydrogen per km² by administrative area.

Appendix H. Economic Analysis of Case Studies

H.1 Connection of the PV Array to the Electrolyser through a Battery Bank for Ghana Case Studies

Metal Hydride Storage

Prices, costs and sensitivity analysis of this scenario can be seen in Tables H.1 to H.3.

Table H.1, Scenario 2a - Distribution of costs

Component	Sizes	Capital Cost (£)	O&M(% of investment costs)	Lifetime (years)
PV System	54kW	49,140	2%	20
Battery bank (Lead Acid)	48V/3500Ah	22,000	2%	10
PEM Electrolyser	2Nm ³ /h per electrolyser 20 cells, 4 stacks	7,673 per Nm ³ /h	2%	10
MH Storage		1,000 per Nm ³	2%	20

Table H.2, Present cost analysis model for the solar hydrogen system, referring to scenario 2a

Life Cycle Cost Evaluation Model for the Different Combinations of the Solar Hydrogen System									
Input Parameters									
PV System Capital Cost (£/kW)	Electrolyser Capital Cost (£ per Nm ³ /h)	Batteries Cost (£ per kWh)	PV system Size (kW)	Size of Batteries (Wh)	Electrolyser Size (Nm ³ /h)	Electrolysers number	PV System Life (ys)	Electrolyser System Life (ys)	Annual Hydrogen Production of the System (kg)
910	7673	0.1	54	220000	2	2	20	10	800
Calculated Parameters									
PV System Capital Cost including battery (£)	Capital Cost of Electrolyser System (£)	Capital Cost of Hydrogen Storage System (£)	O&M Costs of the PV System (£)	O&M Costs of the Electrolyser System (£)	O&M Costs of the Hydrogen Storage System (£)	Discount Rate r	Life Cycle (ys)		
71140	30692	744500	1423	614	14890	0.05	20		
System Size	Year (i)	PV-Electrolyser Capital Cost (£)	O&M of Total system Cost (£)	Total Costs (£)	Present Value (£)	Annual Hydrogen Production (kg)	Unit Cost of H ₂ (£/kg)		
	0	846332	16926.64	863258.64	863258.64				
	1	0	2835.12	2835.12	2700.12				
	2	0	2835.12	2835.12	2571.54				
	3	0	2835.12	2835.12	2449.09				
	4	0	2835.12	2835.12	2332.46				
	5	0	2835.12	2835.12	2221.39				
	6	0	2835.12	2835.12	2115.61				
	7	0	2835.12	2835.12	2014.87				
	8	0	2835.12	2835.12	1918.92				
	9	0	2835.12	2835.12	1827.55				
Battery and Electrolyser replacement	10	26346	2835.12	29181.12	17914.68	800	57.17		
	11	0	2835.12	2835.12	1657.64				
	12	0	2835.12	2835.12	1578.70				
	13	0	2835.12	2835.12	1503.53				
	14	0	2835.12	2835.12	1431.93				
	15	0	2835.12	2835.12	1363.74				
	16	0	2835.12	2835.12	1298.80				
	17	0	2835.12	2835.12	1236.96				
	18	0	2835.12	2835.12	1178.05				
	19	0	2835.12	2835.12	1121.95				
	20	0	2835.12	2835.12	1068.53				
TOTAL						914765			

Table H.3, Sensitivity analysis of the scenario 2a system

Sensitivity Analysis	
System Part	Percentages (%)
PV system	8.4
Electrolyser	3.6
Metal Hydride Storage	88

The total present cost is £914,765 which corresponds to a unit cost of £57.37 per kg of H₂. The sensitivity analysis shows that the metal hydride storage is responsible for the biggest part of the costs.

Compressed Gas Storage Cylinders

Prices, costs and sensitivity analysis of this scenario can be seen in Tables H.4 and H.5.

Table H.4, Present cost analysis model for the solar hydrogen system, referring to scenario 2b

Life Cycle Cost Evaluation Model for the Different Combinations of the Solar Hydrogen System									
Input Parameters									
PV System Capital Cost (£/kW)	Electrolyser Capital Cost (£ per Nm ³ /h)	Batteries Cost (£ per kWh)	PV system Size (kW)	Size of Batteries (Wh)	Electrolyser Size (Nm ³ /h)	Electrolysers number	PV System Life (ys)	Electrolyser System Life (ys)	Annual Hydrogen Production of the System (kg)
910	7673	0.1	54	220000	2	2	20	10	800
Calculated Parameters									
PV System Capital Cost (£)	Capital Cost of Electrolyser System (£)	Capital Cost of Hydrogen Storage System (£)	O&M Costs of the PV System (£)	O&M Costs of the Electrolyser System (£)	O&M Costs of the Hydrogen Storage System (£)	Discount Rate r	Life Cycle (ys)		
71140	30692	20326	1423	614	407	0.05	20		
System Size	Year (i)	PV-Electrolyser Capital Cost (£)	O&M of Total system Cost (£)	Total Costs (£)	Present Value (£)	Annual Hydrogen Production (kg)	Unit Cost of H ₂ (£/kg)		
	0	122158	2443.16	124601.00	124601.00	800	11.01		
	1	0	2835.12	2835.12	2700.12				
	2	0	2835.12	2835.12	2571.54				
	3	0	2835.12	2835.12	2449.09				
	4	0	2835.12	2835.12	2332.46				
	5	0	2835.12	2835.12	2221.39				
	6	0	2835.12	2835.12	2115.61				
	7	0	2835.12	2835.12	2014.87				
	8	0	2835.12	2835.12	1918.92				
	9	0	2835.12	2835.12	1827.55				
and Electrolyser repla	10	26346	2835.12	29181.12	17914.68				
	11	0	2835.12	2835.12	1657.64				
	12	0	2835.12	2835.12	1578.70				
	13	0	2835.12	2835.12	1503.53				
	14	0	2835.12	2835.12	1431.93				
	15	0	2835.12	2835.12	1363.74				
	16	0	2835.12	2835.12	1298.80				
	17	0	2835.12	2835.12	1236.96				
	18	0	2835.12	2835.12	1178.05				
	19	0	2835.12	2835.12	1121.95				
	20	0	2835.12	2835.12	1068.53				
TOTAL						176107			

Table H.5, Sensitivity analysis of the scenario 2b system

Sensitivity Analysis	
Sensitivity Analysis	Percentages (%)
PV system	58.2
Electrolyser	25.1
Compressed Gas Storage	16.6

The total present cost is £176,107 which corresponds to a unit cost of £11.01 per kg of H₂. The sensitivity analysis shows that the PV array is responsible for the biggest part of the costs.

Distribution of Hydrogen through a Piping system

Prices, costs and sensitivity analysis of this scenario can be seen in Tables H.6 and H.7.

Table H.6, Present cost analysis model for the solar hydrogen system, referring to scenario 2c

Life Cycle Cost Evaluation Model for the Different Combinations of the Solar Hydrogen System									
Input Parameters									
PV System Capital Cost (£/kW)	Electrolyser Capital Cost (£ per Nm ³ /h)	Batteries Cost (£ per kWh)	PV system Size (kW)	Size of Batteries (Wh)	Electrolyser Size (Nm ³ /h)	Electrolysers number	PV System Life (ys)	Electrolyser System Life (ys)	Annual Hydrogen Production of the System (kg)
910	7673	0.1	54	220000	2	2	20	10	800
Calculated Parameters									
PV System Capital Cost including battery (£)	Capital Cost of Electrolyser System (£)	Capital Cost of Hydrogen Storage System (£)	O&M Costs of the PV System (£)	O&M Costs of the Electrolyser System (£)	O&M Costs of the Hydrogen Storage System (£)	Discount Rate r	Life Cycle (ys)		
71140	30692	650000	1423	614	13000	0.05	20		
System Size	Year (i)	PV-Electrolyser Capital Cost (£)	O&M of Total system Cost (£)	Total Costs (£)	Present Value (£)	Annual Hydrogen Production (kg)	Unit Cost of H ₂ (£/kg)		
	0	751832	15036.64	766868.64	766868.64	800	51.15		
	1	0	2835.12	2835.12	2700.12				
	2	0	2835.12	2835.12	2571.54				
	3	0	2835.12	2835.12	2449.09				
	4	0	2835.12	2835.12	2332.46				
	5	0	2835.12	2835.12	2221.39				
	6	0	2835.12	2835.12	2115.61				
	7	0	2835.12	2835.12	2014.87				
	8	0	2835.12	2835.12	1918.92				
	9	0	2835.12	2835.12	1827.55				
and Electrolyser replac	10	26346	2835.12	29181.12	17914.68				
	11	0	2835.12	2835.12	1657.64				
	12	0	2835.12	2835.12	1578.70				
	13	0	2835.12	2835.12	1503.53				
	14	0	2835.12	2835.12	1431.93				
	15	0	2835.12	2835.12	1363.74				
	16	0	2835.12	2835.12	1298.80				
	17	0	2835.12	2835.12	1236.96				
	18	0	2835.12	2835.12	1178.05				
	19	0	2835.12	2835.12	1121.95				
	20	0	2835.12	2835.12	1068.53				
TOTAL						818375			

Table H.7, Sensitivity analysis of the scenario 2b system

Sensitivity Analysis	
System Part	Percentages (%)
PV system	9.5
Electrolyser	4.1
Hydrogen Pipeline	86.5

The total present cost is £818,375 which corresponds to a unit cost of £51.15 per kg of H₂. The sensitivity analysis shows that the hydrogen pipeline system is responsible for the biggest part of the costs.

H.2 Jamaica Case Studies Cost Analysis

The Jamaica case studies are sized according to the average daily cooking demand of a typical Jamaican household, which is 1.98kWh or 1.68kg of hydrogen per month, as showed in section 7.3.2, Chapter 7. According to this demand the system is sized as: 63kW PV array the no-battery case, and 50kW PV array and 150kWh battery, the battery case. The unit prices of the system components are the ones presented in section 8.2 of the thesis.

Direct connection of PV Array and Electrolyser: Scenario 1

Metal Hydride Storage

Prices, costs and sensitivity analysis of this scenario can be seen in Tables H.8 and H.9.

Table H.8, Present cost analysis model for the solar hydrogen system, referring to Jamaica scenario 1a

Life Cycle Cost Evaluation Model for the Different Combinations of the Solar Hydrogen System							
Input Parameters							
PV System Capital Cost (£/kW)	Electrolyser Capital Cost (£ per Nm ³ /h)	PV system Size (kW)	Electrolyser Size (Nm ³ /h)	Electrolysers number	PV System Life (ys)	Electrolyser System Life (ys)	Annual Hydrogen Production of the System (kg)
910	7673	63	2	2	20	10	653
Calculated Parameters							
PV System Capital Cost (£)	Capital Cost of Electrolyser System (£)	Capital Cost of Hydrogen Storage System (£)	O&M Costs of the PV System (£)	O&M Costs of the Electrolyser System (£)	O&M Costs of the Hydrogen Storage System (£)	Discount Rate r	Life Cycle (ys)
57330	30692	589,544	1146.6	613.84	11790.88	0.05	20
System Size	Year (i)	PV-Electrolyser Capital Cost (£)	O&M of Total system Cost (£)	Total Costs (£)	Present Value (£)	Annual Hydrogen Production (kg)	Unit Cost of H ₂ (£/kg)
	0	677566	13551.32	691117.32	691117.32	653	56.35
	1	0	2835.12	2835.12	2700.12		
	2	0	2835.12	2835.12	2571.54		
	3	0	2835.12	2835.12	2449.09		
	4	0	2835.12	2835.12	2332.46		
	5	0	2835.12	2835.12	2221.39		
	6	0	2835.12	2835.12	2115.61		
	7	0	2835.12	2835.12	2014.87		
	8	0	2835.12	2835.12	1918.92		
	9	0	2835.12	2835.12	1827.55		
Electrolyser Replacement	10	15346	2835.12	18181.12	11161.63		
	11	0	2835.12	2835.12	1657.64		
	12	0	2835.12	2835.12	1578.70		
	13	0	2835.12	2835.12	1503.53		
	14	0	2835.12	2835.12	1431.93		
	15	0	2835.12	2835.12	1363.74		
	16	0	2835.12	2835.12	1298.80		
	17	0	2835.12	2835.12	1236.96		
	18	0	2835.12	2835.12	1178.05		
	19	0	2835.12	2835.12	1121.95		
	20	0	2835.12	2835.12	1068.53		
TOTAL					735870		

Table H.9, Sensitivity analysis of the Jamaica scenario 1a system

Sensitivity Analysis	
System Part	Percentages (%)
PV system	8.5
Electrolyser	4.5
Metal Hydride Storage	87.0

Compressed Gas Storage

Prices, costs and sensitivity analysis of this scenario can be seen in Tables H.10 and H.11.

Table H.10, Present cost analysis model for the solar hydrogen system, referring to Jamaica scenario 1b

Life Cycle Cost Evaluation Model for the Different Combinations of the Solar Hydrogen System							
Input Parameters							
PV System Capital Cost (£/kW)	Electrolyser Capital Cost (£ per Nm ³ /h)	PV system Size (kW)	Electrolyser Size (Nm ³ /h)	Electrolysers number	PV System Life (ys)	Electrolyser System Life (ys)	Annual Hydrogen Production of the System (kg)
910	7673	63	2	2	20	10	653
Calculated Parameters							
PV System Capital Cost (£)	Capital Cost of Electrolyser System (£)	Capital Cost of Hydrogen Storage System (£)	O&M Costs of the PV System (£)	O&M Costs of the Electrolyser System (£)	O&M Costs of the Hydrogen Storage System (£)	Discount Rate r	Life Cycle (ys)
57330	30692	16079	1147	614	322	0.05	20
System Size	Year (i)	PV-Electrolyser Capital Cost (£)	O&M of Total system Cost (£)	Total Costs (£)	Present Value (£)	Annual Hydrogen Production (kg)	Unit Cost of H ₂ (£/kg)
	0	104101	2082.01	106182.66	106182.66	653	11.56
	1	0	2835.12	2835.12	2700.12		
	2	0	2835.12	2835.12	2571.54		
	3	0	2835.12	2835.12	2449.09		
	4	0	2835.12	2835.12	2332.46		
	5	0	2835.12	2835.12	2221.39		
	6	0	2835.12	2835.12	2115.61		
	7	0	2835.12	2835.12	2014.87		
	8	0	2835.12	2835.12	1918.92		
	9	0	2835.12	2835.12	1827.55		
Electrolyser Replacement	10	15346	2835.12	18181.12	11161.63		
	11	0	2835.12	2835.12	1657.64		
	12	0	2835.12	2835.12	1578.70		
	13	0	2835.12	2835.12	1503.53		
	14	0	2835.12	2835.12	1431.93		
	15	0	2835.12	2835.12	1363.74		
	16	0	2835.12	2835.12	1298.80		
	17	0	2835.12	2835.12	1236.96		
	18	0	2835.12	2835.12	1178.05		
	19	0	2835.12	2835.12	1121.95		
	20	0	2835.12	2835.12	1068.53		
TOTAL					150936		

Table H.11, Sensitivity analysis of the Jamaica scenario 1b system

Sensitivity Analysis	
System Part	Percentages (%)
PV system	55.1%
Electrolyser	29.5%
Compressed Gas Storage	15.4%

Hydrogen Pipeline

Prices, costs and sensitivity analysis of this scenario can be seen in Tables H.12 and H.13.

Table H.12, Present cost analysis model for the solar hydrogen system, referring to Jamaica scenario 1c

Life Cycle Cost Evaluation Model for the Different Combinations of the Solar Hydrogen System							
Input Parameters							
PV System Capital Cost (£/kW)	Electrolyser Capital Cost (£ per Nm ³ /h)	PV system Size (kW)	Electrolyser Size (Nm ³ /h)	Electrolysers number	PV System Life (ys)	Electrolyser System Life (ys)	Annual Hydrogen Production of the System (kg)
910	7673	63	2	2	20	10	653
Calculated Parameters							
PV System Capital Cost (£)	Capital Cost of Electrolyser System (£)	Capital Cost of Hydrogen Storage System (£)	O&M Costs of the PV System (£)	O&M Costs of the Electrolyser System (£)	O&M Costs of the Hydrogen Storage System (£)	Discount Rate r	Life Cycle (ys)
57330	30692	650000	1147	614	32500	0.05	20
System Size	Year (i)	PV-Electrolyser Capital Cost (£)	O&M of Total system Cost (£)	Total Costs (£)	Present Value (£)	Annual Hydrogen Production (kg)	Unit Cost of H ₂ (£/kg)
	0	738022	34260.44	772282.44	772282.44	653	62.56
	1	0	2835.12	2835.12	2700.12		
	2	0	2835.12	2835.12	2571.54		
	3	0	2835.12	2835.12	2449.09		
	4	0	2835.12	2835.12	2332.46		
	5	0	2835.12	2835.12	2221.39		
	6	0	2835.12	2835.12	2115.61		
	7	0	2835.12	2835.12	2014.87		
	8	0	2835.12	2835.12	1918.92		
	9	0	2835.12	2835.12	1827.55		
Electrolyser Replacement	10	15346	2835.12	18181.12	11161.63		
	11	0	2835.12	2835.12	1657.64		
	12	0	2835.12	2835.12	1578.70		
	13	0	2835.12	2835.12	1503.53		
	14	0	2835.12	2835.12	1431.93		
	15	0	2835.12	2835.12	1363.74		
	16	0	2835.12	2835.12	1298.80		
	17	0	2835.12	2835.12	1236.96		
	18	0	2835.12	2835.12	1178.05		
	19	0	2835.12	2835.12	1121.95		
	20	0	2835.12	2835.12	1068.53		
TOTAL					817035		

Table H.13, Sensitivity analysis of the Jamaica scenario 1c system

Sensitivity Analysis	
System Part	Percentages (%)
PV system	7.6
Electrolyser	4.1
Hydrogen Pipeline	88.4

Connection of the PV Array to the Electrolyser through a Battery Bank – Scenario 2

The second scenario for the Jamaica case study includes battery storage in the PV system. According to this demand the system is sized as 50kW PV array and 150kWh battery.

Metal Hydride Storage

Prices, costs and sensitivity analysis of this scenario can be seen in Tables H.14 and H.15.

Table H.14, Present cost analysis model for the solar hydrogen system, referring to Jamaica scenario 2a

Life Cycle Cost Evaluation Model for the Different Combinations of the Solar Hydrogen System									
Input Parameters									
PV System Capital Cost (£/kW)	Electrolyser Capital Cost (£ per Nm ³ /h)	Batteries Cost (£ per kWh)	PV system Size (kW)	Size of Batteries (Wh)	Electrolyser Size (Nm ³ /h)	Electrolysers number	PV System Life (ys)	Electrolyser System Life (ys)	Annual Hydrogen Production of the System (kg)
910	7673	0.1	50	150000	2	2	20	10	627.6
Calculated Parameters									
PV System Capital Cost including battery (£)	Capital Cost of Electrolyser System (£)	Capital Cost of Hydrogen Storage System (£)	O&M Costs of the PV System (£)	O&M Costs of the Electrolyser System (£)	O&M Costs of the Hydrogen Storage System (£)	Discount Rate r	Life Cycle (ys)		
60500	30692	589,544	1210	614	11790.88	0.05	20		
System Size	Year (i)	PV-Electrolyser Capital Cost (£)	O&M of Total system Cost (£)	Total Costs (£)	Present Value (£)	Annual Hydrogen Production (kg)	Unit Cost of H ₂ (£/kg)		
	0	680736	13614.72	694350.72	694350.72	627.6	59.25		
	1	0	2835.12	2835.12	2700.12				
	2	0	2835.12	2835.12	2571.54				
	3	0	2835.12	2835.12	2449.09				
	4	0	2835.12	2835.12	2332.46				
	5	0	2835.12	2835.12	2221.39				
	6	0	2835.12	2835.12	2115.61				
	7	0	2835.12	2835.12	2014.87				
	8	0	2835.12	2835.12	1918.92				
	9	0	2835.12	2835.12	1827.55				
Battery and Electrolyser replacement	10	22846	2835.12	25681.12	15765.98				
	11	0	2835.12	2835.12	1657.64				
	12	0	2835.12	2835.12	1578.70				
	13	0	2835.12	2835.12	1503.53				
	14	0	2835.12	2835.12	1431.93				
	15	0	2835.12	2835.12	1363.74				
	16	0	2835.12	2835.12	1298.80				
	17	0	2835.12	2835.12	1236.96				
	18	0	2835.12	2835.12	1178.05				
	19	0	2835.12	2835.12	1121.95				
	20	0	2835.12	2835.12	1068.53				
TOTAL						743708			

Table H.15, Sensitivity analysis of the Jamaica scenario 2a system

Sensitivity Analysis	
System Part	Percentages (%)
PV system	8.9
Electrolyser	4.5
Metal Hydride Storage	86.6

Compressed Gas Storage

Prices, costs and sensitivity analysis of this scenario can be seen in Tables H.16 and H.17.

Table H.16, Present cost analysis model for the solar hydrogen system, referring to Jamaica scenario 2b

Life Cycle Cost Evaluation Model for the Different Combinations of the Solar Hydrogen System									
Input Parameters									
PV System Capital Cost (£/kW)	Electrolyser Capital Cost (£ per Nm ³ /h)	Batteries Cost (£ per kWh)	PV system Size (kW)	Size of Batteries (Wh)	Electrolyser Size (Nm ³ /h)	Electrolysers number	PV System Life (ys)	Electrolyser System Life (ys)	Annual Hydrogen Production of the System (kg)
910	7673	0.1	50	150000	2	2	20	10	627.6
Calculated Parameters									
PV System Capital Cost (£)	Capital Cost of Electrolyser System (£)	Capital Cost of Hydrogen Storage System (£)	O&M Costs of the PV System (£)	O&M Costs of the Electrolyser System (£)	O&M Costs of the Hydrogen Storage System (£)	Discount Rate r	Life Cycle (ys)		
60500	30692	16079	1210	614	322	0.05	20		
System Size	Year (i)	PV-Electrolyser Capital Cost (£)	O&M of Total system Cost (£)	Total Costs (£)	Present Value (£)	Annual Hydrogen Production (kg)	Unit Cost of H ₂ (£/kg)		
	0	107271	2145.41	109416.06	109416.06	627.6	12.65		
	1	0	2835.12	2835.12	2700.12				
	2	0	2835.12	2835.12	2571.54				
	3	0	2835.12	2835.12	2449.09				
	4	0	2835.12	2835.12	2332.46				
	5	0	2835.12	2835.12	2221.39				
	6	0	2835.12	2835.12	2115.61				
	7	0	2835.12	2835.12	2014.87				
	8	0	2835.12	2835.12	1918.92				
	9	0	2835.12	2835.12	1827.55				
Battery and Electrolyser replacement	10	22846	2835.12	25681.12	15765.98				
	11	0	2835.12	2835.12	1657.64				
	12	0	2835.12	2835.12	1578.70				
	13	0	2835.12	2835.12	1503.53				
	14	0	2835.12	2835.12	1431.93				
	15	0	2835.12	2835.12	1363.74				
	16	0	2835.12	2835.12	1298.80				
	17	0	2835.12	2835.12	1236.96				
	18	0	2835.12	2835.12	1178.05				
	19	0	2835.12	2835.12	1121.95				
	20	0	2835.12	2835.12	1068.53				
					TOTAL	158773			

Table H.17, Sensitivity analysis of the Jamaica scenario 2b system

Sensitivity Analysis	
System Part	Percentages (%)
PV system	56.4%
Electrolyser	28.6%
Compressed Gas Storage	15.0%

Hydrogen Pipeline

Prices, costs and sensitivity analysis of this scenario can be seen in Tables H.18 and H.19.

Table H.18, Present cost analysis model for the solar hydrogen system, referring to Jamaica scenario 2c

Life Cycle Cost Evaluation Model for the Different Combinations of the Solar Hydrogen System									
Input Parameters									
PV System Capital Cost (£/kW)	Electrolyser Capital Cost (£ per Nm ³ /h)	Batteries Cost (£ per kWh)	PV system Size (kW)	Size of Batteries (Wh)	Electrolyser Size (Nm ³ /h)	Electrolysers number	PV System Life (ys)	Electrolyser System Life (ys)	Annual Hydrogen Production of the System (kg)
910	7673	0.1	50	150000	2	2	20	10	627.6
Calculated Parameters									
PV System Capital Cost including battery (£)	Capital Cost of Electrolyser System (£)	Capital Cost of Hydrogen Storage System (£)	O&M Costs of the PV System (£)	O&M Costs of the Electrolyser System (£)	O&M Costs of the Hydrogen Storage System (£)	Discount Rate r	Life Cycle (ys)		
60500	30692	650000	1210	614	13000	0.05	20		
System Size	Year (i)	PV-Electrolyser Capital Cost (£)	O&M of Total system Cost (£)	Total Costs (£)	Present Value (£)	Annual Hydrogen Production (kg)	Unit Cost of H ₂ (£/kg)		
	0	741192	14823.84	756015.84	756015.84	627.6	64.16		
	1	0	2835.12	2835.12	2700.12				
	2	0	2835.12	2835.12	2571.54				
	3	0	2835.12	2835.12	2449.09				
	4	0	2835.12	2835.12	2332.46				
	5	0	2835.12	2835.12	2221.39				
	6	0	2835.12	2835.12	2115.61				
	7	0	2835.12	2835.12	2014.87				
	8	0	2835.12	2835.12	1918.92				
	9	0	2835.12	2835.12	1827.55				
Battery and Electrolyser replacement	10	22846	2835.12	25681.12	15765.98				
	11	0	2835.12	2835.12	1657.64				
	12	0	2835.12	2835.12	1578.70				
	13	0	2835.12	2835.12	1503.53				
	14	0	2835.12	2835.12	1431.93				
	15	0	2835.12	2835.12	1363.74				
	16	0	2835.12	2835.12	1298.80				
	17	0	2835.12	2835.12	1236.96				
	18	0	2835.12	2835.12	1178.05				
	19	0	2835.12	2835.12	1121.95				
	20	0	2835.12	2835.12	1068.53				
TOTAL						805373			

Table H.19, Sensitivity analysis of the Jamaica scenario 2c system

Sensitivity Analysis	
System Part	Percentages (%)
PV system	8.2
Electrolyser	4.1
Hydrogen Pipeline	87.7

H.3 Indonesia Case Studies Cost Analysis

The Indonesia case studies are sized according to the local household cooking demand, which is 2kWh or 2.7kg of hydrogen per month. According to this demand the system is sized as: 54kW PV array the no-battery case, and 36kW PV array and 150kWh battery, the battery case. The detailed tables presenting the cost benefit analysis of Indonesia case studies are presented below.

Direct connection of PV Array and Electrolyser: Scenario 1 - Metal Hydride Storage

Prices, costs and sensitivity analysis of this scenario can be seen in Tables H.20 and H.21.

Table H.20 , Present cost analysis model for the solar hydrogen system, referring to Indonesia scenario 1a

Life Cycle Cost Evaluation Model for the Different Combinations of the Solar Hydrogen System							
Input Parameters							
PV System Capital Cost (£/kW)	Electrolyser Capital Cost (£ per Nm ³ /h)	PV system Size (kW)	Electrolyser Size (Nm ³ /h)	Electrolysers number	PV System Life (ys)	Electrolyser System Life (ys)	Annual Hydrogen Production of the System (kg)
910	7673	54	2	2	20	10	670
Calculated Parameters							
PV System Capital Cost (£)	Capital Cost of Electrolyser System (£)	Capital Cost of Hydrogen Storage System (£)	O&M Costs of the PV System (£)	O&M Costs of the Electrolyser System (£)	O&M Costs of the Hydrogen Storage System (£)	Discount Rate r	Life Cycle (ys)
49140	30692	600000	982.8	613.84	12000	0.05	20
System Size	Year (j)	PV-Electrolyser Capital Cost (£)	O&M of Total system Cost (£)	Total Costs (£)	Present Value (£)	Annual Hydrogen Production (kg)	Unit Cost of H ₂ (£/kg)
	0	679832	13596.64	693428.64	693428.64		
	1	0	2835.12	2835.12	2700.12		
	2	0	2835.12	2835.12	2571.54		
	3	0	2835.12	2835.12	2449.09		
	4	0	2835.12	2835.12	2332.46		
	5	0	2835.12	2835.12	2221.39		
	6	0	2835.12	2835.12	2115.61		
	7	0	2835.12	2835.12	2014.87		
	8	0	2835.12	2835.12	1918.92		
	9	0	2835.12	2835.12	1827.55		
Electrolyser Replacement	10	15346	2835.12	18181.12	11161.63		
	11	0	2835.12	2835.12	1657.64		
	12	0	2835.12	2835.12	1578.70		
	13	0	2835.12	2835.12	1503.53		
	14	0	2835.12	2835.12	1431.93		
	15	0	2835.12	2835.12	1363.74		
	16	0	2835.12	2835.12	1298.80		
	17	0	2835.12	2835.12	1236.96		
	18	0	2835.12	2835.12	1178.05		
	19	0	2835.12	2835.12	1121.95		
	20	0	2835.12	2835.12	1068.53		

Table H.21, Sensitivity analysis of the Indonesia scenario 1a system

Sensitivity Analysis	
System Part	Percentages (%)
PV system	7.2
Electrolyser	4.5
Metal Hydride Storage	88.3

Compressed Gas Storage

Prices, costs and sensitivity analysis of this scenario can be seen in Tables H.22 and H.23.

Table H.22, Present cost analysis model for the solar hydrogen system, referring to Indonesia scenario 1b

Life Cycle Cost Evaluation Model for the Different Combinations of the Solar Hydrogen System							
Input Parameters							
PV System Capital Cost (£/kW)	Electrolyser Capital Cost (£ per Nm ³ /h)	PV system Size (kW)	Electrolyser Size (Nm ³ /h)	Electrolysers number	PV System Life (ys)	Electrolyser System Life (ys)	Annual Hydrogen Production of the System (kg)
910	7673	54	2	2	20	10	670
Calculated Parameters							
PV System Capital Cost (£)	Capital Cost of Electrolyser System (£)	Capital Cost of Hydrogen Storage System (£)	O&M Costs of the PV System (£)	O&M Costs of the Electrolyser System (£)	O&M Costs of the Hydrogen Storage System (£)	Discount Rate r	Life Cycle (ys)
49140	30692	16218	983	614	324	0.05	20
System Size	Year (i)	PV-Electrolyser Capital Cost (£)	O&M of Total system Cost (£)	Total Costs (£)	Present Value (£)	Annual Hydrogen Production (kg)	Unit Cost of H ₂ (£/kg)
	0	96050	1921.00	97971.02	97971.02	670	10.65
	1	0	2835.12	2835.12	2700.12		
	2	0	2835.12	2835.12	2571.54		
	3	0	2835.12	2835.12	2449.09		
	4	0	2835.12	2835.12	2332.46		
	5	0	2835.12	2835.12	2221.39		
	6	0	2835.12	2835.12	2115.61		
	7	0	2835.12	2835.12	2014.87		
	8	0	2835.12	2835.12	1918.92		
	9	0	2835.12	2835.12	1827.55		
Electrolyser Replacement	10	15346	2835.12	18181.12	11161.63		
	11	0	2835.12	2835.12	1657.64		
	12	0	2835.12	2835.12	1578.70		
	13	0	2835.12	2835.12	1503.53		
	14	0	2835.12	2835.12	1431.93		
	15	0	2835.12	2835.12	1363.74		
	16	0	2835.12	2835.12	1298.80		
	17	0	2835.12	2835.12	1236.96		
	18	0	2835.12	2835.12	1178.05		
	19	0	2835.12	2835.12	1121.95		
	20	0	2835.12	2835.12	1068.53		
TOTAL					142724		

Table H.23, Sensitivity analysis of the Indonesia scenario 1b system

Sensitivity Analysis	
System Part	Percentages (%)
PV system	51.2%
Electrolyser	32.0%
CGS	16.9%

Hydrogen Pipeline

Prices, costs and sensitivity analysis of this scenario can be seen in Tables H.24 and H.25.

Table H.24, Present cost analysis model for the solar hydrogen system, referring to Indonesia scenario 1c

Life Cycle Cost Evaluation Model for the Different Combinations of the Solar Hydrogen System							
Input Parameters							
PV System Capital Cost (£/kW)	Electrolyser Capital Cost (£ per Nm ³ /h)	PV system Size (kW)	Electrolyser Size (Nm ³ /h)	Electrolysers number	PV System Life (ys)	Electrolyser System Life (ys)	Annual Hydrogen Production of the System (kg)
910	7673	54	2	2	20	10	670
Calculated Parameters							
PV System Capital Cost (£)	Capital Cost of Electrolyser System (£)	Capital Cost of Hydrogen Distribution System (£)	O&M Costs of the PV System (£)	O&M Costs of the Electrolyser System (£)	O&M Costs of the Hydrogen Storage System (£)	Discount Rate r	Life Cycle (ys)
49140	30692	650000	983	614	32500	0.05	20
System Size	Year (i)	PV-Electrolyser Capital Cost (£)	O&M of Total system Cost (£)	Total Costs (£)	Present Value (£)	Annual Hydrogen Production (kg)	Unit Cost of H ₂ (£/kg)
	0	729832	34096.64	763928.64	763928.64	670	60.35
	1	0	2835.12	2835.12	2700.12		
	2	0	2835.12	2835.12	2571.54		
	3	0	2835.12	2835.12	2449.09		
	4	0	2835.12	2835.12	2332.46		
	5	0	2835.12	2835.12	2221.39		
	6	0	2835.12	2835.12	2115.61		
	7	0	2835.12	2835.12	2014.87		
	8	0	2835.12	2835.12	1918.92		
	9	0	2835.12	2835.12	1827.55		
Electrolyser Replacement	10	15346	2835.12	18181.12	11161.63		
	11	0	2835.12	2835.12	1657.64		
	12	0	2835.12	2835.12	1578.70		
	13	0	2835.12	2835.12	1503.53		
	14	0	2835.12	2835.12	1431.93		
	15	0	2835.12	2835.12	1363.74		
	16	0	2835.12	2835.12	1298.80		
	17	0	2835.12	2835.12	1236.96		
	18	0	2835.12	2835.12	1178.05		
	19	0	2835.12	2835.12	1121.95		
	20	0	2835.12	2835.12	1068.53		
TOTAL					808682		

Table H.25, Sensitivity analysis of the Indonesia scenario 1c system

Sensitivity Analysis	
System Part	Percentages (%)
PV system	6.6%
Electrolyser	4.1%
Hydrogen Pipeline	89.3%

Connection of the PV Array to the Electrolyser through a Battery Bank Scenario 2

In this case, the Electrolyser selected has a maximum production of 1.5Nm³/h, as it consists of 3 stacks, instead of 4 stacks as in all the other scenarios.

Metal Hydride Storage

Prices, costs and sensitivity analysis of this scenario can be seen in Tables H.26 and H.27.

Table H.26, Present cost analysis model for the solar hydrogen system, referring to Indonesia scenario 2a

Life Cycle Cost Evaluation Model for the Different Combinations of the Solar Hydrogen System									
Input Parameters									
PV System Capital Cost (£/kW)	Electrolyser Capital Cost (£ per Nm ³ /h)	Batteries Cost (£ per kWh)	PV system Size (kW)	Size of Batteries (Wh)	Electrolyser Size (Nm ³ /h)	Electrolysers number	PV System Life (ys)	Electrolyser System Life (ys)	Annual Hydrogen Production of the System (kg)
910	7673	0.1	36	150000	1.5	2	20	10	652
Calculated Parameters									
PV System Capital Cost including battery (£)	Capital Cost of Electrolyser System (£)	Capital Cost of Hydrogen Storage System (£)	O&M Costs of the PV System (£)	O&M Costs of the Electrolyser System (£)	O&M Costs of the Hydrogen Storage System (£)	Discount Rate	Life Cycle (ys)		
47760	23019	600000	955	460	12000	0.05	20		
System Size	Year (i)	PV-Electrolyser Capital Cost (£)	O&M of Total system Cost (£)	Total Costs (£)	Present Value (£)	Annual Hydrogen Production (kg)	Unit Cost of H2 (£/kg)		
	0	670779	13415.58	684194.58	684194.58				
	1	0	2835.12	2835.12	2700.12				
	2	0	2835.12	2835.12	2571.54				
	3	0	2835.12	2835.12	2449.09				
	4	0	2835.12	2835.12	2332.46				
	5	0	2835.12	2835.12	2221.39				
	6	0	2835.12	2835.12	2115.61				
	7	0	2835.12	2835.12	2014.87				
	8	0	2835.12	2835.12	1918.92				
	9	0	2835.12	2835.12	1827.55				
Battery and Electrolyser replacement	10	22846	2835.12	25681.12	15765.98	652	56.25		
	11	0	2835.12	2835.12	1657.64				
	12	0	2835.12	2835.12	1578.70				
	13	0	2835.12	2835.12	1503.53				
	14	0	2835.12	2835.12	1431.93				
	15	0	2835.12	2835.12	1363.74				
	16	0	2835.12	2835.12	1298.80				
	17	0	2835.12	2835.12	1236.96				
	18	0	2835.12	2835.12	1178.05				
	19	0	2835.12	2835.12	1121.95				
	20	0	2835.12	2835.12	1068.53				
TOTAL						733552			

Table H.27, Sensitivity analysis of the Indonesia scenario 2a system

Sensitivity Analysis	
System Part	Percentages (%)
PV system	7.1%
Electrolyser	3.4%
Metal Hydride Storage	89.4%

Compressed Gas Storage

Prices, costs and sensitivity analysis of this scenario can be seen in Tables H.28 and H.29.

Table H.28, Present cost analysis model for the solar hydrogen system, referring to Indonesia scenario 2b

Life Cycle Cost Evaluation Model for the Different Combinations of the Solar Hydrogen System									
Input Parameters									
PV System Capital Cost (£/kW)	Electrolyser Capital Cost (£ per Nm ³ /h)	Batteries Cost (£ per kWh)	PV system Size (kW)	Size of Batteries (Wh)	Electrolyser Size (Nm ³ /h)	Electrolysers number	PV System Life (ys)	Electrolyser System Life (ys)	Annual Hydrogen Production of the System (kg)
910	7673	0.1	36	150000	1.5	2	20	10	652
Calculated Parameters									
PV System Capital Cost (£)	Capital Cost of Electrolyser System (£)	Capital Cost of Hydrogen Storage System (£)	O&M Costs of the PV System (£)	O&M Costs of the Electrolyser System (£)	O&M Costs of the Hydrogen Storage System (£)	Discount Rate r	Life Cycle (ys)		
47760	23019	16218	955	460	324	0.05	20		
System Size	Year (i)	PV-Electrolyser Capital Cost (£)	O&M of Total system Cost (£)	Total Costs (£)	Present Value (£)	Annual Hydrogen Production (kg)	Unit Cost of H ₂ (£/kg)		
	0	86997	1739.94	88736.96	88736.96	652	10.59		
	1	0	2835.12	2835.12	2700.12				
	2	0	2835.12	2835.12	2571.54				
	3	0	2835.12	2835.12	2449.09				
	4	0	2835.12	2835.12	2332.46				
	5	0	2835.12	2835.12	2221.39				
	6	0	2835.12	2835.12	2115.61				
	7	0	2835.12	2835.12	2014.87				
	8	0	2835.12	2835.12	1918.92				
	9	0	2835.12	2835.12	1827.55				
Battery and Electrolyser replacement	10	22846	2835.12	25681.12	15765.98				
	11	0	2835.12	2835.12	1657.64				
	12	0	2835.12	2835.12	1578.70				
	13	0	2835.12	2835.12	1503.53				
	14	0	2835.12	2835.12	1431.93				
	15	0	2835.12	2835.12	1363.74				
	16	0	2835.12	2835.12	1298.80				
	17	0	2835.12	2835.12	1236.96				
	18	0	2835.12	2835.12	1178.05				
	19	0	2835.12	2835.12	1121.95				
	20	0	2835.12	2835.12	1068.53				
TOTAL						138094			

Table H.29, Sensitivity analysis of the Indonesia scenario 2b system

Sensitivity Analysis	
System Part	Percentages (%)
PV system	54.9%
Electrolyser	26.5%
CGS	18.6%

Hydrogen Pipeline

Prices, costs and sensitivity analysis of this scenario can be seen in Tables H.30 and H.31.

Table H.30, Present cost analysis model for the solar hydrogen system, referring to Indonesia scenario 2c

Life Cycle Cost Evaluation Model for the Different Combinations of the Solar Hydrogen System									
Input Parameters									
PV System Capital Cost (£/kW)	Electrolyser Capital Cost (£ per Nm ³ /h)	Batteries Cost (£ per kWh)	PV system Size (kW)	Size of Batteries (Wh)	Electrolyser Size (Nm ³ /h)	Electrolysers number	PV System Life (ys)	Electrolyser System Life (ys)	Annual Hydrogen Production of the System (kg)
910	7673	0.1	36	150000	1.5	2	20	10	652
Calculated Parameters									
PV System Capital Cost including battery (£)	Capital Cost of Electrolyser System (£)	Capital Cost of Hydrogen Distribution System (£)	O&M Costs of the PV System (£)	O&M Costs of the Electrolyser System (£)	O&M Costs of the Hydrogen Storage System (£)	Discount Rate r	Life Cycle (ys)		
47760	23019	650000	955	460	13000	0.05	20		
System Size	Year (i)	PV-Electrolyser Capital Cost (£)	O&M of Total system Cost (£)	Total Costs (£)	Present Value (£)	Annual Hydrogen Production (kg)	Unit Cost of H ₂ (£/kg)		
	0	720779	14415.58	735194.58	735194.58	652	60.17		
	1	0	2835.12	2835.12	2700.12				
	2	0	2835.12	2835.12	2571.54				
	3	0	2835.12	2835.12	2449.09				
	4	0	2835.12	2835.12	2332.46				
	5	0	2835.12	2835.12	2221.39				
	6	0	2835.12	2835.12	2115.61				
	7	0	2835.12	2835.12	2014.87				
	8	0	2835.12	2835.12	1918.92				
	9	0	2835.12	2835.12	1827.55				
Battery and Electrolyser replacement	10	22846	2835.12	25681.12	15765.98				
	11	0	2835.12	2835.12	1657.64				
	12	0	2835.12	2835.12	1578.70				
	13	0	2835.12	2835.12	1503.53				
	14	0	2835.12	2835.12	1431.93				
	15	0	2835.12	2835.12	1363.74				
	16	0	2835.12	2835.12	1298.80				
	17	0	2835.12	2835.12	1236.96				
	18	0	2835.12	2835.12	1178.05				
	19	0	2835.12	2835.12	1121.95				
	20	0	2835.12	2835.12	1068.53				
TOTAL						784552			

Table H.31, Sensitivity analysis of the Indonesia scenario 2c system

Sensitivity Analysis	
System Part	Percentages (%)
PV system	6.6%
Electrolyser	3.2%
Hydrogen Pipeline	90.2%

H.4 Marginal Abatement Curves Calculation Methodology

The MAC curves created are based on a format provided by Somar Company in form of a Microsoft Excel spread sheet. The required input data for this software are the project name, capital cost and annual benefit, and can be seen in Figures H.1 to H.3

Marginal Abatement Cost (MAC) Curve Calculator							
						somar	
Discount rate	4%	Ghana Case Study					
Reduction target (thousand tonnes)	0.243						
Project name		No battery - CGS	No battery - Pipeline	No battery - MH	Battery - CGS	Battery - Pipeline	Battery - MH
Capital cost	(£)	121,452	751,126	845,626	122,158	751,832	846,332
Annual benefit/cost	(£)	2,140	2,140	2,140	2,140	2,140	2,140
Annual average CO ₂ savings for project	(tonnes/year)	256	256	256	256	256	256
Project life	(years)	20	20	20	20	20	20
NPV	(£)	91,037	720,711	815,211	91,743	721,417	815,917
MAC (carbon not discounted)	(£/tonne)	0 17.8	140.8	159.2	17.9	140.9	159.4
Discounted life savings of carbon	(tonnes)	0 3,638	3,638	3,638	3,638	3,638	3,638
MAC (carbon discounted)	(£/tonne)	0 25.0	198.1	224.1	25.2	198.3	224.3
Cumulative savings for all projects	(thousand tonnes/year)	0 0.3	0.5	0.8	1.0	1.3	1.5

Figure H.1, Marginal Abatement Curves Calculation for Ghana

Marginal Abatement Cost (MAC) Curve Calculator							
						somar	
Discount rate	4%	Jamaica Case Study					
Reduction target (thousand tonnes)	0.175						
Project name		No battery - CGS	No battery - MH	No battery - Pipeline	Battery - CGS	Battery - MH	Battery - Pipeline
Capital cost	(£)	108,348	677,566	738,022	111,518	680,736	741,192
Annual benefit/cost	(£)	1,000	1,000	1,000	1,000	1,000	1,000
Annual average CO ₂ savings for project	(tonnes/year)	175.00	175.00	175.00	175.00	175.00	175.00
Project life	(years)	20	20	20	20	20	20
NPV	(£)	94,135	663,354	723,810	97,305	666,524	726,980
MAC (carbon not discounted)	(£/tonne)	0 26.9	189.5	206.8	27.8	190.4	207.7
Discounted life savings of carbon	(tonnes)	0 2,487	2,487	2,487	2,487	2,487	2,487
MAC (carbon discounted)	(£/tonne)	0 37.8	266.7	291.0	39.1	268.0	292.3
Cumulative savings for all projects	(thousand tonnes/year)	0 0.2	0.4	0.5	0.7	0.9	1.1

Figure H.2, Marginal Abatement Curves Calculation for Jamaica

Marginal Abatement Cost (MAC) Curve Calculator							
Discount rate	4%	Indonesia Case Study		somar			
Reduction target (thousand tonnes)	0.243						
Project name		No battery - CGS	No battery - Pipeline	No battery - MH	Battery - CGS	Battery - Pipeline	Battery - MH
Capital cost	(£)	96,050	729,832	679,832	86,997	720,779	670,779
Annual benefit/cost	(£)	3,200	3,200	3,200	3,200	3,200	3,200
Annual average CO ₂ savings for project	(tonnes/year)	180	180	180	180	180	180
Project life	(years)	20	20	20	20	20	20
NPV	(£)	50,570	684,352	634,352	41,517	675,299	625,299
MAC (carbon not discounted)	(£/tonne)	0	14.0	190.1	176.2	11.5	187.6
Discounted life savings of carbon	(tonnes)	0	2,558	2,558	2,558	2,558	2,558
MAC (carbon discounted)	(£/tonne)	0	19.8	267.5	248.0	16.2	264.0
Cumulative savings for all projects	(thousand tonnes/year)	0	0.2	0.4	0.5	0.7	0.9
							1.1

Figure H.3, Marginal Abatement Curves Calculation for Indonesia

H.5 Quotation of the metal hydride tanks

Quotation from Pragma Industries regarding the price of the metal hydride tanks can be seen in Figure H.4.



SAS au capital de 1 272 670 €
RCS 478 038 219 00042 - APE 7490 B
TVA intr. FR30 478 038 219
Z.A. de la Négresse - 40 rue Chapelet - 64200 Biarritz, France
Phone : +33 559 512 755 -- Fax : +33 559 230 798
www.pragma-industries.com

Bill To: Miss Evangelia Topriska
Brunel University
Elliott Jaques 087 Building
Uxbridge, Middlesex, UB8 3PH - UK
Evangelia.Topriska@brunel.ac.uk

Quotation

DATE December 5, 2014
Quotation # QUO141205-06A
Customer ID
VAT ID
FC Market ref.

Quotation valid until: January 4, 2015
Prepared by: Christophe Bruniau

Delivery*: 14 weeks

Description	Qty	Unit Price	Amount
MH10M Metal hydride storage tank Capacity: 5 x 2000 sl Tank weight: 150kg	1	15 800,00 €	15 800,00 €
MH10Mhe Stockage d'hydrogène sur hydrures métalliques Capacity: 10000 sl Tank weight: 120kg Heat exchanger design	1	14 390,00 €	14 390,00 €
NET VALUE			
PACKAGING and SHIPPING			TBA
% VAT			
VAT VALUE			
TOTAL VALUE			

INCOTERM:
For all products : tax-exempt intra-Community supply of goods
Country of origin :

Please let us know your VAT-no otherwise we have to charge 20% VAT

Payment
First deal: Payment with the order for first deal
For following orders, 30% is due at order, 70% at reception of the invoice
All payments are made by bank transfer to Pragma Industries account:
CICSB BIARRITZ - 1 Avenue du Maréchal Foch - 64200 BIARRITZ (France) - Account owner Pragma Industries
Account : 10057 19149 00062325701 25 --- IBAN FR76 1005 7191 4900 0623 2570 125 --- BIC (Swift Code) CMCIFRPP
Shipping and insurance charges are prepaid and added to invoice along with handling charges
Thank you for specifying to your banking institution the mention "Complete bank expenses paid by the purchaser"
**Delivery leadtime excludes office closing for holidays.*
If you have any questions concerning this quotation, contact:
christophe Bruniau, +33 559 512 628 chris.bruniau@pragma-industries.com

Thank you for your business

Figure H.4, Quotation from Pragma Industries regarding the price of the metal hydride tanks

Appendix I. Hydrogen Safety Report

ACP/EU Project 2012-2015 - The application of Solar-Powered Polymer Electrolyte Membrane (PEM) Electrolyser for the Sustainable Production of Hydrogen Gas as Fuel for Domestic Cooking

Safety Features for the Burning of Hydrogen Gas supplied from Cylinders

Prepared by Brunel University: Evangelia Topriska, Maria Kolokotroni, Zahir Dehouche

Deliverables of this Report:

1. Provide a solution that gives colour/visibility to hydrogen flame
2. Provide a solution that prevents hydrogen flame blow-back
3. Provide a solution that gives odour to hydrogen gas
4. Provide answers to the following questions:

Questions to be answered:

1. Is the odour agent/mechanism safe for human interaction and environmentally friendly, and how should it be applied?
2. Is the colouring agent/mechanism safe for human interaction and environmentally friendly, and how should it be applied?
3. What is the location of the blow-back prevention mechanism/arrestor w.r.t stove burner?
4. What is the location of the blow-back prevention mechanism/arrestor w.r.t gas cylinder?
5. Is a liquid sealing a part of the blow-back prevention mechanism?
- 6.

Introduction

Hydrogen is very flammable over a wide range of concentrations. Its flammability is much greater than that of common gases such as methane and it burns with a higher flame temperature (2207°C) and speed (1.8m/s). Its minimum ignition energy is 0.017 MJ and auto-ignition temperature 585°C (Gupta, 2009, p. 8). In standard atmospheric conditions hydrogen can be flammable in concentrations between 4-75% when this range for gasoline is 1-7.6%, and is detonable in 15-59% concentration range (Gupta, 2009, p. 10).

In addition to the flammability, hydrogen is colourless and odourless and therefore non detectable in any concentration by the human senses. These factors can therefore set a dangerous set of conditions for any human that is involved with hydrogen processes. The

hazards stemming from the use of hydrogen are related to explosions, fires or hydrogen mixtures with air in concentrations that can be dangerous for human. In more detail:

- Asphyxiation. This is a situation that may happen in cases that hydrogen displaces the air, and causes the oxygen level to lower at concentrations below 19.5% by volume.
- Overpressure injuries. They are injuries that can be caused as a result of overpressure and duration of a hydrogen explosion. There are cases that the lung rupture threshold can be surpassed and thus causing major body function failures.
- Thermal burns. In the case of a hydrogen fire, the radiant heat absorbed by the human body can cause major thermal injury. This is dependent on many factors such as exposure time, burning rate, heat of combustion, size of burning surface, ambient temperature and humidity and wind conditions.
- Cryogenic burns. They are caused in general by exposure of the skin to cold fluids and cold vessel surfaces. Liquefied hydrogen spills can result in such injuries and even hypothermia, in the most extreme case.

(Gupta, 2009, p. 541)

(All the above mentioned hazards are caused in the rare situation that an accident will occur from the mal-use of hydrogen or the physical damage it causes.)

A solution to the above could be the addition of odour to the hydrogen gas so that it can be easily detected by the human senses. Furthermore, the investigation of the addition of colour to the hydrogen flame is of great importance since when hydrogen is burned it produces a faint coloured flame that is difficult to detect under normal conditions.

Odour Agents

Odorization of gas is quite a deep-rooted process in the history of domestic and commercial gas use. It was first introduced in Germany in the 1880s' with the use of ethyl mercaptan to give odour to "blue water gas" in order to detect leaks. It is a method that has been extremely useful for humanity since it can prevent accidents that may occur from possible leaks.

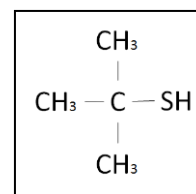
Today, odorization is a process that refers mainly to natural gas, which is the main gas for power production, distributed to be used in heating systems and also used for cooking. According to the current regulations, the presence of gas in the air must be detected by

smell at concentration of 1%. It is performed as a liquid injection of the odour agent or its vaporisation, according to whether the agent is gas or liquid. It is therefore involved in many domestic and human related applications, and has to fulfil basic safety standards. In the United Kingdom the odour agents used for the Natural Gas are mercaptans and triophanes, also known as TBM and DMS (Marcogaz, 2013; College of the Desert, 2001; BOC, 2011).

These odorization agents can also be tried for use suitability with hydrogen gas. More details regarding them are given in the following paragraphs:

TBM-Tertiary Butyl Mercaptan

TBM, whose chemical structure is shown in Figure I.1, is the main mercaptan component used in natural gas odorisation. Its chief characteristics are:



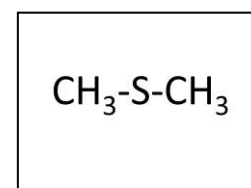
- Low odour threshold
- Gassy odour
- Good soil penetrability
- Highest resistance to oxidation of all the mercaptans

Figure I.1 chemical structure of TBM, source: (Arkema, 2013)

Nevertheless, it has two basic drawbacks that set it on occasions undesirable. It has a high freezing point (1.11°C), and therefore anti-freezing agents are required to be used in combination with it, when used in locations where the temperature falls below this point. Additionally it contains sulphur, which can have a poisonous effect on fuel cells but more importantly on human. If sulphur is burnt it produces sulphur dioxide, SO₂ which is toxic (Emsley, 1998, p. 198).

Dimethyl Sulphide (DMS)

DMS, whose chemical structure is shown in Figure I.2, is usually used sole or in combination with TBM and its main characteristics are:



- Low odour threshold
- Good soil penetrability
- Will not oxidise in the pipelines

Figure I.2, chemical structure of DMS, source: (Arkema, 2013)

DMS is the gas agent used by BOC to provide odour to hydrogen gas (BOC, 2011). They provide a solution in aluminium cylinders and with a current maximum pressure of 150 bar (<James.Brimicombe@boc.com>, 2013).

DMS, even though highly used and effective has also the basic disadvantage of containing sulphur. As mentioned, sulphur when burnt produces sulphur dioxide SO_2 which is a toxic gas hazardous for human and the environment as it is the main contributor to the creation of acid rain. Therefore, the idea to replace the traditional odour agents with non-sulphur ones, has been a dominant one during the last years (Arkema, 2013).

Non sulphur odorization

The world's first non-sulphur gas odorant, created in the R&D departments of Symrise, E.ON Ruhrgas AG of Essen, Germany, and the German Technical and Scientific Association for Gas and Water (Deutscher Verein des Gas- und Wasserfachs e.V. or DVGW), is called GASODOR® S-FREE (Symrise, 2013). Since its first implementation in 2001, GASODOR® S-FREE has been growing in demand and has been widely used all over the planet. It provides a safe and cheap solution to natural gas odourisation as it presents the following important characteristics:

- It has been tested for reaction with a variety of pipe materials and elastomers and has shown reassuring results of no interaction
- GASODOR® S-FREE has a very characteristic, strong and alarming smell that makes it easy to distinguish from everyday smells
- Has proved to be very stable during long periods of gas stagnation

(Schmeer et al., n.d.)

This odour agent could provide a safe solution for odorizing the hydrogen gas.

Acrylate and Acetophenone

Apart from the above, a solution to odourise hydrogen is to add an odorant based on Acrylate and Acetophenone, that has been tested and patented by the European Patent Office (Braun, et al., 2010). However, this patent does not seem to have been commercialised and thus is probably not available for use.

It should be noted that the use of a non-sulphur odour agent is not only safer for humans and the environment by avoiding the SO_2 creation, but also for the equipment involved in the hydrogen usage. As investigated by Imamura et al, (Imamura et al, 2005), sulphur compounds are not always suitable for hydrogen. In their experiments they tested the effect of sulphur and non-sulphur compounds on the performance of a fuel cell. Their results show a major deterioration of the electrical performance with the use of the conventional odoring agent TBM, because of the poisoning of the catalytic membrane. Additionally to mercaptan other sulphide compounds have been proved to be unsuitable for use in fuel cells, because the concentrations predicted by law to ensure the health and safety compliance are poisonous for the catalyst. Oppositely, a variety of sulphur free compounds, such as 2,3-butanedione ($\text{C}_4\text{H}_6\text{O}_2$) and 5-ethylidene-2-norbornene (C_9H_{12}) have been tested to be safe and effect free. Additionally, they present an unpleasant and offensive smell (Imamura et al, 2005).

In the case of the use of any of the above mentioned odorants what should be very carefully examined is the reaction of the odorants with the materials of the storage systems. Kopasz reports that in metal hydride storage the hydrogen absorption may be affected by the blockage of the adsorption sites from reaction with sulphides or other non-sulphur substances (Kopasz, 2006). Another problem with metal hydride storage is that the release of the hydrogen – odorant mix can be dissimilar with the odorant leaving in a more concentrated form in the initial withdrawal than the following ones. This might prove dangerous as the safety of the alarming odour is not guaranteed. Additionally in the case of the compressed gas storage the condensation of the odorant because of the high pressure is the main issue. In this case, this problem can be overcome by choosing an odorant with concentration levels that can prevent condensation (Kopasz, 2006).

Odorisation Methods

The selection of the point of the addition of the odorant to the hydrogen gas is of great significance. According to the existing literature, adding the odorant after the storage system is a solution that guarantees the longevity and good performance of the storage equipment.

The most typical methods of gas odorization that can be used for the case of hydrogen, depending on the nature (gas or liquid) are:

-
- Wick odorizers
 - By-pass systems
 - Pulse by-pass
 - Bourdon tube
 - Drip systems

(Tenkrat et al, 2010)

Recommendation

DMS is the substance that has been traditionally used for gas odorization. The main advantage is that it can be provided by BOC Company as a direct solution along with the addition method.

As a second option, the GASODOR® S-FREE can be tried. In this case more testing is required as it is a relatively new agent that has not been used with hydrogen. However, it has the significant advantage of being sulphur free and thus more environmental friendly than DMS.

In the United Kingdom the threshold of leak detection in air is 1/5 of the lower flammable limit of the gas. Therefore, for hydrogen that the lower flammability level is 4% this threshold is 0.8%. For Natural gas this number is 1% (equivalent to 20 % of LEL). DMS is detectable in air at a level of 10ppm.

Assuming that 10ppm equals to 10 mg/lit =0.01gr/lit and taking into consideration that the density of DMS is 846 gr/lit, in a 50lit hydrogen tank, the concentrations will be:

- 0.5 gr of DMS, which is 0.000591lit, and a 0.001182% of the total tank volume.
- 99.99881% of the hydrogen-DMS mix will be hydrogen.

The odorisation method that will be used depends strongly on the odorant type , the flow rates, the pressures , the pipeline quality in the case of gas transfer and in general the needs of the application. The most adequate methods that can be followed in this case are wick odorisers and bypass systems that are suitable for low flow rates and the main method they follow is vaporisation (Minier). In more details:

Wick odorisers

The device consists of a storage tank with odorant into which the wick extends through a hole, as shown in Figure I.3. The other end of the wick is placed directly in the stream of fuel gas. The regulation of the dosage is done only by the size of the wick. Extra care must

be taken during low flow operation because there exists the possibility of over-odourisation and accordingly odourisation could be insufficient during high gas flow (Tenkrat, et al., 2010).



Figure I.3, Wick odorizer, adjustable and non-adjustable, source: (Tenkrat, et al., 2010)

By-pass system

This method works by strangling the main stream of natural gas in the pipeline (by means of an orifice, Venturi tube, slide or ram pipe with sideway cant embedded into gas stream). In this way difference of pressures is achieved so that a partial flow of fuel gas, proportional to the main stream of fuel gas, passes through the tank with odorant above its surface, saturates with odorant vapours and returns to main gas stream. Odorant dosage can be controlled by the strangling of fuel gas mainstream, as shown in Figure I.4. The device is suitable for both local odourisation and additional odourisation of fuel gas in central odourisation for a flow up 10,000 m³/h (Tenkrat, et al., 2010).

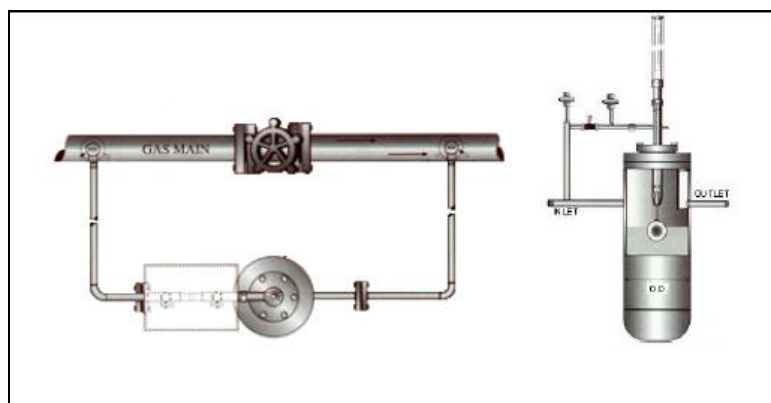


Figure I.4, By-pass odorizer, source: (Tenkrat, et al., 2010)

Colour Agents

According to Schefer et al, emissions from hydrogen flames are visible, despite the common concept of the opposite (Schefer et al, 2009). Nevertheless, this flame visibility occurs in reduced light levels. Schefer tested the hydrogen flames in conditions of 0.33 equivalence ratio of hydrogen and air and inlet velocity 90 m/s, and managed to produce and observe a flame of bluish colour. This phenomenon can also be noted at the launch of the NASA space shuttle, as shown in Figure I.5. The engines of the shuttle run on pure H₂-O₂ fuel mixture and therefore the blue colour is due to the burning of hydrogen (Schefer et al., 2009).



Figure I.5, Space shuttle launch, blue colour for H₂-O₂ fuelled engines, source: (NASA, 2013)

Under normal conditions hydrogen flames are invisible to the human eye, which sets a major danger. It therefore should be examined which solution can add colour to the hydrogen flame. A suggestion could be to test the flame visibility after the addition of the odoring agents. If this fails the next step can be to examine the addition of metal salts that traditionally are used as a mean of flame visibility generators.

As examined by Kaddend sodium chloride (which is the common table salt) and vanadyl sulphate provide a yellow colour to the flames when mixed and burnt with the hydrogen gas (Kaddend, 1966). Kaddend added the metal salt as a spray solution to the hydrogen flame.

There is a variety of flame colorants that are commercialy available and used in industry. Some examples are listed in Table I.1:

Table I.1, typical flame colorants, source: (Kosanke, et al., 2004)

Chemical	Colour
Lithium chloride	Dark red
Strontium chloride	Red
Calcium chloride	Orange
Sodium chloride	Yellow
Borax	Yellowish green
Copper sulphate	Green
Copper chloride	Blue
Potassium chloride	Purple

Critical Factors

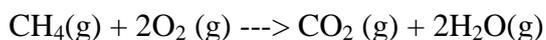
The flame temperature is a critical factor that has to be taken into consideration. The combustion of the substance that will be used as colorant should be examined and its by-products. Methane burns with a flame temperature of 1914°C whereas hydrogen burns with a hotter flame, at 2207°C (Gupta, 2009). The reaction of the above recommended substances with hydrogen under this temperature should be examined. Basic factors that have to be evaluated:

- Reaction between colorant and hydrogen at the combustion temperature
- Percentage of colorant in hydrogen
- Durability of colorant effect. In this aspect the addition of it in the storage medium should be examined.
- When hydrogen burns, the by-product is water. The reaction of the colorant with water has to be taken in consideration also, in the case there will be mixing of them. For example, in the case of metal oxides, the reaction with water producing metal hydroxides that are very strong bases.

The above metal salts can cause skin irradiation while handled and also breathing problems while inhaled. In some cases long-term exposure to them can cause more serious health problems.

The safest of the above substances is Borax, with no reported long-term effects and little risk in handling.

A good and safe solution is the adding of methane to hydrogen gas, for the addition of colour to the flame. This means of course that there will be emissions from the methane burning, but in terms of safety such a compromise is necessary.



Tests have to be performed in order to validate the least possible amount of methane that should be added in order to have a visible flame in daylight. In this case, methane can be added in the cylinders along with the hydrogen gas.

Recommendation

A solution of the above metal salts could be added to the hydrogen gas as an injection or spraying. This should be performed at the entrance to the burner and in any case the concentrations have to be the appropriate ones to ensure a visible flame, verified by testing. The possibility of adding the colouring agent at the same point and with a similar method as the odourant has to be examined. Vital factor is the effect on the storage system, that has to be in any case as minimum as possible. All the suggested colouring agents can be provided by the ScienceLab Company (The Science Lab, 2005).

Solution that prevents hydrogen flame blow-back

In the cases that gas furnaces are not installed properly or are not maintained properly, a gas blow-back may occur. A blow-back is the reverse flow of gases in internal combustion machines and is a very hazardous situation and happens when the gas builds up inside the heater before igniting. A solution to this problem is the installation of an anti-blow-back arrestor or a Flashback arrestor which is a device that stops the flame from burning back up into the equipment and causing damage or explosions. There are usually two types of arrestors:

- **Dry type.** They are mostly used in workshops, homes and portable fuel kits as they work with any orientation and need very little maintenance. They allow free flow of gas through them but take the heat out of the flame front to get it below the ignition temperature of the burning gas mixture.
- **Wet type.** They are liquid barriers following the principle of a siphon where the liquid stops the entering deflagration and/or detonation and extinguishes the flame; their operation is based on passing the gas through a non-flammable and ideally non-gas-absorbing liquid, which is typically water. They stop the flame

by preventing it from reaching the submerged intake. These devices are normally very effective but have the disadvantages of only working in one orientation and of the much larger size than dry type arrestors. This makes them mainly suitable for large or stationary applications and the liquid level needs to be constantly checked (Protego, 2013).

Recommendation

The Flashback arrestor should be placed before the hydrogen burner and after the hydrogen storage system. Depending on the pressure range of the storage- burner system, the adequate arrestor can be selected. There are many commercial products available in the market, that are suitable for use with hydrogen gas. Some typical examples are the following:

- FLASH ARRESTOR SERIES 8491. A product from Specialty Gas Equipment-sgd. It comes with an easily re-settable pressure control which stops gas flow in the event of reverse flow or a flashback that creates 10 psig back pressure. This feature alerts the user that a reverse flow or a flashback of greater than 10 psig has occurred. It is suitable for hydrogen/air mixtures up to 150psig/ 10.3 bar (Specialty Gas Equipment, 2013).
- STAINLESS STEEL FLASH ARRESTOR Model 8492-P4FM. It operates in a similar manner as the previous device, but at lower pressures, 50 psig/ 3.4 bar (Specialty Gas Equipment, 2013)
- Anti Backflash bubbler for hydrogen producing systems (Moreco Energy LLC, 2012).
- Many similar products can be found in eBay and other relevant websites.

Appendix J. Risk Assessment for Hydrogen Lab Work

HAZARDS		ASSESSMENT OF RISK			
	Note The assessment (INSIGNIFICANT, LOW, MEDIUM OR HIGH) is an assessment of the remaining risk <i>AFTER</i> taking the control measures outlined below.	IN-SIGNIF	LOW	MED	HIGH
1	Electrocution from electrical equipment			X	
2	Ingestion of chemicals, nanostructured powders and other hazardous substances		X		
3	Handling compressed gases for energy process (including flammable Hydrogen hazard, Argon, Helium, Nitrogen and Air)		X		
4					
5					
6	Burns (including contacts with furnaces, heating and soldering elements)		X	X	
	Slips, trips and falls		X		
	High energy ball-milling operation (Spex-8000 mixer)				
PRINT Name of Supervisor Dr Zahir Dehouche		PRINT Name of Student: Evangelia Topriska			

DESCRIPTION OF PROJECT AND LOCATION OF WORK:

Investigation of Solar Powered Hydrogen Production for Cooking Applications. The project will be carried out in the Electrical Lab TD404

Planning Controls:

- Use personal protective equipment, e.g. appropriate safety glasses, gloves, fine dust masks and overalls
- Sensitive Hydrogen Detector is installed
- Work in well-ventilated area. Active ventilation system is available to dilute hydrogen leakage and avoid hydrogen confinement
- Use a circuit breaker when using electrical equipment
- All gas cylinders are to be closed after experiments and remaining gas in the line will be purged safely
- High energy ball-milling machine is to be used only under supervision
- Grinding containers should only be opened inside the glove box under inert argon atmosphere

Physical Controls:

- Personal protective equipment, e.g. appropriate safety glasses, gloves, fine dust masks and overalls must be worn during experiments
- when working with flammable chemicals that require extraction the fume hood and the glove box will be used
- for experiments that involve a burning hazard a non-flammable board and mat are available
- Hazards signs regarding high temperature and high pressure apparatuses will be on display
- Floors and walkways shall be generally kept clear of litter, obstructions and trip hazards
- High energy ball-milling machine is equipped with manual lid latch and safety interlock to avoid accidents during operation

Managerial/Supervisory:

- Notify the lab technician and supervisor when carrying out any experiments

Training:

- Anybody without proper training and supervision will not be allowed to carry out experimental work

Signed by Research Student	Date: 21/10/2013
Signed by Supervisor	Date: 21/10/2013
Signed Chief Technician	Date:
With acknowledgments to HASCOM NETWORK LIMITED	

RISK EVALUATION MATRIX

	Insignificant	Minor	Serious	Major
Likely	7 Low	11 Medium	14 High	16 High
Probable	4 Low	9 Medium	13 High	15 High
Possible	2 Insignificant	6 Low	10 Medium	12 Medium
Unlikely	1 Insignificant	3 Insignificant	5 Low	8 Low

NB both severity and likelihood should be evaluated on the basis that all controls specified in the assessment are in place, fully and properly implemented

Severity

Major	e.g. severe burn, fracture requiring hospital admission, fatality
Serious	e.g. a burn or other injury requiring hospital treatment.
Minor	e.g. a cut or other injury requiring first aid.
Insignificant	e.g. a trivial cut or bruises.

Likelihood

Likely	likely to occur in the near future and at frequent intervals
Probable	likely to occur and re occur at intervals
Possible	could occur at some time or other
Unlikely	no more than an extremely remote possibility

Project covered by this evaluation

N B Evaluation AFTER implementation of controls

	Hazards	Severity	Likelihood	Evaluation	Classific'n
1	Electrocution from electrical equipment	Major	Possible	12	Medium
2	Ingestion of chemicals, nanostructured powders and other hazardous substances	Minor	Possible	6	Low
3	Handling compressed gases for energy process (including flammable Hydrogen hazard, Argon, Helium, Nitrogen and Air)	Major	Unlikely	8	Low
4	Burns (including contacts with furnaces, heating and soldering elements)	Serious	Possible	10	Medium
5	Slips, trips and falls	Minor	Possible	6	Low
6	High energy ball-milling operation (Spex-8000 mixer)	Major	Unlikely	8	Low

References

- Moreco Energy LLC, 2012. *The Moreco Hydrogen System*. [Online]
Available at: <http://moregowithhho.com/moreco-hydrogen-system.html>
[Accessed May 2013].
- The Planning Institute of Jamaica & The Statistical Institute of Jamaica, 2007. *Residential Consumer End Use Survey Volume 1- Household Energy & Transport*, Kingston: The Planning Institute of Jamaica & The Statistical Institute of Jamaica.
- University of Wisconsin - Madison, 2012. *TRNSYS 17 Mathematical Reference*, Madison: Solar Energy Laboratory, University of Wisconsin.
- <b.hempel@h-tec.com> Björn Hempel, H.-T., 2012. *email*, s.l.: s.n.
- <F.Salusti@acta-nanotech.com>, F. F. A., 2012. *email*, s.l.: s.n.
- <GVerkoeyen@hydrogenics.com>, G. V., 2012. *email*, s.l.: s.n.
- <James.Brimicombe@boc.com>, J. B., 2013. *email*, s.l.: s.n.
- <pascal.pewinski@ceth.fr>, P. P. C., 2012. *email*, s.l.: s.n.
- <Piers.Capper@boc.com> Capper, P., 2012. *email*, s.l.: s.n.
- <steveh@itm-power.com> Steve Hallett, I., 2012. *email*, s.l.: s.n.
- <TSkoczylas@protononsite.com>, S. T., 2012. *email*, s.l.: s.n.
- Abaoud, H. & Hartmut, S., 1998. The German-Saudi HYSOLAR Program. *International Journal of Hydrogen Energy*, p. 5.
- Air Liquide, 2011. *Air Liquide*. [Online]
Available at: <http://www.uk.airliquide.com/en/products-and-services/specialty-gases/alphagaz.html>
[Accessed November 2012].
- Air Products, 2012. *Air Products*. [Online]
Available at:
http://www.airproducts.co.uk/Prism_Gas_Generation_Systems/Hydrogen_Generators.htm
- Arkema, 2013. *A Basic Understanding of the Chemistry and Characteristics of Natural Gas Odorants*. [Online]
Available at: http://www.arkema-cms.com/user_uploads/site2/brochures/A%20basic%20understanding%20of%20the%20chemistry%20and%20characteristics%20of%20natural%20gas%20odorants.pdf
[Accessed April 2013].
- Arriaga, L., Martinez, W., Cano, U. & Blud, H., 2006. Direct coupling of a solar-hydrogen system in Mexico. *International Journal of Hydrogen Energy*, 32(13), p. 2247–2252.
- ASHRAE, 2008. *ASHRAE IWEC2 Weather Files for International Locations*. [Online]
Available at: <http://weather.whiteboxtechnologies.com/ASHRAE/faq>
[Accessed July 2014].
- Barbir, F., 2005. PEM Electrolysis for production of hydrogen from renewable energy sources. *Elsevier*, p. 9.

-
- BOC, 2011. *BOC Industrial Gases, member of the Linde Group UK*. [Online]
Available at: <http://www.boconline.co.uk/en/index.html>
[Accessed June 2013].
- Braun, N., Muller, D. & Eilers, J., 2010. *EP 1 828 355 B1, ODORANT FOR HYDROGEN BASED ON ACRYLATE AND ACETOPHENONE*, Paris: European Patent Office.
- CETH2, 2012. *5 Nm³/h PEM Electrolyser*. [Online]
Available at: <http://ceth.fr/products-PEM-electrolyser-5-10nm3h.php?PHPSESSID=37ecb40483e1ff86c1f61ffdfbdcafc>
[Accessed November 2012].
- CIBSE, 2007. *Weather, Solar and Illuminance Data-CIBSE Guide J*, London: The Chartered Institute of Building Services Engineers.
- Coleman, H. W. & Steele, G., 1999. *Experimentation and uncertainty analysis for engineers*. 2nd ed. s.l.:John Wiley & Sons.
- Crawley, D. B., 1998. *Which Weather Data Should You Use for Energy Simulations of Commercial Buildings?*, Washington D.C.: ASHRAE.
- Degiorgis, L., Santarelli, M. & Cali, M., 2007. Hydrogen from Renewable Energy: A pilot plant for thermal production and mobility. *Journal of Power Sources*, p. 10.
- Emsley, J., 1998. *The Elements*. New York: Oxford University Press.
- GAISMA, 2014. *GAISMA*. [Online]
Available at: <http://www.gaisma.com/en/info/help.html>
[Accessed May 2014].
- Galli, S. & Stefanoni, M., 1997. Development of a Solar-Hydrogen Cycle in Italy. *International Journal of Hydrogen Energy*, p. 6.
- Gas, L., 2012. *Linde gas generators*. [Online]
Available at: [http://hiq.linde-gas.com/international/web/1g/spg/like351gspg.nsf/repositorybyalias/gg_h2_nm_leaflet/\\$file/Leaflet%20HiQ%20Hydrogen%20NM%20Gas%20Generator.pdf](http://hiq.linde-gas.com/international/web/1g/spg/like351gspg.nsf/repositorybyalias/gg_h2_nm_leaflet/$file/Leaflet%20HiQ%20Hydrogen%20NM%20Gas%20Generator.pdf)
[Accessed November 2012].
- Goetzberger, A., Bopp, G., Griesshaber, W. & Stahl, W., 1993. *The PV/Hydrogen/Oxygen System of the Self-Sufficient House Freiburg*, Freiburg, Germany: Freinhofer Institute for Solar Energy Systems.
- Government of Ghana, 2013. *Government Distributes 8,000 Solar Lanterns To Communities*. [Online]
Available at: <http://ghana.gov.gh/index.php/2012-02-08-08-32-47/general-news/1398-government-distributes-8-000-solar-lanterns-to-communities>
[Accessed November 2014].
- Grasse, W., Oster, F. & Abaoud, H., 1991. HYSOLAR: The German-Saudi Arabian Program in Solar Hydrogen-5 Years of Experience. *International Journal of Hydrogen Energy*, p. 7.
- Gupta, R. B., 2009. *Hydrogen Fuel: Production, Transport and Storage*. Boca Raton: Taylor&Francis Group, LLC.
-

-
- H-TEC Systems, 2012. *H-TEC Systems*. [Online]
Available at: <http://www.h-tec.com/en/systems/el-30-electrolysers/>
[Accessed November 2012].
- Hydro, 2012. *Hydro*. [Online]
Available at: <http://www.hydro.com/en/>
[Accessed November 2012].
- Hydrogenics, 2012. *Hydrogenics- Advanced Hydrogen Production*. [Online]
Available at: <http://www.hydrogenics.com/assets/pdfs/ANNEX%201%20-%20HyLYZER-1.pdf>
[Accessed November 2012].
- Intelligent Energy, 2012. *Intelligent Energy*. [Online]
Available at: <http://www.intelligent-energy.com/>
- Kaddend, A. S., 1966. *Luminescence of Vanadium Oxide particles in Hydrogen Flames*, Surrey: Central Electricity Research Laboratories.
- Kopasz, J., 2006. Fuel Cells and Odorants for Hydrogen. *International Journal of Hydrogen Energy*, p. 5.
- Kosanke, B. J. et al., 2004. *Pyrotechnic Chemistry*. USA: Journal of Pyrotechnics.
- McPhy Energy, 2012. *McPhy Energy*. [Online]
Available at: <http://www.mcphy.com/en/green-hydrogen/carbon-free-hydrogen/>
[Accessed November 2012].
- Meteotest, 2014. *Weather Stations in Meteorology*. [Online]
Available at: <http://meteorology.com/en/>
[Accessed July 2014].
- Meurer, C. et al., 1999. Phoebus- An Autonomous Supply System with Renewable Energy: Six Years of Operational Experience and Advanced Concepts. *Solar Energy*, p. 8.
- Minier, P., n.d.. *Principles of Odourisation, A discussion of odourant, odourizers, and odourization*, Melbourne: OdorEyes Technologies, Inc..
- NASA, 2013. *NASA*. [Online]
Available at:
http://search.nasa.gov/search/search.jsp?nasaInclude=space+shuttle+launch+images&selectedtab=2&entqr=0&output=xml_no_dtd&sort=date%3AD%3AL%3Ad1&ud=1&site=nasa_collection&client=nasa_production&ie=UTF-8&oe=UTF-8&simple_start=&news_start=&images_start=0&v
[Accessed April 2013].
- NOAA - National Oceanic and Atmospheric Administration, 2014. *National Oceanic and Atmospheric Administration*. [Online]
Available at: <http://www.noaa.gov/>
[Accessed July 2014].
- Papagiannakis, I., 2005. *Studying and Improving the Efficiency of Water Electrolysis using a proton Exchange membrane electrolyser*, Glasgow: University of Strathclyde.
- Paul, B., 2009. *DIRECT-COUPLING OF THE PHOTOVOLTAIC ARRAY AND PEM ELECTROLYSER IN SOLAR HYDROGEN SYSTEMS FOR REMOTE AREA*. [Online]
Available at:
-

http://www.google.com/url?sa=t&rct=j&q=&esrc=s&source=web&cd=6&ved=0CFYQFjAF&url=http%3A%2F%2Fresearchbank.rmit.edu.au%2Feserv%2Frmit%3A6771%2FPaul.pdf&ei=MK6zUJO3KuTB0gXZ3YC4BQ&usg=AFQjCNHxTdpO_b18fADAnQoHnDBzn3Bsrg&sig2=bXGZLcLD2trRDHV3ydkPzw
[Accessed November 2012].

Pertamina, 2008. *Kerosene to LP Gas Conversion Programme in Indonesia*, France: World LP Gas Association.

Protego, 2013. *Protego*. [Online]
Available at: <http://www.protego.de/en/products/technical-fundamentals/flame-arresters>
[Accessed May 2013].

Rifkin, J., 2003. *The Hydrogen Economy*. Cambridge: Polity Press.

Sandia National Laboratories, 2014. *Sandia National Laboratories*. [Online]
Available at: <http://www.sandia.gov/>
[Accessed July 2014].

SMA Solar Technology AG, 2013. *Sunny Portal*. [Online]
Available at: <http://www.sunnyportal.com/Templates/Start.aspx?ReturnUrl=%2f>
[Accessed July 2014].

Specialty Gas Equipment, 2013. *FLASH ARRESTOR SERIES 8491*. [Online]
Available at: <http://www.gasequipmentcatalog.net/84.php?id=19>
[Accessed May 2013].

Symrise, 2013. *GASODOR S-FREE, The World's First Sulphur Free Odorant*. [Online]
Available at: http://www.gasodor-s-free.de/fileadmin/user_upload/pdf/Gasodor_englisch.pdf
[Accessed May 2013].

Tenkraat, D., Hlincik, T. & Prokes, O., 2010. *Natural Gas Odorization*. [Online]
Available at: <http://www.intechopen.com/books/natural-gas/natural-gas-odorization>

The Science Lab, 2005. *The Science Lab*. [Online]
Available at: <http://www.sciencelab.com/page/S/CTGY/10403>
[Accessed June 2013].

University of Exeter, 2013. *Weather Files for Current and Future Climate*. [Online]
Available at:
http://emps.exeter.ac.uk/media/universityofexeter/emps/research/cee/lchsmodule1notes/Weather_Files.pdf
[Accessed July 2014].

University of Wisconsin - Madison, 2014. *TRNSYS Standard Component Library Overview*, Madison: University of Wisconsin - Madison.

US Department of Energy, 2013. *Energy Plus Simulation Software - Weather Data for Simulation*. [Online]
Available at:
http://apps1.eere.energy.gov/buildings/energyplus/weatherdata_simulation.cfm
[Accessed July 2014].

User's Manual for TMY2, 2013. *User's Manual for TMY2*. [Online]
Available at: <http://rredc.nrel.gov/solar/pubs/tmy2/appendixa.html>
[Accessed July 2014].

Weather Online, 2015. *Weather Online- Indonesia*. [Online]
Available at: <http://www.weatheronline.co.uk/reports/climate/Indonesia.htm>
[Accessed February 2015].

Wheeler, A. J. & Ganji, A., 1996. *Introduction to Engineering Experimentation*. 3rd ed.
s.l.:Pearson.

Wilcox, S. & Marion, W., 2008. *User's Manual for TMY3 Data Sets*. [Online]
Available at: <http://www.nrel.gov/docs/fy08osti/43156.pdf>
[Accessed July 2014].

Yilanci, A., Dincer, I. & Ozturk, H., 2008. A Review on Solar Hydrogen/Fuel Cell Hybrid Energy Systems for Stationary Applications. *Progress in Energy and Combustion Science*, p. 14.